



00830897 7

ΘΝΕΣ ΣΥΝΕΔΡΙΟ ΘΑΛΑΣΣΙΑΣ  
ΔΙΑΒΡΩΣΗΣ ΚΑΙ ΡΥΠΑΝΣΗΣ  
ΤΩΝ ΥΦΑΛΩΝ ΚΑΤΑΣΚΕΥΩΝ

6th INTERNATIONAL CONGRESS  
ON MARINE CORROSION AND  
FOULING

6ème CONGRES INTERNATIONAL  
DE LA CORROSION MARINE  
ET DES SALISSURES

---

MARINE CORROSION

---

Athens 5-8 SEPTEMBER 1984

GREECE

547.92

MAR

19924

# MARINE CORROSION



574.92  
 MAR  
 19924

DATE DUE

|         |  |  |
|---------|--|--|
| 15-4-23 |  |  |
|         |  |  |
|         |  |  |
|         |  |  |
|         |  |  |
|         |  |  |
|         |  |  |
|         |  |  |
|         |  |  |
|         |  |  |
|         |  |  |
|         |  |  |
|         |  |  |
|         |  |  |
|         |  |  |
|         |  |  |
|         |  |  |
|         |  |  |
|         |  |  |
|         |  |  |

RAECO

6ο ΔΙΕΘΝΕΣ ΣΥΝΕΔΡΙΟ ΘΑΛΑΣΣΙΑΣ  
ΔΙΑΒΡΩΣΗΣ ΚΑΙ ΡΥΠΑΝΣΗΣ 1992 4  
ΤΩΝ ΥΦΑΛΩΝ ΚΑΤΑΣΚΕΥΩΝ

6th INTERNATIONAL CONGRESS  
ON MARINE CORROSION AND  
FOULING

6ème CONGRES INTERNATIONAL  
DE LA CORROSION MARINE  
ET DES SALISSURES

---

MARINE CORROSION

---



DEFENCE INFORMATION SERVICES



00830897 7

Athens 5-8 SEPTEMBER 1984

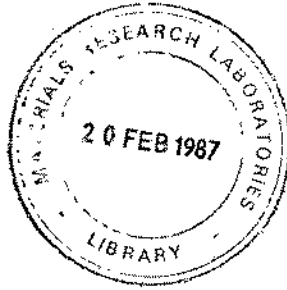
GREECE

87/19924

National Technical University  
Section of Material Science  
Lab. of Physical Chemistry

12-2-87

19924



CORROSION INDUCED BY MECHANICAL EFFECTS  
CORROSION SOUS DES EFFETS MECANIQUES

|   | <u>Pages</u> |
|---|--------------|
| A.M.BECCARIA, E.D.MOR, G.POGGI, T.BARCARO: "Effects of Hydrostatic Pressure on the Corrosion of Copper Alloys in Sea Water" (Italy).....  | 9-25         |
| Th.SKOULIKIDIS, N.KOULOUMBI: "Etude préliminaire de l'influence d'oxydes, électrolytiquement préparés, sur la vie de l'acier subissant corrosion sous contrainte dans une solution de NaCl" (Greece)..... | 25-40        |
| Th.SKOULIKIDIS, Ath.KARAGEORGOS, M.NERSISYAN: "Protection of Al-2.5% Mg Alloy Against S.C.C. in Saline Water by Properly Oriented Anodic Coatings; application to various sheet thicknesses" (Greece)...  | 41-58        |
| H.SHIMADA: "Small Scale Field Test of Steel Wire Ropes in Submerged Sea Water which is Simulating Tension Leg Platform Mooring" (Japan).....  | 59-74        |
| J.M.KROUGMAN, F.P.IJSSELING: "Crevice Corrosion Testing of Stainless Alloys in Seawater" (Netherland).  | 75-96        |
| W.H.HARTT: "Composition and Morphology of Calcareous Deposits Within Simulated Fatigue Cracks in Sea Water" (U.S.A.).....   | 97-111       |

CORROSION STUDIES  
ETUDES SUR LA CORROSION

|   |         |
|---|---------|
| A.R.Di SARLI, N.G.TONEGUZZO, J.J.PODESTA: "Relationships of Different Physicochemical Parameters of Polymeric Coatings Applied on Metal Substrates Obtained by AC and DC Measurements" (Argentina)..... | 115-130 |
|---|---------|

|  | <u>Pages</u>       |
|--|--------------------|
| S.L.GRANESE, E.S.AYLLON, C.BONAZZOLA, B.M.ROSALES:<br>"Atmospheric Marine Corrosion of Fe and Zn" (Argentina).....   | 131-143            |
| H.ROPER: "Durability of Concrete Marine Structures"<br>(Australia).....  | 145-164 <i>Pha</i> |
| C.JIAN: "Materials Selection for Marine Instruments<br>and Alleviation of Corrosion Problems" (China)....  | 165-175            |
| A.J.EDWARDS: "Application of Electrochemical Tech-<br>niques to the Prediction of Environmental Effects<br>on the Corrosion Behaviour of a Ni-Ti Alloy" (En-<br>gland).....  | 177-187            |
| J.C.CHARBONNIER, M.CONFENTE, T.JOSSIC, L.LEMOINE,<br>J.L.PAGNIEZ: "Influence de quelques elements d'al-<br>liage sur la résistance à la corrosion marine d'<br>aciers faiblement alliés" (France).....                                       | 189-204            |
| Ph.BLANCHARD, J.COURTOT-COUPÉZ, L.LEMOINE: "Étude<br>de la corrosion d'aciers en eau de mer par mesure<br>de l'impédance électrochimique" (France).....  | 205-220            |
| D.FESTY, L.LEMOINE: "Effet de la pression hydrosta-<br>tique sur la perméation de l'hydrogène dans l'acier,<br>dans des conditions de chargement électrolytique"<br>(France).....  | 221-232            |
| J.C.LUMARET: "Une nouvelle composition inhibitrice<br>à base de gluconate de zinc pour lutter contre la<br>corrosion marine" (France).....   | 233-248            |
| M.DUPRAT, F.DABOSI, F.MORAN: "Electrochemical Mea-<br>surements Applied to the Corrosion and Protection<br>Study of a Carbon Steel in 3% Sodium Chloride So-<br>lution" (France).....  | 249-268            |
| A.MOLLIKA, A.TREVIS, E.TRAVERSO, G.VENTURA, V.SCOT-<br>TO, G.ALABISO, G.MARCENARO, U.MONTINI, G.de CARO-<br>LIS, R.DELLEPIANE: "Interaction Between Biofouling<br>and Oxygen Reduction Rate on Stainless Steel in<br>Sea Water" (Italy)..... | 269-281            |

|   | <u>Pages</u> |
|---|--------------|
| K.DABROWIECKI, K.BORON: "The Influence of the Surface Treatment on Corrosion of CuNi10Fe1Mn Alloy in Artificial Sea Water" (Poland).....  | 283-289      |
| J.JORBA, P.MOLERA: "Corrosion Marine Resistance of Nitrided Steel" (Spain).....   | 291-296      |
| H.S.PREISER, A.TICKER: "A Novel System for Preserving Hull Areas Obscured by Docking Blocks for Optimum Fuel Savings" (U.S.A.).....   | 297-313      |
| OFF-SHORE   |              |
| TOSHIYUKI YASUI: "Coatings for Offshore Structures and Ships in Frozen Sea" (Japan).....  | 317-331      |
| COATINGS  |              |
| PEINTURES   |              |
| Th.SKOULIKIDIS, P.VASSILIOU: "New Anticorrosive Paints" (Greece).....   | 335-346      |
| A.B.SAMUI, R.K.BANERJEE, DHIRENDRA KUMAR, C.P.DE: "Performance of Metallic and Non-Metallic Coatings in Marine Coastal Zone in India" (India).....                              | 347-360      |
| IWAO MOMIYAMA, HIROSHI KURIYAMA, TADAKAZU KYONO, TSUKASA KURIYAMA: "Investigation on Long-Term Durability of Protective Coatings for Steels in Marine Environment" (Japan)..... | 361-379      |
| F.H. de la COURT: "A Classification System for Anti-fouling Paints Based on a Dynamic Flow Test" (Netherland).....  | 381-400      |
| M.MORCILLO, S.FELIU, J.SIMANCAS, J.M.BASTIDAS: "Application of the AC Impedance Measurements to Predict Paint Systems Performance in Marine Atmospheres" (Spain).....           | 401-415      |
| S.FELIU, F.UTRILLA, M.MORCILLO: "An Impedance Study of Cathodic Delamination in Marine Paints" (Spain).....   | 417-432      |



|   | <u>Pages</u> |
|---|--------------|
| Th.DOWD: "Ablative Antifouling Coating Systems"<br>(U.S.A.).....  | 433-439      |
| S.SKLEDAR: "Behaviour of Pigmented Finishes in Ma-<br>rine Environment" (YUGOSLAVIA).....   | 441-453      |
| CATHODIC PROTECTION<br>PROTECTION CATHODIQUE  |              |
| D.J.TIGHE-FORD, J.N.McGRATH: "Analysis of the Time-<br>Dependent Development of Cathodic Protection Within<br>Pipes" (England).....   | 457-468      |
| D.EUROF DAVIES, K.G.WATKINS: "An Initial Investiga-<br>tion of pH Changes Close to the Surface of Alumin-<br>ium With Prolonged Cathodic Polarisation in Sea Wa-<br>ter" (England).....       | 469-483      |
| J.J.RAMEAU, Ph.GIMENE <sup>3</sup> , M.C.REBOUL: "Rôle de l'in-<br>doum dans la dépassivation des anodes Al-Zn-In u-<br>tilisées en protection cathodique" (France).....                      | 485-499      |
| A.COLOMBO, G.ROCCHINI: "Calculation of Current Den-<br>sity Distrubution for a Correct Application of Ca-<br>thodic Protection" (Italy).....  | 501-516      |
| J.F.TATUM, J.F.TATUM Jr.: "Cathodic Protection With<br>Deep Anode Groundbeds" (U.S.A.).....   | 517-530      |
| S.GRENET, J.GALLAND, M.GROOS: "Etude de la suscepti-<br>bilité à la corrosion marine d'un acier industriel<br>soumis à des impulsions anodiques, sous protection<br>cathodique" (France)..... | 531-540      |

**CORROSION INDUCED BY MECHANICAL EFFECTS**  
**CORROSION SOUS DES EFFETS MECANIKUES**

Effects of hydrostatic pressure on the corrosion of copper alloys in sea water.

A.M. BECCARIA - E.D. MOR - G. POGGI - T. BARCARO

Istituto per la Corrosione Marina dei Metalli

Via della Mercanzia, 4 - 16123 GENOVA - ITALIA

#### Abstract

The electrochemical behaviour of some metals was examined (copper, zinc, 70-30 Cu-Zn, Nickel, 70-30 Cu-Ni) at various hydrostatic pressures.

By increasing pressure, the  $i_{\text{corr}}$  of copper, brass and zinc increases, that of cupronickel alloy remains about constant and that of nickel decreases.

The increase of the corrosion rate with increasing pressure is due to the acceleration of the cathodic reduction process for copper and of the anodic process acceleration for brass alloy and for zinc.

The inhibition of the nickel corrosion was explained with the formation of a passivating layer with a greater dielectric constant than those formed at ambient pressure.

#### Resumé

On a examiné le comportement électrochimique de quelques matériaux métalliques (cuivre, zinc, cuivre-zinc 70-30, nickel, cuivre-nichel 70-30) à de différentes pressions hydrostatiques. On a vu que en augmentant la pression hydrostatique augmente la  $i_{\text{corr}}$  du cuivre, du laiton et du zinc, tandis que la  $i_{\text{corr}}$  de l'alliage cuivre-nichel reste à peu près constante et diminuée celle du nickel.

L'augmentation de la vitesse de corrosion est due à l'accélération du processus cathodique pour le cuivre et à l'accélération du processus anodique pour le laiton et pour le zinc.

L'inhibition de la corrosion du nickel est due à la formation, par effet de la pression hydrostatique, d'un film de passivation ayant une constante diélectrique plus élevée que celles des films formés à la pression ambiante.

### Introduction

On the basis of fieldtests made at various depths in the Pacific Ocean, Reinhart (1-3), De Lucia (4), Morney (5) and Gray (6) deduced that the influence of hydrostatic pressure on the generalized corrosion was negligible for aluminum, iron, nickel and copper.

An increase of the susceptibility of aluminum and its alloys to pitting corrosion and an inhibition of the localized corrosion for nickel-copper alloys was observed.

This effect was suggested (1-3) to be due to a lower concentration of dissolved oxygen (D.O) in deep water (3 ppm) with respect of surface water (6-8 ppm); this may be true for nickel alloys, because it is known (7) that the corrosion resistance of nickel increases with increasing D.O. concentration in sea water, but is not probable for aluminum and its alloys that a low pressure have the same behaviour as nickel.

Recently, Dexter (8-10) suggested that the higher susceptibility of aluminum to pitting corrosion is due to the changes of pH and temperature, rather than to the different D.O. concentration.

This phenomenon is not yet completely elucidated, as Huesler (11) found that in a weakly alkaline environment the corrosion rate of aluminum increases with increasing hydrostatic pressure, being constant temperature and D.O. This was explained with the change of the  $\text{OH}^-$  ions activity and of the corrosion products solubility.

Previous experiments (12-14) made in our laboratory showed that the corrosion rate of some metals (copper and iron) increases with increasing hydrostatic pressure, and that this effect is enhanced by increasing temperature from 5° to 20°C.

This was explained with the acceleration of the cathodic depolarization process for both the examined metals, but the true mechanism and the amount of this effect were not completely elucidated. The increase of the corrosion rate of copper with increasing hydrostatic pressure is in fact much greater (>10%) than the value that can be expected on the basis of the changes of the parameters influencing the cathodic depolarization process (equilibrium constants of systems  $\text{CO}_3^{--}$ ,  $\text{HCO}_3^-$ ,  $\text{CO}_2$ ;  $\text{BO}_3^{--}$ ,  $\text{H}_2\text{BO}_3^{--}$ ,  $\text{HBO}_3^-$ ;  $\text{SO}_4^{--}$ ,  $\text{HSO}_4^-$ , etc.; increase of the conductivity of the solutions; increase of the diffusion coefficient of dissolved gases; decrease of pH).

All these parameters changes less than 5% at 1000 Atm with respect of ambient pressure values.

Some transport processes (dielectric relaxation, diffusion, viscous flow, "normal" conduction, protonic conduction) that are connected with the hydration of ions, their apparent ionic radius and their mobility, assume in the corrosion process a great importance that cannot be completely foreseen on the basis of the available theories. This seem to be confirmed by the results of the researches of Horne on the thermodynamic of sea water (15).

In order to elucidate the effect of hydrostatic pressure on the corrosion of various metals, the electrochemical behaviour, sensitive to pressure, of some metals (e.g. copper) was compared with that of metals whose corrosion is probably not influenced by this parameter (e.g. nickel).

#### Experimental

The composition of the used samples is shown in Table 1. All specimens, polished with abrasive paper (from 180 to 600) and washed with petroleum ether, were immersed in sea water at a pH of 8.1 with a dissolved oxygen concentration of about 7 ppm.

The value of dissolved oxygen content refers also to the pressurized water. The sea water in the pressure vessel had the same content as that measured at ambient pressure because the vessel was pressurized by using a hydropneumatic pump after removing all air bubbles. The liquid used for compression was the same sea water.

Temperature was set at 5 - 10 - 20°C ( $\pm 0,1^\circ\text{C}$ ) for copper and alloy 260 (OT 70-30) and at 20°C ( $\pm 0,1^\circ\text{C}$ ) for other materials.

The pressure vessel used for the experiments was made of stainless steel (AISI 316) coated with alchidic resin, with the electrodes placed in the same position as in the ASTM G5-72 cells, and had a volume of about 3.5 litres.

The working electrode was a rod 25 mm long, 8 mm dia.

The counter electrodes were made with electrically insulated platinum cylinders.

The reference electrode was Ag-AgCl. Potentiodynamic polarization test, measurement of the polarization resistance ( $R_p$ ) and of the electrode capacity ( $C$ ) were made. The potentiodynamic plots were obtained with specimens previously immersed for 2 hours, in free corrosion in the pressurized vessel.

A Tacussel PRT 20-X potentiostat was used, with a scanning speed of 250 mV/h.

The anodic and the cathodic polarization curves were obtained separately, and polarization cycles (cathodic-anodic) were also made with the same scanning speed.

The polarization resistance and the electrode capacity values were measured with a Tacussel Corrovit instrument, connected with a x-y recorder.

Potentiostatic measurements of the  $R_p$  values were made either step by step, by slightly changing the potentials ( $\pm 1.25$ ,  $\pm 2.5$ ,  $\pm 5.0$  mV) and waiting for equilibration, or by cyclically changing the potential ( $\pm 1.25$ ,  $\pm 2.5$  mV) with a frequency of 0.1 Hz. The electrode capacities ( $C$ ) were measured either galvanostatically or potentiostatically, with cycles of 0.1 Hz,  $\pm 250$   $\mu\text{A}$ ,  $\pm 1.25$  mV or  $\pm 1250$   $\mu\text{A}$ , 2.5 mV, depending on the composition of the sample.

### Results and discussion

Table 2 shows the parameters of the corrosion kinetics of copper in sea water obtained in the experiments.

The  $R_{pa}^{-1}$  and  $R_{pc}^{-1}$  values (anodic and cathodic polarization conductance) were obtained with semistationary polarization measurements.

The  $R_p^{-1}$  values shown in the 3rd column of Table 2 are the average of the values obtained by potentiodynamic curves, by semistationary polarization and by cyclic linear polarization measurements.

In the two first cases the Stern and Gray formula was applied, in the latter the method of MacDonald, Syrett and Wing (16) was used for the calculation of  $R_p^{-1}$  with linear cyclic polarization. The  $R_p^{-1}$  values were averaged because their difference was never greater than  $\pm 15\%$ .

The  $i_{corr}$  values (6th column) are the average of the values obtained by applying the Stern and Geary formula to the potentiodynamic polarization curves and to the results of the semistationary polarization tests. The difference between the obtained results was never greater than  $\pm 15\%$ . The  $C$  values (electrode capacitance) are the average of the potentiostatic and galvanostatic results. The two series of values do not differ more than  $\pm 10\%$ .

The results of Table 2 show that the copper corrosion rate increases both with increasing temperature and with increasing hydrostatic pressure. The change of hydrostatic pressure seems also to influence the physico-chemical properties of the passivation layer. The  $R_{pa}^{-1}$  and  $R_{pc}^{-1}$  values show that the cathodic conductance of the electrode increases when the hydrostatic pressure increases from 1 to 150 Atm, and that this increase is greater at 20°C.

The polarization conductance also increases with increasing pressure, showing either a decrease of the thickness of the passivation layer or a change of its composition.

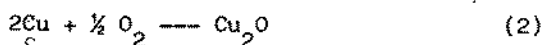
The latter hypothesis is confirmed by the electrode capacitance values, showing that the passivation layer is mainly formed by oxides ( $C \leq 100 \mu F \cdot cm^{-2}$ ).

The potentiodynamic curves (fig. 1) show that the anodic process is not influenced by the increase of hydrostatic pressure that on the contrary increases the cathodic reduction rate (12-13). The cathodic sweep of the potentiodynamic curve of fig. 1 shows two reduction peaks at ambient pressure: at -320 mV (Ag-AgCl) and at -700 mV (Ag-AgCl).

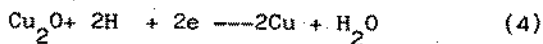
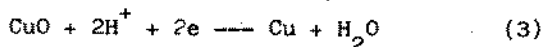
At 150 Atm only a small peak is observed at -300-350 mV (Ag-AgCl). The range of potential at about -300 corresponds to the reduction  $Cu^{++} \rightarrow Cu^+$ , while the -700 mV region is characteristic of the  $Cu^+ \rightarrow Cu$  reduction (17-19).

The cathodic curves of fig. 1 also show that  $Cu^+$  compounds are not detectable on the surface of specimens treated at 150 Atm.

This can be explained by the electrochemical reduction of oxygen on the copper surface that follows the first chemical step (20). Copper reacts with the D.O of seawater to give oxide layers that are easily reduced:



followed by an electrochemical process:



By increasing  $\text{H}^+$  concentration, reaction 3 and 4 are enhanced and the metal is not passivated.

By increasing the hydrostatic pressure the  $\text{H}^+$  ions, whose concentration and contribution to the overall conductivity are small in sea water, increase their mobility more than other ions (21) and therefore increase the reduction rate of copper oxides.  $\text{CuO}$  and  $\text{Cu}_2\text{O}$  are p-type semiconductors with many cationic vacancies (22-23). Cationic transportation processes in the lattice (having a  $\text{Pn3m}$  spatial structure) are enhanced by the high number of cationic vacancies. The electronic resistance is small because the electron transfer between  $\text{Cu}^+$  and  $\text{Cu}^{++}$  ions requires a small energy. Therefore, the decrease of the apparent ionic radius of  $\text{H}^+$  ions, due to hydrostatic pressure, enhances their diffusion in the oxide layer.

Fig. 1 shows that the contribution to the  $i_{\text{cat}}$  given by the reduction intensities of  $\text{Cu}^{++}$  ( $\approx -300$  mV) and  $\text{Cu}^+$  ( $\approx -700$  mV) is appreciably higher when the specimen is under hydrostatic pressure. The intensity of the reduction limiting current ( $i_D$ ), on the contrary, is only 10% greater at 150 than at 1 atm, according with the theoretical calculation.

The intensity of the limit current is connected to the diffusion coefficient of oxygen by the relationship: (24)

$$i_D = \frac{DnFc}{\delta} \quad (5)$$

where  $D$  = diffusion coefficient,  $F$  = Faraday constant,  $c$ : oxygen concentration in the electrolyte,  $\delta$ : diffusion-limited layer thickness,  $n$  = number of electrons passed through the boundary surface.

The diffusion coefficient increases with increasing hydrostatic pressure, but up to 100 Atm the increase is about 6-7%. The increase of the corrosion rate of copper is therefore mainly due to increased activity of  $\text{H}^+$  ions.

The researches of Shams el Din (17) on the behaviour of copper-zinc alloys in alkaline solutions and our previous results (25) on the corrosion of brass in sea water showed that when copper in the alloy

is more than 60%, the alloy undergoes corrosion in the same way as pure copper does.

The electrochemical behaviour of a 70-30 brass at different hydrostatic pressures was therefore investigated to verify if the same effect is also observed at high pressure.

Table 3 shows the main parameters of the corrosive process, measured at 5, 10, 20°C with different pressures. Fig. 2 shows the most significant polarization curves at 150 atm and 20°C.

The values of Table 3 show that, as copper does, the tested alloy increases its corrodibility with increasing pressure, but, while the anodic conductance of copper does not change, both anodic and cathodic conductance of brass change of about 20%, showing that both anodic and cathodic processes are changed.

By increasing the polarization conductance, the electrode capacity for copper decreases, for brass increases. This can be explained by the decrease of the passivation layer on copper and by the change of the structure of the layer on brass, shown by the reduction of  $\text{Cu}^+$  ions at -700 mV at low pressure and at -650 mV at high pressure (polarization curves of Fig. 2).

This fact can be explained with the prevailing formation in this layer of zinc oxydation product that cover the copper oxide layer changing its dielectric properties (electrode capacity) and increasing the anodic conductance. Chemical analyses shown that Cu-Zn ratio is greater (more than +20%) in the corrosion products formed at ambient than at high pressure.

It can therefore be concluded that Cu-Zn alloys that behave in the same way as copper at ambient pressure show a different corrosion process at high hydrostatic pressure.

The same investigation was also made by using zinc specimens, at 20°C and at 1 and 150 Atm, in order to verify the effect of Zn on the behaviour of brass alloys.

Table 4 and fig. 3 show that the electrochemical behaviour at 150 atm is completely different from that of copper because the rate of the anodic corrosion process is increased while the cathodic process remains unchanged. The  $R_{pc}^{-1}$  values are constant while the  $R_{pa}^{-1}$  values appreciably change. The electrode capacity, relatively high and showing the simultaneous presence of zinc oxides and salts, does not change with changing pressure, probably because zinc is a n-type metal without cationic vacancies that act as an electron donor.

The zinc oxides reduction does not depend on the greater diffusion of  $\text{H}^+$  ions into the lattice vacancies of the oxydation products and is therefore near independent on pressure. The small increase ( $\sqrt{5\%}$ ) of the  $i_D$  of cathodic sweep of the polarization curve of fig. 3 is due to the increase of conductivity, of the diffusion coefficient of oxygen, etc., as previously seen for copper.

The anodic process is accelerated, probably owing to the easier



-adsorption of depolarizing anions (as  $\text{Cl}^-$ ) on the passivation layer, that is enhanced at high pressure by the smaller solvation and by the decrease of the apparent ionic radius.

The anion adsorption which introduces electron acceptor levels in the film, will lower the transpassivation potential at the adsorption sites (27) and break the barrier effect. The passive film on n-type (electron-donor) appears to be more stable against anodic polarization than that of p-type, electron-acceptors, oxides.

The hydrostatic pressure probably increases the number of electron-acceptor sites, the film behaves as a p-type compound and is therefore more easily corroded.

In order to verify if the addition of another component (Ni) changes the behaviour of the alloy at high pressure, cupronickel alloy 70-30 with the same copper amount of the previously examined Cu-Zn alloy was tested at  $20^\circ\text{C}$  by comparing the results obtained at 1 and 150 atm. Table 5 and fig. 4 show that pressure does not increase the corrosion rate of this alloy; from the  $i_{\text{corr}}$  and  $R_p^{-1}$  values and from the increase of the equilibrium potential appears that at high hydrostatic pressure the cupronickel corrosion is inhibited ( $\Delta i_{\text{corr}}$  about 50% with respect of ambient pressure).

The potentiodynamic polarization curves of fig. 4 show that at 150 atm the passivation layer is nearly completely formed by a single nickel compound (reduction peak at  $-240$  mV) while at 1 atm several products are detected ( $-240$ ,  $-500$ ,  $-700$  mV).

The passivation of the alloy may be due to the compound formed in both test condition.

The compounds of cupronickel alloys slightly differ from these formed on copper and brass. The reduction peak moves from  $-380$  to  $-500$  mV, probably due to the precipitation of large amounts of  $\text{Ni}^{2+}$  in the  $\text{CuO}$  lattice (28). The low inhibition value (probably due to Ni compounds) can be explained with the amount (30%) of Ni in the alloy. The Ni oxidation products cannot cover the whole surface but only decrease the anodic oxidation sites.

In order to verify if the reduction peaks at  $-240$  mV were due to Ni compounds and to investigate their effect on the corrosion of the alloy, some tests were carried out with pure Nickel (Table 6 and fig. 5). Fig. 5 shows that the  $-240$  mV peak of the cathodic sweep of the cupronickel polarization curves is due to Ni compounds.

Reduction peaks at  $-220$  and  $-240$  mV were in fact observed at ambient pressure and at  $-210$  mV at 150 atm. on nickel.

Values of Table 6 show that the anodic and cathodic conductances are much lower than these of previously studied metals.

This can be explained by the fact that the oxidation compounds of nickel are p-type oxides (29) with cationic vacancies concentrated on the surface only, that do not show ionic transportation processes.

They have a high electronic resistance because the electronic transitions between  $Ni^{++}$  and  $Ni^{+++}$  requires high energy. This decreases the anodic attack of the passivation film, which has n-type characteristics. The value of  $i_{corr}$  is in fact small. The small values of the electrode capacity indicates oxide formation. Moreover, as the electrode capacity at 150 atm is greater ( $42.9 \mu F cm^{-2}$ ) than at ambient pressure ( $6.6 \mu F cm^{-2}$ ) and the electrode conductance and the  $i_{corr}$  are on the contrary much smaller, the compound formed at 150 atm has a greater dielectric constant than that of compound formed at ambient pressure and can therefore better passivate the metallic surface. This is confirmed by the equilibrium potential values  $E_{150 atm} = -81 mV$  and  $E_{1 atm} = -212 mV$ . Fig. 6 shows that hydrostatic pressure does not influence the cathodic reduction process. This can be explained by the fact that the nickel oxydation products have cationic vacancies on their surface only and  $H^+$  ions cannot therefore enter the lattice and are discharged on the electrode. The anodic process is largely inhibited at 150 atm, owing to the formation of a nickel oxydation product (not identified) having a greater dielectric constant than these formed at ambient pressure.

#### Conclusions

The results show that hydrostatic pressure can influence the corrosion kinetic of some metals. This is correlated with the solvation processes connected to transport phenomenon and ionic mobility. The concentration of  $H^+$  in sea water is very low and their contribution to the overall conductivity is negligible, but can play a significant role on the cathodic depolarization of metals, because the protonic mobility largely increases by increasing the hydrostatic pressure. The different mobility of  $Cl^-$  anions also influences the anodic attack, because their hydration degree decreases with increasing hydrostatic pressure.

If the layer formed on metals is a p-type semiconductor with many cationic vacancies in the lattice and high electronic conductivity (e.g. copper) the reduction process due to  $H^+$  ions is enhanced. If the layer is of n-type (e.g. zinc) with an excess of negative charges, its anodic dissolution is increased by the easy anions adsorption. If the layer is of p-type but with few lattice defects and a low protonic and electronic conductivity (e.g. nickel), it is highly resistant to both anodic dissolution and cathodic reduction.

#### Acknowledgement

The authors wish to acknowledge Mrs. Laura Scotti for her collaboration in this work.

TABLE 1 - Weight Percent composition of the examined metals.

| Material                   | Cu   | Zn     | Ni   | Fe   | Pb    | Cd    | Mn    | As    | S      | O   | other elements |
|----------------------------|------|--------|------|------|-------|-------|-------|-------|--------|-----|----------------|
| Electrolytic copper        | 99.8 | 0.0005 | ---  | ---  | 0.001 | 0.003 | ---   | ---   | 0.0015 | --- | ---            |
| Zinc                       | ---  | 99.8   | ---  | 0.02 | 0.05  | 0.003 | ---   | 0.002 | ---    | --- | rem.           |
| Nickel                     | 0.02 | 0.005  | 99.8 | 0.02 | 0.004 | ---   | 0.005 | 0.003 | 0.005  | --- | rem.           |
| Cu-Zn 70-30 Alloy 260 ASTM | 69.5 | 30     | ---  | 0.05 | 0.07  | ---   | ---   | 0.002 | ---    | --- | rem.           |
| Cu-Ni 70-30 Alloy 715 ASTM | 69   | 1.0    | 29.0 | 0.48 | ---   | ---   | 0.52  | 0.002 | ---    | --- | rem.           |

TABLE 2 - Corrosion resistance of copper in sea water

| Temperature<br>°C | Pressure<br>Atm | $R_p^{-1}$<br>$\text{mA}\cdot\text{V}^{-1}\text{cm}^{-2}$ | $R_{Pc}^{-1}$<br>$\mu\text{A}\cdot\text{V}^{-1}\text{cm}^{-2}$ | $R_p^{-1}$<br>$\mu\text{A}\cdot\text{V}^{-1}\text{cm}^{-2}$ | $i_{\text{corr}}$<br>$\mu\text{A}\cdot\text{cm}^{-2}$ | C<br>$\mu\text{F}\cdot\text{cm}^{-2}$ | E<br>mV(Ag-AgCl) |
|-------------------|-----------------|---|--|---|---|---------------------------------------|------------------|
| 5                 | 1               | 120   | 116  | $80 \pm 8$  | $0.150 \pm 0.01$                                      | $38 \pm 2$                            | -200             |
|                   | 150             | 125   | 118  | $85 \pm 4$  | $0.165 \pm 0.02$                                      | $32 \pm 3$                            | -198             |
|                   | 200             | 120   | 128  | $82 \pm 8$  | $0.160 \pm 0.05$                                      | $35 \pm 4$                            | -202             |
|                   | 300             | 130   | 125  | $88 \pm 9$  | $0.162 \pm 0.03$                                      | $37 \pm 5$                            | -196             |
|                   | 1               | 180   | 184  | $110 \pm 7$   | $0.215 \pm 0.06$                                      | $45 \pm 4$                            | -210             |
|                   | 150             | 188   | 196  | $122 \pm 6$   | $0.263 \pm 0.03$                                      | $38 \pm 3$                            | -212             |
| 10                | 200             | 180   | 190  | $120 \pm 9$   | $0.260 \pm 0.07$                                      | $40 \pm 2$                            | -208             |
|                   | 300             | 178   | 192  | $125 \pm 10$  | $0.240 \pm 0.08$                                      | $42 \pm 5$                            | -212             |
|                   | 1               | 265   | 246  | $172 \pm 20$  | $0.380 \pm 0.02$                                      | $62 \pm 5$                            | -235             |
| 20                | 150             | 259   | 295  | $203 \pm 25$  | $0.458 \pm 0.031$                                     | $41 \pm 6$                            | -236             |
|                   | 200             | 260   | 285  | $195 \pm 20$  | $0.420 \pm 0.04$                                      | $56 \pm 3$                            | -237             |
|                   | 300             | 265   | 280  | $190 \pm 22$  | $0.430 \pm 0.04$                                      | $48 \pm 7$                            | -235             |

TABLE 3 - Corrosion resistance of copper-zinc alloy in sea water.

| Temperature<br>°C | Pressure<br>Atm | $R_p$<br>$\mu A.V^{-1} cm^{-2}$ | $R_p$<br>$\mu A.V^{-1} cm^{-2}$ | $R_p$<br>$\mu A.V^{-1} cm^{-2}$ | $R_p$<br>$\mu A.V^{-1} cm^{-2}$ | C             | $i_{corr}$<br>$\mu A.cm^{-2}$ | E<br>mV(Ag/AgCl) |
|-------------------|-----------------|---------------------------------|---------------------------------|---------------------------------|---------------------------------|---------------|-------------------------------|------------------|
| 5                 | 1               | 68                              | 58                              | 46.6 ± 5                        | 31.6 ± 3                        | 0.069 ± 0.002 | -348                          |                  |
|                   | 150             | 67                              | 78                              | 57.2 ± 4                        | 60.4 ± 2                        | 0.072 ± 0.002 | -358                          |                  |
|                   | 200             | 71                              | 75                              | 47.7 ± 5                        | 60.4 ± 2                        | 0.075 ± 0.003 | -358                          |                  |
| 10                | 300             | 87                              | 89                              | 50 ± 3                          | 75.2 ± 2                        | 0.090 ± 0.004 | -362                          |                  |
|                   | 1               | 108                             | 80                              | 62 ± 5                          | 50 ± 7                          | 0.095 ± 0.005 | -363                          |                  |
|                   | 150             | 129                             | 141                             | 87 ± 6                          | 126 ± 8                         | 0.128 ± 0.006 | -373                          |                  |
| 20                | 200             | 89                              | 113                             | 78 ± 5                          | 104 ± 9                         | 0.102 ± 0.005 | -375                          |                  |
|                   | 300             | 115                             | 135                             | 78 ± 7                          | 108 ± 6                         | 0.116 ± 0.007 | -370                          |                  |
|                   | 1               | 103                             | 99                              | 84 ± 7                          | 95.5 ± 9                        | 0.102 ± 0.009 | -358                          |                  |
| 20                | 150             | 155                             | 175                             | 106 ± 5                         | 192 ± 10                        | 0.145 ± 0.007 | -375                          |                  |
|                   | 200             | 158                             | 170                             | 107 ± 5                         | 185 ± 12                        | 0.108 ± 0.006 | -378                          |                  |
|                   | 300             | 148                             | 173                             | 105 ± 7                         | 187 ± 15                        | 0.138 ± 0.007 | -375                          |                  |

TABLE 4 - Corrosion resistance of zinc at 20°C in sea water.

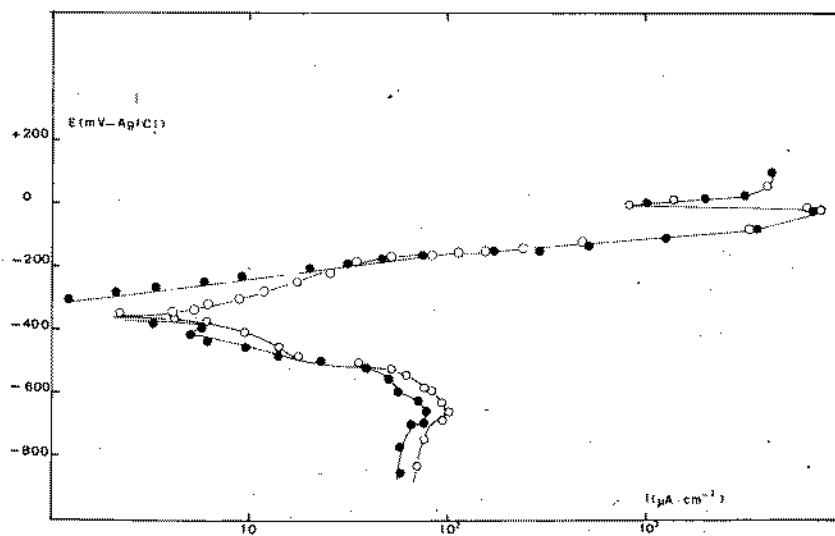
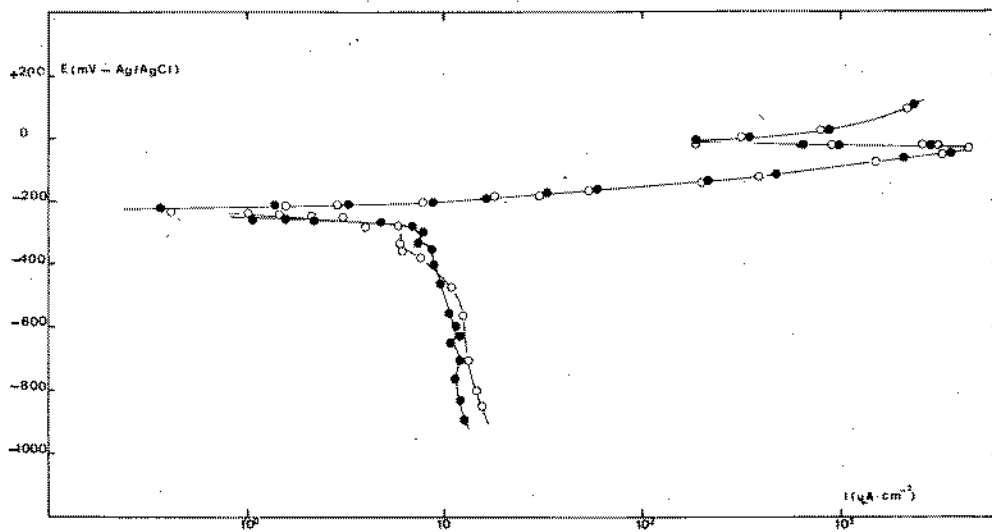
| Pressure<br>Atm | $R_p^{-1}$<br>$\mu A \cdot V^{-1} \cdot cm^{-2}$ | $R_p^{-1}$<br>$\mu A \cdot V^{-1} \cdot cm^{-2}$ | $R_p^{-1}$<br>$\mu A \cdot V^{-1} \cdot cm^{-2}$ | C            | $i_{corr}$<br>$\mu A \cdot cm^{-2}$ | E<br>$mV(Ag/AgCl)$ |
|-----------------|--|--|--|--------------|-------------------------------------|--------------------|
| 1               | 442  | 442  | $295 \pm 7$                                      | $643 \pm 20$ | $0.35 \pm 0.01$                     | -1057              |
| 150             | 567  | 464  | $311 \pm 20$                                     | $630 \pm 12$ | $0.41 \pm 0.03$                     | -1069              |

TABLE 5 - Corrosion resistance of Cu-Ni alloy in sea water at 20°C

| Pressure<br>Atm | $R_p^{-1}$<br>$\mu A \cdot V^{-1} \cdot cm^{-2}$ | $R_p^{-1}$<br>$\mu A \cdot V^{-1} \cdot cm^{-2}$ | $R_p^{-1}$<br>$\mu A \cdot V^{-1} \cdot cm^{-2}$ | C            | $i_{corr}$<br>$\mu A \cdot cm^{-2}$ | E<br>$mV(Ag/AgCl)$ |
|-----------------|--|--|--|--------------|-------------------------------------|--------------------|
| 1               | 609  | 487  | $361 \pm 25$                                     | $533 \pm 20$ | $0.500 \pm 0.07$                    | -212               |
| 150             | 598  | 473  | $327 \pm 5$                                      | $557 \pm 40$ | $0.479 \pm 0.05$                    | -203               |

TABLE 6 - Corrosion resistance of nickel in sea water at 20°C.

| Pressure<br>Atm | $R_p^{-1}$<br>$\mu A \cdot V^{-1} \cdot cm^{-2}$ | $R_p^{-1}$<br>$\mu A \cdot V^{-1} \cdot cm^{-2}$ | $R_p^{-1}$<br>$\mu A \cdot V^{-1} \cdot cm^{-2}$ | C             | $i_{corr}$<br>$\mu A \cdot cm^{-2}$ | E<br>$mV(Ag/AgCl)$ |
|-----------------|--|--|--|---------------|-------------------------------------|--------------------|
| 1               | 13.9   | 16.7   | $8.22 \pm 0.7$                                   | $6.6 \pm 0.5$ | $0.0126 \pm 0.002$                  | -214               |
| 150             | 2.4  | 5.1  | $3.46 \pm 0.3$                                   | $42.9 \pm 1$  | $0.0048 \pm 0.0002$                 | -81                |



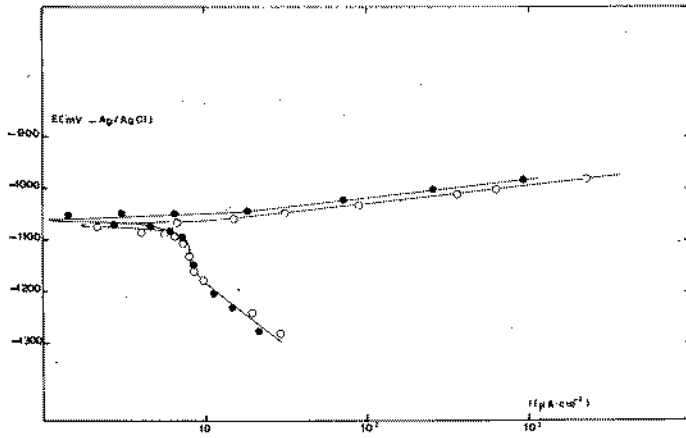


Fig. 3 - Polarisation curves of zinc specimens in sea water at 20°C.

●—●— 1 atm.      ○—○— 150 atm.

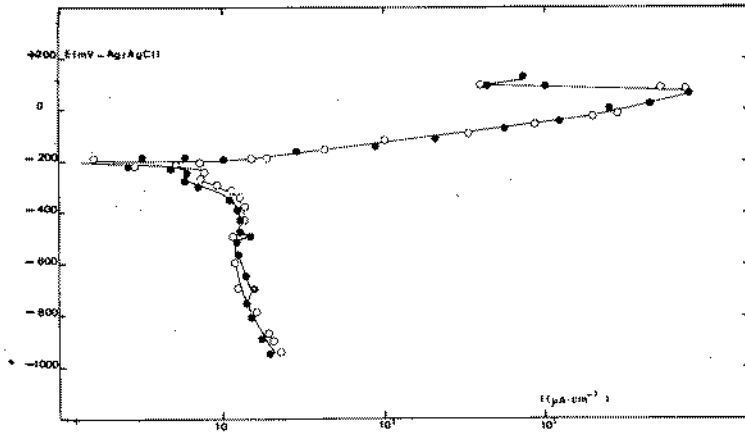


Fig. 4 - Polarisation curves of copper-nickel 70-30 in sea water at 20°C.

●—●— 1 atm.      ○—○— 150 atm.

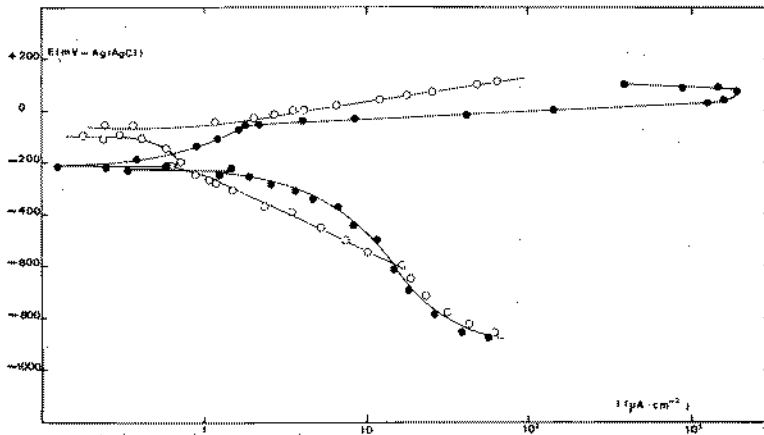


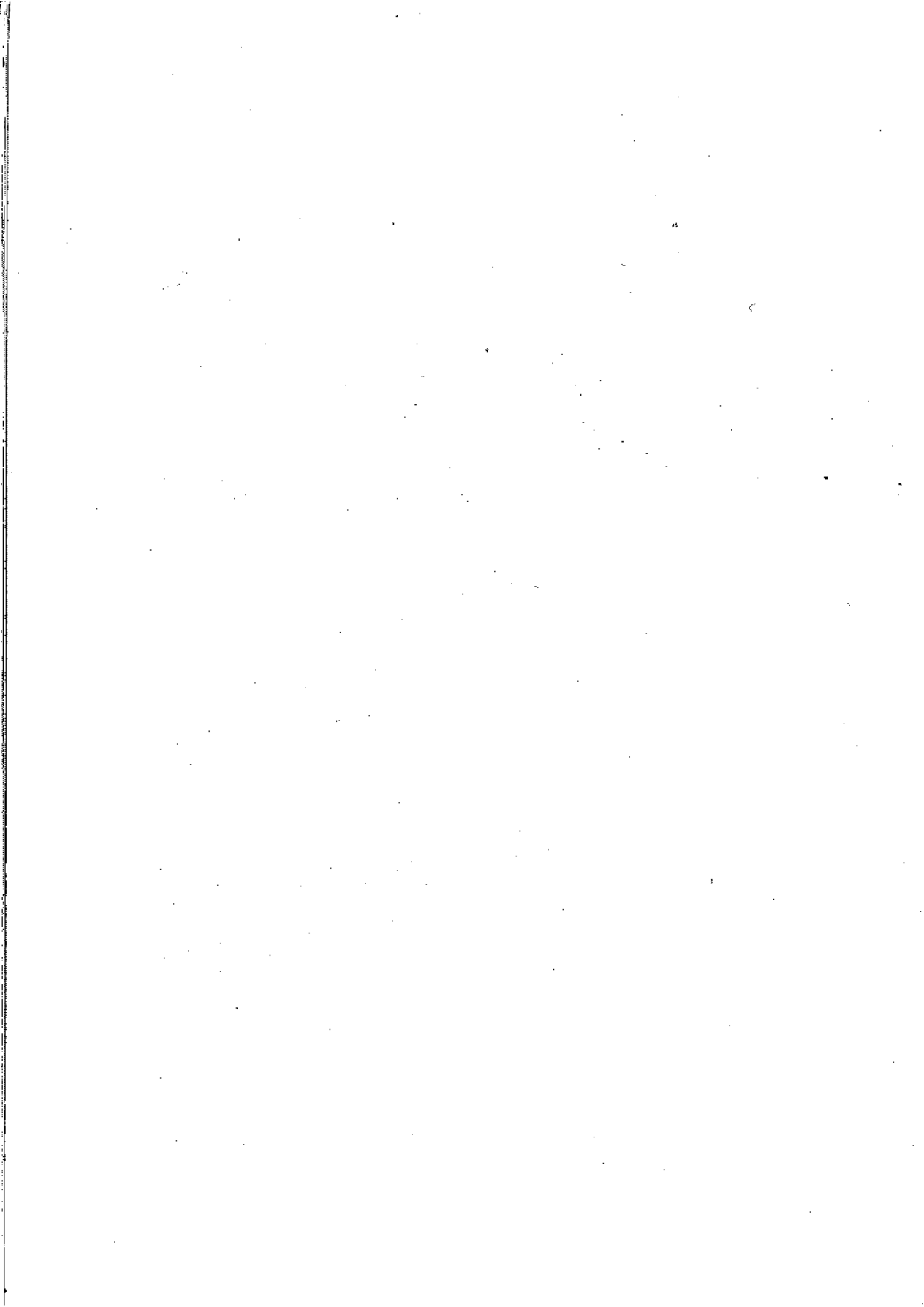
Fig. 5 - Polarisation curves of nickel specimens in sea water at 20°C.

●—●— 1 atm.      ○—○— 150 atm.



### Bibliography

- 1 - Reinhart F.M. : Corrosion of Materials in hydrospace T.R.504-11  
-12 107VS Naval Civil Engineering Laboratory-California Dec. 1966
- 2 - Danck G.J. : Personal communication - U.S. Naval Ship Research  
and Development Center - Annapolis Md. 1971
- 3 - U.S. Naval Engineering Laboratory - Port Heneme - Techn.Rep. R504
- 4 - De Lucia J.J.: Mater. Prot. 1966 8 (5), 49
- 5 - Morney M.T.: Mater. Prot. Perf. 1972, (1), 10
- 6 - Gray K.O. : Mater. Prot. 1964, 7 (3) 47
- 7 - Petrocelli J.V. - V.Hodspadruk - G.A. Di Bari: Plating 1962 49,50
- 8 - Dexter S.C. : Corrosion 1980 36 (8) 423
- 9 - Dexter S.C. : Proceedings 7th International Congress on Metallic  
Corrosion - Rio de Janeiro - Brasil - October 1978 p. 1250-1262
- 10 - Rowland H.T. - Dexter S.C.: Corrosion 1980, 36, 9, 458
- 11 - Huesler K.E. : Werk und Korr. 1967, 18, 1, 11
- 12 - Mor E.D. - Beccaria A.M.: Br. Corros. J. 1978, 13, 3, 142
- 13 - Mor E.D. - Beccaria A.M.: Werk und Korr 1979, 30, 551
- 14 - Mor E.D. - Beccaria A.M.: Proc. Symp. Intern. Corrosion and Pro  
tection Off-Shore - Paris 1979, 124
- 15 - Horne R.A. : Marine Chemistry - Wiley Interscience 1969, 112
- 16 - McDonald - Syrett B.C. - Wing S.S. : Corrosion 1978 34, (9) 289
- 17 - Shams El Din A.M. - F.M. ABD El Wahab: Corros. Sci. 1977, 17 49
- 18 - Shams El Din A.M. - F.M. ABD El Wahab: Electrochim. Acta 1964  
9, 113
- 19 - Al-Kharafi F.M. - Y.A. El-Tantawy: Corros. Sci. 1982 22, 1
- 20 - Bianchi G. - Mazza F. : Corrosione e protezione dei metalli -  
Tamburini 1971, 45
- 21 - Horne R.A.: Marine Chemistry - Wiley Interscience 1969, 119
- 22 - North R.F. - Pryor M.J. : Corros. Sci. 1970 10, 297
- 23 - Kruger : J. Electrochem. Soc. 1961 108 503
- 24 - Barton K. : Protection against Atmospheric Corrosion - John Wiley  
& Sons 1973, 28
- 25 - Beccaria A.M. : Rapporto interno
- 26 - Kortüm G. : Trattato di Elettrochimica - Piccin Padova 1968, 261
- 27 - Sato N. : J. Electrochem. Soc. 1982 129 (2) 255
- 28 - Popplewell J.M. - Hart R.J. - Ford J.A.: Corros. Sci. 1973, 13  
295
- 29 - Wilhelm S.M. - Tanizawa Y. - Chang-Yi-Lin - Hackerman N.: Corros.  
Sci. 1982, 22, 8



ETUDE PRELIMINAIRE DE L'INFLUENCE D'OXYDES, ELECTROLYTIQUEMENT PREPARES, SUR LA VIE DE L'ACIER SUBISSANT CORROSION SOUS CONTRAINTE DANS UNE SOLUTION DE NaCl.

Th. SKOULIKIDIS et N. KOULOUMBI

Université Technique Nationale d'Athènes, Département des Ingénieurs Chimistes, Section de la Science des Matériaux, Athènes, Grèce.

RESUME

Le présent travail concerne une étude préliminaire de l'influence d'oxydes, électrolytiquement préparés, sous des conditions différentes, sur la vie de l'acier qui subit corrosion sous contrainte dans une solution 1N de NaCl. Cette étude s'est basée sur les résultats très favorables en ce qui concerne la protection des alliages d'aluminium par la même méthode. Tous les essais effectués, en variant la densité du courant et la durée de l'anodisation, la température du bain de l'anodisation et sa composition ainsi que l'orientation des éprouvettes dans le bain de l'anodisation ont conduit jusqu'à présent aux revêtements que ne possèdent pas des propriétés protectrices. Ceci pourrait être attribué à deux raisons: Premièrement au fait que dans le cas de l'acier il n'est pas possible de préparer des oxydes orientés normalement à la direction de la future traction des éprouvettes, condition qui est indispensable pour la protection d'aluminium. L'orientation d'oxydes de l'acier est trouvée parallèle à la direction du laminage, indépendamment de l'orientation des éprouvettes pendant l'oxydation anodique. Deuxièmement au mécanisme différent du phénomène, indépendamment ou non de la première explication.

ABSTRACT

The present work is a preliminary study of the influence of electrolytically prepared oxides, under different conditions, against SCC of steel in a 1N NaCl solution. This study is based on the very good results of

## INFLUENCE D'OXYDES ELECTROLYTIQUES SUR LA VIE DE L'ACIER

of protection from SCC of Al-alloys with the same method. All the measurements, by varying the current density, the bath composition and the specimen orientation, lead until now to oxide layers without protective properties. This can be attributed to two reasons: At first in the case of steel it is not possible to prepare oxides oriented normally to the stress direction, a condition that is required for the Aluminum protection. The iron oxide orientation is found to be parallel to the direction of the lamination, independently of the specimen orientation during anodisation. Secondly at the different mechanism of the phenomenon independently or not of the first explanation.

### INTRODUCTION

Il est bien connu que les aciers subissent une fragilisation par l'hydrogène sous une charge, relativement faible, imposé constamment en milieu contenant des ions d'hydrogène. Les surfaces fracturées ont des caractéristiques de fissuration intergranulaire (1-4).

Selon H.P. Van Leeuwen (5) dans ce cas d'abord une fissure peut se former après une certaine période d'incubation. La fissure se propage d'une façon discontinue et si elle atteint une longueur critique, l'éprouvette se rompt. Il y a un seuil de charge au-dessous duquel la fissure ne survient pas.

L'hydrogène tend à se diffuser vers les régions qui subissent les plus fortes tractions. Lorsque une combinaison critique du niveau de la tension et de la concentration en hydrogène est obtenue localement, la fissuration se déclenche. La fissure s'arrête parce que, bien qu'à son fond l'intensité de la tension mécanique soit très élevée, la concentration locale d'hydrogène sera trop basse pour que la fissure avance davantage. Ensuite une diffusion aura lieu jusqu'à ce que les conditions au fond de la fissure soient de nouveau critiques, ce qui provoque un nouveau déclenchement de la fissuration. La répétition de ce procès résulte à la propagation discontinue de la fissure.

Le model de fragilisation par hydrogène est basé sur la suggestion que la concentration maximale en hydrogène se présente au bord de l'enclave plastique. Malgré la différence dans la manière de formation de la voie active, dans la catégorie des métaux et alliages comprenant l'aluminium et l'acier, le fait que dans des études précédentes, concernant la protection de l'aluminium contre la corrosion sous contrainte, des conditions satisfaisantes de protection ont été trouvées (6-10) nous a conduit à appliquer une méthodologie similaire dans

INFLUENCE D'OXYDES ELECTROLYTIQUES SUR LA VIE DE L'ACIER

le cas de l'acier. La protection d'abord et l'optimisation ensuite des conditions de protection dans le cas d'aluminium se sont établies après une série d'essais sans succès (Fig. 1).

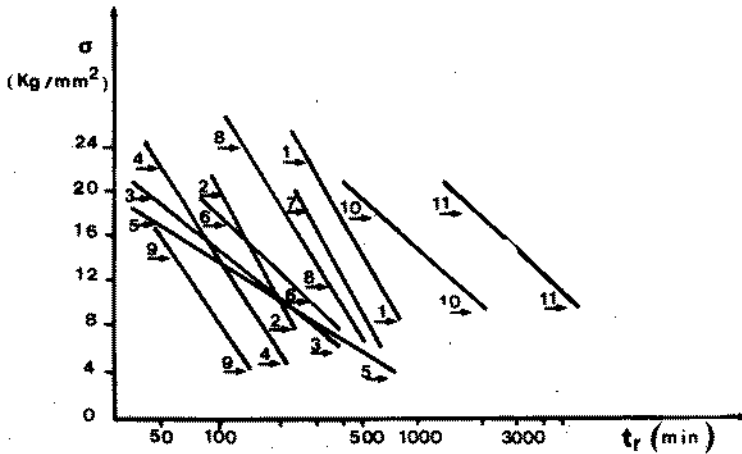


Fig.1. Charge en poids (Kg/mm<sup>2</sup>) des éprouvettes en fonction du logarithme du temps de rupture.

1. Al nu,  $i=2\text{mA/cm}^2$ .
2.  $\gamma_1\text{-Al}_2\text{O}_3 \cdot 3\text{H}_2\text{O}$ // (sans vieillissement)  $i=2\text{mA/cm}^2$ .
3.  $\gamma_1\text{-Al}_2\text{O}_3 \cdot 3\text{H}_2\text{O}$ // (100°C/1,5min vieillissement)  $i=2\text{mA/cm}^2$ .
4.  $\gamma_1\text{-Al}_2\text{O}_3 \cdot 3\text{H}_2\text{O}$ // (50°C/135min vieillissement)  $i=2\text{mA/cm}^2$ .
5.  $\gamma_2\text{-Al}_2\text{O}_3 \cdot 3\text{H}_2\text{O}$ // (sans vieillissement)  $i=2\text{mA/cm}^2$ .
6. Comme (2) = 7. Comme (3) = 8.  $\gamma_2\text{-Al}_2\text{O}_3 \cdot 3\text{H}_2\text{O}$ // (100°C/1,5min vieillissement)  $i=2\text{mA/cm}^2$ .
9. Comme (8) = 10. Al nu;  $i=0,5\text{mA/cm}^2$ .
11.  $\gamma_1\text{-Al}_2\text{O}_3$  (épaisseur égale à 3,4 $\mu\text{m}$ )  $i=0,5\text{mA/cm}^2$ .

De ces études on a conclu que la meilleure protection se réalise avec une couche d'oxyde  $\gamma_1\text{-Al}_2\text{O}_3$  d'une épaisseur de 3,4 $\mu\text{m}$  préparé par l'oxydation anodique dans un bain de 15% d'acide sulfurique à 25°C en imposant une densité du courant d'anodisation de 6A/dm<sup>2</sup>. La condition principale qui offre les propriétés protectrices aux oxydes d'aluminium consiste à l'orientation des cellules d'oxyde normalement vers la future traction (augmentation de la vie des éprouvettes de 220%), condition qui se réalise quand l'éprouvette se place à une position horizon-

INFLUENCE D'OXYDES ELECTROLYTIQUES SUR LA VIE DE L'ACIER  
tôle dans le bain pendant l'anodisation.

Pour cette raison d'une part les premiers essais concernant la protection probable de l'acier ont été effectués aux éprouvettes qui étaient aussi posées horizontalement dans le bain, durant l'oxydation, et d'autre part la direction du laminage était parallèle à la future traction.

### PARTIE EXPERIMENTALE

#### Matériel utilisé. Forme et Dimensions des Eprouvettes

L'acier utilisé (type: black plate, qui correspond à AISI 1006 ou T3) avait la composition nominale suivante (% en poids) C:0,06; Mn:0,36; S:0,2; P:0,14; Fe:99,24, limite élastique égale à 25,70Kg/mm<sup>2</sup>, limite de rupture égale à 36,80Kg/mm<sup>2</sup> et allongement égal à 29,47.

Les éprouvettes étaient coupées d'une tôle (216X10mm) d'une épaisseur de 0,25mm parallèlement à la direction du laminage, qui coïncidait avec la direction de la future traction. La figure 2 représente la forme et les dimensions des éprouvettes.

Des éprouvettes de la même forme ont été utilisées aux travaux précédents (6-10).

#### Conditions d'anodisation

La surface anodisée des éprouvettes se comprend entre les lignes AA' et BB' de la figure 2, bien que le reste de l'éprouvette soit électriquement isolé à l'aide d'un vernis (type Sterling B8-Golden Varnish) et du teflon.

Le bain d'anodisation était composé d'une solution de soude caustique qui contenait CH<sub>2</sub>(OH)SO<sub>2</sub>Na (Rhongallit) comme agent réducteur (11). Pendant nos essais on a varié la composition du bain ainsi que la température et la densité du courant d'anodisation, la durée d'anodisation et l'orientation des éprouvettes dans le bain d'anodisation.

L'anodisation était toujours effectuée imposant un courant alternatif de 220V et de 50Hz. Pendant l'oxydation, chaque éprouvette était posée entre deux électrodes de titane (5X5cm<sup>2</sup>) de telle manière qu'une longueur de 210mm se trouve soit à position horizontale, soit à position verticale (9).

Sous les conditions mentionnées ci-dessus résulte un revêtement uniforme, noir et pas poreux (11). L'oxydation de l'acier dans ces conditions présente par rapport à l'oxydation chimique, aux hautes températures et électrochimique, sous un courant continue, la possibilité

## INFLUENCE D'OXYDES ELECTROLYTIQUES SUR LA VIE DE L'ACIER

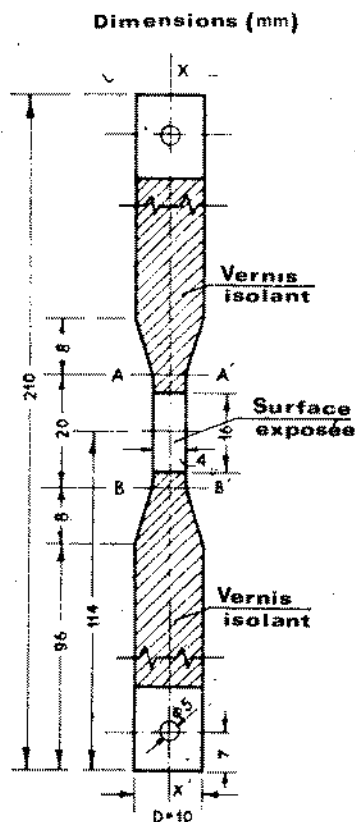


Fig.2. Forme et dimensions des éprouvettes utilisées.

de travailler avec des solutions de soude caustique diluées et aux basses températures. Cet avantage correspond aux demandes énergétiques plus basses, aux valeurs du temps d'oxydation plus faibles et à une appareillage plus simple et plus économique.

#### Appareillage de mesures

L'anode de la cellule électrolytique était l'éprouvette oxydée, entourée par une anneau en aluminium, qui constituait la cathode. Le milieu corrosif était une solution 1N de NaCl circulant avec une vitesse de 70ml/h et se renouvelant. Le phénomène de la corrosion sous contrainte était accéléré à l'aide d'un courant continu imposé de  $0,2\text{mA}/\text{cm}^2$  ou de  $0,5\text{mA}/\text{cm}^2$ . La traction s'imposait aux éprouvettes par un poids défini et constant. Les

## INFLUENCE D'OXYDES ELECTROLYTIQUES SUR LA VIE DE L'ACIER

détails de l'ensemble de l'appareillage, de la manière de la fixation des éprouvettes et de la mesure du temps se trouvent décrits dans la publication précédente (9).

Mesures, résultats et observations1. Influence de la densité du courant et de la durée de l'anodisation.

Le bain d'anodisation avait la composition suivante: 120g/l NaOH + 10g/l Phosgallit. La température d'anodisation était égale à 50°C.

Le paramètre varié au premier lieu était la densité du courant d'anodisation. On a comparé les moyennes géométriques de temps de rupture des éprouvettes oxydées en imposant des différentes densités du courant pour les mêmes Coulomb. Dans chaque cas on a effectué des mesures du temps de la fracture de 6 éprouvettes pour une charge (en poids) moyenne égale à 15Kg/mm<sup>2</sup> et pour une valeur du courant anodique de la corrosion imposée égale à 0,2mA/cm<sup>2</sup>.

La figure 3 représente les résultats de ces mesures. On constate que le temps de rupture passe d'un maximum à une densité du courant de l'anodisation égale à 15A/dm<sup>2</sup>.

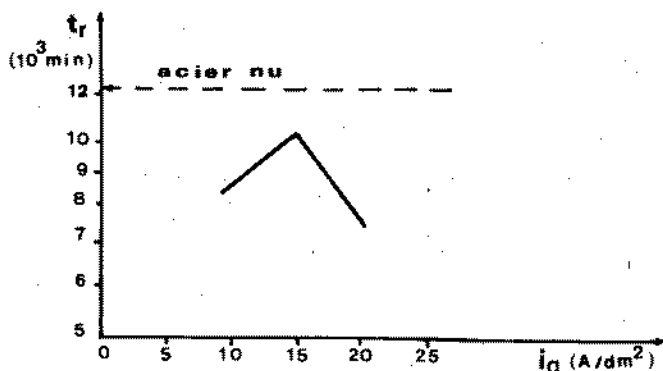


Fig.3. Temps de rupture des éprouvettes anodisées en fonction de la densité du courant de l'anodisation; T=50°C;  $\sigma=15\text{Kg/mm}^2$ ;  $i=0,2\text{mA/cm}^2$ .

On n'a pas anodisé les éprouvettes à une densité du courant plus basse de 10A/dm<sup>2</sup>, étant donné selon la bibliographie (11) que l'épaisseur d'oxyde préparé à 15A/dm<sup>2</sup> pour une durée d'oxydation de 20-25 min à 40-60°C se trouve égale à 1 $\mu\text{m}$ , valeur qui est très basse pour at-



## INFLUENCE D'OXYDES ELECTROLYTIQUES SUR LA VIE DE L'ACIER

tendre des propriétés protectrices satisfaisantes.

À la suite on a évalué l'influence de la durée de l'anodisation sur le temps de rupture des éprouvettes imposant une densité du courant de l'anodisation égale à la valeur moyenne de celle des premières mesures, c.à.d. égale à  $15A/dm^2$ . Toutes les autres conditions expérimentales ont été maintenues comme ci-dessus. On voit les résultats à la figure 4.

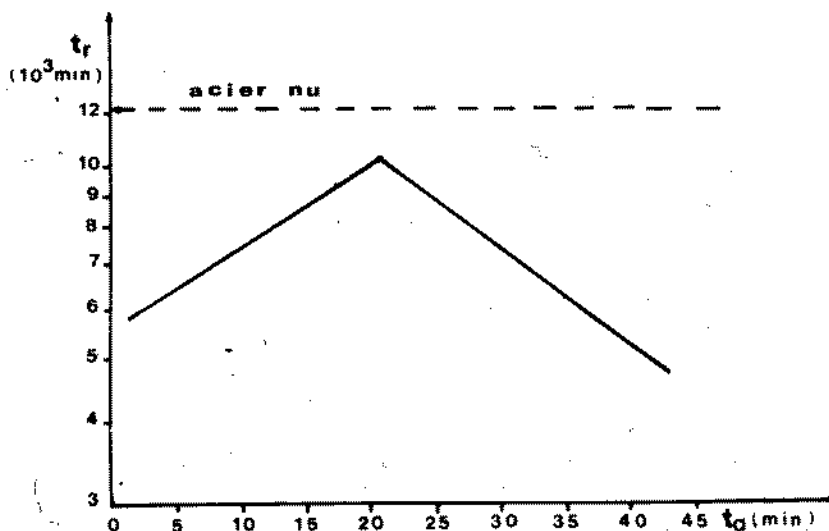


Fig.4. Temps de rupture des éprouvettes anodisées en fonction de la durée de l'anodisation;  $T=50^{\circ}C$ ;  $i_{an}=15A/dm^2$ ;  $\sigma=15Kg/mm^2$ ;  $i=0,2mA/cm^2$ .

Par ce diagramme on constate que, indépendamment de la durée d'oxydation, le temps de rupture des éprouvettes reste toujours plus bas que celui des éprouvettes de l'acier nu. Cependant la vie des éprouvettes augmente en fonction de la durée de l'anodisation et passe par un maximum pour la condition  $t_{an}=20$  min. On constate des phénomènes semblables dans le cas de l'oxydation d'aluminium pour la région d'épaisseur d'oxyde de  $3,4\mu m$  à  $36\mu m$ .

### 2. Influence de la température du bain de l'anodisation.

Sous les mêmes conditions expérimentales à celles du paragraphe 1 on a étudié l'influence de la température du bain d'anodisation sur la vie des éprouvettes lorsque celles-ci étaient anodisées à  $15A/dm^2$  pendant 20 min (condi-

## INFLUENCE D'OXYDES ELECTROLYTIQUES SUR LA VIE DE L'ACIER

tions optimum du paragraphe 1). On a effectué des mesures dans la région de 40°C jusqu'à 60°C étant donné (11) que l'épaisseur du revêtement et sa porosité augmentent en fonction de la température. La figure 5 représente les résultats ressortis.

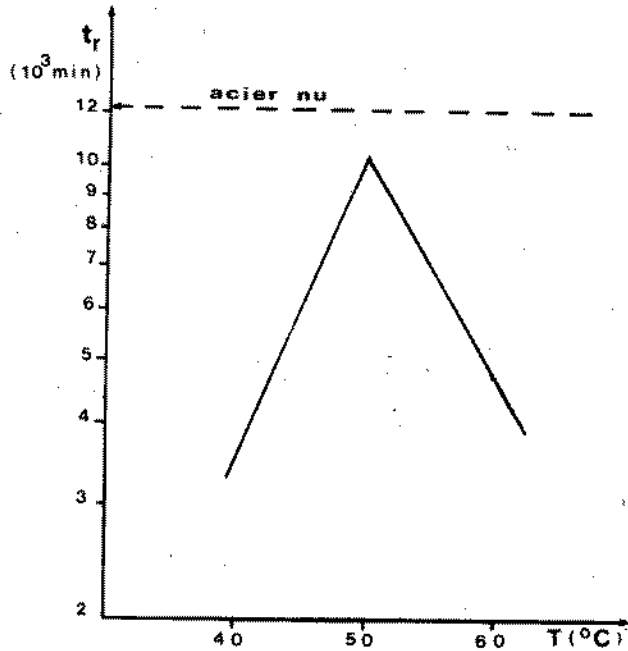


Fig.5. Temps de rupture des éprouvettes anodisées en fonction du bain de l'anodisation;  $i_{an}=15A/dm^2$ ;  $t_{an}=20min$ ;  $\sigma=15Kg/mm^2$ ;  $i=0,2mA/cm^2$ .

La meilleure condition appliquée était celle de 50°C tandis que la vitesse de la corrosion sous contrainte augmente par rapport à celle des éprouvettes de l'acier nu pour l'ensemble des mesures.

### 3. Influence de la composition du bain de l'anodisation.

#### i. Changement de la composition globale.

Les premiers essais sont effectués en changeant en même temps et proportionnellement la concentration en soude caustique et la concentration en Rhongallit, mais en maintenant toutes les autres conditions expérimentales i-

## INFLUENCE D'OXYDES ELECTROLYTIQUES SUR LA VIE DE L'ACIER

dentiques à celles qui précèdent. Par la figure 6 on constate que, bien que la concentration du bain influence la vie des éprouvettes, le temps de rupture reste toujours au-dessous de celui exigé pour l'acier nu. Les meilleurs résultats apparaissent pour la condition NaOH: 120g/l, Rhongallit: 10g/l.

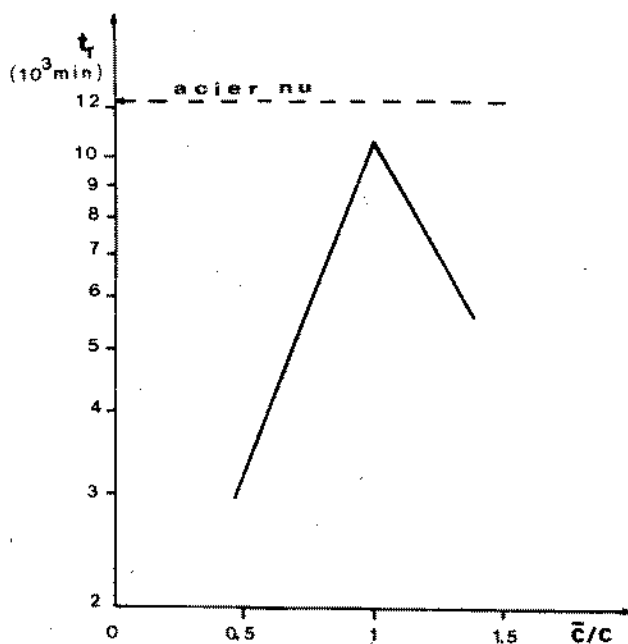


Fig.6. Temps de rupture des éprouvettes anodisées en fonction de la composition globale du bain de l'anodisation;  $\bar{C}$ :NaOH 120g/l+Rhongallit 10g/l;  $T=50^\circ\text{C}$ ;  $i_{an}=15\text{A/dm}^2$ ;  $t_{an}=20\text{min}$ ;  $\sigma=15\text{Kg/mm}^2$ ;  $i=0,2\text{mA/cm}^2$ .

### ii. Changement de la concentration en NaOH.

A la réalisation de ces essais on a varié seulement la concentration en NaOH, la concentration du Rhongallit étant fixe et égale à 10g/l. Ceci résulte soit aux revêtements minces, poreux et pas uniformes soit aux revêtements compacts mais qui ne sont pas en bonne adhésion avec le substrat. Dans tous les cas examinés la vie des éprouvettes anodisées ne dépasse pas celle des éprouvettes nues (figure 7), valeur qui s'est approchée seulement

INFLUENCE D'OXYDES ELECTROLYTIQUES SUR LA VIE DE L'ACIER  
par une concentration en NaOH égale à 120g/l.

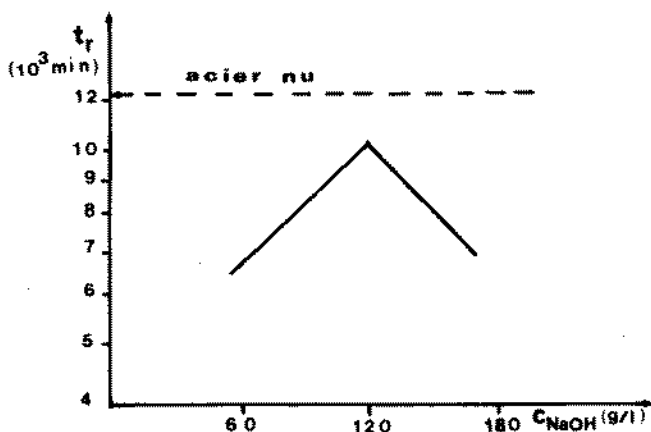


Fig.7. Temps de rupture des éprouvettes anodisées en fonction de la concentration en NaOH;  $C_{Rhongallit} = 10g/l$ ;  $T=50^\circ C$ ;  $i_{an}=15A/dm^2$ ;  $t_{an}=20min$ ;  $\sigma=15Kg/mm^2$ ;  $i=0,2mA/cm^2$ .

iii. Changement de la concentration en Rhongallit (concentration de NaOH constante: 120g/l).

Rhongallit, étant un agent réducteur fort, empêche la formation de l'oxyde  $Fe_2O_3$  et pour certaines limites de concentration améliore l'aspect extérieur d'oxyde formé, et ses propriétés au point de vue de la corrosion généralisée.

Par la figure 8 on peut constater que la présence de Rhongallit dans le bain améliore le temps de rupture des éprouvettes particulièrement pour la région de valeurs de la concentration plus basses (Rhongallit 10g/l: condition optimale). Pourtant la variation même de ce paramètre aussi n'a pas amené aux conditions protectrices.

4. Influence de la température du bain de l'anodisation dans le cas d'oxydes plus épais. Eprouvettes placées verticalement dans le bain de l'anodisation.

Selon la bibliographie qui concerne la méthode d'oxydation utilisée (11) sous une densité du courant plus grande que le  $15A/dm^2$ , des films oxygénés se forment qui possèdent des propriétés différentes contre la corrosion et dont les types ne sont pas déterminés. Pour la détermination de chaque type d'oxyde préparé sous certaine den-

## INFLUENCE D'OXYDES ELECTROLYTIQUES SUR LA VIE DE L'ACIER

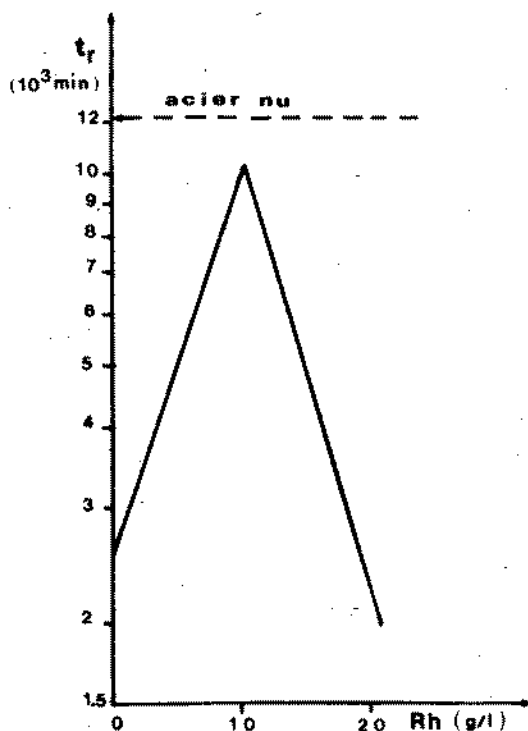


Fig.8. Temps de rupture des éprouvettes anodisées en fonction de la concentration en Rhongallit;  $C_{\text{NaOH}} = 120\text{g/l}$ ;  $T=50^\circ\text{C}$ ;  $i_{\text{an}}=15\text{A/dm}^2$ ;  $t_{\text{an}}=20\text{min}$ ;  $\sigma=15\text{Kg/mm}^2$ ;  $i=0,2\text{mA/cm}^2$ .

sité du courant on a effectué dans notre laboratoire (pour un travail de thèse d'une collaboratrice concernant les propriétés catalytiques des oxydes de fer) des mesures à l'aide d'XRD et de la spectroscopie Mössbauer. La composition des produits de l'oxydation électrochimique de l'acier ainsi trouvée est classée dans le tableau 1. Ces mesures ont en plus montré que les oxydes préparés dans un bain de NaOH (120g/l) et de Rhongallit (10g/l) en imposant une densité du courant de l'anodisation égale à  $100\text{A/dm}^2$  pour un temps égal à 20 min et en température de  $60^\circ\text{C}$  sont noirs et adhérents. Au cours de l'oxydation sous ces conditions les éprouvettes étaient placées verticalement dans le bain de l'anodisation, condition qui

## INFLUENCE D'OXYDES ELECTROLYTIQUES SUR LA VIE DE L'ACIER

Tableau 1: Composition des produits de l'oxydation électrochimique de l'acier.

| T (°C) | i (A/dm <sup>2</sup> ) | Type de produit   |  |
|--------|------------------------|---|--|
|        |                        | Selon Mössbauer   | Selon XRD                                  |
| 40     | 15                     | -   | δ - FeO(OH)                                |
| 60     | 15                     | FeO(OH)   | δ - FeO(OH)                                |
| 60     | 40                     | mélange+(?) Fe <sub>2</sub> O <sub>3</sub>                                      | amorphe                                    |
| 60     | 60                     | intermédiaire γ-Fe <sub>2</sub> O <sub>3</sub> - Fe <sub>3</sub> O <sub>4</sub> | -  |
| 60     | 80                     | γ-Fe <sub>2</sub> O <sub>3</sub> +amorphes                                      | γ-Fe <sub>2</sub> O <sub>3</sub> +amorphes |
| 60     | 100                    | γ - Fe <sub>2</sub> O <sub>3</sub>  | γ - Fe <sub>2</sub> O <sub>3</sub>         |

a été appliquée à cette série de nos mesures. Pour l'accélération de la corrosion sous contrainte on a imposé un courant continu de 0,5mA/cm<sup>2</sup>, valeur supérieure de la précédente parce que les revêtements ainsi préparés étaient plus épais que les surmentionnés.

Premièrement on a varié la température du bain de 5°C à 60°C. Les résultats figurent dans le schéma 9.

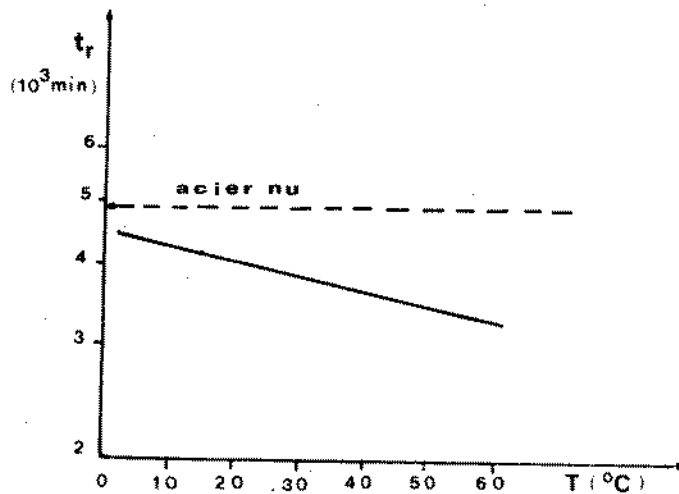


Fig.9. Temps de rupture des éprouvettes anodisées en fonction de la température du bain de l'anodisation; éprouvettes placées verticalement dans le bain d'anodisation;  $i_{an}=100A/dm^2$ ;  $t=20min$ ;  $\sigma=15Kg/mm^2$ ;  $i = 0,5mA/cm^2$ .

## INFLUENCE D'OXYDES ELECTROLYTIQUES SUR LA VIE DE L'ACIER

Les observations macroscopiques des éprouvettes oxydées ont montré que les oxydes à 60°C étaient d'une couleur noire et d'une relativement bonne adhésion sur le substrat tandis qu'à 40°C la couleur devenait plutôt grise et à 30°C des taches de plusieurs couleurs commencent à apparaître. Ces taches dominaient sur la surface pour la région de températures de l'anodisation de 20°C à 5°C.

Par la figure 9 on observe que de 10°C à 60°C le temps de rupture des éprouvettes se diminue un peu, mais la différence n'est pas importante. Ceci pourrait être attribué à une quantité élevée du dégagement en fonction de la température et par conséquent à la formation d'un revêtement plus poreux. On pourrait supposer, selon nos mesures, que les températures de 5°C à 10°C sont les plus favorables, puisque la vie des éprouvettes anodisées approche celle de l'acier nu. Néanmoins on notifie que sous cette condition la vie des éprouvettes de l'acier nu n'est pas dépassée.

Les temps de la rupture de ces oxydes sont comparés à ceux-ci des éprouvettes anodisées sous les mêmes conditions que ci-dessus, sauf l'orientation dans le bain de l'anodisation qui était inversée et à ceux-ci des éprouvettes chimiquement oxydées selon de différentes conditions (12,13). Les résultats montrent que le traitement thermique avant l'anodisation, autant que le traitement chimique, n'améliorent pas la durée de la vie des éprouvettes de l'acier.

### 5. Examen de l'orientation d'oxydes.

Après les séries de mesures sans succès par rapport à notre but, qui était la préparation sur la surface des éprouvettes de couches d'oxydes de fer protectrices contre la corrosion sous contrainte, on a examiné l'orientation des oxydes à l'aide du microscope électronique à balayage lorsque les éprouvettes étaient placées dans le bain d'anodisation soit à position horizontale soit à position verticale.

Les travaux surmentionnés (6-10) concernant la protection des alliages d'Al-2,5% Mg, à l'aide d'oxydes électrolytiquement préparés, ont montré que quand les éprouvettes sont placées horizontalement dans le bain de l'anodisation, elles obtiennent des propriétés protectrices c.à.d. le film d'oxyde ainsi préparé possède des propriétés mécaniques satisfaisantes de telle manière qu'il ne se fissure pas dès qu'on charge les éprouvettes. Dans ce cas les cellules de  $\gamma_1$ -Al<sub>2</sub>O<sub>3</sub> étaient orientées parallèlement à la direction de la gravité mais normalement à la direction de la future traction, tandis que quant aux éprou-

## INFLUENCE D'OXYDES ELECTROLYTIQUES SUR LA VIE DE L'ACIER

vettes normalement placées, les cellules étaient parallèlement à la direction de la gravité et en même temps à la direction de la future traction.

A notre étude on a examiné respectivement au microscope électronique à balayage les oxydes préparés par les deux manières d'emplacement des éprouvettes dans le bain de l'anodisation.

Les figures 10 et 11 sont les figures du microscope électronique à balayage et montrent l'orientation des cellules d'oxyde préparé quand les éprouvettes sont posées horizontalement ou normalement pendant l'anodisation.

Par ces figures on observe que, indépendamment du changement d'orientation de l'éprouvette dans le bain de l'anodisation, l'oxyde qui se forme est toujours orienté parallèlement à la direction des lignes du laminage des tôles de l'acier, direction qui coïncide à celle-ci de la future traction.

Le même phénomène est observé dans le cas d'alliage Al-Si (14) fait qui n'est pas en valeur au cas d'alliage Al-Mg.

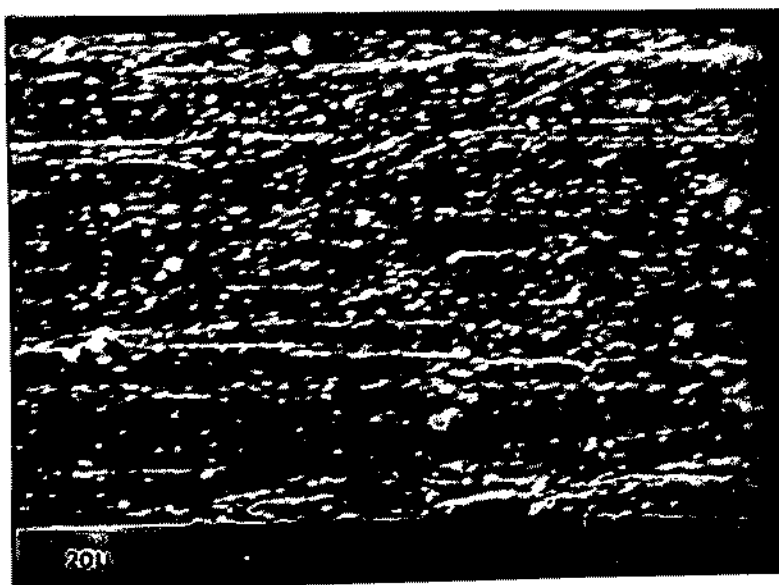


Fig.10. Orientation des cellules d'oxyde de fer quand l'éprouvette est placée horizontalement pendant l'anodisation;  $C_{NaOH}=120g/l$ ;  $C_{Rhongallit}=10g/l$ ;  $T=60^{\circ}C$ ;  $i_{an}=100A/dm^2$ ;  $t_{an}=20min$ ;  $G=1000X$ .



## INFLUENCE D'OXYDES ÉLECTROLYTIQUES SUR LA VIE DE L'ACIER

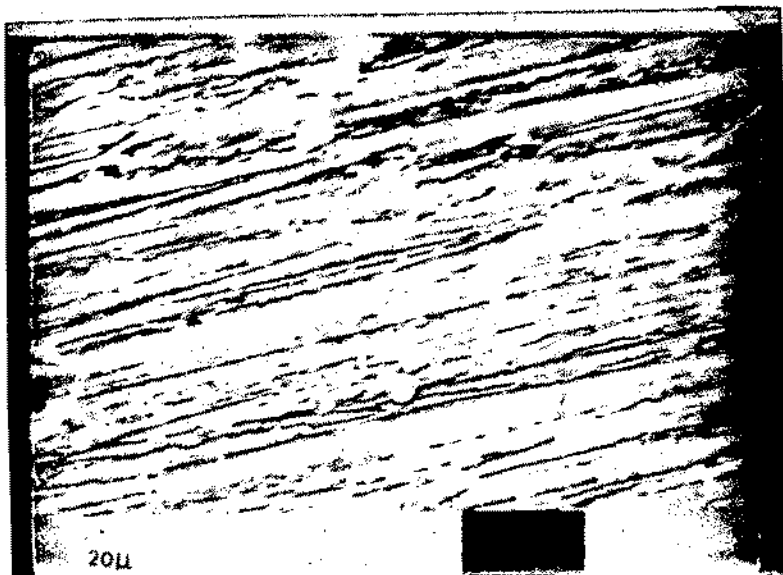


Fig.11. Comme la figure 10. L'éprouvette est placée verticalement pendant l'anodisation.

### CONCLUSIONS ET PERSPECTIVES

1. Dans tous les cas examinés jusqu'à présent, en variant la densité du courant et le temps de l'anodisation ainsi que la composition du bain (partielle et globale) et sa température, on a trouvé que la vie des éprouvettes anodisées diminue par rapport aux éprouvettes nues. Ceci est contraire aux résultats pour le cas d'aluminium.
2. Les résultats de l'examen des surfaces anodisées à l'aide du microscope électronique à balayage montrent que les cellules d'oxydes sont orientées parallèlement à la direction du laminage indépendamment de l'orientation (horizontale ou verticale) des éprouvettes dans le bain de l'anodisation. Ces résultats ne coïncident pas aux résultats au cas d'aluminium où la direction de l'orientation des cellules d'oxydes était toujours parallèle à la direction verticale. Ainsi ayant utilisé des éprouvettes de l'acier coupées parallèlement à la direction du laminage, il ne s'accomplissait pas le cas d'une orientation des cellules d'oxydes normale à la future traction. Ce cas était indispensable pour la protection d'aluminium.

## INFLUENCE D'OXYDES ELECTROLYTIQUES SUR LA VIE DE L'ACIER

Ces résultats:

- a) intensifient l'interprétation donnée pour la protection d'aluminium par des oxydes convenablement orientés,
- b) indiquent que pour la protection de l'acier contre la corrosion sous contrainte il faut utiliser des éprouvettes de l'acier coupées normalement à la direction du laminage.

### RÉFÉRENCES

1. H.P.Van LEEUVEN: "A quantitative analysis of hydrogen-induced cracking" NLR TR 74084 U (1976).
2. H.P.Van LEEUVEN, Materialprüfung, 16, 263 (1974).
3. H.P.Van LEEUVEN, Corrosion, 31, 154 (1975).
4. H.P.Van LEEUVEN, Corrosion, 32, 34 (1976).
5. H.P.Van LEEUVEN, Mémoires Scientifiques Rev. Métallurg., LXXI, No 9 (1974).
6. Th.SKOULIKIDIS et A.KARAGEORGOS, 3me Congrès Internat. sur la Corrosion Marine et des Salissures, Washington D.C. (1972), Compt. Rend. p. 499.
7. Th.SKOULIKIDIS and A.KARAGEORGOS, Br. Corros. J., 10, 17 (1975).
8. Th.SKOULIKIDIS and A.KARAGEORGOS, Br. Corros. J., 13, 28 (1975).
9. Th.SKOULIKIDIS, A.KARAGEORGOS et P.SPATHEIS, 5me Congr. Intern. sur la Corrosion Marine et des Salissures, Barcelona (1980), Compt. Rend. p. 28.
10. Th.SKOULIKIDIS and P.SPATHEIS, Br. Corros. J., 17, 79 (1982).
11. Von Chr.B.PETROW, EK.D.DOBREWA und W.H.BAEWA, Galvanotechnik (Saulgau/Württ.) 60, 257 (1969).
12. Th.SKOULIKIDIS and M.KOUI, Mol. Cryst. Liq. Cryst., 61, 31 (1980).
13. DOS 1928748 (UCB, 1969).
14. Th.SKOULIKIDIS, J.KOLIOS, Acta Metallurgica (à paraître).

PROTECTION OF Al-2.5% Mg ALLOY AGAINST S.C.C. IN SALINE  
WATER BY PROPERLY ORIENTED ANODIC COATINGS; APPLICATION  
TO VARIOUS SHEET THICKNESSES

Th.SKOULIKIDIS, Ath.KARAGEORGOS, M.NERSISYAN

Section of Material Science and Engineering,  
Laboratory of Physical Chemistry and Applied  
Electrochemistry, National Technical Univer-  
sity of Athens, Athens-Greece.

ABSTRACT

In previous works we described a new method for protection of an Al-2.5% Mg alloy against S.C.C. in saline environment by properly oriented anodic coatings, formed in 15% (w/w)  $H_2SO_4$  at  $25^\circ C$  with a current density of  $6.0A/dm^2$ . In the present work the effectiveness of the above method was tested for Al-2.5% Mg alloy sheet of various thicknesses higher than 0.25mm, i.e. 0.50, 1.00, 1.50 and 2.00mm. It was found that, due to the different geometry during anodising, the oxide thickness under the same conditions (current density, temperature, time) is different for different thicknesses of specimens. Taking this into account various (according to their thickness) oxide coatings ( $\gamma_1-Al_2O_3$ ) were prepared for all sheet thicknesses. It was proved that the performance of this protective system is significantly depended upon the thickness of both, the protective anodic coating as well as the metal substrate under protection; in our case it was found that for thicker than  $8.0\mu m$  oxide coatings the T.T.F. has a maximum for a sheet thickness between 1.00 and 0.50mm while for thinner than  $7.0\mu m$  oxide coatings, for a sheet thickness 0.25mm. These led to the suggestion that the employ of 1.00mm thick Al-2.5% Mg alloy coated with an oxide film of  $13.0-35.0\mu m$  results to a better strength and protection than the use of thicker Al-2.5% Mg sheets. Some arguments concerning the interpretation of the anodic oxide coating behaviour are given.

## RESUMÉ

Nous avons décrit dans des travaux précédents une nouvelle méthode de protection d'un alliage Al-2,5% Mg contre la corrosion sous tension en environnement marin, à l'aide des couches anodiques convenablement orientés, formés en solution 15% (w/w) H<sub>2</sub>SO<sub>4</sub>, à 25°C, avec une densité de courant 6,0 A/dm<sup>2</sup>. Dans le présent travail nous avons testé l'efficacité de la méthode ci-dessus, dans le cas d'un alliage Al-2,5% Mg en éprouvettes d'épaisseur supérieure à 0,25mm, c.à.d. 0,50, 1,00, 1,50 et 2,00mm. Il a été trouvé que suivant la géométrie différente de l'anodisation, l'épaisseur de l'oxyde sous les mêmes conditions (densité de courant, température, temps) est différente suivant l'épaisseur différente des éprouvettes. Ainsi nous avons préparé des différentes couches d'oxydes pour tous les épaisseurs des éprouvettes. Il a été prouvé que la performance de ce système de protection dépend d'une manière significative de l'épaisseur du couche anodique ainsi que de l'épaisseur du substrat métallique à protéger. Dans le cas présent, il a été trouvé que, pour des couches plus épaisses que 8,0µm le T.T.F. a un maximum pour une épaisseur d'éprouvette entre 1,00 et 0,50 mm, tandis que pour une épaisseur inférieure à 7,0µm le maximum se présente pour une épaisseur d'éprouvette 0,25mm. Ceci conduit à la suggestion que l'utilisation d'un alliage Al-2,5% Mg d'une épaisseur de 1,00mm couvert d'une couche d'oxyde de 13,0-35,0µm présente une résistance et protection meilleures, comparé à une éprouvette de l'alliage Al-2,5% Mg d'une épaisseur supérieure. Nous présentons quelques arguments concernant l'interprétation du comportement des couches d'oxyde anodique.

## INTRODUCTION

In previous works of ours (1-5) a new method of protection of an Al-2.5% Mg alloy (corresponding to 5052, H. 38) against stress corrosion cracking (S.C.C.) by suitably oriented anodic oxide coatings was suggested. It was found that anodic  $\gamma_1$ - and  $\gamma_2$ -Al<sub>2</sub>O<sub>3</sub> and their hydrates, formed on 0.25mm thick specimens in 15% (w/w) H<sub>2</sub>SO<sub>4</sub> at 25°C, showed satisfactory mechanical properties optimised for an anodic current density,  $i_{an}$ , of 6A/dm<sup>2</sup>. From the various types of the above anodic coatings tested, the porous  $\gamma_1$ -Al<sub>2</sub>O<sub>3</sub> (= means that the oxide cells are built preferentially oriented normal to the future stress direction; such an orientation results from the horizontal arrangement of the specimens during anodising), in a 13.5 µm thick film, was distinguished as possessing the best mechanical strength. This is sufficient to protect the substrate against S.C.C. when tested under accelerated laboratory stress corrosion conditions; a continuously circulating 1M NaCl solution of pH=6.5 and room temperature was used, and an anodic current galvanostatically controlled

at  $0.5 \text{ mA/cm}^2$  was impressed. In such a set of corrosion conditions, an average increase of about 76% of specimen life (that is the time-to-failure, T.T.F.), at three tensile stress levels [constant load of 10, 15 and  $20 \text{ kg/mm}^2$  (\*)] was observed.

The effect of oxide layer thickness on its protective behaviour in the S.C.C. of anodised Al-Mg alloy specimens was revealed by the examination of a large variety of anodic films of  $\gamma_1\text{-Al}_2\text{O}_3$  (from  $0.1 \mu\text{m}$  up to  $35 \mu\text{m}$ ) or  $\gamma_{1,2}\text{-Al}_2\text{O}_3$  [between 36 and  $38 \mu\text{m}$ , recently identified (6)] or  $\gamma_2\text{-Al}_2\text{O}_3$  (above  $38 \mu\text{m}$  up to  $51 \mu\text{m}$ ) produced at  $6 \text{ A/dm}^2$  (7-9). From the T.T.F. records for each anodic film tested under S.C.C. conditions it became clear that the best protective coating is the  $\gamma_1\text{-Al}_2\text{O}_3$ , prepared with a current density of  $6 \text{ A/dm}^2$ , with a thickness of  $3.4 \mu\text{m}$ , and normally oriented to the stress direction; it gives an average T.T.F. increase of 200% compared to the one for bare specimens. From these results, it was found that the protective properties of the three oxides formed are ordered as  $\gamma_1\text{-Al}_2\text{O}_3 > \gamma_2\text{-Al}_2\text{O}_3 > \gamma_{1,2}\text{-Al}_2\text{O}_3$ , and, also, that they are in an inverse relation to their physical sorptive and/or catalytic properties. An interpretation of the mechanical and protective properties of these oxides was also suggested, based on their secondary structure as revealed by EM and SEM (6, 10-12).

The present work aims at further improving the performance of the anodic oxide/aluminium alloy protective system against S.C.C. by studying systematically the role of oxide thickness in relation to the specimen thickness.

## EXPERIMENTAL

### MATERIALS AND DESIGN OF THE SPECIMENS

The commercial Al-Mg alloy tested (type: ASTM 5052, H. 38) conformed to the following nominal composition (in wt-%):

Mg: 2.5; Cr: 0.25; Fe+Si: 0.45; Cu: 0.10; Mn: 0.18; Zn: 0.10, Al: remainder.

The specimens were cut from sheets of suitable thickness ( $e=0.25, 0.50, 1.00, 1.50$  and  $2.00 \text{ mm}$ ), parallelly to the rolling direction (the longitudinal), which coincides with the future stressing direction (i.e. gravity direction), and they were exactly similar to those widely employed for tensile tests having a middle section of re-

---

(\*)  $1 \text{ kg/mm}^2 = 9.8 \text{ N/mm}^2 = 9.8 \times 10^6 \text{ Pa}$

duced width. The same specimens have been used in earlier works (3,4,7-9) and their shape and dimensions have been described in detail in (4). The loading cross-section as well as the total exposed area varied according to the specimen thickness as they are showed in Table I.

TABLE I  
MAIN GEOMETRIC/OPERATIVE CHARACTERISTICS OF THE SPECIMENS

| Specimen thickness<br>mm | Loading cross-section<br>mm <sup>2</sup> | Total exposed area<br>cm <sup>2</sup> |
|--------------------------|--|---------------------------------------|
| 0.25                     | 1  | 1.36                                  |
| 0.50                     | 2  | 1.53                                  |
| 1.00                     | 4  | 1.70                                  |
| 1.50                     | 6  | 1.87                                  |
| 2.00                     | 8  | 2.04                                  |

#### MEASURING ARRANGEMENTS AND CONDITIONS

The measuring arrangements as well as the S.C.C. cell were identical to those already described in detail in the previous work (4). A constantly renewed 1M NaCl solution at room temperature was used as the corroding medium.

The specimens were tested, immersed in the corroding medium and stressed directly by loading them with a certain weight to a definite stress level ( $\sigma=10, 15$  and  $20 \text{ kg/mm}^2$  which corresponds to 98, 147 and  $196 \text{ N/mm}^2$ , respectively) while a galvanostatically controlled anodic current density ( $i=0.5 \text{ mA/cm}^2$ ) was impressed during the test.

Six specimens were tested under each set of conditions and the time that each took to break was recorded; the six individual values are represented by their geometric mean which is referred as the specimen life,  $t$ , or time-to-failure (T.T.F.).

The reproducibility was the same as previously reported (4,7).

#### RESULTS AND DISCUSSION

##### Reference curves

Fig. 1 shows the life curves, as well as their analytical expression, of bare specimens of a different thickness,  $e$ , (considered as "reference specimens") tested as described; these will be used as reference curves with

which one could compare the lives of oxide coated specimens.

The curve for  $e=0.25\text{mm}$  is identical to that earlier-ly reported in (4).

It should be clarified that these curves represent the genuine S.C.C. behaviour of the specimens (between threshold stress and yield point,  $\sigma_{0.2}$ , levels) free of any parasitic effect possibly due to the impressed anodic current (4,13).

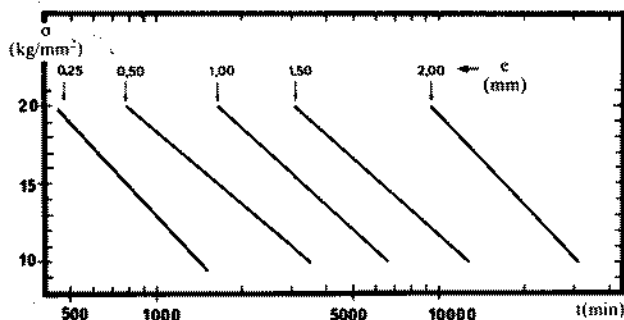


Fig.1. Applied stress,  $\sigma$ , vs  $\log t$ ;  $i=0.5\text{mA}/\text{cm}^2$   
(Reference curves)

$$\begin{aligned} (e=0.25) &\rightarrow \sigma = -17.73 \log t + 67.59 \\ (e=0.50) &\rightarrow \sigma = -15.30 \log t + 64.05 \\ (e=1.00) &\rightarrow \sigma = -16.59 \log t + 73.52 \\ (e=1.50) &\rightarrow \sigma = -16.55 \log t + 77.88 \\ (e=2.00) &\rightarrow \sigma = -19.62 \log t + 97.87 \end{aligned}$$

### Influence of specimen thickness

The effect of specimen thickness on the behaviour under S.C.C. conditions, of the alloy used, was found when the results presented on Fig.1 were transferred to a diagram: specimen thickness,  $e$ , vs  $\log t$  (Fig.2); the curves correspond to the stress levels at which the specimens were loaded. It can be seen that the log of specimen life is a linear function of the thickness,  $e$ , of the form  $e = k \log t - l$  ( $k, l > 0$ ), for a determined stress level. Therefore it becomes evident that the S.C.C. behaviour of bare specimens depends on its thickness rectilinearly in relation to  $\log t$ , as on the stress level following the equation:  $\sigma = -a \log t + b$  ( $a, b > 0$ ) for a determined specimen thickness.

In Fig.2 it is shown that the specimen thickness influences logarithmically its S.C.C. behaviour as any other parameter influencing directly the kinetics of the phenomenon. Such a differentiation in S.C.C. behaviour of the specimens is mainly attributed to the milder electrical/electrochemical and stress conditions predominant in the vicinity of the pit/crack tip in thicker specimens and conse-

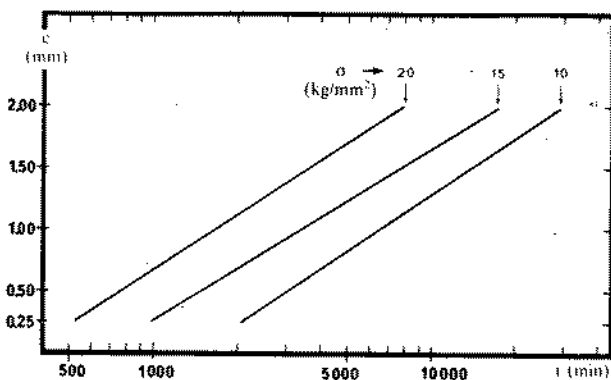


Fig.2. Specimen thickness,  $e$ , vs  $\log t$ ;  $i = 0.5 \text{ mA/cm}^2$

$$(\sigma = 10) \rightarrow e = 1.49 \log t - 3.80$$

$$(\sigma = 15) \rightarrow e = 1.41 \log t - 3.97$$

$$(\sigma = 20) \rightarrow e = 1.53 \log t - 4.81$$

quently to a proportionally less intense active path which in the case of Al-alloys has been proved as a current intensity assisted one (13-18). Thus an important conclusion is that sheet thickness should be considered as a crucial parameter in the behaviour of metals or alloys under S.C.C. conditions as well as the stress factor. This should be taken under consideration when designing or maintaining a construction under S.C.C.

#### Influence of oxide thickness

In previous works (7-9) the relation of the thickness of anodic Al-oxide coatings between 1.7 and  $51 \mu\text{m}$ , to their protective properties of 0.25 mm thick specimens, of the same Al-2.5% Mg alloy, was examined and discussed. The results obtained have been reported in the form of oxide thickness,  $x$ , vs specimen life,  $t$ , curves as shown in Fig. 3 (8); from all three types of surface oxide examined, only  $\gamma_1\text{-Al}_2\text{O}_3$  has been found as giving satisfactory protection to the substrate, with an increasing rate as its thickness decreases, at least in the region of service (up to a minimum thickness of  $3.4 \mu\text{m}$ ).

Aiming at the scope of the present work, i.e. to extend the study of the effect of anodic  $\gamma_1\text{-Al}_2\text{O}_3$  layer thickness on its protective performance to thicker than 0.25 mm sheets, a number of specimens of the same thickness as the reference ones were anodised in a 15% (w/w)  $\text{H}_2\text{SO}_4$  bath at a constant temperature of  $25^\circ\text{C}$ . and at a current density,  $i_{\text{an}}$ , of  $6 \text{ A/dm}^2$ ; anodising times, (proportional) quantities of current passed and  $\gamma_1\text{-Al}_2\text{O}_3$ .



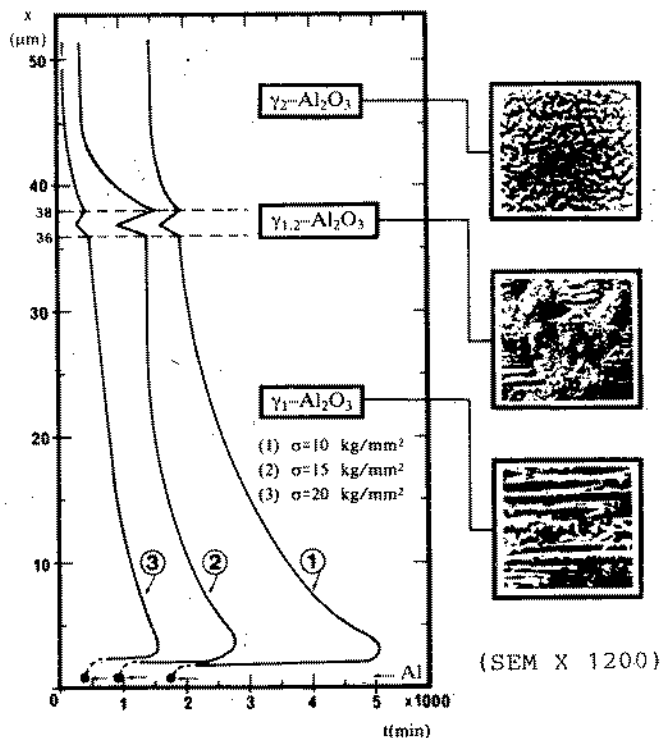


Fig.3. Al-oxide layer thickness,  $x$ , vs specimen life,  $t$ ; specimen thickness  $e=0.25\text{mm}$ ;  $i_{an}=6\text{A/dm}^2$  (in a 15%  $\text{H}_2\text{SO}_4$  bath at  $25^\circ\text{C}$ );  $i=0.5\text{mA/cm}^2$  (8).

thickness produced in each case and directly measured by microscopical examination of cross-sections are indicated in Table II.

During anodising the specimens were held horizontally as it was previously done (4), so that a preferential oxide orientation (indicated =) normal to the rolling direction as well to the future stressing direction resulted, as it is clearly shown in the micrograph of Fig. 4 (19).

It should be noted that the divergence in thickness, observed in Table II for anodic coatings produced under similar anodising conditions, on specimens of different thicknesses, have been already examined in depth and completely elucidated; the results of this study will be

TABLE II  
ANODISING TIME, QUANTITY OF CURRENT AND CORRESPONDING  
 $\gamma_1$ - $\text{Al}_2\text{O}_3$  THICKNESS

| Anodising time, $t_{an}$ , in min | Quantity of current, $Q_{an}$ , in C/dm <sup>2</sup> | $\gamma_1$ - $\text{Al}_2\text{O}_3$ thickness, $x$ , in $\mu\text{m}$ ( $\pm 0.5 \mu\text{m}$ ) |      |      |      |         |
|-----------------------------------|--|--|------|------|------|---------|
|                                   |  | Specimen thickness, $e$ , in mm  |      |      |      |         |
|                                   |  | 0.25   | 0.50 | 1.00 | 1.50 | 2.00    |
| 2.25                              | 810  | 3.4  | 4.2  | 4.7  | 4.9  | 5.5     |
| 9.00                              | 3240   | 13.5   | 16.9 | 18.6 | 19.8 | 22.0    |
| 22.56                             | 8192   | 34.0   | 42.2 | 46.7 | 48.5 | (51.0*) |

(\*) probably  $\gamma_2$ - $\text{Al}_2\text{O}_3$  oxide grain orientation

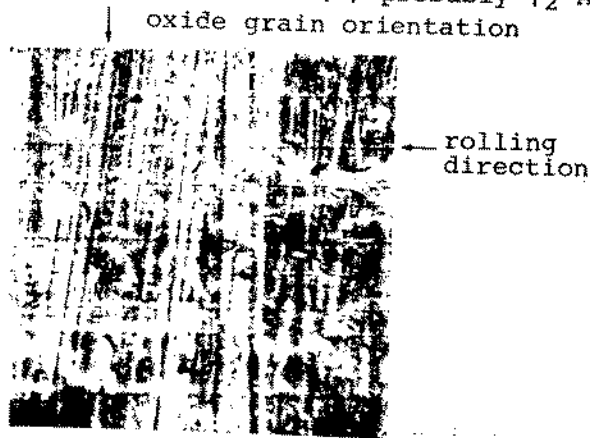


Fig.4. Microphotograph SEM X1200 of  $\gamma_1$ - $\text{Al}_2\text{O}_3$ , normally oriented to the rolling direction;  $i_{an}=6\text{A/dm}^2$ ; oxide thickness  $5\mu\text{m}$  (19).

soon published.

The T.T.F. of anodised specimens corresponding to all cases included in Table II, as well as that of bare ones, are represented according to their thickness  $e=0.50, 1.00, 1.50$  and  $2.00$  mm in the diagrams: oxide thickness,  $x$ , vs specimen life,  $t$ , of Figs 5-8 respectively. From these figures it can be seen that the shape of the resulted curves is generally quite similar to that for  $0.25\text{mm}$  specimens (Fig. 3). It means that  $\gamma_1$ - $\text{Al}_2\text{O}_3$  protects the Al-2.5% Mg specimens against S.C.C. for all oxide thicknesses examined, at all three stress levels 10, 15 and 20  $\text{kg/mm}^2$ , and that the protection increases as the oxide

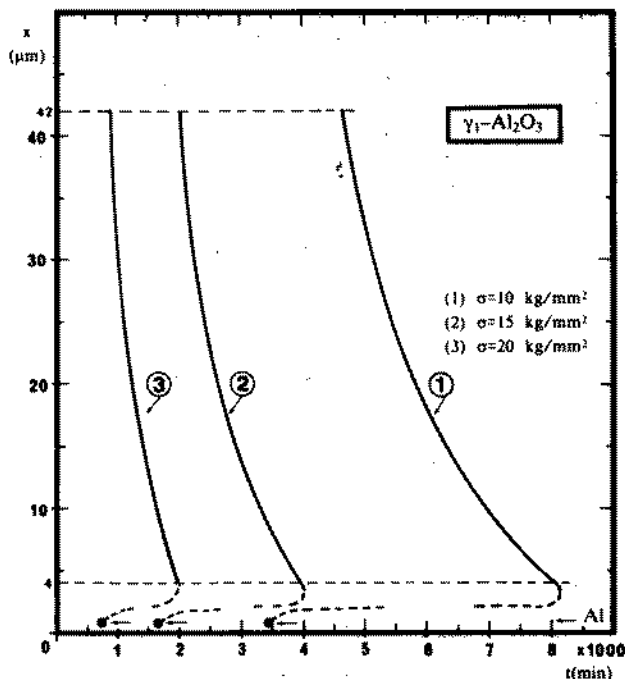


Fig.5.  $\gamma_1\text{-Al}_2\text{O}_3$  thickness,  $x$ , vs specimen lifetime,  $t$ ; specimen thickness  $e = 0.50 \text{ mm}$ ;  $i_{an} = 6 \text{ A/dm}^2$ ;  $i = 0.5 \text{ mA/cm}^2$ .

thickness decreases (the lowest limiting T.T.F. value for  $x \rightarrow 0$  is that of bare specimen at that stress level). This is true for all specimen thicknesses between 0.25 and 1.50 mm but not for the thickness of 2.00 mm; in this latter case  $\gamma_1\text{-Al}_2\text{O}_3$  seems to have lost its protective role offering a small protection only at the stress level of  $20 \text{ kg/mm}^2$  and for oxide thicknesses around the value  $x = 22.0 \mu\text{m}$ .

To obtain a better image of the effect of anodic  $\gamma_1\text{-Al}_2\text{O}_3$  thickness on its protective properties the data presented in Figs 3 and 5-8 are summarized on a diagram: oxide thickness,  $x$ , vs per cent specimen protection,  $p$ , as shown in Fig. 9. This diagram, which fully covers the domain of usual service applications of  $\gamma_1\text{-Al}_2\text{O}_3$ 's, comprises five curves, one for each specimen thickness used. At each anodic oxide thickness tested the corresponding per cent protection has been calcula-

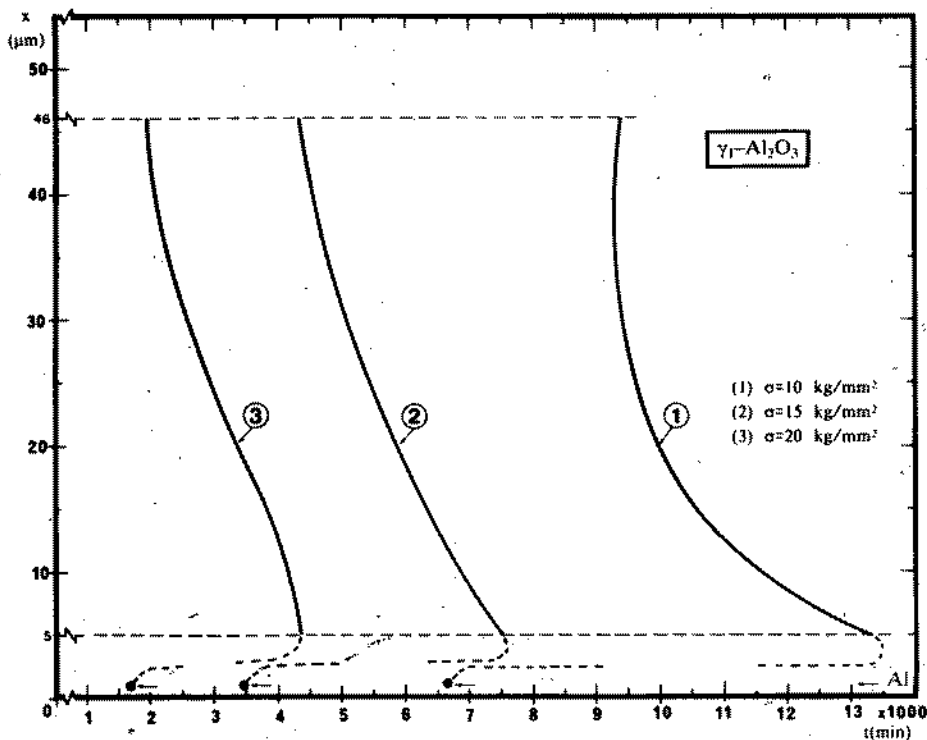


Fig.6.  $\gamma_1\text{-Al}_2\text{O}_3$  = thickness,  $x$ , vs specimen life,  $t$ ; specimen thickness  $e=1.00\text{mm}$ ;  $i_{an}=6\text{A/dm}^2$ ;  $i=0.5\text{mA/cm}^2$ .

ted by dividing the difference (T.T.F. of anodised specimen-T.T.F. of bare specimen) by the T.T.F. of bare specimen ( $\times 100$ ) at each stress level and, thereafter, by averaging over the three stress levels. From Fig. 9 it becomes obvious that the degree of protection offered by  $\gamma_1\text{-Al}_2\text{O}_3$ , as an effective anodic coating against S.C.C., depends not only upon its thickness but moreover upon substrate's thickness. In the comparative Table III, specimen thicknesses are ordered in descending series according to the protection they benefit by a  $\gamma_1\text{-Al}_2\text{O}_3$  layer of a definite thickness. Actually, 1.00mm thick specimens seem to be better protected by anodic oxides of thicknesses between 45.0 and 11.0 $\mu\text{m}$ ; for thinner oxides, between 11.0 and 7.5 $\mu\text{m}$ , the best protection is observed on 0.50 mm thick specimens; and for even thinner oxides, up to the

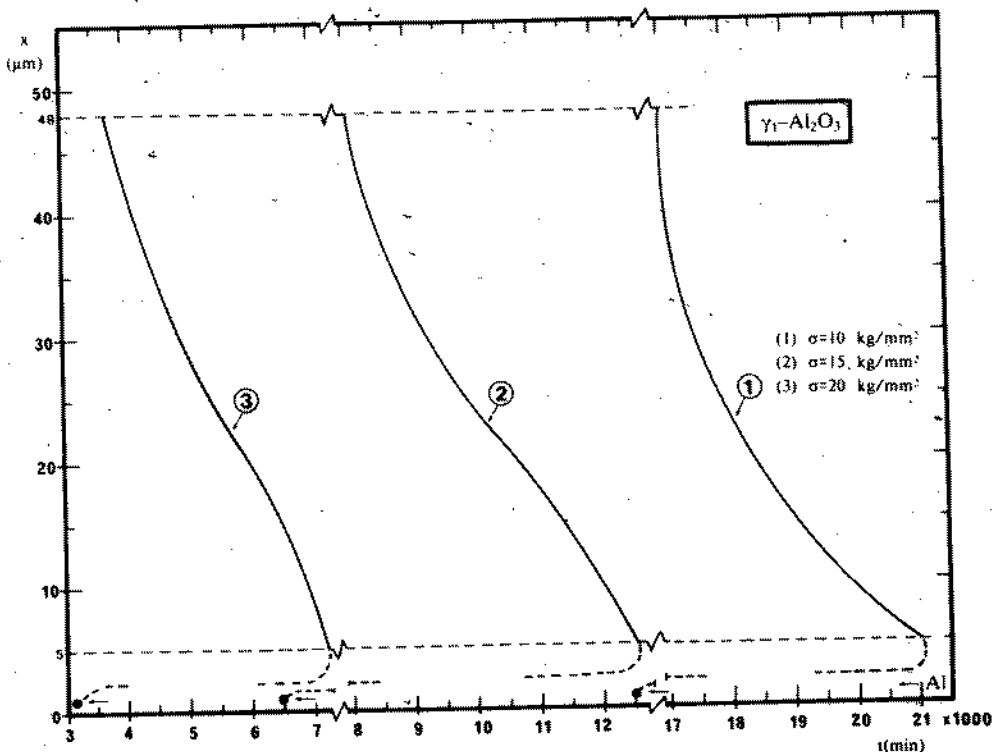


Fig.7.  $\gamma_1\text{-Al}_2\text{O}_3$  thickness,  $x$ , vs specimen lifetime,  $t$ ; specimen thickness  $e=1.50\text{mm}$ ;  $i_{an}=6\text{A/dm}^2$ ;  $i=0.5\text{mA/cm}^2$ .

lower comparable limit of  $5.0\mu\text{m}$ , the best protection is assigned to  $0.25\text{mm}$  thick specimens. Of course,  $2.00\text{mm}$  thick specimens are omitted because their behaviour is not comparable to the rest.

Furthermore, these observations lead to the thought that the degree of protection against S.C.C. that anodic  $\gamma_1\text{-Al}_2\text{O}_3$  offers to Al-2.5% Mg substrate is strongly conditioned by the thicknesses of both the former and the latter. To demonstrate that such a dependence occurs, a diagram (Fig. 10): specimen thickness,  $e$ , vs per cent specimen protection,  $p$ , is drawn, which is derived by successively interpolating the curves of the Fig. 9. Fig. 10 illustrates that, the protection of a specimen against S.C.C. greatly depends upon both the thickness of protective anodic coating as well as

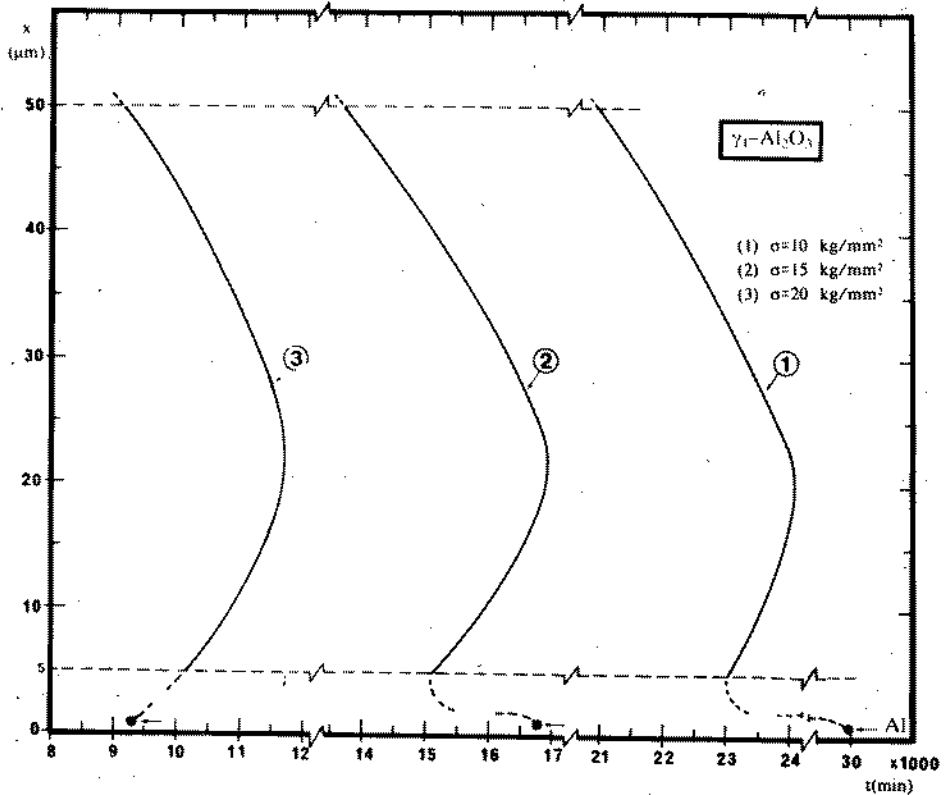


Fig.8.  $\gamma\text{-Al}_2\text{O}_3$  thickness,  $x$ , vs specimen life,  $t$ ; specimen thickness  $e=2.00\text{mm}$ ;  $i_{an}=6\text{A/dm}^2$ ;  $i=0.5\text{mA/cm}^2$ .

its own thickness. This provides a fertile ground to grow up the conception of a "protective system"; so, when evaluating the performance of a protective system in the laboratory, as well as in service, it is necessary to consider as determining parameters, both anodic coating thickness and substrate's thickness and not only the first, as it is usually done. From the curves of Fig. 10 it is, also, seen that the way of performance of the protective system alters a great deal when the oxide thickness changes from 7 to 8  $\mu\text{m}$ . Particularly, for thinner than 7.0  $\mu\text{m}$  oxide coatings the degree of protection is greater the thinner the specimen gets; but for thicker than 8.0  $\mu\text{m}$  oxide coatings the degree of protection is greater for specimens of intermediate thickness. The protection

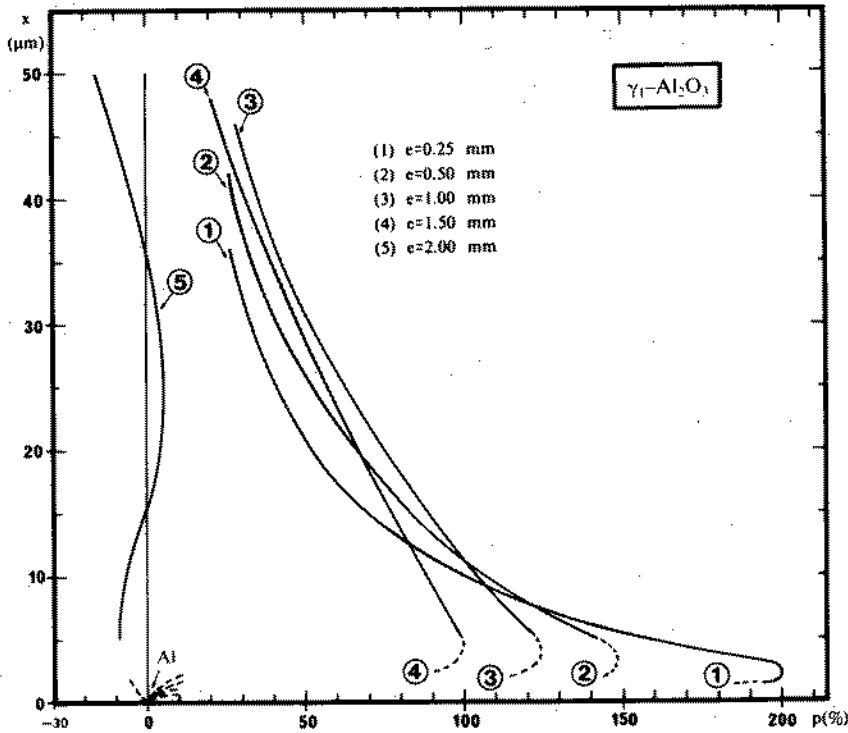


Fig. 9.  $\gamma_1\text{-Al}_2\text{O}_3$  thickness,  $x$ , vs specimen protection,  $p$ ;  $i_{an}=6\text{A/dm}^2$ ;  $i=0.5\text{mA/cm}^2$ .

becomes maximum for 0.50mm thick specimens when  $8.0\mu\text{m} < x < 11.0\mu\text{m}$  and 1.00mm thick specimens when  $x > 12.0\mu\text{m}$ . For example in the case of  $x=15.0\mu\text{m}$  [where thinner anodic coatings tend to thicken under natural conditions, as it is known from experience (5)] the protective system gains an additional yield on its effectiveness if the ratio oxide thickness/metal thickness is 15.0/1.00. This ratio is more realistic and valuable, indeed, in service conditions. Therefore an important suggestion is that thicker than 1.00mm Al-2.5% Mg alloy plates or sheets, as building materials, could be replaced by 1.00mm or thinner ones, which could be more effectively protected.

A suitable interpretation of such alterations obser-

**TABLE III**  
**EVALUATION OF EFFECTIVENESS OF ANODIC OXIDE COATINGS**  
**IN PROTECTING SUBSTRATE AGAINST S.C.C. ACCORDING TO**  
**SPECIMEN THICKNESS**

| Oxide thickness<br>in $\mu\text{m}$ | Order of protection<br>Number in brackets indicates specimen thickness in mm |
|-------------------------------------|--|
| 45.0-20.0                           | (1.00) > (1.50) > (0.50) > (0.25)  |
| 20.0-12.5                           | (1.00) > (0.50) > (1.50) > (0.25)  |
| 12.5-11.0                           | (1.00) > (0.50) > (0.25) > (1.50)  |
| 11.0- 9.0                           | (0.50) > (1.00) > (0.25) > (1.50)  |
| 9.0- 7.5                            | (0.50) > (0.25) > (1.00) > (1.50)  |
| 7.5- 5.0                            | (0.25) > (0.50) > (1.00) > (1.50)  |

ved in protective efficiency of  $\gamma_1\text{-Al}_2\text{O}_3$  according to specimen thickness should be based on each one of the following reasons: (a) The secondary structure (especially the porosity) of  $\gamma_1\text{-Al}_2\text{O}_3$  is affected by the geometry of the electric field during anodising when using thicker specimens (19). (b) Thicker specimens have greater exposed surface; i.e. for a constant current density, they have proportionally higher demands in anodic current during anodising as well as during S.C.C. testing; in addition to this the prolonged exposure under test conditions results to a sensitisation of the substrate in S.C.C. (13). (c) While the form of the stress field at the crack tip shifts from plane stress conditions (specimen thickness 0.25mm) to plain strain ones (marginal specimen thickness 2.00mm), the mechanical properties of anodic coating could hardly be suited to substrate's deformation. This inability is much more pronounced in the case of 2.00mm thick specimens where anodic coating fails to play any protective role.



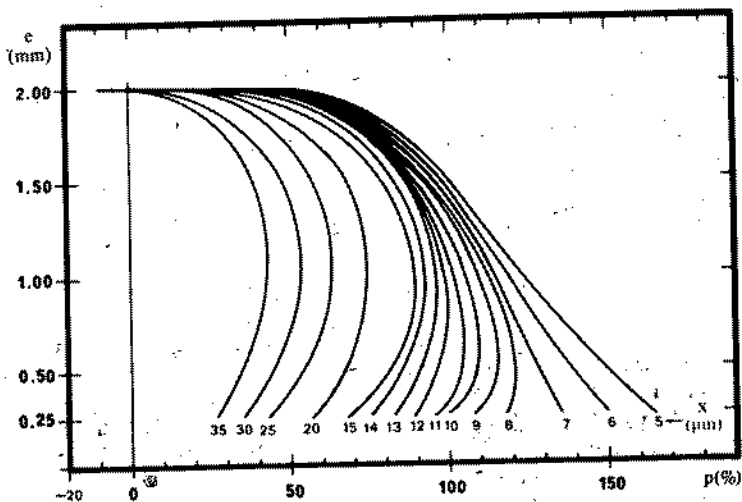


Fig.10. Specimen thickness,  $e$ , vs protection,  $p$ .

### CONCLUSIONS

1. The method of protection of an Al-2.5% Mg alloy against S.C.C. by suitably oriented anodic oxide coatings, which had been suggested in some earlier works of ours and optimized for  $\gamma_1\text{-Al}_2\text{O}_3$  formed on 0.25 mm thick specimens, could be successfully applied on thicker materials up to a thickness of 1.50mm; Thus the time-to-failure of appropriate specimens could be prolonged for two to three times. This method, however, seems to fail so far to protect the substrate when its thickness is 2.00mm.
2. The specimen thickness influences logarithmically its S.C.C. behaviour as any other parameter influencing directly the kinetics of the phenomenon; this is mainly attributed to the milder electrical/electrochemical and stress conditions predominant in the vicinity of the pit/crack tip in thicker specimens, and consequently to a proportionally less intense active path which in the case of Al-alloys has been proved as a current intensity assisted one. Thus an important conclusion is that sheet thickness should be considered as a crucial parameter in the behaviour of metals or alloys under S.C.C. conditions as well as the stress factor. This should be taken under consideration when designing or maintaining a construction under S.C.C.
3. The degree of protection offered by  $\gamma_1\text{-Al}_2\text{O}_3$ , as an effective anodic coating against S.C.C., is strongly depended not only upon its thickness but also upon the substrate's thickness. So, 1.00mm thick specimens

seem to be better protected by anodic coatings of thicknesses between 45.0 and 11.0 $\mu$ m; for thinner oxides, between 11.0 and 7.5 $\mu$ m, the best protection is observed on 0.50mm thick specimens; and, for even thinner anodic coatings, up to 5.0 $\mu$ m, the best protection is assigned to 0.25mm thick specimens. 2.00mm thick specimens do not seem to be protected.

4. Considering the metal substrate and the anodic oxide coating as consisting of a "protective system", the way of performance of this system is significantly affected by the thicknesses of both the protective coating and the under protection substrate. In our particular case it was found that for thinner than 7.0 $\mu$ m coatings the degree of protection is greater the thinner the specimen gets; but for thicker than 8.0 $\mu$ m coatings the degree of protection is greater for specimens of intermediate thickness, becoming maximum for 0.50mm thick specimens when the coating thickness is between 8.0 $\mu$ m to 11.0 $\mu$ m and 1.0mm thick specimens when the coating is thicker than 12.0 $\mu$ m. So, the protective system gains an additional yield on its effectiveness for an appropriate ratio oxide thickness/metal thickness.
5. It is suggested that thicker than 1.00mm Al-2.5% Mg alloy plates or sheets, as building materials, could be replaced by 1.00mm or thinner ones which could be much more effectively protected.

A suitable interpretation of such alterations observed in protective efficiency of  $\gamma_1$ -Al<sub>2</sub>O<sub>3</sub> according to specimen thickness should be based on each one of the following reasons: (a) The secondary structure (especially the porosity) of  $\gamma_1$ -Al<sub>2</sub>O<sub>3</sub> is affected by the geometry of the electric field during anodising when using thicker specimens. (b) Thicker specimens have greater exposed surface, i.e. for a constant current density, have proportionally higher demands in anodic current during anodising as well as during S.C.C. testing which, in addition to prolonged exposure under test conditions, result to a sensitisation of the substrate in S.C.C. (c) While the form of the stress field at the crack tip shifts from plane stress conditions (specimen thickness 0.25mm) to plain strain ones (marginal specimen thickness 2.00mm), the mechanical properties of anodic coating could hardly be suited to substrate's deformation. This inability is much more pronounced in the case of 2.00mm thick specimens where anodic coating fails to play any protective role.

## ACKNOWLEDGMENTS

Dr. A.Karageorgos and M.Nersisyan express their thanks for the research granted by the Research Council of the National Technical University of Athens, that it was also financed by "Aluminium of Greece".

## ABBREVIATIONS AND SYMBOLS

|                  |   |
|------------------|---|
| E.M.             | Electron Microscopy   |
| S.C.C.           | Stress Corrosion Cracking   |
| S.E.M:           | Scanning Electron Microscopy                                      |
| T.T.F.           | Time-to-Failure (specimen life)                                   |
| e                | specimen thickness, in mm   |
| i                | impressed anodic current density, in mA/cm <sup>2</sup>           |
| ian              | anodising current density, in A/dm <sup>2</sup>                   |
| Qan              | quantity of current passed during anodising, in C/dm <sup>2</sup> |
| σ                | stress level (or load of a specimen), in kg/mm <sup>2</sup>       |
| σ <sub>0.2</sub> | yield stress, in kg/mm <sup>2</sup>                               |
| t                | specimen life (T.T.F.), in min                                    |
| tan              | anodising time, in min  |
| x                | anodic coating thickness, in μm                                   |

## REFERENCES

1. TH.SKOULIKIDIS, ATH.KARAGEORGOS, K.LAOUDIS, N.KOULOUMBI, Proc. 30th Confer. of AGARD, Athens, 1970.
2. TH.SKOULIKIDIS: "Propositions sur des thèmes pour discussion", invited paper in the Conference of Ericeira (Portugal) on "The Theory of Stress Corrosion Cracking in Alloys", 1971.
3. TH.SKOULIKIDIS, ATH.KARAGEORGOS, Proc. 3rd Int. Congr. Marine Corrosion and Fouling, Washington, D.C., 1972, p. 499.
4. TH.SKOULIKIDIS, ATH.KARAGEORGOS, Br. Corros. J., 10, 17 (1975).
5. TH.SKOULIKIDIS, P.SPATHIS, *ibid*, 17, 79 (1982).
6. TH.SKOULIKIDIS, F.BATZIAS, Proc. 4th Int. ICSOBA Cong., Athens, 1978, p. 338.
7. TH.SKOULIKIDIS, ATH.KARAGEORGOS, Br. Corros. J., 13, 28 (1978).
8. TH.SKOULIKIDIS, ATH.KARAGEORGOS, *ibid*, 15, 41 (1980).
9. TH.SKOULIKIDIS, ATH.KARAGEORGOS, P.SPATHIS, Proc. 5th Int. Congr. Marine Corrosion and Fouling, Barcelona, 1980, p. 28.
10. TH.SKOULIKIDIS, K.SARROPOULOS, 4th Int. ICSOBA Congr., Athens, 1978, p. 356.
11. TH.SKOULIKIDIS, F.BATZIAS, *ibid*, p. 375.
12. TH.SKOULIKIDIS, G.PATERMARAKIS: "Catalytic Properties of Y<sub>1</sub><sup>-</sup>, Y<sub>1</sub><sub>2</sub><sup>-</sup>, Y<sub>2</sub>-Al<sub>2</sub>O<sub>3</sub>", Dr. Degree Thesis of G. Patermarakis, Laboratory of Physical Chemistry and Applied Electrochemistry, National Technical University of Athens, 1984.

13. ATH.KARAGEORGOS, Proc. 5th Int. Congr. Marine Corrosion and Fouling, Barcelona, 1980, p. 4.
14. TH.SKOULIKIDIS, ATH.KARAGEORGOS, G.BATIS, Br.Corros. J., 11, 143 (1976).
15. TH.SKOULIKIDIS, N.KOULOUMBI, *ibid*, 14, 216 (1979).
16. TH.SKOULIKIDIS, G.BATIS, N.KOULOUMBI, *ibid.*, 15, 152 (1980).
17. TH.SKOULIKIDIS, G.BATIS, N.KOULOUMBI, Proc. 5th Int. Congr. Marine Corrosion and Fouling, Barcelona, 1980, p. 16.
18. TH.SKOULIKIDIS, J.KOLIOS: "Study, predict and explain the behavior of Al-Mg and Al-Si alloys under S.C.C. conditions", Dr. Degree Thesis of J. Kolios, Laboratory of Physical Chemistry and Applied Electrochemistry, National Technical University of Athens, 1983.
19. TH.SKOULIKIDIS, M.NERSISYAN: "Protection of Al-Mg alloys against S.C.C. by properly oriented anodic  $\gamma_1$ -Al<sub>2</sub>O<sub>3</sub> for various sheet thicknesses", Dr. Degree Thesis of M. Nersisyan, Laboratory of Physical Chemistry and Applied Electrochemistry, National Technical University of Athens, 1984.

Small Scale Field Test of Steel Wire Ropes in Submerged Sea Water  
Which is simulating Tension Leg Platform Mooring.

Haruo SHIMADA

R & D LABORATORIES-1, NIPPON STEEL CORPORATION

1618 IDA, NAKAHARA-KU, KAWASAKI 211, JAPAN

Abstract

In order to realize the steel wire rope mooring of T.L.P, it is inevitable to obtain the valuable information as many as possible. For this purpose, we designed the exposure equipment simulated to T.L.P mooring and immersed it into sea water for long term. Through this exposure test in offshore environment, we could make clear the characteristics of such a 4 points mooring as T.L.P, marine fouling and the wire ropes under the extreme variation of tension load due to irregular wave force with lapse of time which is so called the severe corrosion attack. In addition, we showed the possibility of developing the wire rope with high resistance against such attack.

Resumé

Dans le but de réaliser l'ancrage avec des cables d'acier de T.L.P., il est inevitable d'obtenir les informations les plus précieuses et les plus nombreuses. Pour cela nous avons dessiné (construit) l'équipement d'exposition simulé pour l'ancrage de T.L.P. et immergé dans l'eau de mer à long termes. A l'aide de ce test d'exposition en environnement, en mer profonde nous avons pu mettre en évidence les caractéristiques qui correspondent à l'ancrage de 4 points de T.L.P., la salissure marine et les cables d'acier sous les variations extrêmes de la tension de charge qui sont dues à la force irrégulière des vagues dans un lapse de temps qui est appelé "l'attaque severe de la corrosion". Nous avons montré également la possibilité de développer des cables pour présenter une résistance accrue contre une attaque de ce genre.

## 1. Introduction

Concerning the application of wire rope to T.L.P mooring, several reports(1 - 3) have been already discussed. But there are no reports dealing with the behaviour of the wire rope materials exposed to the offshore environments under tension loading. The purpose of this study is to examine the corrosion fatigue and fouling of various steel wire ropes in offshore environments by using the small scale exposure equipment simulated to T.L.P mooring and to obtain the new knowledges in order to realize the steel wire ropes mooring of T.L.P.

## 2. Experiments and Results

### Steel wire ropes prepared for this study

From the preliminary one year corrosion test of various single wires under constant tension load in sea water, we found out that the homogeneous pearlite structure and the bearing of such anti-corrosive elements as Cr, Mo are inevitable in order to increase the corrosion resistance of steel wires in sea water. In addition, we could confirm that the single wire of austenitic stainless steel showed extremely high resistance against sea water corrosion attack but their ropes tended to corrode much more rapidly than the ordinary steel wire ropes due to the severe corrosion attack occurring in crevice of ropes. According to the previous report(4), the bearing amounts of Cr should be decreased under 5% in steel to avoid the crevice corrosion attack in sea water. It is also indicated that the decrease of the inclusions in steel tend to increase the resistance against fatigue deterioration of steel materials. Therefore, we can expect the high resistance against corrosion fatigue of steel materials by decreasing their Sulphur content as low as possible in case of high carbon ordinary steel wire. In referring these knowledges, the following four steel wire ropes were prepared for this study.

Ordinary steel wire ropes SWRS 77B

Ultra low S type ordinary steel wire ropes SWRS 77B

The steel wire ropes with the possibility of high resistance against the sea water corrosion attack

2Cr - 2Co - 0.02Mo bearing wire ropes,

2Cr - 2Co - 0.08Mo bearing wire ropes,

Ordinary steel wire ropes SWRS and ultra low S SWRS are commercial grade wire ropes. 2%Cr bearing steel wire ropes started from 100kg ingot molten in induction furnace. The chemical composition and mechanical strength of these steel wire ropes are shown in Table.1 and Table.2.

### Experimental procedure

Exposure equipment simulated to T.L.P mooring(Fig.1)

We designed this equipment so that we can simulate to T.L.P mooring as near as possible and obtain the valuable informations as many as possible in order to realize T.L.P wire rope mooring in the near future and exposed it to sea water for long term.

The keypoints of this design are represented as follows.

- (1). According to the previous reports of T.L.P design(1 - 5,6), the vertical height of this platform portion located in the submerged zone of sea water is much longer than that of this platform portion located over sea surface in order to increase the stability against wave force.  
To realize that stability in such a very shallow water area as used in this study, it is necessary to keep the platform steadily in the submerged zone of sea water. The most significant factor of the platform of T.L.P is the floating force to give the tension load on the mooring tethers. Accordingly, we set the float steadily in the submerged zone of sea water in our study. The float is consisted of the FRP drums and steel frames.
- (2). The boundary section between the sockets holding steel wire ropes and the wire ropes tends to be deteriorated by corrosion fatigue attack of sea water. In addition, organic resin is recommended as the material poured into the socket (5). Therefore, we selected polyethylene resin and epoxy resin whose water permeability is extremely low as the compound material in the socket. And we covered both the steel socket surface and the steel wire ropes portion connected to the socket in length of about 100mm with the butyl rubber layer in thickness of 5 mm.
- (3). The significant point of T.L.P design is to avoid the torsion force due to wave force as well as possible. Therefore, we set the swivels in all the wire rope mooring lines for this purpose which can absorb that torsion force.
- (4). The other significant point of T.L.P design is to keep the the stability of the anchor installed in the sea bed in order to support the mooring force. Accordingly, we set 4 concrete anchors whose weight is enough for supporting the floating force and wave force.
- (5). In T.L.P mooring, it is necessary to keep the balance of the platform even if the sudden rupture of any mooring rope line occurs. In order to approach to this aim, we prepared simultaneously two wire ropes at each mooring corner. The one is used for mooring the float and therefore exposed to sea water under tension load. The function of the other is to maintain the balance of the float in the sudden rupture of the above wire ropes and therefore exposed to

sea water free from tension load in order to delay its deterioration as long as possible.

In addition, we are connecting the float to 4 steel piles by 4 long chains which are not contributing to mooring the float at all, but are available for preventing the missing of the float even in the negligible small case that all of 8 wire ropes break suddenly.

- (6). In order to apply the wire rope mooring to T.L.P, we have to forecast the life of steel wire ropes under tension load and to obtain the information about the good timing to replace the wire ropes. For this purpose, we set the load cell in each mooring line and checked the tension load force with lapse of time. The outline of this anchors and the float connected to wire ropes with such various parts as sockets, swivels, load cells and shackles is shown in Fig.2a and Fig.2b.

### Results

From this experimental results, we could obtain the following new knowledges.

- 1). 4 point mooring in this study consists of the typical statics indeterminate mooring which represents a couple of wire ropes facing each other under approximately equal tension load, but a couple of the nearest neighbor under different tension load.(Fig.3)
- 2). Each mooring wire rope is exposed to sea water under variable tension load changing with lapse of time. The extreme variation of tension load with time might be due to the irregular wave force.(Fig.4) From these results, it is clear that the mooring wire ropes of T.L.P tends to deteriorate due to corrosion fatigue in sea water.
- 3). The deterioration of spiral wire ropes due to the rupture of the single wire of their surface layer can be checked very easily by divers.(Fig.5)
- 4). 2Cr - 2Co - 0.08Mo bearing wire ropes caused mechanical rupture of one single wire belonging to their surface layer within 3 months after the beginning of exposure test. This might be due to the presence of the residual tiny martensite in the homogeneous pearlite structure which tends to cause mechanical defects resulting in rupture under tension load. Once such rupture occurs, the deterioration of the spiral steel wire ropes tend to be accelerated very rapidly.(Fig.6)
- 5). The ranking of the resistance against marine fouling after 1 year exposure in sea water is described as follows.(Fig.7)



No.1 ; 2Cr - 2Co - 0.02, 0.08Mo bearing wire ropes

No.2 ; Ultra low S SWRS

No.3 ; Ordinary SWRS

- 6). 15 months have elapsed since the beginning of the exposure test of mooring wire ropes, but any of the above mentioned three wire ropes except 2Cr - 2Co - 0.08Mo bearing rope has not shown the rupture due to corrosion fatigue. This might be due to controlling the variable tension load within the range of 0.35 minimum to 5% maximum of the braking force of the wire ropes.
- 7). It is well known that the price of Cobalt element is very expensive. In our additional work, we have succeeded in commercial production trial of cheap 2Cr - 0.05/0.2Co - 0.03Mo bearing steel wire consisting of homogeneous pearlite structure with no residual martensite by using Slow Cooling System and direct cold extrusion. Their mechanical strength is shown in Table.3.

### 3. Conclusion

In order to make clear various problems in T.L.P wire rope mooring, we carried out the long term simulation test in offshore environment by using the special small scale exposure equipment. From this study, it has been revealed that the corrosion fatigue and marine fouling are the most troublesome problems for realizing T.L.P wire rope mooring. In addition, we could indicate the possibility of developing the wire ropes with high resistance against such attack.

### Acknowledgement

The author would like to express their thanks to Dr.Hideya Okada, Managing director of Nippon Steel Corporation, Mr.Motoya Fujii, General manager of Bar Shape & Wire Rod Technical Department of Nippon Steel Corp. and Mr.Yoshiaki Sakakibara, R & D Lab-1 of Nippon Steel Corp.

Table.1 Chemical composition of the steel wire ropes prepared for this study

| Wire ropes      | C(%) | Si(%) | Mn(%) | P(%)  | S(%)  | Al(%) | Co(%) | Cr(%) | Cu(%) | Mo(%) |
|-----------------|------|-------|-------|-------|-------|-------|-------|-------|-------|-------|
| Ordinary SWRS   | 0.75 | 0.25  | 0.80  | 0.016 | 0.014 | 0.004 | -     | -     | -     | -     |
| Ultra lowS SWRS | 0.77 | 0.18  | 0.78  | 0.013 | 0.002 | 0.03  | -     | -     | -     | -     |
| 2Cr-2Co-0.02Mo  | 0.83 | 0.27  | 0.29  | 0.017 | 0.011 | 0.02  | 2.0   | 2.0   | 0.22  | 0.02  |
| 2Cr-2Co-0.08Mo  | 0.86 | 0.29  | 0.26  | 0.017 | 0.011 | 0.03  | 2.0   | 2.0   | 0.22  | 0.08  |

Table.2 Mechanical Strength of Single Wire prepared by cold extrusion of the rods

| Specimens       | Wire Diameter (mm) | Tensile Strength (kg/mm <sup>2</sup> ) | Number of Torsion to Failure in 100D |
|-----------------|--------------------|--|--------------------------------------|
| Ordinary SWRS   | 3.06               | 165.0                                  | 39                                   |
| Ultra lowS SWRS | 3.06               | 163.0                                  | 37                                   |
| 2Cr-2Co-0.02Mo  | 3.06               | 188.5                                  | 33                                   |
| 2Cr-2Co-0.08Mo  | 3.06               | 189.0                                  | 28                                   |

Table.3 Mechanical Strength of Single Wire prepared by cold extusion of the rods produced by SCS process after hot rolling

| Specimens                       | Wire Diameter (mm) | Tensile Strength (kg/mm <sup>2</sup> ) | Number of Torsion to Failure in 100D | R.A (%)   |
|---------------------------------|--------------------|--|--------------------------------------|-----------|
| 2Cr-0.05Co-0.84C-0.23Cu-0.022Mo | 2.9                | 177                                    | 44.8                                 | 28.4-33.5 |
| 2Cr-0.2Co-0.84C-0.24Cu-0.029Mo  | 2.9                | 175-179                                | 44.0                                 | 32        |

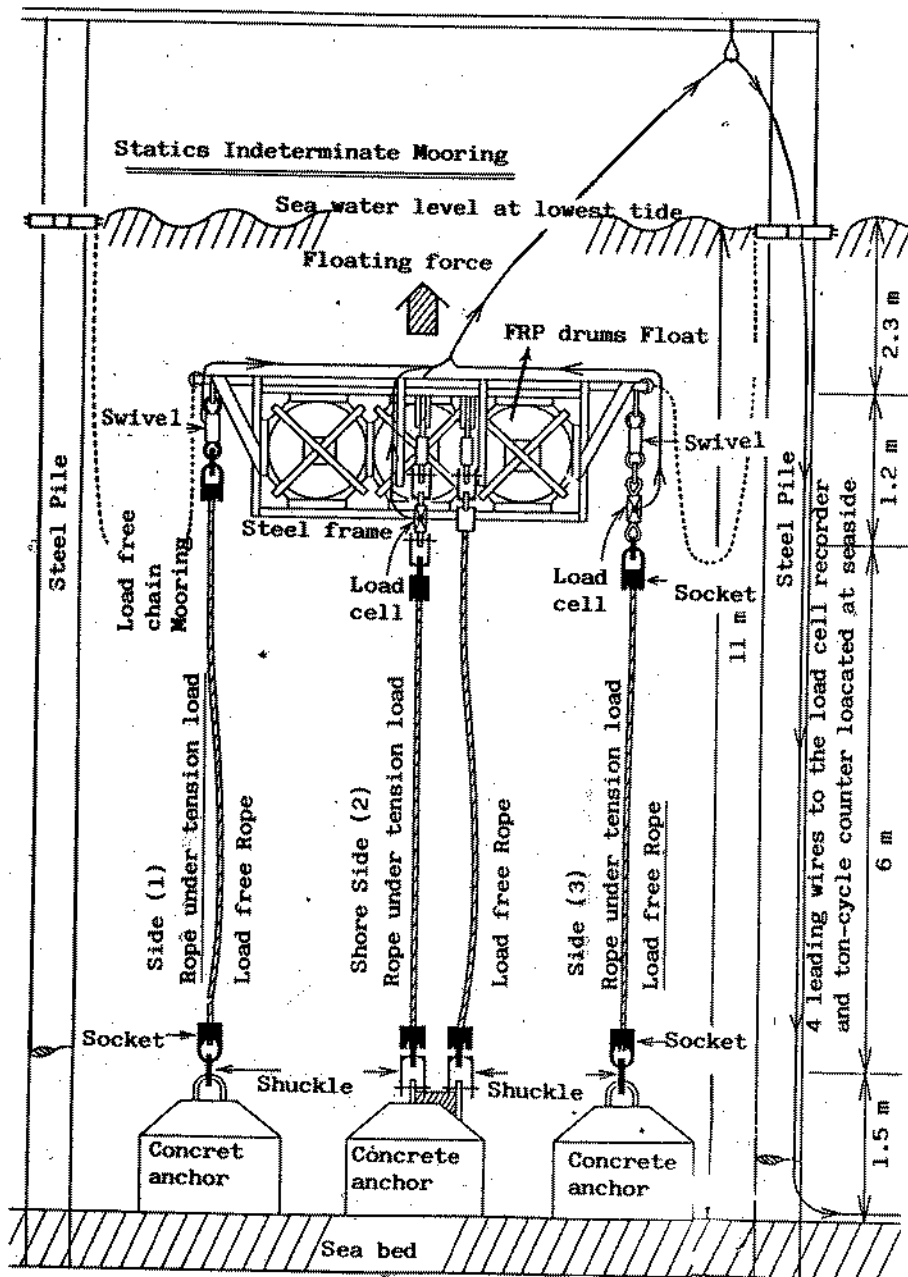
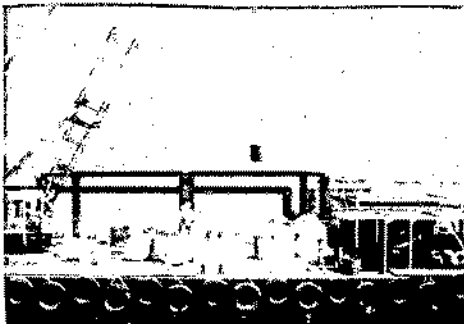
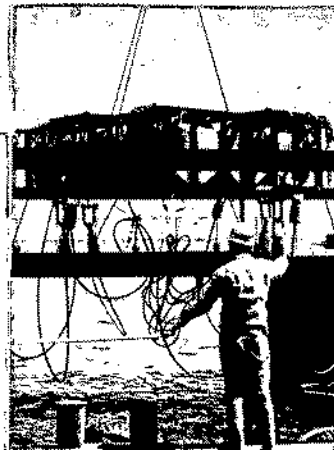


Fig.1 Side view of the exposure equipment simulated to T.L.P. mooring.



Launching of the anchor

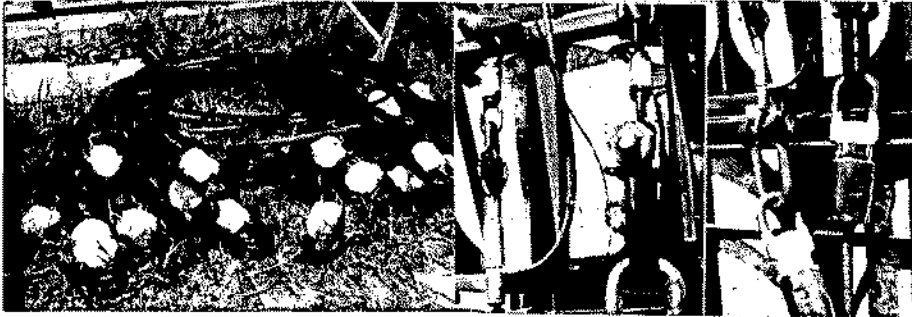


Launching of the float with load cells, sockets, wire ropes and other parts.

Fig.2a Launching of the anchors and the float connected to wire ropes with various parts



Fig.2b Setting work of the exposure equipment simulated to T.L.P mooring into the submerged sea water. The float is moored by 4 wire lines under tension load which are connected to the concrete anchor.



Sockets connecting the float  
and wire ropes

Swivels  
Load cell

Load cell  
Sockets

Fig.2c The view of the sockets connecting wire ropes,  
Swivels and load cells

Load cell



Sockets

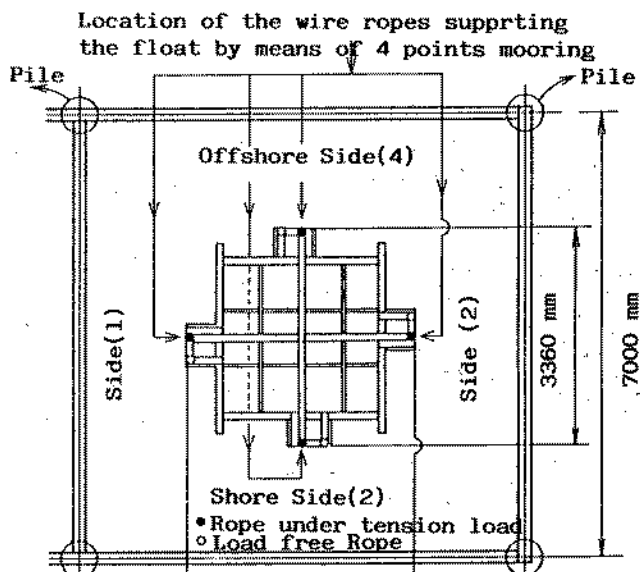


Wire rope under tension load

Wire ropes

Load free wire rope

Fig.2d The view of the sockets, load cell and wire ropes  
of this equipment in sea water observed after 7  
month elapsed.



Plane figure of the exposure equipment simulated to T.L.P Mooring

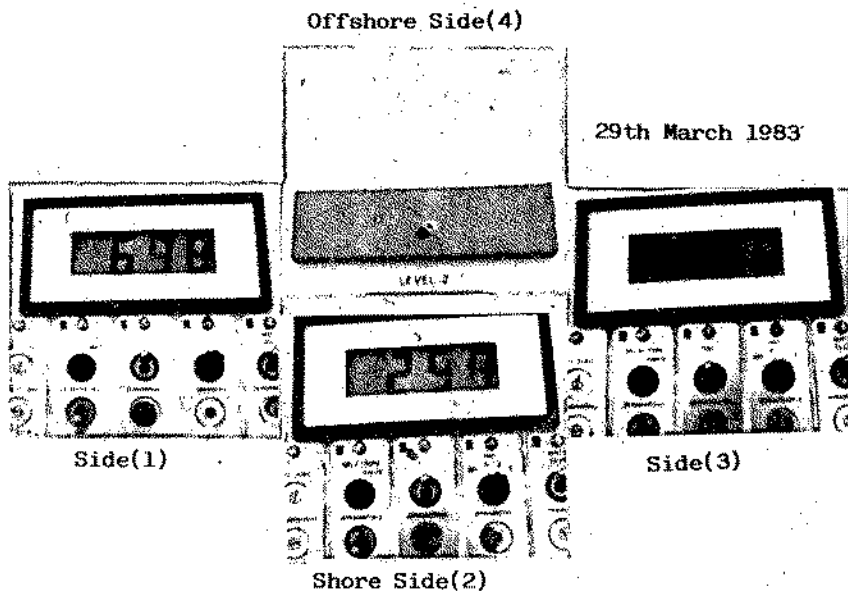
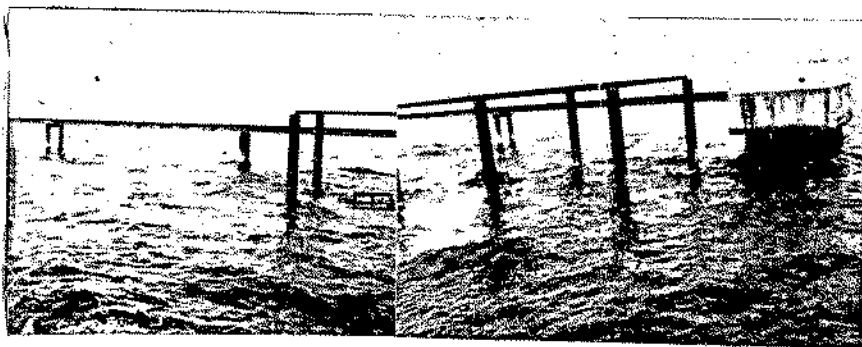


Fig.3 Tension load of each wire rope under 4 points mooring examined by means of load cell and ton-cycle counter.



From 3 to 4 p.m , 29th March 1983    Wind Speed ; 3.2 m - 5.2 m  
 Wind Direction ; N - NNE  
 Tide difference ; Approx. 1.5 m



From 10 to 12 a.m, 26th May 1983    Wind Speed ; 5.5 m - 7.7 m  
 Wind Direction ; NNE

Fig.4a Wave condition of the sea area installing the exposure  
 equipment simulated to T.L.P wire rope mooring.



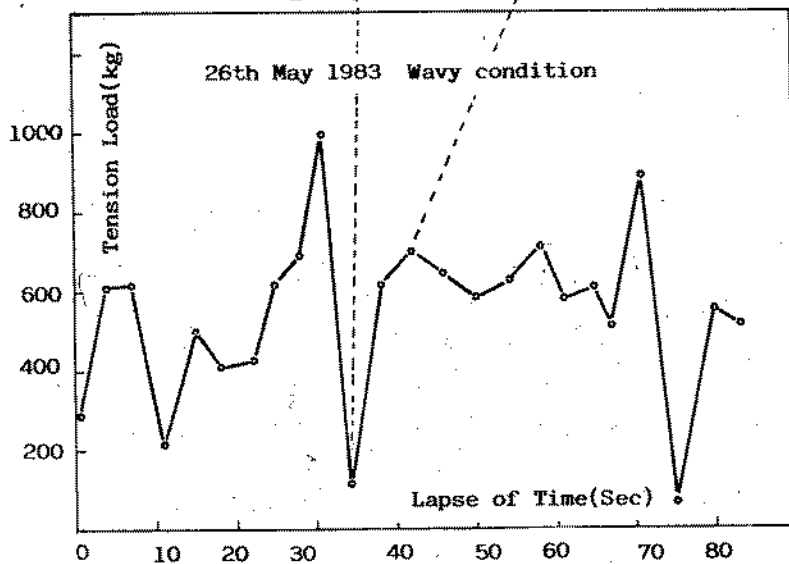
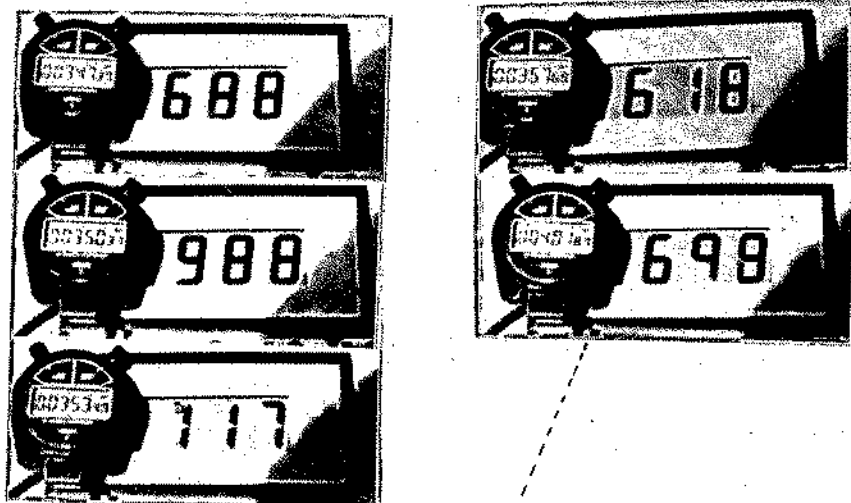
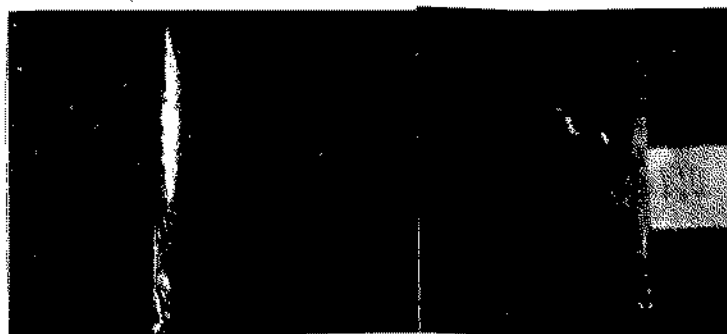


Fig.4b Variation of the Tension Load of the Steel Wire Rope located at the Shore Side(2) with Lapse of Time examined by means of Load Cell.



Fig.5 The deterioration of spiral wire rope checked by diver's inspection.



After 7 months

After 12 months

Fig.6 The deterioration procedure of the spiral wire ropes under tension loading in sea water.

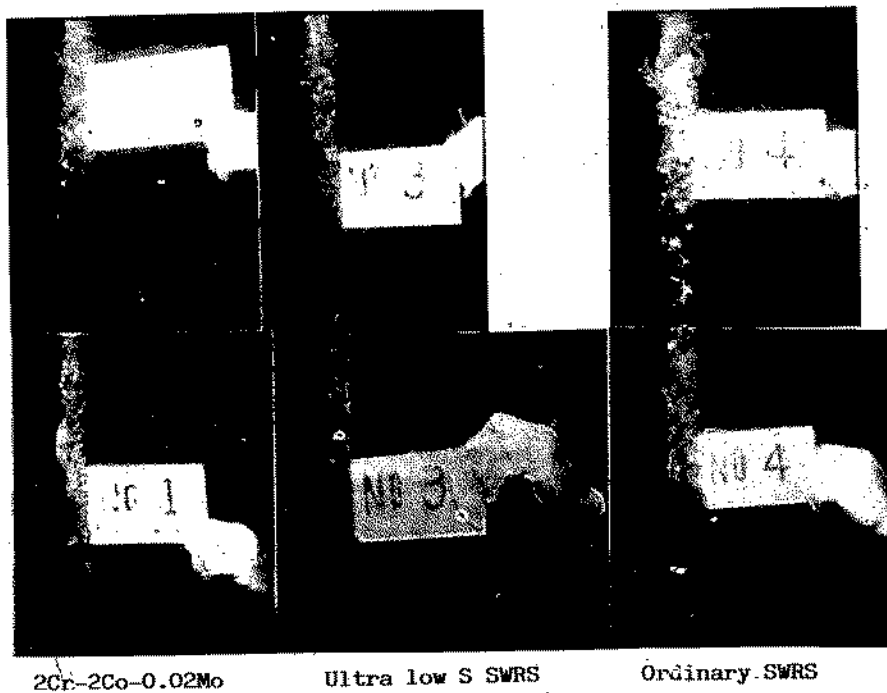


Fig.7 Marine fouling behaviour of various wire ropes immersed in sea water.

Reference

- (1) Graham R.Perrett, Robert M. Webb ; "TETHERED BUOYANT PRODUCTION SYSTEM", Proceedings of 1980 O.T.C (Houston, U.S.A) OTC No 3881 P261/274
- (2) Technical Advancement ; "BP's Tethered Buoyant Platform" Ocean Industry 15(1980)4 P156/157
- (3) Tobin R.McNatt ; "Deep Ocean Mooring Design Technology-Present Status and Future Development", Proceedings of 1982 O.T.C, OTC No 4177 P139/152
- (4) F.M.Reinhart ; "Corrosion of Metals and Alloys at varying Depths" Seawater Corrosion Handbook edited by M Schumacher P 135 (Published by NOYES DATA CORP.,U.S.A, 1979)
- (5) Kenneth T.Ronson ; "ROPES FOR DEEP WATER MOORING", Proceedings of 1980 O.T.C, OTC No 3850 P485/496
- (6) Leonard LeBlanc ; "ANALYZING PLATFORM PRICETAGS", Offshore 40(1980)3 P43/50

## Crevice Corrosion Testing of Stainless Alloys in Seawater

J.M. Krougman  
F.P. IJsseling

Corrosion Laboratory, Royal Netherlands Naval College,  
1781 AC Den Helder, The Netherlands

Crevice corrosion of several stainless steels and nickel alloys under an O-ring has been stimulated by anodic polarization in seawater. In order to favour crevice corrosion initiation the crevice area was provided with scratches.

The influence of alloy composition, particularly the role of molybdenum on the crevice corrosion temperature has been established. The results of these tests have been compared with polarization measurements in simulated crevice solutions and multiple crevice assembly tests in seawater.

Some limitations of the results obtained are highlighted.

La corrosion caverneuse de quelques aciers inoxydables et de quelques alliages de nickel sous une rondelle a été provoquée par la polarisation anodique en eau de mer. En appliquant des rayures dans la région de caverne, l'initiation de la corrosion caverneuse a été stimulée.

L'influence de la composition chimique, en particulier le rôle du molybdène, sur la température de la corrosion caverneuse a été déterminée.

Les résultats de ces essais ont été comparées avec les mesures de polarisation dans des solutions de caverne simulées et des essais d'assemblage de caverne multiple en eau de mer.

Quelques limitations des résultats obtenus sont signalés.

## 1. Introduction.

Successful application of stainless alloys in seawater depends on the absence of crevice corrosion. For this reason corrosion testing of stainless alloys especially concerns this type of localized attack.

A well known problem of crevice corrosion testing is the scatter in test results<sup>1</sup>. This results from the complicated nature of crevice corrosion. Many factors influence this type of attack such as: alloy composition, microstructure, surface condition, geometry, solution chemistry, potential, time. Of all these factors a major one is micro-crevice geometry as was indicated in mathematical modelling studies<sup>2</sup>. For this reason accidental differences in micro-crevice geometry can effect test results considerably.

On this basis two possibilities can be indicated to decrease data scatter. First to carry out testing as careful and reproducible as possible. Second to increase the number of specimens to be tested<sup>3</sup>. This possibility can also be understood as an increase of the number of micro-crevices to be applied on one specimen.

In crevice corrosion testing conditions of maximum severity are recommended<sup>3</sup>. Within given chemical, metallurgical and environmental conditions, crevice corrosion can be stimulated when:

- crevice gap and crevice depth (Fig. 1) to be applied have critical dimensions for crevice corrosion initiation;
- the potential to be applied has the highest value which stainless alloys can reach in seawater;
- the duration of the test is long enough for the crevice solution to reach the critical composition for crevice corrosion initiation.

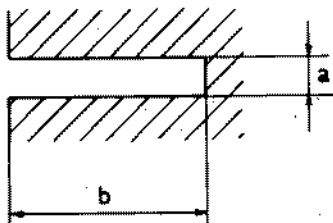


Fig. 1.  
Crevice geometry:  
a = gap and b = depth

The values of critical crevice gap and depth are between 0.1 and 1 micron<sup>4</sup>.

These values conform with the width and depth of grinding scratches. Thus situation of partly covered scratches may stimulate crevice corrosion initiation<sup>5-7</sup>. Moreover application of a great number of micro-crevices is to be preferred above one tiny crevice which is difficult to reproduce<sup>8</sup>. Using a greater number of micro-crevices the influence of accidental variations can be restricted. Moreover the probability of reaching critical conditions for crevice corrosion initiation will be increased, thus diminishing data scatter.

Using rubber for covering the scratches stimulation of crevice corrosion initiation will be optimized<sup>9</sup>.

Crevice corrosion is considered not to initiate at a specific externally applied potential<sup>10</sup>. However considering crevice corrosion to be a particular case of pitting<sup>5</sup> stimulation of crevice corrosion will require exposure at the highest potential stainless alloys can reach in seawater.

Initiation of crevice corrosion of stainless alloys is concerned among other things with local acidification and increase of the

chlorine ion concentration. The time to reach the critical composition for initiation of crevice corrosion may vary from a few seconds to hundreds of hours. This time is proportional to the crevice gap and inversely proportional to the corrosion current density<sup>11</sup>.

Temperature may also effect crevice corrosion initiation, in this respect the crevice corrosion temperature (CCT) has been defined as the temperature below which no localized corrosion will occur<sup>12</sup>.

On this basis it was decided to determine the susceptibility for initiation of various stainless alloys under crevice corrosion stimulating conditions in seawater at different temperatures. The results of these experiments were compared with the results from polarization measurements in simulated crevice solutions, which may indicate the relative resistance to crevice corrosion initiation<sup>13,14</sup>. Moreover the test results have been compared with those of multiple crevice assembly (MCA) exposure tests<sup>15</sup> in seawater.

## 2. Experimental.

### 2.1. Materials.

Two groups of iron and nickel base austenitic alloys with varying molybdenum content were selected for testing. Several commercial stainless steels with the highest available molybdenum contents were added to the program. The compositions of these materials are given in Table 1.

Commercially produced sheet was used in as delivered condition for testing. The thickness varied between 1 and 4 mm.

Table 1. Nominal Chemical Composition for Alloys Tested

| Alloy       | Element % wt |     |     |     |     |           |
|-------------|--------------|-----|-----|-----|-----|-----------|
|             | Cr           | Ni  | Mo  | Cu  | Fe  | Other     |
| AISI 316 L  | 18           | 10  | 2.5 |     | Bal |           |
| 1713 NCN    | 17           | 13  | 4.5 |     | Bal | 0.15 N    |
| A 963       | 17           | 16  | 6   | 1.6 | Bal | 0.15 N    |
| 254 SMO     | 20           | 18  | 6   | 0.7 | Bal | 0.20 N    |
| AL 6X       | 20           | 24  | 6   |     | Bal |           |
| 1925 hMo    | 21           | 25  | 6   | 1.7 | Bal | 0.14 N    |
| INCOLOY 825 | 22           | Bal | 3   | 2.2 | 30  | 1 Ti      |
| HASTELLOY G | 22           | Bal | 6   | 1.8 | 20  | 2 Cb + Ta |
| INCONEL 625 | 22           | Bal | 9   |     | 2.5 | 3 Cb + Ta |

### 2.2. Potentiostatic Exposure tests.

These tests have been carried out with a limited number of specimens each provided with a large number of micro-crevices. From every alloy at least five panel specimens (20 x 20 mm) have been made.

Before testing the specimen was abraded on one side with silicon carbide emery paper (HERMES FLEX 18) up to grit 800 and polished with diamond paste 3  $\mu$ m. Next the specimen was scratched with emery paper

grit 800 to introduce micro-crevices. In four strokes, each stroke with fresh emery paper, the specimen obtained a standard pattern of about 1,500 scratches. The scratching assembly (Fig. 2) consisted of: 1. load of 3 kg; 2. saddle of PVC; 3. emery paper (adjusted under saddle with double sided adhering tape); 4. specimen; 5. specimen holder of PVC (longitudinal section). The direction of scratching was to the right.

After scratching the specimen was rinsed in ethanol, dried in a stream of air and weighed. Next the specimen was inserted in a specimenholder (Fig. 3) which was made of PVC. By means of a plug (4), M 35 x 1, the specimen (3) was pressed against a rubber O-ring (1), BUTA N R118, internal diameter 14.0 mm and thickness 2.6 mm. The plug was fitted with a torque level of 0.9 Nm. Next the contact wire (2) was pressed against the specimen. In this way only the surface of the specimen inside the O-ring could come in contact with seawater.

Before testing the O-rings were cleaned by boiling in distilled water. Every test was carried out with a new O-ring.

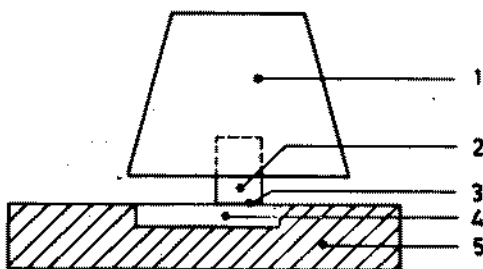


Fig. 2.  
Principle of scratching  
assembly

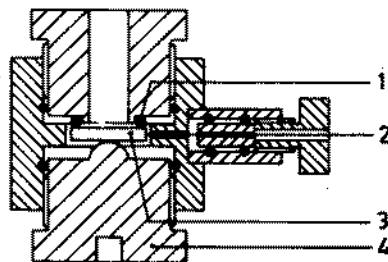


Fig. 3.  
Longitudinal section of  
specimen holder

The holder with the specimen was immersed in a basin with filtered (up to 40  $\mu\text{m}$  particle size) slowly moving, continuously refreshed seawater obtained from the harbour of Den Helder. During the test period the salinity varied between 22.6 and 29.5‰ and the pH between 7.60 and 7.99. The temperature of the seawater was thermostatically maintained at the desired value + 0.5°C. A schematic representation of the test set up is shown in Fig. 4. It consisted of: 1. graphite electrode connected to earth (to suppress interferences); 2. heating element; 3. contact thermometer; 4. platinum electrode, Winkler type (AE); 5. specimen holder (WE); 6. reference electrode (RE). The arrows indicate seawater entry and exit. The reference electrode was a saturated calomel electrode (SCE).

After adjusting the specimen holder in the basin the free corrosion potential was measured against the saturated calomel electrode. After two minutes the specimen was polarized at 500 mV SCE potentiostatically (Wenking MP 75). This potential was chosen because it was about the highest value stainless alloys have reached in seawater<sup>16,17</sup>. The current flowing between specimen and platinum electrode was recorded (Kipp BD 5) via a resistance of 10 ohm as a function of time.



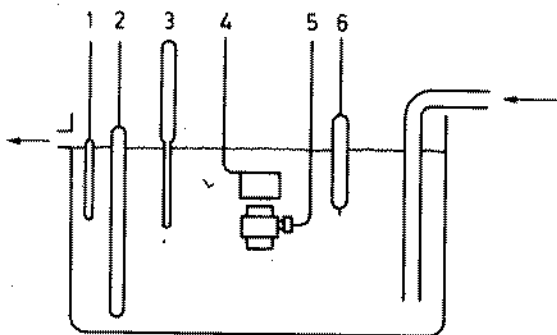


Fig. 4.  
Schematic diagram of test cell

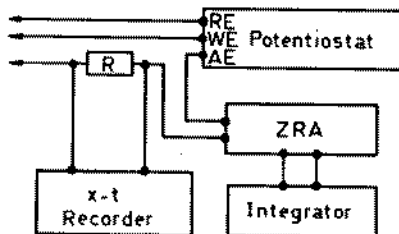


Fig. 5.  
Circuit diagram

Moreover via a zero resistance ammeter (ZRA) the current was integrated to determine the charge transfer or total charge.

The circuit diagram is shown in Fig. 5.

The time up to a sudden increase of the current was regarded as the initiation time. After three hours the test was stopped. The specimen was removed from the holder, rinsed in ethanol and dried, the corrosion products having been dissolved in a 20% v/v solution of nitric acid. Next the specimen was weighed. Finally the maximum penetration depth was determined with a calibrated microscope, magnification 100 x.

At each temperature of 10°, 25°, 40°, 55° and 70°C five tests were carried out. However, the tests were continued in general up to

the crevice corrosion temperature plus 15°C.

One specimen of each alloy tested was used to determine the hardness ( $HV_{30}$ ) and the surface roughness (CLA) in the scratched areas. It appeared that the hardness varied between 160 and 250 and the roughness between 0.10 and 0.40  $\mu\text{m}$ . Although considerable differences exist in hardness no significant differences in surface roughness were observed.

### 2.3. Polarization Measurements.

The electrode consisted of a piece (17 x 17 mm) of the material to be tested on which a rod of brass (length 140 mm and diameter 8 mm) was brazed. These parts were mounted in epoxy resin (EPOFIX). At the top of the rod about 10 cm was left uncoated.

The test cell (Fig. 6) consisted of: 1. electrode; 2. sliding contacts of graphite; 3. pulley drive; 4. shaft with bearings; 5. coupling to electrode; 6. tube for nitrogen bubbling; 7. reference electrode with capillary; 8. auxiliary electrode of platinum; 9. double walled perspex cell with inlet and outlet (see arrows) for thermostated water; electrical connections to working-, auxiliary and reference electrode WE, AE and RE respectively.

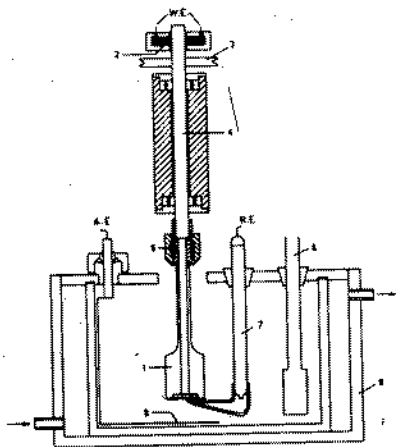


Fig. 6.  
Cell for polarization  
measurements

From a reservoir thermostated water at  $25 \pm 0.5^\circ\text{C}$  was pumped through the double wall.

The basis of the simulated crevice solutions was artificially prepared seawater (according to ASTM standard D-1141-52). The pH of this seawater was about 8.0. The solutions with an extra amount of sodium chloride were prepared prior to the acidification with hydrochloric acid. The amount of sodium chloride depended on the desired final pH. An addition of 146 gram sodium chloride per liter seawater ( $\approx 2.5 \text{ M}$ ) corresponded with pH 2. An addition of 263 gram ( $\approx 4.5 \text{ M}$ ) corresponded with pH 1<sup>14</sup>.

By injecting nitrogen bubbles ( $2 \text{ dm}^3 \text{ min}^{-1}$ ) these solutions were freed from oxygen. The introduction of nitrogen started 30 min prior to immersion and continued

during the measurement. After deaerating the oxygen level was less than 750 ppb.

Several minutes before polarization the working electrode was abraded with grit 220, cleaned with ethanol and dried in a stream of air. An unshielded area of  $1 \text{ cm}^2$  was created, sticking electroplaters tape on the metal surface. Next the electrode was adjusted in the cell.

An electric motor rotated the working electrode at about 1,500 rpm. Electric contact to the working electrode was made using sliding contacts (graphite).

Polarization started 200 mV less noble than the free corrosion potential. The potentiostat (Wenking LT-78), controlled by the Wenking SMP-69-scanner, altered the potential in the noble direction. The scanning rate was 10 steps of  $2 \text{ mV min}^{-1}$ . The current between working and auxiliary electrode was led through a resistance box. A x-t recorder (Kipp BD 8) registered the potential difference over the adjusted resistance. Polarization ceased after reaching a current of 500  $\mu\text{A}$ . All measurements have been carried out at least in duplicate. Every measurement was performed in a fresh solution.

#### 2.4. Multiple Crevice Assembly Exposure Tests.

These tests were carried out with panel specimens (150 x 100 mm). Two surface conditions were applied namely mill finish, and abraded with grade 220 silicon carbide paper. The crevice nuts were fitted with a torque level of 0.7 Nm. In order to be able to carry out electrochemical measurements a connection wire was brazed at an edge of the panel specimens. To avoid galvanic effects from the contact wire the specimens were painted. The specimens in mill finish condition were painted at one side and abraded with grit 800 on the other sides.

The specimens in abraded condition were painted on all edges. The single tests have been performed in seawater at 25°C. More details concerning these exposure tests have been reported elsewhere<sup>17</sup>. After exposure the penetration depths and areas of attack were determined microscopically. From the mean penetration and area of attack the extend of attack was calculated.

### 3. Results and Discussion.

#### 3.1. Potentiostatic Exposure Tests.

##### 3.1.1. Initiation of Crevice Corrosion.

All specimens which initiated localized attack suffered from crevice corrosion under the O-ring preferentially in the scratched areas. Thus it was confirmed that partly covered scratches are effective micro-crevices.

The lowest temperature at which the materials initiated crevice corrosion or the crevice corrosion temperature (CCT) can be derived from Table 2. It appears that with increasing the molybdenum content, the CCT also increases.

Table 2. Number of Specimens Which Initiated Crevice Corrosion in Potentiostatic Exposure Tests

| Material    | 10°C | 25°C | 40°C | 55°C | 70°C |
|-------------|------|------|------|------|------|
| AISI 316 L  | 5    | 5    |      |      |      |
| 1713 NCN    | 0    | 5    |      |      |      |
| A 963       | 0    | 4(1) | 5    |      |      |
| AL 6X       | 0    | 5(1) | 5    |      |      |
| 1925 hMo    | 0    | 0    | 1(2) | 5    |      |
| 254 SMO     | 0    | 0    | 0    | 1    | 2    |
| INCOLOY 825 | 4    | 5    |      |      |      |
| HASTELLOY G | 1(1) | 5(2) |      |      |      |
| INCONEL 625 | 0    | 0    | 0    | 3    | 3    |

(1) Unstable crevice corrosion.

(2) Tendency towards repassivation (3 specimens of HASTELLOY G).

Although A 963, AL 6X, 1925 hMo and 254 SMO contain about the same amount of molybdenum different values of CCT were observed. The alloys A 963 and AL 6X showed the same results. Most resistant alloys are 254 SMO and INCONEL 625 which remained free from crevice corrosion up to 40°C.

The number of material and temperature combinations which initiated crevice corrosion was 17. From 13 of these combinations at least 3 specimens initiated. From 9 combinations 5 specimens initiated. These figures indicate the reproducibility of initiation to be convincing.

After initiation of crevice corrosion three types of propagation could be distinguished: stable propagation, stable propagation with tendency towards repassivation and unstable propagation. The last two

types of propagation preceded stable crevice corrosion at the next higher temperature.

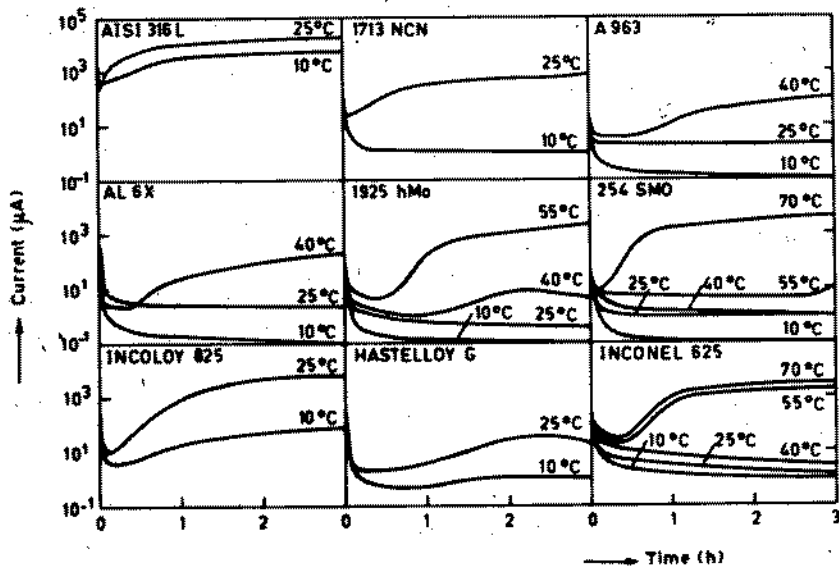


Fig. 7.  
Schematic representation of current as a function of time at 500 mV SCE

From Table 2 and Fig. 7 it can be learnt that stable crevice attack is characterized by an uninterrupted increase of the current. Repassivation is accompanied by a decrease of current. The current-time curve of unstable crevice attack shows an increase of the current which is less than  $1 \mu\text{A}$  while the shape of the curve is the same as in the case of no initiation. For these reasons the initiation time of unstable crevice corrosion could not be determined accurately.

The initiation times at various temperatures are given in Fig. 8. It appears that the initiation times vary between a few seconds and three hours, increasing with the molybdenum content. An increase of temperature tends to decrease the initiation times and to increase the scatter in the initiation times.

From the alloys in the present study CCT values have also been determined by other authors under other conditions. Garner<sup>18</sup> and Nikhil et al.<sup>19</sup> used a 10% ferric chloride solution with redox potential 600 mV SCE, 120 grit specimen finish and rubber and TEFLON crevice devices respectively. Manning<sup>20</sup> used a 4% sodium chloride + 0.01 M hydrochloric acid + 0.1% ferric sulphate solution (oxydizing sodium chloride - hydrochloric acid) with redox potential 630 mV SCE, mill finish and TEFLON multiple crevice assembly).

The results of these studies can be compared with the present tests because the potential range in which the alloys have been tested is about the same.

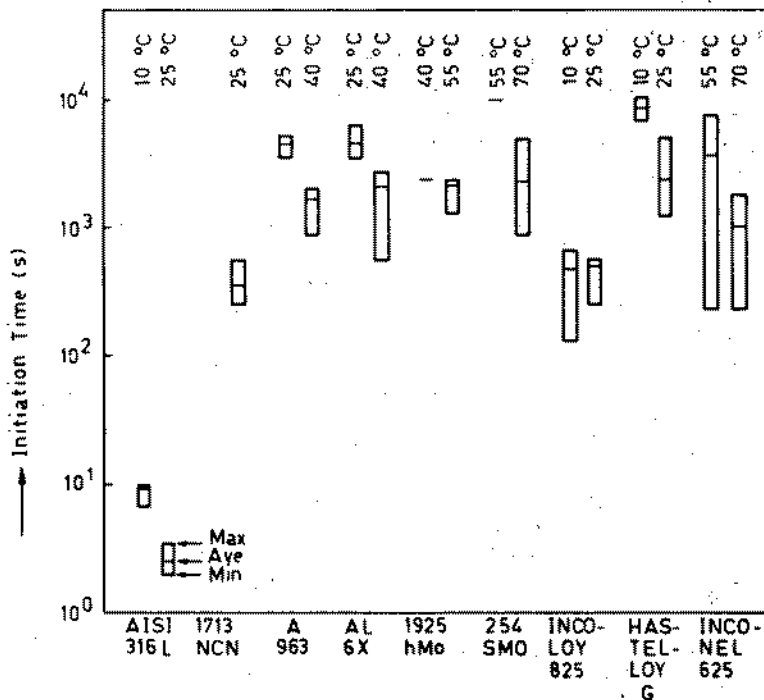


Fig. 8.  
Initiation times of crevice corrosion at 500 mV SCE

Table 3. Initiation of Crevice Corrosion in Ferric Chloride Tests, Oxydizing Sodium Chloride - Hydrochloric Acid Tests and Potentiostatic Tests in Natural Seawater

| Material    | Ferric Chloride<br>Garner | Ferric Chloride<br>Nikhil et al. | Oxydizing Sodium Chloride<br>Hydrochloric Acid | Natural Seawater |
|-------------|---------------------------|----------------------------------|--|------------------|
| AISI 316 L  | -5 - 0°C                  |                                  |  | < 10°C           |
| 1713 NCN    | 10 - 15°C                 |                                  |  | 11 - 25°C        |
| A 963       |                           |                                  |  | 11 - 25°C        |
| AL 6X       | 30 - 35°C                 | 37°C                             | 25°C   | 11 - 25°C        |
| 1925 hMo    | 35 - 40°C                 |                                  |  | 26 - 40°C        |
| 254 SMO     | 40 - 45°C                 | 46°C                             | 30°C   | 41 - 55°C        |
| INCOLOY 825 | -10 - 0°C                 |                                  | < -5°C   | < 10°C           |
| HASTELLOY G | 15 - 20°C                 |                                  | 25°C   | < 10°C           |
| INCONEL 625 | 45 - 50°C                 |                                  |  | 41 - 55°C        |

From Table 3 it appears that the present results fit best with the tests of Garner. In cases of disagreement, AL 6X and HASTELLOY G, the values of CCT in ferric chloride are higher than in seawater but then unstable crevice corrosion was involved.

The same holds for the results of Manning. However the CCT of 254 SMO he found is significantly lower than found in the present and other studies. Nikhil et al. found a significantly higher CCT for AL 6X than in the present study.

The difference between the results cannot be explained with certainty. It is possible that minor attack at temperatures below reported CCT values has been overlooked or regarded as insignificant. Moreover differences in surface finish and crevice device may have influenced the results. However the lower CCT of 254 SMO found by Manning can probably be attributed to the surface condition. In his tests mill finish was used whereas in this and other studies the mill finish was removed by grinding.

In addition the results of the present study may indicate the test method applied to be more sensitive than the others, possibly achieved with the large number of micro-crevices.

### 3.1.2. Propagation of Crevice Corrosion.

The maximum penetration depths, mass losses and total charges are given in Fig. 9.

It appears that propagation as indicated by these measures decreases with molybdenum content. Although the decrease may be partly attributed to longer initiation times (Fig. 8), lower currents after initiation are believed to be the main factor as indicated by comparing AISI 316 L, 1713 NCM and A 963 at 25°C and INCOLOY 825 and HASTELLOY G at 25°C in Fig. 7.

Resemblances and differences in propagation can be observed between the alloys with about 6% molybdenum (Fig. 7 and 9). The propagation of A 963 and AL 6X is almost the same. At 40°C the propagation of 1925 hMo is lower than the propagation of A 963 and AL 6X. At 55°C the propagation of 254 SMO is lower than the propagation of 1925 hMo.

Although 254 SMO and INCONEL 625 behaved almost the same with respect to initiation of crevice corrosion the minimum level of the total charge for INCONEL 625 is significant higher than for 254 SMO. This means that the current at 500 mV SCE is higher for INCONEL 625 than for 254 SMO. A confirmation of this behaviour is found in Fig. 7.

The scatter in penetration depths covers one order of magnitude. The scatter in mass losses and total charges cover two or three orders of magnitude. The difference can be explained by assuming mass loss and total charge to be proportional to the extent of the attack. Penetration depth is related to the extent of the attack, however, not necessarily according to a linear function.

The scatter in the propagation data may be attributed to the relatively short exposure time.

From the plot of the mass loss against the total charge it appears that there is a linear relation between mass loss and total charge (Fig. 10).

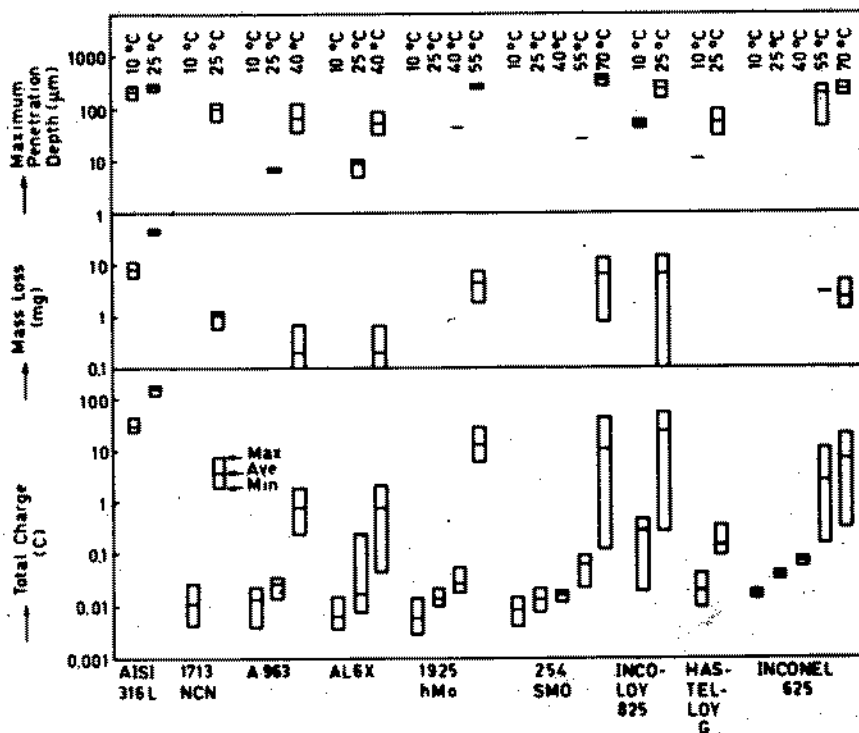


Fig. 9. Maximum penetration depths of crevice corrosion, mass losses and total charges at 500 mV SCE

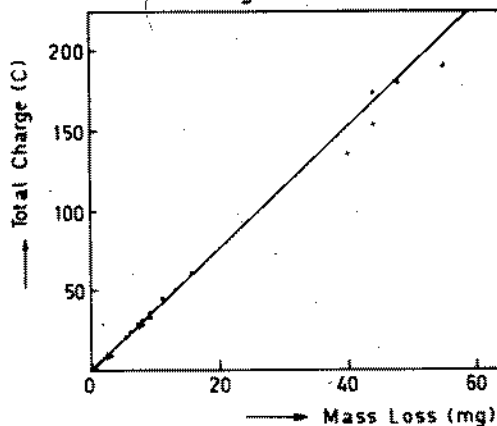


Fig. 10. Comparison of mass loss and total charge in potentiostatic tests at 500 mV SCE

From Fig. 9, it follows that the total charge is a more distinct and sensitive measure for the extent of attack than the mass loss, especially when minor penetrations are involved. When mass loss cannot be determined quantitative data of the extent of attack can be estimated from total charge.

When the alloys remained free from crevice corrosion the total charge varied between 0.004 and 0.030 C for the stainless steels and between 0.010 and 0.090 C for the nickel alloys.

From Fig. 9 it can be derived that initiation of crevice corrosion was not observed below a total charge of 0.008 C. Below 0.018 C stable crevice corrosion did not occur and the maximum penetration depth was 10  $\mu\text{m}$  or less.

In Fig. 11 a survey of the attacked specimens is given. It appears that AISI 316 L also initiated pitting on the unshielded surface. The maximum penetration depth varied between 10 and 420  $\mu\text{m}$ . No other alloy showed macroscopically visible pitting in the unshielded surface.

The influence of temperature on propagation can be derived from Fig. 7, 9 and 11.

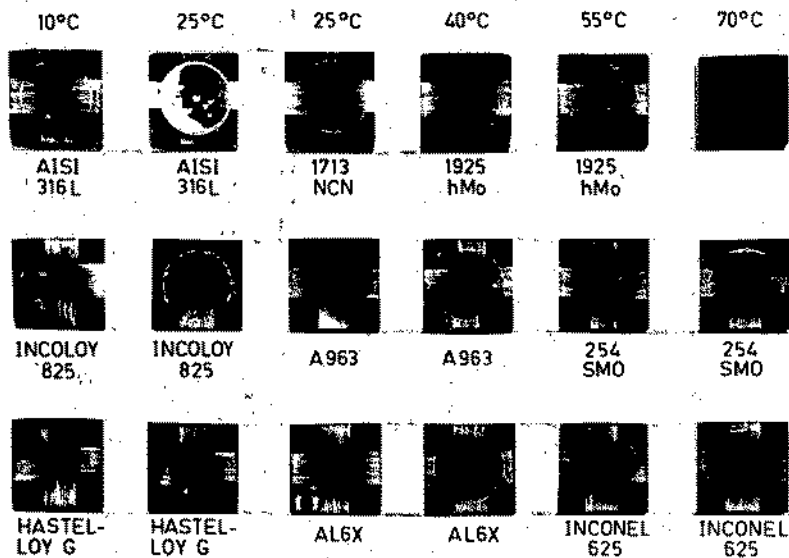


Fig. 11.

Representative examples of attacked specimens from the potentiostatic tests at 500 mV SCE

It appears that propagation of crevice corrosion increases with temperature. However, the maximum penetration depth seems to be less sensitive to temperature variation as shown by comparing the results for AISI 316 L at 10 and 25°C and INCONEL 625 at 55 and 70°C in Fig. 9 and 11.

Comparison of the propagation data with similar data from the studies mentioned under initiation was not possible because the relevant data were not reported.

Redmerski et al.<sup>21</sup> performed crevice corrosion tests in solutions with pH 2, 1,00-10,000 ppm chloride, temperature 60-100°C, using a multiple crevice assembly of ROULON and test duration of 4 months. In these tests the maximum penetration depths which were observed for 254 SMO and INCONEL 625 were 250 and 120  $\mu\text{m}$  respectively. These values were of the same order of magnitude and comparative ratio with the results in the present study which were 400 and 235  $\mu\text{m}$  respectively.



### 3.2. Polarization Measurements.

In the anodic polarization curve of stainless alloys in simulated crevice solutions the critical current density for passivation (CCD) and the breakdown potential (BP) represent characteristic points. In general a high value of CCD and a low value of BP indicate susceptibility for localized attack.

In Fig. 12 the highest values of CCD and the lowest value of BP have been plotted. As a criterion for the breakdown potential a sudden increase of the current or reaching a current density of  $5 \mu\text{A}\cdot\text{cm}^{-2}$  was chosen. In general polarization measurements have been carried out up to the crevice corrosion temperature plus  $15^\circ\text{C}$ .

From Fig. 12 it appears that on increasing the molybdenum content CCD decreases and BP increases. The lower chromium and nickel contents of A 963 as compared with the other steels which contain about 6% molybdenum result in higher values of CCD and lower values of BP in acidified solutions with increased chlorine content.

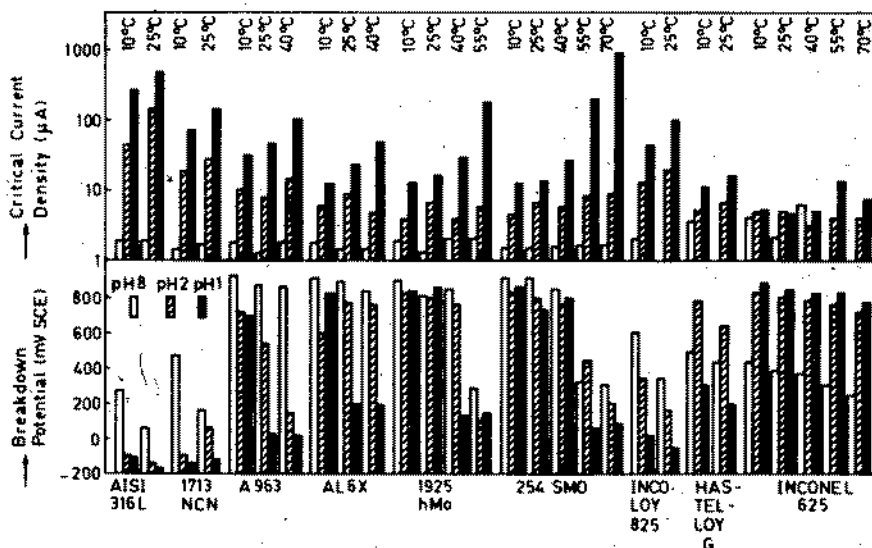


Fig. 12. Results of polarization measurements in simulated crevice solutions

From Fig. 12 it also appears that decreasing the pH and increasing the chlorine ion concentration result in an enlargement of CCD for all alloys. However, the intensity of this effect differs for each alloy. Moreover on increasing the temperature CCD increases.

The effect of decreasing the pH and increasing the chlorine ion concentration on BP is more complicated. In fact five conditions can be distinguished:

1.  $\text{BP} < 500 \text{ mV SCE}$ ;
2.  $\text{BP} (\text{pH } 8) < 500 \text{ mV SCE}$  and  $\text{BP} (\text{pH } 1) < 500 \text{ mV SCE}$ ;
3.  $\text{BP} (\text{pH } 1) < 500 \text{ mV SCE}$ ;

4. BP (pH 8)  $\leq$  500 mV SCE, BP (pH 1)  $>$  BP (pH 2) and BP (pH 2)  $>$  500 mV SCE;  
 5. BP  $>$  500 mV SCE.

Considering crevice corrosion to be a special kind of pitting the conditions 1-3 can be regarded as denoting a tendency for crevice corrosion initiation with reference to exposure in seawater at 500 mV SCE. Condition 4 indicates at pH 8 a tendency for initiation. However, in the acidified solutions this tendency disappears. An alloy with condition 4 will be in the transpassive region when it is polarized just beyond BP in seawater (pH 8). Then general attack at a low rate will take place. Condition 5 represents no tendency for crevice corrosion initiation.

Table 4 summarizes the conditions for the alloys tested. For all alloys but INCONEL 625 the role of temperature is obvious.

Table 4. Conditions (1) of Breakdown Potential in Simulated Crevice Solutions

| Material    | 10 <sup>0</sup> C | 25 <sup>0</sup> C | 40 <sup>0</sup> C | 55 <sup>0</sup> C | 70 <sup>0</sup> C |
|-------------|-------------------|-------------------|-------------------|-------------------|-------------------|
| AISI 316 L  | 1                 | 1                 |                   |                   |                   |
| 1713 NCN    | 1                 | 1                 |                   |                   |                   |
| A 963       | 5                 | 3                 | 3                 |                   |                   |
| AL 6X       | 5                 | 3                 | 3                 |                   |                   |
| 1925 hMo    | 5                 | 5                 | 3                 | 1                 |                   |
| 254 SMO     | 5                 | 5                 | 5                 | 1                 | 1                 |
| INCOLOY 825 | 3                 | 1                 |                   |                   |                   |
| HASTELLOY G | 3                 | 2                 |                   |                   |                   |
| INCONEL 625 | 4                 | 4                 | 4                 | 4                 | 4                 |

(1) Conditions 1-5 correspond with conditions 1-5 mentioned previously.

### 3.3. Multiple Crevice Assembly Exposure Tests.

The MCA tests were part of a different program. Therefore only limited comparison with the potentiostatic tests is possible. Except for one alloy, only one specimen per condition was exposed to natural seawater of 25<sup>0</sup>C. Nevertheless, in our opinion the results of these tests are interesting enough to report here.

In Table 5 results of the MCA tests have been summarized.

#### 3.3.1. Initiation of Crevice Corrosion.

From Table 5 it appears that attack under the crevice nut initiated for AISI 316 L at -150 mV SCE and 140 mV SCE. The other alloys initiated between 100 and 250 mV SCE under the crevice nut. These alloys initiated under the paint between 210 and 460 mV SCE. When stainless alloys remain free from localized attack the corrosion potential increases with increasing exposure time in seawater. Thus initiation

under the paint refers to longer initiation times than under the crevice nut. The maximum corrosion potential varied between 50 and 475 mV SCE.

Table 5. Results of MCA Exposure Tests

| Material    | Surface Finish | Corrosion Potential at Initiation (mV SCE) | Maximum Corrosion Potential (mV SCE) | Initiation Time (d) | Propagation Time (d) | Exposure Time (d) | Maximum Penetration (mm.d <sup>-1</sup> ) | Extent of Propagation (mm <sup>2</sup> .d <sup>-1</sup> ) | Place of Localized Attack |
|-------------|----------------|--|--------------------------------------|---------------------|----------------------|-------------------|---|---|---------------------------|
| AISI 316 L  | mill           | -150                                       | 50                                   | < 1                 | 28                   | 28                | 0.02                                      | 0.11  | under crevice nut         |
| AISI 316 L  | grit 220       | 140  | 140                                  | 3                   | 58                   | 61                | 0.01                                      | 0.05  | under crevice nut         |
|             |                | 75   |                                      | 5                   | 56                   |                   | 0.02                                      | 0.66  | under paint               |
| 1713 NCR    | mill           | 110  | 210                                  | 3                   | 73                   | 78                | 0.01                                      | 0.03  | under crevice nut         |
|             |                | 210  |                                      | 6                   | 72                   |                   | 0.01                                      | 0.69  | under paint               |
| 1713 NCR    | grit 220       | 210  | 460                                  | 3                   | 3                    | 111               | 0.03                                      | 0.13  | under crevice nut         |
|             |                | 460  |                                      | 88                  | 23                   |                   | 0.01                                      | 0.26  | under paint               |
| A 963       | grit 220       |  | 475                                  |                     |                      | 336               |   |   | none                      |
| AL 6X       | mill (1)       | 215  | 325                                  | 5                   | 2                    | 131               | 0.03                                      | 0.10  | under crevice nut         |
|             |                | 325  |                                      | 30                  | 101                  |                   | < 0.01                                    | 0.58  | under paint               |
| AL 6X       | grit 220       |  | 470                                  |                     |                      | 713               |   |   | none                      |
| 254 SMO     | mill           | 250  | 425                                  | 8                   | 5                    | 72                | 0.02                                      | 0.04  | under crevice nut         |
| INCOLOY 825 | mill           | 125  | 155                                  | 1                   | 14                   | 15                | 0.03                                      | 0.36  | under crevice nut         |
| HASTELLOY G | mill           | 215  | 380                                  | 3                   | 13                   | 28                | 0.01                                      | 0.08  | under crevice nut         |
| INCONEL 625 | mill           |  | 600                                  |                     |                      | 336               |   |   | none                      |

(1) Immersed in 10% w/v nitric acid prior to exposure.

The initiation times indicate that increasing the molybdenum content increases the initiation time. The alloys which remained free from localized attack are A 963 and AL 6X with grit 220 finish and INCONEL 625 with mill finish.

The influence of surface finish on initiation is not clear. However, mill finish tends to lower initiation times than found for grit 220 finish.

In MCA tests in seawater at 30°C Kain<sup>22</sup> observed for AL 6X and 254 SMO with mill finish and Hack<sup>8</sup> for AL 6X, 254 SMO, INCOLOY 825 and HASTELLOY G with grit 120 finish initiation times varying between 3 and 16 d and 1 and 28 d respectively. Our results are within the range of these initiation times. In the work of Kain and Hack INCONEL 625 remained free from localized attack thus confirming our result with this alloy.

### 3.3.2. Propagation of Crevice Corrosion.

The propagation rate of crevice corrosion has been expressed in two ways. Firstly the maximum penetration per unit of propagation time. Secondly the extent of propagation per unit of propagation time.

It appears that the maximum penetration covers one order of magnitude and seems to be independent from the molybdenum content. The extent of propagation covers three orders of magnitude and tends to decrease with increasing molybdenum content.

From all alloys which initiated 254 SMO showed the least attack due to a tendency for repassivation.

The extent of propagation under the paint is larger than under the crevice nut because the layer of paint can form crevices with larger width and depth than the crevice nut.

The maximum penetration of AL 6X and 254 SMO as calculated from the results of Kain were almost the same as reported here. The maximum penetration from the results of Hack for AL 6X and 254 SMO are comparable with our results. However the maximum penetrations for INCOLOY 825 and HASTELLOY G are higher than we found. An explanation for this difference may be that precise propagation times were not available.

#### 3.4. Relation Between Potentiostatic Exposure Tests, Polarization Measurements and Multiple Crevice Assembly Exposure Tests.

Generally speaking, the temperature at which the breakdown potential in one or more simulated crevice solutions was 500 mV SCE or lower corresponds with the crevice corrosion temperature in the potentiostatic tests. This agreement confirms that crevice corrosion initiation may also be a special kind of pitting. However two disagreements can be noted. First 1713 NCN did not initiate at 10°C although the breakdown potentials were lower than 500 mV SCE. Additional potentiostatic testing revealed initiation at 12°C. Second at all temperatures the breakdown potential of INCONEL 625 was lower than 500 mV SCE. However up to 40°C this alloy remained free from crevice attack.

In the potentiostatic tests, the polarization measurements and the MCA tests at 25°C AISI 316 L, 1713 NCN, AL 6X, INCOLOY 825 and HASTELLOY G are indicated to be susceptible to crevice corrosion initiation.

Although not initiated in the MCA test A 963 is also susceptible for crevice corrosion initiation according to the other tests. The opposite was found for 254 SMO. This alloy initiated in the MCA tests but indicated resistance to initiation in the other tests at 25°C. However in the MCA test the specimen was in the mill finish condition whereas in the other tests the mill finish was removed. According to the MCA tests of Kain and Hack, however, with 254 SMO crevice corrosion initiated at 30°C in mill finish as well as with grit 120 finish condition. Possibly the conditions in the MCA tests may be more severe than in the potentiostatic tests and vice versa. Moreover exposure of an alloy at 500 mV SCE may result in anodic protection of the crevice when the breakdown potential of the alloy in the crevice solution remains above 500 mV SCE.

In the potentiostatic tests INCONEL 625 initiated crevice corrosion at 55 and 70°C. From all polarization measurements in ASTM seawater (pH 8) it appeared that at 500 mV SCE the alloy was in the area of transpassive corrosion. However in the polarization measurements as well as in the potentiostatic tests the current was higher at 55 and 70°C than at the lower temperatures.

From the maximum corrosion potential in seawater at 25°C and the lowest breakdown potential in ASTM seawater at 25°C for HASTELLOY G and INCONEL 625, both about 400 mV SCE, it follows that 500 mV SCE is too high for the nickel alloys in potentiostatic testing. These results indicate that potentiostatic testing of nickel alloys for seawater use at 25°C has to be carried out up to or below 400 mV SCE,

in other words near the breakdown potential.

At temperatures higher than 25°C it is to be expected that the maximum corrosion potential will be lower than 500 mV SCE for stainless steels and lower than 400 mV SCE for nickel alloys. Additional potentiostatic testing at 400 mV SCE still provoked initiation of crevice corrosion for INCOLOY 825 and HASTELLOY G at 25°C. Testing at 70°C revealed freedom of crevice corrosion for 254 SMO at 300 mV SCE and for INCONEL 625 at 200 mV SCE. However crevice corrosion initiated at 400 mV SCE for 254 SMO and at 300 mV SCE for INCONEL 625.

These results indicate that the maximum corrosion potential stainless alloys can reach at temperatures higher than 25°C have to be determined separately. Thus potentiostatic testing of stainless alloys for seawater use needs to be carried out at different potentials.

Although based on different principles the propagation in the potentiostatic tests and the MCA tests can be compared in a qualitative manner.

From the maximum penetration depth in the potentiostatic tests it appears that on increasing the molybdenum content the penetration decreases. In the MCA tests this influence of molybdenum is not evident. However, the mass loss and total charge of the potentiostatic tests agree better with the extent of propagation for the MCA tests. From this a beneficial effect of molybdenum on propagation of crevice corrosion can be concluded.

The results of all tests point out that molybdenum has a beneficial effect on initiation as well as propagation of crevice corrosion. INCONEL 625 was the most resistant material to crevice corrosion initiation while of the stainless steels 254 SMO performed best.

### 3.5. Limitations of Results Obtained.

The potentiostatic test with micro-creviced specimens is a sensitive and rapid test method which produces acceptably reproducible results. It presents an unambiguous criterion for crevice corrosion susceptibility namely the crevice corrosion temperature. Moreover useful additional data can be obtained such as propagation behaviour and tendency towards repassivation. However, it must be emphasized that the results of this test hold just for the specific test conditions. Therefore application of the results must be carried out with caution.

The data from potentiostatic testing can usefully be applied for ranking purposes. When a material appears to behave inadequately in service it can be replaced by an alloy which gives a better performance in the potentiostatic test.

In the potentiostatic tests scratching of the specimens improved reproducibility of initiation. This means of introducing micro-crevices may improve the reproducibility of other crevice corrosion tests.

The results of the potentiostatic tests and the MCA tests showed some disagreements. Thus highlighting the need to apply different test methods to clarify the behaviour of materials. In this respect polarization measurements in simulated crevice solutions turned out to be useful.

The alloys tested differ in molybdenum content as well as in the content of other elements. However in this study the influence of other elements has been ignored.

Two more general remarks about the applicability of the results of crevice corrosion testing are: first within one specification the corrosion resistance of material from different manufacturers may vary considerably; second the way of producing or the product form of an alloy may notably influence its susceptibility to crevice corrosion. Both limitations will be illustrated.

The first example concerns bar from different manufacturers (A and B) with the same nominal composition as 1713 NCN. The susceptibility for crevice corrosion has been determined by means of polarization measurements in simulated crevice solutions.

Table 6. Lowest Value of Breakdown Potentials (mV SCE) in Simulated Crevice Solutions at 25°C

| Material | ASTM sea-water | ASTM seawater + 2.5 M NaCl + HCl, pH2 | ASTM seawater + 4.5 M NaCl + HCl, pH1 |
|----------|----------------|---------------------------------------|---------------------------------------|
| A        | 370            | 60                                    | -80                                   |
| B        | 225            | -160                                  | -225                                  |

From the lower breakdown potentials of material B (Table 6) it appeared that B was more susceptible to localized attack than A. The cause of this behaviour was the presence of a considerable amount of chi phase (rounded and outlined) and manganese sulphides (dark and elongated) in the austenitic structure of B (Fig. 13).

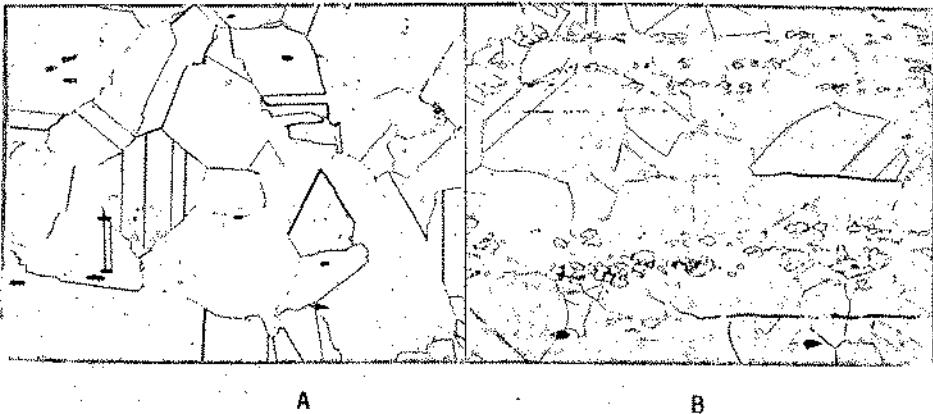


Fig. 13. Microstructure of materials A en B, etchant aqua regia; magnification 200 x

The second example deals with an alloy which nominally contains: chromium 23%, nickel 17%, molybdenum 3.2%, manganese 5.5% and balance of iron.

In the NCA test sheet of this alloy remained free from localized attack in seawater at 25°C during two years. In potentiostatic exposure tests at 200 mV SCE in seawater at 25°C sheet provided with micro-crevices initiated minor pitting. However, bar suffered from severe crevice attack and minor pitting (Table 7).

Table 7. Results of Potentiostatic Exposure Tests in Seawater at 25°C

| Product Form | Exposure Time (h) | Maximum Penetration Depth (µm) | Mass Loss (mg) | Total Charge (C) | Type of Localized Attack   |
|--------------|-------------------|--------------------------------|----------------|------------------|----------------------------|
| Sheet        | 3                 | < 5                            | < 0.1          | 0.04             | Pitting                    |
|              | 3                 | < 5                            | < 0.1          | 0.05             | Pitting                    |
| Bar          | 1.3               | 45                             | 0.8            | 2.69             | Crevice attack and pitting |
|              | 1.3               | 40                             | 0.9            | 2.95             | Crevice attack and pitting |

From polarization measurements in simulated crevice solutions it appeared that for bar the critical current densities were higher and the breakdown potentials were less noble than for sheet (Table 8).

Table 8. Lowest Value of Breakdown Potentials (mV SCE) in Simulated Crevice Solutions at 25°C

| Product Form | ASTM Seawater | ASTM Seawater + 2.5 M NaCl + HCl, pH2 | ASTM Seawater + 4.5 M NaCl + HCl, pH1 |
|--------------|---------------|---------------------------------------|---------------------------------------|
| Sheet        | 890           | 790                                   | 840                                   |
| Bar          | 45            | -70                                   | -140                                  |

These measurements confirm the susceptibility for crevice corrosion of bar.

An explanation for the different behaviour might be found in the microstructure. Sheet had a recrystallized austenitic structure and bar a work hardened one (Fig. 14). The mean hardness of sheet was 253 HV<sub>30</sub> and for bar 350 HV<sub>30</sub>. Schwenk confirmed that work hardening of stainless alloys may increase the susceptibility for localized attack<sup>23</sup>. Another explanation might be the difference in chromium content. Bar contained 3.2% chromium less than sheet.

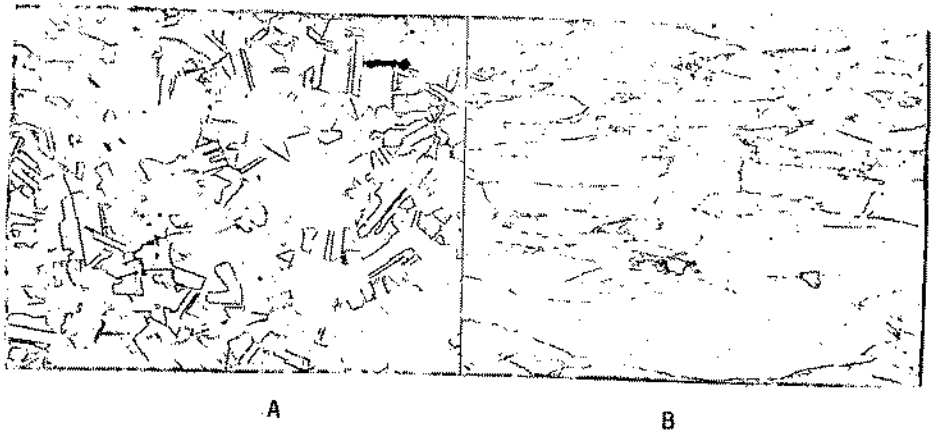


Fig. 14.  
Microstructure of sheet (A) and bar (B); etchant aqua regia;  
magnification 300 x

These examples point out that materials have to be tested in the same condition as to be applied in practical use, including: chemical composition, product form, heat treatment and microstructure. Moreover the examples indicate that statements - such as: "If an alloy contains at least so much of certain elements one need not bother about the corrosion resistance" - must be rejected.

#### 4. Conclusions.

1. Application of micro-crevices in potentiostatic exposure tests efficiently provoked reproducible crevice corrosion.
2. This test method delivers an unambiguous criterion for crevice corrosion susceptibility in seawater namely the crevice corrosion temperature. On this basis ranking of materials can be established.
3. Generally speaking, the results of the potentiostatic tests agreed with the results of the polarization measurements in simulated crevice solutions. The results of the MCA tests supported the results of the potentiostatic tests to some extent. However in both cases disagreements were observed.
4. The results of the potentiostatic tests hold just for the specific test conditions including the metallurgical state of the alloys. In materials selection based on the results of these types of tests one must be aware of this fact.
5. Increasing the molybdenum content in stainless alloys increases the crevice corrosion temperature. In this study 254 SMO and INCONEL 625 performed best. Up to 40°C these alloys remained free from crevice attack at 500 mV SCE in seawater.
6. In this study CCT values have been determined in steps of 15°C, however for ranking purposes the test can be made more sensitive by decreasing the temperature steps.



### Acknowledgement.

The authors are grateful to Messrs De Vrij and Raatsie, co-workers at the corrosion laboratory, who have performed the experiments.

### 5. References.

1. Sydberger, T., Werkstoffe u. Korros., 1981, 32, 119.
2. Kain, R.M., NACE Corros. Conf. Houston, 1982, paper no. 66.
3. Streicher, M.A., NACE Corros. Conf. Houston, 1983, paper no. 70.
4. Oldfield, J.W. and Sutton, W.H., Br. Corros. J., 1978, 13, 13.
5. Szlarska-Smialowska, Z., and Mankowski, J., Corr. Sci., 1978, 18, 953.
6. Mapa, L.B., Richardson, J.A. and Wood, G.C., Proc. EUROCOR, London, 1977, 247.
7. Janik-Czachor, M., Wood, G.C. and Thompson, G.E., Br. Corros. J., 1980, 15, 154.
8. Hack, H.P., NACE Corros. Conf. Houston, 1983, paper no. 65.
9. Brigham, R.J., Corrosion, 1981, 37, 608.
10. Uhlig, H.H., Mat. Perf., 1983, 22, 35.
11. Crolet, J.L. and Defranoux, J.M., Corros. Sci., 1973, 13, 575.
12. Brigham, R.J., Corrosion, 1974, 30, 396.
13. Defranoux, J.M. and Tricot, R., Mem. Scient. Rev. Met., 1972, 69, 317.
14. Oldfield, J.W. and Sutton, W.H., Br. Corros. J., 1978, 13, 104.
15. Anderson, D.B., ASTM Spec. Techn. Publ., 576, 1974, 231.
16. Mollica, A. and Trevis, A., Proc. 4th Internat. Congr. on Marine Corros. and Fouling, Juan-les-Pins, 1976, 351.
17. Krougman, J.M. en IJsseling, E.P., Proc. 5th Internat. Congr. on Marine Corros. and Fouling, Barcelona, 1980, 214.
18. Garner, A., NACE Corros. Conf. Houston, 1982, paper no. 195.
19. Nagaswami, N.S. and Streicher, M.A., NACE Corros. Conf. Houston, 1983, paper no. 71.
20. Manning, P.E., NACE Corros. Conf. Houston, 1982, paper no. 176.
21. Redmerski, L.S., Eckenrod, J.J. and Kovach, C.W., Mat. Perf., 1983, 22, 31.
22. Kain, R.M., OTEC Report ANL/OTEC-BCM-022, 1981.
23. Schwenk, W., Korrosion, Verlag Chemie Weinheim, 1960, 13, 20.



## COMPOSITION AND MORPHOLOGY OF CALCAREOUS DEPOSITS

## WITHIN SIMULATED FATIGUE CRACKS IN SEA WATER

William H. Hartt  
Florida Atlantic University  
Department of Ocean Engineering  
Boca Raton, Florida 33431 USA

## ABSTRACT

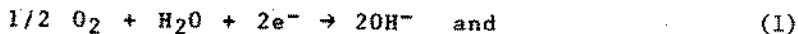
Under certain exposure conditions calcareous deposits may form within fatigue cracks and thereby contribute to crack closure and to reduced crack growth rate or arrestment. On this basis experiments have been performed where cathodically polarized, 1018 steel specimens with a simulated crack have been cycled in sea water. Analysis of the boldly exposed and crack surfaces by SEM and EDAX permitted examination and characterization of the chemistry and morphology of calcareous deposits. The predominant cation in the film was calcium, and magnesium was detected only at isolated locations within the crack at the most negative potential (-1.100 v., SCE). Morphology of the occluded cell deposit was observed to vary with potential and position, whereas this morphology was relatively invariant for the external surface. Significance of these results are discussed with regard to fatigue and crack closure.

## SOMMAIRE

Dans certaines conditions d'expositions, des dépôts calcaires peuvent se former à l'intérieur de fissures d'usure, contribuant à obstruer les fissures et à en réduire le taux de croissance. A partir de cette hypothèse, des expériences furent effectuées sur des spécimens pré-fissurés d'acier 1018 polarisés à la cathode, agités périodiquement en eau de mer. L'analyse au SEM et au EDAX des surfaces fissurées, a permis d'examiner et de caractériser la chimie et la morphologie des dépôts calcaires. Le cation prédominant des dépôts fut du Calcium, tandis que l'on a découvert du Magnésium seulement à des sites isolés dans la fissure, là où les potentiels étaient les plus négatifs (-1.100v., SCE). Il fut observé que la morphologie des dépôts cellulaires situés à l'intérieur variait selon les potentiels et selon leur positions tandis que celle des cellules de surface demeurait relativement stable. La portée de ces résultats fut discutée en regard de la "fatigue" et de l'oblitération des fissures..

## INTRODUCTION

Cathodic Protection and Calcareous Deposits. Corrosion control technology has evolved during the past several decades to the point that the submerged portion of numerous types of marine structures is typically instrumented with a cathodic protection system (1). A unique facet of sea water as an electrolyte is occurrence upon cathodic surfaces of calcareous deposits. These films have been projected to have a beneficial influence upon the effectiveness and efficiency of marine cathodic protection, since they serve as a diffusion barrier to dissolved oxygen and thereby enhance cathodic polarization (2-5). Calcareous deposits occur as a consequence of a cathodic current and the resultant increase in pH of electrolyte adjacent to the metal surface in accordance with either or both of the reactions



and the fact that solubility limit for most inorganics decreases with increasing pH (2-5, 6). Deposit chemistry may be complex and variable depending upon the conditions of formation, but the material is comprised primarily of  $CaCO_3$  and  $Mg(OH)_2$  (2,5,6). Influential variables have been projected to include, but not necessarily be limited to, cathodic current density (2,7), temperature (8), pressure (9), water chemistry (10-12), velocity (7) and nature of the substrate (2,10). A recent review has discussed these factors in detail (13).

Fatigue. Fatigue of steel in sea water has been judged to be a failure mode that may be critical to the integrity and reliability of numerous types of ocean structures, including ships, offshore structures and riser systems (14-16). This is a consequence of wind, wave, current, duty and earthquake loadings, in addition to the possibility of dynamic amplification in the case of deep water structures. Because such structures are often cathodically protected, it is important that any influences of relatively negative polarization upon fatigue be understood (17). In this regard it has been observed that fatigue crack growth rate is either unchanged or slightly reduced for modest amounts of cathodic polarization ( $\phi \sim -0.80v.$ , SCE) but is enhanced progressively with further decrease in potential (18-20). This has been attributed to dissolution of atomic hydrogen into the metal in conjunction with Equation 2 and interaction of this species with dislocations at the crack tip vicinity.

Fatigue and Calcareous Deposits. Hudgins, et al (21) were apparently the first to consider that calcareous deposits might have a beneficial effect upon fatigue of steel in synthetic sea water, although no directly applicable experimental data was obtained to substantiate this. Using compact tension specimens fatigued in sea water, Scott (22) observed for load control tests with positive R, that the maximum crack opening per cycle remained relatively invariant with time, whereas the minimum value progressively increased. He attributed this to calcareous deposit formation within the crack and influence of this matter upon crack closure. The fact that lowering of fatigue crack growth rate typically accompanied this was explained in terms of a reduced effective stress intensity range. Similarly, Royer (23) has observed either a reduction or arrestment of crack propagation in compact tension specimens in sea water in response to potentiostatic control at an increasingly negative potential.

Hooper and Hartt (24,25) considered that calcareous deposits which formed within cracks of notched 1018 specimens fatigued in natural sea water were responsible for "endurance limit enhancement," where for a range of cathodic potentials the fatigue limit was approximately two times greater than in air. This behavior also was attributed to formation of calcareous deposits within cracks and to a corresponding reduction in the effective stress intensity range. Such a process is analogous to that associated with corrosion product accumulation (26,27) and oxide induced crack closure (28-30). It may be reasoned, based upon the above information, that corrosion fatigue cracking of structural steel in sea water or synthetic sea water under conditions of cathodic polarization should not be a problem. However, such reduction or elimination of fatigue crack propagation has not been observed universally, as pointed out above (18-20). Apparently, whether a particular fatigue crack propagates rapidly or not at all is determined by the competing influences of hydrogen and calcareous deposits.

Crack Electrolyte Chemistry. It is generally recognized that chemistry of the electrolyte within local cells can become modified relative to the bulk solution. This results because both convective and diffusional interchange between the two (bulk and occluded cell electrolytes) is restricted due to geometric factors. Corrosion rate within crevices, pits, intergranular paths, filiforms, tuberculations, exfoliations and cracks has been rationalized in terms of localized pH modification (31). For the case of exposure in a near-neutral chloride solution under freely corroding or anodically polarized conditions pH of the occluded cell electrolyte for most metals becomes acidic. Local pH has been shown to increase progressively, however, with increasing cathodic current density and at sufficiently high values to exceed that of the bulk solution (32,33). The potential dependence of

static stress crack growth rate has been interpreted in terms of these local chemistry changes (34).

With regard to corrosion fatigue, it may be argued that the alternate opening and closing of the crack faces may result in a pumping action which should preclude crack electrolyte modification. On the other hand, if one considers the static tension case as simply one extreme of the frequency spectrum, then it may be reasoned that modification should occur for corrosion fatigue also, provided frequency is not excessive. Whether or not the electrolyte within a corrosion fatigue crack becomes distinct in comparison to the bulk is important, since development of calcareous deposits and crack propagation rate should depend upon solution chemistry in this region.

Several observations in the literature, in addition to those reported earlier for the specific case of cathodically polarized steel in sea water, support the projection that electrolyte chemistry modification can occur within corrosion fatigue cracks. For example, Barsom (35) measured pH of such electrolyte to be about three for a 12Ni-5Co-3Mo steel cycled at 0.1 Hz in a near-neutral 3% NaCl - distilled water solution. Similarly, Meyn (36) reported a pH of less than three for the crack electrolyte of Ti-8Al-1Mo-1V specimens fatigued at both 0.5 and 30 Hz. In addition the observation (25) that under certain conditions of fatigue of steel in sea water calcareous deposits form more profusely within the crack than on the bulk surface suggests that pH within the crack can become more alkaline than for the bulk electrolyte adjacent to the freely exposed surface.

Mass Transport within Environmental Fatigue Cracks. In sea water pH is controlled by the carbon dioxide system, as expressed by the reactions



If  $\text{OH}^-$  is added to the system as a consequence, for example, of either Reactions (1) or (2), then



is expected also. This, in turn, promotes calcareous deposit formation, as represented by the reaction



On this basis, it may be reasoned that thermodynamics of the precipitation process are influenced by concentration of  $\text{Ca}^{++}$ ,  $\text{Mg}^{++}$  (not included above),  $\text{OH}^-$  and inorganic carbon. One may envision a complicated interfacing of the above reactions in the vicinity of the metal surface with ionic concentrations being determined by  $\text{OH}^-$  production rate (cathodic current density) and mass transfer rate for the above species. Solving this problem is difficult even for relatively simple geometries such as a flat (37) or tubular members (38). Added complications arise as well when one considers kinetics of the precipitation process. Further, in the case of a fatigue crack, one must also contend with 1) an unknown current and potential distribution as a function of distance into the crack, 2) concentration gradients of critical species in both the crack opening and depth directions, 3) unknown, time dependent hydrodynamics, 4) surface roughness and 5) tortuous path.

Mass transport processes may include both diffusional and convective mixing. While mixing within static stress environmental cracks is expected to occur by diffusion, convective mixing should also be important for applications involving cyclic stresses. For the latter situation (environmental fatigue) it may be reasoned that there are two determinants in rationalizing the concentration and distribution of various species. The first pertains to transport within the crack itself in response to the cyclic electrolyte ejection-ingestion process and the second to the extent of mixing (convective and diffusional) between the crack and the bulk solution as the former exits and reenters the occluded cell on each cycle. With regard to the former it may be reasoned that both convective and diffusional mixing could be important if the flow is laminar, since ion migration is expected to be the predominant transfer mechanism normal to flow lines (perpendicular to the crack walls). However, movements by convection are expected to dominate parallel to streamlines (along the length of the crack). In situations where the ejection-ingestion flow is turbulent, mass transfer by convective mixing is expected to totally dominate that by diffusion in both directions (normal and parallel to the crack faces). No studies have been undertaken to define those conditions for which crack electrolyte flow is turbulent and where it is laminar.

The purpose of the present paper is to present the results of experiments which have addressed the structure and composition of calcareous deposits which formed in sea water within a simulated fatigue crack in a structural steel specimen cathodically polarized in sea water. By so doing it was intended that the properties of calcareous deposits within cracks and how deposits contribute to crack closure effects might be better understood.

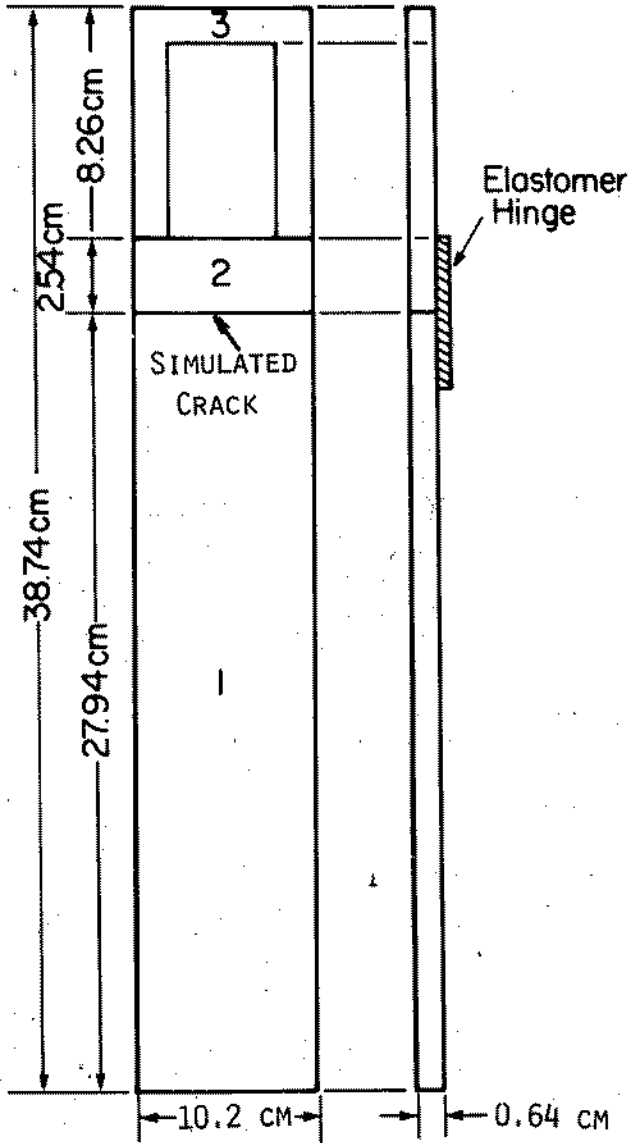


Figure 1: Geometry of simulated fatigue crack specimen.



## EXPERIMENTAL PROCEDURE

The experiment plan was based upon a simulated fatigue crack specimen, as illustrated in Figure 1. This was comprised of three components with the simulated crack being formed by the mating faces of Parts (1) and (2) via an elastomeric hinge (39). The specimens were machined from 6.4 mm thick cold finished 1018 steel plate. The simulated crack faces and the front specimen faces 25.4 mm above and below the crack were surface ground. All surfaces were acetone degreased and with the exception of the ground faces the specimen was coated with aerosol Quelspray. Thus, only the crack and a limited portion of the front surface were bare.

Cyclic opening and closing of the crack was realized by connecting the specimen base to a rigid vise and the top to the drive arm of a modified Fatigue Dynamics Model VSP-150 machine. A calibrated vernier drive on the base, in conjunction with the fatigue machine stroke adjustment, permitted crack opening and closing values to be accurately adjusted. These were set at 0.25 and 0.05 mm, respectively. Frequency of the cyclic process was 0.5 or 1.0 Hz.

Figure 2 illustrates the specimen in perspective to the electrolyte bath and related instrumentation. The bath was of an all plexiglas construction with nylon fittings and was such that electrolyte entered near the base and flowed upward past the specimen at a nominal velocity of 1.6mm/sec. Natural sea water, as is available at the Center for Marine Materials Laboratory, served as the electrolyte (40). A saturated calomel electrode for potential control was positioned in the overflow compartment, while a Pt coated Nb counter electrode was mounted on the bath wall immediately opposite the uncoated specimen face. Potentiostatic control was affected using a Wenking Model 68 FRO.5 potentiostat. Subsequent to testing, calcareous deposits on the crack and boldly exposed faces were examined by scanning electron microscopy, and in some cases the chemistry of these was characterized by EDAX analysis.

## RESULTS AND DISCUSSION

Figures 3 and 4 present multi-SEM micrographs of the simulated crack surface of specimens polarized to  $-0.900\text{v}$ . (SCE) for 168 hours. Near the center of each composite is a low magnification micrograph to which the higher magnification views are referenced and with the crack mouth and tip identified. For comparison, Figure 5 presents a micrograph of deposits which occurred on the boldly exposed surface of the specimen in Figure 3. Two points are apparent from these microstructures: first, deposit morphology within the crack typically differed from that on the external

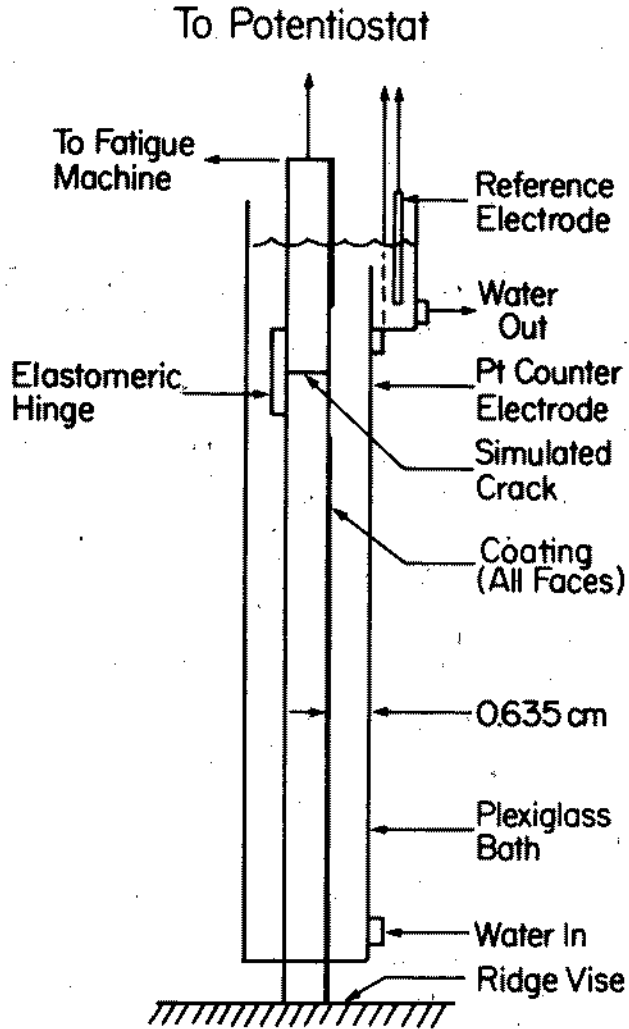


Figure 2: Schematic specimen and sea water bath.

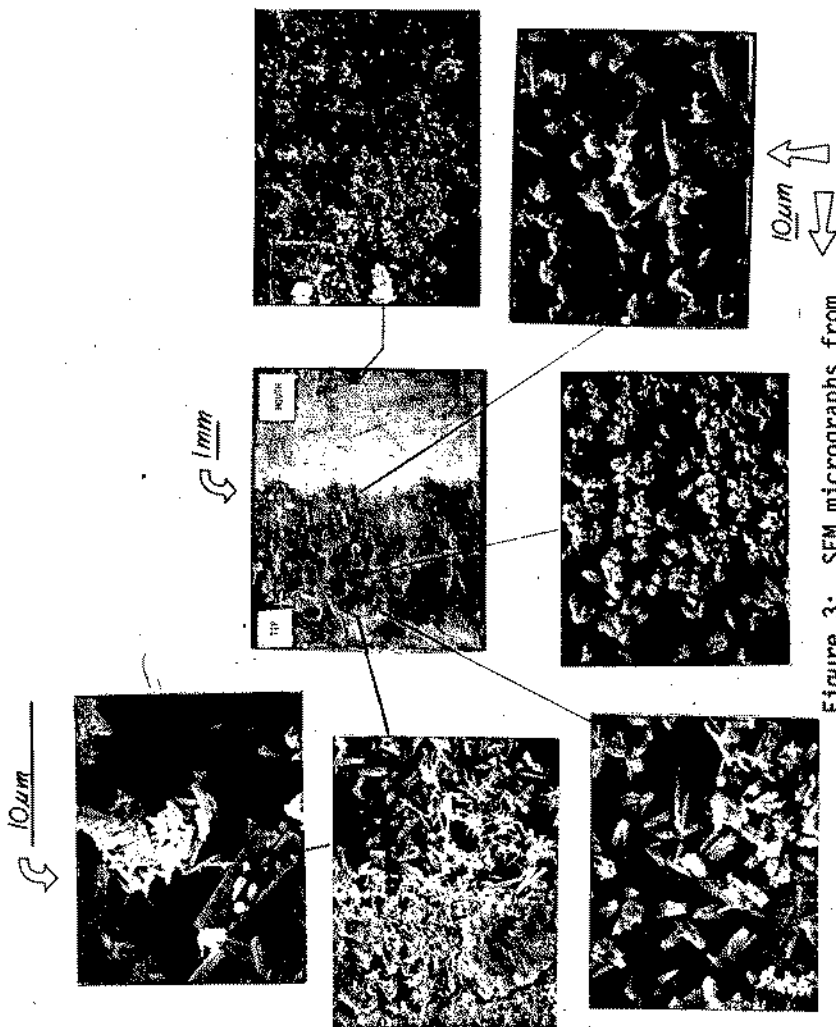


Figure 3: SEM micrographs from different regions within crack for  $-0.900v$ ,  $0.5$  Hz.

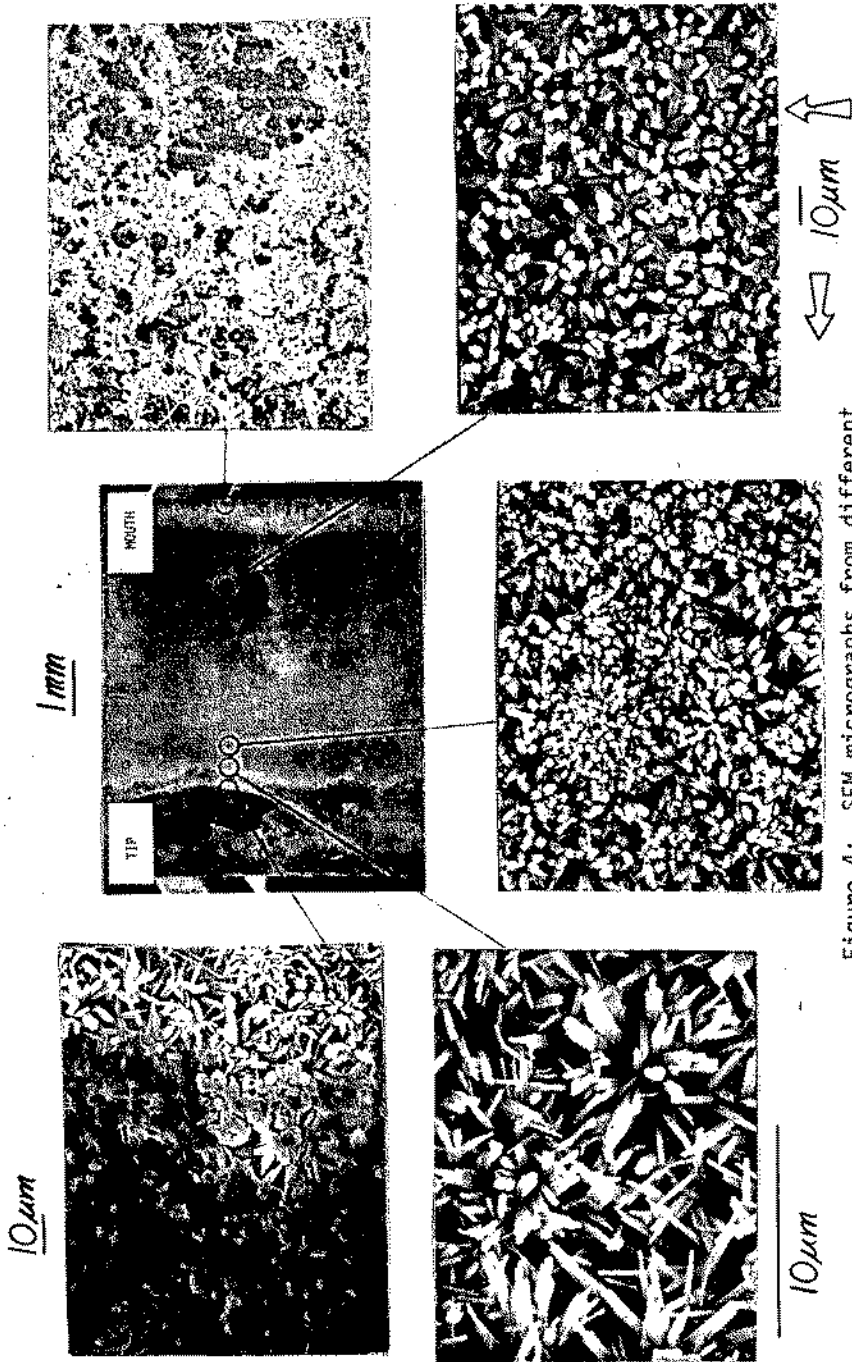


Figure 4: SEM micrographs from different regions within crack for -0.500V., 1.0 Hz.

surface and, second, there existed a transition in morphology with distance into the crack. Limited additional experiments at  $-0.780$ ,  $-1.000$  and  $-1.100$ v. (SCE) were consistent with this. However, deposit morphologies within the simulated cracks were observed to be variable, even for constant experimental conditions, and could not necessarily be reproduced. Consequently it was concluded that the micrographs in Figures 3 and 4 are typical but not necessarily unique to a specific experimental condition.

EDAX analysis indicated that the predominant cation in the deposits was calcium in all cases with little or no magnesium being detected. This was true both within and external to the crack. In the case of the  $-1.100$ v. specimen local, high magnesium regions were encountered; and the morphology of these was similar to what has been reported previously (41).

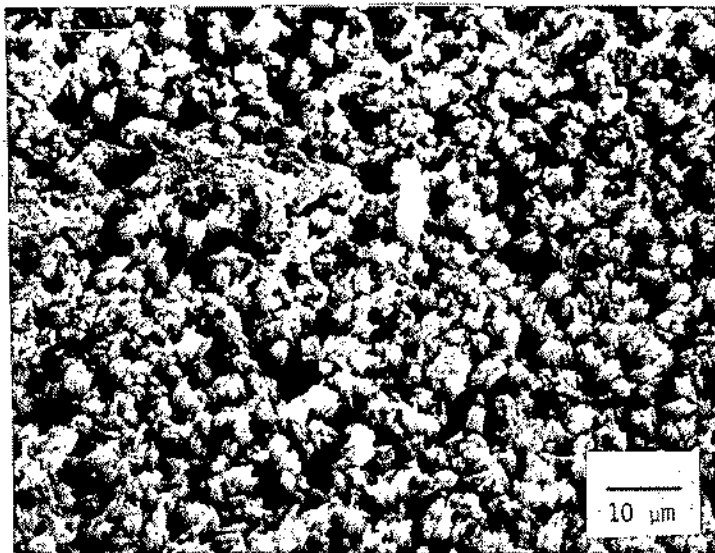


Figure 5: SEM micrograph from boldly exposed specimen surface,  $-0.900$ v. and  $0.5$  Hz.

The problem of rationalizing calcareous deposit structure and properties in terms of variables of formation (potential, temperature, velocity, etc.) is a difficult one, even for a boldly exposed surface. For the case of a fatigue crack the situation becomes even more complex due to unknown and difficult to

characterize hydrodynamics and possible kinetic limitations imposed by a slow rate of reactant replenishment at deposition sites. The fact that deposit morphology within the simulated cracks differed from that on boldly exposed surfaces was probably due to these latter two factors, as was the variable deposit structure along the crack length. The observation that a particular deposit morphology was not necessarily reproducible for experiments performed under apparently identical conditions may reflect the fact that more than one variable can be controlling.

Apparent also from the micrographs near the crack tip in Figures 3 and 4 (particularly Figure 4) is that flattening and compaction of calcareous deposits has occurred, presumably as the deposits grew to a thickness exceeding that minimum crack opening. More indepth experiments are required, however, to determine the resistance of such deposits to crack closing forces and how this resistance might depend upon deposit structure.

#### CONCLUSIONS

1. The morphology of calcareous deposits formed within the simulated fatigue crack of cathodically polarized, 1018 steel specimens exposed to flowing natural sea water was different than for deposits formed on the boldly exposed surfaces. Also the deposit morphology changed with distance into the crack.
2. The morphology of deposits within simulated cracks was not necessarily the same for apparently identical specimens and experimental conditions. This may be due to a competing influence from such factors as mass transport processes (crack hydrodynamics, in particular) and reactant availability.
3. The cation comprising calcareous deposits was primarily calcium with little or no magnesium being detected. An exception was a specimen polarized to  $-1.100v$ . (SCE), where small, local magnesium rich deposits were found within the simulated crack.
4. Areas of compacted calcareous deposits were observed near the crack tip, indicating that within the 168 hour test period the thickness of this material had grown to exceed the minimum crack opening and that the calcareous deposits had interfered with crack closure.

#### ACKNOWLEDGEMENTS

The author is indebted to the Sea Grant National Marine

Corrosion Program for financial support. The assistance of Mr. Keith Davidson in the experimental aspects of this study is appreciated.

#### BIBLIOGRAPHY

1. W. H. Hartt, "Corrosion Prevention of Offshore Structures", in Introduction to Offshore Structures, Ed. D. V. Reddy and M. Arockiasami, Trans Tech Pub., to be published.
2. R. A. Humble, *Corrosion*, Vol. 4, p. 358 (1948).
3. F. L. LaQue, *Corrosion*, Vol. 6, p. 161 (1950).
4. G. L. Doremus and J. G. Davis, *Materials Protection*, Vol. 6, (1), p. 30 (1967).
5. K. G. Compton, "Cathodic Protection of Structures in Sea Water," paper no. 13 presented at CORROSION/75, Toronto, April 14-18 (1975).
6. J. C. Hudson, The Corrosion of Iron and Steel, Van Nostrand Co., Inc., New York, 1940, pp. 158 and 175.
7. S. L. Wolfson and W. H. Hartt, *Corrosion*, Vol. 37, 1981, p. 70.
8. M. A. G. Rodrigo, *Afinidad*, Vol. 23, p. 217 (1966).
9. H. England and R. Heidersbach, "The Effects of Water Depth on Cathodic Protection," paper no. 172 presented at CORROSION/82, March 22-26, 1982, Houston.
10. H. Klas, *Archiv fur das Eisenhüttenwesen*, Vol. 19, p. 321 (1958).
11. C. H. Culberson, "Effect of Seawater Chemistry on the Formation of Calcareous Deposits," paper no. 61 presented at CORROSION/83, Anaheim, April 18-22, 1983.
12. T. L. Nye, S. W. Smith and W. H. Hartt, "Once Through Versus Recirculated Sea Water Testing for Calcareous Deposit Polarization of Cathodically Protected Steel," presented at Intl. Symp. on Laboratory Corrosion and Standards, Nov. 14-16, 1983, Miami. To be published in ASTM Special Technical Publication.
13. W. H. Hartt, C. H. Culberson and S. W. Smith, "Calcareous Deposits upon Metal Surfaces in Sea Water - A Critical Review," paper no. 59 presented at CORROSION/83, Anaheim,

April 18-22, 1983. To be published in Corrosion.

14. J. G. Hicks, "Material and Structural Problems in Offshore Installations," Proceedings Conference on Welding in Offshore Constructions, 1974, p. 1.
15. H. Wintermack, "Materials and Welding in Offshore Constructions," 1975 Portevin Lecture, International Institute of Welding.
16. P. W. Marshall, "Problems in Long-Life Fatigue Assessment for Fixed Offshore Structures," preprint 2638, ASCE National Water Resources and Ocean Engineering Conference, San Diego, April, 1976.
17. W. H. Hartt, Materials Performance, Vol. 20(11), p. 50 (1981).
18. P. M. Scott and D. R. V. Silvester, "The Influence of Mean Tensile Stress on Corrosion Fatigue Crack Growth in Structural Steel Immersed in Sea Water," Interim Tech. Rept. 3/02, Dept. of Energy, U. K. Offshore Steels Research Project, May 25, 1977.
19. P. M. Scott and D. R. V. Silvester, "The Influence of Sea Water on Fatigue Crack Propagation Rates in Structural Steel," Interim Tech. Rept. 3/03, Dept. of Energy, U. K. Offshore Steels Research Project, Dec. 19, 1977.
20. O. Vosikovsky, Closed Loop, Vol. 6 (1), p. 3 (1976).
21. C. M. Hudgins, B. M. Casad, R. L. Schroeder and C. C. Patton, J. Pet. Tech., Mar., 1971, p. 283.
22. P. M. Scott, Materials Development Division, Harwell, England. Personal communication.
23. C. P. Royer, Exxon Production Research Co., Houston. Personal communication.
24. W. C. Hooper and W. H. Hartt, Corrosion, Vol. 34, p. 320 (1978).
25. W. H. Hartt and W. C. Hooper, Corrosion, Vol. 36, p. 107 (1980).
26. G. E. Nordmark and W. G. Frick, J. Test. Eval., Vol. 6, 1978, p. 301 (1978).
27. R. van der Velden, H. L. Ewalds, W. A. Schultze and A. Punter, ASTM Spec. Tech. Pub. 801, 1983, p. 64.



28. R. O. Ritchie, S. Suresh and C. M. Moss, *J. Engr. Mat. Tech.*, Vol. 102, p. 293 (1980).
29. S. Suresh, G. F. Zamiski and R. O. Ritchie, *Met. Trans A.*, Vol. 12A, p. 1435 (1981).
30. R. O. Ritchie and S. Suresh, *Met. Trans. A.* Vol. 13A, p. 937 (1982).
31. B. F. Brown, *Corrosion*, Vol. 26, p. 249 (1970).
32. M. Pourbaix, *Corrosion*, Vol. 26 p. 431 (1970).
33. M. H. Peterson and T. J. Lennox, *Corrosion*, Vol. 29, p. 406 (1973).
34. B. F. Brown, "The Role of the Occluded Cell in Stress Corrosion Cracking of High Strength Steels," *Rapports Techniques CEBELCOR*, Vol. 112, RT. 170 (1970).
35. J. M. Barsom, *Int'l. J. Fr. Mech.*, Vol. 7, p. 163 (1971).
36. D. A. Meyn, *Met. Trans.*, Vol. 2, p. 853 (1971).
37. K. M. McCabe and S. W. Smith, "Effects of Flow Parameters on the Cathodic Protection of a Steel Plate in Natural Sea Water," to be presented at Sea Water Corrosion Symposium, CORROSION/85, Boston, March 25-29, 1985.
38. E. Bardal and P. O. Gartland, "Effects of Flow Conditions on the Current Density Necessary for Cathodic Protection of Steel in 3.5% NaCl Solution and Sea Water," presented at CORROSION/83, April 18-22, 1983, Anaheim.
39. W. H. Hartt and S. S. Rajpathak, "Formation of Calcareous Deposits within Simulated Fatigue Cracks in Sea Water," paper no. 62 presented at CORROSION/83, April 18-22, 1983, Anaheim.
40. W. H. Hartt, "Fatigue of Welded Structural Steel in Sea Water", *Proceedings 13th Offshore Tech. Conf.*, May 4-7, 1981, Houston, p. 87.
41. "Sea Grant Program on Marine Corrosion," Vol. I, Final Report; Program Leaders S. C. Dexter and W. H. Hartt, Sea Grant Office of NOAA, June 30, 1984.



CORROSION STUDIES  
ETUDES SUR LA CORROSION

)

RELATIONSHIPS OF DIFFERENT PHYSICOCHEMICAL PARAMETERS OF POLYMERIC COATINGS APPLIED ON METAL SUBSTRATES OBTAINED BY AC AND DC MEASUREMENTS

A.R.Di Sarli\*, N.G.Toneguzzo\*\* and J.J.Podestá\*\*

\* CIDEPINT - Centro de Investigación y Desarrollo en Tecnología de Pinturas (CIC-CONICET).  
52 entre 121 y 122 - 1900 La Plata - Argentina.

\*\* INIFTA - Instituto de Investigaciones Fisicoquímicas Teóricas y Aplicadas (UNLP-CONICET-CIC).  
Casilla de Correo 16 - Sucursal 4 - 1900 La Plata - Argentina.

ABSTRACT

The diffusivity, permeability and solubility coefficients of water and oxygen by AC and DC techniques respectively were measured for five different varnishes applied on steel plates. Important differences were arised from the measures with DC due to the applied external potential, which enhanced the electrolyte constituents permeation through the membranes by electroendosmosis process.

In AC measures a good agreement was found among corrosion potential ( $E_{corr}$ ), film capacitance ( $C_f$ ) and electrolytic resistance ( $R_m$ ) vs immersion time relationships for all the membranes tested.

From the results obtained for both techniques it was concluded that the varnish mixture formulated with chlorinated rubber grade 20 and a pure phenolic resin (1/1 ratio by weight) showed the greater protective action.

RESUME

Dans ce travail ont été mesurés les coefficients de diffusion, perméabilité et solubilité de l'eau et de l'oxygène au moyen de techniques de courante alterne (AC) et directe (DC), respectivement, pour des plaques d'acier recouvertes par cinq vernis différents.

Des différences importantes ont été établies au moyen des mesures avec DC, dû au potentiel externe appliqué, qui accélère les phénomènes de perméabilité de l'électrolyte à travers les membranes par electroendosmose.

Dans les mesures avec AC on a obtenu une bonne corrélation entre

l'évolution du potentiel de corrosion ( $E_{\text{corr}}$ ), la capacité du "film" ( $C$ ) et la résistance électrolytique ( $R_m$ ), en fonction du temps d'immersion, pour toutes les membranes essayées.

De la comparaison des résultats obtenus au moyen des techniques indiquées on a établi que la membrane correspondante au vernis obtenu avec caoutchouc chloré degré 20 et une résine formophénolique pure (dans le rapport 1/1 en poids) présente le meilleur comportement protecteur.

## INTRODUCTION

The tendency of a coated metal to corrode is a function of three major factors: a) the nature of the substrate metal, b) the character of the interfacial region between the coating and the substrate and c) the nature of the coating. In principle these factors are dependent on the water and oxygen diffusion through the coating, so the rate of reaction may be decreased by reducing the permeability of the coating for these constituents. On the basis of the present knowledge, it appears unlikely to eliminate completely the diffusion of water and oxygen through the coating or through defects in the coating that always are present when the coating is prepared during normal application.

Electrical methods for studying the protective properties of coatings are numerous and many have produced important results. Two reviews on this subject have been published recently (<sup>1,2</sup>) and selected information will be extracted from these reviews and other published sources. Electrical methods as laboratory accelerated tests that prove to be useful in predicting the lifetime of a coating include DC measurements of coating conductivity (<sup>3-5</sup>), of impedance as a function of frequency (<sup>6</sup>), of equivalent AC resistance at constant frequency (<sup>7</sup>). The AC properties of a coating have also been used to estimate the amount of water taken up by a coating (<sup>7-9</sup>).

Corrosion potential measurements and their applicability to coated metals have been summarized by Wolstenholme (<sup>10</sup>) concluding that the movement of the corrosion potential in the noble direction is indicative of an increasing cathodic/anodic surface area ratio and indicates that oxygen and water are penetrating the coating and arriving at the metal/coating interface.

The movement of the corrosion potential in the active direction indicates that the anodic/cathodic surface area ratio is increasing and that the overall corrosion rate is becoming significant. Increasingly positive potentials with time suggest that alkaline conditions caused by the oxygen reduction reaction are developing locally at the metal/coating interface and that delamination is produced. Increasingly active potentials are indicative of rusting in the case of steel substrates representing the signal that the coating lifetime is limited.

Due to coating permeability (which is assumed to act as a semipermeable membrane), when water solubility in the membrane increases (other properties remaining the same), water should be absorbed in increasing amounts for each particular immersion time (<sup>11</sup>) and should stop only when the osmotic pressure gradient between internal and external solu-

tions becomes zero.

Nevertheless, an equilibrium state could be reached if the mechanical pressure exerted on the internal solution and resulting from the film resistance to swelling and deformation, becomes equal to the osmotic pressure. This condition is a function of the mechanical and adhesive properties of the particular coating system under test <sup>(12)</sup> and could explain the influence of the coating nature at the overall system behaviour, since different experiences carried out with several salt solutions <sup>(13)</sup> showed that the material responsible for weight and volume increasing is only pure water absorbed by the coating during immersion in salt solutions.

With respect to the influence of the substrate employed on the protective properties of different coatings, a series of comparative tests has been carried out with films supported on an active or inert substrate and with free films <sup>(5)</sup>. In the latter case it has been found that when films were applied on iron and immersed in a corrosive solution, corrosion takes place at the areas of low film resistance. At these areas the attached film had similar resistance to that determined on the free films.

On the other side, when the films were supported on inert substrates (platinum or passivated iron), their resistance was several orders of magnitude higher than that of free films.

These results can be explained in terms of the penetration of ions into the film, a process which takes place more easily if ions are available from both sides.

In the case of films supported on an inert substrate, ionic penetration can occur only from one side, then, only after the film has taken up water, thereby lowering the film dielectric constant. This uptake of water is retarded in the case of attached films, as contrasted to a free one, by the action of cohesion forces between polymeric chains and adhesion forces to the substrate, which reduce the freedom degrees and oscillation amplitude of the polymeric chains <sup>(14)</sup>.

These observations provide support for Bacon et al <sup>(4)</sup>, which establish that prediction of coatings performance can be made from measurements of electrolytic resistance.

The electrochemical process of corrosion depends not only on the presence of water, since oxygen plays an important role; so, the diffusion processes of these two constituents will be considered.

The aim of this work is to determine the diffusivity, permeability and solubility of water and molecular oxygen through different polymer coated/steel systems by AC and DC techniques. Auxiliary corrosion potentials, capacitance and electrolytic resistance measurements in function of the immersion time were carried out.

## EXPERIMENTAL

### 1. AC measurements

Naval steel plates SAE 1020 of 8 x 16 x 0.2 cm were employed as metallic substrates. Surface was sandblasted to grade Sa 2.5-3 according to SIS 05 59 00-1962 swedish standard. Then, the plates were

TABLE I  
CHARACTERISTICS OF THE COATINGS TESTED

| Membrane type  | Composition<br>(g/100 g)          |      | Elaboration<br>process                                   |
|----------------|-----------------------------------|------|--|
| A <sup>1</sup> | Chlorinated rubber R-20           | 51.8 | Dissolution of resin and plasticizer in toluene          |
|                | Chlorinated paraffin 42 %         | 22.2 |  |
|                | Toluene                           | 26.0 |  |
| B <sup>2</sup> | Tung oil                          | 53.3 | Copolymerization of tung oil and phenolic resin          |
|                | Pure phenolic resin               | 26.6 |  |
|                | Toluene                           | 20.1 |  |
| C <sup>3</sup> | Phenolic varnish (80 % of solids) | 63.8 | Dissolution of varnish, resin and plasticizer in toluene |
|                | Chlorinated rubber R-20           | 17.0 |  |
|                | Chlorinated paraffin 42 %         | 7.2  |  |
|                | Toluene                           | 12.0 |  |
| D <sup>3</sup> | Phenolic varnish (80 % of solids) | 54.6 | Dissolution of varnish, resin and plasticizer in toluene |
|                | Chlorinated rubber R-20           | 21.9 |  |
|                | Chlorinated paraffin 42 %         | 9.4  |  |
|                | Toluene                           | 14.1 |  |
| E <sup>3</sup> | Phenolic varnish (80 % solids)    | 38.6 | Dissolution of varnish, resin and plasticizer in toluene |
|                | Chlorinated rubber R-20           | 30.9 |  |
|                | Chlorinated paraffin 42 %         | 13.3 |  |
|                | Toluene                           | 17.3 |  |

<sup>1</sup> Chlorinated rubber varnish

<sup>2</sup> Oleoresinous varnish

<sup>3</sup> Mixtures of oleoresinous and chlorinated rubber varnishes

cleaned with toluene and, after solvent evaporation, coated with different varnishes, employing a Bird stainless steel applicator. Varnishes characteristics are given in Table I. Wet films of 75  $\mu\text{m}$  thick were obtained. After 72 hours drying at room temperature in a closed vessel (to avoid contamination by atmospheric pollution), dry film thicknesses (15-25  $\mu\text{m}$ ) were determined by means of an electromagnetic gage, us



ing bare steel surface as reference.

The electrochemical cells were built with a PVC (polyvinyl chloride) open tube 10 cm length and 5 cm outside diameter, with one of the edges flattened; a borax-hydrochloric acid buffer solution (pH 8.2) was used as electrolyte.

The varnished plates were fixed to the flattened edge of the cells, using an epoxy resin as adhesive. The geometrical area of all working electrodes was 18.5 cm<sup>2</sup>.

As counterelectrode and reference electrode, respectively a spectroscopic grade graphite cylinder of geometrical area ca. 20 cm<sup>2</sup> and a saturated calomel electrode (SCE) were employed. Impedance modulus ( $|Z|$ ) and phase angle ( $\phi$ ) of the working electrode of the different systems were measured at the corrosion potential and at room temperature, in the frequency range of 5 up to 5.10<sup>5</sup> Hz with a vector impedance meter Hewlett Packard 4800 A.

The coating permeability was determined by measuring the parallel capacitance ( $C_p$ ) at a frequency value of 3.10<sup>4</sup> Hz with a rms potential of 0.027 V.

Data storage treatment, diagrams plot, variables and parameters calculation were carried out by means of an Olivetti P 6060 microprocessor, using a series of programmes developed in this laboratory to obtain the concerned parameters.

#### 5. DC measurements

A conventional electrochemical pyrex glass cell (ca. 0.6 l) with three electrodes was used. The working electrode was a rotating disk type with a naval steel cylinder 0.8 cm outside diameter embeded in a PTFE rod. The free surface (0.5 cm) was coated with the varnishes mentioned in Table I. The counterelectrode was a platinum wire of ca. 10 cm<sup>2</sup> and the reference electrode was a SCE (15).

A borax-hydrochloric acid buffer solution (pH 8.2) saturated with different oxygen partial pressures ( $C_s$ ), from 21% up to 100%, was employed as electrolyte.

A potentiostatic pseudo-stationary technique with IR compensation was used to obtain the diffusional-convective current density ( $i_d$ ) at different rotation rates with angular speeds ( $\omega$ ) from 20 up to 126 s<sup>-1</sup>.

The permeability coefficient ( $P_m$ ) of molecular oxygen of the different systems was graphically obtained plotting  $C_s/i_d$  vs  $\omega^{-1/2}$  (Fig.1). By extrapolation to  $\omega^{1/2} \rightarrow \infty$  the molecular resistivity ( $x_m$ ) is obtained according to equations 1 and 2.

$$\lim_{\omega^{1/2} \rightarrow \infty} i_d = n F P_m C_s \quad (1)$$

$$P_m = 1 / x_m \quad (2)$$

A transient coulombimetric technique with a step change of the oxygen partial pressure was employed for the determination of the dif

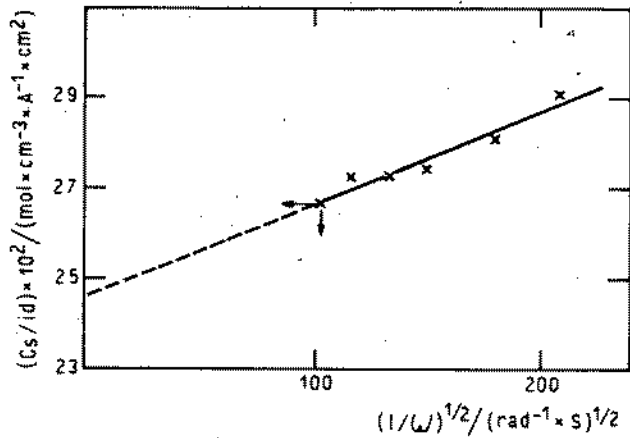


Fig. 1.-  $C_s/id$  vs  $1/\omega^{1/2}$  of coated naval steel (varnish C, 45  $\mu\text{m}$  thickness) immersed in borax-hydrochloric acid buffer solution (pH 8.2) saturated with oxygen, at 30°C

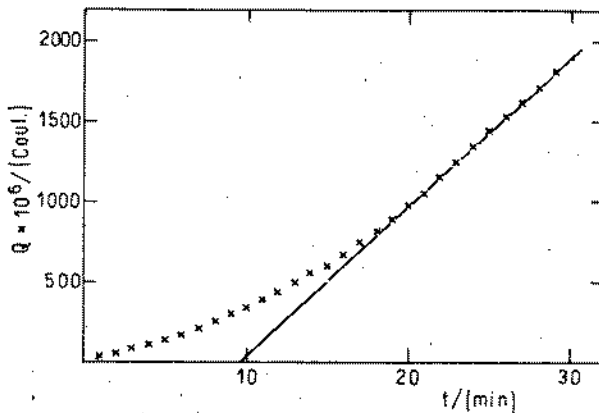


Fig. 2.- Relationship between charge  $Q$  ( $\mu\text{coul}$ ) and time  $t$  (min) for oxygen concentration changes (system C) and angular disk rotation rate  $126\text{ s}^{-1}$

fusivity coefficient of molecular oxygen in the membranes ( $D_m$ ) according to Barrer's equation (<sup>16</sup>):

$$D_m = \frac{\delta_m^2}{6 \Theta} \quad (3)$$

where  $\delta_m$  is the thickness of the coating and  $\Theta$  the lag time. The lag time  $\Theta$  was graphically determined from the relationship between the charge ( $Q$ ) and the time ( $t$ ) (Fig. 2).

The value of  $P_m$  can be assessed from the slope  $\Delta Q/\Delta t$  and can be compared with those figures calculated from the potentiostatic pseudo-stationary technique.

The solubility coefficients ( $S$ ) were calculated by means of equation 4:

$$P_m = S D_m \quad (4)$$

## RESULTS

### A) Corrosion potential measurements

The stabilized corrosion potential values versus the immersion time relationships are showed in Fig. 3 for the different systems.

System A (plasticized chlorinated rubber) depicts for the first day of immersion a  $E_{corr}$  value of  $-0.26$  V/SCE, shifting to more positive steady values during some days. After that,  $E_{corr}$  fluctuates in a range of various tenths of millivolts for finally overcome the value of  $-0.7$  V/SCE.

System B (oleoresinous varnish) exhibits a markedly different behaviour. During the first ten days of immersion  $E_{corr}$  takes positive values, however, they change to slightly negative ones at longer immersion times, with a tendency to stabilization at  $-0.05$  V/SCE after 50 days.

Systems C, D and E (mixtures of oleoresinous varnish and chlorinated rubber resin systems) showed, in some cases, significative changes of the  $E_{corr}$  values.

Systems C and D (with oleoresinous varnish/chlorinated rubber varnish relations of 4/1 and 2.5/1 by weight respectively) show less positive  $E_{corr}$  values than system B. Slightly negative  $E_{corr}$  values are observed for system E, corresponding to a relation varnish/chlorinated rubber 1/1 by weight.

After 15 days immersion systems C, D and E showed the same value for the corrosion potential ( $-0.075 \pm 0.025$  V/SCE).

For long immersion times, system E maintains the same value, instead systems C and D shift sharply to more negative potentials.

### B) Impedance measurements

The impedance behaviour of the five different coated systems in the buffer solution were measured at the moment of immersion and then

TABLE II

DIFFUSIVITY (D), PERMEABILITY (P) AND SOLUBILITY COEFFICIENTS OF WATER AND OXYGEN FOR COATED STEEL OBTAINED WITH AC AND DC TECHNIQUES RESPECTIVELY.

| System<br>Parameters                              | A                    | B                    | C                    | D                    | E                    |
|---|----------------------|----------------------|----------------------|----------------------|----------------------|
| $D_{M_{H_2O}}$<br>(AC)<br>( $cm^2 \cdot s^{-1}$ ) | $1.8 \cdot 10^{-11}$ | $1.1 \cdot 10^{-10}$ | $1.0 \cdot 10^{-10}$ | $4.1 \cdot 10^{-11}$ | $6.2 \cdot 10^{-11}$ |
| $D_{M_{O_2}}$<br>(DC)<br>( $cm^2 \cdot s^{-1}$ )  | $1.7 \cdot 10^{-7}$  | $3.3 \cdot 10^{-8}$  | $1.2 \cdot 10^{-8}$  | $6.0 \cdot 10^{-9}$  | $4.5 \cdot 10^{-9}$  |
| $P_{M_{H_2O}}$<br>(AC)<br>( $cm^2 \cdot s^{-1}$ ) | $8.6 \cdot 10^{-13}$ | $2.7 \cdot 10^{-12}$ | $3.0 \cdot 10^{-12}$ | $7.6 \cdot 10^{-13}$ | $6.4 \cdot 10^{-13}$ |
| $P_{M_{O_2}}$<br>(DC)<br>( $cm^2 \cdot s^{-1}$ )  | $5.7 \cdot 10^{-8}$  | $6.8 \cdot 10^{-8}$  | $2.3 \cdot 10^{-8}$  | $4.7 \cdot 10^{-8}$  | $7.9 \cdot 10^{-10}$ |
| $S_{H_2O}$<br>(AC)                                | 0.048                | 0.024                | 0.029                | 0.019                | 0.019                |
| $S_{O_2}$<br>(DC)                                 | 0.34                 | 0.33                 | 2.00                 | 6.80                 | 0.20                 |

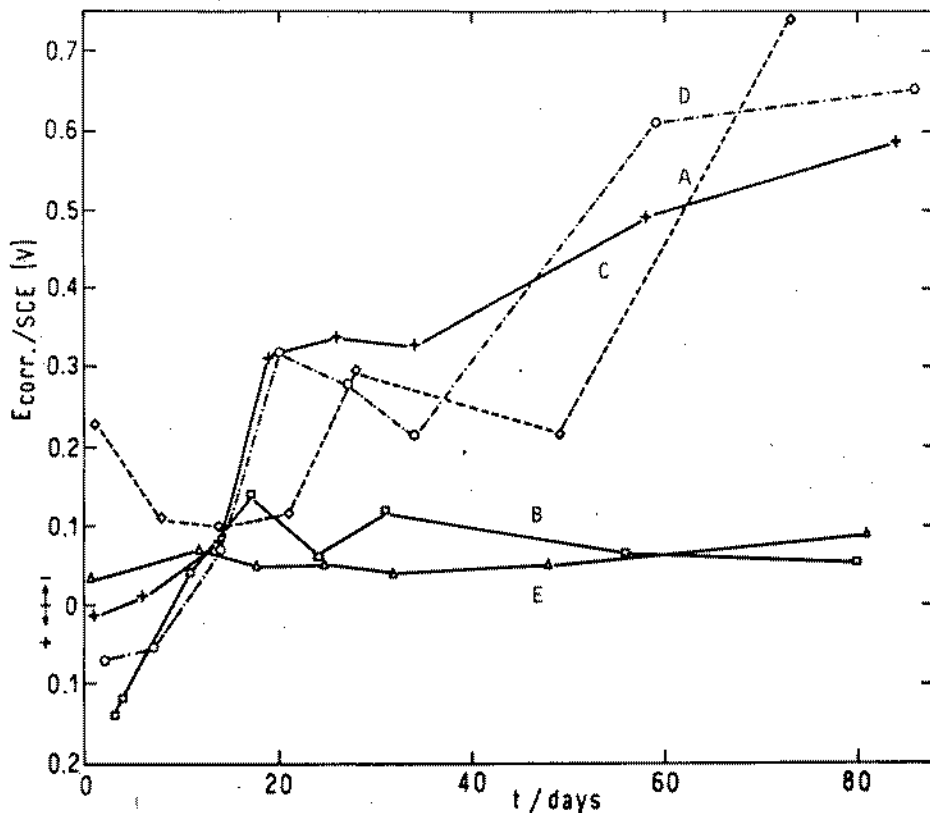


Fig. 3.- Corrosion potential ( $E_{\text{corr}}$ ) vs immersion time of coated naval steel immersed in borax-hydrochloric acid buffer (pH 8.2) at room temperature, for systems A (20  $\mu\text{m}$ ), B (24  $\mu\text{m}$ ), C (20  $\mu\text{m}$ ), D (16  $\mu\text{m}$ ) and E (15  $\mu\text{m}$ ).

periodically during the following weeks until 83 days of test.

The impedance Nyquist diagram obtained during each run for a particular system in function of the immersion time is shown in Fig. 4.

Similar curves were obtained for the other systems, allowing the calculation of the capacitance and electrolytic resistance for each system at increasing immersion times. All curves showed a high frequency semicircle which can be attributed to the varnish film properties associated with capacitance values similar to those reported by other authors for different organic coatings ( $10^{-13}$ ).

The different behaviour of the capacitance values vs immersion time for the tested systems (Fig. 5) are related to the interactions of the

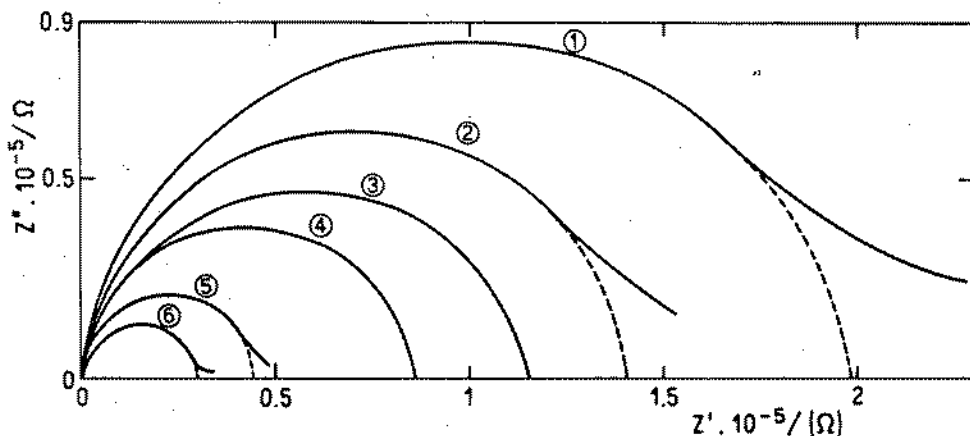


Fig. 4.- Impedance diagrams of naval steel coated with varnish E (15  $\mu\text{m}$  thickness), immersed in borax-hydrochloric acid buffer (pH 8.2) at room temperature, for 12 days immersion (1), 19 days (2), 27 days (3), 32 days (4), 48 days (5) and 81 days (6).

electrolytic medium on the organic varnishes acting as membranes.

Within the first 20 days, systems C and D present high values of capacitance, but later a sharp decrease was observed up to reach a value of ca.  $0.5 \text{ nF cm}^{-2}$ , similar to that of B and E systems, which remain constant during a certain time.

The variation of the capacitance to high values for the A, D and C systems, are demonstrative of the progressive and marked deterioration of the coatings in function of the immersion time.

The relation of the ionic resistance ( $R_m$ ) with the immersion time in the five coatings tested is shown in Fig. 6.

The  $R_m$  values were obtained graphically from the semicircles with a diameter equal to  $R_m$  ( $\Omega \cdot \text{cm}^2$ ).

All systems initially exhibit  $R_m$  values of various  $\text{M}\Omega \cdot \text{cm}^2$ , reaching lower values of some orders of magnitude with the time increase. The rate and magnitude of such differences depends on the coating composition, being minimum for system E and maximum for system D with, at least, two orders of magnitude for  $R_m$  values at the end of the test.

#### C) Diffusivity, permeability and solubility coefficients of water with AC technique

The diffusion, permeability and solubility coefficients of water in the coatings were obtained from measures of the parallel capacitance as a function of exposure time<sup>(9)</sup>. The results obtained for system C are shown graphically in Fig. 7.

From linear regression of Carpenter equation<sup>(17)</sup> the diffusion, permeability and solubility coefficients were calculated<sup>(18)</sup>.

Values of the diffusion, permeability and solubility coefficients of water and oxygen obtained with AC and DC techniques, respectively, are shown in Table II for different systems.

D) Diffusivity, permeability and solubility coefficients of oxygen with DC techniques

The permeability coefficient of oxygen is in agreement with the values obtained by stationary and transient techniques. In general it was observed an increment of the permeability coefficients for varnishes with oleoresinous resin in relation to the chlorinated rubber varnish.

In the mixtures, differences among their values cannot be appreciated; except that exists an order of magnitude more elevated than for chlorinated rubber and the same order less than the pure oleoresinous resin.

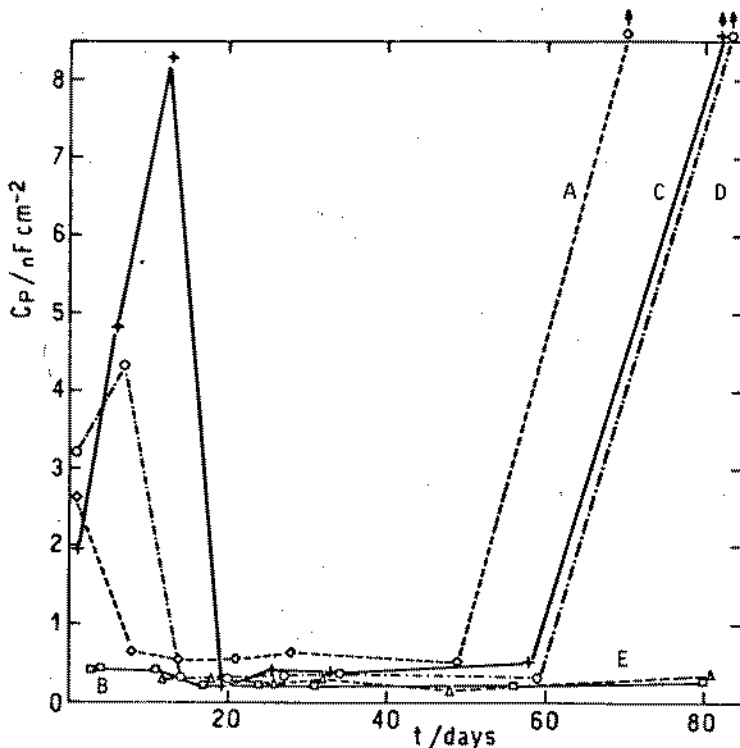


Fig. 5.- Capacitance ( $nF cm^{-2}$ ) vs immersion time of coated naval steel immersed in borax-hydrochloric acid buffer (pH 8.2) at room temperature, for systems A, B, C, D and E.

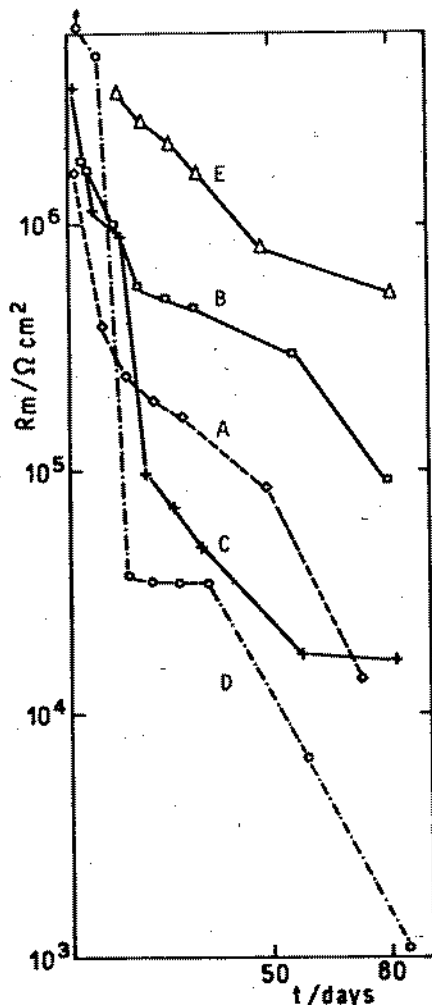


Fig. 6.- Electrolytic resistance  $R_m$  ( $\Omega \text{ cm}^2$ ) vs immersion time of coated naval steel immersed in borax-hydrochloric acid buffer. (pH 8.2) for the different systems tested.

The diffusivity coefficients of oxygen in the membranes decrease when content of chlorinated rubber in the varnish increases. The permeability coefficient of system E is two orders of magnitude less than the rest of the other systems.

#### DISCUSSION

The interfacial region consists of the steel substrate, a thin oxide coating on the metal, perhaps a water layer and finally the organic coating. The bond between the organic coating and the substrate is difficult to interpret specially when water and oxygen permeates



the coating and becomes available for adsorption or electrochemical reactions in the interfacial region.

According to the results obtained by other authors<sup>(9, 19, 20)</sup>, the values shown in Table II for the different coefficients corresponding to water and oxygen demonstrate the existence of a controlled diffusional process by the water flow through the membrane.

In the present work noticeable differences among such coefficient values obtained by means of AC and DC electrochemical techniques, respectively, are attributed not only to particular interactions of each reagent with the membrane but also to the fact that for parameters determination corresponding to oxygen, by measures of the diffusional-

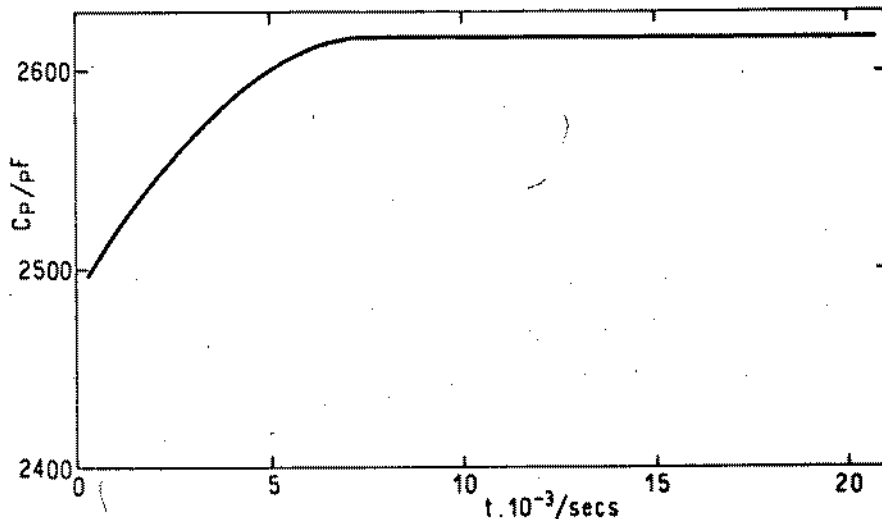


Fig. 7.- Parallel capacitance  $C_p$  ( $nF\text{cm}^{-2}$ ) vs immersion time (seconds) of coated naval steel (varnish C) immersed in borax-hydrochloric acid buffer (pH 8.2) at room temperature

convective currents, a cathodic potential ( $-0.850$  V/SCE) was applied, while for the water permeation measurement, it was necessary to introduce an electric perturbation of a few millivolts.

Then, from a simple comparison of the results, arise as a first conclusion that an important factor to be taken into account in this type of studies is the technique to be used since, as it is demonstrated, it affects noticeably the barrier effect proportionated by the organic films and in consequence their protective capacity. This is due to the presence of an electric potential gradient, whose value depends on the externally applied potential which enhanced the water flow through the membrane by the mechanism of electroendosmosis<sup>(18)</sup>. The

high water dielectric constant permits water to act as coating plasticizer and to diminish the cohesion forces among polymeric chains and favours, sometimes, oxygen flow<sup>(21, 22)</sup>. This probably occurs owing to the polymeric film swelling, with which the necessary reagents for cathodic reaction complementary of metallic dissolution reach with greater rapidity the metal/membrane interface, depolarizing the reactions that produce the corrosion phenomenon, in comparison with what happens when the system changes naturally.

According to the results of Table II it is evident that the validity of the same obtained from DC measures, in the case of metallic protection by organic films, it is limited to those coating systems that use cathodic protection as complement.

Other factors to take into account in data interpretation are temperature and immersion time. AC tests were realized at room temperature (about 20°C) while DC measures were done at 30°C in thermostated bath; it is generally accepted that<sup>(14)</sup> an increase of this variable affects the values of solubility, diffusivity and then permeability coefficients, increasing them as consequence of a greater mobility in polymeric chains. With respect to immersion time, to avoid errors that may be introduced by the accumulation of interfacial water as suggested by Funke<sup>(22)</sup>, AC measurements for parameter determination corresponding to water flow were realized within the first four hours of immersion.

While those corresponding to oxygen (DC technique) were done at five days, since during the first immersion hours it is not observed a net current passage owing to the lack of membrane dampening, proving that the membrane acts as a dielectric.

The oleoresinous varnish B due to its greater polar character possesses a higher solubility with respect to water than in the chlorinated rubber varnish A case. The aggregate to oleoresinous varnish in increasing proportions of chlorinated rubber varnish, is accompanied by a reduction of water and oxygen diffusion coefficient in approximately one order of magnitude. This decreasing is attributed to a hydrophilic character decreasing for the mixture system compared with the corresponding to the oleoresinous varnish, that becomes more evident as diminishes the relative proportion of this binder, since for a mixture 1:1 (system E) the water diffusion coefficient value is about the same that for pure chlorinated rubber (system A) which in practice cannot be employed as only binder because for large immersion times it is deteriorated in contact with an aqueous medium, thus losing its protective capacity.

It seems remarkable that the behaviour of system with varnish A does not follow the above mentioned tendency with respect to oxygen diffusion rate, considering that its high value is due to an electro-osmotic effect with later delamination, since, previous to obtain experimental data it was necessary to apply the cathodic potential to accelerate the membrane dampening rate, which demanded a long time in natural conditions owing to the water low activity in the electrolyte and the high impermeability of organic coating (order of  $10^{-13}$  cm<sup>2</sup>/s) to short immersion times.

In figures 4, 5 and 6 are summarized the experimental results obtained from impedance measures for the five coatings employed.

Comparatively, it can be seen that a close relationship exists among the evolution of corrosion potential ( $E_{\text{corr}}$ ), membrane capacitance ( $C_p$ ) and electrolytic resistance ( $R_m$ ) in function of immersion time for all studied systems.

So, more positive  $E_{\text{corr}}$  values (less metallic substrate activity) are correlated with the highest electrolytic resistance values (less electrolytic permeation rate) and lower capacitance values (less electrolyte enter to film and then less dielectric constant increase). As the immersion time increases, the change in these electric parameter values exhibit the behaviour modifications of the different coatings, as a consequence of their deterioration by interactions with the medium in which they are submerged.

It is important to remark that, independently of the time considered, the above mentioned correlation among these parameters was maintained for all systems up to conclude the test and provided the electrical perturbation necessary to accomplish the measurements have very low amplitude, such results are demonstrative of the natural evolution suffered by these systems. According to the above mentioned results, that take into account different factors influencing the metal/coating/medium interfaces behaviour, it may be stated that, from the low values obtained for system E, constituted by 50 per cent/W of oleoresinous and 50 per cent/W of chlorinated rubber varnishes supported on a naval steel plate and submerged in a borax-hydrochloric acid buffer solution, this system possesses the highest protective behaviour.

These results are coincident with preliminary experiments realized by Rascio et al<sup>(2,3)</sup> with the same varnishes employed as binders of anticorrosive formulations for marine use.

#### ACKNOWLEDGEMENTS

The authors thank E.E. Schwiderke for his valuable assistance in computer programming. This work was partially sponsored by the SENID (Navy Research and Development Service of Argentina).

#### REFERENCES

- (1) Leidheiser, H. Jr.- Prog. Organic Coatings 7, 79 (1979).
- (2) Sato, Y.- Prog. Organic Coatings 9, 85 (1981).
- (3) Kinsella, E.M. and Mayne, J.E.O.- Brit. Polym. J. 1, 173 (1969).
- (4) Bacon, R.C., Smith, J.J. and Rugg, F.M.- Ind. Eng. Chem. 40, 161 (1948).
- (5) Mayne, J.E.O. and Mills, D.J.- J. Oil Colour Chem. Assoc. 58, 155 (1975).
- (6) Leidheiser, H.Jr. and Kendig, M.W.- Corrosion 32, 69 (1976).
- (7) Touhsaent, R.E. and Leidheiser, H. Jr.- Corrosion 28, 435 (1972).
- (8) Brasher, D. M. and Kingsbury, A.H.- J. Appl. Chem. 4, 62 (1954).
- (9) Holtzman, K.A.- J. Paint Technol. 43, N°554, 47 (1971).

- (10) Wolstenholme, J.- Corros. Sci. 13, 521 (1973).
- (11) Lowry, H.H. and Kohman, G.T.- J. Phys. Chem. 31, 23 (1927).
- (12) Guruviah, S.- J. Oil Col. Chem. Assoc. 53, 669 (1970).
- (13) Kittelberger, W.W. and Elm, A.C.- Ind. and Eng. Chem. 38, 7 (1946).
- (14) Kumins, Ch.A.- J. of Coat. Tech. 52, 664 (1980).
- (15) Toneguzzo, N.G., Podestá, J.J. and Arvía, A.J.- Anales Asoc. Quím. Argentina 71, 381 (1983).
- (16) Barrer, R.M.- Diffusion in and through solids. Cambridge University Press, London (1941).
- (17) Carpenter, A.S.- Trans. Faraday Soc. 43, 529 (1947).
- (18) Kittelberger, W.W. and Elm, A.C.- Ind. and Eng. Chem. 39, 7 (1947).
- (19) Funke, W., Machunsky, E. and Handloser, G.- Farbe u. Lacke 84, 493 (1978).
- (20) Haagen, H. and Funke, W.- J. Oil Col. Chem. Assoc. 58, 359 (1975).
- (21) Yaseen, M. and Funke, W.- J. Oil Col. Chem. Assoc. 61, 284 (1978).
- (22) Funke, W.- J. Oil Col. Chem. Assoc. 46, 10 (1963).
- (23) Rascio, V. and Caprari, J.J.- Corrosión y Protección (Spain) 5(1), 145 (1974).

ATMOSPHERIC MARINE CORROSION OF Fe and Zn

S. L. GRANESE, E. S. AYLLON, C. BONÁZZOLA and B. M. ROSALES

CEICOR - CITEFA/CONICET

Zufriategui 4380 - (1603) Villa Martelli - Buenos Aires/Argentina

**ABSTRACT** - The initial and propagation stages of the atmospheric corrosion of Fe, Zn and some of their alloys were analyzed in marine environment. Natural and laboratory exposures to the marine salt spray were performed to correlate the morphology and magnitude of the attack with the composition and metallurgical characteristics of the metal.

**RESUME** - On analyse les etapes d'initiation et propagation de la corrosion atmospherique du Fe, Zn et quelques unes de leur alliages dans du milieu marin. Des expositions naturels et de laboratoire à la brouillard saline marine ont été faites pour corrélationner la morphologie et magnitude de l'attaque avec la composition et caractéristiques métallurgiques du métal.

**INTRODUCTION** - In previous papers we had analyzed the atmospheric corrosion of steel<sup>1,2,3</sup> having observed that the natural pollutant of the marine environment produces the highest corrosion rates<sup>4</sup>.

It is well known that the stability of a metal in a given environment is due to the protective properties of the film always present on its surface. The chemical composition and structure of the film determines its behaviour as a barrier, controlling the corrosion rate and type of attack.

Localized corrosion appears as a consequence of chemical heterogeneities at the metal surface, like non-metallic inclusions, second phase particles, impurities segregated at grain boundaries, etc.<sup>5</sup>. Passive films formed on heterogeneous alloys are not uniform containing weak points because the passive film

cannot be formed on the chemically heterogeneous points of the surface<sup>6</sup>.

In previous papers<sup>1,4</sup> we showed that not only the nucleation but also the propagation of the atmospheric corrosion occurs through localized attacks. The knowledge of the detrimental effect of those metal heterogeneities could suggest some ways to improve the stability of films formed on technological alloys.

This information is specially useful in marine environment where the role of the aggressive  $\text{Cl}^-$  ions has extensively been discussed.

**EXPERIMENTAL** - Outdoor exposures of commercial Fe and Zn base alloys were performed in a marine site having a  $[\text{Cl}^-] = 0.4 \text{ g.dm}^{-2}.\text{y}^{-1}$ , for periods up to 48 months. Hot rolled A 52 steel (C 0.21, Si 0.30, Mn 1.20, P 0.014, S 0.022, Cr 0.115, Ni 0.08, Mo 0.015, V 0.174); Rolled Zn 99.965% (Fe 0.0062, Cd 0.026, Cu 0.0013, Pb, Ni and Mn  $< 0.0001$ ); Cast Zn 99.9967% (Fe 0.0016, Cd 0.0006, Pb, Ni, Cu and Mn  $< 0.0001$ ). The meteorologic information of the test site is given in Table I.

**TABLE I: CLIMATIC CHARACTERISTICS OF THE OUTDOOR TEST SITE**

|                                    | MARINE   |
|------------------------------------|--|
| T. (°C) Max.                       | 27.6   |
| Min.                               | 2.1  |
| Av.                                | 14.8   |
| R.H.(%) Max.                       | 96.3   |
| Min.                               | 58.0   |
| Av.                                | 77.0   |
| Rain (mm)                          | 887.7  |
| (hs.)                              | 629.1  |
| Dew (hours)                        | 2,784  |
| Sun (hours)                        | 2,505  |
| Radiation ( $\text{cal.cm}^{-2}$ ) | 137,416  |
| Mean Environment<br>Pollution      | 0.4 $\frac{\text{mgCl}^-}{\text{cm}^2.\text{y}}$ |
| Rain water pH                      | 6.5  |
| Location Lat.                      | 37°56' S   |
| Long.                              | 57°35' WG  |

Test samples of 100 x 300 x 1 mm. were sand blasted (only the steels), degreased with acetone, weighed to 0.1 mg and ex

posed facing N, at 30° respect to the horizontal. The corrosion products were eliminated in pickling solutions of 50% HCl with 1% urotropine, for steels and 200  $\text{gl}^{-1}$   $\text{CrO}_3$  for Zn alloys.

Cross sections of a wire 99.999% Fe and sheets of the rolled and cast Zn alloys were used for short term tests to compare the results for pure metal and commercial alloys. Outdoor tests up to 5 days and expositions in salt spray box up to 10 hours were performed on polished to 0.25  $\mu\text{m}$  samples. SEM and EDAX were applied to study the nucleation of the attack.

Cross sections of the test sheets submitted to long term natural exposures were also observed by SEM to determine the profiles after some years at the atmosphere.

**RESULTS** - In the Fig. 1 the weight loss is shown as a function of time for periods up to 48 months in the outdoor marine testing site.

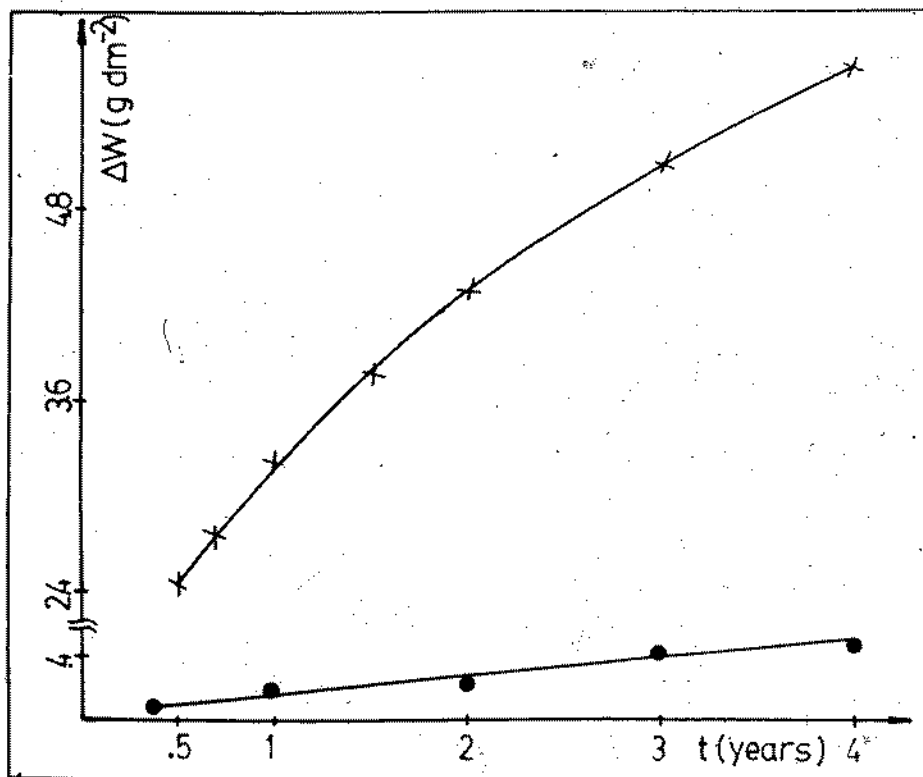


Fig. 1 Weight loss as a function of time at the marine atmosphere.  
 x steel      ● Zinc alloy

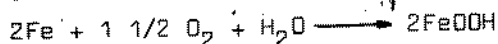
The mathematic expressions fitting the experimental results obtained, were:

$$\text{for A 52 steel: } \Delta W = kt^n \quad k = 3.23 \quad n = 0.41 \quad (1)$$

$$\text{for rolled Zn alloy: } \Delta W = k't \quad k' = 0.13 \quad (2)$$

where  $k$  and  $n$  were calculated by regression.

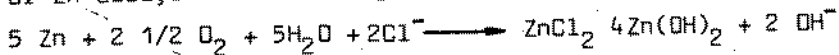
The corrosion products grown on steels in marine environment are formed by large amounts of  $\alpha$ -FeOOH,  $\beta$ -FeOOH and  $\text{Fe}_3\text{O}_4$  with  $\delta$ -FeOOH as minor product<sup>7,8,9</sup>, with the following global reaction:



where the NaCl would act as a catalizer of the process through a cycle implying the formation and regeneration of HCl<sup>10</sup>. In some points at the steel/rust interphase the following reaction takes place<sup>11</sup>.



which is again oxydized by the atmospheric oxygen to FeOOH. For Zn alloys the following reaction was proposed<sup>12</sup>.



Analysis by X Ray diffraction was intended to characterize them but the low chrystallinity of Fe corrosion products produced uncertain results for the natural exposures.

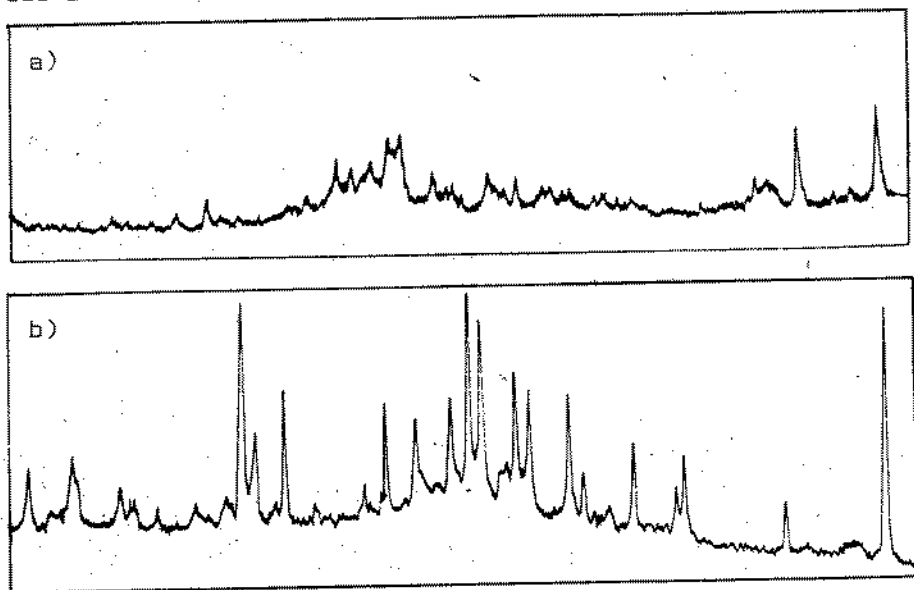


Fig. 2 X Ray diffraction of Zn corrosion products a) In the marine site; b) In salt spray box.



On Zn, on the contrary, the principal peaks are well enough defined to assure the presence of the mentioned corrosion product. For the salt spray tests the crystallinity of the corrosion products is greater than the found in the natural environment, as is shown for Zn in Fig. 2.

The nucleation of the attack is shown in Fig. 3 for pure Fe as compared to steel and in Fig. 4 for pure and alloyed Zn:

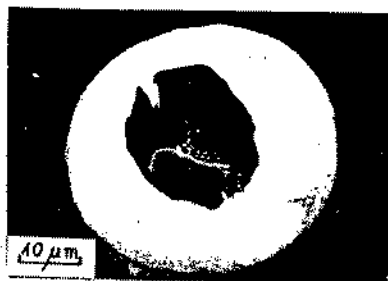
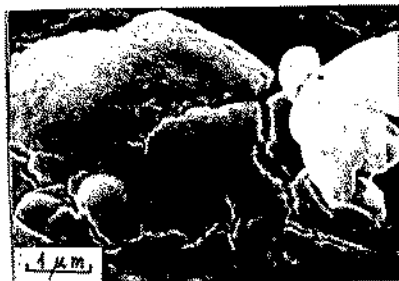


Fig. 3: a) Pure iron, 7 minutes in salt spray box



b) A 52 steel, 2 days at the marine site.

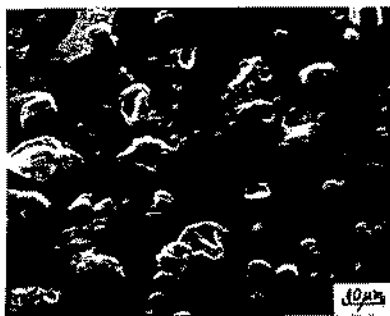
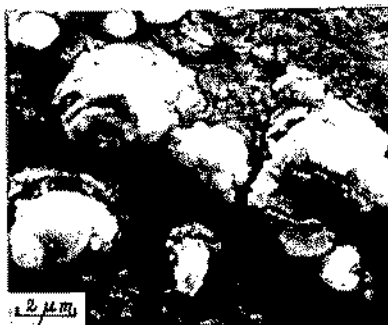


Fig. 4: a) Pure cast Zn in salt spray.



b) Zn rolled and cast alloys 1 day at the marine site.

In the next figure the structure of the corrosion products formed on the Zn alloys after exposures to the natural and laboratory marine media can be compared.

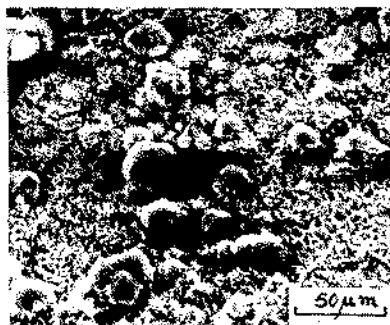


Fig. 5: a) Zn alloy after 5 days at the marine site.



Fig. 5: b) Zn alloy after 4,5 hs. at the salt spray box.

The aspect of the surfaces submitted to incipient attack in the marine or salt spray environments are shown in the next photographs.

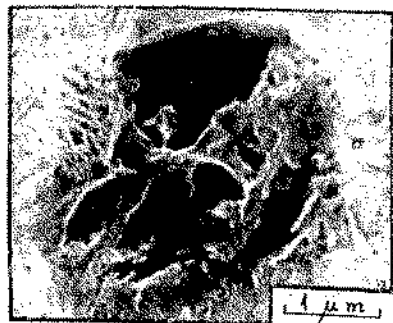
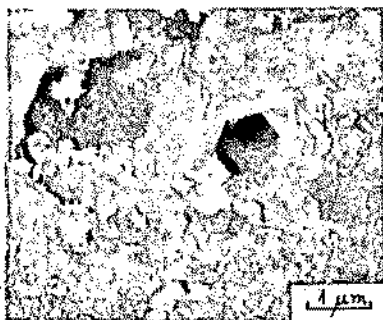


Fig.6: a) A 52 steel after 2 days in the marine site.



b) Cast Zn alloy after 4 1/2 hs. in the salt spray.

DISCUSSION - The results exposed show great similarities in the atmospheric corrosion of both metals and their alloys. Specially the initiation, which was clearly shown to occur on discrete points of the metal as blistering of the surface. Those discrete points have previously<sup>1</sup> been related to surface heterogeneities for the case of steels. Those heterogeneities were secondary phase, as cementite, and non-metallic inclusions, which in fact were generally found associated to the attack nucleation. In the case of high purity Fe and Zn small defects, not detectable with the available techniques, could act as nucleation centers. In this case the phenomenon should be treated on an stochastic basis. This is also valid for the Zn base alloys tested because the secondary phases are too small to be related to the nucleation of pits using MEB with EDAX analysis as can be seen in Fig. 8. The last possibility for a non-statistic initiation of the attack could be the grain boundaries. This was tested using the cast Zn, whose big grains provided very clear conclusions, which were in a previous paper also informed for steel<sup>1</sup>. In the next photographs the aspect of samples submitted to the marine pollutant do not show any preferential attack at grain boundaries.

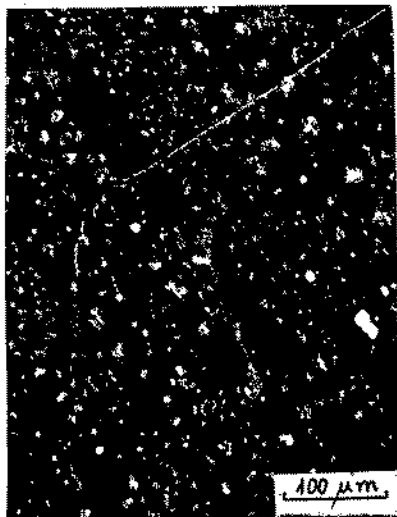
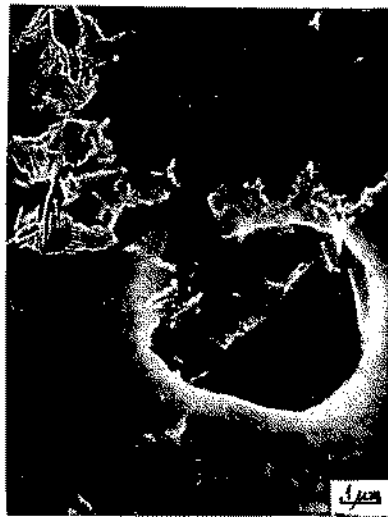


Fig. 7: a) Cast Zn exposed in salt spray box.



b) Steel exposed 3 days at the marine site.

Also the propagation of the attack produces very similar structures to those observed for steels<sup>4</sup>, evidencing the existence of preferential penetration sites as can be seen in the next figures.



a) Skyward phase



b) Groundward phase

Fig. 8: Cross section of the rolled Zn after 2 years exposition at the atmosphere.

The second micrograph shows a more intense localized attack than the first one due to the longer times of wetness of this phase than the skyward one.

Among the differences appreciated in the corrosion of the distinct alloys, the most remarkable is the lower aggressivity of the marine environment on Zn than on Fe ones, (Fig. 1). The greater protectiveness of the corrosion products film for-

med on Zn than on Fe in this medium could be attributed to its chemical composition. In the first one the pollutant is captured in the protective film while the non-protective FeOOH does not inhibit the negative effect of the  $\text{Cl}^-$ , which accumulates in the bottom of the pits in the steel. This had been verified by EPMA<sup>4</sup> and reproduced in the following photograph:



Fig. 9: EPMA of Cl in a cross section of a steel after natural exposition during 30 months<sup>4</sup>.

From Fig. 1 it is also evident the distinct law of change with time of the corrosion rates. According to equations (1) and (2) it decreases as the time of exposition increases, for steels, being time independent for Zn alloys.

The morphologies of the attacks nucleated on the alloys surfaces in the natural marine environment are well reproduced in the salt spray box tests. This is useful for the analysis of the influence of composition or metallurgical changes in the alloys. The results thus obtained are easily reproducible because of the fixed environmental variables in the box, and are not modified by the fluctuations in the climate of a test site. Even when the concentration of the  $\text{Cl}^-$  ion be different its qualitative effect on the selectivity of the areas and morphology of the attack can be established. For the corrosion products on the contrary, the great differences in morphology observed indicates that the film growth is highly dependent of the climatic variables. They determine, as much as the pollutant, its protective properties.

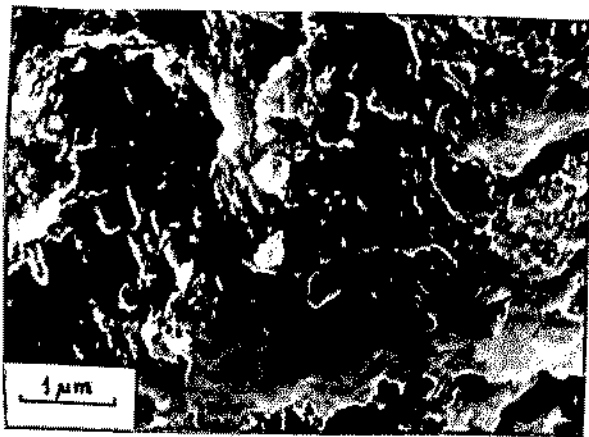
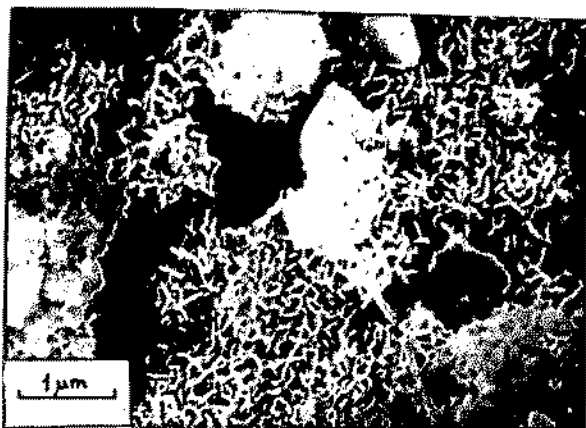
A good correlation was observed among the susceptibility to localized attack of both metallic alloys and the sites where  $\text{Cl}^-$  accumulates.

The compactness of the corrosion products film, limiting the migration of the aggressive species, determines the morphology and kinetics of propagation of the attack. For plain C steels in the marine environment the accumulation of the pollutant at

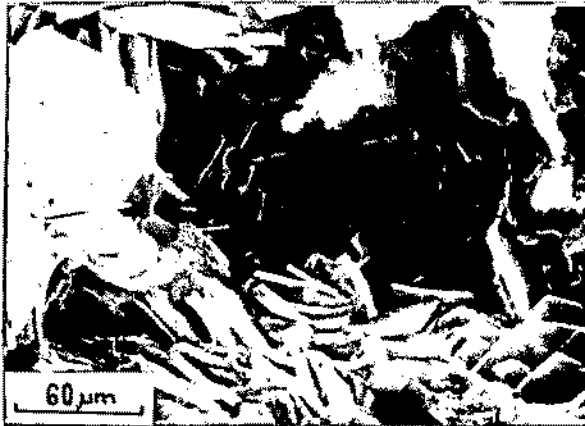
the bottom of the pits, shown in Fig. 9, maintain them depassivated promoting the penetration at the initial sites. The more protective films grown on Zn base alloys do not completely inhibit the  $Cl^-$  migration. It was also found at the bottom of pits but in much lower amounts than in steels.

The time of wetness has lower effect on the Zn alloy than on the steel. Test samples of the last show a remarkable difference between the side near the coast and the opposite one. The predominant winds promote an accelerated drying on the sea side, producing an almost double reduction in thickness on the opposite side.

The aspect of the corrosion products formed in the marine site on the tested Fe and Zn alloys is shown in the next photographs.



a) A 52 steel after 2 years exposition



b) Rolled Zn alloy 2.5 years exposition.

Fig. 10: MEB of the corrosion products of the alloys.

More packed structures on the steel do not produce by themselves more protective rusts than the grown on the Zn alloy.

After pickling the samples evidenced the localized, chrysta llographic attacks on the steel, that can be seen in the next figure.

In the Zn alloy the pickling solution does not allow the analogous observation because it produces a too much heavy attack having a leveler effect.

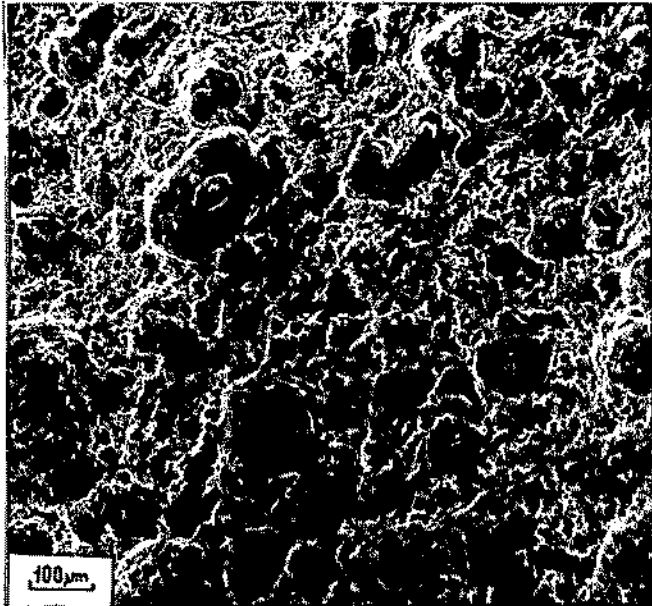
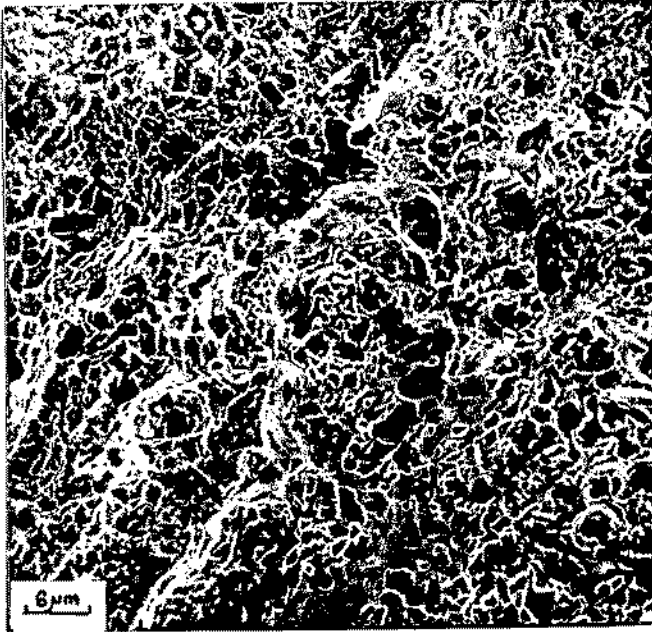


Fig. 11 MEB of the steel shown in Fig. 10, after pickling.



REFERENCES

1. B. M. Rosales and E. S. Ayllón, Atmospheric Corrosion, W.H. Ailor Ed., J. Wiley, New York, Atmospheric Marine Corrosion of Structural Steels, chap. 29, (1982).
2. B. M. Rosales and E. S. Ayllón, Atmospheric Corrosion, W.H. Ailor Ed., J. Wiley, New York, Controlling Factors in the Atmospheric Corrosion of Steel, chap. 35. (1982).
3. B. M. Rosales and E. S. Ayllón, Atmospheric Corrosion, W.H. Ailor Ed., J. Wiley, New York, Urban-industrial Atmospheric Corrosion of a Weathering Steel, chap. 28, (1982).
4. B. M. Rosales, E. S. Ayllón, R. T. Bonard, S. L. Granese and J. L. Ikehara. Factors Affecting the Atmospheric Corrosion of Steel, 8th. International Congress on Metallic Corrosion, Mainz, Germany, p. 317-322, (1981).
5. M. Janik-Czachor and A. Szummer, Effect of Chemical Heterogeneity within the Metal Phase on the Stability of the Passivating Film on Iron Alloys, Proceedings of the 5th. Int. Symposium on Passivity Bombannes, France, p. 547-554, (1983).
6. K. Hashimoto, Supplement to Passivation of Amorphous Metals Idem previous, p. 247-252.
7. P. Keller, Werkstoffe Korros. 22, 32, (1971).
8. J. E. Hiller, Werkstoffe Korros. 17, 943, (1966).
9. L. G. Sillén, Svensk Kem. Tidskr. 75, 161, (1963).
10. K. Barton, T. D. Cuc y S. Bartonova, Werkstoffe Korros. 28, 17, (1977).
11. V. R. Evans, C. A. J. Taylor, Corr. Science, 12, p. 227-246 (1972).
12. W. Feitknecht, Principes Chimiques et Termochimiques de la corrosion des Metaux dans une Solution Aqueuse, Démonstrés par l'exemple du Zinc, Metaux et corrosion, 23, p. 192-203, (1947).



## DURABILITY OF CONCRETE MARINE STRUCTURES

HAROLD ROPER

ASSOCIATE PROFESSOR  
SCHOOL OF CIVIL AND MINING ENGINEERING  
THE UNIVERSITY OF SYDNEY, AUSTRALIA

**ABSTRACT:** The durability problems of reinforced and prestressed concrete marine structures are considered. Degradation processes include chemical attack, physical erosion, freeze-thaw damage and fatigue effects on the concrete and corrosion and fatigue of the reinforcement. Methods to overcome or minimise these phenomena are discussed.

Les problèmes de durabilité des structures marines de béton armé et précontraint sont jugés être des processus de dégradation comme l'attaque chimique, l'érosion physique, le dommage de l'eau glacée, les effets de la fatigue sur le béton et la corrosion et la fatigue de l'armature. Plusieurs méthodes sont considérées pour surmonter ou minimiser ces phénomènes.

### 1 INTRODUCTION

The properties of concrete required in marine structures are adequate strength, long-term durability and appropriate economy. As well the concrete must provide physical and chemical conditions under which steel reinforcement either remains passive or corrodes sufficiently slowly not to cause distress during the design life period. These concrete properties are achieved by the selection of suitable materials, the choice of mix proportions and the use of proper methods of placement and curing. The three aspects interact, as mix proportions and placement methods depend on material selection.

## 2 GENERAL DURABILITY SURVEYS

Browne and Domone (1) have discussed a series of structures which include ships and barges, built between 1918 and 1944, harbours and jetties built from the 1890's but particularly in the 1920's and '30s and the Nab defence tower in the Solent, a 55 year old structure in sound condition, which is one of the earliest examples of an offshore structure, built onshore, floated to its final location and fixed to the sea-bed by its dead weight only. In recent years this method has been successfully used for lighthouses, loading berth and oil rig construction.

Bury and Domone (2) carried out surveys of pile and beam types of structures up to 70 years old, and Mulberry Harbour Units used in the Allied invasion of Normandy. They concluded that in general the structures had suffered only a limited degree of degradation which took the form principally of corrosion of reinforcement and spalling of the concrete cover. They suggest that no degradation has occurred in permanently immersed concrete, even in structures where severe corrosion occurred in the splash zone.

From actual measurements on the structures areas of corrosion and spalling were found to be associated with:

- (i) High positive e.m.f. [up to 300 mV relative to non-spalled areas compared to about 30mV in non-corroding structures (values relative to copper sulphate half cells)].
- (ii) Low concrete resistivity (about 3,000-5,000 ohm cm, c.f. 13,000 to 15,000 ohm cm for non-spalled areas).
- (iii) High chloride content (about 1.5% by weight of cement).
- (iv) Low cover, below 10 mm compared with normal design figures of at least 25 mm.

Mehta (3) discusses examples of concrete exposed for considerable periods to sea water in mild climates. The influences of materials types, richness of mix and workmanship were all shown to be of considerable importance to the durability or corrosion of such concretes.

Seki (4) discussed the results of field observations of the deterioration of plain concrete in Japan. One of the most interesting findings is the lack of durability of cold joints. The breakdown at such joints was generally severe, and could lead to significant problems.

Prestressed concrete, developed since the Second World War, has been successfully used for marine structures throughout the world, again with excellent durability. One of the most recent large successful structures was the Ekofisk oil storage tank, a prestressed concrete structure, which has shown this type of structure to be viable and economic for North Sea conditions. Current offshore oil production platforms for the North Sea have a design life of thirty years.

From such surveys it is concluded that the behaviour of concrete in seawater is significantly different in three different zones namely:

- (i) the zone above high-tide level, where build up of salts can occur in evaporative drying cycles and where an abundance of atmospheric oxygen is available;
- (ii) the inter-tidal zone, where the concrete is kept saturated but is subject to cyclic exposure to air and is subject to abrasion and attachment of some organisms;
- (iii) the totally submerged zone where oxygen availability is limited, and as depth increases, more rapid penetration of sea water into concrete is brought about by hydrostatic pressure

In zones (i) and (ii), world wide surveys show that the greatest problems of durability arise from the corrosion of reinforcing steel rather than from chemical or physical disintegration of the concrete (1; 5). Disintegration of concrete per se, if it does occur, is much influenced by the ambient temperatures. As for zone (iii) there is little evidence of degradation in permanently immersed concrete. However there always exists the possibility that in this zone embedded steel may be losing metal to form either low oxygen compounds which are less liable to disrupt the concrete, or mobile products which appear elsewhere.

### 3 CHEMICAL ATTACK ON CONCRETE BY SEA WATER

When chemical attack does occur in sea water the influence of high water cement ratios and high permeability often due to low contents of cementitious phases is often noted. The precise reactions and phases formed may be disputed, but generally it is agreed that magnesium sulphate and carbon dioxide play important roles.

Sea water contains significant amounts of magnesium sulphate. Biczok (6) quotes a figure of 2800 mg/l

as the average concentration of  $\text{SO}_4^{2-}$  ions in Atlantic ocean water, a figure which according to the U.S. Bureau of Reclamation, puts such water into the 'severe' range as far as sulphate attack is concerned (7). Two mechanisms of sulphate attack can occur with this level of sulphate concentration. In the splash zone the salt concentrations can be higher than in the surrounding sea water. The use of sulphate resisting cement, low in  $\text{C}_3\text{A}$ , does not necessarily therefore produce structures free of disintegration. The increased protection to steel observed when high  $\text{C}_3\text{A}$  contents are used should also be noted. It is difficult to generalise on the resistance of different cements to sea water attack. The resistance is related to the mineralogical composition. The differences are due to the presence of sulphates other than  $\text{CaSO}_4$ , and to the presence of foreign ions in the basic compounds (8). Two forms of  $\text{C}_2\text{S}$  exist ( $\alpha, \beta$ ) with the  $\alpha$ -form containing alkali in solid solution and two forms of  $\text{C}_3\text{A}$  (cubic and orthorhombic) again with the orthorhombic containing alkali. The cubic form has been found to have greater resistance to attack by magnesium sulphates. Cement fineness can also affect resistance. In coarsely ground cement, encased  $\text{C}_3\text{A}$  in grains can react with sea water to produce ettringite at a stage when the cement paste has already hardened. Local stress and cracking then results.

Mehta (3) has discussed the reactions which he believes occur due to the action of magnesium salts on cementitious minerals. Also important are the reactions related to the presence of  $\text{CO}_2$  in sea water. In both cases the products lead to strength losses of their paste. Alkali-aggregate reaction may also be enhanced in sea water (9).

Blast furnace slag cements have been found generally to improve the resistance of concrete to sea water attack. To achieve this improvement, a considerable proportion of slag is required. In France cements containing more than 65% slag are admitted by the Permanent Commission on Hydraulic Binders and Admixtures (COPLA) as marine cements. Alternatively pozzolans may be used to improve resistance, but not all pozzolans are equally effective.

It should be stressed that if sound impermeable concrete with adequate cement content is properly mixed and placed durable structures over design lifetimes can be produced. A water-cement ratio of less than 0.45 and preferably less than 0.40 and a cement content of  $390 \text{ kg m}^{-3}$  are recommended by Gerwick (10) to prevent attack from sea water.

#### 4                    PHYSICAL EROSION OF CONCRETE

Sea waves present problems of a physical nature in that their continual action gives rise to attrition of concrete which may lead to cavitation and erosion.

Erosion may be due to solid particles carried by water. Pits develop from implosion of cavities in fast flowing water. Size, shape, quantity and hardness of carried particles will influence the rate of erosion as will the velocity of flow. Concrete with large aggregate erodes less than a mortar of similar strength, whilst hard aggregate increases the abrasion resistance.

Cavities formed by pressure changes cause pitting when they collapse on entering areas of higher pressure. The rapid entry of water into these spaces produces great pressures which is most significant in eddies. The surface of the concrete as a result will be irregular and pitted in contrast with the smoothly worn surface eroded by water-borne solids. The rate of damage increases after an initial period where damage is slight.

The ACI Committee 210 recommends under cavitation conditions that the mix should be designed such that  $f_c > 40$  MPa and a good bond obtained to avoid plucking out of large aggregate. The quality of the concrete at or near the surface provides the erosion resistance - initially it depends on the quality of the matrix, but should this be eroded away, the nature of coarse aggregate assumes importance. The coarse aggregate should be limited to 20 mm in size.

#### 5                    FREEZE-THAW AND AIR ENTRAINMENT

Air entrainment offers not only advantages in terms of durability under freeze-thaw conditions but furthermore improves the workability of the mix, and placement of concrete. This indirectly improves the durability as well, since better compaction lessens the possibility of differential cells resulting from segregation and bleeding, and slows the formation of a laitance layer.

From the viewpoint of marine structures the most important change in properties brought about by air entrainment is that the permeability of concrete to aqueous liquids is reduced. The permeability (K) affects the rate at which salts and oxygen in the environment penetrate into the concrete, and also the rate at which materials are leached from the cementitious phase. In the actual structure compaction of the concrete is a most important factor and may result in a difference of  $10^5$  times between site and laboratory compacted concrete.

It is now generally accepted that concrete under repeated loadings does not have an endurance-limit up to 10 million cycles. Furthermore to date the greatest number of cycles that have been applied to concrete in research is about 20 million.

Hsu (11) points out that research projects on fatigue of concrete have been confined to a narrow range of cycles, thus limiting the use of rules and equations. Studies in the range of low cycle fatigue in seismic research cannot be extrapolated to the high cycle range, as there is no continuity between them. Based on tests in the high cycle region it has been suggested by some investigators (12 to 15), that the fatigue strength is independent of the rate of loading. Others (16, 17) who have made tests in the low cycle region have found loading rate to have a strong influence on strength. Awad and Hilsdorf (16) furthermore found that the fatigue strength in the low-cycle region was strongly time dependent.

With respect to offshore concretes Waagaard (18) quotes Dutch work which shows that submerged concrete has a shorter fatigue life than air dried concrete, the longer the storage time in water, the shorter is the fatigue life (effect of saturation), and that the frequency affects the fatigue life, the lower the frequency, the shorter the fatigue life. Such information leads to further complications in design considerations. The relationship between fatigue strength of concrete  $S$  and the number of cycles of repeated loading,  $N$ , are given in many design codes. Fig. 1 after Hallam (19) is a sample  $S$ - $N$  curve for concrete given in a document intended to provide members of the CIRIA underwater engineering group with guidance on the dynamic design of fixed structures subject to wave and current action. It is stated that "Fatigue problems have rarely been encountered with concrete structures.  $S$ - $N$  curves show a long fatigue life for concrete even when subjected to large stress ranges. It is likely, for the stress levels worked to in structural concrete design, that the fatigue life of most marine concrete structures will exceed their design life. However, it is recommended that a fatigue check be performed for all dynamically loaded structures."

In a structure properly designed and constructed for the appropriate conditions of use, there should be no problem of steel corrosion in concrete within the design life. Unfortunately, these highly desirable conditions are not always achieved.



## 7.1 Corrosion Mechanisms in Marine Structures

Browne and Geoghegan (20) summarise the initiation and controlling factors of splash zone corrosion as the following:

- (1) Chloride levels exceeding 0.4% by weight of the cement.
- (2) Permeability and concrete cover to the reinforcement (e.g. 50 mm cover, high permeability (w/c 0.7); corrosion activation in 6 months).
- (3) Moisture content of the concrete affecting both the resistivity and oxygen permeability, and hence the time to spall, (e.g. 25 mm cover, high permeability, partially dry:spalling in 2½ years).

Gjorv (21) states that observations indicate that detrimental amounts of chloride ions are capable of penetrating into high quality concrete beyond what would be a practical limit for the thickness of a concrete cover. Hence for concrete structures in ocean environments it is necessary to look for preventative measures in addition to good concrete cover. He suggests that therefore in addition to taking preventative measures during design and construction, techniques should also be applied in order to periodically monitor the presence or absence of steel corrosion before it becomes too late.

Probably the most comprehensive series of papers on the topic of steel corrosion in concrete, is available in a recent publication of the American Concrete Institute to which the reader is referred (22).

## 8 FATIGUE AND CORROSION FATIGUE OF REINFORCED CONCRETE

During the last few years there has been an intensification of interest in the fatigue behaviour of steel reinforcement in concrete structures. Although fatigue has not proved to be a problem to date, loading cycles and corrosive conditions are becoming increasingly severe so that the margin of reserve strength is progressively being reduced, (23). Fatigue endurance of reinforcement can be influenced by type of steel, geometry and size of bars, nature of the loading cycle, welding and presence of corrosive liquids. A recent review paper, chiefly related to highway bridges has been presented by Tilly (24).

Data available on the life of offshore structural concrete has been presented by Browne and Domone (25). They state that in composite reinforced or prestressed concrete sections, the levels of stress in the steel are a greater percentage of the ultimate stress than for

concrete and it is therefore generally sufficient to consider the fatigue properties of the steel as controlling the fatigue performance of the structural element. Gerwick and Venuti (26) suggest that as opposed to bridges, typical concrete sea structures are more influenced by low-cycle high amplitude fatigue than by high cumulative usage. They state that when concrete is cracked and then is cycled repeatedly into the "crack re-opening" tensile range, the steel is subjected to significantly increased stress ranges. As a result bond is progressively lost particularly along smooth bars, strand and wire. Adequate fatigue capacity of the steel must therefore be assured in design for such conditions.

With regard to crack propagation in steel, two models, which have been proposed to account for the enhanced crack growth rates of carbon steel in sea water compared to air, are illustrated schematically in Fig.2. The anodic dissolution model (Fig. 2a) is based essentially on the thesis that the increment of crack extension on each stress cycle is enhanced, without change of mechanism, in a corrosive environment like sea water due to dissolution of the yielding metal at the crack tip. On the other hand, the hydrogen embrittlement model (Fig.2b) involves postulating that hydrogen, produced by the cathodic reduction reaction at or near the crack tip and possibly favoured by low pH in the crack, promotes increased crack growth rates either by reducing the cohesive energy at the crack tip and embrittling it - possibly by causing decohesion at carbides or other inclusions.

At the University of Sydney an extensive test program is underway to assess the influence of bar properties on corrosion fatigue in sea water at 6.7 Hz. The beam dimensions are given in Fig. 3, the test setup in Fig.4, and some results in Figs. 5, 6 and 7. Coated bars have been extensively tested, and it appears that whereas nickel coating has little effect on the fatigue properties, galvanizing plays an important role in increasing the fatigue endurance of such bar. The interested reader is referred to a series of papers by Roper et al (27, 28). In the course of this work it was found that epoxy coated bars may perform less than satisfactorily when subjected to fatigue loadings in the presence of sea water.

The effects of slower cycle rates which would be encountered by a marine structure, together with the effects of concrete crack blocking by continued hydration or even reaction products remain as yet of interest. It appears that in certain cases crack blocking may reduce the stress range in the steel to such low levels as to

dispel any fears of crack propagation. However in other situations such blocking may not be effective due to the geometry of the structural member. For a discussion of the crack blocking effects the reader is referred to papers by Arthur et al (29, 30).

## 9 CORROSION OF PRESTRESSING STEELS IN MARINE STRUCTURES

Discussing the durability of prestressed ocean structures Gerwick (31) suggests that the disruption of concrete may take several forms, and includes amongst these corrosion of prestressing tendons and tendon anchorages. He states that despite all real and potentially adverse factors, prestressed concrete is inherently extremely durable in the sea water environment and has given outstanding performance in sea structures ranging from the tropical environment to the Arctic. Durability and freedom from maintenance are prime reasons for specifying prestressed concrete for ocean structures.

In both ordinary reinforcement and prestressed tendons, a thin layer of general corrosion product is acceptable. The development of very local cells, leading to pitting, hence reduction of area is particularly worrying in prestressed tendons. The development of pits may be due to bad storage conditions of tendons prior to installation as described by Fountain et al (32), or to the corrosive conditions active in service as described by Phillips (33) for wires from the Geehi aqueduct. In both cases the mechanism can be described as in Fig.8. It should be noted that at the pit, the site of corrosion, the area is depleted in oxygen and the process is autocatalytic in nature. From the first reference it is apparent that although corrosion inhibitors may be useful in certain cases, the particular one chosen leads in part to the problem, and the authors suggest that strongly hydrophilic inhibitors, particularly sulphates, should not be used for protection of tendons prior to installation. In both the first and second cases the influence of the structure of the steel is shown to be important. In the first paper it is noted that in the case of the Wylfa pits, growth is to a limiting pit depth, after which continued growth is in a direction parallel to the axis of the wire. In the second it is stated that "slight corrosion-pitting, to a maximum depth of 0.05 mm was observed, as were cracks which originated at the inner surface of the core winding where rust deposits were apparent. The cracks were at right angles to the wire surface".

Pitting is the expected corrosion phenomenon for pre-stressing tendons if chlorides do gain access to the

steel in marine structures. In this regard it is worthwhile to consider Gjov's (21) statements on prestressing:

"Great efforts have been made in developing protective methods for arresting steel corrosion in concrete. However, a recent survey of literature indicates that at the time being, there is no method generally applicable and economically reasonable. A number of research laboratories are still engaged on the problem. The efforts are mainly concentrated on cathodic protection, either in the form of metallic coatings (zinc and cadmium) or in the form of impressed polarization from an external generator."

Although a somewhat depressing outlook is taken, Gjov does not suggest the cessation of use of the material for marine structures but exhorts the concrete technologist to seek ways to economically further protect and extend the life of such structures.

At Sydney University, work is being pursued to assess the protection capabilities of zinc sheeting cast in mortar, as an encapsulating, expendable anode in a marine environment. This system is being monitored with respect to potentials, current flow and by visual assessment of corrosion phenomena. This procedure may lead to a technique of arresting corrosion in reinforced concrete structures after it has commenced.

#### 10 FATIGUE AND CORROSION FATIGUE OF PRESTRESSED CONCRETE

This topic is well covered in reports of the American Concrete Institute Committee 215 (34) and of the F.I.P. Commission on Concrete Sea Structures (35).

#### 11 FUTURE DEVELOPMENTS IN CORROSION CONTROL

Probably the three most important unfolding developments in corrosion control are the use of very low permeable concretes using superplasticisers, the use of nitrites as inhibitors and the cathodic protection techniques, all of which may eventually be used to improve durability of an already successful composite material.

#### REFERENCES

1. BROWNE, R. D. and DOMONE, P. L. J. - "The Long Term Performance of Concrete in the Marine Environment". Symposium on Offshore Structures, Inst. Civil Engineers, London, 1975.
2. BURY, M. R. C. and DOMONE, P. L. J. - "The Role of Research in the Design of Concrete Offshore."

- Structures". Sixth Annual Offshore Technology Conference, Texas, Paper No. OTC 1949., 1974.
3. MENTA, K. - "Durability of Concrete in Marine Environment - A Review". American Concrete Institute Publication SP-65, 1980.
  4. SEKI, H. - "Deterioration of Coastal Structures in Japan". American Concrete Institute, Special Publication 49, 1975.
  5. GJORV, O. E. - "Control of Steel Corrosion in Concrete Sea Structures". American Concrete Institute Publication SP-49, 1975, pp 1-9.
  6. BICZOK, I. - "Concrete Corrosion, Concrete Protection". Chemical Publishing Company, New York 1967, pp 178 and 353.
  7. U.S. BUREAU OF RECLAMATION - Concrete Manual, U.S. Dept. of the Interior, 8th Edition, 1975, p 11.
  8. REGOURD, M. - "Physico-chemical Studies of Cement Pastes, Mortars and Concretes Exposed to Sea Water". American Concrete Institute, Publication SP-65, 1980, pp 63-82.
  9. REGOURD, M., BISSERY, P., EVERS, G., HORNAIN, H. and MORTUREUX, B. - "Ettringite et Thaumasite dans le Mortier de la Digue du Large du Port de Cherbourg". Annales de l'Institut Technique du Batiment et des Travaux Publics. No. 358, 1978, pp 1-14.
  10. GERWICK, B. - "Practical Method of Ensuring Durability of Prestressed Concrete Ocean Structures". American Concrete Institute, Publication SP-47, 1975, pp 317-324.
  11. HSU, T. T. C. - "Fatigue of Plain Concrete". Journal American Concrete Institute, Proc. V78 No. 4, July-Aug 1981, pp 292-305.
  12. SPOONER, D. C. - "The Stress-strain Relationship for Hardened Cement Paste in Compression". Magazine of Concrete Research, Vol. 24, No.79, June 1972, pp 85-92.
  13. GRAF, O. and BRENNER, E. - "Versuche zur Ermittlung der Widerstandsfähigkeit von Beton gegen oftmals Wiederholte Druckbelastung". Deutscher Ausschuss für Eisenbeton, Bulletin No.76, 1934 (Part I); Bulletin No.83, 1936 (Part II).
  14. KESLER, C. E. - "Effect of Speed of Testing on Flexural Fatigue Strength of Plain Concrete". Proceedings, Highway Research Board V. 32, 1953, pp 251-258.

15. ASSIMACOPOULOS, B. M., WARMER, R. F. and EKBERG, C. E. - "High Speed Tests on Small Specimens of Plain Concrete". Journal of the Prestressed Concrete Institute. Vol.4, No.2, Sept. 1959, pp 53-70.
16. AWAD, M. E. and HILSDORF, H. K. - "Strength and Deformation Characteristics of Plain Concrete Subjected to High Repeated and Sustained Loads". Structural Research Series No. 373, Department of Civil Eng., University of Illinois, Urbana, February 1971.
17. SPARKS, P. R. and MENZIES, J. B. - "The Effect of Rate of Loading upon the Static and Fatigue Strengths of Plain Concrete in Compression". Magazine of Concrete Research (London), Vol.25, No.83, June 1973, pp 73-80.
18. WAAGAARD, K. - "Fatigue Strength Evaluation of Offshore Concrete Structures". American Concrete Institute Convention in Dallas. February 8-13, 1981.
19. HALLAM, M. G., HEAF, N. J. and WOOTTON, L. R. - "Dynamics of Marine Structures: Methods of Calculating the Dynamic Response of Fixed Structures subject to Wave and Current Action". Report UR 8, CIRIA Underwater Engineering Group. October 1978.
20. BROWNE, R. D. and GEOGHEGAN, M. P. - "The Corrosion of Concrete Marine Structures - The Present Situation". Soc. of Chemical Industry Symposium, Corrosion of Steel Reinforcement in Concrete Construction, London, Feb. 1978.
21. GJORV, O. E. - "Durability of Concrete Structures in the Ocean Environment". Proceedings of FIP Symposium Concrete Sea Structures, Tbilisi, Sept 1972, pp 141-147.
22. MALHOTRA, V. M. - Editor. - "Performance of Concrete in Marine Environment". Special Publication No. SP-65, American Concrete Institute, Detroit 1980. 640 pp.
23. THURLIMAN, B. - "Thurliman on Design". CIA News, Concrete Institute of Australia, Vol.6 No. 4, Dec. 1980.
24. TILLY, G. P. - "Fatigue of Steel Reinforcing Bars in Concrete: A Review". Fatigue of Engineering Materials and Structures, Vol.2, 1979, pp 251-268.
25. BROWNE, R. D. and DOMONE, P. L. - "Permeability and Fatigue Properties of Structural Marine Concrete at Continental Shelf Depths". Int. Conference on Underwater Construction Technology. University College, Cardiff, Wales. April 1975.

26. GERWICK, B. C. and VENUTI, W. J. - "High and Low Cycle Fatigue Behaviour of Prestressed Concrete in Offshore Structures". Trans. of the Society of Petroleum Engineers. Vol. 269, Aug. 1980, pp 304-310.
27. ROPER, H. and HETHERINGTON, G. B. - "Fatigue of Reinforced Concrete in Air, Chloride Solution and Sea Water". American Concrete Institute 1982, SP-75, pp 307-331.
28. ROPER, H. - "Reinforcement for Concrete Structures Subject to Fatigue". International Association for Bridge and Structural Engineering, Colloquium on Fatigue of Steel and Concrete Structures, Lausanne, Switzerland. March 1982, pp 239-246.
29. ARTHUR, P. D., EARL, J. C. and HODGKIESS, T. - "Fatigue of Reinforced Concrete in Seawater". Concrete, May 1979.
30. ARTHUR, P. D., EARL, J. C. and HODGKIESS, T. - "Corrosion Fatigue in Concrete for Marine Applications". Paper presented at the 1980 Fall Convention, ACI, San Juan, Puerto Rico.
31. GERWICK, B. - "Practical Method of Ensuring Durability of Prestressed Concrete Ocean Structures". American Concrete Institute, Special Publication 47, 1975.
32. FOUNTAIN, J. J., BLACKIE, D. and MORTIMER, D. - "Corrosion Protection of Prestressing Tendons". Int. Conf. on Experience in the Design, Construction and Operation of Prestressed Concrete Pressure Vessels and Containment for Nuclear Reactors. Institution of Mechanical Engineers (University of York), England, 1975.
33. PHILLIPS, E. - "Survey of Corrosion of Prestressing Steel in Concrete Water-retaining Structures". Australian Water Resources Council, Technical Paper No. 9, 1975.
34. AMERICAN CONCRETE INSTITUTE COMMITTEE 215 - "Consideration for the Design of Concrete Structures Subjected to Fatigue Loading". Journal of the American Concrete Institute Proceedings Vol. 71, No.3, March 1974, pp 97-121.
35. FIP COMMISSION ON CONCRETE SEA STRUCTURES - "Recommendations for the Design and Construction of Concrete Sea Structures". Federation Internationale de la Precontrainte, Wexham Springs, Slough, Nov. 1974.

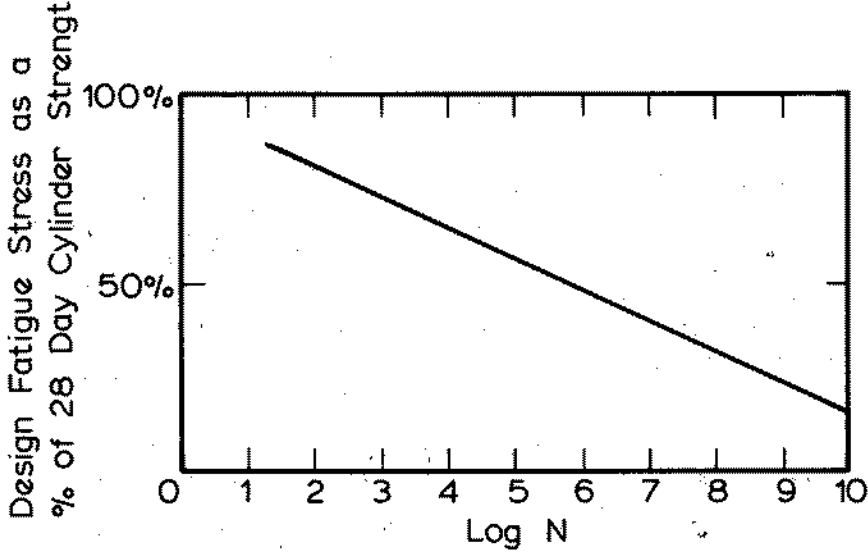


FIG.1 SAMPLE S-N CURVE FOR CONCRETE

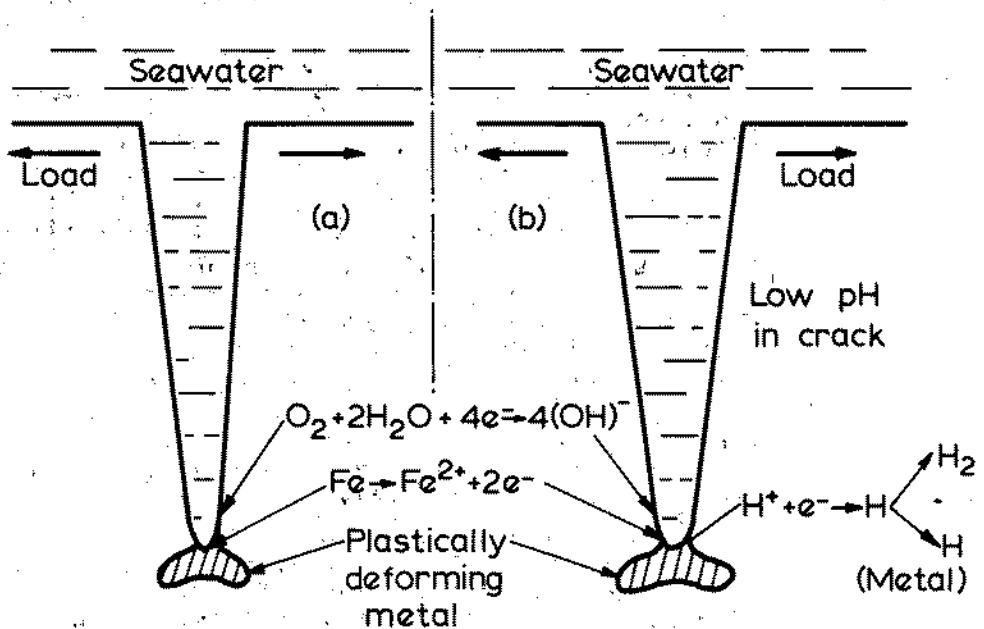
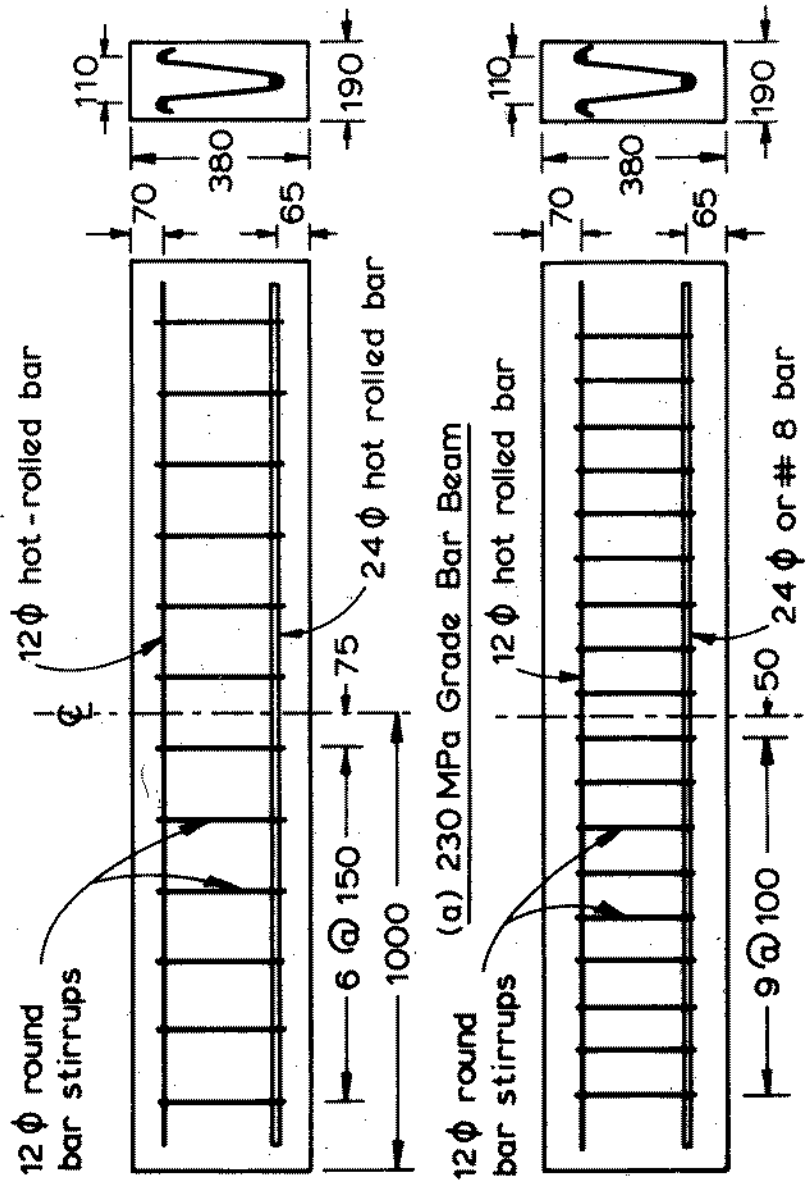


FIG.2 SCHEMATIC REPRESENTATION OF PROCESSES OCCURING DURING FATIGUE CRACK PROPAGATION IN SEAWATER





(a) 230 MPa Grade Bar Beam  
(b) 410 and 413 Grade Bar Beam

FIG.3 BEAM DIMENSIONS AND REINFORCEMENT

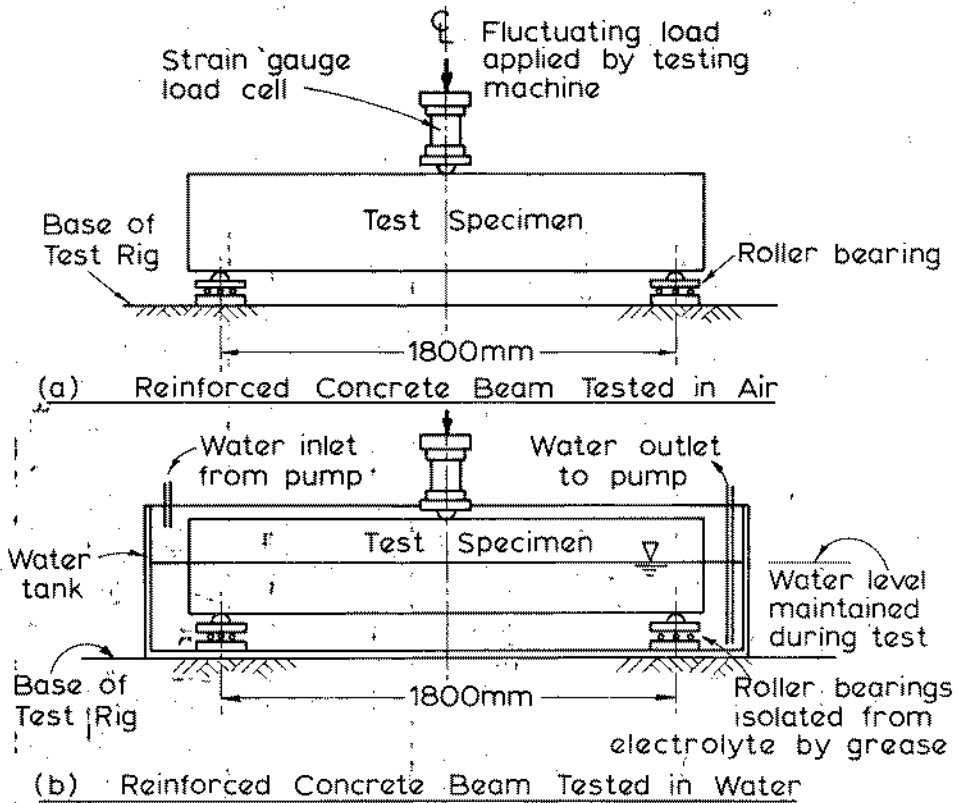
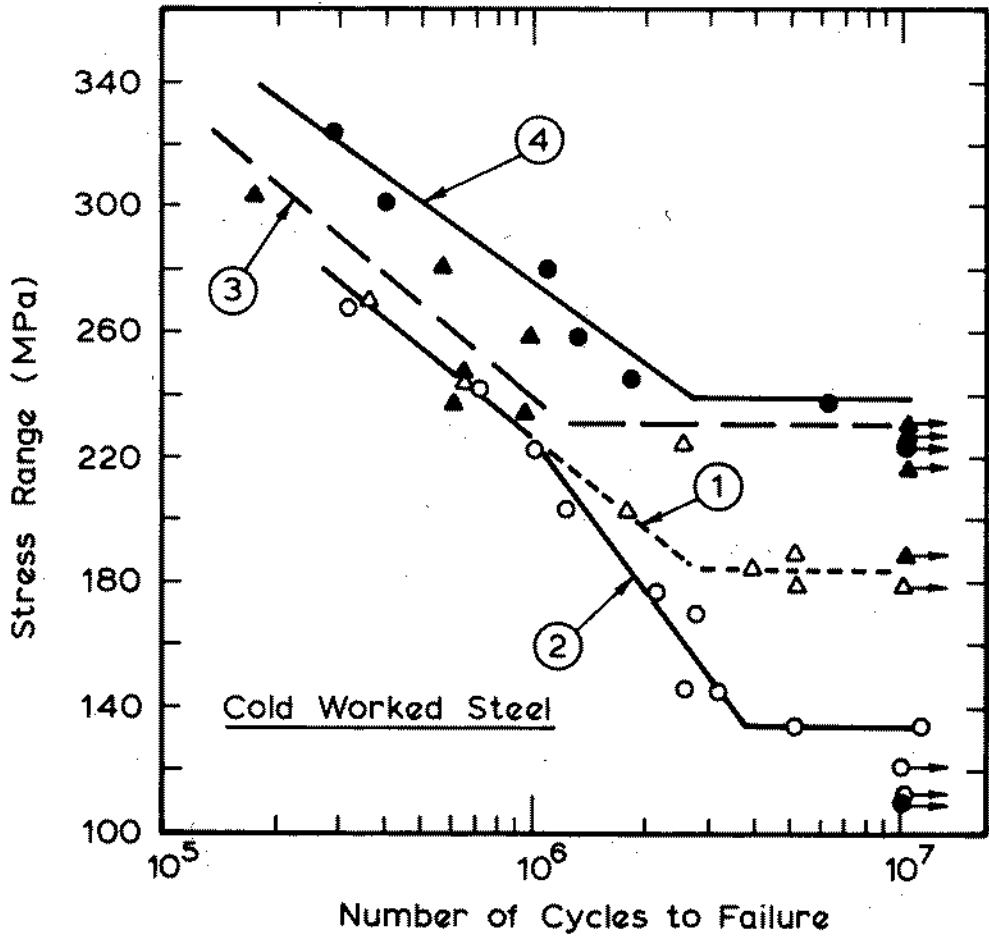
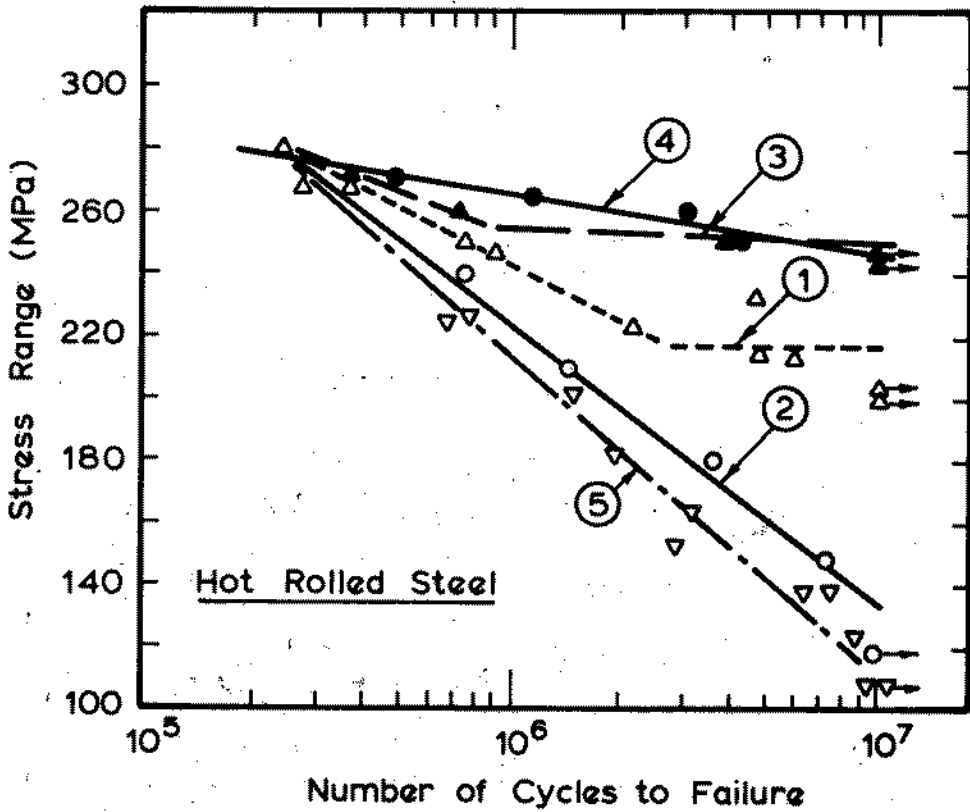


FIG. 4 TEST LAYOUT OF FATIGUE SPECIMENS



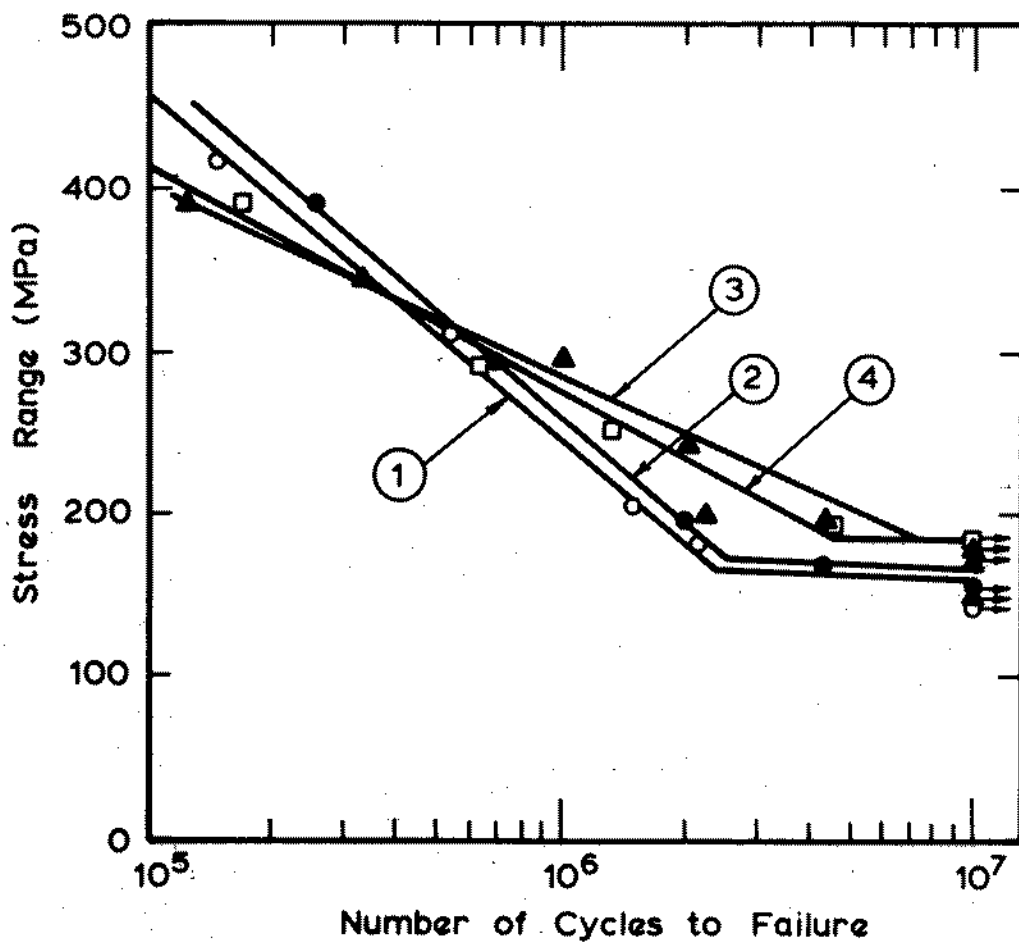
|   |   | Coating    | Environment |
|---|---|------------|-------------|
| △ | 1 | None       | Air         |
| ○ | 2 | None       | Sea Water   |
| ▲ | 3 | Galvanized | Air         |
| ● | 4 | Galvanized | Sea Water   |

**FIG.5 S-N CURVES FOR BEAMS**



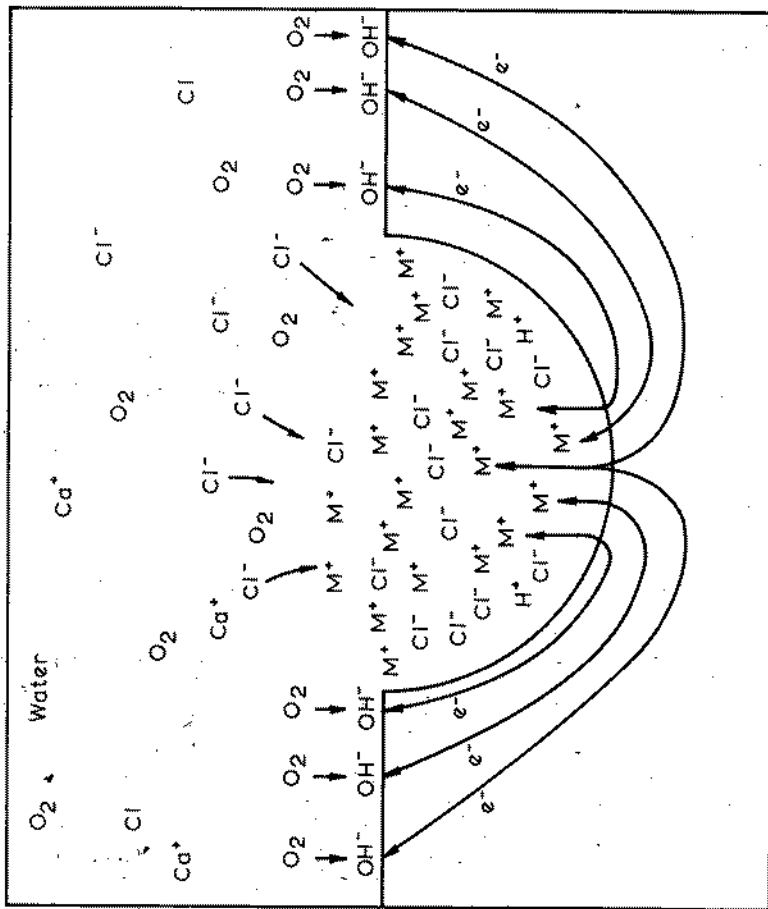
|   |   | Coating    | Environment   |
|---|---|------------|---------------|
| △ | 1 | None       | Air           |
| ○ | 2 | None       | Sea Water     |
| ▲ | 3 | Galvanized | Air           |
| ● | 4 | Galvanized | Sea Water     |
| ▽ | 5 | None       | NaCl Solution |

FIG. 6 S-N CURVES FOR BEAMS



|   |   | Coating     | Environment |
|---|---|-------------|-------------|
| ○ | 1 | None        | Sea Water   |
| ● | 2 | Nickel Clad | Sea Water   |
| ▲ | 3 | Epoxy       | Sea Water   |
| □ | 4 | Galvanized  | Sea Water   |

FIG.7 S-N CURVES FOR BEAMS-AMERICAN BAR



**FIG. 8** PITTING CORROSION OF A METAL IN A SALT SOLUTION. Note the development of the oxygen concentration cell pitting. The pitting process tends to be autocatalytic in nature because, as the pit grows, the region formed is depleted of oxygen, leading to an increasing corrosion rate.

MATERIALS SELECTION FOR MARINE INSTRUMENTS  
AND ALLEVIATION OF CORROSION PROBLEMS

Chen Jian  
Institute of Ocean Technology, NBO  
Tianjin, China

ABSTRACT

A brief discussion is presented in the paper on materials selections, which is of prime importance to the reliable operation of marine instruments. In an attempt to choose corrosion resistant materials, sea immersion tests were conducted in the waters off Qingdao and Xiamen for periods ranging from three months to three years. Results of these tests are presented. Comparisons were performed between LY12 aluminum alloy and 1Cr18Ni9Ti stainless steel and results show that the former is more resistant to seawater attack. Comparisons between 3J53 constant elastic materials and niobium-base constant elastic alloy show that 3J53 is susceptible to corrosion while niobium-base alloy experienced little weight loss after exposure to seawater for a period of 3 years. Methods for alleviating corrosion problems through cathodic protection and application of coating compounds are also described in this paper and examples are provided.

RESUME

Nous présentons ici une discussion brève concernant la sélection des matériaux, qui est d'une grande importance relative à l'opération sûre de sélection des instruments marins. Dans ce but de sélectionner des matériaux résistants à la corrosion nous avons effectué des tests d'immersion dans l'eau de mer de Qingdao et de Xiamen de 3 mois à 3 ans. Nous présentons les résultats de ces tests. Les comparaisons sont faites entre l'alliage de l'aluminium LY12 et l'acier inoxydable 1Cr18Ni9Ti et les résultats ont montré que le premier est plus résistant contre l'attaque de l'eau de mer. Les comparaisons qui ont été réalisées entre les matériaux élastiques constant 3J53 et les alliages élastique "constant" à base de niobium montrent que 3J53 est susceptible à la corrosion alors que l'alliage à base de niobium montre une légère perte de poids après exposition à l'eau de mer et cela pendant 3 ans. Dans cette communication nous décrivons également des méthodes pour alléger les problèmes de la corrosion pendant la protection cathodique et pour appliquer des revêtements et nous donnons des exemples correspondants.

## INTRODUCTION

Marine instruments are subject to corrosion when exposed to seawater. Great attention should be paid to the selection of materials for the housings and attachments of instruments for marine application, and many factors should be considered, including corrosion resistance, availability, cost and physical and mechanical properties. Selection criteria vary with needs. Materials for ship-board instruments should be of low specific gravity because of handling problems and those with compass need non-magnetic housings and some require constant elastic materials.

For the purpose of corrosion alleviation, protective coats are commonly used and to instruments designed for long-term operation in the sea, sacrificial anodes are often attached so as to restrict both local and uniform attacks.

Full immersion panel tests and in-situ tests on instruments suspended from test units were carried out in an attempt to select corrosion resistant materials.

### SELECTION OF MATERIALS FOR PRESSURE HOUSINGS OF MARINE INSTRUMENTS

The most common oceanographic measurements include temperature, salinity, depth, current direction and speed, wave, DO and pH, with which the periods of instruments' exposure to marine environments vary, ranging from days to weeks or years and the sites for instrument deployment change, some on the surface in the coastal waters and some in the deep waters hundreds or thousands of meters deep below surface. In order to be compatible to the hostile environments, instruments should be made of materials



resistant to corrosion and to high pressure and therefore the materials selected should provide the combination of good corrosion resistance performance and high strength. Non-metals can meet the corrosion requirement but they have poor strength and fabricability, thus resulting in undersized dimensions of the housing. In some cases, instruments for shallow water application can be made of plastic materials with great strength, but so far no suitable non-metal materials for the construction of instruments for deep water application have been developed. As a result, metal materials become the first choice.

The commonly-used metal materials are apt to electrical-chemical corrosion. Thus corrosion resistance is the first consideration in selecting materials for marine service. In addition, many other factors, such as cost, specific gravity, magnetism and the specific requirements of various instruments should be taken into account. These factors make aluminum alloy, carbon steel and stainless steel the most acceptable ones. Aluminum alloy has moderate or high strength and is non-magnetic and its corrosion resistance to seawater can be greatly enhanced by anodic oxidation. These performances make aluminum alloy the most popular materials. The advantages of carbon steel over aluminum alloy is low cost and good weldability, but it is of higher specific gravity and susceptible to formation of rust film. It is rarely used for shipboard instruments. Stainless steel is suitable for some kind of devices such as water sampler, which is designed to operate in the sea intermittently for several hours each time and can be rinsed with freshwater after recovery from the water.

Carbon steel is susceptible to uniform attack. If an annual corrosion rate of less than 0.13mm and an annual pitting depth of 1.02 mm are considered in addition to

corrosion allowance when instruments are designed, no perforation will occur and reliable operation can be maintained during the designed life time.

Aluminum alloy and stainless steel are apt to suffer local attack such as pitting corrosion and crevice corrosion. Those corrossions are more harmful than uniform attack. Some local pits or holes will lead to the leakage of the housing and cause complete failure. Therefore in-situ tests are necessary for the selected materials and even the processed and machined housings to gain information on their corrosion resistance.

Aluminum alloys are categorized into Al-Mg series, Al-Cu series and Al-Zn series, etc. Al-Mg series, having good resistance to seawater corrosion but poor strength, are not suitable for construction of housings for operation in the deep ocean where great pressure exists. Because of the addition of 3% -5% Cu, the tensile strength of Al-Cu series aluminum alloy has been significantly increased but corrosion resistance decreased. LY12 is one of the most commonly used alloys. Al-Zn series aluminum alloy is superior to Al-Cu in terms of strength and corrosion resistivity, but has not found wide application because it is limited in sizes and forms.

1Cr18Ni9Ti is one of the stainless steels widely used. For comparative purpose between LY12 aluminum alloy and 1Cr18Ni9Ti stainless steel, full immersion tests were conducted by Xiamen Laboratory, China Ships Company, in Xiamen Harbor between June 10, 1982 and November 4, 1982, when surface temperature there ranged from 12.0°C to 29.1°C and salinity from 17.3‰ to 29.7‰. Results are given in Table 1.

Panels of the two materials stated above were tested under the same conditions, by suspending from the same

test unit and immersing in the same area. Results of the two panels were not identical, demonstrating that Al-Cu alloy is superior to 1Cr18Ni9Ti in terms of corrosion resistance. These two materials are commercially available in a variety of forms and sizes and thus have found wide acceptance. However, tests indicate that LY12 is more preferable because of its low specific gravity and low cost.

Some stainless steels have been developed to provide good combination of corrosion resistance and strength. For example, ultra low carbon stainless steel 00Cr20Ni125-Mo5N was exposed for a period of three years in the waters off Zhanjing and very slight corrosion was observed on the panels. This alloy has overall desired performances but is limited in sizes and forms, and also very expensive.

Table 1. Corrosion Comparison of Panels  
Immersed in Xiamen Harbor

| Panel No.       | Compositions  | Thick-ness | Exposure (day) | Corrosion rate        | Maximum pitting depth |
|-----------------|---|------------|----------------|-----------------------|-----------------------|
| LY12            | Cu 3.8-4.9%,<br>Mg 1.2-1.8%,<br>Mn 0.3-0.9%,<br>balance--Al.  | 2 mm       | 174            | 0.74mm<br>per<br>year | 0.4 mm                |
| 1Cr18-<br>Ni9Ti | Cr 17.0-19%<br>Ni 8-10.5%<br>Ti 0.80%<br>Mn 2%<br>balance--Fe | 2 mm       | 174            |                       | perfora-<br>tion      |

#### SELECTION OF MATERIALS FOR MARINE SENSORS

In materials selection for marine sensors, the first

consideration is the oceanographic parameters to be determined. For example, the flow tube in the sensor of a conductive salinometer for salinity determination should exhibit minimum linear expansion coefficient so as to ensure least variation in the physical dimensions of the flow tube when temperature fluctuates. Strict selection of corrosion resistant materials is of great significance to the dimensional stability of the flow tube. Among non-metal materials, glass exhibits expansion coefficient of  $5.5 \times 10^{-6} / ^\circ\text{C}$ , which is an order less than that of plexiglass and has better dimensional stability. This resulted in the selection of glass for the construction of the flow tube.

Materials for depth sensor should display good elasticity, and constant elastic metals are most acceptable. Furthermore, they should be resistant to seawater corrosion which will result in reduction of elasticity. Full immersed panel tests were performed by Qingdao Laboratory of Institute of Iron and Steel, Ministry of Metallurgical Industry. Salinity there was about 31‰, and average temperature was  $15^\circ\text{C}$ , with temperature from January to June being  $7.8^\circ\text{C}$  and from July to December  $21.5^\circ\text{C}$ , DO ranged from 5.67 ml/l to 8.0 ml/l and pH from 8.3 to 8.6.

The commonly-used constant elastic material is 3J53, and it was tested in the waters off Qingdao and results are given in Table 2, which demonstrates that 3J53 displayed high rates of attack. Cracking had developed before exposure time reached 118 days. Because precision will be greatly reduced when depth sensor is slightly corroded and complete failure will occur when cracking develops, 3J53 is not suitable for construction of instruments designed for long term operation in the marine environment.

Niobium-base materials were exposed to seawater for

three years in the waters off Qingdao and very little weight loss was observed. Results are illustrated in Table 3.

Table 2. Fully Immersed Panel Tests Near  
Qingdao

| Alloy | Composition   | Thickness            | Jan.14,1980          | Feb. 26,1980                                   |
|-------|---|----------------------|----------------------|--|
| 3J53  | Ni 41.5-43%<br>Cr 5.1-5.9%<br>Ti 2.2-2.8%<br>Al 0.4-0.8%<br>Balance--Fe | 0.375 mm<br>0.575 mm | cracking<br>observed | complete<br>breaking and<br>partial separation |

\* Exposure time: September 18, 1979.

Table 3. Corrosion Experiments of Niobium-base  
Materials Near Qingdao

| Weight(g)  | Panel number |          |          |
|--|--------------|----------|----------|
|  | 1            | 2        | 3        |
| Weight before immersion<br>April 1, 1978                 | 28.588g      | 28.500g  | 27.670g  |
| Weight after 12 months<br>April 2, 1979                  | 28.5667g     | 28.5376g | 27.6733g |
| Weight after 23 months<br>Feb.26, 1980                   | 28.5621g     | 28.5340g | 27.6701g |
| Weight after three years<br>full immersion<br>April 1981 | 28.5610g     | 28.5336g | 27.6700g |

\* Exposure time: April 1, 1978

The niobium-base materials tested contain Nb 54.5%, Ti 40% and Al 5.5% and is of thickness of 0.33 mm. Exposure tests began April 1, 1978 in the waters off Qingdao. In April 2, 1979 and February 26, 1980, the tested panels were recovered from the test sites for visual

inspections and photography. After being cleaned, dried and weighed, they were re-immersed. Results of repeated inspections were similar and show that extensive marine growths were developed on the surface of the panels. After removal of the foulants, brightness was restored and no local attack was found. Results of weighings of the cleaned and dried panels demonstrated no weight loss.

The above experiments show that niobium-base materials have good to excellent resistance to seawater local attack and uniform attack even under full immersion conditions. This can be attributed to the fact that the alloy contains high percentage of niobium and titanium which are highly resistant to corrosion. A very stable oxide film can be developed on the surface of the titanium materials and this film will provide protection, thus the resistance performance of the alloy can be increased.

Comparison of the two constant elastic materials reveals that niobium-base alloy is superior to 3J53 and therefore can be preferably used for marine instruments.

#### PROTECTIVE MEASURES AGAINST CORROSION

In addition to the housings of the instrument, emphasis should also be given to minor components of the instrument such as frames, shafts, screws and nuts. It is a common practice that when selecting materials for these attachments, the first consideration is strength. This tends to cause contact corrosion between different metals. For example, when carbon steel wire or chain is used to connect instrument whose housing is not made of carbon steel to buoy or drilling platform, contact corrosion will inevitably occur because of the difference of the housing and the wire. From January to November 1980, a current meter with a housing of copper alloy was attached to a mooring

system with carbon steel structure in the south China sea and no insulating barrier was provided to the junction between the current meter and the mooring chain. After exposure of six months, the chain was seriously damaged and eventually got broken, resulting in the loss of the current meter as a result of contact corrosion. A temperature-salinity sensor with a housing of aluminum alloy was also connected to the mooring system and no insulating measures were taken. The aluminum alloy, whose potential was more negative than that of carbon steel, became the anode while the chain became cathodic, resulting in the formation of corrosion cell and thus an acceleration of corrosion. Finally the aluminum alloy housing (Mg 9.0%, Mn 0.56% and Al ) with thickness of 8 mm was perforated in ten months exposure in seawater.

In order to minimize contact corrosion between different metals, insulating materials such as nylon or rubber should be introduced. If instrument is supposed to be attached to buoys, nylon rings or sleeves should be used between the instrument and the chain. Nylon or rubber sleeves should also be used for screws, nuts or shafts made of different materials for the purpose of corrosion restriction.

Sacrificial anode is effective for providing cathodic protection of instrument designed to operate in marine environment. Materials for sacrificial anode are commonly made of alloys containing Al (0.3-0.6%), Cd (0.05-0.15%) and Zn, or containing Zn (2.5%), In (0.02%), Cd (or Sn) (0.01%) and Al. These anodes feature in good current efficiency (over 90%), high solubility and excellent smelting behavior.

Furthermore, instruments for marine application should be painted with protective coats. The following are ex-

amples showing the status of instruments after long-term exposure to seawater.

Model SCL 2-1 Well-less Tide Gauge is an device with a housing of carbon steel. Protection was provided by applying three-layer of epoxy tar primer, four-layer of chlorinated rubber intermediate film, three-layer of toxic  $Cu_2O$  topcoat and a sacrificial anode with thickness of 30 mm and weight of 1.2 kg to the housing. It was deployed for one year from 1980 to 1981 in the tidal zones near Xiamen and Shanwei. Little marine growth developed and no evident attack occurred on the housing. The topcoat remained nearly undamaged.

From June 17, 1983 to October 11, 1983, a magnetic recording current meter with a housing of LY12 aluminum alloy and a frame of 00Cr20Ni25Mo5N non-magnetic stainless steel was tested under full immersion conditions. Protective coatings and sacrificial anode were also applied. Inspection showed that the instrument suffered no severe attack and remained watertight. Only four isolated barnacles were observed.

From September 26, 1982 to January 16, 1983, an acoustic release with LY12 aluminum alloy housing was tested under complete immersion conditions in the waters off Qingdao. No visible corrosion and marine fouling occurred. No attack developed between the carbon steel shaft and the housing. The instrument displayed good watertight performance under 25 atmospheric pressure. In the period from June 16, 1983 to October 11, 1983 this instrument was tested again in the waters off Qingdao by suspending from a test unit under full immersion conditions. Result was identical to that obtained in 1982. The acoustic release experienced two full immersion tests for a total period of 229 days, little corrosion and marine growths



were observed, demonstrating that the protective measure was very effective.

#### SUMMARY

Corrosion of marine instruments can be effectively controlled if strict selection of materials are observed and necessary protective measures are taken. However, negligence will lead to complete failure.

#### References

- Dexter, S.C., Handbook of Oceanographic Engineering Materials, 1979.
- Fink, F.W. and Boyd, W.K., The Corrosion of Metals in Marine Environments, 1970.
- Chen Jian., Journal of Instrument Materials, 1982, 13(3), P72.



APPLICATION OF ELECTROCHEMICAL TECHNIQUES TO THE PREDICTION OF  
ENVIRONMENTAL EFFECTS ON THE CORROSION BEHAVIOUR OF A NI-TI ALLOY

ANN J EDWARDS

ADMIRALTY RESEARCH ESTABLISHMENT

HOLTON HEATH, POOLE, DORSET UK

SUMMARY

Potentiostatic techniques have been used to study the effects of changes in pH and chloride concentration to seasalt solutions on the corrosion behaviour and, in particular, pitting corrosion resistance of a 52Ni, 45Ti, 3Fe alloy. The alloy, known to be susceptible to crevice corrosion in seawater, was also found to be susceptible to pitting corrosion in acidified concentrated seasalt solutions and subject to rapid uniform corrosion in hydrochloric acid solutions.

RESUME

Des techniques potentiostatiques ont été utilisées pour étudier les effets de changements dans le pH et la concentration de chlorure dans des solutions de sel marin sur le comportement de l'alliage 52 Ni, 45 Ti et 3 Fe en présence de corrosion, et en particulier sur sa résistance à la piqûre par corrosion. Cet alliage, connu pour sa prédisposition à la corrosion fissurante dans l'eau de mer, s'est également avéré sensible à la corrosion en piqûre dans des solutions acidifiées de sel marin concentré et sujet à une corrosion uniforme rapide dans des solutions d'acide chlorhydrique.

The relationship between these values and the pitting corrosion behaviour of the alloy in a given environment is shown in the schematic polarisation curves in Figure 2.

- a. The alloy is unlikely to pit if  $E_{\text{corr}}$  is significantly active in relation to  $E_p$ ,  $E_r$  is more noble than  $E_{\text{corr}}$  and the current density of the reverse scan falls rapidly from  $I_s$ , ie pits will not propagate at the rest potential.
- b. Pitting will occur if  $E_p$  and  $E_{\text{corr}}$  are close or equal,  $E_r$  is more active than  $E_{\text{corr}}$  and the current density of the reverse scan at  $E_{\text{corr}}$  remains at  $I_s$ , ie pits once initiated could propagate at the rest potential.
- c. Pitting may occur if  $E_{\text{corr}}$ ,  $E_p$  and  $E_r$  are all close and any small change in conditions which would alter these values could initiate pitting. Under these conditions the scan rate must be sufficiently slow to allow repassivation to occur.

In order to obtain the values required to assess the alloys tendency to pitting and to study its general corrosion behaviour, anodic polarisation curves for the alloy in the solutions shown in Table 2 were plotted. Hydrochloric acid and sodium hydroxide were used to adjust the pH to 2 and 12 respectively. The natural seawater having a chloride concentration of 0.55 M was obtained from Portland Harbour and seasalt used to produce solutions of higher  $\text{Cl}^-$  concentration was made by evaporating seawater from the same source. A Wenking potentiostat and stepping motor control with Bryans XY recorder were used to plot the polarisation curves. The cell comprised a platinum auxiliary electrode and silver/silver chloride reference electrode. The test electrodes were in the form of bar immersed in the solution to a measured depth. This technique was adopted because it was considered that the reduction in accuracy of surface area measurement was preferable to the presence of crevices in a mounted electrode. The potential was scanned in the region  $-500$  mV to  $+520$  mV at a stepping rate of 30 mV/min and the minimum current measured on the log  $i$  scale was  $0.1 \mu\text{A}/\text{cm}^2$ .

## RESULTS AND DISCUSSION

Table 2 summarises the characteristics of  $E_{\text{corr}}$ ,  $E_p$ ,  $E_r$  and a comparison of  $I_s$  and  $I$  at  $E_{\text{corr}}$  on the reverse scan. From these results it can be seen that in seawater (0.55 M chloride) at pH 2 pitting is unlikely, but is likely to occur at 1.09 M chloride at pH 2 and higher concentrations as illustrated in Figures 3 and 4. The anodic polarisation curve for the alloy in 1.09 M  $\text{Cl}^-$  seasalt solution at pH 2 where  $E_p$  equals  $E_{\text{corr}}$ ,  $E_r$  is more active than  $E_{\text{corr}}$ , and the current density of the reverse scan at  $E_{\text{corr}}$  is equal to  $I_s$  is shown in Figure 4.

## INTRODUCTION

The purpose of this investigation was to predict the behaviour of the alloy under conditions likely to arise in specific service applications. In this particular instance there was a likelihood that condensation from a marine atmosphere could occur on the material which might subsequently evaporate leaving a deposit of concentrated brine on the surface. Yet another environmental possibility was that acidic or alkaline deposits could form on the surface as a result of contamination from other equipment. The Ni-Ti alloy (52Ni/45Ti/3Fe) has an austenitic structure and like stainless steels is dependent on an adherent surface oxide film for its corrosion resistance.

The alloy was previously found to be susceptible to crevice corrosion in seawater. Figure 1 shows a sample of the alloy after exposure in an INCO crevice jig<sup>(1)</sup> in Langston Harbour for 9 months. The open circuit potentials of the alloy with reference to an Ag/AgCl reference electrode in static solutions of seawater and seasalt solutions are shown in Table 1.

## EXPERIMENTAL

As the alloy was known to be susceptible to crevice corrosion a study of its pitting corrosion behaviour was undertaken. The technique adopted was one which has been proposed by Sedriks in the study of pitting of stainless steels<sup>(2)</sup>.

The parameters of interest are the breakdown potential  $E_{\text{corr}}$ , pitting potential  $E_p$  and repassivation potential  $E_r$ , determined from an anodic polarisation curve with a reverse scan from a predetermined potential.

The definition of these potentials as shown in Figure 2 are as follows:

- a. Breakdown potential  $E_{\text{corr}}$  - breakdown of passive film.
- b. Pitting potential  $E_p$  - initiation of pits.
- c. Repassivation potential  $E_r$  - potential at which no current flows after reversal of scan.

Assessment of the tendency for pitting of the alloy in a given environment is based on:

The separation of  $E_{\text{corr}}$  and  $E_p$ ; the value of  $E_r$  in relation to  $E_{\text{corr}}$  and the current density  $I_s$  at which the potential scan is reversed.

In all the other seawater solutions tested, ie pH 8.5-9.5 and pH 12 the alloy showed no propensity to pitting at its rest potential. These observations were confirmed by visual examination of the test electrode after completion of the test. Tests in hydrochloric acid solutions indicated that the alloy was susceptible to pitting corrosion at its rest potential in 5.5 M hydrochloric acid as indicated in Figure 5 but not in the lower concentrations tested. However, on visual examination of the electrode after testing in 5.5 M hydrochloric acid there was no evidence of pitting corrosion, only rapid general corrosion had occurred masking any localised attack.

Predictions from electrochemical results are consistent with results obtained with drops of various electrolytes on the alloys' surface.

### CONCLUSIONS

The use of this technique has shown that using simple and relatively quick electrochemical measurements, predictions of the pitting corrosion behaviour of any alloy in a given environment can be made from polarisation curves. Thus, with the aid of a few simple confirmatory exposure tests, the method can be used to survey the behaviour in a wide range of environments.

### REFERENCES

1. ANDERSON D. B. 'Statistical Aspects of Crevice Corrosion in Seawater' ASTM-ASM Symposium on Pitting Corrosion, Detroit, USA. 23 October 1974.
2. SEDRIKS A JOHN. 'Corrosion of Stainless Steels' Corrosion Monograph Series 1979, pp 63-65.

TABLE 1  
OPEN CIRCUIT POTENTIALS FOR THE ALLOY IN  
SEAWATER AND SEASALT SOLUTIONS

| SOLUTION           | CHLORIDE<br>CONCENTRATION<br>(Moles) | pH  | Temp<br>°C | OPEN CIRCUIT<br>POTENTIAL<br>mV vs Ag/AgCl |
|--------------------|--------------------------------------|-----|------------|--|
| Seawater           | 0.55 M                               | 8.2 | 20         | + 44                                       |
| Seawater + Seasalt | 1.09 M                               | 9.0 | 20         | + 1  |
| Seawater + Seasalt | 3.13 M                               | 9.2 | 20         | + 10                                       |
| Seawater + Seasalt | 3.13 M                               | 2   | 20         | +140                                       |
| Seawater + Seasalt | 3.13 M                               | 2   | 30         | + 20                                       |

TABLE 2

SUMMARY OF POLARISATION CHARACTERISTICS OBTAINED FOR THE ALLOY IN VARIOUS TEST SOLUTIONS

| SOLUTION           | CHLORIDE CONCENTRATION (Moles) | pH      | Temp °C | E <sub>corr</sub> (mV) | E <sub>p</sub> (mV) | E <sub>r</sub> (mV) | I <sub>s</sub> (µA/cm <sup>2</sup> ) | I at E <sub>corr</sub> on Reverse Scan (µA/cm <sup>2</sup> ) |
|--------------------|--------------------------------|---------|---------|------------------------|---------------------|---------------------|--------------------------------------|--|
| Seawater           | 0.55                           | 2       | 20      | -160                   | +430                | 0                   | 40                                   | -  |
| Seawater + Seasalt | 1.09                           | 2       | 20      | +280                   | +280                | 0                   | 120                                  | 120  |
| Seawater + Seasalt | 1.56                           | 2       | 20      | +110                   | +415                | -25                 | 112                                  | 116  |
| Seawater + Seasalt | 3.13                           | 2       | 20      | +110                   | +110                | -65                 | 132                                  | 130  |
| Seawater           | 0.55                           | 8.5-9.5 | 20      | -225                   | +170                | +5                  | 132                                  | -  |
| Seawater + Seasalt | 1.09                           | 8.5-9.5 | 20      | -370                   | +515                | -30                 | 4                                    | -  |
| Seawater + Seasalt | 1.56                           | 8.5-9.5 | 20      | -380                   | +260                | -20                 | 124                                  | -  |
| Seawater + Seasalt | 2.34                           | 8.5-9.5 | 20      | -360                   | +300                | -100                | 116                                  | -  |
| Seawater + Seasalt | 3.13                           | 8.5-9.5 | 20      | -250                   | +170                | -140                | 126                                  | -  |
| Seawater + Seasalt | 3.13                           | 8.5-9.5 | 30      | -445                   | +25                 | -405                | 140                                  | -  |
| Seawater           | 0.55                           | 12      | 20      | -430                   | -                   | +130                | 3.4                                  | -  |
| Seawater + Seasalt | 1.09                           | 12      | 20      | -300                   | -                   | +70                 | 22                                   | -  |
| Seawater + Seasalt | 1.56                           | 12      | 20      | -460                   | +235                | -100                | 130                                  | -  |
| Seawater + Seasalt | 3.13                           | 12      | 20      | -335                   | +335                | -105                | 124                                  | -  |
| Hydrochloric Acid  | 0.5                            | 0.48    | 20      | -105                   | -                   | +185                | 5                                    | -  |
| Hydrochloric Acid  | 0.75                           | 0.3     | 20      | -90                    | -                   | +145                | 9                                    | -  |
| Hydrochloric Acid  | 1.1                            | -0.05   | 20      | -115                   | +300                | 0                   | 112                                  | -  |
| Hydrochloric Acid  | 2.0                            | -0.3    | 20      | -150                   | -                   | -85                 | 27                                   | -  |
| Hydrochloric Acid  | 3.13                           | -0.49   | 20      | -125                   | +440                | -95                 | 65                                   | -  |
| Hydrochloric Acid  | 5.5                            | -0.74   | 20      | -430                   | -430                | -445                | 92                                   | 80   |



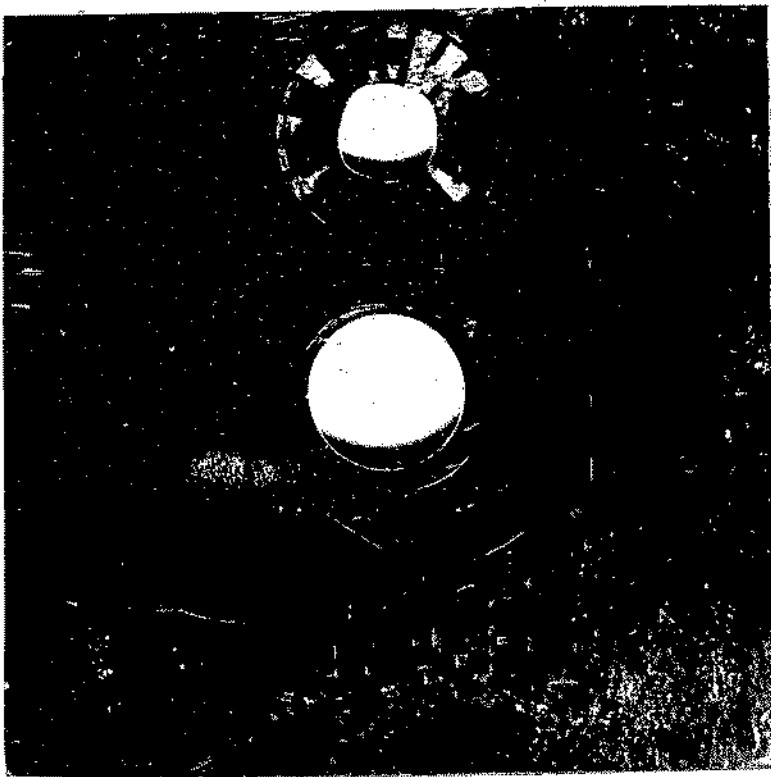


Figure 1      Crevice Corrosion After 9 Months Exposure  
in an INCO Crevice Jig

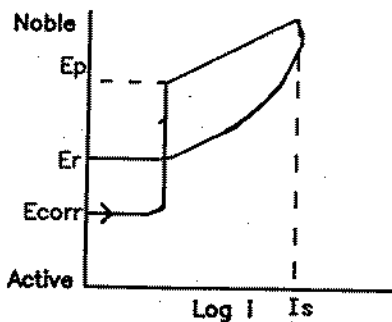
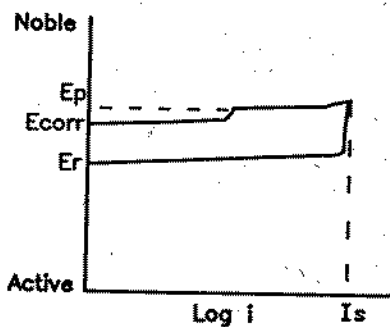
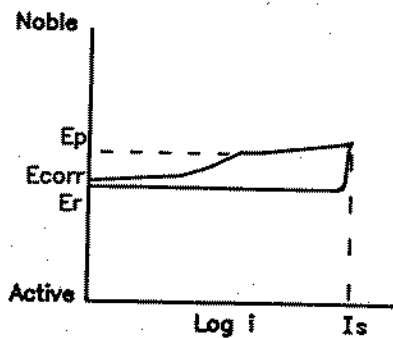
a) Pitting unlikely at  $E_{corr}$ b) Pitting will occur at  $E_{corr}$ c) Pitting may occur at  $E_{corr}$ 

Figure 2. Schematic Polarisation Curves

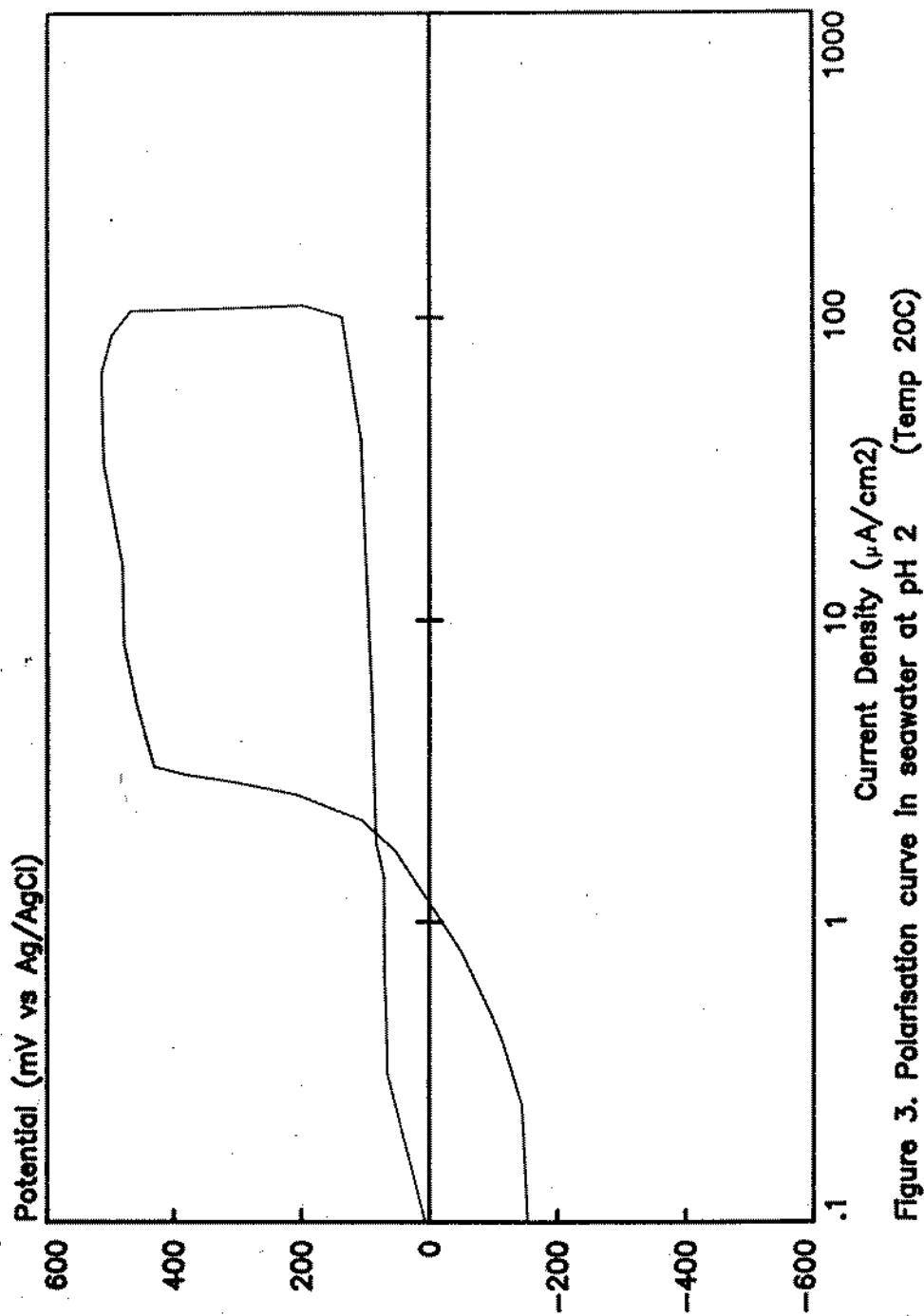


Figure 3. Polarisation curve in seawater at pH 2 (Temp 20C)

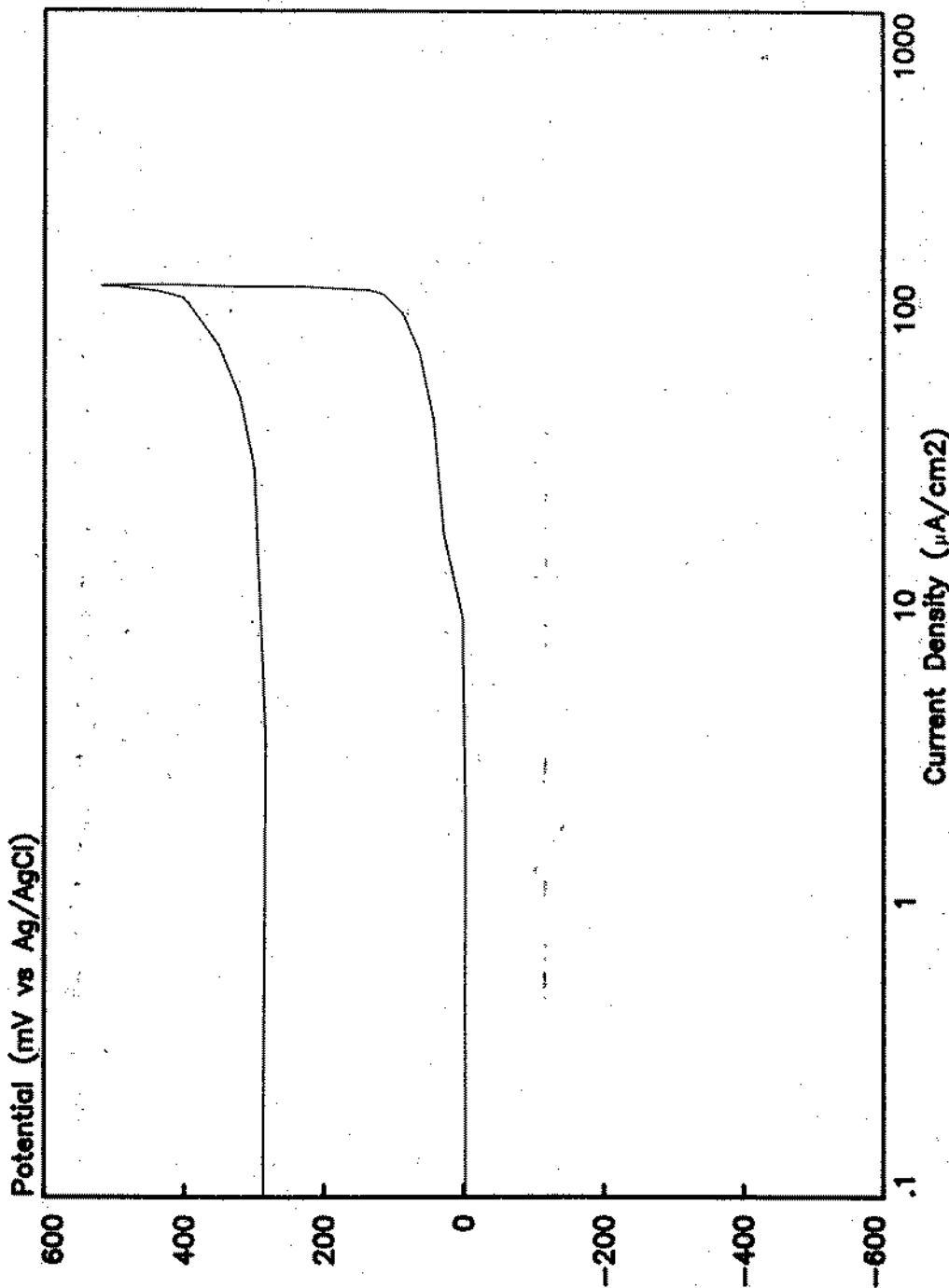


Figure 4. Polarisation curve in pH2 1.09M seasalt at 20C

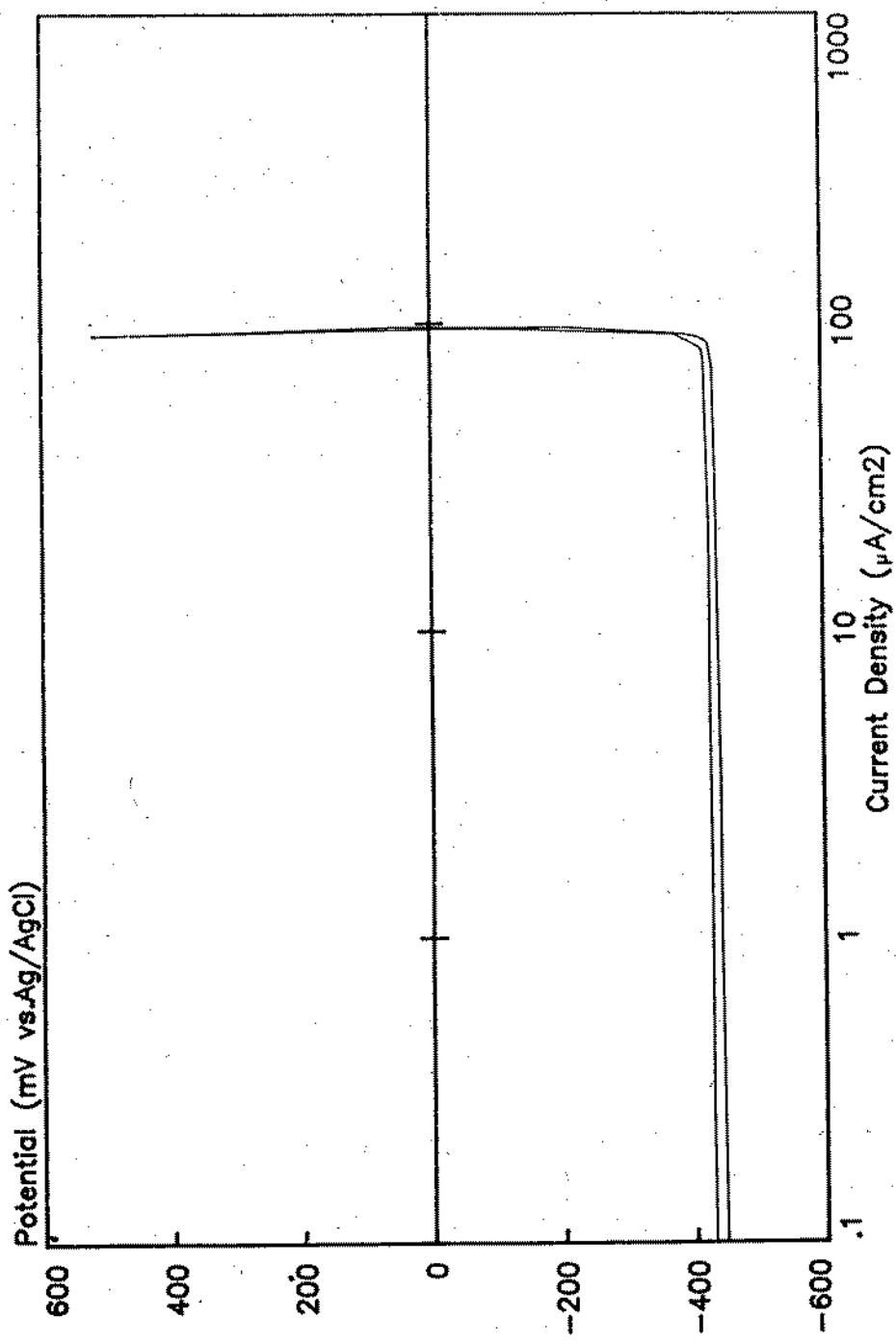
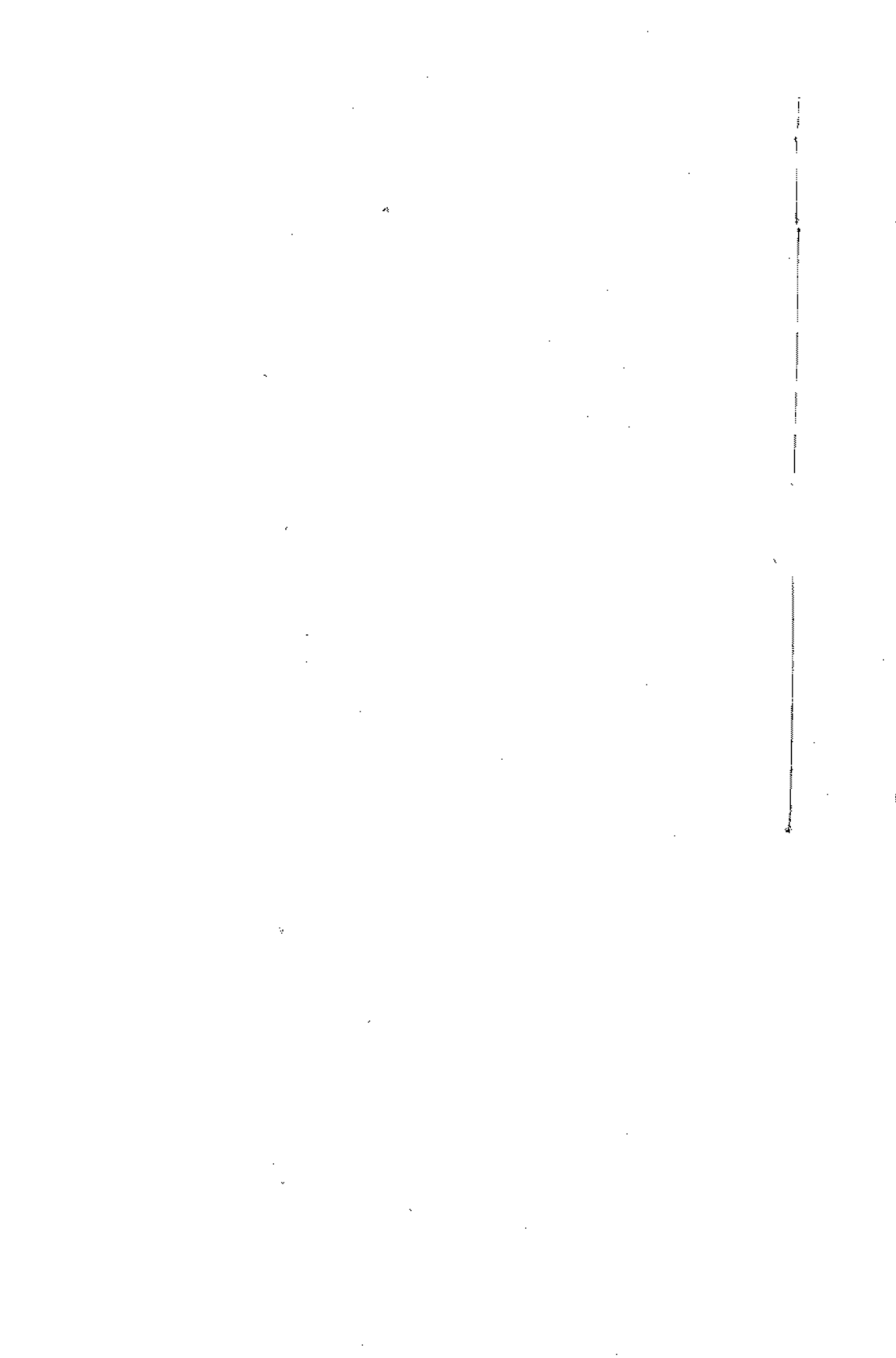


Figure 5. Polarisation curve in 5.5M Hydrochloric acid at 20 C



INFLUENCE DE QUELQUES ELEMENTS D'ALLIAGE SUR LA RESISTANCE  
A LA CORROSION MARINE D'ACIERS FAIBLEMENT ALLIES

MM CHARBONNIER\* - CONFENTE\*\* - JOSSIC\* - LEMOINE\*\*\* - PAGNIEZ\*\*\*\*

\*IRSID St Germain en Laye - \*\*SNAP Pompey

\*\*\*CNEOX Brest - \*\*\*\*CITAG Paris

L'influence du chrome, de l'aluminium, du molybdène et du nickel sur la résistance à la corrosion marine d'aciers faiblement alliés a été étudiée.

Des coulées industrielles d'acier doux et d'aciers faiblement alliés ont été élaborées avec des teneurs en :

Cr : entre 1,5 et 4% - Al : entre 0,2 et 1%  
Mo : 0,5 et 1% - Cu : 0,4% - Ni : 0,2%

Des essais en eau de mer vivante ont été effectués dans les stations de l'IRSID à BIARRITZ et du COB à BREST.

L'addition d'éléments tels que le chrome et l'aluminium diminue la masse d'acier corrodée (perte de poids), mais provoque le développement de corrosion localisée. Il est montré que le meilleur compromis de résistance à la corrosion généralisée et localisée est obtenu avec un acier de type 2% Cr - 1% Al. Le molybdène limite la tendance aux corrosions localisées par plaques en généralisant la corrosion sur toute la surface de l'éprouvette. L'addition de nickel est favorable pour la tenue dans les zones de marée. Les éléments d'alliage interviennent essentiellement en modifiant les caractéristiques d'étanchéité des rouilles vis-à-vis de l'environnement.

The influence of chromium, aluminum, molybdenum and nickel on the marine corrosion resistance of low alloyed steels was investigated.

Industrial heats of carbon steel and low alloyed steels were manufactured with contents in :

Cr : between 1.5 and 4% - Al : between 0.2 and 1%  
Mo : 0.5 and 1% - Cu : 0.4% - Ni : 0.2%

Corrosion experiments were conducted in the test sites of BIARRITZ and BREST.

The addition of elements, such chromium and aluminum, reduces the mass of corroded steel (weight loss), but promotes the development of localised corrosion. It is shown that the best compromise between general and local corrosion resistance is obtained with the 2% Cr - 1% Al steel. Reducing the tendency to localised corrosion, molybdenum favours the development of general corrosion. The addition of nickel increases the corrosion resistance in tidal zones. The alloying elements act essentially by modifying the sealing properties of rust with regard to environment.

## 1 - INTRODUCTION

Le développement d'aciers à tenue à la corrosion améliorée en environnement marin présente un intérêt certain pour de nombreuses applications telles que l'industrie pétrolière offshore, l'exploitation des océans (aquaculture et ressources minérales), et d'une façon générale, toutes les installations de complexes industriels en bord de mer.

L'acier est en effet un matériau économique et intéressant du point de vue de ses caractéristiques mécaniques. Il est toutefois sensible à la corrosion en milieu marin mais certaines techniques telles que la protection cathodique ou la protection par peinture permettent d'éviter ou de limiter cette corrosion. On peut aussi chercher à améliorer la résistance à la corrosion de l'acier en lui ajoutant des éléments d'alliage, en faible quantité, pour des raisons économiques.

Les données publiées montrent que certains éléments tels que le chrome, l'aluminium, le nickel, le cuivre, etc ... sont susceptibles d'améliorer la tenue à la corrosion des aciers. Cependant, leurs effets ne sont pas additifs et dépendent des sites d'emploi. Par ailleurs, l'acier peut présenter des formes de corrosion différentes, généralisée ou localisée par plaques. Le problème est alors d'éviter les corrosions locales, les plus pernicieuses, tout en minimisant l'attaque généralisée ; ceci avec des ajouts d'éléments d'addition en quantité compatible avec un développement industriel rentable du point de vue économique.

Cette recherche a fait l'objet d'un programme d'essais et de développement dont les premiers résultats sont présentés ici.

## 2 - MATERIAUX ETUDIÉS

### 2 - 1 - Composition chimique

Au total, neuf coulées différentes ont été étudiées. Le tableau 1 indique en % pondéral la composition chimique des différentes nuances.

Il convient de distinguer :

- les sept premières nuances à teneurs variables en chrome et aluminium (53 à 59) et dont une contient 1 % de molybdène. Ces coulées, d'environ 1 tonne chacune, ont été élaborées par la Société CREUSOT-LOIRE. Après laminage à chaud et prélèvement d'échantillons, les éprouvettes ont subi un traitement de normalisation dans les conditions suivantes : chauffage en bain de sel de 30 mn à 950°C et refroidissement lent à l'air, de façon à avoir des structures aussi voisines que possible pour les différents aciers ;



| Repère | Nuance abrégée          | C     | Mn    | Si    | S     | P     | Ni    | Cr   | Mo    | Cu    | Al    |
|--------|-------------------------|-------|-------|-------|-------|-------|-------|------|-------|-------|-------|
| 53     | Acier doux de référence | 0,102 | 0,280 | 0,175 | 0,006 | 0,010 | 0,035 | 0,14 | 0,030 | 0,020 | 0,017 |
| 54     | 2Cr                     | 0,096 | 0,320 | 0,190 | 0,006 | 0,009 | 0,030 | 2,09 | 0,020 | 0,020 | 0,014 |
| 55     | 2Cr-0,3Al               | 0,110 | 0,380 | 0,290 | 0,005 | 0,009 | 0,075 | 2,15 | 0,020 | 0,020 | 0,340 |
| 56     | 2Cr-1Al                 | 0,115 | 0,390 | 0,300 | 0,005 | 0,009 | 0,030 | 2,14 | 0,007 | 0,010 | 0,920 |
| 57     | 2Cr-1Mo                 | 0,098 | 0,350 | 0,200 | 0,008 | 0,012 | 0,024 | 2,10 | 1,060 | 0,010 | 0,032 |
| 58     | 3Cr                     | 0,100 | 0,340 | 0,195 | 0,007 | 0,012 | 0,032 | 3,11 | 0,020 | 0,015 | 0,026 |
| 59     | 4Cr-1Al                 | 0,115 | 0,400 | 0,350 | 0,007 | 0,012 | -     | 4,10 | 0,020 | 0,015 | 0,010 |
| 60     | 1,5Cr-1,5Al-0,5Mo       | 0,010 | 0,490 | 0,340 | 0,005 | 0,007 | 0,010 | 1,39 | 0,480 | 0,010 | 1,513 |
| 61     | 1,5Cr-0,2Al-0,4Cu-0,2Ni | 0,15  | 0,620 | 0,280 | 0,008 | 0,010 | 0,20  | 0,98 |       | 0,320 | 0,20  |

Tableau 1  
Composition chimique des coulées étudiées

- les aciers 60 et 61 ont été étudiés, à titre de comparaison, dans le cadre d'un programme communautaire européen\*. La nuance 60 est à bas carbone et contient un peu de molybdène. Après laminage à chaud, un traitement thermique à 900°C (5 mn) a été appliqué. La coulée 61 permet d'étudier l'influence d'un ajout de cuivre et de nickel. L'acier 61 n'a pas subi de traitement thermique après laminage à chaud.

## 2 - 2 - Structure

Les différents aciers étudiés présentent des structures du type ferrite-perlite. Par rapport à l'acier de référence (53) qui possède une structure ferritique grossière, l'ajout de 2 % de chrome (nuance 54) accroît la quantité de perlite par action sur la teneur en carbone de l'eutectoïde et sur la trempabilité. L'augmentation de la teneur en aluminium (55 et 56) provoque un affinement du grain. Les aciers 2Cr-1Mo (57) et 3Cr (58) présentent des structures voisines : ferrito-perlitiques avec quelques plages de type bainitique. L'acier 4Cr-1Al (59) est homogène avec une structure de type ferrite-perlite à grains très fins.

Afin de déceler une éventuelle influence de la microstructure sur la tenue à la corrosion, certaines éprouvettes de l'acier 2Cr-1Mo ont subi une trempe à l'huile afin d'obtenir une structure de type

\* Nous remercions MM BLEKKENHORST (HOOGVENS GROEP P.V.) et BRÜNO (CSM) qui nous ont fourni ces échantillons.

martensitique (repérée par la suite 57M). Cette microstructure a été choisie afin de nous placer dans des conditions extrêmes pour mieux examiner l'influence de la microstructure. Les aciers 60 et 61 présentent respectivement une structure ferritique et ferrito-perlitique..

### 2 - 3 - Caractéristiques mécaniques

A titre indicatif, le tableau 2 rassemble les caractéristiques mécaniques de l'ensemble des aciers étudiés. Le traitement thermique effectué sur les aciers 53 à 59, choisi pour obtenir des structures semblables pour les différentes nuances, n'est pas en effet le plus adéquat du point de vue des caractéristiques mécaniques. L'acier 60 (traitement de 900°C/5 mn) et l'acier 61 (brut de laminage) ont des caractéristiques mécaniques plus élevées.

| Repère | Nuances                    | Re<br>MPa | Rm<br>MPa | A <sub>80</sub> % |
|--------|----------------------------|-----------|-----------|-------------------|
| 53     | Acier doux<br>référence    | 242       | 366       | 38,5              |
| 54     | 2Cr                        | 242       | 432       | 32,7              |
| 55     | 2Cr-0,3Al                  | 250       | 448       | 31,7              |
| 56     | 2Cr-1Al                    | 280       | 438       | 28,3              |
| 57     | 2Cr-1Mo                    | 280       | 578       | 24,9              |
| 58     | 3Cr                        | 235       | 460       | 28,3              |
| 59     | 4Cr-1Al                    | 241       | 462       | 25,3              |
| 60     | 1,4Cr-1,5Al-0,5Mo          | 471       | 565       | 11,5              |
| 61     | 1,5Cr-0,2Al-0,4Cu<br>0,2Ni | 512       | 724       | 9,8               |

Tableau 2  
Caractéristiques mécaniques des nuances étudiées

### 3 - RESULTATS EXPERIMENTAUX

Des essais in situ ont été effectués en eau de mer vivante pour apprécier les formes et les cinétiques des phénomènes de corrosion pouvant apparaître sur les aciers faiblement alliés exposés en zones de marnage et d'immersion.

Au laboratoire, des essais électrochimiques et des analyses de rouille ont été réalisés afin de tenter d'expliquer le rôle et le mode d'action des éléments d'addition à partir des résultats obtenus in situ dans les stations de corrosion.

#### 3 - 1 - Essais in situ

Les essais d'exposition en milieu naturel ont été réalisés en deux sites différents :

- à Biarritz dans les cuves alimentées en eau de mer naturelle (immersion) ;
- à Brest sur la station d'essais en mer de Saint Anne du Portzic (immersion et marnage).

Des plaques sablées de 200 x 300 x 4 mm ont été exposées pendant 4 périodes différentes : 6, 12, 18 et 24 mois ; 3 échantillons ont été utilisés par nuance et pour chaque durée d'exposition.

Après chaque relevage, les échantillons ont été examinés visuellement. Des prélèvements de produits de corrosion ont été effectués pour analyse ainsi que des mesures de perte en poids et de profondeur de piqûres.

3 - 1 - 1 - En immersion permanente (fig. 1 et 2), les mesures de perte en poids obtenues sur les 2 sites, montrent qu'à Brest les vitesses de corrosion sont, pour l'ensemble des nuances, plus importantes qu'à Biarritz. Ceci peut être attribué à des courants marins plus violents à Brest, ainsi qu'à l'absence de macrosalissures à Biarritz.

Cependant, le classement respectif de chaque nuance vis à vis de la corrosion généralisée est le même pour les 2 stations.

. Les nuances 2Cr-1Al (56), 1,5Cr-1,5Al-0,5Mo (60), 4Cr-1Al (59), ont le meilleur comportement ;

. Les aciers 2Cr (54), 2Cr-0,5Al (55), 2Cr-1Mo (57) 3Cr (56) ont des pertes en poids plus élevées ; pour l'acier 2Cr-1Mo on n'observe pas, à Biarritz, de différences très importantes entre la structure ferritique (57F) et martensitique (57M) ;

. La nuance de référence et l'acier 61 (1Cr-0,2Al-0,2Ni-0,4Cu) ont le plus mauvais comportement.

Des vitesses de corrosion très basses sont mesurées après 2 ans d'exposition. Les pertes de poids correspondent à des réductions d'épaisseur de l'ordre de 0,025 mm/an avec les nuances 56, 59 au Cr-Al. L'acier de référence se corrode à une vitesse de 0,1 mm/an. Cependant, les mesures de pertes de poids ne suffisent pas à caractériser convenablement le comportement en immersion de ces matériaux. En effet, l'observation macrographique des éprouvettes (photos 1 et 2) montre que les pertes de poids correspondent à une réduction d'épaisseur à peu près homogène dans certains cas (nuances 53 et 54 par exemple) mais sont en rapport, dans d'autres cas, avec des zones de corrosion localisée d'étendues plus ou moins larges (nuances 58 et 59 par exemple).

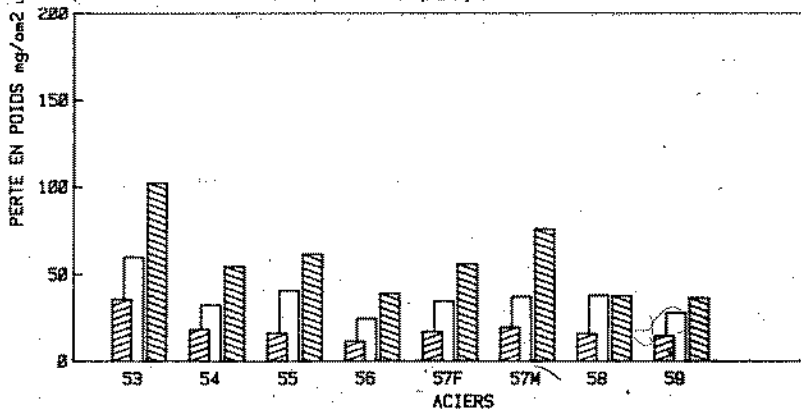


Figure 1

Pertes de poids par immersion à Biarritz pendant 6,12,18 mois

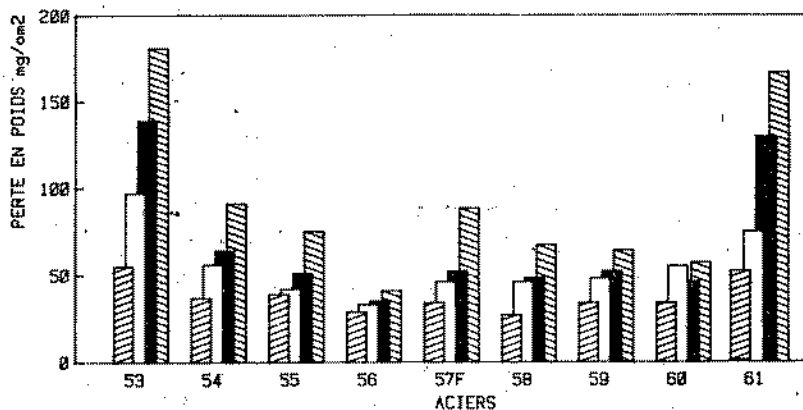


Figure 2

Pertes de poids par immersion à Brest pendant 6,12,24 mois



Photo 1

Immersion à Biarritz  
pendant 3 ans  
Acier 53 ( Référence)

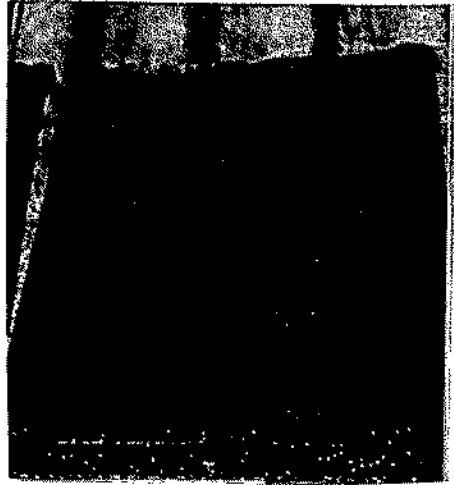


Photo 2

Immersion à Biarritz  
pendant 3 ans  
Acier 59 (4Cr-1Al)

Il est possible d'évaluer la profondeur des "piqûres" (corrosion localisée) présentes sous la rouille. La figure 3 rassemble les mesures effectuées sur l'ensemble des nuances.

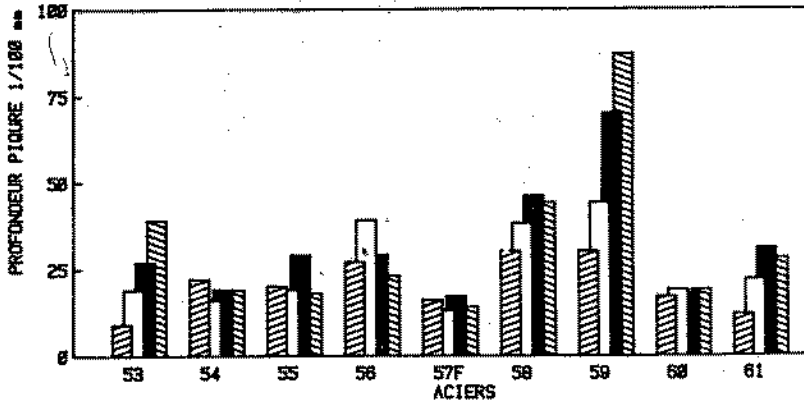


Figure 3

Évaluation des profondeurs de piqure après  
immersion à Brest pendant 6,12,18,24 mois

L'examen des résultats montre que les aciers les plus riches en chrome 4Cr-1Al (59) et 3Cr (58) sont ceux qui présentent les piqûres les plus profondes. A part l'acier à 2Cr-1Al (56) qui a un comportement intermédiaire, les autres nuances ont des profondeurs de piqûres inférieures à celles existant à la surface de l'acier de référence. Il est important de noter que les aciers au molybdène (57 et 60) sont ceux qui souffrent le moins de corrosion localisée.

3 - 1 - 2 - En zone de marnage, les aciers testés présentent un plus mauvais comportement qu'en immersion. Ce résultat n'est pas conforme avec certaines observations réalisées sur des palplanches où la vitesse de corrosion est généralement du même ordre de grandeur en immersion qu'en marnage. Il convient cependant de considérer que nos essais sont réalisés dans des conditions assez différentes. D'une part, on utilise des petites éprouvettes où des effets galvaniques entre la zone immergée et la zone de marnage ne peuvent pas se produire. D'autre part, du fait des conditions météorologiques assez sévères rencontrées sur le site de Brest, la zone de marnage se trouve être une zone très agressive avec une action érosive des vagues et des courants.

Les pertes de poids mesurées sont rassemblées à la figure 4.

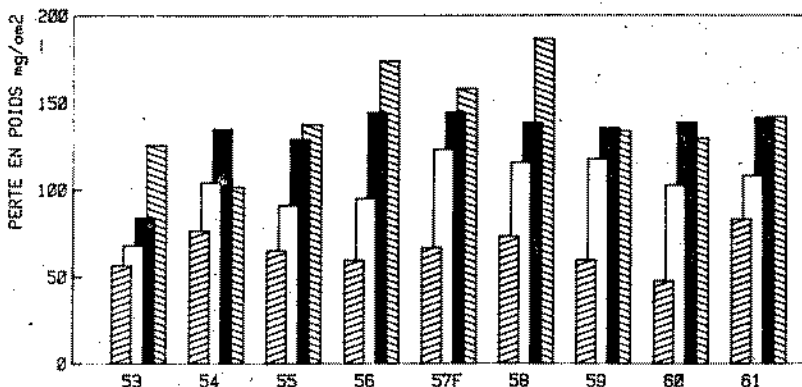


Figure 4  
Perte de poids en zone de marnage à Brest  
pendant 6, 12, 18 et 24 mois

On constate que les vitesses de corrosion sur les aciers alliés sont plus importantes que celles que nous avons obtenues avec l'acier de référence. Il apparaît donc que les éléments d'alliage Cu-Al-Mo ne sont pas bénéfiques dans ces conditions. Cependant, des essais réalisés sur des nuances au Cr-Al-Ni (4Cr-1Al-1Ni) (1) ont montré l'intérêt de l'ajout du nickel pour une augmentation de la résistance à la corrosion des aciers en zone de marnage.

L'examen de la figure 5, où sont reportées les mesures de profondeur des piqûres qui existent sous la rouille, montre qu'en zone de marnage, comme dans le cas des essais en immersion, les aciers 3Cr (58) et 4Cr-1Al (59) sont les plus sensibles aux phénomènes de corrosion localisée.

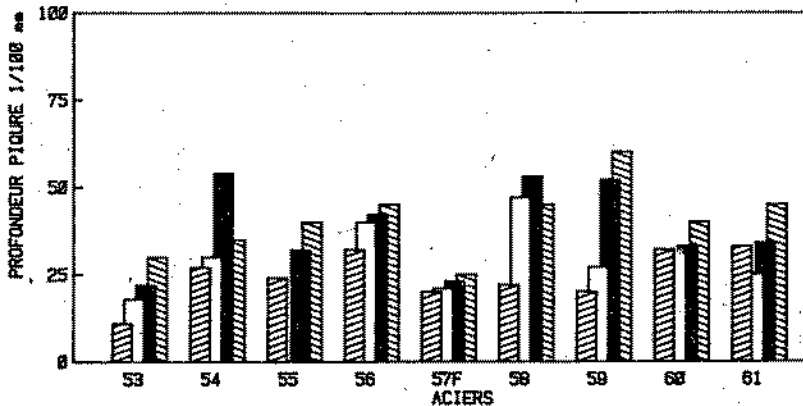


Figure 5

Evaluation des profondeurs de piqûres en zone de marnage après 6,12,18 et 24 mois

### 3 - 2 - Essais en laboratoire

#### 3 - 2 - 1 - Essais électrochimiques

Des mesures électrochimiques ont été effectuées sur des échantillons de métal nu ou préalablement enrouillés (2). Les mesures électrochimiques instantanées ne suffisent pas à rendre compte du comportement réel des aciers en eau de mer, ce qui montre que l'effet des éléments d'alliage sur la corrosion est obtenu essentiellement par la modification des caractéristiques des couches de rouille.

En revanche, les mesures électrochimiques (courants de corrosion et courants limites de diffusion) faites sur des échantillons pré-enrouillés 6 et 12 mois en eau de mer vivante conduisent à des classements proches de ceux que fournissent les essais in-situ.

#### 3 - 2 - 2 - Analyse des rouilles

La rouille qui se forme lors de la corrosion marine de l'acier est principalement constituée, selon différents auteurs (3 à 6) de :

- αFeOOH (goethite)
- γFeOOH (lepidocrocite)

$\beta$  FeOOH (akaganéite)

Fe<sub>3</sub>O<sub>4</sub> (magnétite)

et d'une phase amorphe dont l'un des principaux constituants serait d'après (3)  $\delta$  FeOOH.

La diffraction des rayons X et la spectrométrie d'absorption infrarouge ont été utilisées pour détecter la présence de ces phases dans les rouilles formées en immersion et en zone de marnage. La spectroscopie de diffraction infrarouge a permis d'obtenir des données qualitatives sur le pourcentage des différentes phases observées.

La microsonde électronique a donné par ailleurs des informations sur la répartition des éléments d'additions dans les couches de rouille formées à la suite d'une immersion de deux ans. Par spectrométrie d'émission de rayons X (fluorescence X), il est possible de doser ces éléments d'alliage.

On peut distinguer deux couches de rouille à la surface du métal. Pour tous les aciers étudiés, la couche la plus externe (en contact avec le milieu extérieur) est essentiellement constituée de goéthite ( $\alpha$  FeOOH) et de lepidocrocite ( $\gamma$  FeOOH). Il est intéressant de noter qu'après 18 mois en immersion, la goéthite se trouve en plus grande proportion ( $\approx 70$  %) que la lepidocrocite. En revanche, après 18 mois d'exposition en zone de marnage, la couche de rouille est essentiellement constituée de lepidocrocite  $\gamma$  FeOOH (pratiquement 100 %).

Dans la couche de rouille interne, la magnétite Fe<sub>3</sub>O<sub>4</sub> est le seul oxyde de fer identifié avec certitude, par les méthodes d'analyse employées (représentant 30 à 60 % des phases présentes).

L'étude de la répartition des éléments d'alliage met en évidence plusieurs points :

. En immersion, on observe généralement un enrichissement en éléments d'alliage dans la partie inférieure de la couche de rouille.

A partir des examens effectués à la microsonde électronique dont quelques exemples sont représentés aux figures 6, 7 et 8, les aciers peuvent être classés en 3 catégories :

- ceux qui présentent un enrichissement significatif par rapport au métal de base en Cr, Al et Mo (aciers 2Cr-1Al, 3Cr, 4Cr-1Al, 2Cr-1Mo) dans les couches de rouille.

- ceux qui sont recouverts d'une couche de rouille peu ou pas enrichie en éléments d'addition.



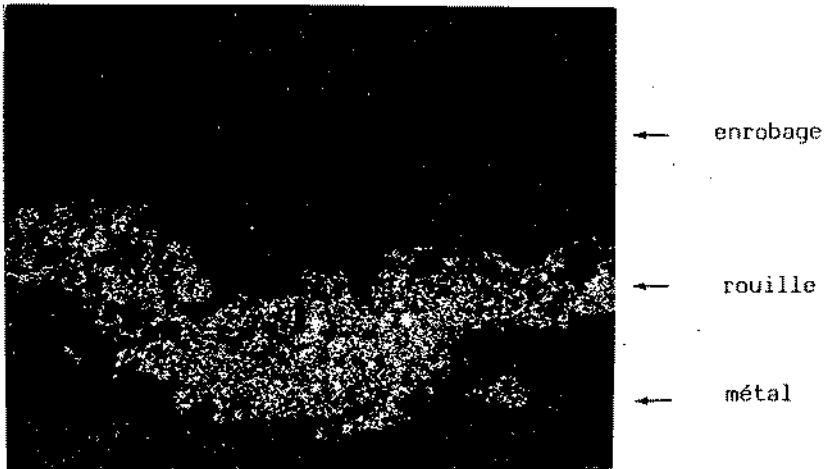


Image Cr

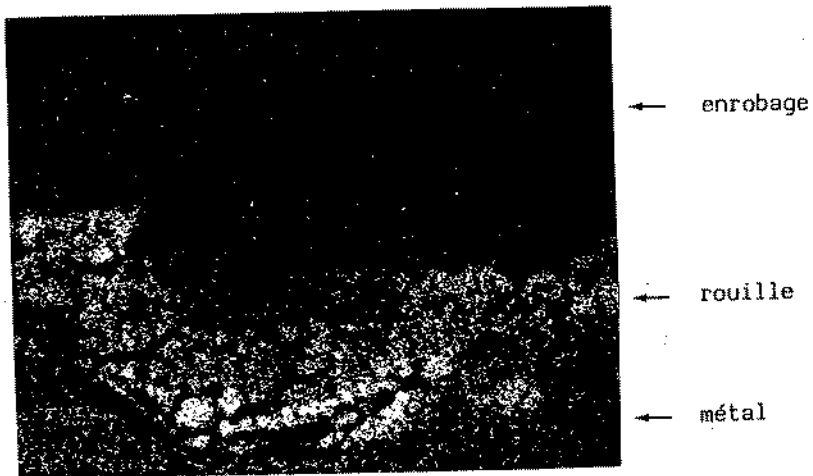


Image Mo

zCr-1Mo (57)

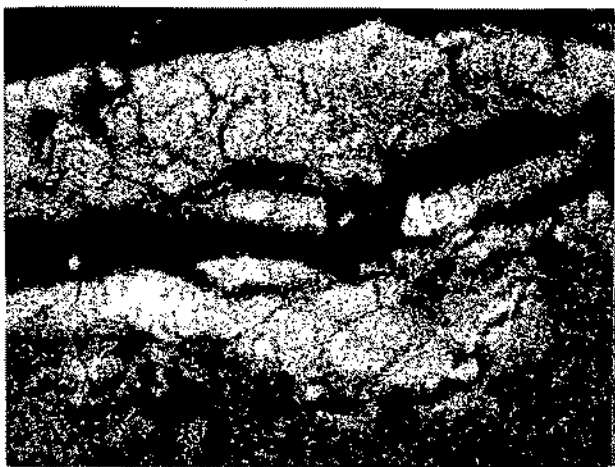
Figure 6

Observations à la microsonde électronique  
des couches de rouille formées après 2 années  
d'immersion à Biarritz



← rouille

← métal

Image Cr

← rouille

← métal

Image Al

2Cr-1Al (56)

Figure 7

Observations à la microsonde électronique  
des couches de rouille formées après 2 années  
d'immersion à Biarritz



Image Cr

3Cr (58)

Figure 8

Observations à la microsonde électronique  
des couches de rouille formées après 2 années  
d'immersion à Biarritz

L'enrichissement en éléments d'addition peut être localisé à l'interface métal-couche de rouille et former ainsi une "barrière" (exemple acier 2Cr-1Mo). On observe aussi des enrichissements en "strates" (aluminium dans l'acier 2Cr-1Al) plus ou moins homogène (chrome dans l'acier 3Cr).

D'une manière générale, l'enrichissement en chrome est d'autant plus important que la teneur de départ dans l'acier est élevée. L'enrichissement en Cr ne dépasse pas 10 %. Celui en aluminium n'excède pas une teneur de 15 %. La concentration des différents éléments évoluent beaucoup pendant les 18 premiers mois de l'immersion.

Les aciers 56 et 60 qui présentent les pertes de poids les plus faibles sont aussi ceux qui ont une teneur en aluminium plus importante que la teneur en chrome dans la couche de rouille.

. En zone de marnage, l'enrichissement en éléments d'alliage après deux années d'exposition reste faible en regard des concentrations mesurées en immersion, et ceci malgré une vitesse de corrosion élevée et de ce fait une dissolution importante des éléments d'alliage.

#### 4 - DISCUSSION ET CONCLUSION

Les essais in situ effectués sur les sites de Brest et de Biarritz conduisent à des résultats cohérents : les aciers les plus alliés 4Cr-1Al, 2Cr-1Al et 3Cr donnent les pertes de poids les plus faibles tandis que les aciers 2Cr, 2Cr-0,3Al et 2Cr-1Mo révèlent un comportement intermédiaire entre les trois premiers et l'acier doux de référence qui subit la corrosion généralisée la plus importante. Les additions de Cr et de Al réduisent d'un facteur 3 à 4 ( $\approx 0,025$  mm/an) les taux de corrosion de la nuance de référence non alliée.

Cependant, tous les aciers ne subissent pas les mêmes formes de corrosion, et les aciers les plus riches en Cr connaissent les corrosions localisées les plus importantes. Parmi les nuances étudiées, celles à 2Cr-1Al présentent à l'issue de deux années d'exposition, le meilleur compromis de résistance aux deux formes de corrosion précitées.

En immersion, les éléments d'alliage exercent un effet essentiellement en modifiant les caractéristiques des couches de rouille qui adhèrent au métal, et qui sont principalement constituées de magnétite ; les éléments Cr, Mo et surtout Al sont enrichis dans ces couches et ceci d'autant plus que le métal de base est plus allié. Ces couches internes, enrichies en éléments d'alliage, adhérentes et compactes, doivent constituer un écran protecteur contre la corrosion. Les phénomènes d'enrichissement sont beaucoup plus faibles dans les zones de marnage.

200

Les raisons de la tendance à la corrosion localisée des nuances les plus alliées ne sont pas complètement éclaircies. Il est vraisemblable que les inclusions  $MnS + Al_2O_3$ , que nous avons décelées (2) dans l'acier 4Cr-1Al par exemple<sup>2</sup>, peuvent intervenir sur l'amorçage des piqûres (7,8). Toutefois, les dimensions des zones de corrosions localisées et des inclusions ne sont pas du tout du même ordre de grandeur.

Il semble bien certain que les phénomènes d'acidifications prononcées ( $pH \leq 3,8$ ) qui ont été mis en évidence par plusieurs auteurs (9,10,11) contribuent beaucoup au développement des corrosions, lorsque celles-ci sont amorcées. Dans cette optique toutefois, le mécanisme d'action des éléments Al et Mo n'apparaît pas encore nettement. Sur le plan pratique cependant, le molybdène tend à généraliser la corrosion sur l'ensemble de la surface de l'éprouvette.

Un phénomène important à prendre aussi en compte nous paraît être celui du couplage galvanique entre les zones cathodiques "passivées" et les zones anodiques corrodées, zones que l'on décèle à l'oeil nu sur les nuances les plus alliées. Un tel couplage est en effet de nature à porter, en milieu acide, le métal à des potentiels où il peut subir des corrosions par "piqûres" et à exalter la dissolution anodique (2).

En définitive, l'addition d'éléments judicieusement choisis permet :

- de réduire de façon importante la corrosion généralisée des aciers dans l'eau de mer ;
- de trouver un compromis entre la résistance à la corrosion généralisée et la corrosion localisée.

Les taux de corrosion observés sont alors tels que la protection cathodique ou par peinture n'est plus indispensable.

Nos travaux se poursuivent pour améliorer encore les compositions des nuances à base de chrome et d'aluminium.

REFERENCES

- (1) M. CONFENTE, L. BELLOT, E. ANTOINE, J. GULZENNCE, L. LEMOINE  
Ve Congrès de la Corrosion Marine et des Salissures  
Barcelone, 1980
- (2) J.C. CHARBONNIER, M. CONFENTE, T. JOSSIC, L. LEMOINE,  
J.L. PAGNIEZ  
A paraffre
- (3) T. MISAWA  
Corrosion Science, 1974, Vol. 14, pp 279
- (4) J.E. HILLER  
Werkstoffe und Korrosion, 1966, Vol. 17, p. 943
- (5) P. KELLER  
Werkstoffe und Korrosion, 1969, Vol. 20, p. 102
- (6) A. TAKAMURA, K. ARAKAWA, W. FUJIWARA, H. MIROTE  
Proceedings of the 5th International Congress on Metallic  
Corrosion, Tokyo, 1972, NACE
- (7) A. SAARINEN, K. ONELA  
Corrosion Science, 1979, vol. 10, p. 809
- (8) R. STROMMEN  
Communication présentée à l'assemblée annuelle 1975 de l'ins-  
titut International de Soudure - Tel Aviv.
- (9) R. BRUNO  
Meccanismo d'azione deivari elementi di lega nez controllo  
dei ferromeni di corrosione localizzata e generalizzat  
Conventien 7210 KB/404 n°4.
- (10) N. LUKOMSKI, K. BOHNENKAMP  
Werkstoffe und Korrosion, 30, 1979, p. 482
- (11) Y. H. LEE, Z. TAKEHARA, S. YOSHIZAWA  
Corrosion Science, 21, 1981, P. 391

## ETUDE DE LA CORROSION D'ACIERS EN EAU DE MER PAR MESURE DE L'IMPEDANCE ELECTROCHIMIQUE

Ph. Blanchard\* J. Courtot-Coupez\*, L. Lemoine\*\*

\* Laboratoire de Chimie Analytique

LA. CNRS n° 322, UBO, 29283 BREST CEDEX (France)

\*\* CNEXO/COB

BP 337, 29273 BREST CEDEX (France)

### RESUME

Le comportement de diverses nuances d'aciers a été observé en milieu eau de mer naturelle dans des conditions d'immersion pendant une durée de deux années, ainsi qu'en cellule à circulation.

Le mécanisme de la corrosion a été étudié. Une comparaison a également été entreprise entre les différentes méthodes de suivi de la corrosion ; notamment les différents paramètres pouvant être extraits de la mesure de l'impédance électrochimique ont été confrontés aux valeurs obtenues pour les pertes de poids.

### ABSTRACT

Behaviour of various mild steels has been investigated in natural seawater under immersed conditions and in flowing cells, during two years.

Corrosion mechanism has been studied. A calibration has been done between different electrochemical methods. Particularly, electrochemical impedance data have been compared with weight losses.

### INTRODUCTION

Les études de corrosion d'aciers en eau de mer mettent le plus souvent en jeu des mesures de pertes de poids et de profondeurs d'attaque ainsi que le tracé des courbes intensité-potentiel.

Actuellement, la technique des impédances électrochimiques, permettant de dissocier les mécanismes fait l'objet de développements. Cependant

malgré sa puissance, elle n'est encore que peu utilisée car elle nécessite, pour une bonne interprétation des résultats, une méthodologie de dépouillement délicate de mise en oeuvre.

Dans ce contexte, une expérimentation a été entreprise pour étudier la résistance à la corrosion marine de trois aciers différents, immergés pendant deux ans en eau de mer naturelle. L'évolution de la corrosion a été suivie par les différentes méthodes citées précédemment et une interprétation des diagrammes d'impédance a été recherchée.

## 1 - RAPPEL BIBLIOGRAPHIQUE

Les mécanismes de corrosion d'aciers en milieu marin et dans les milieux de pH voisins de la neutralité sont rendus très complexes par la croissance à la surface d'épais dépôts de produits de corrosion. En effet, l'eau de mer contenant environ 8 mg/l d'oxygène permet d'oxyder le fer à des degrés supérieurs à deux. Les oxyhydroxydes ferriques produits, très peu solubles, forment des couches de rouille dont la composition et la structure peuvent être déterminées par spectrophotométrie infrarouge ou diffraction de rayons X. C'est ainsi que la couche externe est essentiellement constituée d'un dépôt peu adhérent pouvant former d'épais renflements de couleur rouge brique à brun foncé ; les constituants qu'elle renferme sont principalement la goethique ( $\alpha$ -FeOOH), la plus stable et la lépidocrocite ( $\gamma$ -FeOOH). La couche interne dont la croissance intervient plus tard (dans des conditions d'oxygénation plus faibles), plus fine et très adhérente, renferme principalement de la magnétite ( $\text{Fe}_3\text{O}_4$ ). [5]

Les examens des produits de corrosion obtenus laissent prévoir plusieurs mécanismes possibles pour leur formation et donc pour la corrosion des aciers dans l'eau de mer.

La réaction de dissolution du fer est au départ couplée avec la réduction de l'oxygène et l'on a formation d'une couche d'oxyhydroxydes ferriques, surtout de structure  $\alpha$  au départ (seule cette structure est stable au pH de l'eau de mer, un milieu plus acide étant nécessaire à la formation de la forme  $\gamma$ ). L'oxygénation diminuant, l'on a ensuite formation d'une couche interne de magnétite, pouvant elle-même être oxydée dans une étape ultérieure ; la corrosion devient alors plus lente.

La poursuite du processus se ferait ensuite par réduction de l'oxygène migrant à travers les couches peu conductrices de FeOOH et oxydation, soit de la magnétite en FeOOH à l'interface entre ces deux oxydes, soit du fer avec croissance de la couche interne à l'interface fer/magnétite ou migration d'ions ferreux à travers la magnétite.

Une deuxième possibilité pour la réaction cathodique réside dans la réduction de l'oxyhydroxyde en magnétite, qui imposerait la vitesse. Le front entre les deux oxydes se rapprochant de la surface, on pourrait avoir de nouveau réoxydation par l'oxygène en solution.

Il faut également noter que dans le cas d'aciers faiblement alliés, la couche interne de magnétite s'enrichit en éléments d'alliages qui peuvent



modifier ainsi ses propriétés vis à vis des réactions cathodiques et anodiques [1,2,4,5].

## 2 - MATERIELS ET TECHNIQUES

### 2.1 - Préparation des éprouvettes

Les matériaux testés sont des aciers doux. La composition élémentaire est donnée par le tableau 1.

Les éprouvettes carrées (9x9 cm) ont été découpées dans des tôles brutes de laminage de chaque nuance. Elles n'ont pas subi de traitements thermiques, ni de rectification ou de polissage. Après décapage quelques heures dans HCl 5N contenant 5g/l d'hexaméthylènetétramine, elles ont été rincées à l'eau distillée puis à l'alcool éthylique avant d'être séchées à l'étuve. Chaque échantillon est raccordé, par soudure à l'étain, à un conducteur électrique ; les surfaces non destinées à l'étude (partie arrière, bordure, zone de soudure) sont ensuite recouvertes de résine epoxy. La surface exposée est alors dans tous les cas proche de 50 cm<sup>2</sup>. Le poids initial déterminé, les éprouvettes sont immergées verticalement sur des cadres de PVC en bassin avec renouvellement continu d'eau de mer. Ce bassin étant situé à l'intérieur d'un bâtiment, la croissance des salissures biologiques est partiellement inhibée.

Des échantillons de 10 cm<sup>2</sup> environ et polis jusqu'au papier numéro 800 ont été exposés en cellules à circulation d'eau de mer naturelle après une préparation identique. Un écoulement laminaire a été obtenu et la vitesse de l'eau est proche de 0,1 m/s.

Les éprouvettes sont relevées après des périodes d'exposition de 3, 6, 12 et 18 mois après avoir subi les diverses mesures électrochimiques.

### 2.2 - Mesures effectuées

Les potentiels libres de corrosion sont mesurés hebdomadairement par rapport à une électrode de référence Ag/AgCl/Cl<sup>-</sup>edm (potentiel 5 mV au-dessus de l'électrode ECS) à l'aide d'un millivoltmètre haute impédance Tacussel Axiès 20 000.

Les courbes intensité-potentiel sont tracées à l'aide d'un potentiostat et d'un pilote de tension Tacussel. L'acquisition des données a été automatisée par l'emploi d'un ensemble composé d'un calculateur servant également au traitement des données, d'un millivoltmètre mesurant d'une façon alternée le courant et la tension et d'une table traçante digitale. L'électrode de référence est une électrode ECS tandis qu'une plaque de titane platiné constitue la contre-électrode.

Les courbes sont tracées à partir du potentiel de corrosion, à la vitesse de 5 mV/mn, vitesse pouvant être considérée comme compatible avec un état quasi-stationnaire. Une correction de chute ohmique est effectuée.

Les diagrammes d'impédance sont obtenus à l'aide d'un ensemble Schlumberger-Solartron, analyseur de fonction de transfert 1172 et potentiostat ECI 1186. L'enregistrement a lieu en mode potentiostatique avec une tension surimposée de 10 mV efficaces. La gamme de fréquences s'étend entre 10 KHz et 0,1 mHz à raison de 5 mesures par décades, la durée totale d'acquisition est alors d'environ 15 heures.

Les données sont stockées sur ordinateur pour faire l'objet de divers traitements : transformations plan de Nyquist - plan de Bode, ajustements de modèles et simulations. Les diagrammes présentés sont paramétrés en fréquences, par décades depuis la valeur 1 pour 10 KHz jusqu'à 9 pour 0,1 mHz.

### 3 - RESULTATS

#### 3.1 - Pertes de poids et morphologie des attaques

La figure 1 représente la perte de poids observée pour les différents aciers en fonction de la durée d'immersion. Cette mesure est effectuée après élimination des produits de corrosion dans une solution décapante contenant un inhibiteur. Pour l'acier au carbone, la vitesse d'attaque semble relativement constante autour de 5 g/dm<sup>2</sup>/an ; l'attaque est uniformément répartie sur la surface. Pour les autres aciers, un net infléchissement est constaté après environ 6 mois. Dans nos conditions, la perte de poids est environ 3 fois plus faible, au bout de 18 mois d'essais, pour l'acier 3 que pour l'acier de référence. Il faut de plus noter que sur les aciers alliés, l'attaque n'est pas uniforme mais donne lieu à une séparation entre des zones anodiques rouillées, et cathodiques recouvertes de dépôt calcomagnésien.

#### 3.2 - Suivi du potentiel

A l'immersion en eau de mer stagnante, le potentiel se situe en général autour de - 700 mV/ECS. Une valeur très stable est obtenue au bout d'une cinquantaine de jours. Un ennoblissement très lent et régulier est alors constaté durant une année, suivi d'une stabilisation. Nos résultats sont sur ce plan en accord avec ceux récemment publiés pour un même type de matériau [7]. Les nuances alliées présentent des potentiels plus élevés. Il ne semble cependant pas exister de rapport direct en vitesse de corrosion et potentiel d'abandon pour les aciers testés.

#### 3.3 - Courbes intensité-potentiel

Les caractéristiques intensité-potentiel ont été tracées dans les conditions d'exposition des éprouvettes à des temps d'immersion de 0, 3, 6, 12 et 18 mois.

| Nuance | C     | Mn   | S     | Ni    | Cr   | Mo    | Cu    | Al    |
|--------|-------|------|-------|-------|------|-------|-------|-------|
| 1      | 0,102 | 0,28 | 0,006 | 0,035 | 0,14 | 0,03  | 0,02  | 0,017 |
| 2      | 0,100 | 0,34 | 0,007 | 0,032 | 3,11 | 0,02  | 0,015 | 0,026 |
| 3      | 0,115 | 0,39 | 0,005 | 0,032 | 2,14 | 0,007 | 0,01  | 0,925 |

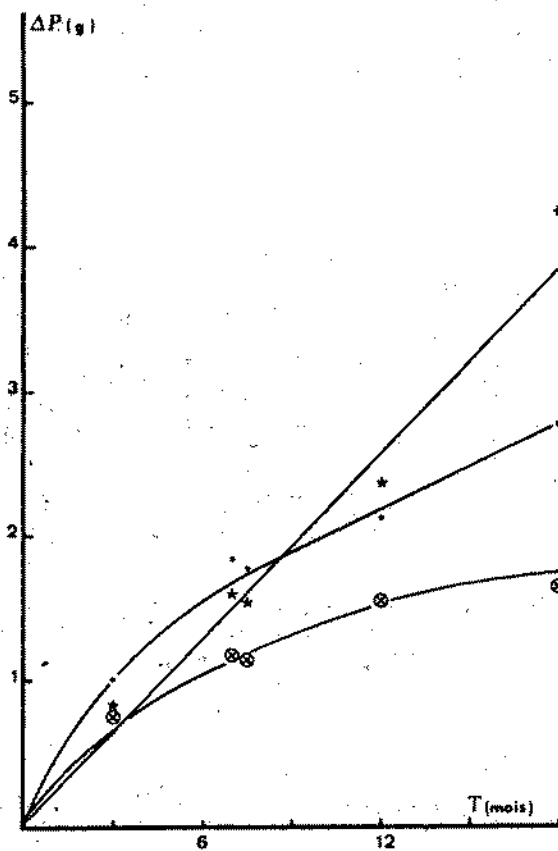
**Tableau 1** : Composition élémentaire des aciers étudiés.

| Nuance | Potentiel (mV/ECS) | Début | 3 mois | 6 mois | 18 mois |
|--------|--------------------|-------|--------|--------|---------|
| 1      | - 850              | 17,5  | 11,43  | 5,05   | 5,00    |
|        | - 800              | 13    | 9,52   | 5,00   | 5,10    |
| 2      | - 850              | 19    | 18,3   | 17,80  | 5,13    |
|        | - 800              | 16    | 15,5   | 11,26  | 4,07    |
| 3      | - 850              | 15    | 15,18  | 7,85   | 7,49    |
|        | - 800              | 13    | 11,88  | 6,48   | 6,55    |

**Tableau 2** : Evolution en fonction du temps, du courant de diffusion de l'oxygène à 2 surtensions cathodiques (en  $\mu\text{A cm}^{-2}$ ).

|   | Début          |                |                |                | 6 mois         |                |                |                | 12 mois        |                |                |                | 18 mois        |                |                |                |
|---|----------------|----------------|----------------|----------------|----------------|----------------|----------------|----------------|----------------|----------------|----------------|----------------|----------------|----------------|----------------|----------------|
|   | C <sub>2</sub> | R <sub>2</sub> | C <sub>3</sub> | R <sub>3</sub> | C <sub>2</sub> | R <sub>2</sub> | C <sub>3</sub> | R <sub>3</sub> | C <sub>2</sub> | R <sub>2</sub> | C <sub>3</sub> | R <sub>3</sub> | C <sub>2</sub> | R <sub>2</sub> | C <sub>3</sub> | R <sub>3</sub> |
| 1 | .24            | 4.6            | -              | -              | 6.7            | 2.65           | -              | -              | 28.8           | 3.4            | -              | -              | 1630           | 1.9            | -              | -              |
|   | -              | -              | -              | -              | 11.0           | 2.79           | -              | -              | 22.8           | 2.9            | -              | -              | -              | -              | -              | -              |
| 2 | .58            | 3.30           | 29.4           | 4.0            | 9.7            | 2.5            | -              | 1.5            | 11.7           | 4.9            | 355            | 2.8            | 82.5           | 6.8            | -              | -              |
|   | -              | -              | -              | -              | 0.7            | 3.3            | -              | -              | -              | -              | -              | -              | -              | -              | -              | -              |
| 3 | .57            | 3.6            | -              | -              | .34            | 4.2            | -              | -              | 0.26           | 1.6            | 1.4            | 9.8            | .61            | 7.3            | 37.7           | 6.5            |
|   | -              | -              | -              | -              | .64            | 2.7            | -              | -              | 1.0            | 2.8            | 8.0            | 1.8            | .55            | 6.5            | 3.9            | 4.4            |

**Tableau 3** : Evolution des paramètres de l'impédance électrochimique avec le temps.  
(capacités en  $\text{mFcm}^{-2}$ , résistances en  $\text{K}\Omega\text{cm}^2$ )



**Figure 1 :** Evolution de la perte de poids des échantillons avec le temps ;  
\* nuance 1, . nuance 2, ⊗ nuance 3.

### 3.3.1 - Courbes cathodiques

Dès l'immersion, en l'absence de produits de corrosion, ces courbes mettent en évidence la présence d'un palier de diffusion de l'oxygène dissous s'étendant du potentiel libre jusqu'à environ  $-1000$  mV/ECS (figure 2a). Le courant limite de diffusion de l'oxygène est d'environ  $20 \mu\text{Acm}^{-2}$ . Il est à noter qu'à ce stade aucune différence importante n'existe entre les nuances, hormis le potentiel de corrosion.

Ces courbes évoluent au cours du temps (figure 2b) et correspondent probablement à 2 réactions de réduction simultanées : celle de l'oxygène dissous et celle probablement des produits de corrosion, à des potentiels inférieurs à  $-800$  mV/ECS. Cette dernière réaction subsiste lors du tracé de la courbe en eau de mer désoxygénée quelques heures auparavant. L'apparition de produits de corrosion réductibles ne peut être mise en évidence dans le cas de la nuance comportant du chrome et de l'aluminium.

L'évolution du courant limite la diffusion de l'oxygène (courant en milieu oxygéné - courant en milieu désoxygéné) en fonction du temps est donnée dans le tableau 2. Celui-ci diminue au cours du temps mais d'une manière moins rapide dans le cas des nuances alliées. Ce phénomène peut être attribué à la différence des faciès d'attaque entre l'acier 1, uniformément rouillé, et les aciers 2 et 3 corrodés par plaques. Le dépôt calco-magnésien semble donc être plus perméable à l'oxygène que les couches de rouilles.

Dans le cas de l'acier au carbone, la vitesse de corrosion en  $\mu\text{A/cm}^2$ , estimée à l'aide de la loi de Faraday à partir des pertes de poids, a sensiblement la même valeur que le courant limite de diffusion de l'oxygène ( $5 \mu\text{A/cm}^2$ ). Pour les autres aciers, on se situe très probablement aux conditions de corrosion, dans la zone mixte activation-diffusion de la vague de diffusion de l'oxygène.

### 3.3.2 - Courbes anodiques

L'allure des courbes anodiques dans la gamme de courants  $0 - 0,2 \text{ mA cm}^{-2}$  est représentée sur la figure 3. Ces courbes n'évoluent pratiquement pas dans le temps pour l'acier au carbone, tandis qu'une nette diminution du courant apparaît dans le cas des aciers alliés. Ces courbes ne présentant pas de pentes de Tafel, cette diminution du courant est difficile à attribuer à une modification du mécanisme électrochimique. L'hypothèse d'une diminution de la surface mise en jeu semble devoir être rejetée, l'aptitude à la corrosion localisée ayant tendance à s'estomper avec le temps [5]. Les causes les plus probables sont soit la diminution du paramètre  $b_a$  de Tafel par une variation de la nature de l'interface, soit la formation de produits de corrosion de grande résistance électrique, déformant la courbe intensité-potentiel.

L'évaluation de la vitesse de corrosion à partir de ces courbes ne peut être effectuée ni par méthode graphique, ni par ajustements de paramètre à l'aide de programmes récemment publiés dans la littérature [8].

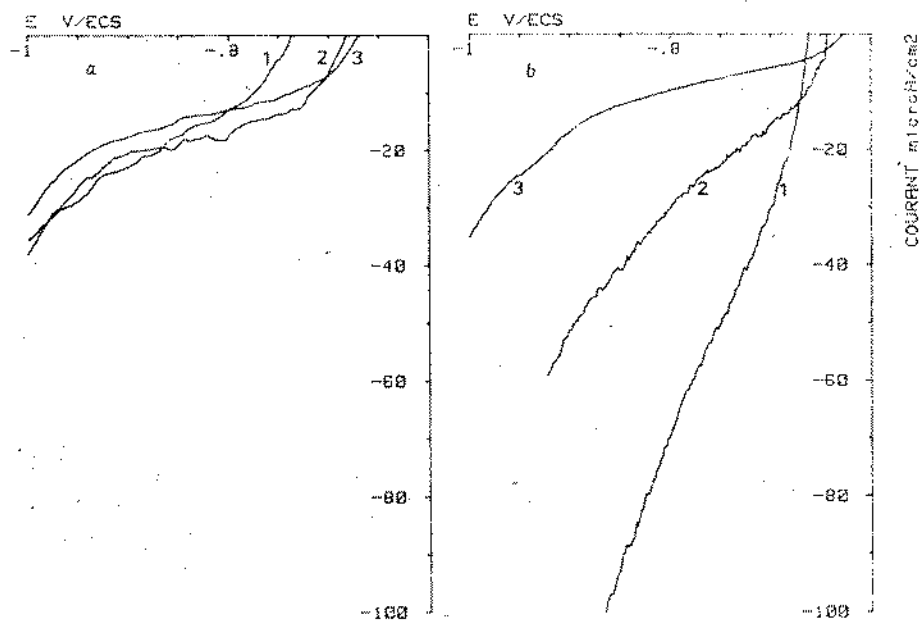


Figure 2 : Courbes intensité-potentiel cathodiques ;  
a : 3 mois en immersion, b : 18 mois en immersion.

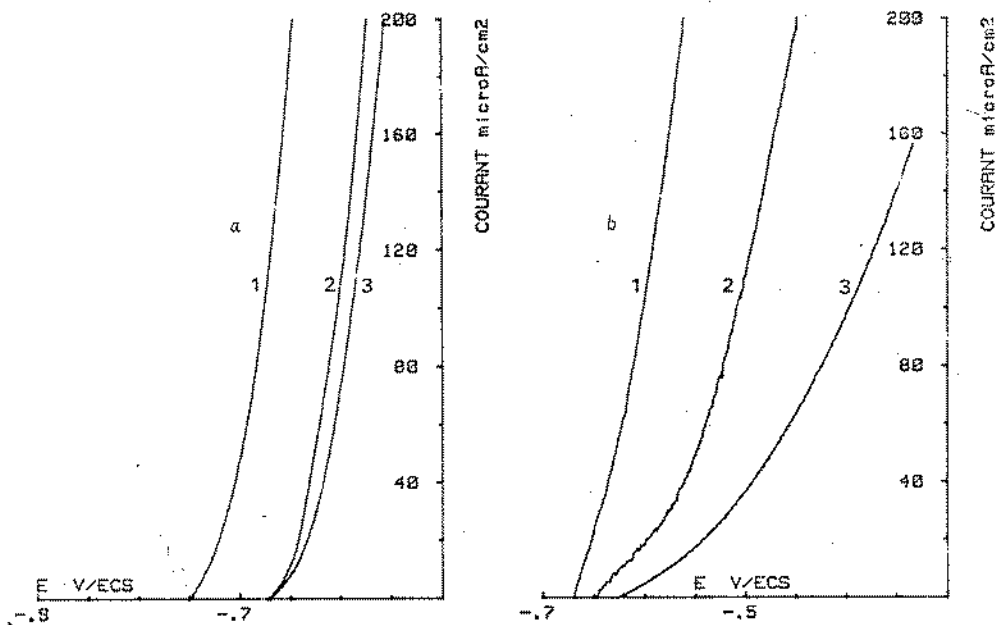


Figure 3 : Courbes intensité-potential anodiques ;  
a : 3 mois en immersion, b : 6 mois en immersion.

### 3.3.3 - Discussion

Sauf dans le cas de la nuance au carbone, ces courbes ne permettent pas de calculer le courant de corrosion et donc de caractériser la tenue à la corrosion de nos aciers. Toutefois, il a pu être mis en évidence des différences de réactivité entre les courbes de rouille, apportées par la présence d'éléments d'alliage. Ainsi, l'ensemble des propriétés cathodiques et anodiques, de même que l'évolution des potentiels dans le temps, permettent de penser que la vitesse d'attaque des aciers alliés est pour une large part sous contrôle anodique.

### 3.4 - Diagrammes d'impédance électrochimique

Des diagrammes ont été tracés en potentiel de corrosion pour diverses durées tout au long du vieillissement des éprouvettes. Les principaux types obtenus sont représentés sur la figure 4. La forme de ceux-ci, notamment ceux relevant des nuances alliées, implique qu'ils contiennent plusieurs boucles ; résistance de transfert ( $R_t$ ) et résistance de polarisation ( $R_p$ ) n'ont donc pas dans notre cas la même signification. Ceci peut expliquer l'absence de droites de Tafel sur les courbes intensité potentiel.

Les diverses boucles présentes relèvent de temps de relaxation très voisins ; selon l'ordre décroissant des fréquences, on peut toutefois envisager de décomposer les diagrammes en différents secteurs : - A hautes fréquences (de 10 KHz à 10 Hz), il existe une boucle dans le domaine capacitif qui voit son influence augmenter avec le temps. Celle-ci est suivie d'une seconde boucle capacitive à des fréquences comprises entre 1 Hz et 10 mHz, selon les aciers et les temps d'immersion, et dont le centre est situé très en dessous de l'axe des réels. Il est généralement possible d'observer d'autres boucles à fréquences très basses, particulièrement sur la nuance alliée au chrome et à l'aluminium. Elles présentent généralement un caractère inductif pour les temps d'immersion inférieurs à 6 mois et capacitif pour les temps plus longs.

#### 3.4.1. Méthode d'exploitation des diagrammes

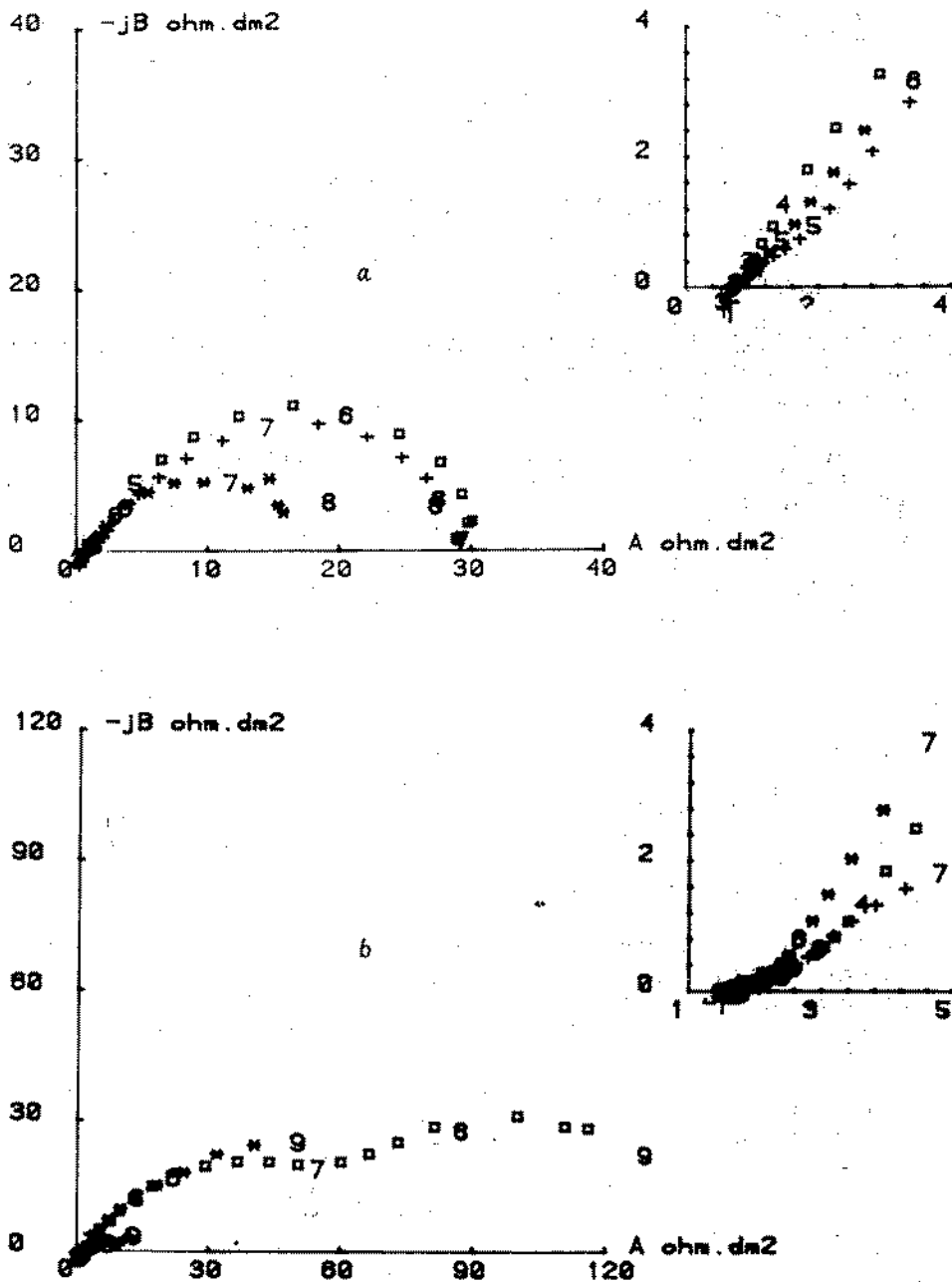
Une corrélation a été recherchée entre un paramètre pouvant être extrait de l'impédance avec les données de pertes de poids. Pour cela, il faut alors noter que pour les diagrammes obtenus dans notre étude, aucune détermination de paramètres ne peut être effectuée par une méthode simple. La transformation selon la technique de Bode [9] facilitant généralement l'exploitation d'impédances composées d'éléments conventionnels (capacités et résistances indépendantes de la fréquence) n'a pas apporté de grandes améliorations.

Une méthode de calcul a donc été employée [10], qui consiste en l'ajustement de portions de cercles ou de droites. Celle-ci fait appel au calcul de l'ellipse décrite par les variables centrées réduites :

$$\theta_1 = \frac{x - E(x)}{\sigma_x}$$

$$\theta_2 = \frac{y - E(y)}{\sigma_y}$$





**Figure 4 :** Diagrammes d'impédance électrochimique au potentiel de corrosion ; a : 3 mois en immersion, b : 18 mois en immersion (+ : nuance 1, \* : nuance 2, □ : nuance 3).

où  $E(x)$  et  $E(y)$  représentent la moyenne des variables  $x$  et  $y$  affectées respectivement à la partie réelle et imaginaire de l'impédance.  $\sigma_x$  et  $\sigma_y$  représentent les écarts-types calculés sur ces mêmes variables.

La détermination de cette ellipse d'équation :

$$\frac{\theta_1^2}{A} + \frac{\theta_2^2}{B} = 1$$

où  $A$  et  $B$  sont estimés par une méthode de moments, constitue une voie générale permettant d'accéder à l'ajustement de parties de droites pouvant mettre en évidence la présence d'impédance de diffusion ou de caractériser une surface poreuse [11], ou de parties de cercles relatifs à des capacités.

Cette méthode fournit alors la valeur du rayon, la position du centre dans le cas d'un cercle, la valeur de la pente dans le cas d'une droite et l'analyse du choix du modèle par discrimination.

Cet ajustement a été, dans la mesure du possible, appliqué à l'analyse de chaque arc capacitif dans un domaine de fréquences (partie haute fréquence) où il n'y a pas de perturbations trop importantes par les arcs voisins. La résistance associée à chaque arc est alors donnée par la valeur comprise entre les deux intersections du cercle avec l'axe des réels. La capacité, à 1 Hz, a été calculée selon la technique proposée par Cole and Cole [12]

$$\text{Log} \frac{|R-Z|}{|Z|} = (1-\alpha)(\text{Log}(R.C) + \text{Log}(\omega))$$

avec  $R$  : Résistance associée à l'arc

$C$  : Capacité " "

$Z$  : Impédance à la fréquence  $\omega/2\pi$

$\alpha$  : argument du vecteur (origine du diagramme centre du cercle).

en utilisant l'ajustement d'une droite.

Le diagramme total peut alors être progressivement simplifié par suppression des éléments calculés. Dans le cas de la suppression d'une capacité en parallèle, le diagramme résultant peut être obtenu à l'aide de la relation

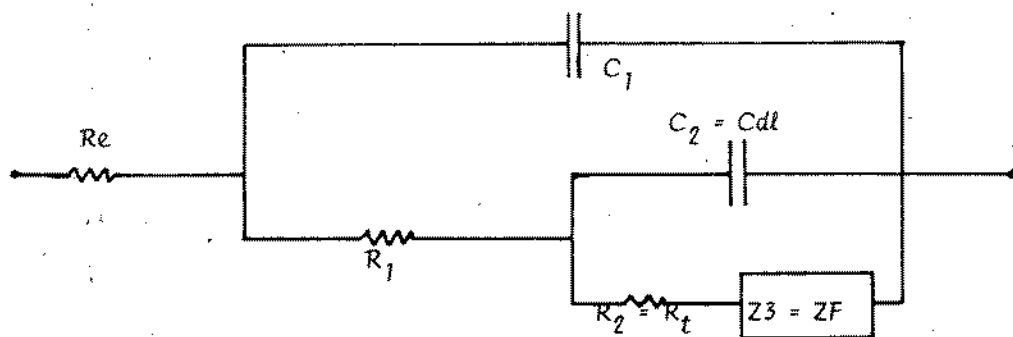
$$\frac{1}{Z} = \frac{1}{Z_{\text{tot}}} - jC(\omega)$$

où  $C_\omega$  représente la valeur de la capacité à fréquence donnée, pouvant être obtenu selon :

$$C(\omega) = \frac{(R.C)^{1-\alpha} \cdot \omega^{-\alpha}}{R} (\cos \alpha \frac{\pi}{2} - j \sin \alpha \frac{\pi}{2})$$

### 3.4.2 - Interprétation et relation avec la vitesse de corrosion

A partir des résultats des ajustements effectués ainsi que des interprétations données par différents auteurs, il est possible de proposer le schéma équivalent représenté sur la figure 5.



**Figure 5 :** Schéma équivalent utilisé.

$R_1$  et  $C_1$  peuvent être attribués à l'influence d'un dépôt à la surface de l'électrode [13]. La mesure du produit  $R_1$  à plusieurs potentiels sur des échantillons rouillés en cellules à circulation durant 4 mois donne des valeurs assez proches de celles attendues pour le produit  $R_t \cdot I$  (de 120 à 160 mV pour la partie cathodique et de 20 à 40 mV pour la partie anodique). Ceci justifie donc le choix de la seconde boucle comme celle représentant la capacité de double couche en parallèle sur la résistance de transfert.

Les résultats des ajustements sont donnés dans le tableau 3.

Les valeurs de la capacité de double couche sont généralement très grandes (de l'ordre du mF cm<sup>-2</sup>). Celle-ci augmente de façon quasi linéaire avec le temps dans le cas de la nuance non alliée et de façon moins importante pour les autres. Ces différences traduisent très certainement des modifications des couches de rouille par les éléments d'alliage.

Il faut signaler que la forme de la seconde boucle capacitive, notamment dans le cas de l'acier au carbone, peut s'éloigner notablement d'un cercle dans sa partie haute fréquence. Ce phénomène a déjà été signalé [7] comme pouvant provenir de l'influence d'une couche de magnétite poreuse et conductrice.

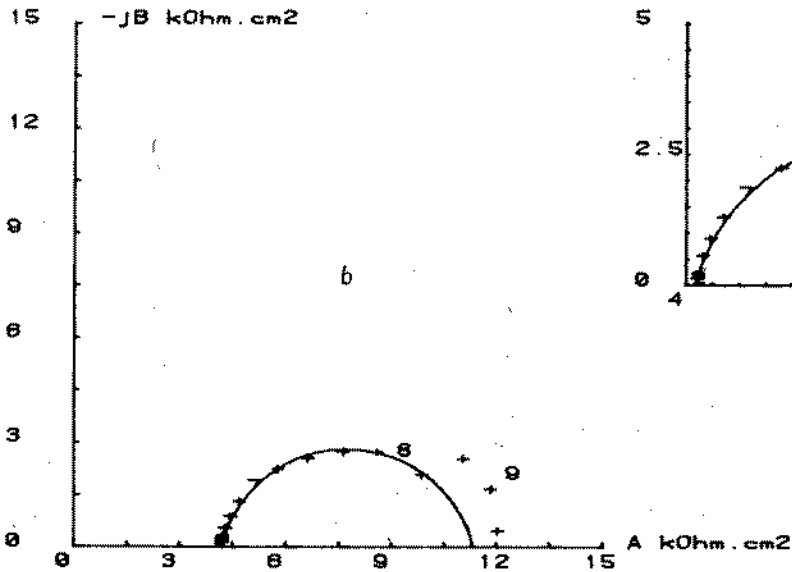
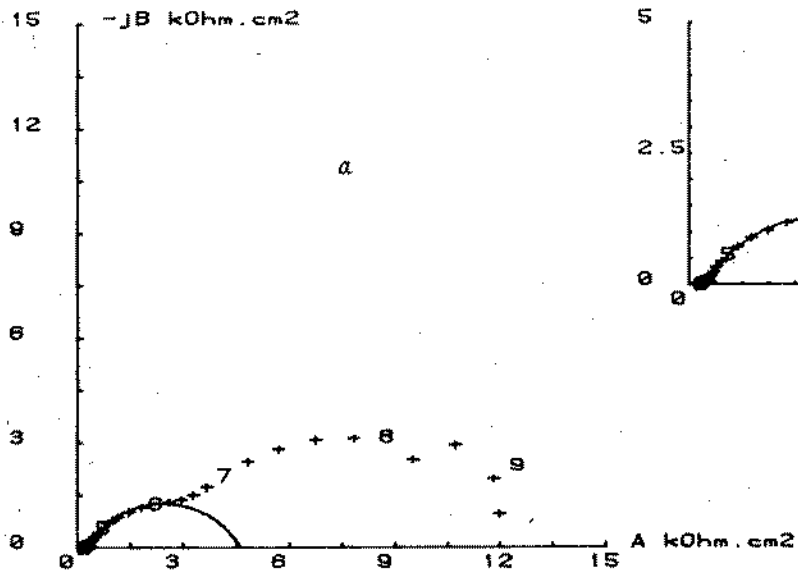
Bien que la vitesse de circulation de l'eau ait une influence importante sur la vitesse de corrosion de nos aciers, il n'a pas été possible de mettre en évidence la présence d'une impédance de diffusion. L'impédance faradique ( $Z_3$  ou  $Z_F$ ), obtenue par suppression des deux premières boucles se ramène, après 6 mois environ, à une simple résistance pour les aciers 1 et 2 tandis qu'une boucle capacitive peut généralement être obtenue pour l'acier 3 (figure 6).

La vitesse de corrosion constante au cours du temps pour l'acier au carbone peut être associée à la résistance de transfert qui reste quasi-invariante tout au long de l'immersion. Un étalonnage semble également réalisable entre  $R_t$  et la vitesse de corrosion par l'acier 2, tandis que le comportement de l'acier 3 semble mieux corrélé avec la somme  $R_2 + R_3$  (ou  $R_t + R_F$ ) qu'avec  $R_t$ .

## CONCLUSION

Une méthode de calcul des composants de l'impédance a été proposée, qui ne fait pas appel aux grandes approximations généralement effectuées pour des diagrammes présentant des boucles de formes non conventionnelles. La validité des paramètres ainsi extraits peut être renforcée par la bonne corrélation généralement obtenue entre diagrammes expérimentaux et diagrammes simulés.

Une relation empirique peut être obtenue entre la vitesse de corrosion et la résistance de polarisation. Toutefois, la grande complexité des diagrammes obtenus et les différentes hypothèses émises quant à l'attribution des différentes boucles nécessitent encore des études fines du rôle électrochimique des différentes couches présentes sur l'électrode par l'intervention de facteurs tels que porosité, résistivité, capacités. Des travaux sur des couches uniformes de dépôt calcomagésien et de produits de corrosion sont actuellement en cours.



**Figure 6 :** Exemple d'exploitation des diagrammes ;  
cas de l'acier n° 3.  
a) Ajustement du second arc capacitif ;  
b) Tracé et ajustement de l'impédance faradique.

**BIBLIOGRAPHIE**

- [01] N. AZZERI, R. BRUNO, L. SPLENDORINI  
*Corrosion Science*, 21, 11, (1981), 78.
- [02] G.M. FERRARI,  
Convention 7210 KB/604, Foundation for materials research in the  
sea, Netherlands, 1980.
- [03] A. BONNEL, F. DABOSI, C. DESLOUIS, M. DUPRAT, M. KEDDAM,  
B. TRIBOLLET,  
*J. Electrochem... Soc.*, 130, 4, (1983), 753.
- [04] L. LEMOINE, E. ANTOINE,  
Convention 7210 KB/303, CNEXO, 1980.
- [05] B. LE BOUCHER,  
*Corrosion marine et effets protecteurs des produits de corrosion*,  
6ème colloque sur l'Exploitation des Océans, Paris, 1974.
- [06] J.C. CHARBONNIER,  
Convention 7210 KB/302, IRSID, 1982.
- [07] M.H. PETERSON, T.J. LENNOX,  
*Mat. Performance*, 23, 3, (1984), 15.
- [08] N.D. GREENE, R.H. GANDHI,  
*Mat. Performance*, 7, (1982), 34.
- [09] F. MANSFELD,  
*Corrosion* 37, 5, (1981), 301.
- [10] J. LABEVRIE  
*Discrimination de droites et d'arcs de cercle dans un diagramme d'impédance électrochimique. Rapport CNEXO 84/GO/R10.*
- [11] J.P. CANDY, P. FOUILLOUX, M. KEDDAM, H. TAKENOUTI,  
*Electrochim. Acta*, 26, 8, (1981), 1029.
- [12] K.S. COLE, R.H. COLE,  
*J. Chem. Phys.*, 9, (1941), 341.
- [13] D.G. JOHN, P.C. SEARSON, J.L. DAWSON,  
*Br.Corr. J.*, 2, (1981), 108.

EFFET DE LA PRESSION HYDROSTATIQUE SUR LA PERMEATION DE L'HYDROGENE  
DANS L'ACIER, DANS DES CONDITIONS DE CHARGEMENT ELECTROLYTIQUE

FESTY Dominique, LEMOINE Lionel

CNEXO-COB

BP 337 - 29273 BREST CEDEX (France)

RESUME

Afin de connaître le comportement des aciers à haute résistance mécanique utilisé en grande profondeur, une étude a été entreprise pour qualifier l'effet de la pression hydrostatique sur la perméation de l'hydrogène dans les aciers. Une cellule de perméation spécifique a été développée. Les expérimentations sont réalisées sur du fer Armco et de l'acier 42CD4 dans un électrolyte agité ( $0,1N H_2SO_4$ ) jusqu'à 800 bar. Les résultats obtenus mettent en évidence que la pression n'affecte pas le coefficient de diffusion mais augmente le flux d' $H_2$ , dans ces conditions d'essais. Un risque accru de fragilisation est à prévoir pour des aciers protégés cathodiquement sous forte pression.

INTRODUCTION

L'extension en grande profondeur de la recherche et de l'exploitation des ressources minérales et fossiles en milieu marin nécessitent et nécessiteront l'emploi d'aciers à haute résistance mécanique.

Dans de tels milieux, une fiabilité accrue du matériel est nécessaire compte tenu des coûts d'intervention.

En milieu marin la protection cathodique est généralement utilisée pour assurer une durée de vie maximale aux matériels. Cependant, la réduction cathodique de l'eau produit de l'hydrogène susceptible de fragiliser les aciers, ce qui va à l'encontre du critère de fiabilité.

Parmi les travaux effectués sur la fragilisation par l'hydrogène sur l'influence des paramètres d'environnement, l'effet de la pression

hydrostatique a été étudié par deux auteurs (1,2). Tout d'abord Nanis et Deluccia (1) ont travaillé sur du fer Armco dans une solution de chargement  $0,1 \text{ N H}_2\text{SO}_4 + 0,001 \text{ N HCL}$  à  $21^\circ\text{C}$ . Ils ont utilisé une cellule de perméation (type Devanathan (3)) conçue pour travailler sous pression hydrostatique. La mesure du taux de perméation et l'évaluation du coefficient de diffusion à différentes densités de courant et différentes pressions leur ont permis d'arriver aux résultats suivants :

- 1/ Le taux de perméation de l'hydrogène résiduel (sans protection cathodique) croît linéairement avec la pression jusqu'à 420 bar. La croissance s'accroît entre 420 et 550 bar. (figure 1)
- 2/ Les effets de la pression sur la perméation de l'hydrogène sont réversibles dans un domaine allant de 0 à 570 bar.
- 3/ Le coefficient de diffusion est indépendant de la pression appliquée jusqu'à 430 bar.
- 4/ La solubilité de l'hydrogène dans le fer Armco est proportionnelle à la pression appliquée jusqu'à 420 bar.

Ils concluent donc à l'intérêt de tenir compte du rôle de l'hydrogène dans la rupture d'aciers devant être utilisés à grande profondeur. D'autre part, l'absence d'effet de la pression hydrostatique sur le coefficient de diffusion indique une distorsion minime du réseau et peut apporter des éléments dans la description de la migration d' $\text{H}_2$  dans le cas de contraintes statiques.

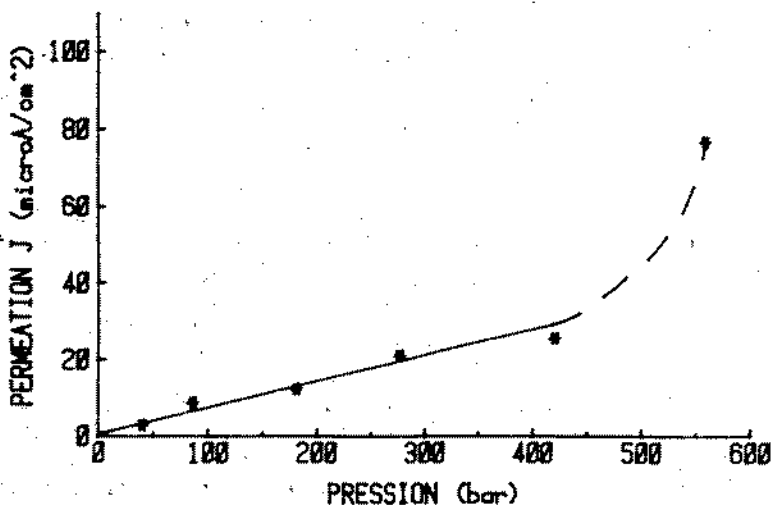


Figure 1: Courant de perméation résiduel en fonction de la pression hydrostatique à  $21^\circ\text{C}$  (1)



Blundy et Schreier reprennent la même technique expérimentale en ajoutant un système d'agitation afin d'isoler l'effet de la pression partielle de l'hydrogène  $\text{PH}_2$ .

Ils ont étudié la perméation de l'hydrogène à travers l'acier dans  $0,1 \text{ mol dm}^{-3} \text{ NaOH}$  et dans  $0,05 \text{ mol dm}^{-3} \text{ H}_2\text{SO}_4$ , dans des conditions de densité de courant et de pression appliquées constantes et différentes pressions partielles en hydrogène. Ils ont montré que :

- Si l'hydrogène dégazé à la cathode peut diffuser dans la solution, la pression partielle n'est pas affectée par la pression hydrostatique et les risques de fragilisation ne sont pas plus grands qu'à pression atmosphérique. (figure 2)

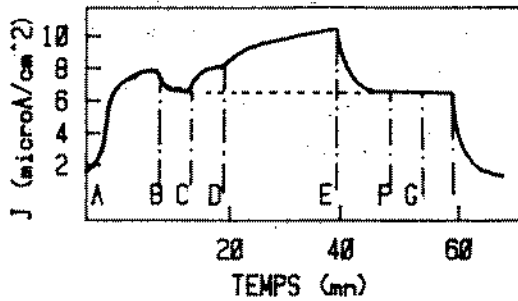


Figure 2: Courant de perméation en fonction de l'agitation et de la pression hydrostatique (2).

A:  $P=1 \text{ atm}$ , agité; B:  $P=1 \text{ atm}$ , agité; C:  $P=1 \text{ atm}$ , non agité; D:  $P=12 \text{ atm}$ , non agité; E:  $P=125 \text{ atm}$ , agité; F:  $P=500 \text{ atm}$ , agité; G:  $P=1 \text{ atm}$ , agité

## LA METHODE EXPERIMENTALE

### Choix de la méthode

A partir de ces résultats, les objectifs de cette étude sont de développer un moyen d'essai permettant d'étudier l'effet de la pression hydrostatique sur la perméation de l'acier dans différentes solutions de chargement électrolytique, afin de pouvoir disposer d'un outil permettant de qualifier l'agressivité d'un chargement.

Dans le but de qualifier notre méthode, nous nous sommes attachés à retrouver les résultats fournis par la littérature sur le fer Armco dans des solutions  $H_2SO_4$ .

Différentes méthodes peuvent être utilisées pour étudier la fragilisation de l'acier par l'hydrogène (dosage de l'hydrogène par dégazage de l'échantillon à température croissante, essais mécaniques : striction d'éprouvettes chargées ou non en  $H_2$ , également rupture différée d'éprouvette chargée en hydrogène sous contrainte statique).

Mais dans le cas de l'étude de l'influence d'un paramètre d'environnement, en l'occurrence la pression hydrostatique, la cellule de perméation apparaît comme bien adaptée. Cette méthode permet l'étude de la diffusion de l'hydrogène, généré électrolytiquement, à travers une membrane de fer par oxydation anodique de l'hydrogène sur la face de sortie et mesure du courant de perméation (l'hydrogène est produit cathodiquement à la face d'entrée). Elle a l'avantage d'être rapide et de mesurer en continu le flux d'hydrogène ayant diffusé, permettant ainsi d'observer l'évolution de ce phénomène avec la pression.

D'autre part, seul un essai de courte durée peut être envisagé du fait de l'impossibilité de renouveler les électrolytes dans un caisson hyperbar.

### Description

La cellule en polymétacrylate est constituée de deux compartiments que sépare l'échantillon métallique (figure 3). Chaque compartiment est équipé :

- . d'une membrane souple assurant la mise en équipression
- . d'une électrode de référence du type Ag/AgCl et d'une électrode auxiliaire PdH (celle-ci utilisée en tant qu'anode évite la production d'oxygène dans la solution (2).)

Le compartiment cathodique est relié à une pompe électrique immergeable qui permet de renouveler en circuit fermé l'électrolyte à la surface de l'échantillon.

L'échantillon d'un diamètre de 28 mm est disposé de telle manière que la surface non utilisée et le contact électrique soient protégés par de l'huile non conductrice dans un compartiment permettant de supporter les variations de pression. La surface utile de l'échantillon est de 2,84 cm<sup>2</sup>.

La mise en pression est assurée par un caisson métallique de 125 litres de capacité utile. La pression est réglable de 0 à 1000 bar, la température en est régulée. Des connecteurs électriques permettent d'assurer le contrôle de l'expérimentation.

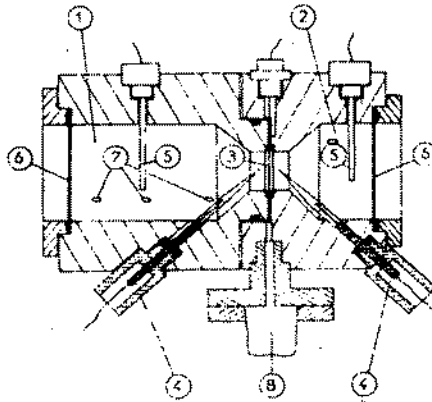


Figure 3: Cellule de perméation. 1 et 2: compartiments anodique et cathodique; 3: échantillon; 4 et 5: électrode Ag/AgCl et Pd/H; 6 et 8: membrane d'équipression; 7: orifice de remplissage et d'agitation

Des adaptateurs basse impédance placés dans le caisson hyperbar assurent la liaison des électrodes de référence. Afin d'accroître l'isolation de la cellule, celle-ci est placée dans une enceinte remplie d'eau distillée (figure 4).

Le circuit de contrôle et de mesure est constitué d'un générateur de courant continu (chargement), d'un potentiostat (détection) et d'un système d'acquisition automatique de données piloté par un micro-ordinateur.

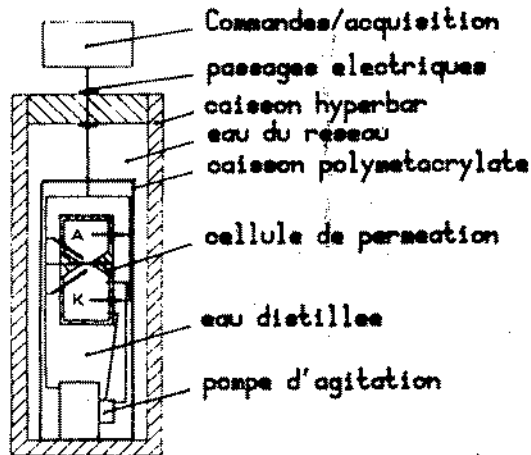


Figure 4: Dispositif expérimental

Les échantillons (sous la forme de disque de 28 mm de diamètre et 1 ou 1,5 mm d'épaisseur) sont polis à la pâte diamant (2,5  $\mu\text{m}$ ) et subissent un traitement thermique (recuit sous vide à 500°C pendant 1 heure et refroidissement dans le four). L'indice des grains obtenus est de l'ordre de 7 (NFAO4-102). Les échantillons de 42CD4 sont quant à eux uniquement polis à la pâte diamant (2,5  $\mu\text{m}$ ).

Chaque échantillon reçoit sur une de ses faces un revêtement de palladium déposé par électrolyse dans une solution de  $\text{PdCl}_2$ , afin d'éviter l'oxydation du fer par la polarisation anodique.

Avant mise de l'échantillon dans la cellule, celui-ci est dégraissé dans de l'acétone pur, décapé dans une solution de méthanol, HCl (2%) pendant 1 minute, rincé au méthanol pur, décapé dans du méthanol à 2% d' $\text{H}_2\text{SO}_4$  pendant 3 minutes, rincé et séché.

Dans le compartiment détection l'électrolyte est constitué d'une solution de 0,1 mole  $\text{dm}^{-3}$  NaOH et 0,01 mole  $\text{dm}^{-3}$  NaCl. L'addition de NaCl a pour but de maintenir constant le potentiel de l'électrode de référence Ag/AgCl.

La solution cathodique utilisée a été principalement une solution de 0,1 N  $\text{H}_2\text{SO}_4$  + 0,001 N HCl.

Les solutions sont préparées 24 heures à l'avance. Elles sont pré-électrolysées et un barbotage d'argon est effectué pendant une douzaine d'heures pour éviter la présence d'oxygène.

La cellule dégraissée, l'échantillon est monté (côté palladié dans le compartiment détection). Avant remplissage, un flux d'argon est maintenu dans les différentes parties de la cellule. Le compartiment anodique est d'abord rempli. L'échantillon est polarisé à un potentiel de l'ordre de -50 mV/ECS et le compartiment cathodique est rempli quand le courant mesuré dans le compartiment détection s'est stabilisé à une valeur inférieure au  $\mu\text{A}/\text{cm}^2$ .

La cellule est alors introduite dans le caisson hyperbar, les circuits électriques sous tension.

### Exploitation des données

L'exploitation des données s'appuie sur la théorie de la diffusion largement publiée dans la littérature.

L'hydrogène est supposé diffuser à travers le fer sous forme atomique sous l'effet d'un gradient de concentration. Pour un échantillon d'épaisseur  $L$  la concentration en hydrogène à la face d'entrée est  $C_0$ , sur la face de sortie, la concentration  $C_L$  est égale à zéro.

La résolution des équations de Fick permet de connaître la concentration en hydrogène dans l'échantillon à différents temps et à différentes abscisses.

Deux formules donnant le rapport  $J_t/J_\infty$  sont disponibles ( $J_t$  flux de perméation à l'instant  $t$ ,  $J_\infty$  flux de perméation à l'état stationnaire,  $D$  coefficient de diffusion).

$$- J_t/J = \frac{2L}{\sqrt{\pi Dt}} \sum_{n=1}^{\infty} (-1)^n \exp \left[ - \left( \frac{L(2n+1)}{4Dt} \right)^2 \right]$$

Cette formule est obtenue par la méthode des transformées de Laplace. En ne gardant que le premier terme, et en l'exprimant en fonction du nombre sans dimension  $Z = Dt/L^2$  l'équation devient :

$$J_t/J_\infty = \frac{2}{\sqrt{\pi Z}} \exp - \frac{1}{4Z}$$

Cette solution n'étant valable que dans le domaine où  $Z$  est compris entre 0 et 0,4.

$$- J_t/J_\infty = 1 + 2 \sum_{n=1}^{\infty} (\cos n\pi) \exp -n^2 Z \pi^2 \quad \begin{array}{l} \text{(obtenue par la} \\ \text{méthode de} \\ \text{Fourier)} \end{array}$$

En ne gardant que le premier terme, l'équation devient :

$$J_t/J_\infty = 1 - 2 \exp (-\pi^2 Z)$$

et donne une bonne résolution pour  $0,14 < Z < 1$ .

Par l'expérimentation, la courbe donnant  $J_t/J_\infty = f(t)$  est obtenue.

Par les formules mathématiques, une correspondance entre  $J_t/J$  et est établie, et il est possible en des points donnés de calculer le coefficient de diffusion  $D$  en connaissant l'épaisseur de l'échantillon par exemple pour des valeurs de  $J_t/J_\infty$  de 0,63 ou 0,83 (valeurs couramment utilisées).

L'emploi d'un système d'acquisition de données permet de réaliser ces calculs pour un grand nombre de points et d'établir le tracé de  $Z = f(t)$  qui est théoriquement une droite de pente  $D/L^2$ . L'allure du tracé fournit une première information sur la qualité de la perméation. Un calcul du coefficient de diffusion est obtenu par régression au premier degré de la courbe  $Z = f(t)$  (figure 5).

## RESULTATS EXPERIMENTAUX

### Fer ARMCO en solution sulfurique

- Effet de l'agitation de la solution à pression atmosphérique :  
Des courbes de perméation ont été tracées avec et sans l'agitation de la solution du compartiment de chargement,  
(0,1N  $H_2SO_4$  + 0,01 N HCl /  $20 \pm 1^\circ C$  /  $i_K$  1mA/cm<sup>2</sup>/e = 1 mm)

### Acier faiblement allié : effet de la pression hydrostatique

L'épaisseur des disques d'acier faiblement allié 42CD4 est d'environ 0,7 mm. Ces essais ont été réalisés en milieu sulfurique (0,1 N  $H_2SO_4$  + 0,01 N HCl).

Cependant, en raison du comportement de l'acier testé dans la solution cathodique (piquration rapide et profonde), il n'a pas été possible de déterminer l'effet de la pression hydrostatique sur le flux résiduel de perméation. (potentiel libre)

Entre 0 et 50 bar, une augmentation sensible du courant est notée (20% environ), au-delà de 50 bar l'augmentation du flux est moins importante ( $4 \mu A/cm^2$  entre 100 et 600 bar) (figure 7).

La valeur mesurée du coefficient de diffusion dans nos conditions d'essais est faible pour le 42CD4, soit de l'ordre de  $10^{-8} cm^2.s^{-1}$ , ce qui nécessite pour atteindre un état permanent une période d'1 heure 20 minutes (pour un échantillon de 0,7 mm d'épaisseur) après chaque montée en pression.

La courbe obtenue ne doit pas être considérée réalisée à l'état stationnaire (attente de 20 minutes à chaque palier). Des essais de plus longue durée auraient pour conséquence de modifier la composition de la solution.

Après mise au point, le dispositif expérimental permet d'obtenir des courbes de perméation en milieu aqueux sous des pressions hydrostatiques allant jusqu'à 800 bar. L'actuel dispositif est limité dans ses performances pour des essais de longue durée, vu l'impossibilité de renouveler les électrolytes sous pression. Dans ces conditions, le fer Armco possédant un coefficient de diffusion plus important que le 42CD4 se prête mieux à de telles études, aussi les principaux résultats concernent donc le fer Armco.

L'agitation de la solution de chargement a effectivement pour effet d'abaisser le flux de perméation (2). La remise en solution de l'hydrogène produit sur l'échantillon maintient plus homogène la concentration en hydrogène.

En l'absence d'agitation, le flux à l'état stationnaire ne se stabilise pas dans le temps.

Le coefficient de diffusion de l'hydrogène mesuré dans le fer Armco est de l'ordre de  $6.10^{-5} cm^2/s$  (les valeurs fournies dans la bibliographie varient entre  $10^{-6}$  et  $8.10^{-5} cm^2/s$  pour le fer à température ambiante) et n'est pas affecté par la pression hydrostatique les pressions utilisées ne modifiant pas le réseau cristallin dans le domaine élastique.

Dans nos expérimentations, le flux d'hydrogène est affecté par la pression hydrostatique, ce qui correspondrait à une augmentation de la pression partielle (2).

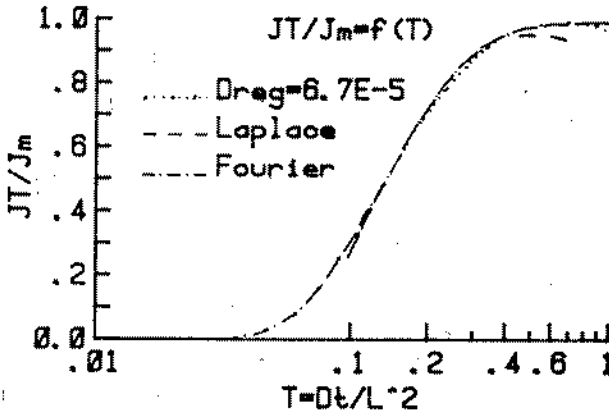
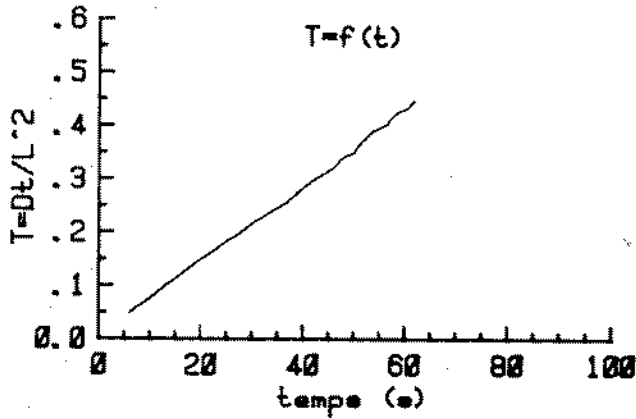


Figure 5: Traitement des données. Fer Armco,  $a = .96\text{mm}$ ,  $0.1\text{N H}_2\text{SO}_4$ ,  $i_k = 1\text{mA/cm}^2$

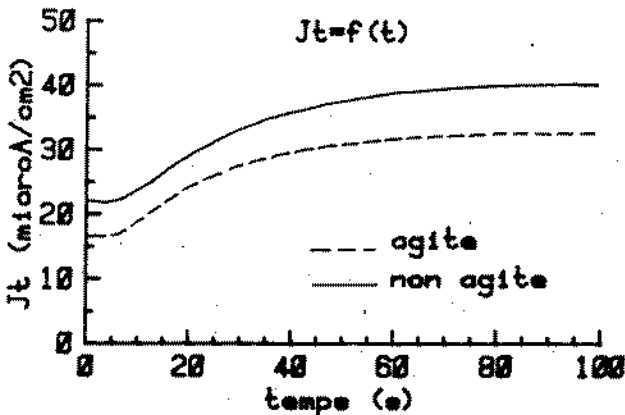


Figure 6: Effet de l'agitation.

L'agitation a pour effet d'abaisser les flux de perméation de l'ordre de 10 à 15%. (figure 6)

- Effet de la pression hydrostatique :

Des courbes de perméation ont été tracées à différentes pressions par palier de 200 bar sur des échantillons différents et dans des conditions de chargement identiques aux précédentes avec une agitation permanente de la solution.

Une certaine dispersion a été observée sur la valeur des coefficients de perméation. La valeur moyenne est de l'ordre de  $6 \cdot 10^{-5} \text{ cm}^2 \text{ s}^{-1}$  et ne varie pas de manière très sensible avec la pression. La valeur de la surtension imposée à  $1 \text{ mA/cm}^2$ , de l'ordre de 130 mV, n'est pas affectée par la pression.

L'étude de l'évolution du courant de perméation résiduel en l'absence de polarisation (potentiel de corrosion) a été effectuée avec une montée en pression par palier de 50 bar (figure 7).

Entre 0 et 50 bar l'effet de la pression hydrostatique est très marqué, soit une augmentation de 15% du courant résiduel de perméation. Au-delà de 50 bar, l'augmentation du courant résiduel va en s'accroissant avec l'augmentation de la pression ( $8 \mu\text{A/cm}^2$  de 100 à 800 bar). La descente en pression a pour effet de diminuer le courant résiduel de perméation. Celui-ci reste cependant plus élevé qu'à la montée. Ce qui peut s'expliquer par une augmentation de la pression partielle d' $\text{H}_2$  dans la solution compte tenu de la durée de l'essai et à une modification de l'état de surface de l'échantillon.

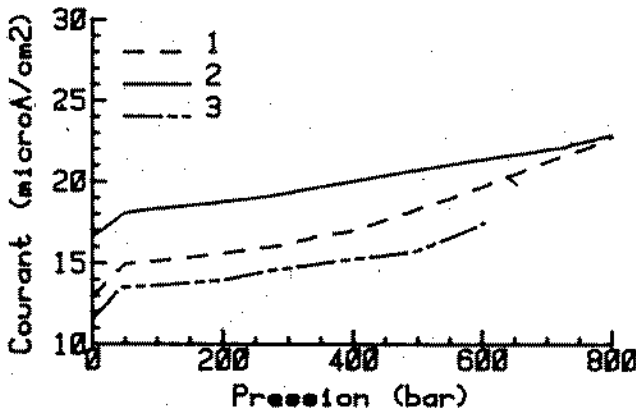
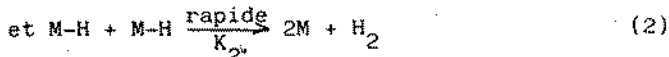
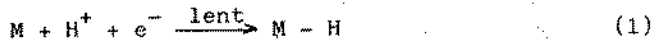


Figure 7: Effet de la pression sur les courants de perméation. 1: fer Armco, I résiduel, montée en pression; 2: fer Armco, I résiduel, descente; 3: acier 42CD4, J infinie, montée.



La réaction d'évolution de l'hydrogène cathodique dans une solution d' $H_2SO_4$  à 0,1 N suit un mécanisme de décharge-désorption chimique couplé, pour un taux de recouvrement d'hydrogène absorbé faible ( $\Theta_H < 0,1$ ) (2).



En sachant qu'un accroissement de la pression partielle d'hydrogène implique un accroissement du taux de recouvrement :

$$(J = K\Theta_H \text{ et } \partial J / \partial P_{H_2} > 0 \longrightarrow \frac{\partial \Theta_H}{\partial P_{H_2}} > 0),$$

et que la pression hydrostatique ne peut avoir d'effet sur la réaction de décharge, Blundy et Shreir avancent que la pression doit avoir une répercussion sur les constantes  $k_2$  et  $k_{-2}$  de la réaction de désorption chimique. Cela se traduirait par une diminution de  $k_2$  et un accroissement de  $k_{-2}$ , donc un accroissement du taux de recouvrement  $\Theta_H$ .

La courbe donnant le flux résiduel en fonction de la pression n'est pas la même que celle obtenue par Nanis et Deluccia, ceci peut s'expliquer par un effet de l'agitation.

L'effet observé entre 0 et 50 bar demande à être confirmé car cela peut s'avérer important pour des applications pratiques.

## CONCLUSION

Le dispositif mis en oeuvre a permis de qualifier l'effet de la pression hydrostatique sur la perméation de l'hydrogène dans l'acier en milieux aqueux :

- Le coefficient de diffusion de l'hydrogène dans le fer Armco ( $6 \cdot 10^{-5} \text{ cm}^2 \text{ s}^{-1}$ ) n'est pas modifié par la pression hydrostatique.
- L'agitation de la solution de chargement a pour effet de diminuer le flux de perméation et de le stabiliser.
- Le flux de perméation est affecté par la pression :  $\partial J / \partial P_{H_2}$  est positif. La réaction d'évolution de l'hydrogène dans un électrolyte acide étant celle d'une décharge-désorption couplé, ces résultats sont expliqués par une augmentation de l'adsorption, donc un accroissement du taux de recouvrement en fonction de la pression hydrostatique.

En conclusion, au vu des résultats obtenus, les essais réalisés au cours de cette étude laissent présager un risque accru de fragilisation par l'hydrogène des aciers à hautes résistances mécaniques utilisés par grande profondeur.

Ces risques sont aggravés par l'absence d'agitation du milieu associés à la protection cathodique.

Le dispositif expérimental étudié et mis au point à l'occasion de cette étude nous permet de qualifier le comportement d'alliage métallique en milieu aqueux, sous chargement électrolytique et sous pression hydrostatique jusqu'à 800 bar. Nous avons réalisé ainsi des essais sur du fer Armco et acier à haute résistance mécanique 42CD4 en milieu sulfuré.

#### BIBLIOGRAPHIE

(1) Nanis et Deluccia

"The effects of hydrostatic pressure to 8250 psi on electrolytic hydrogen in Iron"

Department of the Navy Naval Air Development Center, Johnsville, 24 24 Janvier 1968.

(2) Blundy et Shreir

"The effect of pressure on the permeation of hydrogen through steel" City of London Polytechni, London, November 1975.

(3) Devanathan, Stachurski et Beck

"A technique for the evaluation of hydrogen embrittlement characteristics of electroplating baths"

Electrochemistry Laboratory, University of Pennsylvania, Philadelphia, Pennsylvania.

Aeronautical Materials Laboratory, Naval Air Engineering Center, Philadelphia, Pennsylvania, January 1963.

(4) Hitoshi Murayama, Masao Sakashita et Norio Sato

"H<sub>2</sub>S - Catalysed hydrogen absorption in iron"

Electrochemistry Laboratory Faculty of Engineering Hokkaido University, Sapporo, Japan.

(5) J. O'M. Bookris

"On hydrogen damage and the electrical properties of interfaces".

UNE NOUVELLE COMPOSITION INHIBITRICE A BASE  
DE GLUCONATE DE ZINC POUR LUTTER CONTRE  
LA CORROSION MARINE

J.C. LUMARET  
ROQUETTE FRERES  
62136 LESTREM - FRANCE

Résumé

L'intérêt porté à l'eau de mer, nouvelle source d'eau utilisable comme fluide de transfert d'énergie ou encore dans certaines opérations de forage pétrolier fait qu'il devient important de trouver une composition qui permette de prévenir de manière efficace la corrosion des métaux tels que l'acier au contact de ces solutions.

On a étudié par perte de masse et par des techniques électrochimiques, le caractère inhibiteur de corrosion vis-à-vis de l'acier d'une combinaison de gluconate de zinc et d'hexaméta-phosphate de sodium dans différents milieux : eau de mer synthétique aérée, eau chlorée aérée, eau de mer synthétique polluée par différentes bactéries sulfato-réductrices.

Abstract

The interest in sea water as a new water source usable as energy transfer fluid or in some oil drilling processes is so that it becomes important to find a composition to prevent efficiently the corrosion of metals such as steel in contact with these solutions.

By measuring weight loss and using electrochemical techniques, we have studied the corrosion inhibiting power on steel with a composition consisting of zinc gluconate and sodium hexametaphosphate in different media such as : aerated synthetic sea water, aerated chlorinated water, synthetic sea water polluted by different sulfate reducing bacteria.

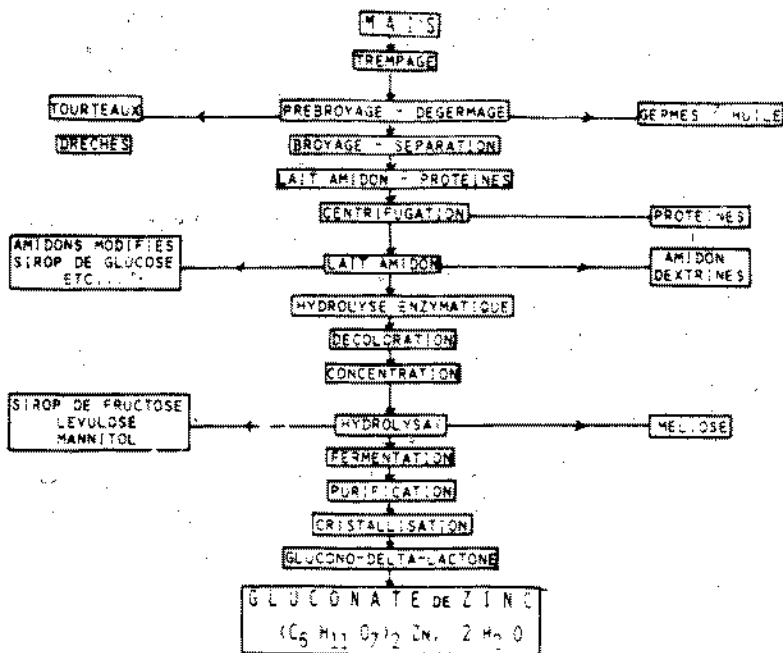
## I - HISTORIQUE

Depuis 1933, ROQUETTE FRERES est devenu l'un des plus importants producteurs d'amylacés. Ayant débuté par la fécule de pomme de terre, ROQUETTE FRERES a su au fil des années diversifier ses productions : 1946 - le maïs, 1956 - l'amidon de blé.

Aujourd'hui, ses laboratoires de recherche, ses filiales disposant d'unités de production (Italie, Espagne, Etats-Unis) ou de forces de vente (R.F.A, Grande-Bretagne, Etats-Unis), ses quatre usines françaises, fruits d'une politique d'investissements font de ROQUETTE FRERES la 103ème entreprise industrielle française. Par ses activités exportatrices, ROQUETTE FRERES s'est classée en 1982, au 59ème rang des entreprises françaises et au 2ème rang des industries parachimiques. Il est en outre le premier producteur mondial de sorbitol (1).

C'est dans le cadre de nos travaux de développement que nous nous sommes intéressés aux traitements de surfaces et tout particulièrement à la mise au point d'une nouvelle composition inhibitrice pour la corrosion marine.

Cette nouvelle orientation pour ROQUETTE FRERES a été motivée par la publication en 1976, d'un article rédigé par le Professeur MOR faisant état de l'utilisation comme inhibiteur de corrosion pour les milieux salins du gluconate de zinc, (2) produit fabriqué à partir du maïs :



Nos propres travaux ont été basés sur l'élaboration d'une composition à base de gluconate de zinc pouvant être indifféremment employée dans :

- 1) un milieu aérobie
- 2) un milieu anaérobie

C'est le détail de cette étude que nous nous proposons de présenter.

## II - MILIEU AEROBIE

La détermination de l'efficacité de la composition en question, en tant qu'inhibiteur de corrosion vis-à-vis de l'acier pour le milieu considéré résulte en fait de deux sous-études :

- d'une part, la recherche par simple mesure de pertes de poids dans une eau de mer synthétique aérée, des conditions optimales d'utilisation de la dite composition,
- d'autre part, dans les conditions définies précédemment, la détermination de la nature de l'inhibition dans une eau chlorée aérée.

### II-1 Eau de mer synthétique aérée

L'intérêt porté à l'eau de mer, nouvelle source d'eau utilisable comme fluide de transfert d'énergie, par exemple dans des installations de refroidissement notamment en circuit fermé, fait qu'il devient important aujourd'hui de trouver une composition qui permette de prévenir de manière efficace, la corrosion des métaux tels que l'acier au contact de ces solutions.

Si l'eau de mer est déjà extrêmement corrosive de par le haut degré de dissociation des sels qui la composent et sa grande conductivité, elle le sera d'autant plus en présence d'oxygène dissous.

Il a déjà été proposé de réduire la corrosion par l'addition, à l'eau de mer au contact de substrats métalliques, des substances minérales telles que les polyphosphates, les chromates... Or, l'utilisation de ces sels présente de sérieux inconvénients.

En effet, les polyphosphates se reconvertissent sous l'action d'une chaleur modérée en orthophosphates qui peuvent réagir avec les sels de l'eau pour favoriser la formation de boues. Il en résulte une diminution très nette du rendement de la transmission de chaleur et éventuellement une accélération de la corrosion.

Par ailleurs, la présence de polyphosphates donne lieu au phénomène bien connu d'eutrophisation des eaux.

Les chromates qui sont des inhibiteurs de corrosion très efficaces, ont l'inconvénient d'être très toxiques ; l'eau contenant des chromates ne peut être évacuée sans avoir subi un traitement d'épuration préalable souvent onéreux.

De plus, il a été constaté que dans certaines circonstances, les chromates peuvent accélérer la corrosion, notamment par le phénomène dit " de piqûre ", lorsqu'ils sont présents à de faibles concentrations. Cette corrosion par piqûres peut être très sévère et peut entraîner une perforation du substrat métallique.

On a également proposé l'utilisation, comme inhibiteur de la corrosion, des gluconates de métaux alcalins ou alcalino-terreux ou encore d'ammonium, le gluconate de sodium étant le sel le plus souvent retenu. Le pouvoir inhibiteur du gluconate de sodium utilisé seul ayant néanmoins été jugé insuffisant, il a été souvent proposé en combinaison avec des " agents " dits synergiques, choisis parmi les acides organiques, les acides aromatiques, les silicates, les phosphates, les tannins, le et le sulfate de zinc (3 - 4 - 5).

Nous avons constaté au cours des nombreux essais que nous avons effectués pour comparer le comportement de ces différentes compositions inhibitrices connues, que ni le système " gluconate de sodium - polyphosphate - sulfate de zinc ", ni le " gluconate de zinc seul " ne permettaient d'obtenir une inhibition parfaite de la corrosion et que bien au contraire, elles conduisaient dans certains cas, après une inhibition temporaire de la corrosion à une accélération de celle-ci. De plus, nous avons trouvé que la corrosion des substrats métalliques par l'eau de mer pouvait être inhibée avec une efficacité inconnue jusqu'alors en ayant recours à un mélange de :

" GLUCONATE de ZINC et HEXAMETAPHOSPHATE de SODIUM "  
noté (GZ - HMPP)

Cette composition a fait l'objet d'un dépôt de demande de brevet le 31 août 1981 au nom de ROQUETTE FRERES, publiée sous le numéro 2.512.072 (6).

### II-1.1 - Quelques exemples

La méthode d'expérimentation utilisée consiste à mesurer et à comparer les pertes de métal enregistrées pour des échantillons métalliques identiques dont l'un joue le rôle d'échantillon témoin et est placé dans l'eau de mer synthétique saturée en oxygène dissous, l'autre jouant le rôle d'échantillon d'essais placé dans la même eau dans laquelle on a introduit les compositions à tester.

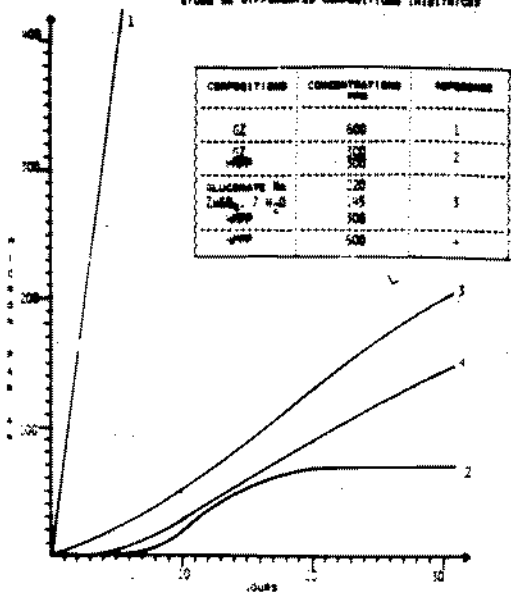
Ces échantillons métalliques sont en acier E 24-1 (0,22 % C - 0,075 % P - 0,062 % S).

Avant l'expérimentation, ces échantillons sont polis, dégraissés chimiquement, décapés dans une solution d'acide chlorhydrique et rincés. Ils sont ensuite séchés et pesés.

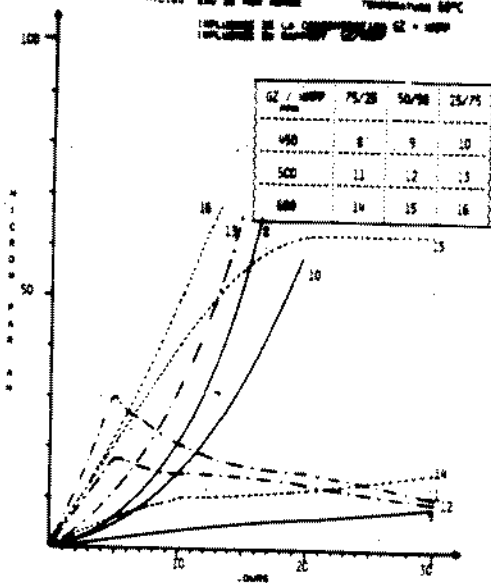
Les pertes de masse enregistrées pour chacun des essais ont été converties en vitesse de corrosion exprimée en  $\mu$ /an. La durée de l'expérimentation a été de 30 jours.

L'ensemble des résultats obtenus est donné ci-après sous forme de courbes :

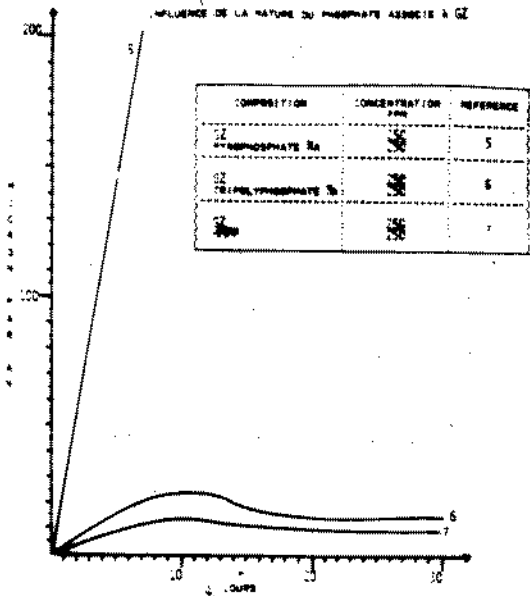
MILIEU EAU DE MER AEREE TEMPERATURE 50°C  
 ETUDE DE DIFFERENTES COMPOSITIONS INHIBITRICES



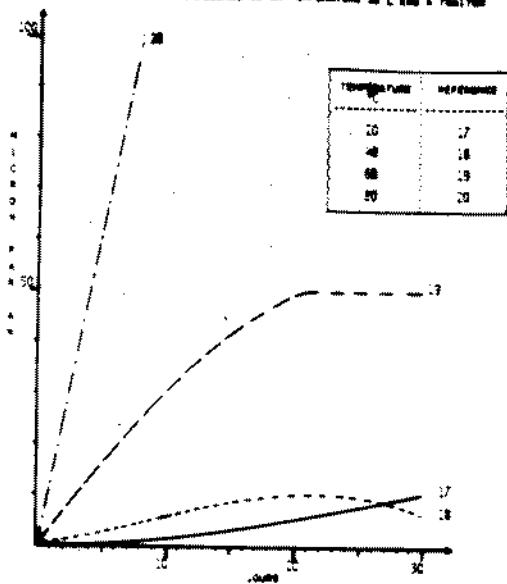
MILIEU EAU DE MER AEREE TEMPERATURE 60°C  
 INFLUENCE DE LA COMPOSITION GE + ZnP



MILIEU EAU DE MER AEREE TEMPERATURE 60°C  
 INFLUENCE DE LA NATURE DU PHOSPHATE ASSOCIE A GE



MILIEU EAU DE MER AEREE GE + ZnP 50/50 500ppm  
 INFLUENCE DE LA TEMPERATURE DE L'EAU A TITRES



Au regard des performances obtenues avec les compositions conformes à l'art antérieur, la combinaison GZ - HMPP s'est avérée nettement plus efficace, d'autant que l'observation des solutions d'essais nous a permis de constater qu'après 30 jours de tests aucun trouble n'était apparu.

A l'inverse, les circuits où seul l'hexamétaphosphate était présent, contenaient une quantité importante de boues qui avaient tendance à précipiter et de ce fait à obturer les installations.

La concentration préférée de cette composition est de l'ordre de 450 à 500 ppm pour un mélange 50/50. 80

### II-2 - Eau chlorée aérée

En collaboration avec le Docteur HOCH du Laboratoire de Corrosion de l'Ecole Nationale Supérieure des Techniques Industrielles et des Mines de Douai, nous avons déterminé la nature de l'inhibition obtenue avec le mélange gluconate de zinc - hexamétaphosphate de sodium à l'aide de mesures de valeurs des constantes de TAFEL (cathodique CTC et anodique ATC). Elles ont été couplées à des mesures de la résistance de la polarisation dont la valeur est directement convertible en vitesse de corrosion régulière en fonction du temps (7 jours, 14 jours, 3 semaines, 1 mois).

Compte tenu des travaux précédemment exposés, nous avons examiné afin de vérifier les proportions optimales, trois niveaux du rapport GZ / HMPP et trois niveaux de la concentration

|   |                       |         |         |         |
|---|-----------------------|---------|---------|---------|
| ( | :                     | :       | :       | )       |
| ( | RAPPORT GZ / HMPP (%) | 40 / 60 | 50 / 50 | 60 / 40 |
| ( | -----                 | -----   | -----   | -----   |
| ( | :                     | :       | :       | )       |
| ( | CONCENTRATION (ppm)   | 450     | 500     | 550     |
| ( | :                     | :       | :       | )       |

Si nous avons choisi comme milieu d'essai une eau adoucie contenant 1 000 ppm d'ions chlorures, c'est que nous pensions que l'eau de mer étant très agressive, cela pouvait risquer de " masquer " l'influence de l'inhibiteur surtout au début du contact métal/eau à cause des interférences dans la décomposition concurrentielle inhibiteur - ions. Les solutions d'essais ont été aérées par barbottage d'air, maintenues à 40°C et leur pH stabilisé respectivement à une valeur égale de 4 et 7.

Quant aux échantillons métalliques, tous les essais ont été effectués sur de l'acier A-42 recuit dont la composition chimique est donnée ci-après.



(Analyse effectuée par spectrophotométrie à l'aide d'une lampe à décharge lumineuse)

| ELEMENT ( % en poids ) |      |      |       |       |       |      |
|------------------------|------|------|-------|-------|-------|------|
| C                      | Mn   | Si   | P     | S     | Cu    | Al   |
| 0,07                   | 0,28 | 0,03 | 0,017 | 0,023 | 0,045 | 0,04 |
| :                      | :    | :    | :     | :     | :     | :    |

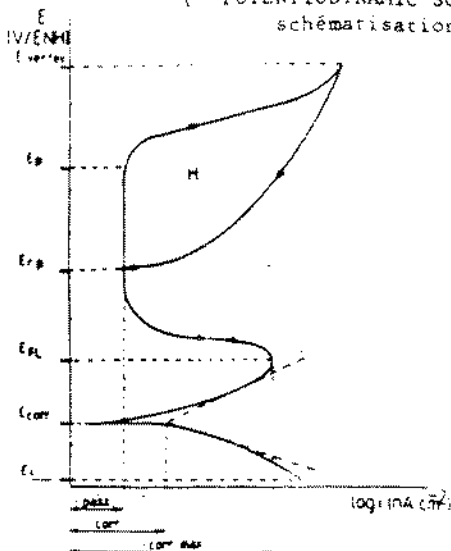
La face en contact avec le milieu d'essai avait une surface de 16,25 cm<sup>2</sup> et a été préalablement polie sur papiers abrasifs jusqu'aux grains 600 (mesh/inch<sup>2</sup>), lavée, dégraissée à l'alcool pur et séchée.

### II-2.1 - Les mesures

Ces mesures ont été effectuées à l'aide d'un potentiostat de type EG x G, modèle 350 (Princeton Research). Le branchement était à 3 électrodes. Les potentiels imposés sur l'échantillon ont été mesurés par rapport à une électrode de référence au sulfate mercurique saturé (Hg<sub>2</sub> SO<sub>4</sub>). Ces potentiels imposés étaient en pratique mesurés au centre de l'échantillon immergé à l'aide d'un capillaire de HABER-LUGGINS rempli d'une solution de sulfate de potassium saturée. Les électrodes auxiliaires étaient en graphite.

a) pour le temps d'immersion  $t = 0$

FONCTION  $i = f(E)$  " COMPLETE "  
 (" POTENTIODYNAMIC SCAN ")  
 schématisation USA



Les fonctions  $i = f(E)$  " complète " (" Potentiodynamic Scan ") identiques à celles présentées ci-contre ont été tracées en aller et retour pour le domaine du potentiel compris entre le potentiel initial,  $E_i$  (-0,250mV/E<sub>cor</sub>) et le potentiel final  $E_f$  (+ 1,5 V/E<sub>NH</sub>).

Ces fonctions ont permis de relever les valeurs :

- . du potentiel de corrosion  $E_{cor}$
- . des droites de TAFEL,  $ATC = \frac{\alpha nF}{RT}$  et  $CTC = \frac{\beta nF}{RT}$
- . du courant de corrosion,  $i_{cor} = \frac{ATC \cdot CTC}{2,3 (ATC + CTC) R_p}$  (7)
- . de la résistance de polarisation,  $R_p$
- . du potentiel de rupture,  $E_{..}$
- . des potentiels de picûres,  $E_p$  et de repassivation,  $E_{RP}$
- . d'hystérésis (sensibilité du métal vis-à-vis d'une corrosion localisée

$$H = \int_{E_{cor}}^{E_p} i(E)_{\text{retour}} - \int_{E_{cor}}^{E_f} i(E)_{\text{aller}}$$

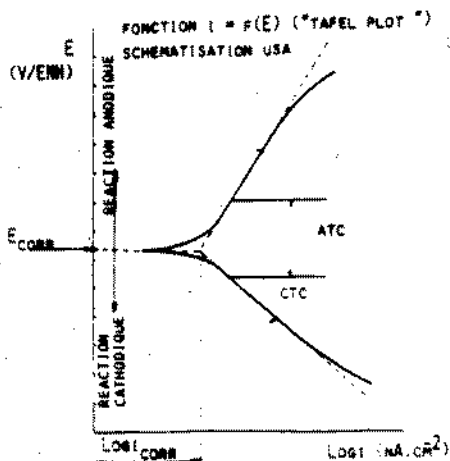
ou encore

$$R = \frac{\int_{E_{cor}}^{E_f} i_{AN.ALL} (E)}{\int_{E_{cor}}^{E_f} i_{AN.RET} (E)}$$

avec :

- $\alpha, \beta$  : coefficient de transfert
- $n$  : nombre d'électron participant à la réaction
- $F$  : nombre de Faraday
- $T$  : température absolue ( $^{\circ}K$ )
- $R$  : constante universelle des gaz
- $i_{AN.ALL}$  ou  $i_{AN.RET}$  : intensité du courant anodique aller ou retour

b) Pour les durées d'immersion de 1,2,3 et 4 semaines

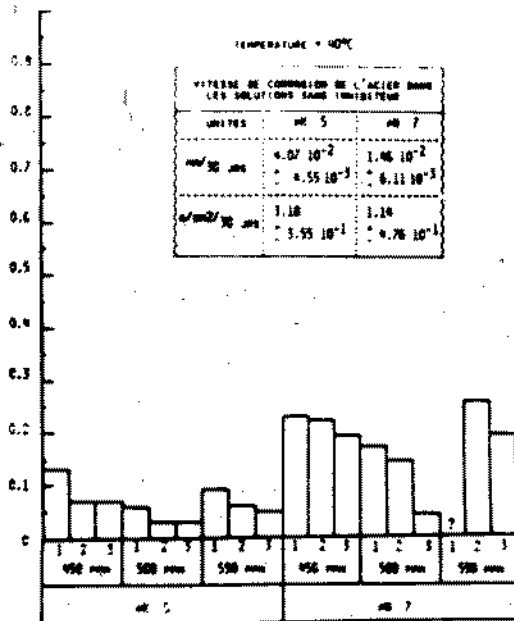


Les fonctions  $i = f(E)$  tracées dans le domaine des potentiels compris entre  $-0,250 \text{ V}/E_{\text{COR}}$  et  $+0,250 \text{ V}/E_{\text{COR}}$  ont permis de relever les valeurs de  $E_{\text{COR}}$ , ATC, CTC,  $i_{\text{COR}}$  et  $R_p$ . (programme "TAFEL PLOT")

### II-2.2 - Traitement des résultats

Il ressort de cette étude que toutes les combinaisons de concentrations totales (450, 500 et 550 ppm) et de rapports GZ/HMPP (40/60, 50/50, 60/40) ont manifesté dans les solutions aqueuses contenant 1 000 ppm de chlorures, aux paramètres examinés (pH 5 et 7 - température  $40^\circ\text{C}$ ) une efficacité d'inhibition de la corrosion de l'acier.

|                                    |                   |
|------------------------------------|-------------------|
| $i_{\text{COR}}$ (Avec Inhibiteur) | 1 - GZ/HMPP 40/60 |
| $i_{\text{COR}}$ (Sans Inhibiteur) | 2 - GZ/HMPP 50/50 |
|                                    | 3 - GZ/HMPP 60/40 |



Il semble que le mécanisme de cette inhibition soit basé sur le blocage à la fois des sites anodiques (corrosion) et des sites cathodiques (dépolarisation). En d'autres termes, les inhibiteurs examinés réduisent les courants d'échange relatifs à la réaction de dissolution et à la réaction de dépolarisation. Il est donc bien possible qu'une partie des inhibiteurs réagisse par adsorption à la surface et l'autre par réduction du corps dépolarisant, qui en principe, dans ces solutions serait l'oxygène dissous.

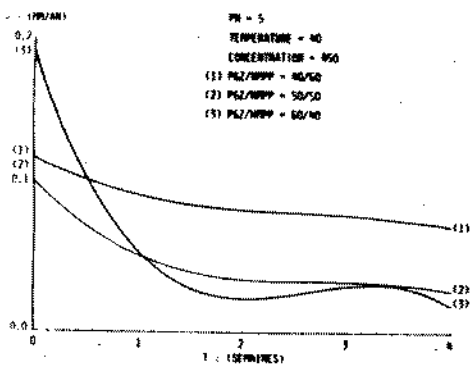
A quelques exceptions près, aucune corrosion par piqûres ne s'est manifestée dans les solutions avec les inhibiteurs. Les exceptions où  $R < 1$  ne peuvent pas être prises en considération car dans aucun des cas étudiés, les fonctions  $i = f(E)$  ne prennent la forme d'hysteresis positive. Ces exceptions résultent du fait que le potentiel de corrosion mesuré lors du tracé " retour " est inférieur à celui déterminé lors du tracé " aller ". Ce phénomène n'a aucune relation avec la corrosion par piqûres.

| CONCENTRATION |                 | PH 5         |              |      | PH 7         |              |      |
|---------------|-----------------|--------------|--------------|------|--------------|--------------|------|
| TOTALE PPM    | RAPPORT %Z/HMPP | I'AN ALL     | I'AN RET     | R    | I'AN ALL     | I'AN RET     | R    |
| 450           | 40/60           | 1.829 $10^2$ | 1.084 $10^2$ | 1.69 | 1.001 $10^2$ | 0.811 $10^2$ | 1.23 |
|               | 50/50           | 2.633 $10^2$ | 1.404 $10^2$ | 1.45 | 1.38 $10^2$  | 0.581 $10^2$ | 2.37 |
|               | 60/40           | 1.075 $10^2$ | 0.519 $10^2$ | 2.07 | 1.372 $10^2$ | 2.086 $10^2$ | 0.95 |
| 500           | 40/60           |              |              |      | 1.691 $10^2$ | 0.796 $10^2$ | 2.07 |
|               | 50/50           |              |              |      | 1.147 $10^2$ | 0.633 $10^2$ | 1.81 |
|               | 60/40           |              |              |      | 0.828 $10^2$ | 0.687 $10^2$ | 1.20 |
| 550           | 40/60           |              |              |      | 0.546 $10^2$ | 0.988 $10^2$ | 0.91 |
|               | 50/50           |              |              |      | 0.763 $10^2$ | 1.078 $10^2$ | 0.71 |
|               | 60/40           |              |              |      | 0.970 $10^2$ | 0.478 $10^2$ | 2.03 |

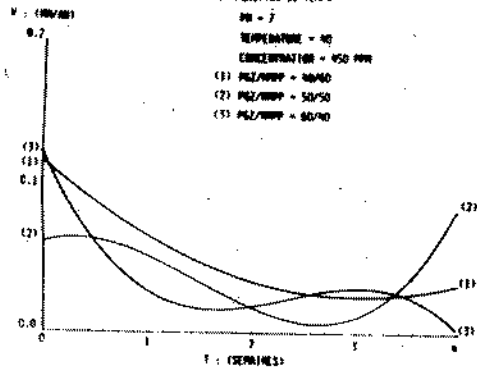
Tandis que les surfaces des échantillons d'acier qui ont été immergés dans les solutions à 1 000 ppm de chlorures  $Cl^-$ , se sont couvertes de produits de corrosion typiques de ces milieux (du type magnétite hydratée,  $Fe_3O_4 \cdot x H_2O$ , d'une couleur brun noirâtre), dans un laps de temps de 2 à 3 jours, ces mêmes surfaces ont conservé l'aspect métallique peu terni lors de toute la durée de l'immersion (28 jours) dans les solutions avec inhibiteur. Ces surfaces d'acier selon les observations approfondies ont été recouvertes lors de l'immersion par des couches minces de produits plus ou moins visqueux qui fournissent après séchage à l'air des couches gris jaunâtre.

Ceci peut expliquer que les effets des inhibiteurs commencent à se manifester pratiquement dès le début de l'immersion mais qu'ils sont davantage prononcés à partir de 5 à 7 jours. La durée de ces effets inhibiteurs dépasse dans les conditions étudiées la durée maximale des essais, c'est-à-dire quatre semaines.

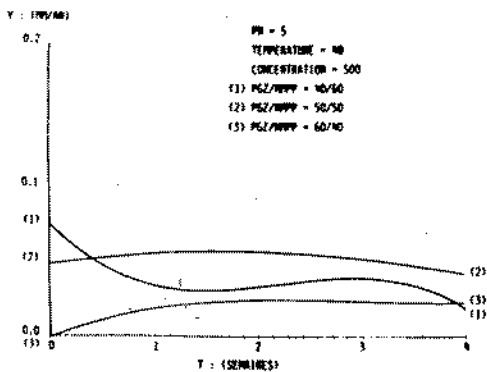
VITESSE DE CORROSION EN FONCTION DU TEMPS



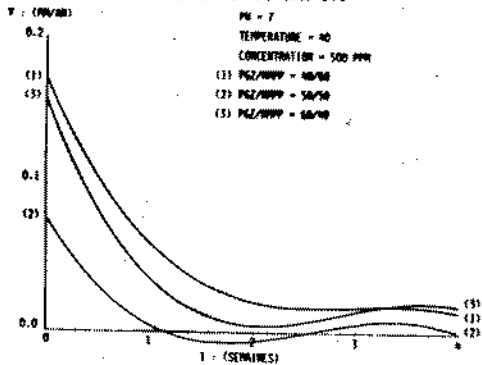
VITESSE DE CORROSION EN FONCTION DU TEMPS



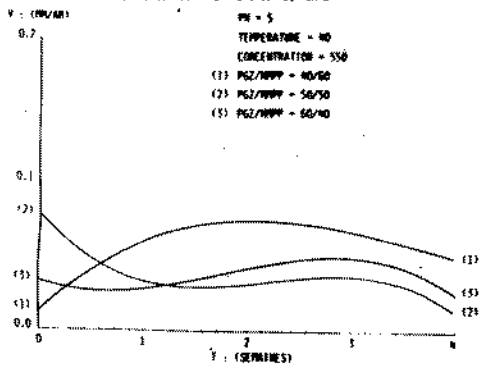
VITESSE DE CORROSION EN FONCTION DU TEMPS



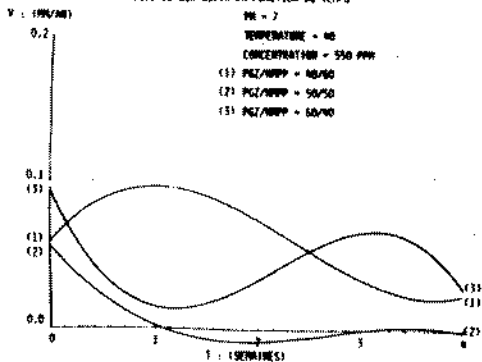
VITESSE DE CORROSION EN FONCTION DU TEMPS



VITESSE DE CORROSION EN FONCTION DU TEMPS



VITESSE DE CORROSION EN FONCTION DU TEMPS



### III - MILIEU ANAEROBIE

Il s'est agi plus particulièrement d'étudier le comportement des compositions inhibitrices en question face aux phénomènes de corrosion bactérienne rencontrés notamment dans certaines opérations de forage pétrolier comme le transfert en off shore (8).

Une des classes de bactéries les plus souvent rencontrées dans ces milieux sont les bactéries sulfatoréductrices (9 - 10).

Dès 1923, Von Wolzogen Kühr décrivait le rôle important joué par ces bactéries. Autant que l'on puisse savoir, ces bactéries ne font partie que d'un seul groupe de Spirillacées dont le représentant est Desulfovibrio desulfuricans.

Etant anaérobies strictes, on les trouvera soit sous les couches de rouille au contact du métal, soit au contact de substances métalliques immergées dans des solutions non oxygénées.

Le type de corrosion qu'elles génèrent, se caractérise par l'apparition de trous dans le fer ou l'acier. Au début du processus, les bactéries sulfatoréductrices enlèvent le film d'hydrogène qui recouvre normalement tout métal immergé et qui empêche sa dissolution.

Le processus se poursuit alors avec la formation de sulfure, composé corrosif issu de la transformation due à ces bactéries des sulfates en hydrogène-sulfure qui se combine avec les sels ferreux pour donner naissance à ces dits sulfures.

#### III-1 - Principe des essais

Afin de simuler ces phénomènes de corrosion bactérienne, nous avons opéré de la façon suivante.

Dans des flacons remplis d'eau de mer synthétique, on a introduit une plaque métallique d'acier E 24-1 (3 x 10 cm) préalablement dégraissées, décapées, séchées à l'acétone puis pesées.

Chacune des solutions a étéensemencée avec un cocktail de bactéries anaérobies récoltées au niveau d'un forage pétrolier en milieu marin, et adjuvantées de différentes compositions du mélange GZ / HMPP :

| RAPPORT GZ / HMPP | CONCENTRATION | REFERENCES |
|-------------------|---------------|------------|
| -                 | Témoin 0      | 1          |
| 100 - 0           | 500           | 1          |
| 75 - 25           | 500           | 2          |
| 50 - 50           | 500           | 3          |
| 25 - 75           | 500           | 4          |
| 75 - 25           | 1 000         | 5          |
| 50 - 50           | 1 000         | 6          |
| 25 - 75           | 1 000         | 7          |

Ces solutions ont ensuite été stochées à l'obscurité à 30°C. Elles ne seront pas oxygénées tout au long de l'essai.

### III-2 - Exploitation des résultats

Après un mois de culture, une mesure de la perte de poids des échantillons métalliques a été effectuée.

| REFERENCES | PERTE de POIDS (%) |
|------------|--------------------|
| T          | 0,381              |
| 1          | 0,103              |
| 2          | 0,066              |
| 3          | 0,084              |
| 4          | 0,087              |
| 5          | 0,085              |
| 6          | 0,156              |
| 7          | 0,117              |

Au regard de ces résultats, on constate que dans les cas étudiés, la composition GZ/HMPP a présenté un caractère inhibiteur de la corrosion bactérienne, le meilleur résultat ayant été obtenu avec 500 ppm du mélange 75 GZ - 25 HMPP. Aucune trace de corrosion par perforation n'a été décelée à la surface des échantillons d'acier.

L'observation visuelle des solutions d'essais a montré que les milieux étaient restés parfaitement translucides à l'exception du témoin.

#### III-2.1 - Remarque

Un essai similaire à celui précédemment exposé a été réalisé, mais en introduisant dans le milieu d'essai de l'hydrogène-sulfure. Les résultats en sont après 33 jours :

| COMPOSITION   | CONCENTRATION PPM | % EFFICACITE                                   |  |
|---------------|-------------------|--|--|
|               |                   | EAU DE MER NON OXYGENEE + BACTERIES ANAEROBIES | EAU DE MER + BACTERIES ANAEROBIES + H <sub>2</sub> S |
| GZ            | 200               | 17   | -  |
| HMPP          | 200               | 20   | -  |
| GZ-HMPP 50-50 | 200               | 44   | 78   |

III-2.2 - Etude du caractère bactéricide des compositions  
à base de gluconate de zinc en milieu anaérobie

A défaut de matériel adapté à la fermentation anaérobie, les numérations sur gélose se sont révélées difficiles et n'ont pas donné de résultats reproductibles.

Mais disposant dans nos laboratoires d'un appareil de mesure d'ATP (adenosine triphosphate), la contamination microbiologique a été évaluée en quantité d'ATP.

a) Méthode

- Préparation d'une gamme d'étalons d'ATP standard avec un tampon glycine
- Extraction de l'ATP
- 0,1 ml de la prise d'échantillon + 0,9 ml de DMSO pur (diméthylsulfoxyde)
- Agitation
- Temps de contact : 2 minutes
- A 0,5 ml de la dilution obtenue, on ajoute 2,5 ml de tampon MOPS (morpholino-propan sulfonic acid)
- Agitation
- Temps de contact : 2 minutes
- Après extraction, on effectue le dosage :
  - 100 µl de l'extraction
  - + 100 µl de l'enzyme de dosage de l'ATP - lecture
  - + 10 µl d'ATP standard - lecture.

b) Les milieux de croissance (9)

Les milieux choisis sont des milieux bactériologiques de référence pour la culture des anaérobies.

| Milieu VL                |       | MILIEU SA   |            |
|--------------------------|-------|-------------|------------|
| Tryptone                 | 10 g  | Tryptone    | 10 g       |
| Extrait de viande        | 5 g   | pH          | non ajusté |
| Dextrose                 | 2 g   | qsp 1 litre |            |
| Amidon soluble           | 5 g   |             |            |
| Chlorhydrate de cystéine | 0,4 g |             |            |
| pH                       | 7,4   |             |            |
| qsp 1 litre              |       |             |            |

Ces milieux ont été ensemencés avec les mêmes bactéries que précédemment.

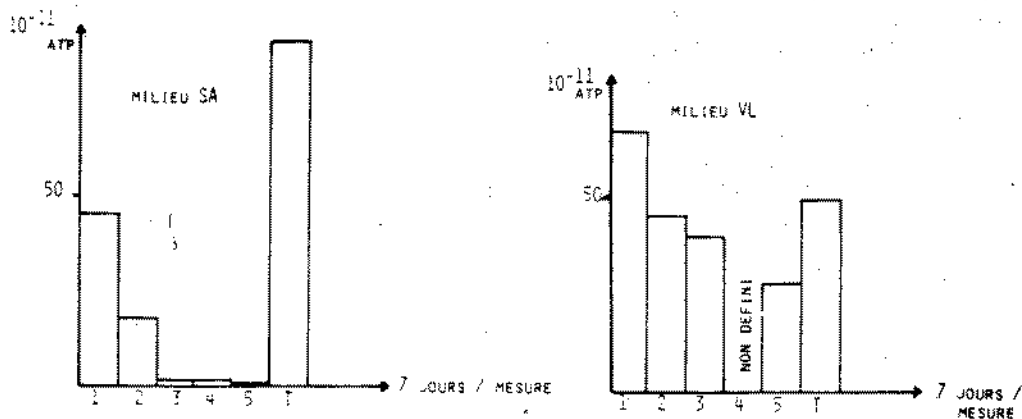


## c) Les compositions testées

| RAPPORT<br>GZ - HMPP | CONCENTRATION<br>ppm | REFERENCE |
|----------------------|----------------------|-----------|
| -                    | 0                    | T         |
| 0 - 100              | 500                  | 1         |
| 25 - 75              | 500                  | 2         |
| 50 - 50              | 500                  | 3         |
| 75 - 25              | 500                  | 4         |
| 100 - 0              | 500                  | 5         |

## d) Les résultats

Ils sont indiqués dans les courbes ci-après.



Dans le présent essai, il s'avère que le gluconate de zinc seul est la composition la plus efficace.

D'une manière générale, toutes les compositions contenant du gluconate de zinc peuvent être considérées comme étant des inhibiteurs de bactéries anaérobies. En ce qui concerne l'HMPP, les résultats obtenus sont médiocres.

IV - CONCLUSIONS

L'ensemble des travaux que nous venons d'exposer permet de conclure que le gluconate de zinc en association avec l'hexamétaphosphate de sodium est une excellente composition inhibitrice de la corrosion de l'acier au contact de solutions salines et ce, qu'il s'agisse de milieux aérés ou non.

BIBLIOGRAPHIE

- (1) L'Expansion - Déc. 1983 - 54
- (2) E.D. MOR and C. WRUBL - Br Corros J. 1976 - Vol. 11 n° 4  
" Zinc gluconate as an inhibitor of the corrosion of mild steel in sea water "
- (3) GB Patent 1.302.738 - Zizis Andrew FOROULIS - ESSO RESEARCH
- (4) GB Patent 1.434.804 - APPLIED CHEMICAL Pty Ltd
- (5) US Patent 3.116.105 - H. KERST
- (6) FR Patent 2.512.072 - ROQUETTE FRERES
- (7) Valeur induite de la théorie de STERN et GEARY
- (8) M.H. SANIEZ - ROQUETTE FRERES  
" Inhibition de la corrosion bactérienne " (résultats non publiés)
- (9) J. CHANERAU - Technique et Documentation  
" Corrosion bactérienne - Bactéries de la corrosion "
- (10) INSTITUT PASTEUR de LILLE (FRANCE)  
" Les bactéries sulfato-réductrices " (cours de microbiologie)

ELECTROCHEMICAL MEASUREMENTS APPLIED TO THE CORROSION AND PROTECTION  
STUDY OF A CARBON STEEL IN 3 % SODIUM CHLORIDE SOLUTION.

Michel DUPRAT, Francis DABOSI

E.R.A. CNRS 263, Laboratoire de Métallurgie Physique  
E.N.S. CHIMIE 118 Route de Narbonne 31077 TOULOUSE FRANCE  
and Francis MORAN

Union Chimique et Industrielle de l'Ouest  
24, Boulevard de Strasbourg 75010 PARIS FRANCE

**ABSTRACT :** The electrochemical behaviour of a carbon steel rotating disc electrode in 3 % NaCl solution has been investigated using both steady-state (plotting of current-voltage curves) and transient (impedance measurements) electrochemical techniques. The protection by various inhibitive compounds added to the aggressive medium or by application of a coating on the metal has been also studied using the same techniques. In the absence of any protection mass transport of oxygen occurs not only in the liquid phase but also through a porous layer of corrosion products and the corrosion rate is controlled by the reduction of oxygen under either purely diffusional or mixed control depending on the experimental conditions. Both organic (diamino-1,2-ethane ; oleylamino-propylene amine + amino-tri (methyl-phosphonic) acid) and mineral (zinc monofluorophosphate) compounds have been examined as inhibitors. It has been shown that diamino-1,2-ethane acts in mainly reducing the anodic area whereas the two others act in forming relatively thick and compact protective films. A glycerylphthalate type paint has been applied on variously pre-treated (phosphatation, phosphatation + post-treatment by monofluorophosphates) electrodes. Impedance measurements have allowed one to follow the evolution, as a function of the immersion time, of the parameters influencing the corrosion performance of the different coatings ; the favourable effect of the pre-paint surface treatment has been exhibited for long immersion times.

**RESUME :** L'étude du comportement électrochimique d'une électrode à disque tournant en acier au carbone a été menée par des méthodes électrochimiques à la fois stationnaires (relevé des courbes courant-tension) et transitoires (mesure de l'impédance). La protection par divers composés inhibiteurs additionnés au milieu agressif ou par application

d'un revêtement sur le métal a été également étudiée à l'aide de ces mêmes techniques. En l'absence de toute protection, le transport de l'oxygène se fait non seulement en phase liquide mais aussi à travers une couche poreuse de produits de corrosion et la vitesse de corrosion est soit sous contrôle purement diffusionnel soit sous contrôle mixte selon les conditions expérimentales. Des composés à la fois organiques (diamino-1.2-ethane, oleylamino-propylène amine + acide amino-tri (methyl-phosphonique)) et minéraux (monofluorophosphate de zinc) ont été étudiés en tant qu'inhibiteurs. Il a été montré que le diamino-1.2-ethane agissait principalement en réduisant l'aire anodique alors que les deux autres formaient des films protecteurs relativement épais et compacts. Une peinture de type glycerophthalique a été appliquée sur des électrodes différemment pré-traitées (phosphatation, phosphatation + post-traitement par les monofluorophosphates). Les mesures d'impédance nous ont permis de suivre l'évolution, en fonction du temps d'immersion, des paramètres influençant la performance vis à vis de la corrosion des différents revêtements ; pour des longs temps d'immersion, l'effet favorable du traitement de surface avant peinture a été mis en évidence.

### INTRODUCTION

In the literature many studies have been devoted to corrosion and protection in acidic media in order to measure the corrosion rate or to identify the elementary steps involved in the overall processes. However relatively few studies have been carried out in neutral aerated media (1) ; this may be explained by the following features : i) the cathodic reaction which predominates at the corrosion potential is no more the hydrogen evolution reaction the mechanism of which is relatively well-known, but in this case the dissolved oxygen reduction reaction the mechanism of which has been studied thoroughly on noble metals only (2). ii) such interfaces generally show strong time dependence induced by the progressive deposit of insoluble corrosion products which makes their study more complex (3,4). In this paper are reported some examples of the application of both steady-state (plotting of the current-voltage curves) and transient (impedance measurements) electrochemical methods to the corrosion kinetics study of a carbon steel in 3% sodium chloride solution simulating sea water. The influence of various inhibitive compounds added to the medium as well as the effect of a coating (conversion treatment + paint) application on the metal surface have been also examined using the same techniques.

### EXPERIMENTAL

The steel sample selected for the study is the N 80 type according to the API standards, and has the following composition by percent weight : C = 0.4 ; Mn = 1.38 ; P = 0.013 ; S = 0.024 ; Si = 0.19 ; Cu = 0.04 ; Ni = 0.03 ; Cr = 0.09 ; Mo = 0.19 and Fe to 100. The working electrode consists of the cross section of a cylindrical rod of 1 cm<sup>2</sup> area, a thermoretractable sheath preventing the cylindrical area from making contact with the solution, the electrode surface

being only the cross section. In order to avoid possible crevice conditions between the metal rod and the sheath induced by the successive polishings, the sheath was renewed after each run. The surface is polished with a silicon carbide emery cloth (grade 80), then rinsed with water, and finally dried in pulsed warm air after an ultrasonic washing in ethanol. This electrode is screwed into a conducting rotating shaft. The reference electrode is a saturated calomel electrode (SCE) and the auxiliary electrode is a platinum grid of large area. Current-voltage curves have been obtained either in potentiostatic or galvanostatic mode with a TACUSSEL electrochemical set up including a potentiostat, a chart recorder and a high impedance electronic millivoltmeter. Impedance measurements have been performed by means of a frequency response analyser (SCHLUMBERGER-SOLARTRON 1174) included in an experimental set up described in detail elsewhere (5). The corrosive medium is a 3 % solution of NaCl (pro analysis grade) dissolved in distilled water ; it is in contact with air and at ambient temperature ( $\sim 20^{\circ}\text{C}$ ).

Diamino-1.2-ethane ( $\text{H}_2\text{N}-(\text{CH}_2)_2-\text{NH}_2$ ) is a "Pro analysis" grade (MERCK) product ; zinc monofluorophosphate ( $\text{ZnPO}_3\text{F}$ ,  $2.5 \text{ H}_2\text{O}$ ) is a laboratory synthesized product the use of which as inhibitor has been patented (6) ; the inhibitor mixture, oleylamino-propylene amine + amino tri(methyl phosphonic) acid, consists of current chemical products and has been also previously patented (7). The paint applied is a glycerylphthalate type of near constant thickness ( $40 - 50 \mu$ ) whereas the pre-treatment procedures before painting have been previously described in detail elsewhere (8).

## RESULT AND DISCUSSION

### I - N 80 carbon steel/3 % NaCl

#### I.1. Steady-state measurements

1.1.1. Current-voltage curves : Prior to any experiment, the electrode is held at zero current for a given angular velocity  $\Omega$  (rpm) of the disk till the corrosion potential is stabilized. The steady state occurs rather slowly and the current-potential curves are, therefore, plotted point by point in a quasi steady-state mode. As an example, two cathodic plots after a hold time at zero current of 30 min and 2 hr are displayed in Fig. 1. A shift of  $E_{\text{corr}}$  towards more cathodic potentials and a decrease of the diffusion current with an increasing hold time at zero current are concurrently observed. From a detailed analysis of these curves (9), this diffusion plateau was ascribed to dissolved oxygen. Moreover, the variations of the limiting current density with the hold time have been explained by hindrance to diffusion due to the progressive deposit of corrosion products.

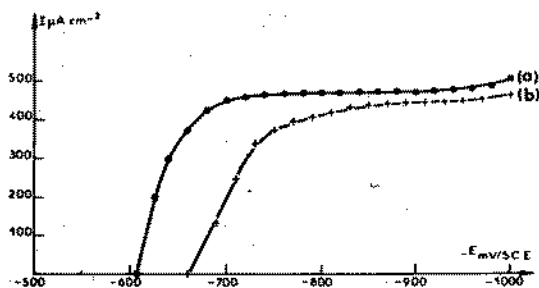


Fig. 1 - Cathodic current-voltage curves obtained in potentiostatic mode at  $\Omega = 1000$  rpm. Hold time at  $E_{\text{corr}}$  : (a) 30 min, (b) 2hr

It has been verified that for anodic overpotentials, the current even at some tens of  $\text{mA} \cdot \text{cm}^{-2}$  is not dependent on the angular velocity of the disk (Fig. 2).

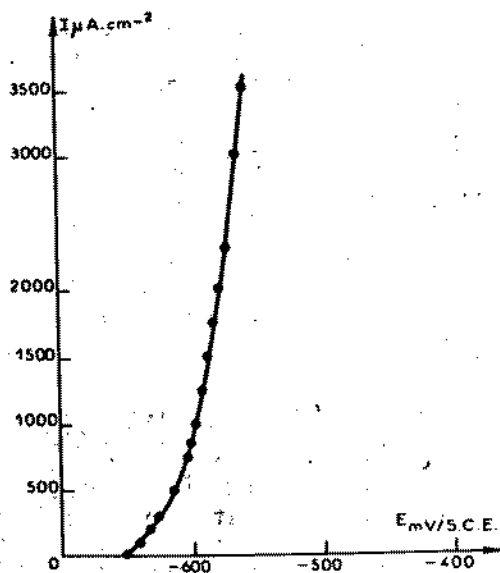
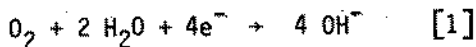


Fig. 2 - Anodic current-voltage curve obtained in galvanostatic mode at  $\Omega = 1000$  rpm. Hold time of  $E_{\text{corr}}$  : 2 hr.

I.1.2. Cathodic mass transport study : The elementary cathodic reaction may be written as



The variations of the diffusional component vs.  $\Omega$  were measured, in potentiostatic regulation, for cathodic and anodic overpotentials, and for the corrosion potential. The results are reported in Fig. 3.

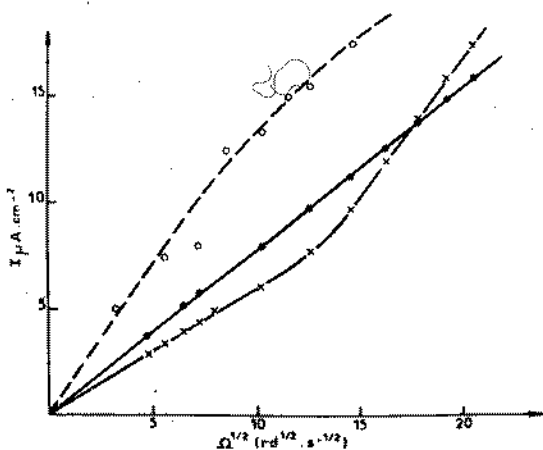


Fig. 3 - Diffusion component of the current density vs.  $\Omega^{1/2}$ .

O: E corresponds to  $I_d = 250 \mu\text{A cm}^{-2}$  at  $\Omega = 1000 \text{ rpm}$   
 ●: E = -914 mV/SCE  
 X: E =  $E_{\text{corr}}$  ( $\Omega = 1000 \text{ rpm}$ ).  
 Actual diffusional components are obtained by multiplying the above value by:  
 4 (O), 20 (X), 100 (●).

At the cathodic diffusion plateau ( $E_c = -914 \text{ mV/SCE}$ ) the diffusion current values (●) plotted as function of  $\Omega^{1/2}$  fall on a straight line intersecting the origin of the axis. The experimental slope value is in agreement with that deduced from the Levich equation (10)

$$I_L = 0.62 n F c_{\infty} D^{2/3} \nu^{-1/6} \Omega^{1/2} A \quad 2$$

for the set of values at  $20^\circ\text{C}$ :  $c_{\infty} = 2.10^{-7} \text{ mol.cm}^{-3}$ ;  $\nu = 10^{-2} \text{ cm}^2.\text{sec}^{-1}$ ;  $D = 1.74.10^{-5} \text{ cm}^2.\text{sec}^{-1}$  this value has been deduced from that measured at  $25^\circ\text{C}$ ,  $2.10^{-5} \text{ cm}^2 \text{ sec}^{-1}$  (11) where: n, the number of electrons transferred, is taken as 4, F is the Faraday,  $c_{\infty}$  the oxygen concentration in the bulk,  $\nu$  the kinematic viscosity of the solution, D the molecular diffusion coefficient of oxygen, and A the electrode area ( $\text{cm}^2$ ). This result indicates that the whole electrode area is active in regard to the cathodic reaction.

At the corrosion potential (X) (Fig. 3), a linear plot through the origin is first observed up to 1500 rpm, but the slope is lower than that corresponding to Eq. [2]. Beyond 1500 rpm, a sharp increase of the current occurs, the data being fitted by a second linear plot whose extrapolation intersects the  $\Omega^{1/2}$  axis at a positive abscissa. However, if the angular velocity is decreased, the current values lie again on a straight line going through the origin of the axis but with a higher slope than previously found between 0 and 1500 rpm. A fraction of the electrode area is then covered by a thick layer (9). The bare portions of the disk are bounded by logarithmic spirals issued from the rotation axis which accounted for a hydrodynamic shearing of the layer formed during the hold time at zero current, under the flow action. Therefore, below 1500 rpm a low portion of the interface remains bare and gives rise to a dependence  $I_d \propto \Omega^{1/2}$ , which can be expected for an active surface delimited by a convex contour on a rotating disk in laminar flow. Above 1500 rpm, the layer disruption becomes significant and, therefore, the increasing bare sur-

face leads to a jump in the diffusion current.

After a hold time of 2 hr at an anodic current of  $250 \mu\text{A}\cdot\text{cm}^{-2}$  ( $\Omega = 1000 \text{ rpm}$ ), the plot  $I_d$  vs.  $\Omega^{1/2}$  (O) (Fig. 3) is curved. If the same data are replotted in the  $i^{-1}$ ,  $\Omega^{-1/2}$  coordinates, a straight line is found again, but it does not go through the origin of the axis (Fig. 4).

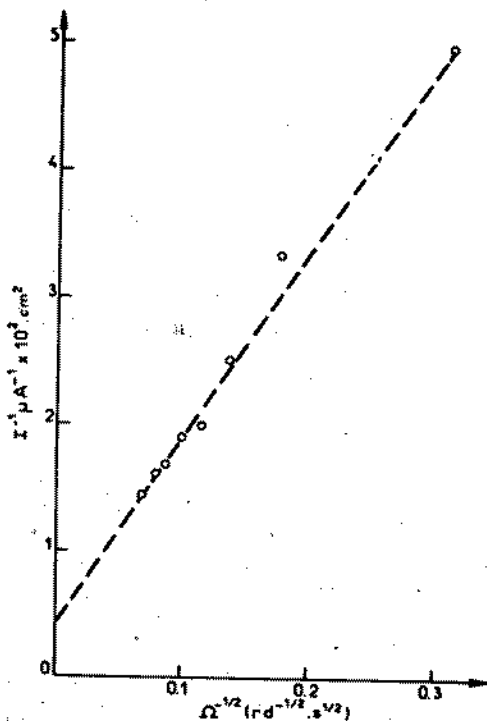


Fig. 4 - Reciprocal values of the diffusional component vs.  $\Omega^{-1/2}$  corresponding to the data (O) of Fig. 3.

Different causes are known to separately produce such an effect: (i) mixed kinetics, i.e. electron transfer-mass transfer, for the cathodic reaction (10) (ii) the existence of a porous layer in which mass transport only depends on molecular diffusion, in addition to the convective diffusion transport in the liquid phase (12) and (iii) a partial blocking of the interface, i.e., a decrease of the active area (13, 14). Under the imposed hold time conditions, the metal is wholly covered by a colloidal layer of rust. It can be easily washed out under a water jet, and there remains an underlying black powdery layer. If one imposes then a cathodic polarization ( $E = -914 \text{ mV/SCE}$ ) on this surface, the measured diffusion current corresponds to that previously obtained on an active surface. The occurrence of a partial blocking of the interface must then be ruled out. This second layer can be also removed by an ultrasonic cleaning.



There only remains the role of a porous layer played by the colloidal layer, conceivably ferric hydroxide, in regard to oxygen diffusion. The mass transport of dissolved oxygen would proceed by both convective diffusion in the liquid phase (classical Nernst layer) and by molecular diffusion through the colloidal layer. Moreover, if one assumes a mixed kinetics control for the oxygen consumption, the total current resulting from the different series processes involved may be written as

$$I^{-1} = I_k^{-1} + I_{\Omega \rightarrow \infty}^{-1} + I_L^{-1} \quad [3]$$

where  $I_k$  is the "kinetic current" of oxygen, i.e., which would be measured at the corrosion potential on a bare surface in the absence of a mass transfer control.  $I_{\Omega \rightarrow \infty}$  is the plateau current with the colloidal layer for an infinite angular velocity. Given  $\delta'$  and  $D'$ , respectively, the thickness layer and the molecular oxygen diffusion coefficient in this layer, then

$$I_{\Omega \rightarrow \infty} = c_{\infty} D' / \delta' \quad [3']$$

Finally  $I_L$  is given by Eq. [2].

Equation [3] provides then a linear relationship between  $I^{-1}$  and  $\Omega^{-1/2}$ , the slope of which must be identical to the reciprocal of that appearing in the Levich equation (Ref. (10)). Now, the experimental slope value of  $0.15 \mu\text{A}^{-1} \text{rd}^{1/2} \text{sec}^{-1/2}$  is at variance with the theoretical value of 0.0125. This discrepancy may be explained if the consumption of dissolved oxygen by the chemical oxidation reaction of ferrous to ferric ions is considered (15). This leads to the overconsumption of oxygen during anodic dissolution and therefore explains the steep decay of the diffusional component at small anodic overvoltages in apparent contrast with the wide range of mixed kinetics observed at a platinum electrode (Fig. 5).

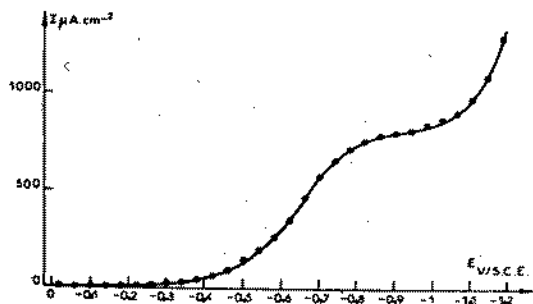


Fig. 5 - Cathodic current-voltage curve obtained in potentiostatic mode at  $\Omega = 1000$  rpm on a Pt electrode ; 3 % NaCl solution.

## II.2. Electrochemical impedance measurements

Electrochemical impedance measurements are carried out by using a small amplitude sine wave (less than 20 mV peak to peak). Fig. 6 shows in the complex plane two impedance diagrams for two different

rotation speeds (600 and 2400 rpm). Previously to the measurement the electrode is allowed to undergo corrosion at its free corrosion potential for 2 hours at 1000 rpm. Impedance measurements are then performed under potentiostatic control at the same potential. Both diagrams exhibit two capacitive loops with fairly low characteristic frequencies. In an attempt to establish an analogy with the impedance of a redox system, the low frequency loop should be attributed to the relaxation of mass transport. Even though the low frequency loop is somewhat sensitive to hydrodynamic conditions it does not look like an usual diffusion impedance (16) nor it watches a more important feature, the proportionality of the characteristic frequency to the speed of rotation. This is consistent with the data of the mass transport study according to which diffusion occurs not only in the liquid phase but also in a layer of corrosion products.

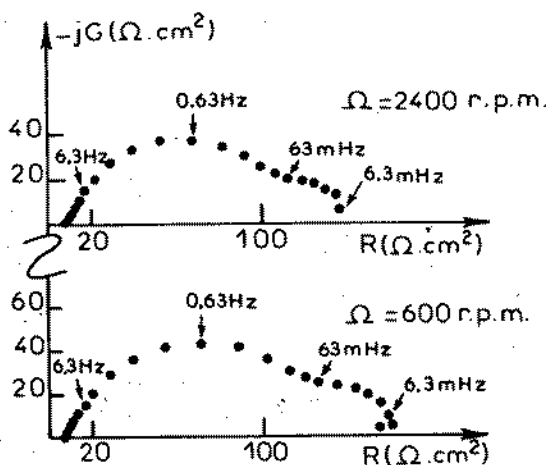
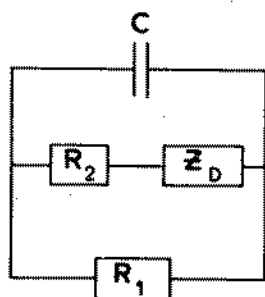


Fig. 6 - Electrochemical impedance diagrams obtained in potentiostatic mode ( $E = E_{\text{corr}}$  when  $I = 0$  at  $\Omega = 1000$  rpm) at different rotation speeds.

Accordingly, the frequency response of the system must be quite different from that of an ideal Nernst diffusion layer (16). Moreover it can be noted that the longer the time for free corrosion before impedance measurement, the larger the low frequency loop. In order to estimate the contribution of mass transport to the electrode impedance at a mixed potential, impedance diagrams have been simulated by assuming the equivalent circuit in Fig. 7.  $R_1$  and  $R_2$  are respectively the transfer resistance for the anodic and cathodic processes,  $C$  the parallel capacitance and  $Z_D$  the diffusion impedance (according to the Nernst layer model) related to the cathodic current. The calculated diagram in Fig. 8 is fairly similar to those provided by experiments. In terms of the circuit used in the simulation, the high frequency loop is  $\frac{R_1 R_2}{R_1 + R_2}$  in diameter so that at constant potential, in agreement with experimental findings, its size is slightly (mixed

control) or no dependent (diffusion control) on  $\Omega$ . This tends to support, as assumed in a previous paper (9) a mixed or purely diffusional control of the corrosion rate.



$$Z_D = R_D \frac{\tanh(j\omega \frac{\delta^2}{D})^{1/2}}{(j\omega \frac{\delta^2}{D})^{1/2}}$$

Fig. 7 - Equivalent circuit of the interface carbon steel/3% NaCl solution, in the vicinity of the corrosion potential.

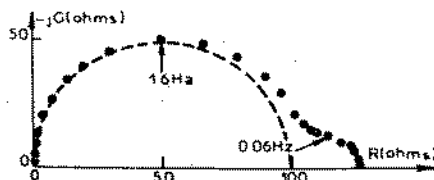


Fig. 8 - Simulated electrochemical impedance diagram according to the equivalent circuit of Fig. 7  
 $R_1 = 150 \Omega$ ;  $R_2 = 300 \Omega$ ;  $R_D = 500 \Omega$   
 $\delta^2/D = 20 \text{ sec}$ .

In addition, experimental data obtained around the corrosion potential - where two capacitive loops are still observed - corroborate the validity of equivalent circuit reported in Fig. 7:

- i) in the cathodic range the low frequency (L.F) loop size increases with overpotential
- ii) in the anodic range, the dimensions of both loops decrease with overpotential.

The capacitance  $C$  associated to the high frequency (HF) loop of diameter  $R_1$  has been roughly estimated - since this loop is not centered on the real axis - from the relationship  $C = (R_1 \omega_c)^{-1}$ , where the characteristic pulsation  $\omega_c = 2 \pi f_c$  corresponds to the maximum value of the imaginary component. The obtained value is abnormally high ( $\sim 2 \text{ mF cm}^{-2}$ ) since  $C$  is likely to be considered as the double layer capacitance. The frequency dispersion - leading to a flattening of the loop (17) - and the high value of the capacitance may be ascribed to the surface heterogeneity and the porous and conductive nature (18) of the deposited corrosion products layer generated during the preliminary hold time at the free corrosion potential.

Finally, this work carried out by both steady-state and transient measurements leads to the following conclusions: i) during the corrosion of a carbon steel in aerated 3% NaCl solution mass transport occurs not only in the liquid phase but also through a corrosion products porous layer, ii) the corrosion rate is controlled

by the reduction of dissolved oxygen under either purely diffusional or mixed control depending on the experimental conditions ; consequently, the systematic use of the polarization resistance (19) in order to determine the corrosion rate may lead to erroneous values (20).

## II - N 80 carbon steel/inhibited 3 % NaCl

### II.1. N 80 carbon steel/3 % NaCl + $\text{H}_2\text{N} - (\text{CH}_2)_2 - \text{NH}_2$ ( $10^{-2}$ M)

Diamino-1,2-ethane exerting a strong alkalinizing effect, the pH of the NaCl solution reaches the value 10.85 instead of 6.20 without inhibitor. For this reason, a comparative test has been performed by adjusting the pH to the same value as that of an inhibitor free solution by means of a small addition of 0.5 M NaOH.

The electrochemical impedance diagram, obtained in galvanostatic regulation at zero d-c current and in the presence of diamino-1,2-ethane ( $10^{-2}$  M) is reported in Fig. 9.a. By comparison with results from an uninhibited solution (fig. 9.c) it is observed that : (i) there only remains one capacitive loop, the second loop previously ascribed to the molecular diffusion of dissolved oxygen through a corrosion products porous layer having vanished, ii) the polarization resistance is greatly increased. To examine the intrinsic influence of the inhibitor alkalinity, impedance measurements have been carried out in the uninhibited solution but at the same pH (10.85) adjusted by NaOH : the relevant diagram reported in Fig. 9.b presents the same shape as that of Fig. 9.a but with a decreased polarization resistance.

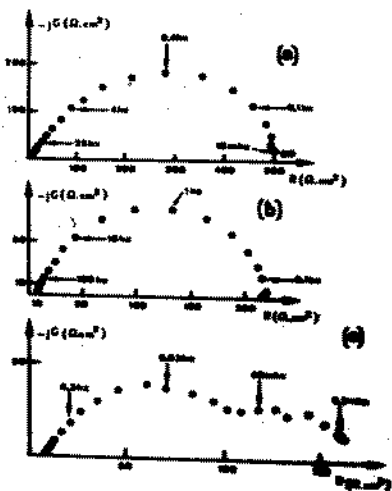


Fig. 9 - Electrochemical impedance diagrams in galvanostatic mode at  $I = 0$  and  $\Omega = 1000$  rpm.

- 3 % NaCl +  $\text{H}_2\text{N} - (\text{CH}_2)_2 - \text{NH}_2$  ( $10^{-2}$  M)  
pH = 10.85
- 3 % NaCl ; pH = 10.85 adjusted by NaOH.
- 3 % NaCl.

The corresponding steady-state cathodic current-voltage curves are shown in Fig. 10. A comparison of curves a and c shows that the inhibitor gives rise to a shift of the corrosion potential to more

positive values and to a more marked region of mixed kinetic control of oxygen reduction ; moreover; in contrast with the uninhibited situation, it should be mentioned that the limiting current density in presence of the inhibitor is very close to the value predicted by LEVICH (10) for a uniformly active surface. From the point of view of both corrosion potential and limiting current density, curve b is located between a and c.

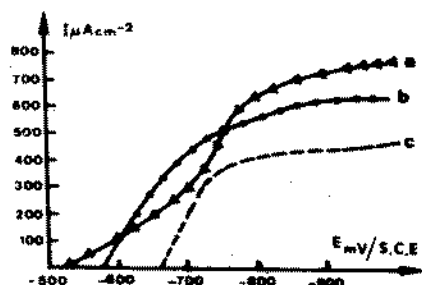


Fig. 10 - Steady - state cathodic current-voltage curves at  $\Omega = 1000$  rpm. a), b), c) as Fig. 9.

In the immediate vicinity of the corrosion potential the cathodic current is poorly dependent on the rotation speed of the electrode while the impedance diagrams at the free corrosion potential are not influenced by the disk angular velocity. These results suggest that at the free corrosion potential, the rate of oxygen reduction is mainly under charge transfer control ; consequently, polarization resistance measurements can therefore be used to evaluate the corrosion rate.

Finally a better insight of the action mode of this type of inhibitor can be afforded by considering the following features :

- at high cathodic overpotentials the interface behaves as a bare surface ; in particular the LEVICH equation applies on the cathodic plateau which precludes any meaningful hindering process taking place at the interface.
- the impedance diagrams of Fig. 9-a and 9-b exhibit the same shape, and, hence the electrochemical behavior of carbon steel in both solutions is presumably identical, though the pH increase alone does not provide such an protective effect as that due to diamino-1,2-ethane. The inhibitor action can be then clearly described as a reduction of the active area of dissolution without modification of the anodic mechanism.

This analysis corroborates previous assumptions regarding the inhibiting action of such a type of compounds (21, 22) ; the inhibitor is able, by a chelation mechanism, to strengthen and fill in the "pre-passive" layer of  $\text{Fe}(\text{OH})_2$  formed by the pH increase of the solution as well as to directly make bonds with the metallic atoms of the bare fraction of the metal.

II.2. N 80 carbon steel/3 % NaCl + 1 g l<sup>-1</sup> + oleylamino-propylene amine + amino tri (methyl-phosphonic) acid :

Because the previous inhibitor and those of the same type (22) are basic in nature, their use must be prevented in some practical situations. So we have developed, in collaboration with industry, a neutral inhibitive formulation composed of a fatty amine (oleylamino-propylene amine) and a phosphonic acid (amino-tri (methyl phosphonic) acid) (7, 23) ; it should be mentioned that this choice of composition was dictated by your aim in associating a corrosion inhibitor (fatty amine) and a scaling inhibitor (phosphonic acid). The chosen formulation will be denoted in this article : FA + TMPA.

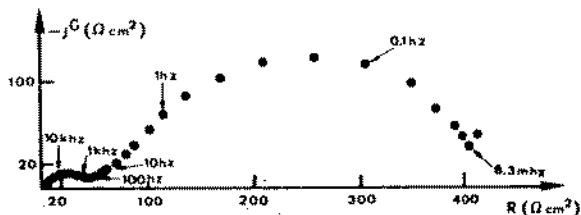


Fig. 11 - Electrochemical Impedance diagram in galvanostatic mode at  $I = 0$  and  $\Omega = 1000$  rpm ; 3 % NaCl + 1 g l<sup>-1</sup> (FA + TMPA).

The electrochemical impedance diagram obtained in galvanostatic regulation at zero d.c. current and in the presence of 1 g.l<sup>-1</sup> (FA + TMPA) is reported in Fig. 11. It is characterized by two well-separated capacitive loops as in the absence of inhibitor (Fig. 9-c or 6) but the characteristic frequencies associated to each loop are different. In particular, the capacity associated to the high frequency (HF) loop has a very low value  $C_{HF} \sim 1 \mu F/cm^2$ . Consequently we are lead to believe that this very low value can be ascribed to either i) the change of the dielectric constant of the double layer the value of which would be modified by the strong hydrophobic effect of this compound ii) the formation of a more compact and protective film similar to a paint film.

Indeed, the first assumption must be disregarded in so far as the low value of the HF associated resistance  $R_{HF} (\sim 35 \Omega cm^2)$ , in comparison to that obtained with the blank solution ( $\sim 115 \Omega cm^2$ ), would indicate an increase of corrosion rate at variance with the observed inhibitive effect (23).

Moreover, this is also corroborated by the steady-state results reported in fig. 12. Indeed in the cathodic plateau region, the current  $I$  corresponding to dissolved oxygen reduction in both the inhibited and blank solution is lower than that,  $I_L$ , predicted by LEVICH (10) on a uniformly active surface. In the blank solution, this effect has been previously ascribed to the progressive deposit of insoluble cor-

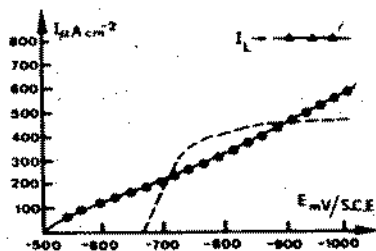


Fig. 12 - Steady-state cathodic current-voltage curves at  $\Omega = 1000$  rpm.

3% NaCl  
 3% NaCl +  $1 \text{ g l}^{-1}$  (FA + TMPA)  
 $I_L$  deduced from LEVICH equation.

rosion products acting as a diffusion barrier. In the inhibited solution the difference between the cathodic current and  $I_L$  appears more marked in the potential range - 700 to - 900 mV/SCE although there is no accumulation of corrosion products on the metal surface. Moreover in presence of the inhibitor no diffusion plateau clearly appears, the inhibitor seeming to induce a shift of the hydrogen evolution wave towards less cathodic potentials. Separate experiments carried out with inhibitor mixture of different composition have shown that phosphonic acid is responsible for this shift by lowering the interfacial pH while the bulk solution pH remains nearly the same as that in absence of the inhibitor. Thus, the inhibitor action may therefore be explained in terms of film effect, which is also suggested by the fact that the impedance diagram reported in Fig. 11 resembles those relative to the same electrode covered by a paint film as it will be shown in the following section (Fig. 15 and 16). The protective film can be then characterized by  $R_{HF}$  and  $C_{HF}$  obtained from electrochemical impedance measurements. The value of  $R_{HF}$  increases with immersion time whereas the value of  $C_{HF}$  slightly decreases; when the oxygen concentration is decreased; - the medium being then less aggressive - the HF loop only appears for long immersion times (Table I).

| Hold time at $E_{corr}$ (min) |                                    | 20  | 80  | 210 |
|-------------------------------|------------------------------------|-----|-----|-----|
| AERATED                       | $R_{HF}$ ( $\Omega \text{ cm}^2$ ) | 7   | 25  | 35  |
| MEDIUM                        | $C_{HF}$ ( $\mu\text{F cm}^{-2}$ ) | 2.3 | 1.6 | 1.2 |
| PARTIALLY DEAERATED           | $R_{HF}$ ( $\Omega \text{ cm}^2$ ) | —   | —   | 22  |
|                               | $C_{HF}$ ( $\mu\text{F cm}^{-2}$ ) | —   | —   | 2.6 |

TABLE I - 3% NaCl +  $1 \text{ g.l}^{-1}$   
 (FA + TMPA) ;  $\Omega = 1000$  rpm.

Finally, when the inhibitor concentration is reduced to  $375 \text{ mg.l}^{-1}$  the size of the HF loop is greatly reduced even for long immersion times; for this concentration it has been shown elsewhere

(23) that the inhibitor is poorly efficient (~ 20 % instead of ~ 80 % at  $1 \text{ g.l}^{-1}$ ). In conclusion, it appears that the inhibitor mixture (FA + TMPA) acts by building up a film of a dielectric nature, the protective efficiency of which is increased with the inhibitor concentration and presumably enhanced by the initial corrosion products.

### II.3. N 80 carbon steel/3 % NaCl + $\text{ZnPO}_3\text{F} \cdot 2.5 \text{ H}_2\text{O}$ ( $10^{-2} \text{ M}$ )

In view of the promising results obtained with monofluorophosphates as post-treatment agents of phosphated metallic surfaces before painting (see the following section), we have also studied their action as inhibitors when they are directly added to the aggressive medium. Zinc monofluorophosphate,  $\text{ZnPO}_3\text{F} \cdot 2.5 \text{ H}_2\text{O}$ , appeared to be the best inhibitor against corrosion of carbon steel in 3 % NaCl solutions (24, 25).

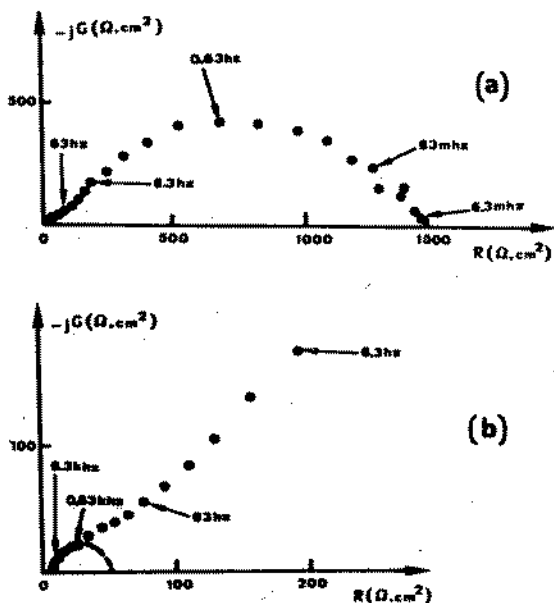


Fig. 13 - Electrochemical impedance diagrams in galvanostatic mode at  $I = 0$  and  $\Omega = 1000 \text{ rpm}$  3 % NaCl +  $\text{ZnPO}_3\text{F} \cdot 2.5 \text{ H}_2\text{O}$  ( $10^{-2} \text{ M}$ ) (Detail of HF range in (b)).

The electrochemical impedance diagram obtained in galvanostatic regulation at zero d.c. current and in the presence of  $\text{ZnPO}_3\text{F} \cdot 2.5 \text{ H}_2\text{O}$  ( $10^{-2} \text{ M}$ ) is shown in Fig. 13.a - By comparison with results from the blank solution (fig. 9.c or 6) it is observed that the corrosion resistance is very greatly increased. In the HF range (Fig. 13.b), a capacitive loop is also observed; the value of the associated capacity  $C_{\text{HF}}$  is about  $5 \mu\text{F}/\text{cm}^2$  which is well below of the usual value of the double layer capacity, whereas the value of the associated resistance  $R_{\text{HF}}$  is about  $45 \Omega\text{cm}^2$ .



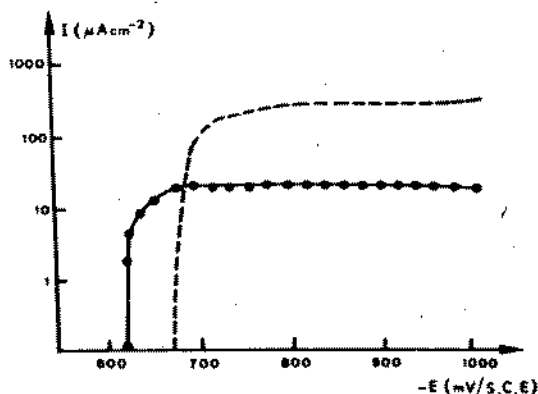


Fig. 14 - Semi-logarithmic representation of the steady-state cathodic curves at  $\Omega = 1000$  rpm  
 : 3 % NaCl +  $ZnPO_3F \cdot 2.5 H_2O$  ( $10^{-2}$  M)  
 : 3 % NaCl

In addition steady-state measurements (Fig. 14) show that in the presence of  $ZnPO_3F \cdot 2.5 H_2O$  the cathodic current is greatly reduced: the limiting current density  $I_L$  decreases from about  $350 \mu A/cm^2$  to about  $30 \mu A/cm^2$ . These observations suggest that the HF loop is representative of a thick film formed by the inhibitor on the metal surface. By comparison with the inhibitor (FA + TMPA) the value of capacity is greater suggesting that this film is less thick or/and of a less dielectric nature in agreement with the mineral nature of the inhibitor. Such high frequency time constants have been already mentioned in the case of the iron protection by sodium nitrite (26, 27) but not clearly ascribed to thick protective film effects.

In conclusion, of this section it appears that electrochemical impedance measurements carried out at the corrosion potential ( $I = 0$ ) may provide valuable information on the corrosion inhibition mechanisms which cannot be obtained from only steady-state measurements. However, it is obvious that impedance measurements carried out in the cathodic and anodic ranges are necessary in the case of more complete studies involving in particular the precise determination of the inhibitive efficiency.

### III - Coated N 80 carbon steel/3 % NaCl

In a previous work (28) the influence of chemical conversion surface treatments on the corrosion protection of a carbon steel in 3 % NaCl solution has been investigated using steady-state electrochemical methods whereas the composition and the morphology of the protective layers has been determined by physico-chemical analysis (Chemical analysis, S.E.M., E.S.C.A.). It has been shown that all surface treatments reduce the corrosion rate of the metallic substrate but great differences in protection magnitude were encountered depending upon the nature of the treatment. The present work deals in detail with the effect of a paint layer application on the following surface treatments of the steel: zinc phosphatation, zinc phosphata-

tion + potassium monofluorophosphate ( $K_2PO_3F$ ) post-treatment, zinc phosphatation + zinc monofluorophosphate ( $ZnPO_3F - 2.5 H_2O$ ) post-treatment.

### III.1. Steady-state measurements

In table II are reported the values of the corrosion potential  $E_{corr}$ , the corrosion current density  $i_{corr}$ , the current density at  $-1000$  mV/SCE  $i_{(-1000)}$  and of the polarization resistance  $R_p$ . The  $i_{corr}$  values have been determined according a critical analysis of the cathodic steady-state current-voltage curves described in a previous paper (9) whilst  $i_{(-1000)}$  values may provide some information on the degree of the coating's porosity (29). A good correlation is obtained between  $i_{corr}$ ,  $i_{(-1000)}$  and  $R_p$  showing that the paint directly applied on the bare metal affords the better protection which casts doubt on the generally accepted benefits of the prepaint surface treatments. Nevertheless it should be mentioned that these measurements only take account of instant corrosion rates (about 1 hour after the electrode immersion).

| Nature of coating   | $E_{corr}$<br>(mV/ECS) | $i_{corr}$<br>( $\mu A \cdot cm^{-2}$ ) | $i_{(-1000)}$<br>( $\mu A \cdot cm^{-2}$ ) | $R_p$<br>( $K\Omega \cdot cm^2$ ) |
|---|------------------------|---|--|-----------------------------------|
| Bare steel + paint  | $-525 \pm 75$          | $0,07 \pm 0,01$                         | $0,86 \pm 0,10$                            | $310 \pm 70$                      |
| Zinc phosphatation + paint  | $-510 \pm 10$          | $0,22 \pm 0,17$                         | $1,5 \pm 0,8$                              | $120 \pm 10$                      |
| Zinc phosphatation + $K_2PO_3F$ post-treatment + paint            | $-630 \pm 70$          | $1,2 \pm 0,6$                           | $2,9 \pm 0,5$                              | $65 \pm 35$                       |
| Zinc phosphatation + $ZnPO_3F - 2,5 H_2O$ post-treatment + paint. | $-510 \pm 10$          | $0,16 \pm 0,08$                         | $1,3 \pm 0,2$                              | $200 \pm 130$                     |

TABLE II - Instant corrosion resistance characteristics of the variously treated and painted steels.

So, in order to verify the validity of these extrapolated rapid steady-state data to the conditions met in actual practice, we have examined the influence of the immersion time in the aggressive medium on the corrosion resistance of the various coatings. For this purpose, electrochemical impedance measurements have been carried out.

### III.2. Electrochemical impedance measurements

Because they are based on small amplitude perturbations, impedance measurements have the advantage of being non-destructive and therefore more suited to continuous monitoring, and may in addition provide some information on the mechanisms involved in the coated metal degradation. For these reasons, there is a growing interest in the use of this type of measurements for evaluating the corrosion performance of coated metals immersed in aggressive media (30-36). Experimental impedance diagrams can be analysed to obtain individual components of an equivalent electrical circuit which best approximates the coated metal/solution interface.

III.2.1. Experimental impedance data : impedance measurements were carried out in galvanostatic mode at the free corrosion potential ( $i = 0$ ) ; the results were then plotted in the complex plane. The diagrams generally exhibit two more or less well separated capacitive loops, depending on the immersion time in the aggressive medium.

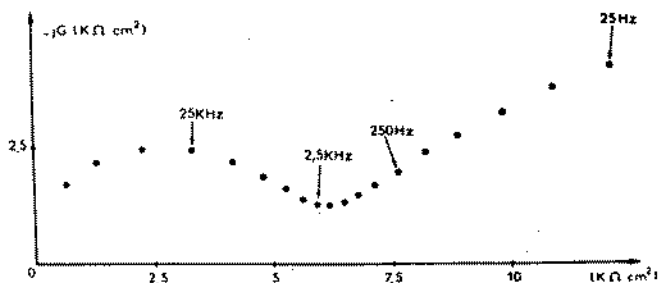


Fig. 15 - High frequency part of the impedance diagram - Zinc phosphatation +  $K_2PO_3F$  post-treatment + paint -  $i = 0$ .

Fig. 15 shows a typical high frequency part of a diagram obtained in the case of a paint layer applied on a  $K_2PO_3F$  post-treatment steel ; the very low value ( $\sim 1 \text{ nF.cm}^{-2}$ ) of the capacity associated with this loop excludes the possibility that it can be ascribed to charge transfer.

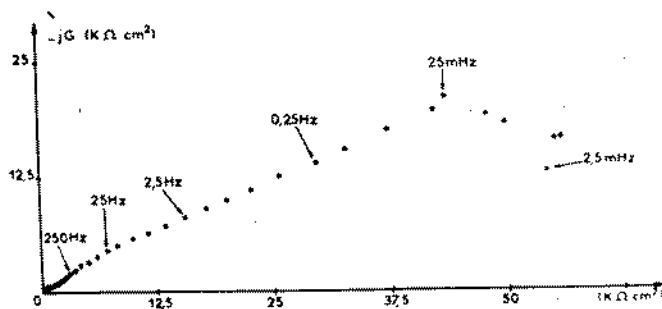


Fig. 16 - Impedance diagram - Zinc phosphatation +  $ZnPO_3F - 2.5 \text{ H}_2O$  post-treatment + paint ;  $i = 0$ .

As can be seen in the case of the paint layer applied on a  $ZnPO_3F - 2.5 \text{ H}_2O$  post-treated steel after about 45 min. immersion (fig. 16), the low frequency part is very depressed and cannot be ascribed with certainty to a single relaxation time. Such a shape is roughly similar to that obtained in the case of the bare metal under identical conditions as represented in fig. 9.c or 6 ; this diagram has been considered in the first section as representing both charge-transfer and mass transport taking place not only in the liquid phase but also through a porous layer of corrosion products.

As the very low value of the capacity associated with the high frequency loop (fig. 15) allows us to ascribe it to the insulating paint

film, the equivalent electrical circuit shown in fig. 17 (31) can therefore be used to describe the experimental results. This equivalent circuit consists of the electrolyte resistance  $R_E$ , the capacitance  $C_p$  of the intact film, the electrolyte resistance  $R_E^i$  through the pores, the double layer capacitance  $C$  in parallel with the faradic impedance  $Z_F$  which represents the corrosion of the metallic substrate.

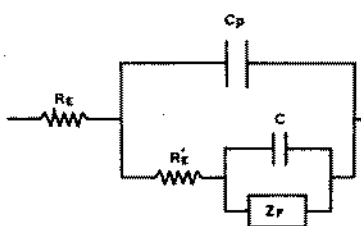


Fig. 17 - Electrical equivalent circuit of a coated metal/solution interface after (31).

$R_E$  = electrolyte resistance

$C_p$  = Intact film capacity

$R_E^i$  = Electrolytic resistance through the pores.

$C$  = double layer capacity

$Z_F$  = Faradic impedance

III.2.2. Corrosion resistance evaluation of the different coatings : Using the suitable interface model of fig. 17, values of its individual components at different immersion times have been determined for the different coatings. In table III are reported the values of  $R_E^i$ ,  $C_p$  as well as  $R_p$  which corresponds to the intercept on the real axis of the lower frequency limit of the impedance. It can be observed that whatever the type of surface treatment, when immersion time in the aggressive medium increases  $R_E^i$  decreases, whereas  $C_p$  slightly increases : this corresponds to the degradation of the coating. In addition,  $R_p$  varies roughly in the same manner as  $R_E^i$ . For long immersion times, it appears that the treatment of the metal before painting is, in all cases, favourable to corrosion resistance. The better protection afforded, for short immersion times, by the paint directly applied on the metal can be assigned to the fact that the paint layer is generally thicker in this case than that applied on the treated surface.

Finally, from a mechanistic point of view, the following points may be emphasized i) we have never observed - even for short immersion times - a purely capacitive behaviour of the interface which would be characteristic of an intact coating covering the whole surface, ii) the coated metal dissolution occurs as on the bare steel but over a greatly reduced active surface.

| Immersion time in the aggressive medium (hours) | Bare steel + paint          |  |  | Zinc phosphatation + paint  |  |  | Zinc phosphatation + $H_2O_2$ post-treatment + paint |  |  | Zinc phosphatation + $ZnO_2$ 7.5 $H_2O_2$ post-treatment + paint |  |  |
|---|-----------------------------|--|--|-----------------------------|--|--|--|--|--|--|--|--|
|   | $R_p^1$ ( $\mu\text{m}^2$ ) | $C_p^1$ ( $\mu\text{F}\cdot\text{cm}^{-2}$ ) | $R_p^2$ ( $\text{K}\Omega\cdot\text{cm}^2$ ) | $R_p^1$ ( $\mu\text{m}^2$ ) | $C_p^1$ ( $\mu\text{F}\cdot\text{cm}^{-2}$ ) | $R_p^2$ ( $\text{K}\Omega\cdot\text{cm}^2$ ) | $R_p^1$ ( $\mu\text{m}^2$ )                          | $C_p^1$ ( $\mu\text{F}\cdot\text{cm}^{-2}$ ) | $R_p^2$ ( $\text{K}\Omega\cdot\text{cm}^2$ ) | $R_p^1$ ( $\mu\text{m}^2$ )                                      | $C_p^1$ ( $\mu\text{F}\cdot\text{cm}^{-2}$ ) | $R_p^2$ ( $\text{K}\Omega\cdot\text{cm}^2$ ) |
| 0.5   | 4500 ± 500                  | 0.3 ± 0.1                                    | 240 ± 20                                     | 2000 ± 300                  | 1.15 ± 0.3                                   | 48 ± 5                                       | 8000 ± 600   | 0.40 ± 0.1                                   | 45 ± 5                                       | 950 ± 150  | 1.7 ± 0.5                                    | 63 ± 8                                       |
| 3   | 3800 ± 400                  | 1.25 ± 0.3                                   | 45 ± 5                                       | 200 ± 30                    |  | 20 ± 3                                       | 1000 ± 150   | 0.30 ± 0.1                                   | 50 ± 5                                       | 400 ± 100  |  | 55 ± 5                                       |
| 8   | 2500 ± 300                  | 1.0 ± 0.3                                    | 38 ± 5                                       | 150 ± 20                    |  | 20 ± 3                                       | 750 ± 150  |  | 78 ± 8                                       | 210 ± 30   |  | 33 ± 5                                       |
| 16  | 2000 ± 200                  | 1.25 ± 0.3                                   | 28 ± 3                                       | 135 ± 20                    |  | 22 ± 3                                       | 600 ± 100  |  | 70 ± 8                                       | 200 ± 30   |  | 37 ± 5                                       |
| 31  | 1300 ± 150                  | 1.72 ± 0.3                                   | 26 ± 3                                       | 120 ± 15                    |  | 20 ± 3                                       | 550 ± 100  |  | 77 ± 8                                       | 140 ± 20   |  |  |
| 49  | 38 ± 4                      |  | 10 ± 2                                       | 115 ± 15                    |  | 17 ± 3                                       | 2300 ± 300   | 1.1 ± 0.3                                    | 50 ± 5                                       | 160 ± 20   |  | 30 ± 5                                       |
| 72  | 30 ± 5                      |  | 7.5 ± 1                                      | 115 ± 15                    |  | 12 ± 2                                       | 4000 ± 500   | 1.15 ± 0.3                                   | 44 ± 5                                       | 220 ± 30   |  | 24 ± 5                                       |
| 97  | 20 ± 5                      |  | 2.4 ± 0.5                                    | 110 ± 15                    |  | 17 ± 3                                       | 2400 ± 300   | 1.4 ± 0.3                                    | 54 ± 5                                       | 210 ± 30   |  | 20 ± 4                                       |
| 121   | 20 ± 5                      |  | 2.4 ± 0.5                                    | 95 ± 15                     |  | 18 ± 3                                       | 1600 ± 200   | 1.4 ± 0.3                                    | 28 ± 3                                       | 200 ± 30   |  | 19 ± 3                                       |
| 147   | 20 ± 5                      |  | 1.8 ± 0.3                                    | 100 ± 15                    |  | 17 ± 3                                       | 1250 ± 150   | 1.3 ± 0.3                                    | 28 ± 3                                       | 280 ± 50   |  | 15 ± 3                                       |

TABLE III - Corrosion resistance, as a function of immersion time, of the variously treated and painted steels.

#### REFERENCES

- (1) D.D. MacDONALD, B.C. SYRETT and S.S. WING, Corrosion 34, 289 (1978) ; *ibid* 35, 367 (1979).
- (2) J.P. HOARE in "Advances in Electrochemistry and Electrochemical Engineering" Editors P. DELAHAYE and C.W. TOBIAS Interscience, New York p. 201 (1971).
- (3) R.D. AMSTRONG and A.C. COATES, J. Electroanal. Chem. 50, 303 (1974).
- (4) K.G. BOTO and L.F.G. WILLIAMS, J. Electrochem. Soc. 124, 656 (1977).
- (5) C. GABRIELLI and M. KEDDAM, Electrochim. Acta 19, 355 (1974).
- (6) F. MORAN, S. ROCHER, J. DURAND, L. COT, M. DUPRAT et F. DABOSI, French Pat. n° 82-09426.
- (7) F. MORAN, U.S. Pat. 4, 276, 089 Jun. 30, 1981.
- (8) J.L. PAYEN, University Thesis, MONTPELLIER (1978).
- (9) M. DUPRAT, N. BUI et F. DABOSI, J. Appl. Electrochem. 8, 455 (1978).
- (10) V.G. LEVICH "Physicochemical Hydrodynamics" Prentice Hall, Englewood Cliffs, New Jersey (1962).
- (11) B.E. CONWAY "Electrochimica Data "Elsevier Publishing Company AMSTERDAM (1952).
- (12) M. DELAMARE, I. MINH CHAU PHAM, P.C. LACAZE and J.E. DUBOIS, J. Electroanal. Chem. 108, 1 (1980).
- (13) F. SCHELLER, S. MULLER and R. LANDSBERG, *ibid* 19, 187 (1968).
- (14) E. LEVART, D. SCHUHMANN, O. CONTAMIN and M. ETHAN, *ibid*, 70, 117 (1976).
- (15) H. TAMURA, K. GOTO and M. NAGAYAMA, Corr. Sci. 16, 197 (1976).

- (16) C. DESLOUIS, I. EPELBOIN, M. KEDDAM et J.C. LESTRADE, *J. Electroanal. Chem.* 28, 57 (1970).
- (17) S.H. GLARUM and J.H. MARSHALL, *J. Electrochem. Soc.* 126, 424 (1976).
- (18) J.P. CANDY, P. FOUILLOUX, M. KEDDAM and H. TAKENOUTI, *Electrochim. Acta* 28, 1029 (1981).
- (19) M. STERN and A.L. GEARY, *J. Electrochem. Soc.* 104, 56 (1957).
- (20) I. EPELBOIN, M. KEDDAM and H. TAKENOUTI, *J. Appl. Electrochem.* 2, 71 (1972).
- (21) M. DUPRAT, N. BUI and F. DABOSI, *Corrosion* 35, 392 (1979).
- (22) M. DUPRAT and F. DABOSI, *ibid* 37, 89 (1981).
- (23) M. DUPRAT, F. DABOSI, F. MORAN and S. ROCHER *ibid* 37, 262 (1981).
- (24) A. BONNEL, Thèse de Docteur-Ingénieur, TOULOUSE (1981).
- (25) M. DUPRAT, A. BONNEL, F. DABOSI, J. DURAND et L. COT, *J. Appl. Electrochem.* 13, 317 (1983).
- (26) A. MARSHALL, *Corrosion*, 37, 214 (1981).
- (27) F. MANSFELD, M.W. KENDIG and S. TSAI, *Corr. Sci.* 22, 455 (1982).
- (28) J.J. ROBIN, J. DURAND, L. COT, A. BONNEL, M. DUPRAT et F. DABOSI, *J. Appl. Electrochem.* 12, 701 (1982).
- (29) R.W. ZURILLA and V. HOSPARADUK, Paper n° 780187 National S.A.E. Meeting. DETROIT (1978).
- (30) I. EPELBOIN, M. KEDDAM and H. TAKENOUTI, Extended Abstract 144<sup>th</sup> Meeting Electrochem. Soc. p. 168 and 181 BOSTON (1973).
- (31) L. BEAUNIER, I. EPELBOIN, J.C. LESTRADE et H. TAKENOUTI, *Surf. Technol.* 4, 237 (1976).
- (32) G. REINHARD and K. HAHN, *Neue Hütte* 24, 299 (1979).
- (33) G. WALTER, *J. Electroanal. Chem.* 118, 259 (1981).
- (34) F. MANSFELD, M.W. KENDIG and S. TSAT, Extended Abstracts 160<sup>th</sup> Meeting Electrochem. Soc. p. 373 and 376 DENVER (1981).
- (35) J. HUBRECHT, M. PIENS and J. VERECKEN, *ibid* p. 369.
- (36) J.D. SCANTLEBURY, K.N. HO and D.A. EDEN in "Electrochemical Corrosion Testing" Ed. F. MANSFELD and U. BERTOCCI, ASTM STP 727 p. 187 (1981).

INTERACTION BETWEEN BIOFOULING AND OXYGEN REDUCTION RATE  
ON STAINLESS STEEL IN SEA WATER

Mollica, A.-Trevis, A.-Traverso, E.-Ventura, G.-  
Scotto, V.-Alabiso, G.-Marcenaro, G.-Montini, U.  
De Carolis, G.-Dellepiane, R.

Istituto per la Corrosione Marina dei Metalli  
Consiglio Nazionale delle Ricerche.

Via della Mercanzia 4 - 16123 Genova-Italy

SUMMARY - Field tests on stainless steel pipe specimens exposed to natural sea water flowing at a rate of 1.1 and 2.2 m/s at a temperature in the range of 24 to 36°C were made to study at the same time the behaviour of these stainless steels and of the slime developed on these steels. Slime formation was assessed by thickness measures, by analysis of the organic and inorganic content, ETS activity and Chl a content. Steel behaviour was observed by free corrosion potential measures, by determining the weight loss and galvanic currents between a stainless steel and a sacrificial anode. It was found that bacterial settlements increase the oxygen reduction rate which, in turn, stimulates the corrosion of stainless steel in sea water.

RESUME - Le comportement des aciers inoxydables et la formation de biosalissures sur leur surfaces ont été étudiés au cours des essais pratiques effectués sur des aciers inoxydables exposés à l'eau de mer s'écoulant à une vitesse de 1,1 et 2,2 m/s et à une température ambiante dans le domaine de 24 à 36°C. La composition du film microbien a été évalué moyennant des mesures d'épaisseur, des teneurs en substances organiques et inorganiques, de l'activité ETS et de la teneur en Chl a. Le comportement des aciers a été observé en mesurant le potentiel de libre corrosion, les pertes de poids et les courants galvaniques entre un acier inoxydable et un anode sacrificielle.

## BIOFOULING AND OXYGEN REDUCTION RATE

On a ainsi pu démontrer que la formation des films microbien augmente la vitesse de réduction d'oxygène et que cette augmentation stimule la corrosion de l'acier inoxydable dans l'eau de mer naturelle.

### INTRODUCTION

In our previous paper(1), we observed an increased oxygen reduction rate on stainless steel surfaces when they were covered by slime during their immersion in flowing natural sea water. We also brought evidence that this increase may corroborate the observations made by several authors(2,3,4) according to which the corrosivity of natural sea water is greater than that of sterile sea water, as far as stainless steel is concerned.

In this paper, we want to explain more in detail the correlation existing between the modified oxygen reduction rate and slime composition and to verify the consequences of this alteration on stainless steel corrosion.

The data reported in this paper are part of a research work financed by ANSALDO IMPIANTI(Genoa,Italy) to assess the reliability of recently formulated stainless steels when used to manufacture sea water cooled condenser tube nests.

### METHODOLOGY

The test equipment used for this purpose is illustrated in fig.1.

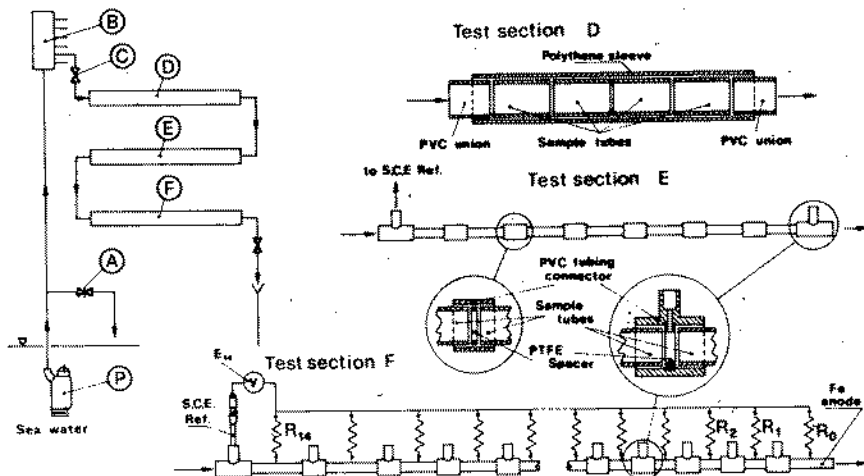


Fig.1 - General layout of the test apparatus.



## BIOFOULING AND OXYGEN REDUCTION RATE

A submersible pump P is pumping the sea water and, after elimination of the excess water by means of the by-pass A, this water is conveyed to a distribution tank B, from which ducts, all similar to the one illustrated schematically in the figure, are branched off. The flow rate in each duct is adjusted by the cock C and the water thus enters stainless steel pipes each having an I/D of 24 mm and arranged in series inside the test sections D, E and F.

The section D is grouping a set of test specimens on which to assess slime formation; the section E is used to determine the stainless steel crevice corrosion resistance, whereas the section F is dedicated to an evaluation of the galvanic currents circulating between the stainless steel pipe and the sacrificial anode. This test apparatus was used for two test series each lasting 92 days.

The sea water was pumped from the tailrace of a Power Plant cooling system located inside the Port of Genoa.

A proper selection of the starting dates made it possible to make these tests in two different temperature ranges ( $24^{\circ}\leq T\leq 32^{\circ}\text{C}$  and  $31^{\circ}\leq T\leq 36^{\circ}\text{C}$ ) in the course of one year.

Furthermore, each test series had the aim to study the effect of the two different flow rates (1.1 and 2.2 m/s) on the parameters under consideration. Since the flow in each duct was affected by variations friction coefficient generated by slime formation, the opening of the cocks C had to be periodically adjusted.

Finally, the actual flow rate values were ranging between 0.9 and 1.2 m/s and between 1.9 and 2.2 m/s.

### Slime evaluation

The 5 cm long specimens placed inside test section D were periodically removed to assess the evolution and composition of slime by means of the following measures:

- wet weight of the settlement obtained after letting the specimen drip for a few minutes;
- weight of the slime after drying for 1 hour at  $100^{\circ}\text{C}$  to eliminate imbibition water, weight after drying for one hour at  $420^{\circ}\text{C}$  to remove the organic fraction, and weight of the slime after 1 hour holding time at  $900^{\circ}\text{C}$  to eliminate chlorides;
- respiratory ETS (Electron Transport System) activity to determine the maximum respiratory capacity of the settled biomass (5) after having removed the slime by sonization of the specimen in phosphate buffer.
- Chlorophyll a (Chl a) content by spectrophotometry (6) in anhydrous methanol.

### Crevice Corrosion Resistance

The crevice on the 10 cm long specimens fitted into test

## BIOFOULING AND OXYGEN REDUCTION RATE

section E was obtained by a polythene tube watertight pressed on the outer surface of the test specimen. The crevice corrosion resistance of each specimen was assessed as follows:

- by periodical free corrosion potential measures during exposure;
- by weight loss determination and visual inspection at the end of exposure.

Galvanic currents

In each duct, a stainless steel tube having a "formal" length of 1.2 m (test section F) was consisting of 14 test specimens of various length  $l_n$  ( $1 \leq n \leq 14$ ). Each specimen was connected to a zero resistance conductor by means of resistors  $R_n$  ( $1 \leq n \leq 14$ ) equal to 10 Ohm.

This conductor was connected to a tubular iron anode by means of a resistor  $R_0$ . This assembly permitted to evaluate not only the total galvanic current  $I_0$  and the mixed potential  $E_0$ , but also the output current values  $I_n$  from the various specimens and the distribution of the potentials  $E_n$  along the pipe. The data thus obtained permitted to plot the cathodic oxygen reduction curve pointwise on the stainless steel surface, by means of the values:

$$\left( \frac{I_n}{2\pi r l_n}; \frac{E_{n-1} + E_n}{2} \pm \frac{E_n - E_{n-1}}{2} \right)$$

## RESULTS AND DISCUSSION

Slime formation rate

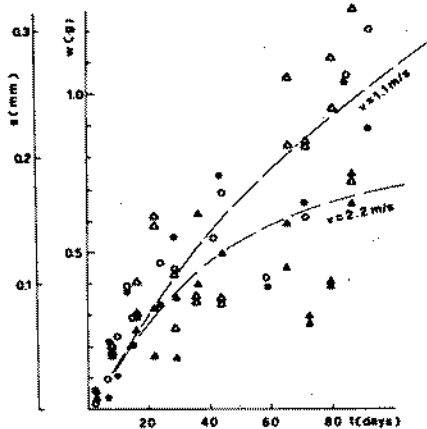
The wet slime weights  $w$  for all test conditions are reported in fig.2 as a function of time.

After drying, the weight is reduced by more than 30% thus indicating that the slime is essentially consisting in a stagnant water film entrapped in a matrix of organic and inorganic matter.

By approximation and assuming the slime mass totally made up of water, we can translate the wet weight into average thickness values  $s$  (second ordinate in the figure) and conclude that the slime thickness increases with time to reach an average value of about 300  $\mu\text{m}$  after three months, at a flow rate of 1.1 m/s and a thickness of 200  $\mu\text{m}$  at a flow rate of 2.2 m/s.

The percentage of organic matter in the dry residue is shown in fig.3. This graph also shows that the organic fraction is prevailing in initial settlement phases then to remain at about 40% when exposure time increases.

## BIOFOULING AND OXYGEN REDUCTION RATE



○ v=1.1 m/s, ● v=2.2 m/s,  $24^{\circ} \leq T \leq 32^{\circ} \text{C}$   
 △ v=1.1 m/s, ▲ v=2.2 m/s,  $31^{\circ} \leq T \leq 36^{\circ} \text{C}$

Fig.2 - Wet weight and slime thickness vs time.

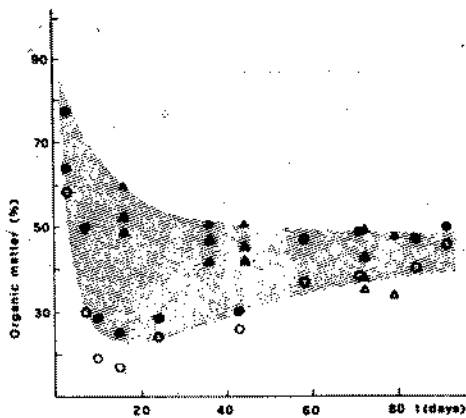
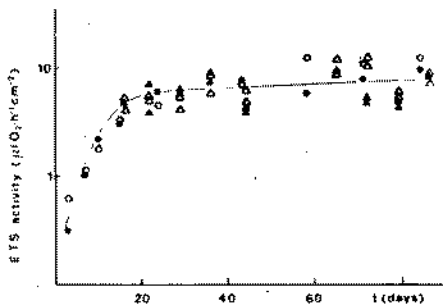


Fig.3 - Organic matter content in the dry residue vs time.

Respiratory ETS activity is plotted against time in fig.4. According to these data, colonization of the surface achieved in about 15 days in all test conditions and the number of micro-organisms doesn't differ much from the quantity measured at the end of the test period. Finally, fig.5 shows the ETS and Chl a values measured in specimens sampled at the same time. The straight line, indicated by Packard (7),  $\text{ETS} = 3.28 \text{ Chl a}$  representing a phytoplankton dominated ecosystem is also plotted in this graph.



○ v=1.1 m/s, ● v=2.2 m/s,  $24^{\circ} \leq T \leq 32^{\circ} \text{C}$   
 △ v=1.1 m/s, ▲ v=2.2 m/s,  $31^{\circ} \leq T \leq 36^{\circ} \text{C}$

Fig.4 - ETS activity vs time.

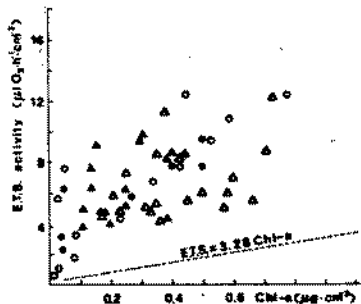


Fig.5 - Relationship between ETS activity and Chl a.

## BIOFOULING AND OXYGEN REDUCTION RATE

The same relationship was also proved on algal dominated microfouling in a preparatory study (8). The position of our data as compared with this straight line, shows that our microfouling is potentially more oxygen consuming than producing; with respect to a prevailingly algal population. The data here submitted together with the observations from other Authors (9,10) who studied such settlements in conditions similar to ours, can be summarized as follows:

- a bacterial settlement occurs on the stainless steel walls; these bacteria reach their maximum viability after two weeks exposure;
- a growing amount of inorganic matter then progressively is entrapped on the slimy mucilage;
- the slime mass increases with the length of exposure time.

### Oxygen reduction kinetics on stainless steel surfaces

Fig. 6a shows the trend of the galvanic currents circulating between a stainless steel tube (20Cr18Ni6Mo) and an iron anode measured by the potential drop on the resistor  $R_0$  set at 10 Ohm (fig. 1) during the test performed in the range of 24° to 32°C. These trends show that galvanic currents, irrespective of the flow rate, are starting from 0.5 mA to increase, in about two weeks, by one order of magnitude, then to settle down, as the test continues, at a value of 5÷6 mA. This means that the trend of  $I_g$  at a given time interval follows the trend of ETS rather than that of the biomass, thus suggesting a close correlation between

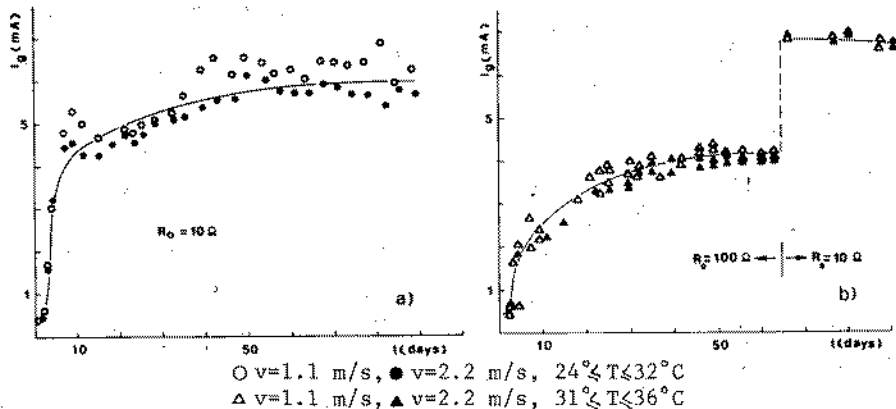


Fig. 6a, b - Galvanic currents vs time between a stainless steel pipe ( $I/D=24 \text{ mm}, l=1.2 \text{ m}$ ) and an iron anode.

## BIOFOULING AND OXYGEN REDUCTION RATE

the development of bacterial settlements and alteration of the oxygen reduction kinetics on stainless steel from which the amount of galvanic currents finally depends. The trend of galvanic currents observed during the test at  $31 \leq T \leq 36^\circ\text{C}$  (fig.6b) is absolutely similar. The presence of slime on the steel surface is an essential prerequisite for modification of the oxygen reduction kinetics. This can also be observed in fig.7a, in which the galvanic currents are plotted vs time, measured on the test specimens on which the slime was repeatedly removed during the last 20 days of test by two manual cleaning systems.

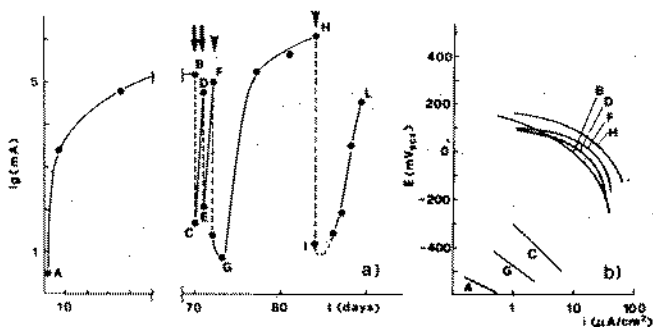


Fig.7a,b - Effect of cleaning with a nylon brush, either followed (↓) or not (∇) by flushing with ethyl alcohol on the galvanic current (a) and on oxygen reduction kinetics (b).  
 $v = 1.1 \text{ m/s}$ ,  $24 \leq T \leq 32^\circ\text{C}$ .

In the first case, nylon brushes of a slightly larger size than the pipes ( phases BC and DE ) were used for slime removal, while in the second, nylon brushes and cotton wool wads soaked in ethyl alcohol ( phases FG and HI ) were used for cleaning. The first cleaning system was adopted without interrupting the flow inside the duct, while in the second case, the flow was interrupted for about 5 minutes.

The graph shows that;

- galvanic currents suddenly drop by almost one order of magnitude when the slime is removed;
- the greater the accuracy in cleaning, the smaller will be bacterial residues settled on the steel surface and the more time will be required for galvanic currents to reach once more their steady state value.

Fig.7b shows the calculated oxygen reduction current density as a function of the potential according to the methodology described in previous pages, during various slime development phases. These graphs show that the oxygen reduction curve can start from type A, G, C levels on clean,

## BIOFOULING AND OXYGEN REDUCTION RATE

or recleaned steels, up to type B, D, F, H levels on bacteria colonized or recolonized surfaces. Bacterial settlements thus set a mechanism in motion speeding up the oxygen reduction rate up to cathodic current values of  $10 \mu\text{A}/\text{cm}^2$  already at potentials ranging between 0 and 100 mV(SCE). For completion of the information hitherto gathered on the correlation existing between slime and cathodic current modifications, the trend of galvanic currents measured in a special test is plotted in fig.8a.

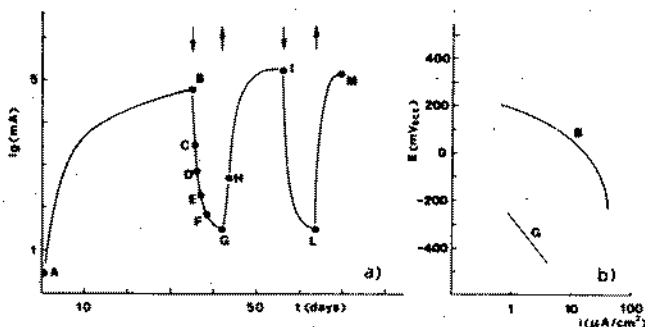


Fig.8a,b - Effect of disconnection ( $\downarrow$ ) and reconnection ( $\uparrow$ ) of the anode on galvanic current (a) and on the cathodic current density (b).  
 $v=1.1 \text{ m/s}$  ,  $24^\circ\text{T} \leq 32^\circ\text{C}$ .

The slime was left to develop freely on the steel surface for 35 days on end in flowing water before the stainless steel tube was disconnected from the iron anode. Connection was restored after one day and after 10 minutes the usual current and potential values were measured along the pipe. The connection was then once more interrupted. This procedure was repeated for 5 days on end. The CDE curve shows the decay of the galvanic currents as time goes by, due to these operations. The EFG curve shows that galvanic current values increase when the steel pipe and iron anode are once more permanently connected. The oxygen reduction curves calculated during the various test phases are shown in fig.8b. From the mass of these data it can be inferred that, even in the presence of slime, the oxygen reduction kinetics and, hence, the galvanic current value may fluctuate between two extreme levels that are similar to the levels plotted in fig.7. The presence of slime on the stainless steel surface is therefore an essential factor for alteration of the oxygen reduction curve although it is insufficient to determine the instantaneous trend of this curve which is also effected by the "history" of the test specimen before

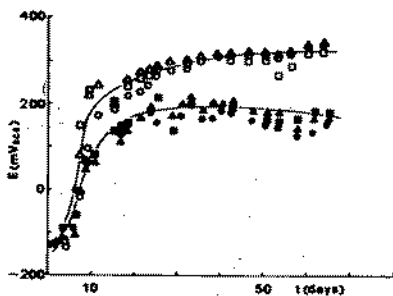
## BIOFOULING AND OXYGEN REDUCTION RATE

measuring. The interpretation of this phenomenon will be studied at a later stage; for the moment we want to highlight the fact that as soon as the connection between the slime covered stainless steel tube and the iron anode is re-established, galvanic currents will return to their maximum value within a few days. However, the findings of this particular test are only valid for a short transient period and are therefore of little importance for the determination of bimetal couple behaviour in long-term tests.

### How is the modified oxygen reduction kinetics affecting the corrosion resistance of stainless steels.

For simplification purposes, we'll first highlight how the modified oxygen reduction kinetics, caused by bacterial settlements, is affecting the behaviour of both passive and active steel specimens.

The typical behaviour of passive test specimen determined by measuring the free corrosion potential, is illustrated in fig.9. These data refer to a 20Cr18Ni6Mo steel chosen from the test specimen not showing any localized corrosion at the end of the test cycle. The figure only shows the potential values of sea water exposed test specimens at a flow rate of about 1.1 m/s, but the values obtained from specimens exposed at a flow rate of 2.2 m/s are virtually identical.



○△○▽=1.1 m/s, 24° ≤ T ≤ 32°C  
●▲■▽=1.1 m/s, 31° ≤ T ≤ 36°C

Fig.9 - Free corrosion potentials of passive test specimens vs time.

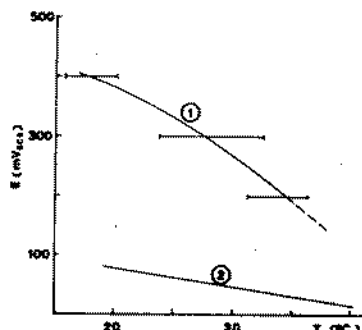


Fig.10 - Corrosion potential vs temperature of passive specimens in natural sea water (1) and in 3% NaCl (2).

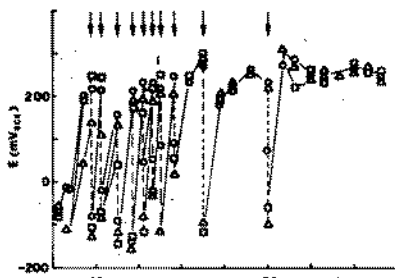
It can be observed that free corrosion potentials are fast ennobled during the first two weeks of exposure still coinciding with the bacterial settlement development phase. The values reached by these potentials after stabilisation of the settlement will depend on the sea water tempera

## BIOFOULING AND OXYGEN REDUCTION RATE

ture. The graph in fig.10 was plotted by integrating these values with those of previous tests(1,11) showing how the temperature is affecting the corrosion potential values measured on slime covered passive test specimen.

The same graph also shows the free corrosion potential values measured on a passivated steel type immersed in a 3% Na Cl solution. Their comparison shows that the presence of slime has a strong effect at ambient temperature and that the difference between natural and artificial sea water tends to vanish, in agreement with LaQue(4) when the temperature rises towards 50°C.

The influence of slime on corrosion potential values is further demonstrated in fig.11. This graph shows the strongly decreasing potential value when the slime is removed with a nylon brush ( $\Delta V=300\pm 400$  mV in the temperature range  $24^\circ \leq T \leq 32^\circ \text{C}$ ). The high free corrosion potential levels



O Δ □ v=1.1 m/s,  $24^\circ \leq T \leq 32^\circ \text{C}$

Fig.11 - Effect of slime removal( $\downarrow$ ) by manual cleaning on the corrosion potential of passive stainless steels.

of steel reached in natural sea water at near to ambient temperature values may contribute to explain the increased initiation probability of localized corrosion as compared with the synthetic sea water(3,4).

The effect of slime on localized corrosion growth rate is shown in the graphs of the figures 12 and 13. The  $E_{corr}$ -t curves plotted in fig. 12 show the behaviour of 4 out of 8 21Cr2.5Mo steel specimens exposed in natural sea water, with pre-formed crevice, for 92 days. All specimens resulted corroded at the end of this test.

The sudden drop of the corrosion potential, observed in almost all test specimens after about 20 days, indicates the initiation of crevice corrosion.

During the propagation stage, the potential tends to reach a steady state at about +100 mV(SCE). The average weight loss of the test specimens was  $1.6 \pm 0.5$  g.

Another set of 8 test specimens of the same steel type, exposed in the same test conditions, was repeatedly cleaned and the slime was removed with a nylon brush during the first 50 days of the test period. At the end of experience 6 specimens were corroded. The trend of the free corrosion potential of 4 out of 8 samples is shown in fig.13. In this case, the decrease of the potential due to removal of the slime, is partly overlapping and masking the decrease caused by crevice corrosion initiation, so making diffi-



## BIOFOULING AND OXYGEN REDUCTION RATE

cult to define the incubation time of the attack.

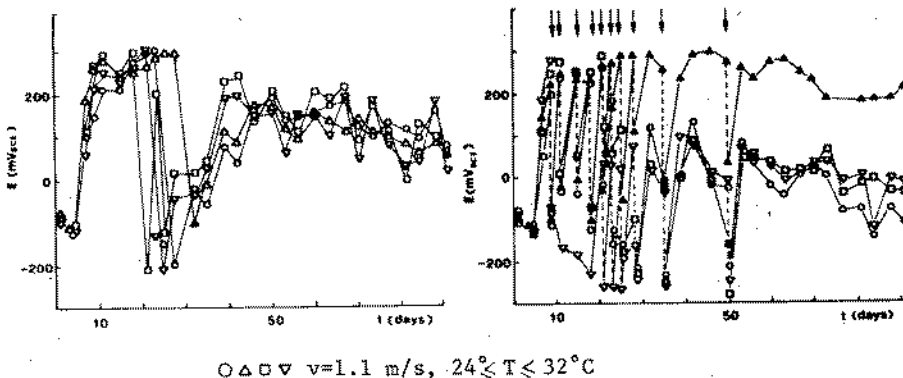


Fig.12 - Trend of the potential on 4 of 21Cr2.5Mo specimens in free corrosion. All specimens were corroded.

Fig.13 - Effect of repeated slime removal(↓) on free corrosion potential of 4 21Cr2.5Mo specimens.  
▲ uncorroded, ○△□ corroded

It should, however, be noted that the specimens that resulted corroded at the end of the test maintained their potential at less noble levels than the uncorroded specimens from the first month of their exposure. This leads us to assume that corrosion was initiated within this period. The potential of the corroded specimens, which has a value ranging between -200 and -250 mV (SCE) immediately after cleaning, rises to  $-100 \pm 0$  mV (SCE) when the cathodic surface of the steel is left undisturbed for the remaining 40 days of the test period and is then once more colonised with bacteria. The average weight loss of these specimens was found to be  $0.6 \pm 0.3$  g.

We can therefore conclude that frequent slime removal from cathodic areas during the first 50 days of the 92 day test period, not only slightly decreases initiation probability, but also reduces by half the average weight loss. The effect of the presence and absence of slime on the overall behaviour of stainless steels will be more easily understood with the help of the scheme in fig.14 in which two cathodic curves B and C are plotted.

The first of these curves refers to a cathodic surface with settlement and the second to a cleaned cathodic surface as already seen in fig.7. The same figure also shows two anodic curves, the first of which (1) describes a steel in passive conditions with passivity currents estimated at  $10^{-7}$  A/cm<sup>2</sup>, while curve (2) represents a steel in active conditions.

## BIOFOULING AND OXYGEN REDUCTION RATE

The cross potential between the latter curve and the two cathodic curves are fixed taking the results reported in fig.13 into account. The sharp decrease of the corrosion potential in the test specimen in passive state can be immediately observed together with the lowering by about two orders of magnitude of the corrosion currents in an active specimen after cleaning of its cathodic surfaces. On this subject, it should be noted that this graph was plotted with the implicit assumption that a cathodic area of  $1 \text{ cm}^2$  is available outside the anodic area. This reasoning can be repeated with similar conclusions also for a generic cathodic area.

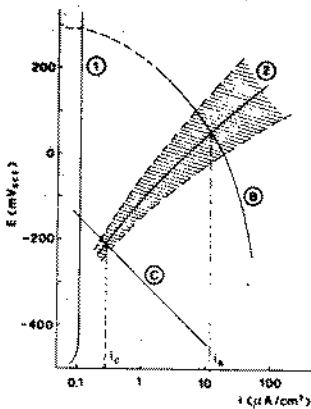


Fig.14 - Schematic outline of how the presence or absence of slime is affecting the behaviour of stainless steels:

- ⓑ cathodic current in presence of slime
- ⓒ cathodic current in absence of slime
- ① anodic current in passivity conditions
- ② anodic current in activity conditions

## CONCLUSIONS

The inner surfaces of stainless steel tubes subjected to once through natural sea water at the rate of 1.1 and 2.2 m/s at temperature ranging between  $24^\circ$  and  $36^\circ\text{C}$ , were covered with slime reaching stationary conditions after two weeks of exposure. The development of bacterial settlement is coinciding with a strong increase of the oxygen reduction rate on the stainless steel surfaces.

The practical consequences of this phenomenon can be synthesized as follows :

- increased corrosion rate of sacrificial anodes connected to the steel surface. In particular, when coupling a stainless tube to an iron anode, the corrosion rate of the sacrificial anodes was found to increase by one order of magnitude ( from 0.5 mA measured on a clean tube to 6 mA measured on a slime covered tube ) ;
- greater probability of localized corrosion initiation, due to strong ennobling of the free corrosion potential induced on specimens in passivity conditions.

The potential increase observed in the temperature ran

## BIOFOULING AND OXYGEN REDUCTION RATE

- ge taken into examination was about 300 mV;
- increase of the localized corrosion rate up to about two orders of magnitude.

The continuous removal of the slime from the stainless steel surfaces exposed in natural sea water was found to be efficient as an anticorrosion measure through a mechanism which can be somehow compared with the cathodic inhibition mechanism.

## REFERENCES

1. Mollica, A.; Trevis, A.: Proc. 4th Int. Congr. on Marine Corrosion and Fouling, Juan-Les-Pins, 1976, 351.
2. Compton, K.G.: Corros., 1970, 26, 448.
3. Lagutina, A.G.; Danilchenko-Shevchenko, O.F.; Barannik, V.P.: Zashchita Metallov, 1970, 6, 1, 48.
4. LaQue, F.L.: Mater. Perform., 1982, april, 13.
5. Owens, T.G.; King, F.D.: Mar. Biol., 1975, 30, 27.
6. Talling, J.F.; Driver, D.: Proc. Conf. of Primary Productivity Measurements, 1963, Hawaii TID, 7633, 142.
7. Packard, T.T.; Harmon, D.; Boucher, J.: Tethys, 6, (1-2), 1974, 213.
8. Alabiso, G.; Marcenaro, G.; Scotto, V.: Boll. Mus. Ist. Biol. Univ., Genova, 50 suppl. 1982, 91.
9. Tarbuck, L.A.; Wyborn, C.H.E.: Proc. Symp. Condens. Biofouling Control, 1979, Publ. 1980, Garey.
10. Pope, D.H.; Soracco, R.J.; Wilde, E.W.: Mater. Perform., 1982, July, 43.
11. Mollica, A. et al.: unpublished data.



The Influence of the Surface Treatment on Corrosion  
of CuNi10Fe1Mn Alloy in Artificial Sea Water.

K.DABROWIECKI, K.BORON

Technical University

ul. Smoluchowskiego 25  
50-372 Wrocław POLAND

Abstract.

The corrosion resistance of condenser tubes made of CuNi10Fe1Mn alloy, which have differently treated surfaces i.e. annealed under a protective gas atmosphere and chemically etched, was examined. It was found that, the CuNi10Fe1Mn alloy tubes annealed with no protective atmosphere, but etched in nitric acid characterize in a higher corrosion resistance than the tubes annealed with no protective gas.

CuNi10Fe1Mn alloy is commonly used for condenser tubes in heat exchangers exploited in sea water. Corrosion resistance of these tubes depends, in a considerable degree, on the technological conditions of their obtainment.

The purpose of this paper was to investigate the corrosion resistance, in artificial sea water, of the condenser tubes made of CuNi10Fe1Mn alloy of variously processed surface /applying the protective atmosphere during annealing, various methods of chemical surface etching/.

Experimental method.

The commercial condenser tubes of CuNi10Fe1Mn alloy were under investigations with the surface prepared in the following way:

1. Annealed without the protective atmosphere.  
Annealing was carried out at the temperature  $740 \pm 5^{\circ}\text{C}$ , for 45 min, with cooling in the air.

2. Annealed without the protective atmosphere and etched in sulphuric acid. The tubes were annealed as in the 1 manner, and then they were etched in sulphuric acid of 10% concentration, temperature 60°C for 15 min.
3. Annealed without the protective atmosphere and etched in nitric acid. The tubes were annealed as in the 1 manner, and then they were etched in concentrated nitric acid at room temperature for 30 sec.
4. Annealed under the protective argon atmosphere. Annealing was conducted at the temperature  $740 \pm 5^\circ\text{C}$  for 45 min. During annealing and cooling the kiln was filled with argon.

The artificial sea water of pH 8,2 [1] was used for the investigations. The corrosion rate was designated with the gravimetric measurements in stationary conditions and in the conditions imitating the flow of solution. The conditions imitating the flow of solution were achieved applying the method of a rotating cylinder. Linear speed of the sample surface in relation to the electrolyte was 2,5 m/s. Solutions during the measurements were aerated.

Potentiokinetic measurements of polarization were conducted in synthetic, aerated sea water at room temperature with the potential sweep rate 0,06 V/min.

Results of the investigations and discussion.

Morphology of tubes' surface.

The appearance of tubes' surface after having applied the manners of its preparation was presented in Fig. 1-4.

Surface of the tube annealed without the protective atmosphere was covered with a thick layer of oxidation products.

The surface film showed two types of the numerous cracks: tiny, arranged in an irregular network and considerably deeper, arranged according the direction of tube's drawing. The surface appearance of the tubes etched after annealing in sulphuric acid /the 2 manner/ shows, that the layer was dissolved during etching, was not, however, removed completely. Surface of the tube etched after annealing in nitric acid /the 3 manner/ was smooth and brilliant, that

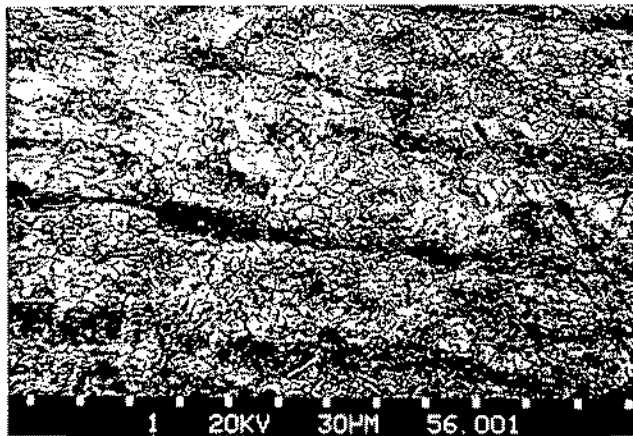


Fig.1. The surface of a tube of CuNi10Fe1Mn annealed without the protective atmosphere /according to the 1 manner/.

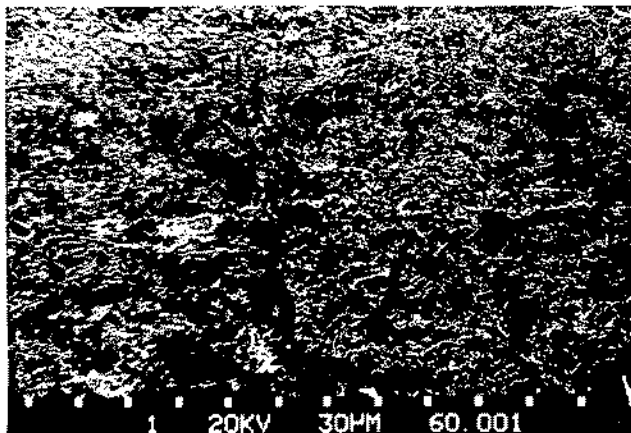


Fig.2. The surface of the tube of CuNi10Fe1Mn annealed without the protective atmosphere and etched in sulphuric acid /according to the 2 manner/.

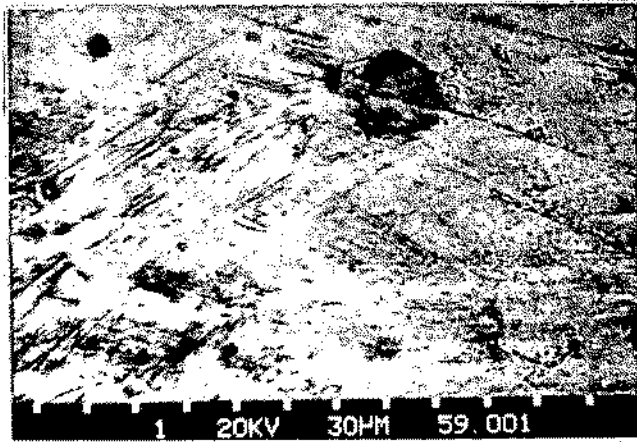


Fig.3. The surface of a tube of CuNi10Fe1Mn annealed without the protective atmosphere and etched in nitric acid /according to the 3 manner/.

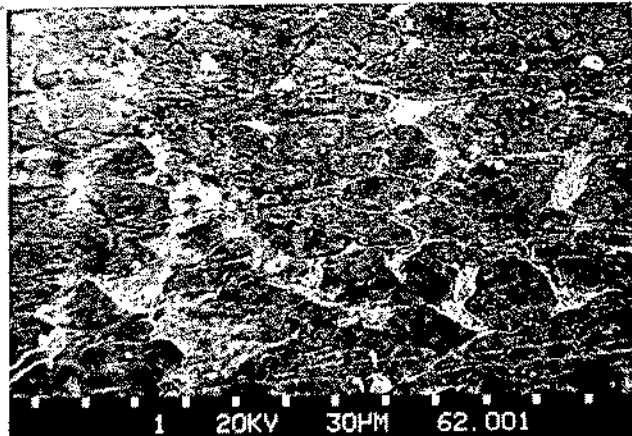


Fig.4. The surface of a tube of CuNi10Fe1Mn annealed in the argon atmosphere /the 4 manner/.

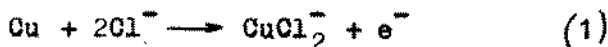


proves a total removal of the surface layers that were formed during annealing. Surface of the tube annealed in the argon atmosphere /the 4 manner/ was covered with a cracked layer, that did not form a continuous film.

#### Potentiokinetic polarization curves.

In the Fig.5 there were presented potentiokinetic polarization curves of CuNi10Fe1Mn alloy of surface processed according to the four presented manners and for the sake of comparison, potentiokinetic polarization curve of CuNi10Fe1Mn alloy of just cleaned with emery-paper No600 surface /the 5 manner/.

Anode polarization curves achieved for the mechanically cleaned surface of cupro-nickel /the 5 curve/ are similar. The run of anode polarization curve of CuNi10Fe1Mn alloy of surface prepared according to the 1 manner differs considerably from the remaining curves in lower current values and a wider passive area. The run of anode polarization curves shows that, the presence of oxide layers on CuNi10Fe1Mn alloy surface retards the anode reaction or hinders the transport of ions taking part in the anode process. The Tafel slopes of the anode reaction for CuNi10Fe1Mn alloy of surface prepared according to the 2 and 3 manners /resulting in 0,06 and 0.065 V respectively/ are very close to the Tafel slope for pure copper in chloride solutions /0,06 V according to [2] /. It points to the dominating anode reaction in Tafel region.



The values of Tafel slopes for CuNi10Fe1Mn alloy of surface prepared according to the 4,5, manners show that reaction (1) may be one of the anode reactions of alloy's dissolution.

Considerably higher values  $b = 0,09$  V for CuNi10Fe1Mn of surface prepared according to the 1 manner suggests, other mechanism of the anode process than for cupro-nickel of surface prepared according to the remaining manners.

Distinguishable on cathode curves border diffusion currents prove distinctly, that in the initial conditions, oxygen reduction is the dominant cathode reaction. Lack of border diffusion currents on cathode polarization curve of CuNi10Fe1Mn alloy

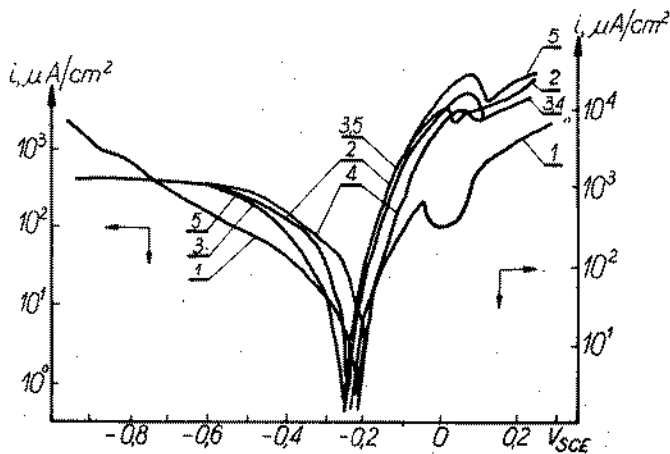
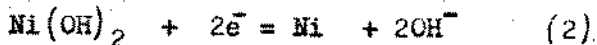


Fig.5. Potentiokinetic polarization curves of CuNi10Fe1Mn alloy in artificial sea water 1,2,3,4,- CuNi10Fe1Mn of the mentioned above manners of preparing the surface, 5-CuNi10Fe1Mn of just cleaned surface.

annealed without the protective atmosphere suggests appearance of the other cathode reaction than only oxygen reduction, one of the possible reactions is:



that in sea water of pH = 8,2 is possible with potential about -0,65 V [3].

Gravimetric investigations.

In the investigations samples were covered with a green-celadon layer. According to [4] it may contain  $\text{Cu}_2(\text{OH})_3\text{Cl}$ .

Corrosion rate designated during the investigations in the stationary and imitating flow of sea water conditions was presented. in Fig.6.

In the stationary conditions CuNi10Fe1Mn alloy annealed without the protective atmosphere, etched in nitric acid /the 3 manner/ shows considerably higher corrosion resistance than the alloy prepared according to the remaining manners. Corrosion resistance of the alloy prepared according to the 1,2,4 manner

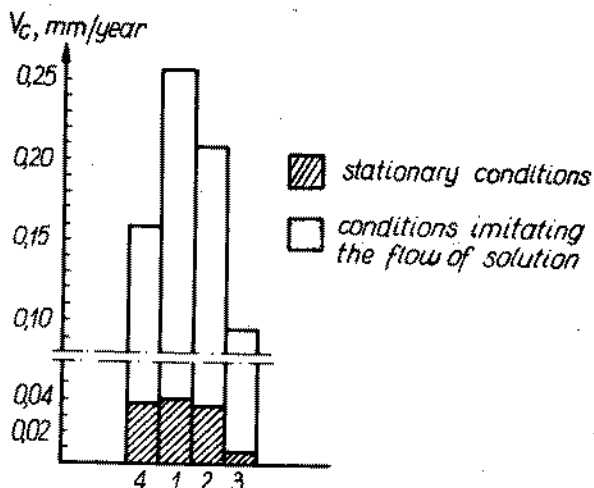
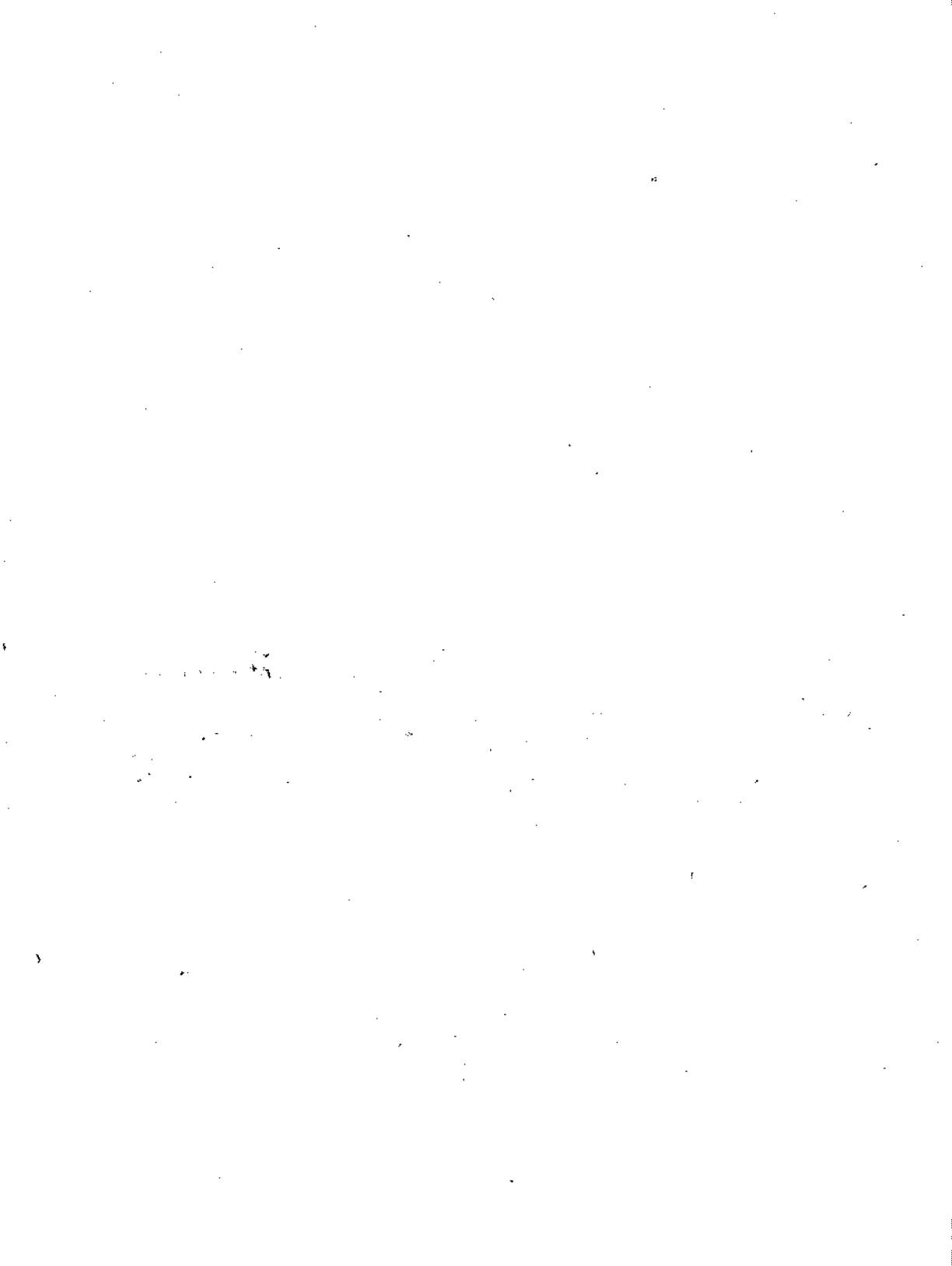


Fig.6. Corrosion rate designated in gravimetric measurements.

practically does not differ. Corrosion resistance in the conditions imitating flow is differentiated and depends on the manner of surface processing. The alloy of surface etched in nitric acid /the 3 manner/ shows the greatest corrosion resistance. Consequently diminishing corrosion resistance reveal the samples annealed in argon /the 4 manner/, etched in sulphuric acid /the 2 manner/ and annealed without the protective atmosphere /the 1 manner/.

#### REFERENCES

1. Polish Standard PN-66/C-06502
2. Kato C., Ateya B.G., Castle J.E., Pickering H., *J. Electrochem. Soc.*, 127, 1980, (1980).
3. Dobos D., *Electrochemical Data*, Akademiai, Kiado, Budapest.
4. Kato C., Castle J.E., Ateya B.G., Pickering H.W., *J. Electrochem. Soc.*, 127, 1897, (1980).



Corrosion Marine Resistance of Nitrided Steel

J. Jorba and P. Molera

Dept. Metal.lúrgia. Fac. Química.

Universitat de Barcelona.

Abstract.

The results of investigations into the effect of nitriding on the sea-water corrosion behaviour of F-1740 steel are presented and discussed. The electrochemical results have been correlated with observations of the surficial zone obtained by optical microscopy and SEM. The formed phases during nitriding processes has been identified by X-ray diffraction. The protector effect of nitriding may be imputed principally to the presence of a continuous layer formed into the surface during the treatment.

Résumé

Dans la présente communication se propose de décrire les résultats obtenus pour mettre en évidence l'influence de la nitruration dans la conduite de l'acier F-1740 à la corrosion par l'eau de mer. Les résultats électrochimiques ont des relations avec l'observation des zones superficielles par microscopie optique et microscopie électronique (SEM). Les phases, qu'ont été créés pendant la nitruration, elles ont été identifiées par diffraction de rayons-X. La bonne résistance a la corrosion de l'acier nitruré est attribué a la présence d'une couche continue sur la surface métallique.

## Introduction.

Nitriding is surface treatment method whereby nitrogen is introduced into the surface of a solid ferrous alloy in order to beneficially modify the surface-sensitive properties as surface hardness, fatigue, wear and sometimes corrosion. It has been reported (1-4), that, depending on the composition of the corrosive environment and alloy type, corrosion resistance of surface steels may be decreased or increased through nitriding.

The aim of the present investigation has been to gain information on the modification of corrosion behaviour in sea-water of aluminum-containing low-alloy steel treated in salt-bath, gas nitriding and ion nitriding processes by determining

- a) the potentiodynamic polarization curves in sea-water media and,
- b) the microstructure of the formed layer and the present phases in surficial zone.

## Experimental method.

The nominal composition of the type F-1740 steel used in the present work was: C, 0.35-0.40%; Si, 0.20-0.50%; Mn, 0.50-0.80%; P, less than 0.035%, S, less than 0.035%; Cr, 1.50-1.80% Mo, 0.25-0.40%; Al, 0.80-1.20%, Fe, balance.

The material was in form of 25 mm diameter rod and was water quenched from 900°C and tempered at 550°C to 46 Rc hardness. To produce tests specimens, the rod was skimmed down to 20 mm diameter and then cut into discs 8 mm thick. One face of each of these discs was then wet-ground down on No. 600 silicon carbide paper before nitriding. The nitriding conditions are given in Table I.

The present phases in the surficial zone were determined by X-ray diffraction directly applied on the nitrided surface, and optical and Scanning Electron Microscopy were used to examine the morphology of the nitrided zone after conventional metallographic preparation and Nital 2% attack.

The effect of nitriding on the corrosion behaviour of the F-1740 steel was investigated using the potentiodynamic polarization technique at room temperature. Rigid and insulated connections were secured into back faces of specimens and a circular area of 10 mm diameter was exposed at aqueous media. The corrosion studies were carried out in air-saturated sea-water with 52 mS conductivity and air-saturated solution with 50 mS conductivity formed with 26.514 g Sodium Chloride; 2.247 g Magnesium Chloride; 3.305 g Magnesium Sulphate; 1.141 g Calcium Chloride; 0.725 g Potassium Chloride; 0.202 g Sodium Bicarbonate and 0.083 g Sodium Bromide.

Table I. Treatment conditions.

| Treatment           | Media  | Time       | Temp.          | Pressure         | Gas flow                 |
|---------------------|--|------------|----------------|------------------|--------------------------|
| Salt-bath           | 3% cyanate<br>22% cyanide  | 4 h        | 823 K          | 101.3 kPa        | ----                     |
| Gas nitriding       | ammonia  | 44 h       | 783 K          | 101.3 kPa        | 25-30% dis-<br>sotiation |
| Ion<br>nitriding I  | 50% N <sub>2</sub> +50% H <sub>2</sub>   | 6 h        | 753 K          | 170 Pa           | 1.1-2.1<br>l/min.        |
| Ion<br>nitriding II | 15% N <sub>2</sub> +50% H <sub>2</sub><br>40% N <sub>2</sub> +60% H <sub>2</sub> | 6 h<br>2 h | 803 K<br>803 K | 170 Pa<br>170 Pa | 1.1-2.1<br>l/min.        |

A standard potentiostatic circuit and a conventional polarization cell was used. The constant weep rate applied was ~ 600 mV/h and the open-circuit potential was recorded after 55 min immersion.

### Results and Discussion.

The effect of nitriding processes on current density vs potential in sea-water and prepared solution was the same. The open-circuit potential are summarized in Table II and the complete potentiodynamic curves of nitrided and unnitrided specimens in sea-water are shown in fig. 1. The examination of all treated samples revealed heavy pitting after the test. The compound layer was perforated and corrosion grew into diffusion zone with layer breakdown (fig. 2). In other side, the examination of unnitrided specimens revealed general corrosion without pitting evidence.

The observation of gas nitriding samples, by optical microscopy and SEM, revealed a 'white layer' ~25 μm thick with a continuous surficial layer ~2 μm thick (fig.3). Only Fe<sub>2</sub>N phase was identified by X-ray diffraction. Salt-bath treatment produced a continuous layer ~2 μm thick identified as Fe<sub>3</sub>C (fig.4). In both ion nitriding processes were determined Fe<sub>2-3</sub>N and Fe<sub>4</sub>N phases, but only the ion nitriding II process produced a continuous layer 4-5 μm thick. This difference has been imputed at higher temperature and longer process.

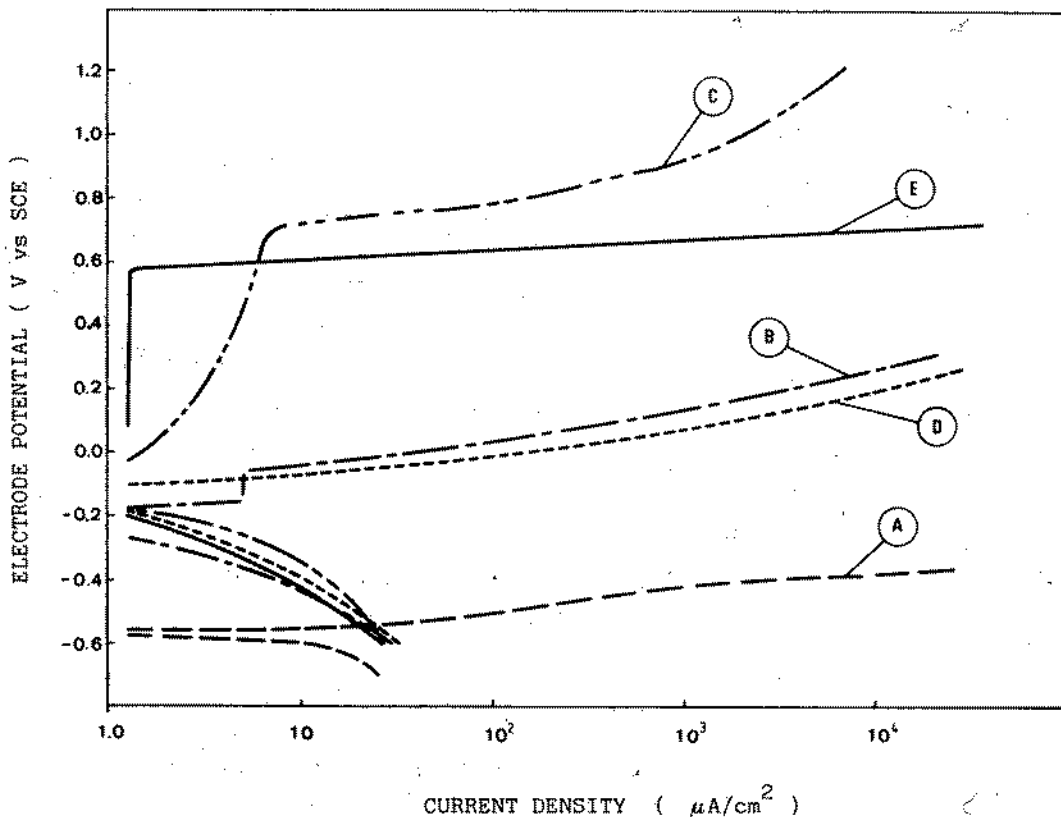


Fig. 1 Potentiodynamic curves in sea-water. A, untreated; B, salt-bath; C, gas nitriding; D, ion nitriding I; E, ion nitriding II.

The different electrochemical behaviour may be imputed principally to the presence of a continuous layer formed into the surficial zone during the treatment and to the present phases. So, the presence of a continuous layer formed by  $\text{Fe}_2\text{N}$  or  $\text{Fe}_{2-3}\text{N-Fe}_4\text{N}$  permit to get high potential values before a sharp increase in the current density. But, the presence of the same phases  $\text{Fe}_{2-3}\text{N}$  and  $\text{Fe}_4\text{N}$  in ion nitriding I samples does not have been enough to get the same behaviour. In all cases, the resistance corrosion of unnitrided specimens has been the lowest.



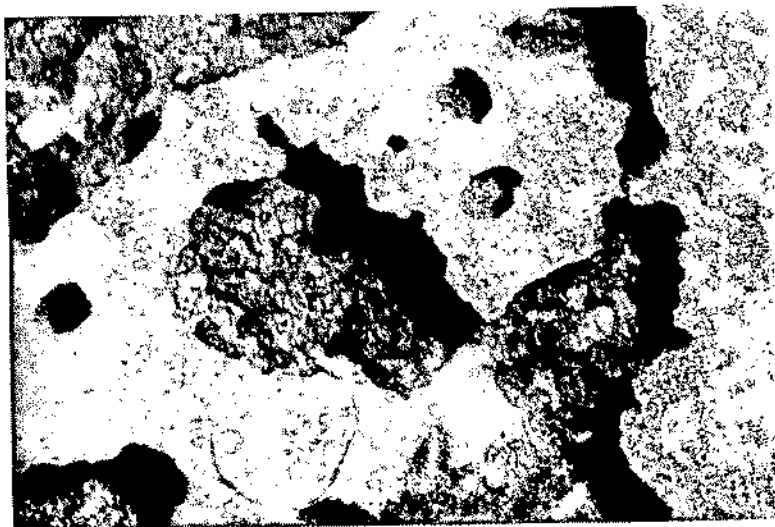


Fig. 2 Optical micrograph of pits and breakdown layer in a gas nitriding specimen after potentiodynamic polarization in air-saturated sea-water; original magnification x 100.



Fig. 3 Scanning electron micrograph of surficial zone in gas nitriding specimen showing the 'white layer' and the continuous surficial layer; original magnification x 400.

Table II. Open-circuit potentials vs SCE.

| Untreated | Salt-bath | Gas nitriding | Ion nitriding I | Ion nitriding II |
|-----------|-----------|---------------|-----------------|------------------|
| -0.59 V   | -0.22 V   | -0.01 V       | -0.14 V         | -0.10 V          |



Fig. 4 Scanning electron micrograph of surficial zone in salt-bath specimen showing the continuous surficial layer identified as  $Fe_3C$ ; original magnification  $\times 1700$ .

#### Acknowledgements

We gratefully acknowledge the financial support of the CIRIT of Generalitat de Catalunya. We also thank the equipment support of the Servei de Microscòpia of Universitat de Barcelona.

#### References

- 1.- "Metals Handbook", vol. 4, ASM, Metals Park 1981.
- 2.- J. Bidlen, Zoroze Ochr. Mater, 19. (5), 103 (1975).
- 3.- P. Süry, Br. Corros, J, 13, (1), 31 (1978).
- 4.- C. Núñez, P. Molera, J. Jorba. "I Congreso Iberoamericano de Corrosión y Protección". Revista Iberoamericana de Corrosión y Protección. Madrid 1983.

## A NOVEL SYSTEM FOR PRESERVING HULL AREAS OBSCURED

## BY DOCKING BLOCKS FOR OPTIMUM FUEL SAVINGS

H.S. PREISER AND A. TICKER

U.S. Department of the Navy; 2 Revell Rd, Severna Park, MD 21146 USA

Consulting Corrosion Specialist, Private practice; 12117 Maddox Lane,  
Bowie, MD 20715 USA

## ABSTRACT

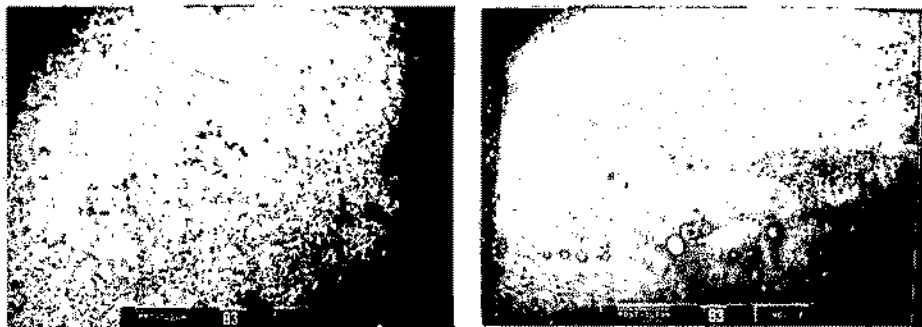
A novel hull coating system, designed to facilitate application of complete coating system in areas normally obscured by the docking blocks supporting the ship in drydock, has been developed and demonstrated. This concept is known as the DOK-BLOK Hull Coating System. The materials and application process are described, modifications and alternate procedures are given, laboratory and shipboard tests are detailed, test results are reported, and ship performance and economic advantages of this system are discussed. To date, all available test data indicate the DOK-BLOK Hull Coating System to be a potentially successful, cost effective system, well suited to accomplish the task for which it was designed.

## Resume

On explique la mise au point d'un nouveau système de revêtement de carène conçu pour faciliter l'application d'un revêtement complet dans des zones normalement cachées par les cales de dock qui soutiennent le bateau en cale sèche. Le nom donné à ce système de revêtement de carène est celui de DOK-BLOK. On décrit les matériaux utilisés et la procédure d'application, on donne les modifications apportées et les modes opératoires alternés, on décrit en détail les essais effectués en laboratoire et à bord du bateau, on donne les résultats des essais et l'on discute du fonctionnement du bateau et des avantages économiques de ce système. Toutes les données des essais dont on dispose à ce jour montrent que le système de revêtement de carène DOK-BLOK est virtuellement une réussite. C'est un système efficace pour son coût; il est bien adapté pour accomplir la tâche pour laquelle il a été conçu.

## INTRODUCTION

Operating Naval ships are routinely drydocked every 3 to 5 years to renew hull bottom anticorrosion (AC) and antifouling (AF) paint systems and to effect necessary repairs to the underwater hull, appendages and submerged equipment. During this reconditioning of the ship bottom by blast cleaning and repainting, the areas of the hull resting on the docking blocks are inaccessible and therefore cannot be preserved. Consequently, when the ship is undocked these areas remain unprotected and thus corrode and foul excessively resulting in increasing fuel consumption and reduced ship performance. In addition these areas serve as nuclei for the creep of fouling onto areas which would normally remain protected. Figure 1 shows typical accumulation and creep of fouling in such an unprotected area. By contrast, note the generally clean and foul free appearance of the adjacent protected hull areas. New approaches are therefore needed to preserve these inaccessible docking block areas during periods between drydockings.



Fouling Extends Beyond  
Unprotected Block Area

Cleaned Block Area Showing Sharp  
Demarcation At Unprotected Edge

Figure 1 - Typical Fouling Accumulation on Unprotected Block Area Before and After Cleaning

## ECONOMIC BENEFITS

Considerable economic benefits can be derived from protecting hull areas obscured by docking blocks. Docking blocks obstruct a significant portion of the underwater hull, affecting from about 5% for a high performance ship, to as much as 20% of the underwater area in the case of a supertanker. Figure 2 shows some large ships resting on arrays of docking blocks in drydock. Note the number of blocks involved. Projected prolonged drydocking intervals make these unprotected docking blocks areas even more vulnerable to corrosive attack and roughening by the marine environment, thus impairing eff-

icient ship operation and increasing the danger of structural damage. The penalty for not painting hull areas obstructed by the docking blocks is increased consumption to maintain a given speed of a partially fouled ship. This fuel penalty occurs either during intervals between routine underwater hull cleanings or during the entire time between drydocking in the case where long term AF paints are used. This direct economic loss is in addition to the intangibles associated with ship safety due to possible increased corrosion at the unprotected areas, where cathodic protection systems may be inadequate.

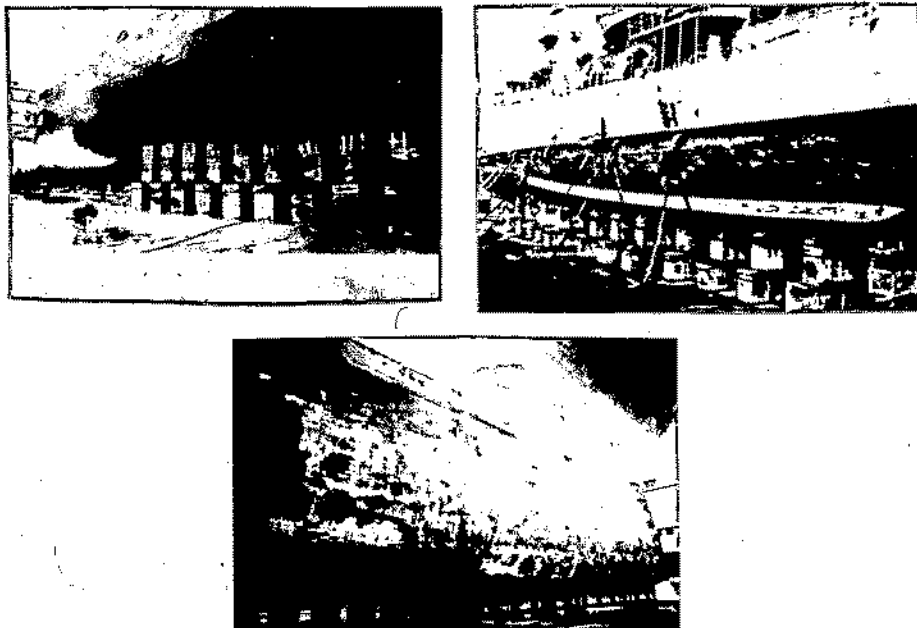


Figure 2 - Typical Large Ships in Dry Dock Resting on Blocks.  
(Area Covered by Blocks Vary from 5-20% F Hull)

A recent paper presented at the 20th Annual ASE Technical Symposium<sup>(1)</sup> described a study designed to determine fuel savings gained if keel and side block areas on aircraft carriers are preserved. The hull areas considered in this investigation ranged from a lower limit of 4% of the total wetted area (area just covered by the docking blocks) to an upper limit of 11% of the total wetted area (area completely affected by the spread of fouling from unpreserved block areas). Calculations based on results obtained in this study predict fuel savings of 1.0 to 2.3 million dollars per carrier over the 5 year period between drydockings where periodic underwater cleaning is

used. Similar calculations indicate fuel savings of about \$160,000 for destroyers and \$110,000 for frigates, per ship over a 5 year period<sup>(2)</sup>. When the calculations are carried out for ships having a long term, high performance, unattended AF coating installed, the fuel savings increase by approximately a factor of two.

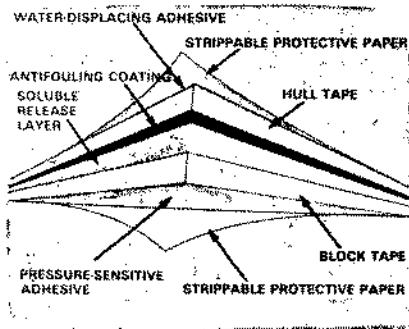
The DOK-BLOK system offers an economical means for overcoming this problem. It is estimated that to apply this method on new construction and during extended overhaul (5 year intervals), the cost of the prepackaged coating system, including application, should not exceed \$15 per square foot. For a typical frigate, having an underwater area of 22,500 square feet of which 5% is docking block area, the cost of DOK-BLOK protection should be about \$16,875 per ship, once every 5 years, or \$3,375 per year. Using the figures for destroyers generated in the above study, a net saving of \$28,625 per year per ship is indicated, in addition to increased mission capability and ship safety. To put it another way, for each dollar invested in the DOKBLOK system, nine dollars of fuel would be saved where periodic cleaning takes place and as much as \$18 of fuel saved where long term, unattended AF systems are used.

#### INVESTIGATION

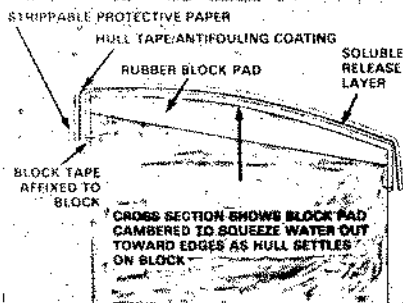
##### Description of the DOK-BLOK System

The DOK-BLOK Hull Coating System is a simple, cost effective procedure for applying an appropriate coating system to the underwater hull areas obstructed by the docking blocks. Basically, the system consists of two tapes separated by a water soluble material to form a prepackaged sandwich. Each tape features a water repelling adhesive which is covered by an easy release protective paper. The bottom tape, termed the "block tape," serves to anchor the unit to the docking block. The top tape, termed the "hull tape" consists of a polymer-faced tape which has been previously coated with a suitable antifouling paint. It is the hull tape which adheres to the ship's hull and ultimately becomes an integral part of the ship's bottom paint system. The water soluble layer between the two tapes provides mechanical protection to the AF coating during the docking of the ship. It also functions as a plane of separation between the tapes when the ship is undocked.

In practice, after positioning of the docking blocks in the pumped out drydock, each block is fitted with a properly sized DOK-BLOK tape sandwich unit which is fastened to the docking block. Just prior to reflooding the drydock, the top protective paper is removed to expose the hull tape adhesive surface. The system is now ready to receive the docking ship. After the ship has been drydocked and is resting on the docking blocks, overlapping portions of the hull tape are faired onto the adjacent hull and painted over during the regular hull painting operation. When the ship lifts off of the docking blocks during undocking the sandwich separates within the water



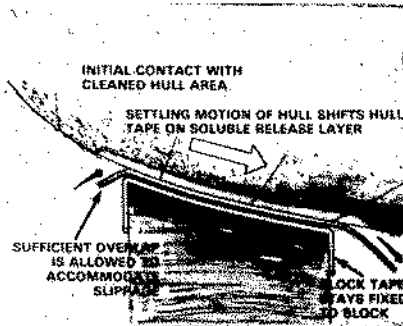
### 1. TAPE SANDWICH STRUCTURE



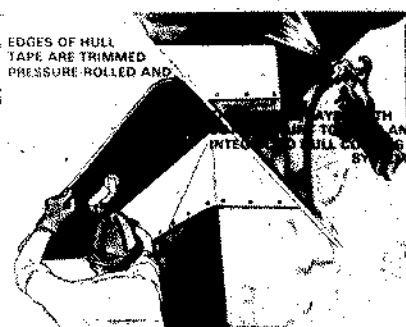
### 2. PREDOCKING BLOCK PREPARATION



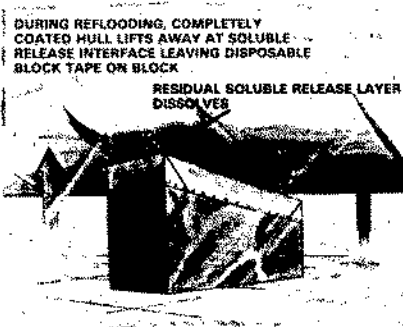
### 3. UNDERWATER HULL SURFACE PREPARATION



### 4. INITIAL DRYDOCKING



### 5. DRYDOCK OPERATIONS



### 6. UNDOCKING

Figure 3 - Schematic Application Sequence of Dok-Blok Hull Coating System. US Patents 4,321,101 & 4,420,533

soluble layer with the hull tape remaining on the hull as an integral part of the total hull paint system. Figure 3 shows a series of schematic sketches of the DOK-BLOK tape and sandwich structure being applied to a ship hull during drydocking operations. The process is further described in the literature<sup>(3-5)</sup>.

### Materials Selection

Industry was surveyed for commercially available candidate materials, suitable for use in the DOK-BLOK system. Table I lists candidate materials acquired and tested, either individually or in various combinations as DOK-BLOK sandwiches. In some instances, duplicate materials were obtained from several sources. Early hull tape samples were thin and quite drapeable, leading to some concern that under the settling ship's weight these materials may tend to wrinkle or roll up, rather than slide evenly as a unit. For this reason, subsequent hull tape samples were thicker, reinforced sheet materials capable of sufficient pliability to follow the curvature of a ship hull.

TABLE I  
CANDIDATE MATERIALS FOR DOK-BLOK SYSTEM

| <u>MATERIALS<br/>(GENERIC)</u>            | <u>FORM</u>                         | <u>THICKNESS<br/>(MILS)</u> |
|---|-------------------------------------|-----------------------------|
| <u>ADHESIVE MATERIALS</u>                 |                                     |                             |
| OIL MODIFIED RUBBER RESIN<br>ACRYLIC FOAM | FILM                                | 17                          |
|   | TAPE                                | 20                          |
| <u>HULL MATERIALS</u>                     |                                     |                             |
| VINYL                                     | TAPE                                | 2                           |
| VINYL                                     | SHEET                               | 10                          |
| VINYL                                     | SHEET                               | 15                          |
| VINYL                                     | SHEET                               | 20                          |
| POLYURETHANE                              | SHEET                               | 12                          |
| POLYETHERIMIDE                            | SHEET                               | 20                          |
| POLYETHYLENE TEREPHTHALATE                | SHEET                               | 10                          |
| POLYETHYLENE                              | SHEET                               | 20                          |
| POLYESTER COATED GLASS-REINFORCED         | FABRIC                              | 10                          |
| <u>BLOCK MATERIALS</u>                    |                                     |                             |
| POLYESTER                                 | TAPE                                | 2                           |
| ACRYLIC                                   | TAPE                                | 3                           |
| POLYURETHANE                              | SHEET                               | 12                          |
| <u>WATER SOLUBLE MATERIALS</u>            |                                     |                             |
| POLYVINYL ALCOHOL                         | FILM                                | 1                           |
| POLYVINYL ACETATE                         | FILM                                | 1                           |
| <u>BLOCK PAD MATERIALS</u>                |                                     |                             |
| NATURAL GUM RUBBER                        | SHEET                               | 250                         |
| NEOPRENE RUBBER                           | (35-40 DUROMETER)<br>OPEN CELL FOAM | 500                         |
|   | (5-9% SOLID)                        |                             |



### Dry Docking Load Simulator (DDLS) Machine

To facilitate reliable evaluation of candidate DOK-BLOK component materials, the DDLS machine was designed and constructed. This machine under controlled laboratory conditions, simulates the conditions that the materials would encounter in actual service; i.e., vertical loading of approximately 235 pounds square inch and the slight movement of a ship as it cradles on a docking block prior to coming to rest. The machine accommodates a sample DOK-BLOK sandwich, 11 inches by 11 inches and consists of a hydraulic cylinder which exerts a variable vertical loading (ram) force on a water submerged simulated drydock block bearing surface. A second cylinder provides a slow horizontal oscillating force to a platform supporting the simulated docking block assembly, causing the block assembly to move horizontally back and forth over a 2 inch span. The hydraulic control system includes gauges and regulators which allow both the adjustment and monitoring of a wide range of loading parameters. An electrical control system provides appropriate control of the various motions generated within the machine. A schematic diagram of the DDLS machine is shown in Figure 4. The control systems are not indicated.

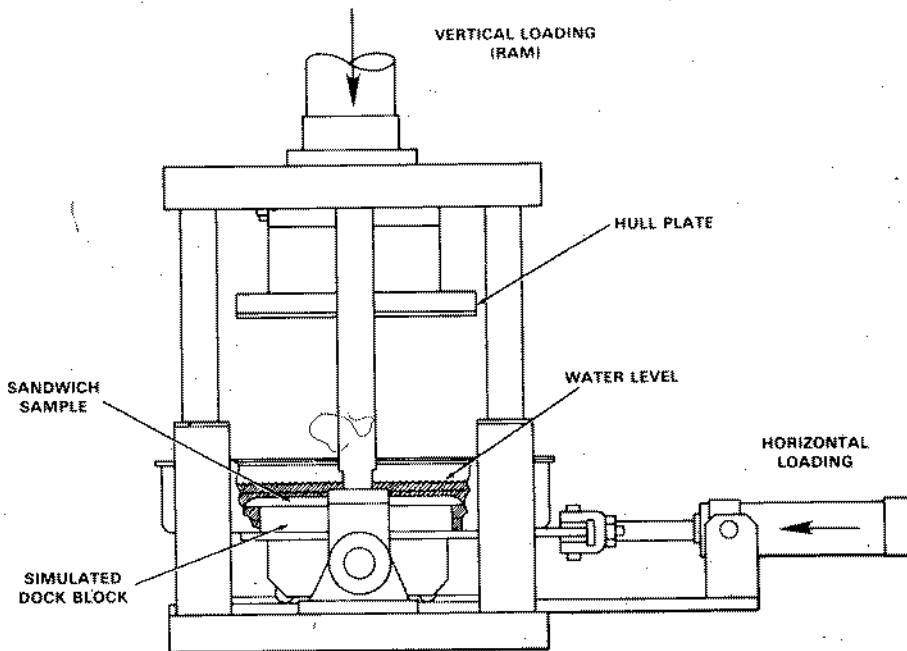


Figure 4 - Schematic Diagram of Drydock Load Simulator (DDLS)

### Laboratory Tests

Initial laboratory tests established the feasibility of this process to transfer the hull tape from a submerged docking block to a ship hull, with good adhesion of the transferred tape. These tests consisted mainly of applying a tape system to a submerged (tap water or 3% salt solution) simulated docking block (wooden block) and pressing a weighted steel panel onto the submerged hull tape adhesive. Lifting the panel off the block assembly revealed the transferred hull tape. Timing cycles, weight loads as well as the condition of the panel surfaces were varied. Steel surfaces tested were: blast cleaned; tight rust and mill scale; painted; painted, fouled and wire brushed; etc. Many of the adhered tape samples were subjected to 1 inch wide 90° peel tests at a peel rate of 12 inches per minute. The adhesion values varied from about 6 to 3 pounds per inch width.

The Dry Docking Load Simulator (DDLS) machine, described earlier, provided considerable information regarding the selection of satisfactory candidate materials. Physical properties of individual candidate materials were examined and those found unsuitable were discarded. The adhesive film was then applied to the various plastic sheets and DOK-BLOK tape sandwiches of appropriate size to fit the DDLS machine were constructed. The sandwich was then positioned and attached to the simulated block in the water pan of the machine. The protective paper was removed from the hull tape adhesive and the pan was filled with water to a level covering the block and sandwich assembly. A 14 inch by 14 inch steel hull plate was bolted to the vertical force component (ram) of the DDLS. The ram cylinder pressure was adjusted to exert a 235 psi load on the 11 inch square sandwich sample. The ram was slowly lowered onto the sandwich/block assembly which was moving laterally, back and forth over a two inch span. The horizontal oscillation was set to 60 seconds for each cycle. The horizontal cycling was continued under full load for 5 minutes and then stopped. The water was drained from the pan one hour after the ram load was induced on the sample, but the ram load was continued for an additional seven hours. Figure 5 is a photograph of the DDLS machine showing the rising hull plate after an undocking cycle. The separated water soluble layer is clearly visible on the adhered tape. Figure 6 is a close-up photograph of a typical transferred hull tape to the metal substrate. Here again one inch width sections of the tape were subjected to 90° peel tests at a peel rate of 12" minute. The force to peel the tape averaged about 10 pounds per inch width. By comparison, results on a similar test performed on a F-121 vinyl AF paint film on a bare metal substrate indicated that 3 pounds per inch width was required to peel the paint from the substrate. This aspect is under further study to determine peel strength of AF coatings on various AC painted substrates.

In a second dynamic laboratory test, the ram of the DDLS was used to apply a leading candidate hull tape to one face of five steel disks, 9 inches diameter. Each disk presented a different surface

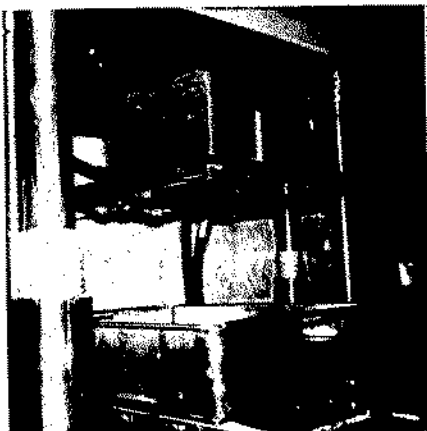


Figure 5 -  
DDLS Machine Showing Rising  
Hull Plate After Simulated  
Undocking Cycle



Figure 6 -  
Close-up of Typical Transferred  
Hull Tape (The Separated Water  
Soluble Layer is Clearly  
Visible on the Face of  
Adhered Tape)

condition to the tape adhesive; i.e., bare metal (abrasive blasted); tight rust; Navy Epoxy AC paint (F-150); copper-based Navy AF paint (F-121); and a commercial ablative AF paint system. The back of each disk was coated with an epoxy AC paint system. The adhered tape on each disk was trimmed to conform to the disk perimeter and the taped flat surface of each disk was scribed to bare metal to form pie shaped sections. Alternate sectors of tape on each disk were removed as shown in Figure 7. The leading edge of each tape section was either feathered or faired into the disk surface, painted over, or left as a stepped edge. Each disk was then installed on a variable speed rotating disk machine and rotated underwater at a preset constant speed. The rotational speed was periodically increased and the test tapes were inspected at the end of each speed cycle for evidence of tape deterioration. Figure 8 shows the variable speed rotating disk machine with a disk in place. This machine is also instrumented to measure hydrodynamic drag generated by the various tape surfaces and/or edge configurations. The results of rotation of a glass-reinforced polyester tape adhered to the rusted disk are summarized in Table II. Other data generated in these experiments for adhesion of the tape to different substrates were quite similar. The gross failure of separation of the tape from the adhesive has led to the suspicion that silicone parting compounds commonly used in the manufacture of the glass-reinforced polyester tape contaminated the surface sufficiently with a low energy material so as to interface with its adhesion strength to resist high rotational speeds. The presence of surface contaminants indicative of silicone has been confirmed by x-ray photoelectron spectroscopy (XPS)

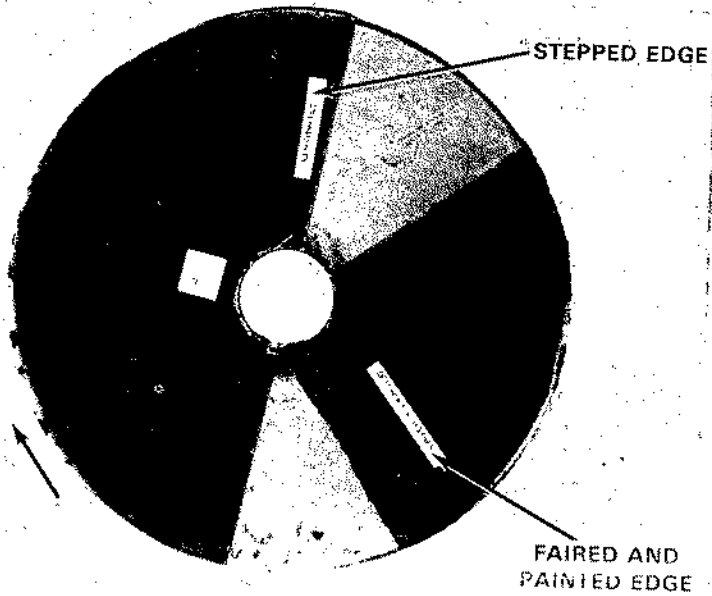


Figure 7 - Typical Rotating Disk Showing Hull Tape in Place with Exposed and Painted Edges

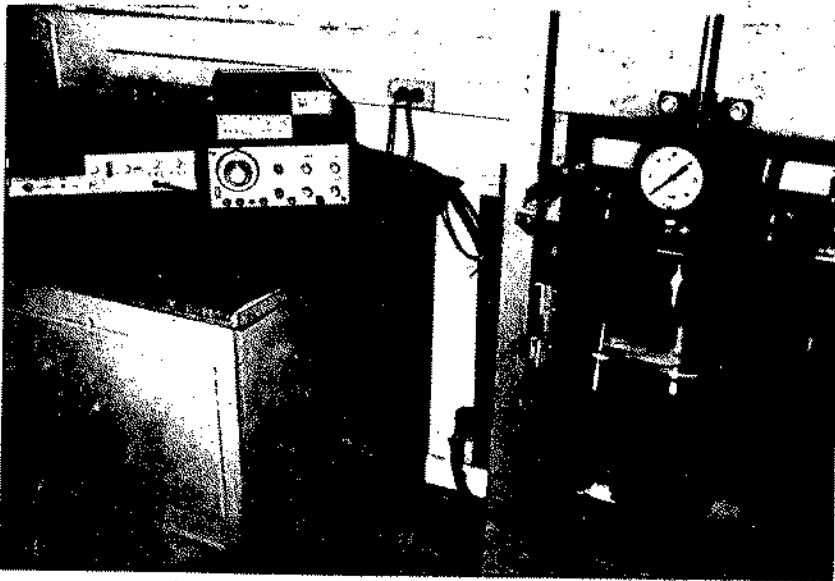


Figure 8 - Variable Speed Rotating Disk Machine in Operation with Test Specimen in Place

TABLE II  
EFFECT OF HIGH SPEED FLOW ON ADHESION OF HULL TAPE TO RUSTED STEEL  
(ROTATING DISK TEST, 9" DIA.)

| PERIPHERAL<br>SPEED<br>KNOTS | HOURS | LOSS OF ADHESION<br>UNPAINTED EXPOSED EDGE |          | LOSS OF ADHESION<br>PAINTED FAIRED EDGE |          | NOTES |
|------------------------------|-------|--|----------|---|----------|-------|
|                              |       | FABRIC                                     | ADHESIVE | FABRIC                                  | ADHESIVE |       |
| 5                            | 6     | N  | N        | N                                       | N        |       |
| 10                           | 6     | N  | N        | N                                       | N        |       |
| 15                           | 6     | 1  | 0        | N                                       | N        | (a)   |
| 20                           | 6     | F  | 1        | N                                       | N        | (b)   |
| 25                           | 6     | F  | 2        | N                                       | N        | (c)   |
| 30                           | 6     | F  | 2        | N                                       | N        | (d)   |
| 40                           | 6     | F  | 4        | N                                       | N        | (e,f) |

SCALE: N - NO EDGE LIFTING

- 1 - BEGINNING EDGE LIFTING (1-8mm<sup>2</sup> AREA)
- 2 - MODERATE EDGE LIFTING (8-50mm<sup>2</sup> AREA)
- 3 - SUBSTANTIAL EDGE LIFTING (51-200mm<sup>2</sup> AREA)
- 4 - SEVERE EDGE LIFTING (201-450mm<sup>2</sup> AREA)
- F - FAILED TAPE (OVER 50% OF AREA LIFTED OFF)

- NOTES: (A) FABRIC OVERLAPPING THE CIRCUMFERENCE OF THE DISC HAD SEPARATED FROM THE ADHESIVE, CONSEQUENTLY THE OVERLAP WAS TRIMMED FLUSH TO THE EDGE OF THE DISC WITH A RAZOR KNIFE.
- (B) A SIGNIFICANT SECTION OF THE FABRIC DELAMINATED FROM THE ADHESIVE; THE FOILED SECTION WAS CUT AWAY FORMING A NEW LEADING EDGE.
- (C) THE NEW LEADING EDGE OF THE FABRIC REMAINED INTACT FOR 6 HOURS BUT BEGAN TO SHOW RAPID DELAMINATION AT THE BEGINNING OF THE 30 KNOT CYCLE. SOME LIFTING OF THE ADHESIVE AT THE LEADING EDGE NEAR THE PERIFERY HAD OCCURRED.
- (D) NO FURTHER DEGENERATION OF THE ADHESIVE WAS OBSERVED.
- (E) SEPARATION OF THE ADHESIVE FROM THE SUBSTRATE INCREASED STEADILY.
- (F) THE LEADING EDGE OF FABRIC AND ADHESIVE SYSTEM WERE INTACT THROUGHOUT THE ENTIRE EXPERIMENT.

techniques. The adhesion of the pressure sensitive adhesive on the rusted steel was excellent with slight evidence of edge peeling beginning to show at 25-30 knots peripheral speeds. In all cases where the leading edge of the hull tape was sealed and faired by careful overlay painting, no evidence of edge lifting could be ascertained over the 5 day test period. The work is continuing and further progress will be reported as the data become available.

#### Field Tests

Based on a highly successful laboratory test program, field test studies were initiated. A ferryboat scheduled for drydocking was selected and three keel blocks and two side blocks were designated for this test. These were identified as keel blocks Nos. 34, 39 and 44 with the two side blocks on both sides of keel block #34. The schematic layout of these blocks are shown in in Figure 9. On 17 September 1983, relevant test areas on the ship's hull were cleaned by divers and on 20 September 1983, the pre-positional blocks were prepared for the test. A 1/4-inch thick gum rubber pad was fastened to the crush boards of one keel block and one side block, followed by

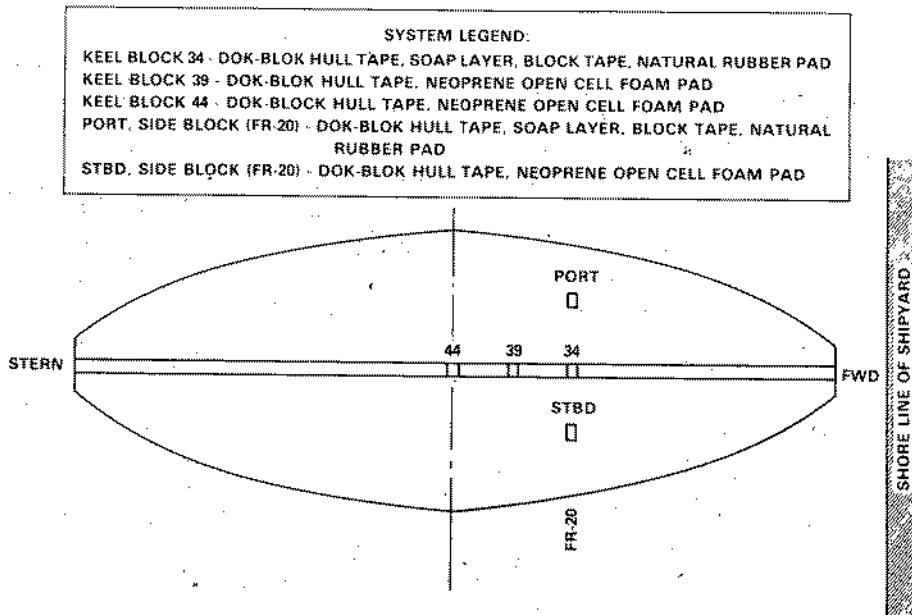


Figure 9 - Schematic Layout of Test Blocks on Ferry Boat



Figure 10 - Typical Dok-Blok Tape System on the Side Block of the Ferry Boat, Before and After Dry Docking

the block tape, a layer of water soluble paste, and finally the hull tape. The entire system was fastened to the dockin block. The other two keel blocks and one side block were fitted with 1/2-inch thick open cell foam rubber pads. The hull tapes were applied directly over these foam rubber pads and the entire system was fastened to the crush boards on each block. Figures 10 and 11 illustrates the appearance of the DOK-BLOK system applied to a side docking block and to a keel block before and after docking.



Figure 11 - Typical Dok-Blok Tape System on Keel Block of Ferry Boat, Before and After Dry Docking

The ferryboat was scheduled for drydocking on 21 September 1983. Prior to flooding the drydock, the protective paper was removed from the hull tape adhesives, but left intact around the sides of the blocks to prevent the overlapped adhesive from contamination by dirt and debris in both the air and water. A videotape camera was installed on one keel block to record the interaction of the settling hull with the DOK-BLOK system installed on the block. In addition, many still photographs were taken of the installation process. The drydock was then flooded, the ship was brought into the drydock and positioned, and the dock was pumped down again exposing the underwater hull of the ship. The following day, the overlapped hull tape was adhered to the ships hull and trimmed to approximately 1 inch of the block edges. Figures 12 and 13 show a technician using a plastic roller to remove tape wrinkles and trapped air or water as he adheres the overlapped tape to the hull. These exposed edges of the adhered hull tape were then painted with one coat of Navy formula 121 antifouling paint. A wooden frame, 2 inches wide, was constructed on 4 of the 5 test blocks, to protect the trimmed edges of the hull tapes during abrasive blasting operations. The tape edges on the fifth block, block 44, were left exposed to observe if the blasting operation could be used as an alternative for trimming the exposed hull tape edges. The protective wooden battens were removed prior to the painting of the ship hull. During the reconditioning process, the hull was abrasive cleaned to bare metal and an ablative AF coating system was applied. The exposed hull tape edges were over coated with this system. A typical applied hull tape is shown in Figure 14.

#### RESULTS AND DISCUSSION

The basic DOK-BLOK systems is described earlier in this paper, however, many modification and variations of this process are possible<sup>(4,5)</sup> some of which include:



Figure 12 -  
Hand Rolling Edge of Trimmed  
Overlap Tape Adhered to Hull



Figure 13 -  
Checking Adhesion of Hull Tape  
Edge After Hand Rolling  
Operation

- a. Elimination of the block tape and the water soluble layer and applying the hull tape directly over the foam rubber pad.
- b. Applying a water soluble coating; such as polyvinyl alcohol or polyvinyl acetate, over the AF coating on the hull tape.
- c. Incorporating a suitable AF material, either chemically or physically, into the polymer facing of the hull tape.
- d. Incorporating suitable corrosion inhibiting materials into the hull tape adhesive.
- e. Underwater application of a very thin hydrophobic film, such as a paste wax, to the cleaned hull prior to contact with the hull tape adhesive. It has been observed that this tends to increase adhesion.



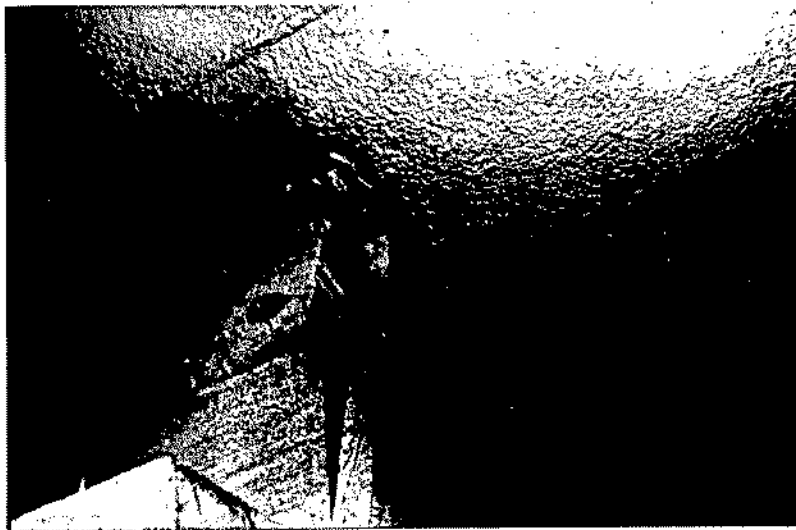


Figure 14 - Typical Applied Dok-Blok Hull Tape After Trimming, Rolling and Blending into Ship Hull Paint System

#### Laboratory Tests

Early static panel tests indicated superior qualities for the DOK-BLOK tape system as compared to actual Navy paint systems. In many instances, hull tapes showed adhesion values on steel or painted panels, three times greater than for control Navy paint systems. In addition, 90° tensile peel tests indicated that tape adhesive bond strength on steel panels previously painted, fouled and wire brushed, exceeded the cohesive strength of the paint films. This was considered significant since experience has shown that hydrodynamic shear forces exerted on hull paints do not exceed its cohesive strength, that is, the paint films do not normally disintegrate but retain their film stability. It therefore appeared that the adhesion of this tape to the hull would be at least as good if not better than the adhesion of the original paint system to the hull. Experiments utilizing the DDLS machine revealed that the adhesive film could be successfully applied to a wide range of polymer materials. Numerous DOK-BLOK sandwiches, employing various combinations of hull tape polymers and other candidate materials, were constructed and satisfactorily tested on the DDLS machine. The final choice of polymer backing for the hull tape revolved mainly about material strength, compatibility with submerged seawater performance, compatibility with Navy AF paint systems and with shipboard cathodic protection systems. Persistent positive laboratory test results established the feasibility of transferring the hull tape from the drydock block to the ship's hull. Dynamic tests on a variable speed rotating disk machine showed a definite

advantage for fairing the leading edges of the tape into the adjacent paint system.

### Field Tests

As stated earlier, a ferryboat was selected for a trial application of the DOK-BLOK Coating System. The ferryboat was approximately 242' long with a 65' beam and a draft of 8-1/2'. Its speed is listed at 13 knots. It has a "vee" shaped hull and a 6' wide flat keel. Permission was granted to install the DOK-BLOK system on port and starboard bilge blocks adjacent to keel block 34. The hull configuration is symmetrical about the fore and aft center line and the center keel block is at position 44. The keel blocks are on 4 foot centers so that block 34 is located 40 feet forward of the center of the ship.

Prior to docking the ferryboat, the services of a diving team was utilized to inspect and clean the ship bottom in hull areas where the DOK-BLOK system would be applied. The hull paint system was reported to be in relatively good condition, with main areas of fouling growth found in patches on the keel where the blocks prevented application of antifouling hull paints on previous drydockings. This growth was about 1/2 inch thick and could be scraped off with a wide putty knife. A light slime on the hull coating was also present. The cleaning operation removed all fouling growths and slimes and any loose paint or corrosion products.

The test docking blocks were prepared with several modified versions of the DOK-BLOK system, as previously described, and the ship was docked in a routine manner. Inspection of the test areas and examination of the videotape showed no apparent problems with the positioning or deployment of the DOK-BLOK tape systems during the dry-docking process. In all cases, the tapes remained in place with no tears or strains. Some minor difficulties were encountered in adhering the overlapped tape edges to the ship's hull. This is attributed to contamination of the tape adhesive by floating dirt, oil or debris. A better method for protecting the adhesive on the overlapped tape edges will be devised before the next shipboard test. However, these edges were cleaned up and were made to adhere to the ship hull, trimmed to approximately one inch of the block and preserved as part of the overall hull paint system. Short term examination by divers of the applied DOK-BLOK coatings, after one month of exposure pier-side showed some softening and peeling of the AF paint on the hull tape but no fouling. Unprotected block areas nearby were beginning to foul profusely as shown in Figures 15 and 16 respectively.

### Conclusions

o The preliminary field test demonstrated the feasibility of shipyard deployment of the DOK-BLOK hull coating system.

o Optimization studies are required to refine and simplify application procedures.

o Component materials and adhesives need to be upgraded to achieve long term performance of this unique coating process. Work is underway to accomplish these objectives.

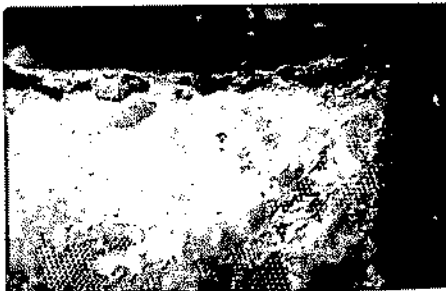


Figure 15 -  
Underwater Close-up Photo of Dok-Blok Hull Tape Showing of Fouling After One Month Exposure in Harbor

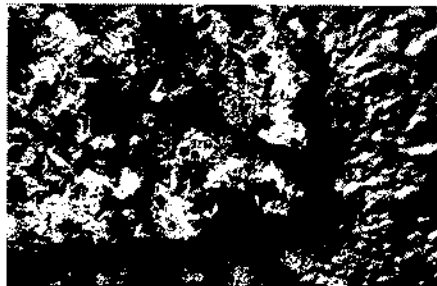


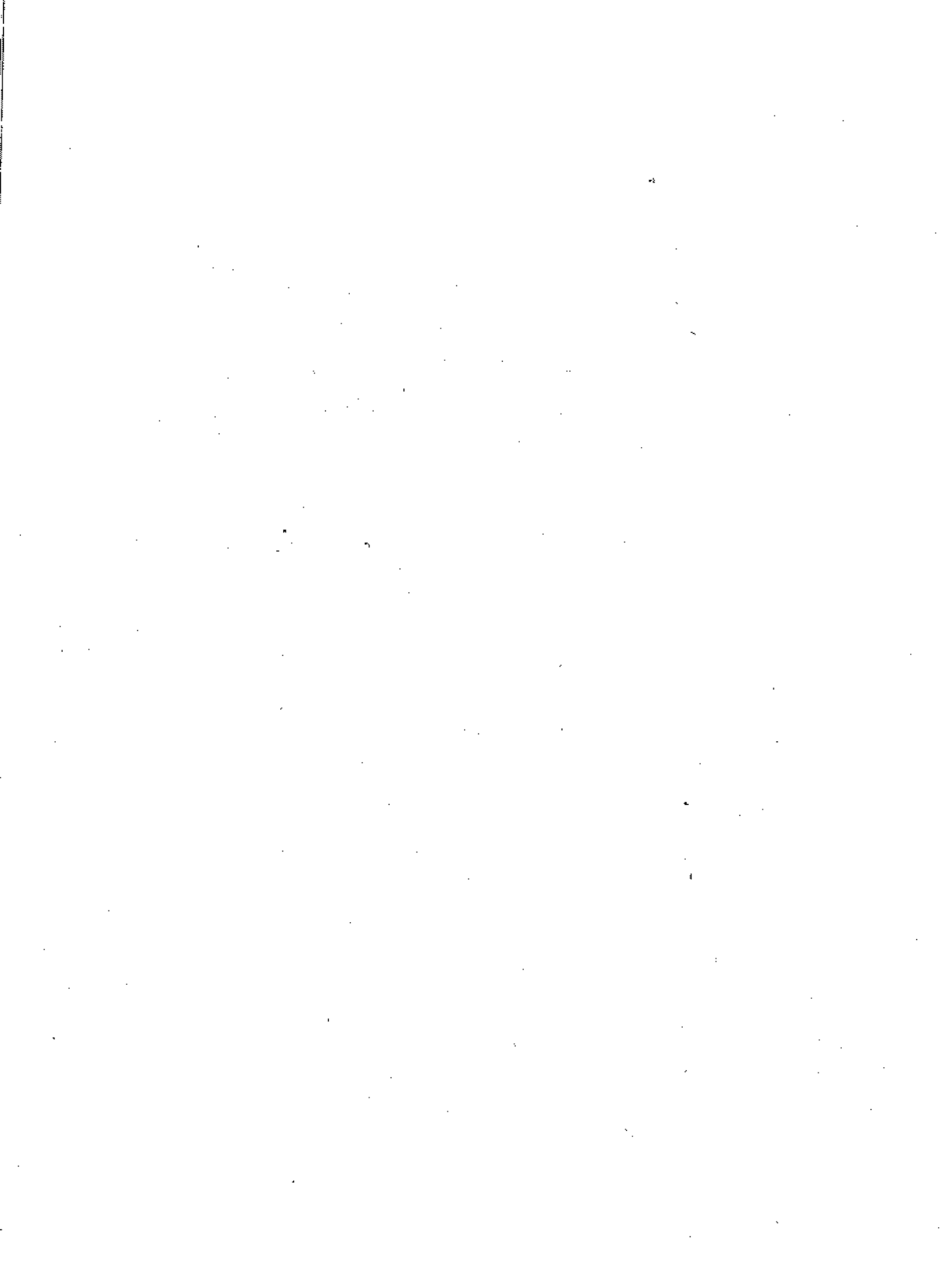
Figure 16 -  
Underwater Close-up Photo of Adjacent Unprotected Block Area of Hull Showing Profuse Fouling Attachment After One Month Exposure in the Harbor

#### References

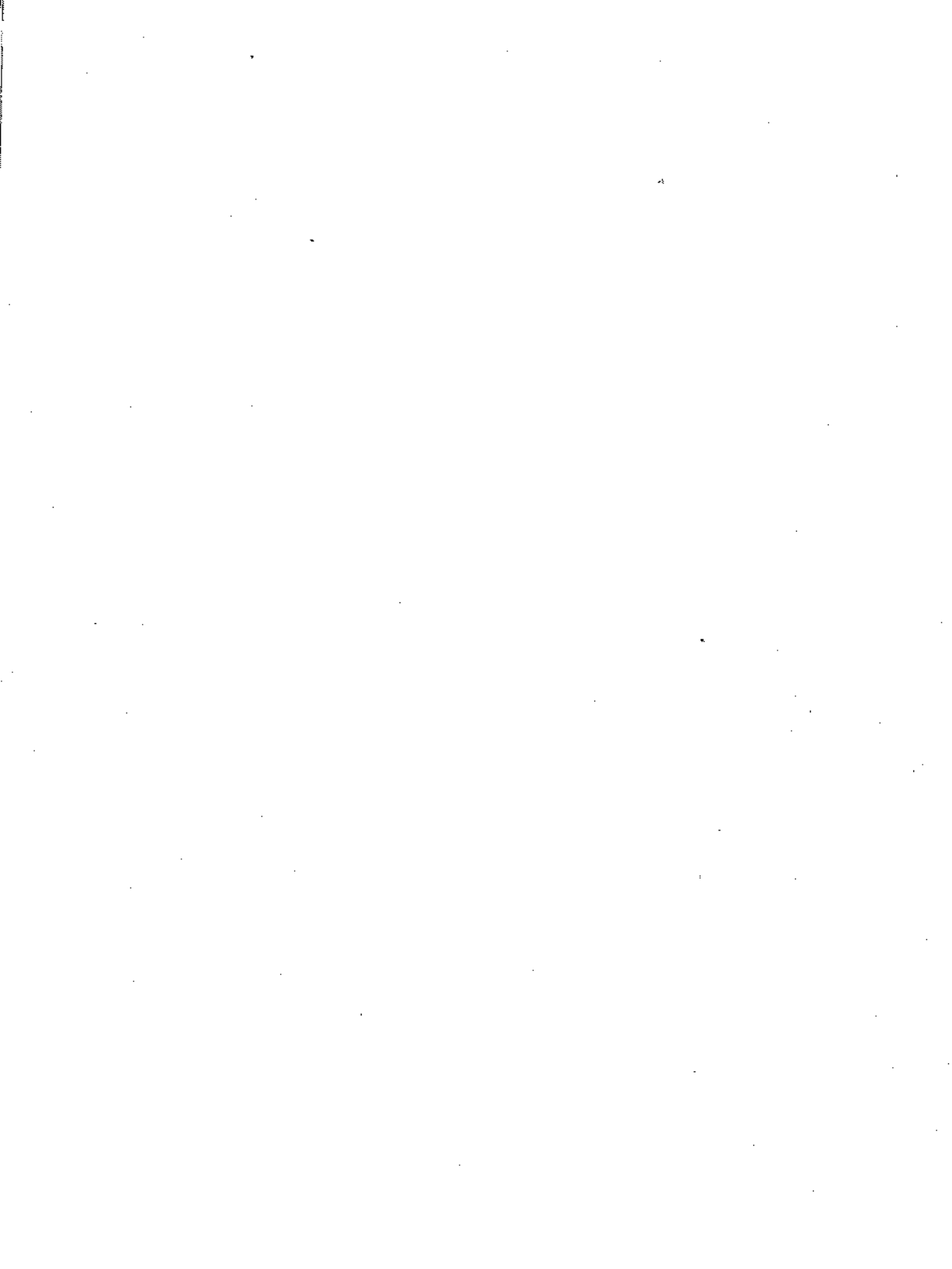
1. Healy, G. and Hough, J.J., "Determination of Fuel Savings if Keel and Side Block Areas on Aircraft Carriers are Preserved." Paper published in 20th Anniversary Technical Symposium, Association of Scientists and Engineers of the Naval Sea Systems Command, Department of the Navy, Washington, DC 20362, 1983.
2. "DOK-BLOK" Hull Coatings System Saves Fuel, Money," The Center Line, DTNSRDC, Bethesda, Maryland 20084, 16 March 1984.
3. "Coating the Hull Without Moving Ship or Blocks," Marine Log, May 1982.
4. U.S. Patent 4,321,101.
5. U.S. Patent 4,420,533.

We wish to acknowledge the assistance of Neil A. Smith and the Navy Research Dive Team in carrying out the underwater documentation of this project and Thomas D. Gracik who conducted the rotating disk experiments.

The opinions expressed herein are solely those of the authors and do not necessarily express the official views of the Navy Establishment at large.



OFF SHORE 



## COATINGS FOR OFFSHORE STRUCTURES AND SHIPS IN FROZEN SEA

TOSHIYUKI YASUI

Technical Research Center, Nippon Kokan

1-2 Chome, Suehiro-cho, Tsurumi-ku, Yokohama, Japan

## SUMMARY

Ice-resistant coatings are required to have special performance of low friction against ice and toughness against ice abrasion. The performance of several coatings were investigated, and the correlation between friction coefficients of the coatings and surface property was obtained. The friction coefficients depend on roughness, hardness and hydrophobicity of the coating film surface. The practical wearing behavior of coatings on the hull of an ice-breaker was tried to simulate by the ice-abrasion tests in laboratory. The experimental results agreed with full-scale performance tests which were conducted using Japanese Antarctic ice-breaker "Fuji" for five years. The laboratory testing method to evaluate effectively the performance of ice-resistant coatings were established. The special application procedures for ice-resistant coatings were also established.

## RESUME

La peinture résistante à la glace doit avoir des caractéristiques particulières telles que faible frottement contre la glace, résistance à l'usure due à la glace, etc. Les caractéristiques des diverses peintures ont été soumises aux études, et cela nous a permis de comprendre la corrélation entre le coefficient de frottement et l'état de surface. Le coefficient de frottement dépend de la rugosité, la dureté et l'hydrophobicité d'une couche de peinture. Nous avons effectué les essais d'abrasion au laboratoire en créant les conditions simulées, afin de saisir le comportement d'usure de la couche de peinture appliquée sur la coque de brise-glace. Les résultats obtenus sont largement d'accord avec ceux des essais faits pendant cinq ans sur le brise-glace japonais "Fuji". Nous avons ainsi pu établir la méthode d'essai en laboratoire permettant d'évaluer effectivement les caractéristiques de peinture résistante à la glace, ainsi que la méthode d'application particulière de la peinture de ce genre.

## 1. INTRODUCTION

There has been little study of review of corrosion protecting method for those areas of structures and ships in frozen sea which come in contact with ice. Previously it was believed that there were no appropriate anti-corrosion methods available; conventional paint film peeled within a short time due to incessant contact and scraping with ice. To deal with this problem, an extra thickness of the steel plate has been increased as a corrosion allowance. As resource development in the Arctic has made progress, paint manufacturers have started developing paint for the bottom of ships navigating in frozen seas (to be hereafter referred to as ice-resistant paint). Recently, ice-resistant paint which is sufficiently durable in frozen sea areas has become available. It has been used for ships navigating in the Baltic Sea, for guard-ships on the Great Lakes, for polar expedition ships of various countries and for offshore drilling structures and icebreakers used in the Arctic. Also, NKK has applied this paint to the new Japanese Antarctic observation vessel, "Shirase", to the Japanese ice-breaking patrol vessel, "Soya", and to "Ikaluk", an ice breaking supply vessel. The functions required to ice-resistant paint are anti-corrosion performance, reduction of friction resistance against ice and the prevention of icing. It is said that friction between the hull and ice leads to a substantial increase in ice breaking resistance. However, ice-resistant paint applied on ship bottoms can be expected to reduce the friction resistance of ship, to increase their ice breaking ability and to improve their fuel consumption. Moreover, the prevention of icing improves navigational stability of ship as well as reduces external forces acting on offshore structures.

Since 1978, we have been conducting a full-scale test of ice-resistant paint on the "Fuji", the Antarctic exploration vessel, together with laboratory tests of properties such as friction, ice release and abrasion. The laboratory test methods to evaluate effectively the performance of many kinds of ice-resistant coating were established. Also, film properties which are necessary for ice-resistant paint were clarified.

Seven brands of ice-resistant paint, as shown in Table 1, were selected in the test, as well as three brands of mastic-type paint containing glass flakes and two brands of conventional hull paint.

## 2. FRICTION TEST

### 2-1 TEST METHOD

An ice friction test apparatus were designed as shown in Fig. 1. The test paint was coated on end of a cylindrical test piece with 30mm inner diameter and 50mm outer diameter. By pressing the sample against an ice surface at an  $8 \text{ kgf/cm}^2$  pressure and then rotating it using a DC motor, three kinds of friction coefficients were measured: breakaway (static friction coefficient after pressing the



sample against the ice for 10 minutes), static and kinetic friction coefficients. The breakaway and static friction were measured by rotating the sample at a rate of 1.31 cm/sec, and the kinetic friction was measured at 39.3 cm/sec. The ice was made by freezing distilled water. The temperature of ice and sample was kept at -20°C by spraying liquid nitrogen into the thermostatic chamber.

Furthermore, it was desired to investigate the surface properties of paints necessary for low friction coatings. So three properties were measured; surface roughness (ISO-R.468), hardness (Knoop hardness number, ASTM-D-1474) and hydrophobicity (contact angle). Using a stylus type roughness meter, surface roughness measurements were made on 10 point height. The contact angle of distilled water droplet on the sample surface were measured to estimate hydrophobicity. Moreover, to clarify the relationship between surface properties and friction further, friction test were conducted on not only paint materials but also 8 kinds of plastic materials.

## 2-2 TEST RESULTS AND EVALUATIONS

Test results for paint, unpainted steel and plastics are shown in Table 2, while an extraction of the results for the first two is given in Fig. 2. The friction coefficient of ice-resistant paint was found to be only about 50% to 75% of that of conventional paint. On the other hand, unpainted steel, with a surface roughness of about 100  $\mu\text{m}$ , exhibits breakaway and static friction coefficients of nearly 5 to 8 times of ice-resistant paint. If the surface roughness of bared steel plate increases due to corrosion, increase of the friction coefficients is expected. Based on these results, it was confirmed that the protection of the hull from corrosion and the keeping of a smooth surface provided by the application of ice-resistant paint contribute noticeably to the reduction of friction resistance to ice.

Furthermore, the relationship between the friction coefficient and the surface properties of the paint film (surface roughness, hardness and contact angle with water) was considered. Multiple regression (index regression) analysis was made in accordance with the following formula (1).

$$\mu = A \cdot R^a \cdot H^b \cdot \theta^c \quad \dots (1)$$

where,

|   |  |
|---|--|
| A   | : Constant   |
| $\mu$ ( $\mu\text{B}$ , $\mu\text{S}$ , $\mu\text{K}$ ) | : Breakaway, Static and Kinetic friction coefficient |
| R   | : Surface roughness (10 point height)                |
| H   | : Knoop hardness                                     |
| $\theta$  | : Angle of contact with distilled water              |

The results are shown in Table 3. The relationship between friction coefficient and surface properties is shown in Fig. 3. It may be

seen from Fig. 3 and Table 3 that the friction coefficient of the hull against ice becomes smaller if the surface roughness is lower, if the hardness and contact angles become large, and if the hydrophobicity becomes high. In other words, when attention is paid to friction reduction, desirable ice-resistant paints are those which provide a smooth surface (not more than  $5 \mu\text{m}$  of 10 point height), hardness exceeding Knoop Hardness Number 4, and high hydrophobicity (exceeding 90 degree contact angle). Based on these surface properties, the friction properties of a paint film can be evaluated.

Table. 1 The paint tested

| No. | Type                    | Main component           | Coating method          |
|-----|-------------------------|--------------------------|-------------------------|
| 1   | Ice-resistant paint     | Nonsolvent type epoxy    | Dual flow airless spray |
| 2   |                         | Epoxy                    | Airless spray           |
| 3   |                         | "                        | "                       |
| 4   |                         | "                        | "                       |
| 5   |                         | "                        | "                       |
| 6   |                         | Nonsolvent type urethane | Dual flow airless spray |
| 7   |                         | Urethane                 | Airless spray           |
| 8   | Mastic type paint       | Epoxy glassflake         | Special air spray       |
| 9   |                         | Polyester glassflake     | Airless spray           |
| 10  |                         | "                        | "                       |
| 11  | Conventional hull paint | Epoxy                    | "                       |
| 12  |                         | Coal tar epoxy           | "                       |

Table. 3 Results of multiple regression analysis.

|               | a      | b       | c               |
|---------------|--------|---------|-----------------|
| $\mu\text{B}$ | 0.177* | -0.132  | -0.130          |
| $\mu\text{S}$ | 0.080  | -0.107  | -0.156 $\Delta$ |
| $\mu\text{K}$ | 0.073* | -0.077* | -0.144**        |

Error rate :  $\Delta$  10%, \* 5%, \*\* 1%

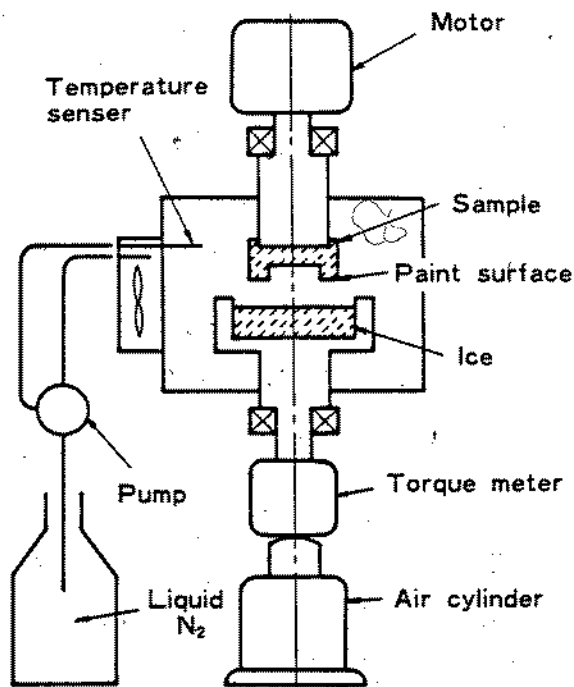


Fig. 1 Ice friction test apparatus

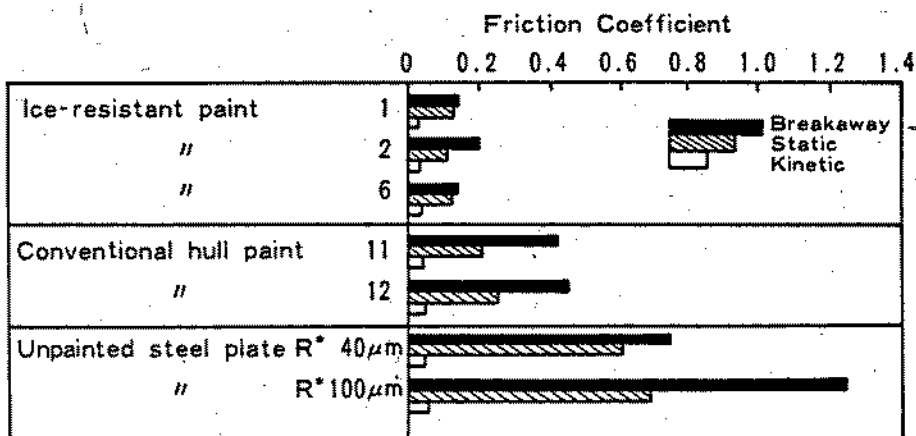


Fig. 2 Friction coefficient of coatings

• R: Surface roughness (Defined by 10 points height)

\* Table. 2 Results of ice friction test

| Type                    | No.                               | Friction coefficient |        |         | Surface roughness $\mu\text{m}$ | Knoop hardness | Contact angle degree |
|-------------------------|-----------------------------------|----------------------|--------|---------|---------------------------------|----------------|----------------------|
|                         |                                   | Breakaway            | Static | Kinetic |                                 |                |                      |
| Ice resistant paint     | 1                                 | 0.141                | 0.130  | 0.027   | 1.0                             | 4.05           | 64                   |
|                         | 2                                 | 0.211                | 0.079  | 0.033   | 1.0                             | 5.02           | 63                   |
|                         | 4                                 | 0.221                | 0.120  | 0.027   | 1.5                             | 8.62           | 62                   |
|                         | 5                                 | 0.327                | 0.156  | 0.027   | 14.5                            | 11.20          | 44                   |
|                         | 6                                 | 0.199                | 0.110  | 0.028   | 1.8                             | 3.80           | 102                  |
|                         | 7                                 | 0.562                | 0.342  | 0.039   | 13.8                            | 0.30           | 84                   |
|                         | 10                                | 0.404                | 0.252  | 0.030   | 15.3                            | 0.88           | 86                   |
| Conventional hull paint | 11                                | 0.422                | 0.207  | 0.043   | 23.0                            | 3.67           | 72                   |
|                         | 12                                | 0.448                | 0.250  | 0.041   | 17.5                            | 1.93           | 63                   |
| Unpainted steel plate   |                                   | 0.534                | 0.434  | 0.033   | 39.2                            | 614.4          | 62                   |
|                         |                                   | 0.740                | 0.602  | 0.042   | 59.6                            |                |                      |
|                         |                                   | 1.247                | 0.680  | 0.048   | 99.1                            |                |                      |
| Polyacetal              |                                   | 0.123                | 0.084  | 0.027   | 3.0                             | 23.21          | 83                   |
|                         |                                   | 0.367                | 0.154  | 0.037   | 37.4                            |                |                      |
| 6-6 Nylon               |                                   | 0.212                | 0.103  | 0.025   | 3.0                             | 12.41          | 64                   |
|                         |                                   | 0.453                | 0.176  | 0.041   | 38.9                            |                |                      |
| Polyethylene            |                                   | 0.230                | 0.112  | 0.029   | 3.3                             | 10.70          | 95                   |
|                         |                                   | 0.561                | 0.217  | 0.032   | 57.3                            |                |                      |
| Polypropylene           |                                   | 0.225                | 0.144  | 0.033   | 6.1                             | 5.84           | 85                   |
|                         |                                   | 0.335                | 0.158  | 0.045   | 31.0                            |                |                      |
| Plastic                 | Ultra high molecular polyethylene | 0.132                | 0.084  | 0.026   | 9.9                             | 5.20           | 96                   |
|                         |                                   | 0.251                | 0.079  | 0.042   | 45.5                            |                |                      |
|                         | 6 Nylon                           | 0.094                | 0.073  | 0.037   | 10.4                            | 4.89           | 58                   |
| Teflon                  |                                   | 0.191                | 0.089  | 0.041   | 54.3                            | 2.86           | 108                  |
|                         |                                   | 0.073                | 0.063  | 0.028   | 8.5                             |                |                      |
| Polyurethane rubber     |                                   | 0.204                | 0.079  | 0.034   | 48.0                            | 0.32           | 84                   |
|                         |                                   | 0.457                | 0.141  | 0.050   | 16.8                            |                |                      |
|                         |                                   | 0.532                | 0.193  | 0.053   | 34.9                            |                |                      |

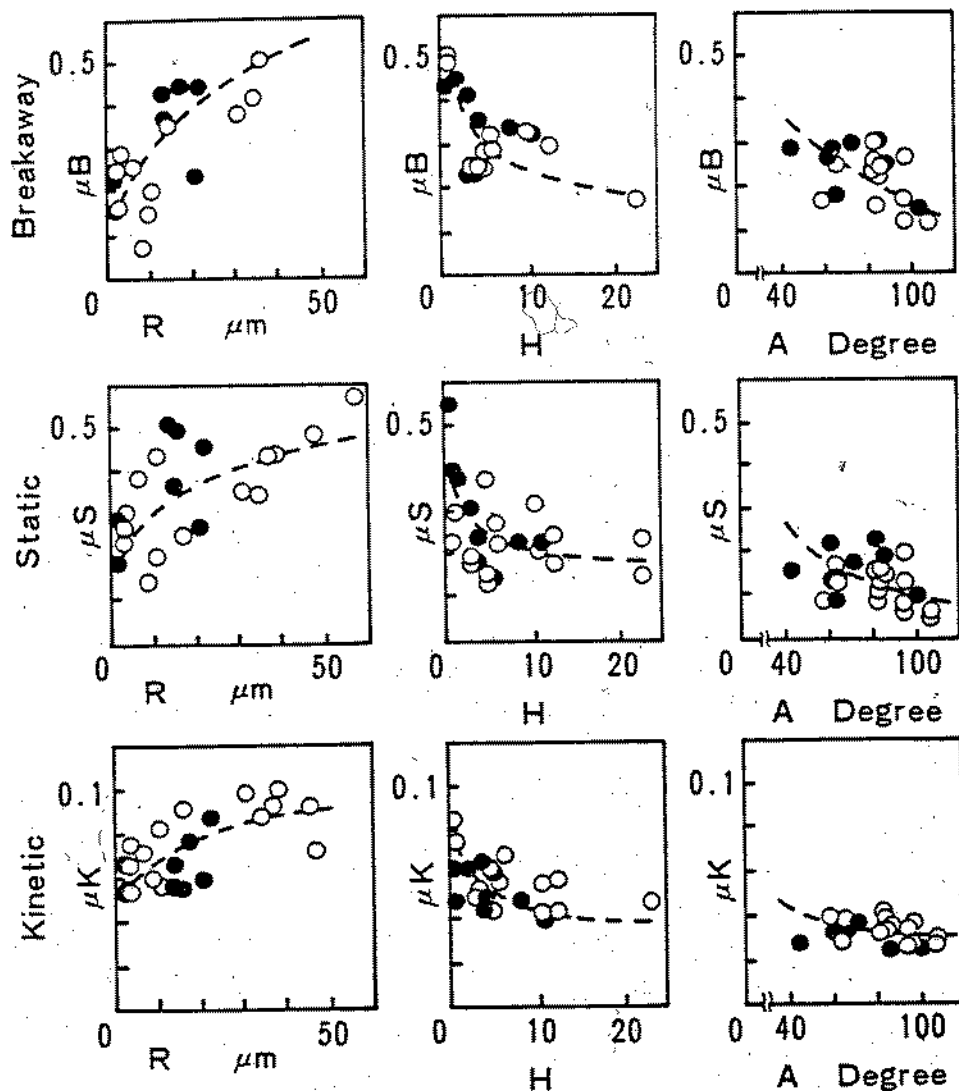


Fig. 3 The relationship between friction coefficients and surface properties

Friction coefficient  
 $R$  : Surface roughness       $\mu_B$  : Breakaway  
 $H$  : Knoop hardness         $\mu_S$  : Static  
 $A$  : Contact angle             $\mu_K$  : Kinetic

● Paint      ○ Plastic

Broken Line : Calculated from regression formula

### 3. ICE-RELEASE TEST

#### 3-1 TEST METHOD

The adhesive strength of ice on the paint film was measured by a tensile tester. As shown in Fig. 4, distilled water was frozen in a stainless cylinder with 30mm outer diameter resting on a paint film. The adhesive strength was then measured by pulling the stainless cylinder vertically from the surface of the paint film at a strain rate of 1 mm/min. and at a temperature of -20°C.

#### 3-2 TEST RESULTS AND EVALUATIONS

The adhesive strength of ice both to the paint film and to unpainted steel is shown in Fig. 5. The adhesion strength of ice to the ice-resistant paint surface is 1/2-1/3 lower than that of unpainted steel, and is 2/3 lower than that of the conventional paint. Thus, the ice releasing effects of ice-resistant paint can generally be seen.

According to the test results on unpainted steel, as the surface roughness increases, ice adhesion strength also increases. Of all the ice resistant paints shown in Fig. 5, No.5 has the greatest surface roughness and consequently exhibits the highest ice adhesion strength.

Furthermore, the relationship between ice adhesion strength and contact angles both of paint and plastic materials with distilled water (or hydrophobicity) is shown in Fig. 6. It has been confirmed that, the adhesion strength of ice decreases, as contact angles increase causing an increase in hydrophobicity. This means that, the paint film surface releases ice more effectively by repelling water better. As these results, it will be concluded that desirable ice-resistant paints to prevent icing are those which provide smooth roughness and high hydrophobicity.

### 4. ABRASION TEST

Several full scale tests have been made with respect to the abrasion of the painted film on steel in ice-friction. In these tests, coatings were applied to the bottom of ice-breakers so that the effects of abrasion could be observed after the service in frozen sea. Though these tests (under actual conditions) were proved to be very reliable, they are quite time consuming. Thus, development of laboratory tests which will simulate the deterioration behavior of paint films on ships during navigation in frozen sea is strongly required.

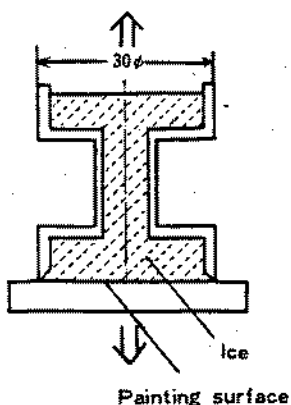


Fig. 4 Ice adhesion strength measuring apparatus

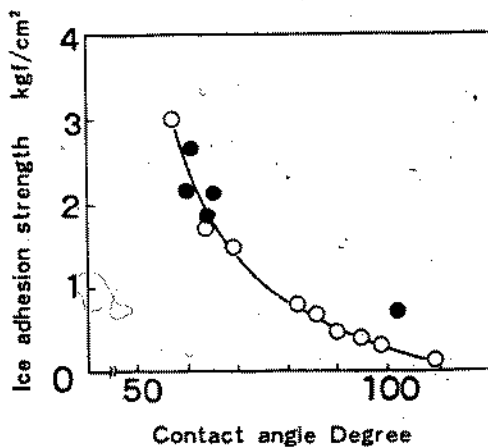


Fig. 6 Ice adhesion strength vs. contact angle

● Paint ○ Plastic

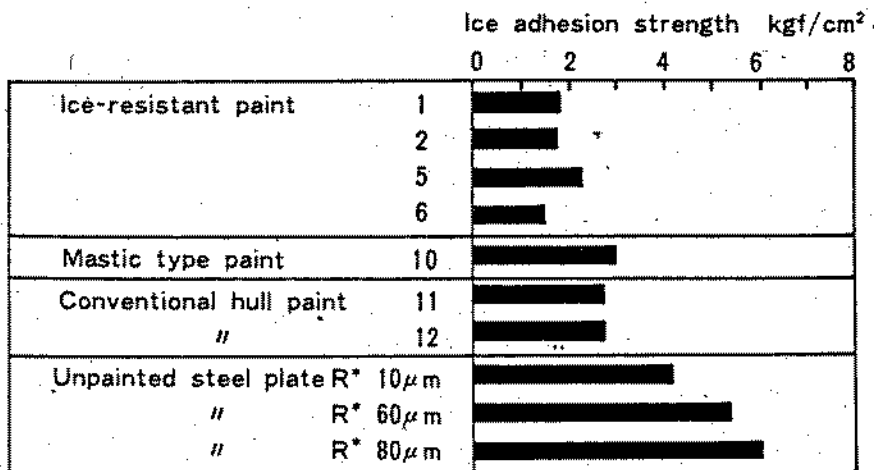


Fig. 5 Ice adhesion strength of coatings

• R : Surface roughness (Defined by 10 points height)

#### 4-1 TEST METHOD

The abrasion test apparatus is shown in Fig. 7. Test samples were steel pipes, with the outer painted surfaces. Ice was pressed against the side of the samples at a surface pressure of 13 - 65 kgf/cm<sup>2</sup>. The samples were rotated at a speed of 10 cm/sec and at an ice temperature of -20°C. The abrasion behavior of the films was periodically observed.

#### 4-2 TEST RESULTS AND EVALUATIONS

After a test period of six hours, several samples were damaged, making it possible to evaluate abrasion resistance. The test results are shown in Table 4. As shown in the table, ice-resistant paint is generally superior to conventional paint. A typical surface appearance is shown in Photo 1. Test results for the deterioration behavior of test samples show that film thickness does not decrease gradually, but that the microscopic area of the film peels off, followed by the expansion of the peeled portion. This deterioration behavior is quite consistent with the behavior of paint films observed in full-scale performance tests under actual conditions.

Film abrasion behavior can be explained as follows. Firstly, minor defects occur on film surfaces. These defects include not only the mechanical damage caused by sharp angled ice masses or other floating objects, but also, due to the intrinsic nature of the film itself, such as holidays. These defective portions, because of the thin film, tend to have greater water permeability and oxygen permeability as compared to other sound part. Thus, the adhesion strength of the film in these portions decreases in short period, and these tend to peel from substratum. Since these defects are generally concave, the compressed ice is liable to deform into it. So the defective area may easily expand due to the moving ice. It was possible to confirm this kind of behavior from the occurrence of peeling in the notched samples and from the fact that after dipping in saline water the blistered film easily peeled off.

On the other hand, abrasion resistance and adhesion strength are shown in Table 4. From this table, it can be concluded that the abrasion resistance of samples has relation with the adhesion strength.

### 5. FULL-SCALE PERFORMANCE TEST

#### 5-1 TEST METHOD

During each of the "Fuji" five Antarctic voyages, carried out from July 1978 to May 1983, full-scale tests were carried out on a 400 m<sup>2</sup> area of the bottom. After each voyage, film deterioration was investigated, and film thickness and surface roughness were measured. Fig. 8 shows the test area, which extended from the bottom of the bow, along the draft line.



Table. 4 Results of ice abrasion test

| No. | Type                    | Paint film after dipping in brine |                                       | Paint film after abrasion test |
|-----|-------------------------|-----------------------------------|---------------------------------------|--------------------------------|
|     |                         | Appearance of paint film          | Adhesion strength kgf/cm <sup>2</sup> |                                |
| 1   |                         | no damage                         | 28 - 40                               | no damage                      |
| 2   |                         | no damage                         | 21 - 29                               | no damage                      |
| 3   |                         | blisters on whole surface         | 5 - 8                                 | totally peeled off             |
| 4   | Ice-resistant paint     | blisters on whole surface         | 6 - 11                                | 70% peeled off                 |
| 5   |                         | several blisters                  | 10 - 18                               | 10% peeled off                 |
| 6   |                         | no damage                         | 18 - 34                               | no damage                      |
| 7   |                         | no damage                         | 3 - 10                                | totalled peeled off            |
| 10  | Mastic type paint       | no damage                         | 6 - 11                                | convex surface worn            |
| 11  | Conventional hull paint | blisters on whole surface         | 10 - 17                               | 30% peeled off                 |
| 12  |                         | several blisters                  | 14 - 22                               | 40% peeled off                 |

## 5-2 TEST RESULTS AND EVALUATIONS

The results on visual observation of paint films are shown in Table 5. Measurement results of film thickness are shown in Fig. 9. An example of the deterioration of the paint film after a voyage to the Antarctic is shown in Photo 2. It appears that the forward areas suffered more severe damage than the midship areas. Also, the paint film slightly below the draft line showed more severe damage than other areas. Most of the paints sampled showed deterioration of the film, indicating that damaged areas become larger as time elapses. The two kinds of film deterioration observed were peeling and rusting. Numerous minor cracks were noticed through observation of rusting. Thus, two kinds of deterioration are considered to occur consecutively and seem to be closely related. In any case, no tendency of gradual decrease of film thickness was noticed. Both minor cracking and minor peeling occurred in the film were gradually becoming larger. These results were satisfactorily consistent with those of abrasion tests. Nonsolvent type epoxy based ice-resistant paint showed to be superior in resistance. It was also confirmed that conventional paint films peeled and rusted in many areas within a short period of time.

## 6. PROCEDURES FOR APPLICATION OF ICE-RESISTANT PAINT

Test results for various ice-resistant paints show that paint with a superior performance tends to be a nonsolvent type. Since they must be applied almost immediately after mixing (they have a very short pot life), an ordinary painting applicator cannot be used. The applicator should be of the dual flow type, allowing the basic component and hardener to be sent at a required ratio to the mixer located near the spray gun. Also, since ice-resistant paints have a higher viscosity than that of other types of paint at ambient temperature and are thus harder to atomize, they should be heated to decrease their viscosity before spraying.

Since paint film performance greatly depends on both the mixing ratio of the basic component and hardener and the mixing function of the mixer. Only mixing ratio errors of up to  $\pm 5\%$  are allowable. Any errors beyond these limits may adversely affect film performance. Also, it is necessary to use mixers with division layers (an index showing mixing function) of more than 1000. Using the applicators which has allowable errors in the mixing ratio and mixers with enough division layers, the specified film performance can be obtained.

## 7. CONCLUSION

The above covers the performance of ice-resistant paints, and the summary of results detained in as follows.

- (1) A test method was established for friction property evaluation. The ice-resistant paint film greatly contributes to decrease of forces due to friction. Friction decreasing effects are greatly varied by paint surface roughness, hardness, and hydrophobicity. In other words, paint film with a smooth surface, adequate hardness and hydrophobicity is effective in reducing friction.
- (2) Effects of prevention icing are clearly related to hydrophobicity of paint film surface, and ice-resistant paint is extremely effective in preventing icing.
- (3) The durability of ice-resistant paint was confirmed through actual ship tests of five years.
- (4) As for abrasion resistant property, evaluation test method was also established. By using the ice abrasion test apparatus, the abrasion resistance of various paint films could be evaluated in the laboratory, and correlation with actual ship tests were confirmed. The paint film deterioration behavior was observed as a process, that was not gradually losing of paint film thickness due to ice-abrasion but gradual development of film defects, which were initially existed in the micro portion of paint surface.
- (5) In case of applying nonsolvent type ice-resistant paint, the dual flow type applicator, the special coating machine, has to be used. About the performance of coating machine, the terms to be accepted for making effective paint films are clarified.

## 8. REFERENCES

- (1) Narita, S. and Ishibashi, Y.: Model Tests of Twin-screw Icebreaker Hull Forms in Ice Model Basin, Nippon Kokan Technical Report No.83 (1979).
- (2) Tsushima, K.: Friction Measurement of Sea Ice on Flat Plates of Metals, Plastics and Coatings, FOAC '79 (1979)
- (3) Calabrese, S. et al: Low Friction Coatings for Icebreakers, Coast Guard report CG-D-107-74 (1974), CG-D-32-76 (1976), CG-D-69-78 (1978)
- (4) Makinen, E. et al: Influence of Friction on Ice Resistance, Ice Tech. 75 (1975)
- (5) Takeuchi, M.: Shear Experiment on Ice Adhered to Road Surface, Seppyo, Vol.35, No.3 (1973)
- (6) Jellinek, H.: Ice Releasing Block Copolymer Coatings, Colloid & Polymer Sci., No.256 (1975)

Table. 5 Appearance of paint film after Antarctic voyage

| No. | Type                    | Number of voyages | Appearance of paint film    |
|-----|-------------------------|-------------------|-----------------------------|
| 1   | Ice-resistant paint     | 1                 | no damage                   |
|     |                         | 3                 | 5% peeled off               |
|     |                         | 5                 | 30% peeled off              |
| 2   |                         | 2                 | 10% peeled off              |
|     |                         | 4                 | 70% peeled off              |
| 3   |                         | 1                 | totally peeled off          |
|     |                         | 2                 | 10% peeled off              |
| 5   | 4                       | 60% peeled off    |                             |
| 6   |                         | 1                 | no damage                   |
| 7   |                         | 1                 | totally peeled off          |
| 8   | Mastic type paint       | 1                 | 5% peeled off, 40% rusting  |
| 9   |                         | 1                 | 15% peeled off, 30% rusting |
| 10  |                         | 1                 | 20% peeled off              |
| 11  | Conventional hull paint | 1                 | 40% peeled off              |
| 12  |                         | 1                 | 50% peeled off              |

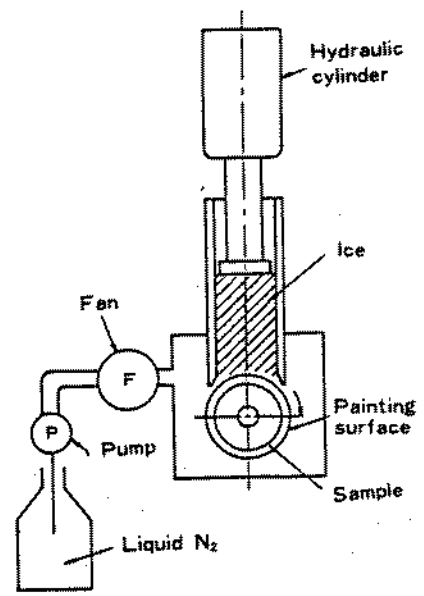


Fig. 7 Ice abrasion test apparatus



Photo. 1 Typical surface appearance after ice abrasion test

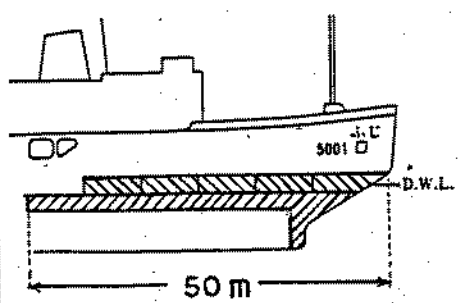


Fig. 8 Test area of ice-breaker "Fuji"

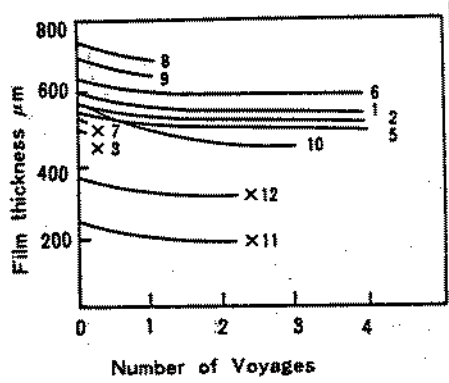
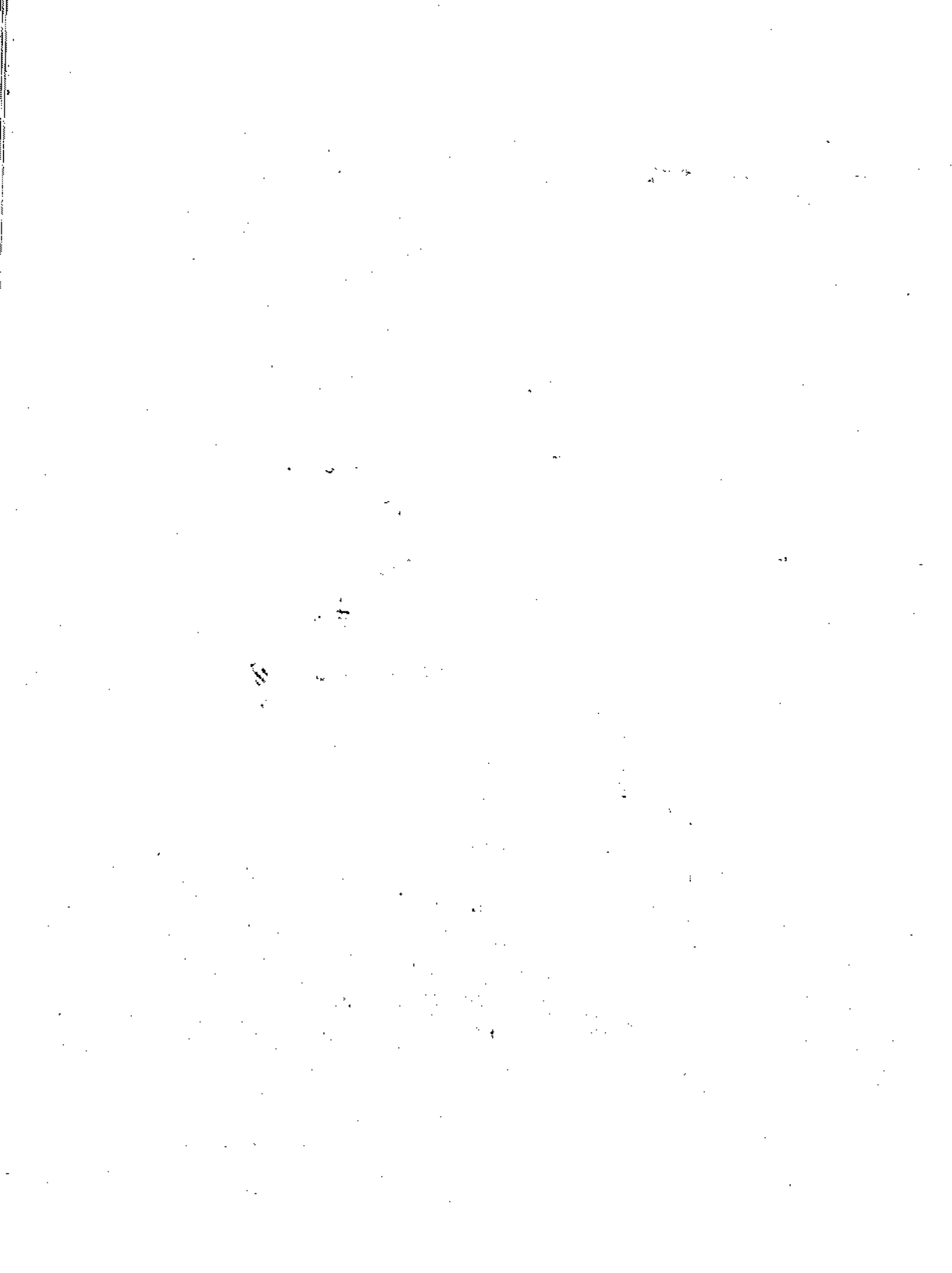


Fig. 9 Film thickness after Antarctic voyage

X --- Totally worn out

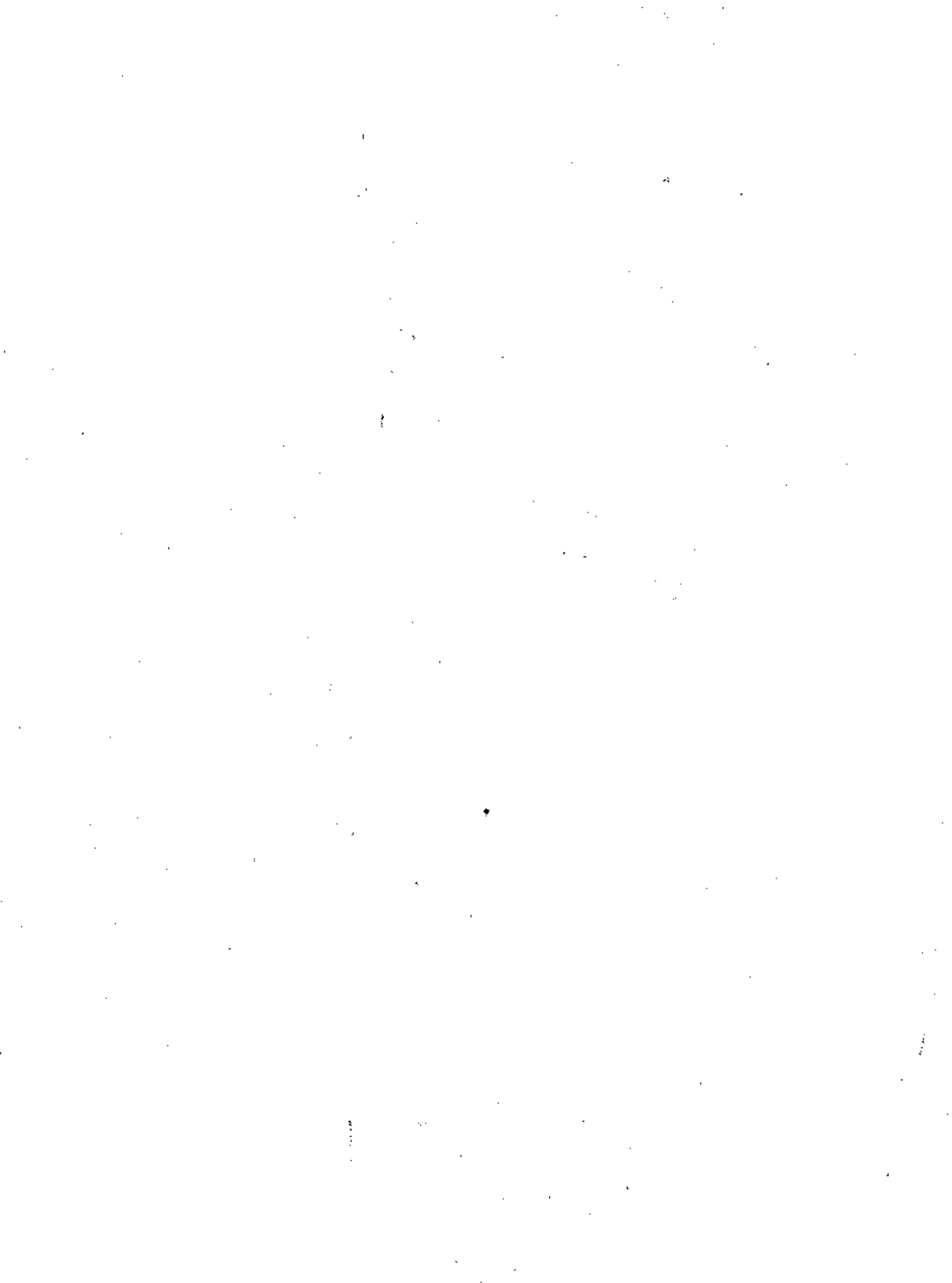


Photo. 2 Typical appearance of ice-breaker "Fuji" after Antarctic voyage



COATINGS  
PEINTURES







## NEW ANTICORROSIVE PAINTS \*

Th. N. SKOULIKIDIS and P. VASSILIOU

National Technical University of Athens, Laboratory of Physical Chemistry and Applied Electrochemistry, Athens-106 82, GREECE

ABSTRACT

A new type of anticorrosive paint has been produced where the pigment is not a sacrificial metal less noble than the protected substrate or paint with dipole molecules or with great electrical resistance, but pigments metal oxides with intense n-semiconductor properties. These pigments by offering electrons to the protected substrate metal protect it much longer than the usual practice. The n-semiconductor properties are given by preparing metal oxide pigments with anodic oxidation. The tests have been carried out in a laboratory scale employing the weight loss method rather than electrical measurements that have been proved unreliable.

RESUME

Un nouveau type des peintures anticorrosives a été produit où le pigment n'est pas un metal sacrifié moins noble que le metal pour protection ou peinture avec des molecules dipoles ou avec une grande résistance électrique, mais pigments oxydes des metaux avec des propriétés intenses n-semiconductrices imposées. Ces pigments en offrant les électrons au metal le protègent plus longtemps que la pratique d'aujourd'hui avec d'autres types des peintures. Les propriétés n-semiconductrices sont imposées en préparant comme pigments les oxydes des metaux avec oxydation anodique sous des con-

\*Patent No 67384/3-7-81

## NEW ANTICORROSIVE PAINTS

ditions appropriées. Les essais ont été faites au laboratoire en employant la méthode de la perte de poids et pas par des mesures électriques qui sont prouvées non-reliable.

INTRODUCTION

As it is known the effective factor in the anticorrosive paints are the properties of the pigments in the polymeric support. The pigments act either as electron donor [sacrificial Zinc (Zinc Rich Epoxy), Aluminum of Magnesium powders] or by the polarity of their molecules and the electrical resistance of the system (Coal Tar Epoxy), or only by the electrical resistance of the system (Chlorinated Rubber). It is obvious that the more effective system is the electron donor system which is a type of cathodic protection. On the other hand it is known that the passivation of the metals is due to the n-semiconductor properties of their corrosion products (mainly oxides). Combining the two above mentioned facts we thought of preparing pigments of metal oxides (some of them are already used for this purpose) with pronounced n-semiconducting properties. To accomplish this we employed preparation conditions for these oxides that in previous works of ours were found to offer intense catalytic n-semiconductor properties, that is by anodic oxidation of powder metals such as  $Al_2O_3$ ,  $ZnO$ ,  $Fe_2O_3$ . These oxides were prepared under different density and preparation time and were mixed with the epoxy support and were tested as protective coating for mild steel in artificial sea water at  $30^\circ C$  for two months in comparison with bare specimens and Zinc Epoxy (90% Zinc powder) coated specimens.

The measure of corrosion was the weight loss because it was found that the electrochemical prediction of corrosion compared to the weight loss results is wrong.

Thus the anticorrosive properties of the pigments were optimized.

It was found that the best anticorrosion behaviour was shown by the Zn powder oxidized by a current density of  $1.5A/dm^2$ , for 90 min at  $28^\circ C$  and with a content of 30% in the epoxy vehicle; it shows the same protection as Z. R.E. (90%).

The use of these pigments has the following advantages:

- long term protection compared to the 90% Zinc epoxy commercial paint, due to the sacrifice of the Zinc powder during protection for the latter.

## NEW ANTICORROSIVE PAINTS

### 1. EXPERIMENTAL AND RESULTS

#### 1.1. Materials, Shape and Dimensions of Specimens

The steel specimens  $5 \times 7 \text{ cm}^2$  were cut from steel sheet of thickness 0.25mm. The steel conformed to the following nominal composition in wt-%: Fe 99.28; C 0.12; Mn 0.5; S 0.05; P 0.05.

As corroding medium a static bath of 3.5% NaCl solution, thermostated at  $30^\circ\text{C}$  by a circulating thermostat was used for a period of two months.

The paint vehicle was epoxy resin and the following pigments at different concentrations in wt-% were used:  $\text{ZnO}$ ,  $\text{Fe}_2\text{O}_3$ ,  $\text{Fe}_3\text{O}_4$  and  $\text{ZnO}$  on Zn powder. The powdered oxides and the metal powder were analytical reagents.

The specimens cleaned, weighed and marked were painted by brush and the average thickness of the dry epoxy coating was  $70 \mu\text{m}$ . A painter's holiday was always left on each specimen.

Ten specimens were used for each experiment to ensure reproducibility of the measurements.

The electrical measurements taken were V-t (potential-time) and V-i (potentiostatic polarization) using a SCE (Saturated Calomel Electrode) as a reference electrode.

One of these specimens were connected to a potential recorder that recorded continuously the potential for the span of the two months that the experiment lasted. The V-i experiments were made by a potentiostat at  $30^\circ\text{C}$  with a stepwise procedure. At the end of the 60 days the specimens were removed, washed with water, left in the thinner of the resin and the paint removed by a ple-xiglass tool, the oxides removed by inhibited hydrochloric acid, washed with water, alcohol, acetone and dried. The specimens were weighed for the weight loss experiment that lasted two months (60 days).

### 2. RESULTS

#### 2.1. Weight-loss Measurements

The weight loss measurements are shown in the following table (Table 1).

#### 2.2. V-t Measurements

The electrical measurements V-t for the above experiments are shown in Fig. 1.

## NEW ANTICORROSIVE PAINTS

TABLE 1  
Weight loss in g of metal specimens after  
2 month immersion in 3.5% NaCl at 30°C

|         | Blank spec. | Blank with epoxy coating |
|---------|-------------|--------------------------|
| 1       | 0.8631      | 0.3665                   |
| 2       | 0.6567      | 0.3079                   |
| 3       | 1.1863      | 0.3567                   |
| 4       | 0.8466      | 0.3309                   |
| 5       | 0.8747      | 0.2419                   |
| 6       | 0.6342      | 0.3163                   |
| 7       | 1.3702      | 0.3313                   |
| 8       | 1.3346      | 0.4372                   |
| 9       | 2.1098*     | 0.3961                   |
| 10      | 1.2177      | 0.3532                   |
| Average | 0.9982      | 0.3438                   |
| St.Dev. | ±0.0940     | ±0.0527                  |

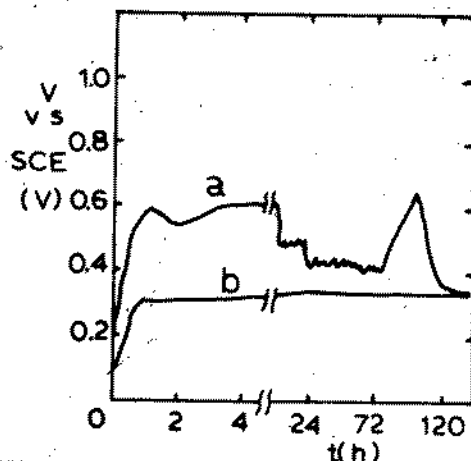


Fig.1. V-t diagram for steel specimens at 30°C in 3.5% BaCl solution: a. Epoxy coated; b. Bare steel specimens.

\*On this specimen V-t measurements were taken for 2 months.

## NEW ANTICORROSIVE PAINTS

2.3. V-i Measurements

The V-i measurements of the specimens are shown in Fig. 2.

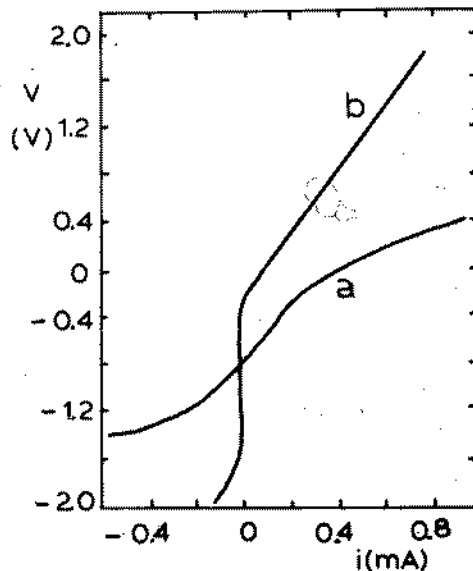


Fig.2. V-i diagram for steel specimens at 30°C in 3.5% NaCl solution:  
a. Bare, b. Epoxy coated specimens.

The weight loss measurements for a pigment concentration in the paint of 30% are shown in the following table (Table 2).

The V-t measurements are shown in Fig. 3.

The V-i measurements are shown in Fig. 4.

## NEW ANTICORROSIVE PAINTS

TABLE 2  
Weight loss in g or painted steel specimens after 2  
month immersion in 3.5% NaCl solution, at 30°C

|         | 30% Fe <sub>2</sub> O <sub>3</sub> | Fe <sub>3</sub> O <sub>4</sub> |
|---------|------------------------------------|--------------------------------|
| 1       | 0.4291                             | 0.1034                         |
| 2       | 0.4594                             | 0.1078                         |
| 3       | 0.5096                             | 0.0964                         |
| 4       | 0.4375                             | 0.0843                         |
| 5       | 0.4888                             | 0.0800                         |
| 6       | 0.3624                             | 0.0962                         |
| 7       | 0.3236                             | 0.0948                         |
| 8       | 0.2466                             | 0.0939                         |
| 9       | 0.3951                             | 0.1324*                        |
| 10      | 0.3823                             | 0.0918                         |
| Average | 0.4034                             | 0.0942                         |
| St.Dev. | ±0.0793                            | ±0.0085                        |
| Protec. | 50%                                | 90.5%                          |
|         | Al <sub>2</sub> O <sub>3</sub>     | ZnO                            |
| 1       | 0.1823                             | 0.2795                         |
| 2       | 0.1872                             | 0.2703                         |
| 3       | 0.1788                             | 0.2458                         |
| 4       | 0.1768                             | 0.2638                         |
| 5       | 0.1583                             | 0.2508                         |
| 6       | 0.1761                             | 0.2355                         |
| 7       | 0.2189                             | 0.2158                         |
| 8       | 0.2017                             | 0.2742                         |
| 9       | 0.5695*                            | 0.2236                         |
| 10      | 0.1493                             | 0.2136                         |
| Average | 0.1810                             | 0.2473                         |
| St.Dev. | ±0.0208                            | ±0.0245                        |
| Protec. | 81.2%                              | 75.2%                          |

\*On this specimen V-t measurements were taken for 2 months.

## NEW ANTICORROSIVE PAINTS

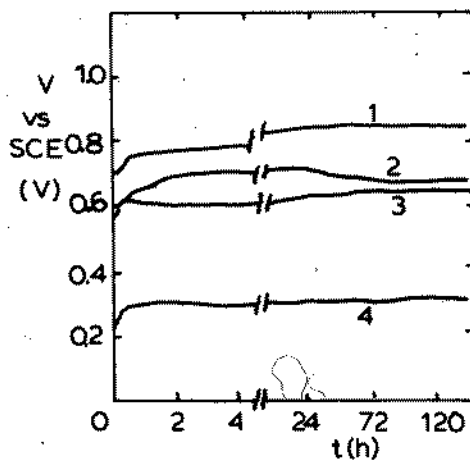


Fig. 3. V-t diagram of steel specimens painted with epoxy paint and 30% pigments:  
1:  $\text{Fe}_3\text{O}_4$ , 2:  $\text{Al}_2\text{O}_3$ , 3:  $\text{ZnO}$ , 4:  $\text{Fe}_2\text{O}_3$ .

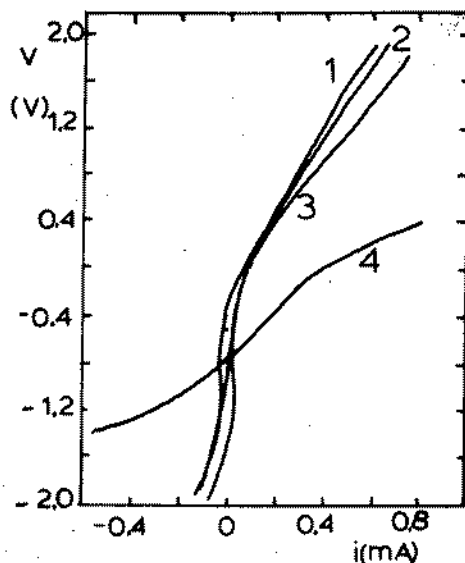


Fig. 4. V-i diagram of steel specimens painted with epoxy paint and 30% pigments:  
1:  $\text{ZnO}$ , 2:  $\text{Al}_2\text{O}_3$ , 3: epoxy paint,  
4: bare.

## NEW ANTICORROSIVE PAINTS

The results of weight loss for Zn powder at 30% wt-% in the epoxy are shown in table 3 compared to the ones with 90% concentration.

TABLE 3

Weight loss in g after 2 month immersion  
in 3.5% NaCl solution at 30°C

|          | Zn 30%  | Zn 90%  |
|----------|---------|---------|
| 1        | 0.0587  | 0.1388  |
| 2        | 0.0630  | 0.2233  |
| 3        | 0.0539  | 0.2040  |
| 4        | 0.0375  | 0.1866  |
| 5        | 0.0767  | 0.1927  |
| 6        | 0.0488  | 0.2401  |
| 7        | 0.0427  | 0.2961  |
| 8        | 0.0582  | 0.1376  |
| 9        | 0.0524  | 0.1357  |
| 10       | 0.0264  | 0.1455  |
| Average  | 0.0518  | 0.1900  |
| St.Dev.  | ±0.0140 | ±0.0531 |
| Protect. | 95%     | 80.9%   |

The weight loss results from the oxidized Zn powder under anodic oxidation conditions (1.5 A/dm<sup>2</sup>) are shown in the following diagram (Fig. 5) compared to ZnO, to Zn(m) 30% bare and the plain epoxy coated specimens.



## NEW ANTICORROSIVE PAINTS

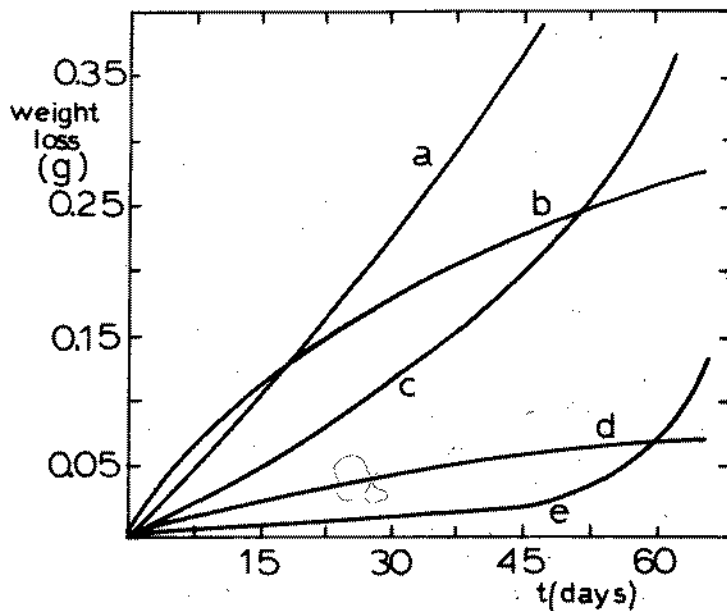


Fig.5. Corrosion rate of steel specimens in 3.5% NaCl solution at 30°C painted with ZnO, Zn and ZnO<sub>elect</sub>. compared to corrosion rates of bare metal and epoxy coated metal.

a. bare metal, b. 30% ZnO, c. epoxy coated, d. 30% electrolytically prepared ZnO, e. 30% Zn<sub>metal</sub>.

### 3. DISCUSSION

If we assume that changes in corrosion rate are chiefly due to changes in anodic polarization, so that a more noble corrosion potential indicates a lower corrosion rate (C) from the measurements of the potential of the blank or painted specimens as a function of time (Figs 1, 3) we can conclude that the corrosion rates are of the following order:

(Fig. 1)  $C_{\text{corrosion blank}} \equiv C_{\text{epoxy painted}}$

(Fig. 3)  $C_{\text{Fe}_2\text{O}_3} > C_{\text{ZnO}} \geq C_{\text{Al}_2\text{O}_3} > C_{\text{Fe}_3\text{O}_4}$

From the V-i measurements (Figs 2,4) we can conclude:

(Fig. 2)  $C_{\text{blank}} > C_{\text{epoxy painted}}$

(Fig. 4)  $C_{\text{blank}} > C_{\text{epoxy}} \geq C_{\text{ZnO}} \equiv C_{\text{Al}_2\text{O}_3}$

But from the weight loss measurements (Tables 1,2) we

## NEW ANTICORROSIVE PAINTS

have that the order is the following:

(Table 1)  $C_{\text{blank}} > C_{\text{epoxy painted}}$

(Table 2)  $C_{\text{Fe}_2\text{O}_3} > C_{\text{ZnO}} > C_{\text{Al}_2\text{O}_3} > C_{\text{Fe}_3\text{O}_4}$

This discrepancy implies that the corrosion rate as it is resulted by electrical measurements is an ambiguous way to check the metal corrosion behaviour and the weight loss measurements is the only mean to check this behaviour. The corrosion rate is significantly affected by cathodic polarization.

In previous works (1-3) we argued that the presence of holders or powders or polymeric materials in contact to the metal affect the electric field in the neighborhood of the specimens. Also the electric measurement per se influences the corrosion rate of the specimen.

In Table 1 we see that the epoxy paint offers a slight protection to the metal.

In Table 2 we have the weight loss or protection of the metal by some typical n-semiconductor oxides employed as pigments in the paint. It is a well established fact that  $\text{Fe}_2\text{O}_3$  and  $\text{Fe}_3\text{O}_4$ ,  $\text{ZnO}$  and  $\text{Al}_2\text{O}_3$  are n-semiconductors (4) i.e. they have mobile electrons that are easily offered.

The 30% pigment concentration in the epoxy vehicle has been chosen after a series of tests where different concentrations or pigment were employed (5) to test the paint behaviour. These experiments showed a promising anticorrosion behaviour of the paint at 30% in pigment concentration.

The protection mentioned in Tables 2 and 3 is derived by the comparison of the weight loss (W.L.) of each type of painted specimen to the W.L. of bare steel. We also notice that the epoxy paint with no pigment protects the metal more than the  $\text{Fe}_2\text{O}_3$  at a 30% (wt) pigment concentration in the epoxy. This is due to a high concentration of pigment in the paint and to conditions of overprotection. A lower pigment concentration shows protection as it has been found in another work (5).

In Table 3 we see a comparison of weight loss when as pigments have been used Zn at 90% and 30% concentration. For the period of two months at 30°C the protection by the lower zinc concentration is better. After the two months it will diminish and will not protect the metal and the opposite might happen (Fig. 5).

In Fig. 5 we have a diagram where the protection of-

## NEW ANTICORROSIVE PAINTS

ferred by zinc oxidised anodically (anodic current density  $1.5A/dm^2$  in a NaOH bath at  $35^\circ C$  with platinum cathodes) at 30% pigment concentration, as a function of time i.e. its corrosion rate is shown. It is also compared to the corrosion rates of bare metal painted with epoxy, with 30% ZnO and with 30% Zn metal.

The protection of the ZnO produced on the Zn metal powder is attributed to its n-semiconductor properties, enhanced by the controlled conditions of the anodic oxidation. ZnO has very good catalytic properties (6) because of its semiconductivity properties. Thus acting as pigment it releases its mobile electrons on the surface of the metal and gives a cathodic protection on the metal. It does not act by metal dissolution, thus it can stay active much longer than the metal pigment that sacrifices itself.

This is shown in the diagram where the protection of zinc 30% at a certain time falls dramatically, the weight loss increases but the oxide protection stays almost constant since it obtains the form of corrosion regulated by a parabolic law.

### 4. CONCLUSIONS

By employing electric measurements V-t and V-i we cannot predict corrosion of steel either blank or painted with epoxy paints. A generalized explanation for these electric measurements is presented based on the disturbance of the spontaneously established electric corrosion field.

The use of weight loss measurements as a measure of corrosion is established. The especially proposed n-semiconductor metal oxides can, as pigments in the epoxy vehicle, replace the metal powders in the anticorrosive paints. The tested pigment is ZnO electrolytically prepared and its superiority consists on the fact that n-semiconductors have a facility to offer electrons and this property does not change with time, the same was that their catalytic properties by electron exchange do not alter with time, but only slightly because of fatigue. On the contrary in the zinc powder paints the metal (zinc) is sacrificed and consumed during protection.

### REFERENCES

1. Skoulikidis Th., Vassiliou P. and Symniotis E., Br. Corros. J., 14, 149 (1979).
2. Skoulikidis Th., Vassiliou P., *ibid*, 17, 142 (1982).
3. Skoulikidis Th., Vassiliou P., Balkan Chemistry Days,

## NEW ANTICORROSIVE PAINTS

- Athens, 1980.
4. Kubaschewski O., Hopkins B.: "Oxidation of Metals", Butterworths, London, 1953.
  5. Vassiliou P., Ph. D. Thesis, NTU, Athens, 1981.
  6. Krylov O.V.: "Catalysis by Non-Metals", Acad. Press, 1970.

## PERFORMANCE OF METALLIC AND NON-METALLIC COATINGS IN MARINE COASTAL ZONE IN INDIA

A.B. Samui, R.K. Banerjee, Dharendra Kumar & C.P. De  
Naval Chemical and Metallurgical Laboratory  
Tiger Gate, Ballard Estate, Bombay 400 023

### ABSTRACT

The protection of metallic structures located in coastal areas is of vital importance for technological as well as economical reasons. The behaviour of various protective systems at a particular site, depends upon severity of environmental conditions including industrial pollution. A study was undertaken at this laboratory to assess the performance of metallic and non-metallic coatings at the laboratory's exposure site located in Bombay. The place is characterised by presence of higher humidity, temperature and rainfall as well as sulphurous pollutants.

Amongst metallic coatings investigated, electroplated cadmium, sprayed zinc and aluminium afforded protection from corrosion for a period of 84 months. Coatings based on tin, nickel and chromium were found to be unsuitable for protection in view of their electrochemical nature and porosity. Passivation of the coatings generally improved their performance.

Organic coatings system comprising epoxy zinc primer and epoxy finishing grey showed protection to mild steel for a period of seventeen months. Phosphated mild steel panels protected with organic coatings were found to be free from corrosion even after a period of 84 months.

### INTRODUCTION

The tropical coastal surf zones, particularly those with high degree of atmospheric salinity and pollution, are known for inducing severe corrosion. Performance assessment of commonly used metallic as well as organic anticorrosive coatings in coastal environment has been recognised as a long felt necessity and the tropical port cities with

the growing industrialisation is a case in point. The data on exposure tests under such conditions has been published for several port cities in the literature. However, since the performance of coating differs from one environment to another, the need for generating information for important maritime cities of India has now been felt.

In order to generate data on the performance of various protective systems intended to be used in coastal locations, NCML undertook a study of exposure of metallic and organic anticorrosive coatings. This paper incorporates the observations on coating systems exposed for a period of seven years in Bombay.

## MATERIALS AND METHODS

### Exposure Site

The exposure site selected for the present study is located at a distance of about 25 kms from Bombay city, latitude 18.58°N (Figure 1). The site represents a tropical marine-cum-industrial atmosphere having appreciable amount of sulphur dioxide. The position for exposure site was chosen about 50 metres away from the sea, ensuring the direct spray of seawater on exposed systems. A summary of the meteorological conditions for the site is given in Table I.

### Metallic and non-metallic coatings :

Protective systems based on metallic and non-metallic coatings for commonly used substrate, mild steel (BS 970 EN 8) have been studied in detail. A few systems were also exposed on non-ferrous substrates such as zinc and aluminium. The observations were also made to ascertain as to what extent the phosphating of mild steel surfaces would improve the performance of organic coatings.

Metallic coatings investigated were based on their cathodic and anodic behaviour with respect to the metals. These included tin, zinc, aluminium, cadmium and copper/nickel combinations. Organic coatings based on epoxy and chlorinated rubber resins were applied on bare as well as metal coated substrates. In the present investigations, 400 specimens were exposed including bare panels of mild steel, zinc, brass and aluminium to evaluate their rate of corrosion at the site.

### Methods for application of coatings

Metallic coatings and phosphating on test specimens were prepared in consultation with the manufacturers of these products. Prior to application of coatings bare metal surfaces were degreased and pickled in suitable solutions. Zinc coated specimens were prepared by electroplating, hot-dipped galvanising and metal spraying. The coating of aluminium was applied by metal spraying. Cadmium, tin, copper, nickel and chromium were applied by electroplating.

Few of the specimens with electroplated cadmium and zinc coatings

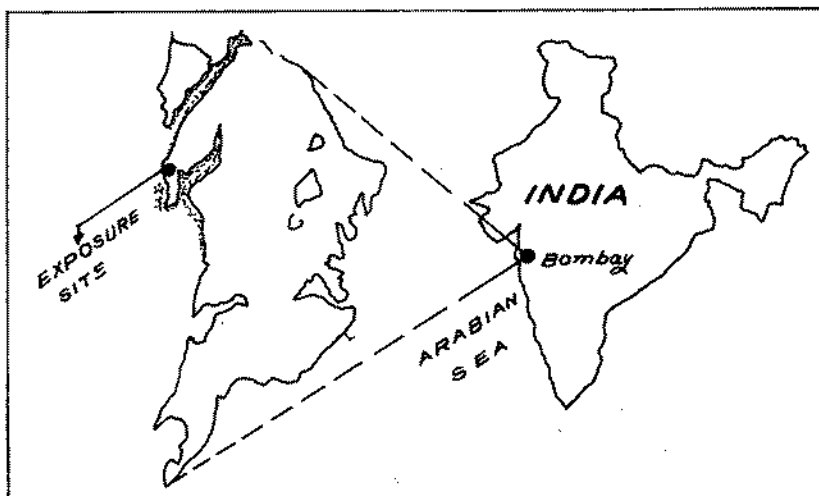


Figure 1 :  
Location of exposure site in Bombay, Latitude 18.58°N

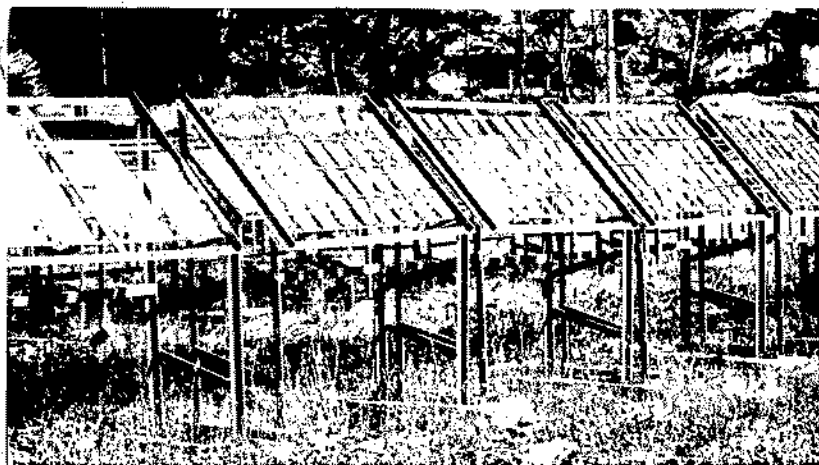


Figure 2 :  
A close view of exposure site in Bombay

were passivated by acid dichromate solutions. Passivation of electroplated tin was done in alkaline chromate solution. The mild steel surface was phosphated by dipping in dilute phosphoric acid solution of primary phosphates.

Organic coatings were applied by brushing under laboratory conditions. On metal coated steel and aluminium specimens, the surfaces were treated with a thin coat of etch primer before application of paints. The paint systems comprised of four coats including primer, undercoat and finishing coats. The thicknesses of organic and metallic coatings were measured by magnetic and B.N.F. jet respectively.

### Specimens

The size of flat panel specimens used for metallic coatings was 6"x4"x1/8" and for organic coatings was 6"x8"x1/8". Precautions were taken to ensure as even a coating as possible. Before exposure, all specimens were degreased.

### Exposure of Specimens

The specimens were secured with plastic fasteners on racks supported at an angle of 45° to horizontal, facing sea wind at a 3-5 feet above ground level. The exposure racks were fixed on galvanised and painted steel frames (Figure 2).

## METHODS OF ASSESSMENT

### Salinity and sulphur dioxide

The wet candle method employed by Ambler [1] was followed for the determination of atmospheric salt content. Sulphur dioxide was measured by lead oxide candle in Stevenson screen. The data on sulphur dioxide and salinity for one year are given in Figures 3 and 4 respectively.

### Corrosion

The performance of coated specimens were assessed by visual examination at monthly intervals, as earlier executed by Hudson [2]. No attempt was made to measure thickness of specimens on their withdrawal since the surface was generally covered with corrosion products of metallic coatings or of base metal.

The rate of corrosion suffered by bare metals was determined by measuring weight loss due to corrosion after cleaning with stripping solutions at room temperature. For mild steel, the specimens were immersed in concentrated hydrochloric acid containing 5% stannous chloride and 2% antimony trioxide. Zinc was derusted by dipping in 10% chromic acid solution. The solution used for aluminium and brass were concentrated nitric acid and 5% sulphuric acid respectively.



**Table I**  
 Meteorological data around the exposure site at Bombay

| Atmospheric conditions     | Wet period | Dry period |
|----------------------------|------------|------------|
| Relative humidity, percent | 72-82      | 55-65      |
| Temperature, °C            | 18.0-30.0  | 25.0-34.5  |
| Rainfall, mm               | 3000       | 200        |
| Total number of rainy days | 100        | 20         |

**Table II**  
 Corrosion rates of bare metals at exposure site in Bombay

| Metal      | Corrosion loss of metal<br>mg/dm <sup>2</sup> /year |
|------------|---|
| Mild steel | 5325  |
| Zinc       | 214   |
| Brass      | 65  |
| Aluminium  | 32  |

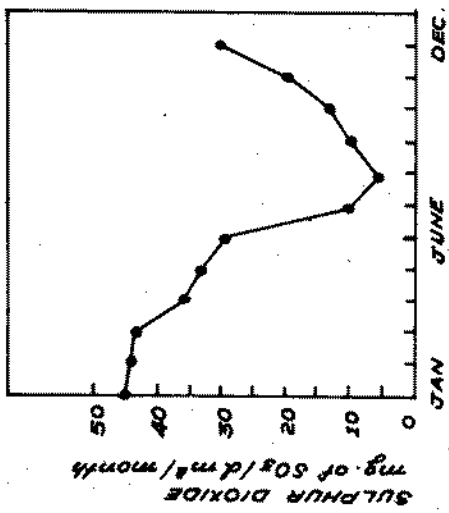


Figure 3 :  
Sulphur dioxide content in Bombay atmosphere

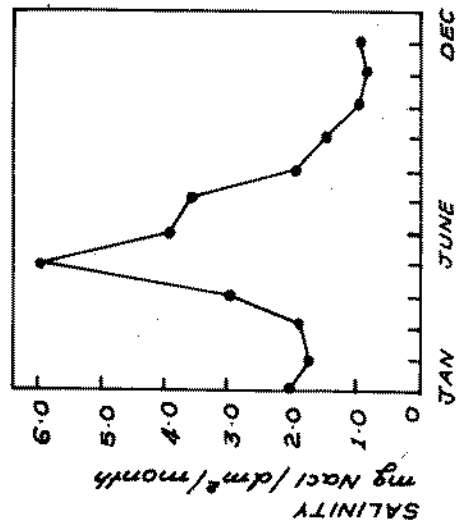


Figure 4 :  
Salinity in Bombay atmosphere

## RESULTS AND DISCUSSION

Both maximum and minimum humidity values at Bombay are higher than the critical humidity value of 70% reported to be conducive for corrosion of iron [3, 4] for nine and seven months respectively in a year. Further, there is heavy rainfall (3,000 mm per year) distributed over six months and the total number of rainy days is about 120 days. The maximum and minimum temperatures recorded are 34.5°C and 18°C respectively. The salinity of the atmosphere recorded was high (average 2.4 mg NaCl/dm<sup>2</sup>/month). The concentration of sulphur dioxide is fairly high (average 27 mg SO<sub>2</sub>/dm<sup>2</sup>/month). Strong winds prevalent at the site reduce gaseous and suspended impurities from the atmosphere accounting for lower values observed in some months. The site is, thus, characterised by heavy rain fall, high humidity, fairly high temperature and high degree of industrial sulphurous pollution favouring increased corrosion rates of metals.

### Corrosion rate of bare metals

Corrosion rates of mild steel, zinc, brass and aluminium are recorded in Table II. It is seen that rates are much higher than the values reported earlier [5]. These variations in corrosion rates of mild steel and zinc may be attributed to the severity of corrosive atmosphere. The distribution of corrosion over mild steel surface was uneven. Brass and aluminium were least corroded. The corrosion of the top surfaces directly exposed to the atmosphere was found to be higher than the other side.

### Performance of metallic coatings on mild steel

It will be seen from the results given in Table III that electroplated as well as electroplated-passivated cadmium coatings have performed very well during the exposure period of 84 months. Similar observations have also been made on specimens coated by spraying zinc and aluminium metals. The followings are the comments on the performance of each type of coatings studied.

### Zinc coatings

The mild steel surface was coated with zinc metal at varying thicknesses by employing different techniques of application. Electroplated (25 microns) and hot-dipped galvanised (100 microns) coatings have shown identical performances. Here the corrosion was observed only on the edges after a period of twelve months. The spreading rate of corrosion was very slow in both cases, covering 5% area in seventy eight months (Figure 5a). The edge corrosion evidently was due to the defects in coating and subsequent consumption of zinc giving sacrificial protection to the base metal. Passivation of electroplated zinc coating rendered no beneficial effects. No sign of corrosion of base metal sprayed with zinc (125 microns) was observed at the end of 84 months of exposure (Figure 5b). All zinc coatings, irrespective of thicknesses, have shown surface roughness due to erosion of corrosion products by wind.

**Table III**  
Performance of metallic coatings during 7 years of exposure  
in Bombay

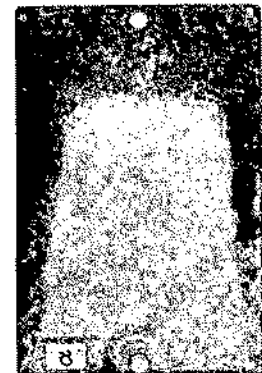
| Substrate                        | Coating                        | Thickness<br>in<br>microns | Mode of<br>application          | Observations in months   |                              |
|----------------------------------|--------------------------------|----------------------------|---------------------------------|--------------------------|------------------------------|
|                                  |                                |                            |                                 | Onset<br>of<br>corrosion | Since 5%<br>area<br>corroded |
| Mild Steel                       | Copper+<br>Nickel              | 25 + 15                    | Electroplating                  | 1                        | 1                            |
|                                  | Nickel +<br>Copper +<br>Nickel | 15+25+15                   | Electroplating                  | 1                        | 1                            |
|                                  | Tin                            | 25                         | Electroplating                  | 1                        | 1                            |
|                                  | Zinc                           | 25                         | Electroplating                  | 78                       | 84                           |
|                                  | Cadmium                        | 22                         | Electroplating                  | 84                       | 84                           |
|                                  | Tin                            | 25                         | Electroplating +<br>Passivation | 42                       | 48                           |
|                                  | Zinc                           | 25                         | "                               | 78                       | 84                           |
|                                  | Cadmium                        | 22                         | "                               | 84                       | 84                           |
|                                  | Zinc                           | 100                        | Hot-dipped<br>galvanising       | 78                       | 84                           |
|                                  | Zinc                           | 125                        | Metal spraying                  | 84                       | 84                           |
|                                  | Aluminium                      | 125                        | Metal spraying                  | 84                       | 84                           |
|                                  | Zinc +<br>Aluminium            | 70 + 60                    | Metal spraying                  | 84                       | 84                           |
|                                  | Zinc                           | Copper +<br>Nickel         | 30 + 20                         | Electroplating           | 6                            |
| Copper +<br>Nickel +<br>Chromium |                                | 30 + 20<br>0.3             | Electroplating                  | 6                        | 6                            |



(c) Specimen coated with electroplated cadmium (22 microns) showing full protected surface and uniform texture.



(b) Specimen coated with metal sprayed zinc (125 microns) showing full protected surface.



(a) Specimen coated with electroplated zinc (25 microns) showing bare surface

Figure 5 :  
Performance of metallic coatings on mild steel specimens after 84 months of exposure period, in Bombay.

### **Aluminium and zinc-aluminium coatings**

Metal sprayed coatings of aluminium (125 microns) and combined zinc-aluminium (70/60 microns respectively) have protected the surface without any corrosion of the base metal. However, the surface roughness was observed in both coatings.

### **Cadmium coatings**

Cadmium coatings applied at a thickness of 22 microns by electroplating showed no signs of corrosion after 84 months exposure period (Figure 5c). Passivation treatment did not show difference in protective behaviour during this period. The surface of the coating remained perfectly smooth throughout the exposure period.

### **Tin coatings**

Tin was applied as cathodic coating to mild steel at a thickness of 25 microns by electroplating. Corrosion of the base metal commenced within one month from the date of exposure. The failure here could be attributed to electrolytic action under humid atmospheres that initiates in the pores of the coating. Porosity of the coating at the thickness investigated is inherent and unavoidable.

Passivation of electroplated tin coating has shown considerable improvement in the protective life. The passivated coating afforded protection to the base metal for forty eight months. This improvement in protective behaviour may be explained on the basis of sealing of pores by passivation treatment.

### **Nickel, copper and chromium coatings**

Nickel, copper and chromium were applied in varying thicknesses by electroplating as cathodic coatings. Different combinations of these coatings examined, failed within a span of one month since the commencement of exposure and were not considered suitable for the coastal areas having comparable atmospheric conditions as the present exposure site.

### **Performance of metallic coatings on zinc**

The metallic coatings based on nickel, copper and chromium were applied on zinc substrate. All systems commenced failing within seven to nine months thereby revealing their limited protective efficiency. Coatings on zinc surface developed adherent, wide spots of corrosion products.

### **Performance of organic coatings**

#### **Coatings on mild steel**

The performance of organic coating systems on mild steel is given in Table IV. All the systems under study have shown chalking on the surfaces. Epoxy paint systems consisting of priming paint with zinc dust showed marginally better performance of seventeen months (Figure 6)

**Table IV**  
Performance of organic coatings on mild steel during 7 years of  
exposure in Bombay

| Coatings   | Thickness<br>in<br>microns | Observations in<br>months |                           |
|--|----------------------------|---------------------------|---------------------------|
|  |                            | Onset of<br>corrosion     | Since 5% area<br>corroded |
| Epoxy zinc chromate primer<br>(2 coats) +<br>Epoxy finishing grey (2 coats)                              | 90                         | 13                        | 15                        |
| Epoxy zinc primer (2 coats) +<br>Epoxy finishing grey (2 coats)  | 90                         | 15                        | 17.                       |
| Epoxy zinc chromate primer<br>(2 coats) +<br>Epoxy undercoat (1 coat) +<br>Epoxy finishing grey (1 coat) | 90                         | 13 .                      | 18                        |
| Epoxy zinc primer (2 coats) +<br>Epoxy undercoat (1 coat) +<br>Epoxy finishing grey (1 coat)             | 90                         | 15                        | 18                        |
| Chlorinated rubber primer<br>(2 coats) +<br>Chlorinated rubber base weatherwork<br>paint grey (2 coats)  | 90                         | 84                        | 84                        |
| Coal tar epoxy (2 coats) +<br>Epoxy finishing grey (2 coats)   | 100                        | 84                        | 84                        |



Figure 6  
Performance of epoxy zinc primer and epoxy finishing grey on mild steel specimen after 17 months

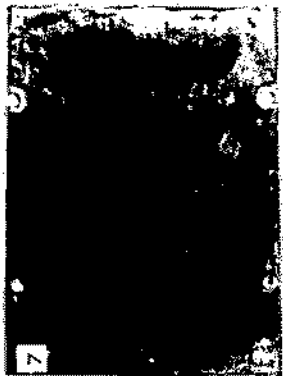


Figure 7  
Panel showing bleeding phenomena of coaltar epoxy paint on mild steel specimen after 84 months.

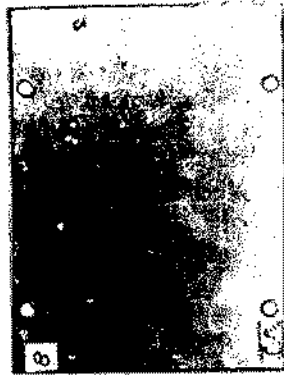


Figure 8  
Panel showing checking behaviour of chlorinated rubber paints after 84 months



than the system with zinc chromate pigment. Application of the under-coat in both cases showed no appreciable improvement in protective behaviour. Loss of gloss was found to be very rapid in all exposed systems. Coal-tar epoxy paint as priming coat and epoxy finishing grey as top coat have given the protective life exceeding a period of 84 months. However, the bleeding phenomenon was observed as expected (Figure 7). Chlorinated rubber based paints on mild steel showed a protective life of more than 84 months and their rate of gloss loss was found to be very slow. However, the occurrence of checking of this paint on the surface limits its utility (Figure 8).

### Coatings on aluminium

Four paint systems commented earlier with respect to mild steel were also applied on aluminium specimens. All the systems have ensured a protective life of 84 months. However, cracking and peeling-off of the zinc chromate pigmented epoxy top coat, bleeding of coal-tar epoxy paint and checking of chlorinated rubber based finishing paint were observed during the exposure period.

### Coatings on metal coated mild steel

Metal coated mild steel specimens were painted with organic coatings mentioned in Table IV with a view to reinforcing the protection and to give desired colour shades. Three coatings namely, hot-dipped galvanised zinc (100 microns), sprayed composite coating comprising zinc and aluminium (70 and 60 microns respectively) and phosphated mild steel together with organic coatings were studied. The performances of these protective systems for the period of 84 months had been almost identical as far as their corrosion protection abilities were concerned. The observations in respect of surface defects of paint top coats were similar to those commented earlier.

### Conclusions

The average annual corrosion rates of mild steel, zinc, brass and aluminium, at marine-cum-industrial site at Bombay, were found to be 5325, 214, 65 and 32 mg/dm<sup>2</sup> respectively.

Amongst the metallic coatings exposed on mild steel substrates, cadmium coating behaved most efficiently in respect of corrosion protection as well as appearance. Sprayed coatings in the thickness range of 125-130 microns of zinc, aluminium and zinc/aluminium protected the surface satisfactorily for a period of 84 months and beyond. Passivation of electroplated tin coating improved the protection compared to non-passivated surface. Copper/nickel/chromium coatings were not considered suitable for protection of mild steel and zinc substrates in environmental conditions prevailing at the site in view of their cathodic behaviour towards base metals as well as porosity.

The protection of base mild steel surface for a period of about 15-17 months was obtained by use of epoxy primers based on zinc dust and zinc chromate, the latter being slightly inferior in performance. Chlori-

nated rubber resin based paints, though imparted protection for a period of more than 84 months, suffered from checking of the top coat. Bleeding of coaltar epoxy coatings makes it unsuitable where decorative appearance of the surface is a consideration.

More prolonged exposure studies are required to assess as to which of the organic coatings on metal coated surfaces would be appropriate for the coastal surf zones.

### References

1. Ambler, H.R. and Bair, A.A., J. Appl. Chem., 5, 437, 1955.
2. Hudson, J.C. and Banfield, T.A., J. Iron & Steel Inst. (London) 154 229, 1946
3. Vernon, W.H.J., Trans. Faraday Soc., 23, 162, 1927.
4. Vernon, W.H.J., Trans. Faraday Soc., 27, 264, 1931.
5. Sanyal, B., Nandi, A.N., Natarajan, A. and Bhadwar, D., J. Sci. Ind Res (India), 18A, 127, 1959.

### RÉSUMÉ

D'après les études faites dans la situation où est situé le laboratoire de Bombay, sur le fonctionnement des enduits métalliques et non-métalliques, caractérisés par la présence de la haute humidité, de la température, de la pluie et des agents de la pollution sulphureuse, on a eu les résultats suivants : le cadmium d'argenture électrique, le zinc pulvérisé et les enduits d'aluminium ont protégé l'acier doux pendant 84 mois. Les enduits d'étain, de nickel et de chrome n'étaient pas propres. Les peintures d'époxy ont pu protéger l'acier doux pendant 17 mois et le traitement de phosphate sur l'acier doux a amélioré, d'une manière générale, le fonctionnement des enduits organiques.

INVESTIGATION ON LONG-TERM DURABILITY OF PROTECTIVE  
COATINGS FOR STEELS IN MARINE ENVIRONMENT

IWAO MOMIYAMA\* HIROSHI KURIYAMA\*

TADAKAZU KYUNO\*\* TSUKASA IMAZU\*\*

\* KANSAI PAINT CO., LTD., 3-12-1 MINAMIROKUGO,  
OHTA-KU, TOKYO, JAPAN

\*\* KAWASAKI STEEL CORPORATION, HIBIYA KOKUSAI BLDG.,  
2-2-3 UCHISAIWAI-CHO, CHIYODA-KU, TOKYO, JAPAN

ABSTRACT

For the purpose of establishing long term durability of offshore steel structures, ten-year exposure tests and analytical investigations were conducted at two locations on the Pacific coast of Japan from 1969 to 1979. The results of the studies are summarized as follows:

At the splash zone, where the corrosive attack was found severest, a long-lasting corrosion protective performance was achieved by the following three coating systems; (a) a duplex system of epoxy zinc primer and two-pack epoxy coating, (b) an extreme high-build non solvent epoxy coating and (c) a high-build inorganic zinc rich paint. Such factors as the use of zinc-rich primer, the increase of film thickness and the high grade of surface preparation contributed to a remarkable improvement of corrosion protective coating systems. The degree of the defect of paint films was found related to the corrosion loss of uncoated steel, of which the measurement of the latter would enable the durability of coating systems to be estimated to some extent.

EPMA analysis confirmed that a great deal of Cl existed in rust layers under the coated film. This fact may warrant the assumption that Cl-ion permeated through the coated film and accelerated the corrosion reaction under the film.

Dans le but d'étudier la durabilité à long terme des structures maritimes en acier, des essais d'exposition sur dix ans et des études analytiques ont été réalisés en deux endroits de la côte pacifique du Japon, entre 1969 et 1979. Le résultat de ces études

peut être résumé comme suit:

Dans la zone d'éclaboussage, là où l'attaque de la corrosion a été observée comme étant la plus grave, un effet de protection anti-corrosion à long terme a été obtenu au moyen des trois systèmes de revêtement suivants; (a) système duplex avec première couche d'apprêt d'époxyde-zinc et revêtement époxyde à deux composants, (b) revêtement époxyde non-solvant extrêmement épais et (c) revêtement épais de peinture inorganique riche en zinc. Ces différents facteurs, tels que l'emploi d'une couche d'apprêt riche en zinc, l'augmentation de l'épaisseur du film et la qualité supérieure de la préparation de surface, ont contribué à l'obtention d'une amélioration remarquable dans la protection anti-corrosion de ces systèmes de revêtement.

On a trouvé une relation entre le degré de déféctuosité des films de peinture et la perte par corrosion de l'acier non-revêtu, la mesure de cette dernière permettant d'estimer quelque peu la durabilité des systèmes de revêtement.

L'analyse EPMA a confirmé la présence d'une grande quantité de Cl dans les couches de rouille présentes sous le film de revêtement. Ce fait peut confirmer l'hypothèse que le ion Cl a pénétré à travers le film de revêtement, accélérant la réaction de corrosion sous le film de protection.

#### INTRODUCTION

To know the durability of corrosion-protective coating systems, much research and field exposure testing has been conducted for coated steel plates; for example, research on accelerated weathering test methods and substitute test methods for laboratorially reproducing the coating deterioration which may occur in an actual environment, in a short period, and research 1) for measuring interfacial phenomena between steel plates and the coating and the electrochemical, optical and physical properties of the coating. Under present conditions, however, these laboratory methods cannot produce data of sufficiently high reliability to permit determination of the durability of coating systems. Therefore at present, achieving a more exact durability assessment requires a long-term test of exposure to the actual environment. However, data obtained by long-term exposure testing will play an important role in judging the reliability of durability-assessing technology to be developed in the future.

Standing on these backgrounds, this research was conducted for about ten years from April, 1969 to May, 1979 in the marine environments, which are Chikura Beach of Chikura-cho, Awa-gun, Chiba Prefecture (hereinafter called Chikura) and Chiba Ironworks Beach of Kawasaki Steel Corporation, Chiba City, Chiba Prefecture (hereinafter called Chiba). To confirm the relation between test environment and corrosion and deterioration behavior of various steel plates and coating systems, measurement of the amount of sea salt particles and analysis of seawater were conducted at intervals at each test site.

Taking into consideration the types of environments in which marine structures are installed, the environment of the actual exposure test was classified into four zones: atmospheric, splash, tidal and submerged zones. In each zone, specimens were installed separately. These exposure tests employed eight kinds of steel plates which had been used in marine structures and harbor facilities.

The corrosion-protective performance of coated film may be greatly influenced by various factors, including surface condition, that is the degree of surface preparation of the steel plates, the welding and shop primer used in the assembly and erection stage of the marine structure or cathodic protection after installation, as well as the characteristics of the coating material itself. Therefore, these tests used coating systems combining as many of the above-mentioned factors as possible in application to various steel plates, to investigate their influence on the corrosion-protective coating performance.

During ten years exposure, test operations were restricted mainly to observation of aging appearance and photographing, to hold coating damage to a minimum. After exposure tests, various measurements and analyses were carried out and the relation between the exposure environment, the coating system and the corrosion-protective performance of the coating was analyzed.

#### EXPERIMENTAL PROCEDURE

Specimens:

Table 1 shows the chemical composition of steel plates used.

Table 1 Chemical Composition of Specimen (wt %)

| Steel                                 | No. | C    | Si   | Mn   | P     | S     | Cu   | Ni   | Cr   | Mo    | Nb    | V     |
|---------------------------------------|-----|------|------|------|-------|-------|------|------|------|-------|-------|-------|
| Mild Steel                            | A1  | 0.15 | 0.03 | 0.81 | 0.014 | 0.034 |      |      |      |       |       |       |
| Sheet Pile                            | A2  | 0.25 | 0.03 | 0.43 | 0.011 | 0.023 | 0.32 | 0.01 | 0.01 | 0.002 |       |       |
| High Strength Steel                   | A3  | 0.18 | 0.46 | 1.14 | 0.019 | 0.012 | 0.01 | 0.01 | 0.02 |       |       |       |
|                                       | A4  | 0.14 | 0.34 | 1.33 | 0.015 | 0.014 | 0.03 | 0.09 | 0.04 | 0.004 |       | 0.039 |
| Atmospheric Corrosion Resistant Steel | A5  | 0.10 | 0.33 | 0.62 | 0.068 | 0.019 | 0.33 | 0.31 | 0.27 |       | 0.023 |       |
|                                       | A6  | 0.14 | 0.33 | 0.83 | 0.026 | 0.018 | 0.34 | 0.14 | 0.28 |       | 0.013 |       |
| Resistant Steel                       | A7  | 0.11 | 0.42 | 0.90 | 0.026 | 0.012 | 0.25 | 0.14 | 0.18 | 0.060 | 0.016 | 0.027 |
| Sea Water Corrosion Resistant Steel   | A8  | 0.12 | 0.04 | 0.81 | 0.088 | 0.019 | 0.49 | 0.47 |      |       |       |       |
|                                       |     |      |      |      |       |       |      |      |      |       |       |       |

Size of uncoated specimen is 6-8 x 50 x 100 (mm). Coated specimens consist of three types of shapes and sizes as shown in Fig. 1

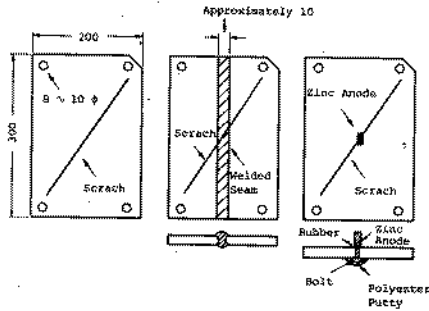


Fig. 1 Shape and Dimension of Coated Specimens (mm)

(Note) The ratio of area between zinc anode and steel to be protected is approximately 2:1000.

On both surfaces of specimens, scratches reaching steel plates were given with a sharp-edged tool.

### Coating systems:

Table 2 shows experimental factors and levels adopted in coating systems.

Table 2 Test Plan

| Factor                 | Level            |   | Factor | Level  |
|------------------------|------------------|---|--------|--|
| A: Steel               | A1               | Mild Steel                                    | F1     | Coal-tar Epoxy (200 $\mu$ m)                       |
|                        | A2               | Sheet Pile                                    | F2     | Coal-tar Epoxy (500 $\mu$ m)                       |
|                        | A3 <sup>*1</sup> | High Strength Steel                           | F3     | Coal-tar Epoxy (1,000 $\mu$ m)                     |
|                        | A4 <sup>*2</sup> |   | F4     | Epoxy (180 $\mu$ m)                                |
|                        | A5 <sup>*1</sup> | Atmospheric Corrosion Resistant Steel         | F5     | High Build Epoxy (400 $\mu$ m)                     |
|                        | A6 <sup>*1</sup> |   | F6     | Polyamide Epoxy <sup>*4</sup> (2,500 $\mu$ m)      |
|                        | A7 <sup>*2</sup> |   | F7     | Vinyl (150 $\mu$ m)                                |
|                        | A8               |   | F8     | Chlorinated Rubber (190 $\mu$ m)                   |
| B: Surface Preparation | B1               | Sea Water Corr. Resist. Steel                 | F9     | Epoxy Modified Polyurethane (200 $\mu$ m)          |
|                        | B2               | Shot Blast Cleaning                           | F10    | Polyurethane (180 $\mu$ m)                         |
|                        | B3               | Sand Tool Cleaning                            | F11    | Coal-tar Polyurethane (200 $\mu$ m)                |
|                        | B4               | R1 + Epoxy Zinc-rich Primer (15 $\mu$ m)      | F12    | Phenol HQ (125 $\mu$ m)                            |
|                        | B5               | R3 + Welding + R2                             | F13    | Inorganic Zinc-rich Paint (75 $\mu$ m)             |
| C: Site                | C1               | Coat Blast Cleaning + Zinc Spray (75 $\mu$ m) | F14    | Vinyl Powder (300 $\mu$ m)                         |
|                        | C2               |   | F15    | Epoxy Powder (200 $\mu$ m)                         |
| D: Zone                | D1               | Chikuro                                       | F16    | Hot Nit Type Petroleum Resin Paint (1,000 $\mu$ m) |
|                        | D2               | Chiba   | F17    | None   |
|                        | D3               | Atmospheric Zone                              |        |  |
|                        | D4               | Splash Zone                                   |        |  |
| E: Sacrificial Anode   | E1               | Tidal Zone                                    |        |  |
|                        | E2               | Submerged Zone                                |        |  |
|                        | E1               | Zinc Anode                                    |        |  |
|                        | E2               | None  |        |  |

(Note) <sup>\*1</sup> 50kg/m<sup>2</sup> class  
<sup>\*2</sup> 60kg/m<sup>2</sup> class  
<sup>\*3</sup> 58kg/m<sup>2</sup> class  
<sup>\*4</sup> Compound to be applied and cured under water

Table 3 shows the actual coating systems. As for coating method, airless spray coating, electrostatic powder coating and hot dip coating (approx. 120°C) were used for epoxy and inorganic zinc-rich primer, epoxy powder and petroleum resin, respectively. Other types of paints were applied using a brush.

Table 3 Coating Systems

| No. | Coating System  | Total Film Thickness ( $\mu\text{m}$ ) |
|-----|---|--|
| T1  | TE (100 $\mu\text{m}$ x 2)  | 200                                    |
| T2  | TE (120 $\mu\text{m}$ x 4)  | 480                                    |
| T3  | TE (140 $\mu\text{m}$ x 7)  | 980                                    |
| T4  | EZP (15 $\mu\text{m}$ x 1) + TE (100 $\mu\text{m}$ x 2)   | 215                                    |
| E1  | EP-Pr. (50 $\mu\text{m}$ x 2) + EP (40 $\mu\text{m}$ x 2)   | 180                                    |
| E2  | EZP (15 $\mu\text{m}$ x 1) + EP-Pr. (60 $\mu\text{m}$ x 4) + EP (40 $\mu\text{m}$ x 2)  | 335                                    |
| E3  | HEP-Pr. (80 $\mu\text{m}$ x 3) + HEP (80 $\mu\text{m}$ x 5)   | 640                                    |
| E4  | EP-Compound (2500 $\mu\text{m}$ x 1)  | 2500                                   |
| V1  | VY-Pr. (30 $\mu\text{m}$ x 3) + VY (30 $\mu\text{m}$ x 2)   | 150                                    |
| V2  | EZP (15 $\mu\text{m}$ x 1) + VY-Pr. (30 $\mu\text{m}$ x 3) + VY (30 $\mu\text{m}$ x 2)  | 165                                    |
| C1  | CR-Pr. (40 $\mu\text{m}$ x 3) + CR (35 $\mu\text{m}$ x 2)   | 190                                    |
| C2  | EZP (15 $\mu\text{m}$ x 1) + CR-Pr. (40 $\mu\text{m}$ x 3) + CR (35 $\mu\text{m}$ x 2)  | 205                                    |
| C3  | Zinc Spray (75 $\mu\text{m}$ ) + Etch.-Pr. (10 $\mu\text{m}$ x 1) + CR-Pr. (40 $\mu\text{m}$ x 1) + CR (35 $\mu\text{m}$ x 2)     | 195                                    |
| U1  | PU-Pr. (50 $\mu\text{m}$ x 2) + PU (45 $\mu\text{m}$ x 2) (Epoxy Modified)  | 190                                    |
| U2  | PU-Pr. (50 $\mu\text{m}$ x 2) + PU (40 $\mu\text{m}$ x 2)   | 180                                    |
| U3  | EZP (15 $\mu\text{m}$ x 1) + PU-Pr. (50 $\mu\text{m}$ x 2) + PU (40 $\mu\text{m}$ x 2)  | 195                                    |
| T5  | TU (100 $\mu\text{m}$ x 2)  | 200                                    |
| M1  | Zinc Spray (75 $\mu\text{m}$ ) + Etch.-Pr. (10 $\mu\text{m}$ x 1) + PH-Pr. (35 $\mu\text{m}$ x 1) + PH-MIO (40 $\mu\text{m}$ x 2) | 200                                    |
| Z1  | IZP (15 $\mu\text{m}$ x 1) + IZP (75 $\mu\text{m}$ x 1)   | 90                                     |
| Z2  | IZP (75 $\mu\text{m}$ x 1)  | 75                                     |
| P1  | EP-Pr. (10 $\mu\text{m}$ x 1) + VY-Powder (300 $\mu\text{m}$ x 1)   | 310                                    |
| P2  | EP-Powder (200 $\mu\text{m}$ x 1)   | 200                                    |
| H1  | Hot Melt Type Petroleum Resin Paint (1000 $\mu\text{m}$ x 1)  | 1000                                   |

(Note) TE: Coal-tar Epoxy, EZP: Epoxy Zinc-rich Primer, EP: Epoxy, Pr.: Primer, HEP: High Build Epoxy, VY: Vinyl, EP-Compound: Polyamide Epoxy, Under-Water-Hardening Type, CR: Chlorinated Rubber, Etch.-Pr.: Etching Primer, PU: Polyurethane, TU: Coal-tar Polyurethane, PH: Phenol, MIO: Microsilica Iron Oxide, IZP: Inorganic Zinc-rich Primer, VY-Powder: Vinyl Powder, EP-Powder: Epoxy Powder

### Specimen positioning and environment:

Fig. 2 shows the positions of specimens of Chikura and Chiba.

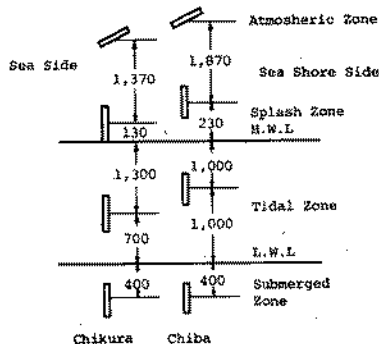


Fig. 2 Position of Specimens (mm)

The amounts of sea salt particles measured at the positions of specimens in atmospheric zone were 0.6 - 8.6  $\text{mg}/\text{dm}^2 \cdot \text{day}$  at Chikura and 0.8 - 2.5  $\text{mg}/\text{dm}^2 \cdot \text{day}$  at Chiba, much less than that of Chikura, which faces the open sea.

As for quality of seawater, it is well known that  $\text{Cl}^-$  concentration and dissolved oxygen content are reduced, COD increases, and the composition ratio of the seawater component changes as the pollu-

tion advances 2). At the early stage of the exposure test, the seawater of Chiba showed a notable reduction in  $\text{Cl}^-$  concentration, increase of COD, presence of  $\text{NH}_4^+$  and  $\text{NO}_3^-$  changes in the composition ratio, proving it to be polluted water. However, concentrations of  $\text{Cl}^-$  and  $\text{SO}_4^{2-}$  increased as time went by, and the degree of pollution was reduced at the late stage of exposure. According to the analytical result, the seawater of Chikura can be considered clean.

## RESULTS

Test results with uncoated specimens:

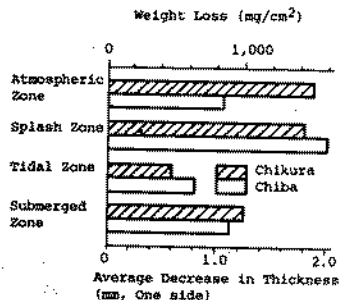


Fig. 3 Weight Loss of Mild Steel in Each Test Zone (after 10 years exposure)

Fig. 3 shows weight loss of uncoated mild steel in each test zone at Chikura and Chiba.

Concerning rust condition, at Chikura, an approx. 5 - 10mm reddish rust layer was formed on the entire surface of each steel. However, no differences in rust appearance were observed between steel grades. At Chiba, an approx. 2 - 3mm reddish rust layer, containing some yellowish rust, was formed on the surfaces of mild steel, sheet pile and high strength steel. This rust layer was fragile and

poor in adhesion, while black-brown rust, formed on atmospheric corrosion resistant steel and seawater corrosion resistant steel, had good adhesion, forming no laminary rust as observed on mild steel.

Table 4 and Fig. 4 show weight loss and average decrease in thickness of uncoated specimens obtained over ten years in the atmospheric zone.

At Chikura, there was only a slight difference in weight loss among steel grades in any test period. For all steel grades, weight loss was slightly reduced after three years had passed. However, even atmospheric corrosion resistant steel did not form the corrosion restricting stable rust usually observed in atmospheric corrosion resistant steel in atmospheric zones at other sites. For mild steel, sheet pile and high strength steel (A6) at Chiba, corrosion increased rapidly until the third year, but had slowed considerably after the fifth year. For atmospheric corrosion resistant steel and seawater corrosion resistant steel, there was only a slight increase in corrosion after two years had passed. This means that stable rust had formed over the two years. In terms of atmospheric corrosion resistance, 50 kg/mm<sup>2</sup> class steel (A5) containing P, Cu, Ni and Cr was the best, followed by 58 kg/mm<sup>2</sup> class steel (A7) containing Cu, Ni and Cr, 50 kg/mm<sup>2</sup> class steel (A6) and sea-



Table 4 Average Decrease in Thickness of Specimens  
(after 10 years exposure, atmospheric zone)

| Steel                                 | No. | Chikura                         |                         | Chiba                           |                         |
|---------------------------------------|-----|---------------------------------|-------------------------|---------------------------------|-------------------------|
|                                       |     | Ave. Decrease in Thickness (mm) | Ratio to Mild Steel (%) | Ave. Decrease in Thickness (mm) | Ratio to Mild Steel (%) |
| Mild Steel                            | A1  | 1.90                            | 100                     | 1.06                            | 100                     |
| Sheet Pile                            | A2  | 1.81                            | 95                      | 0.76                            | 71                      |
| High Strength Steel                   | A3  | 1.84                            | 97                      | 0.86                            | 81                      |
|                                       | A4  | 1.74                            | 91                      | 0.51                            | 48                      |
| Atmospheric Corrosion Resistant Steel | A5  | 1.76                            | 93                      | 0.17                            | 16                      |
|                                       | A6  | 1.73                            | 91                      | 0.20                            | 19                      |
|                                       | A7  | 1.53                            | 81                      | 0.18                            | 17                      |
| Sea Water Corrosion Resistant Steel   | A8  | 1.74                            | 91                      | 0.22                            | 21                      |

(Note) Average decrease in thickness (one side) is calculated from the value of weight loss.

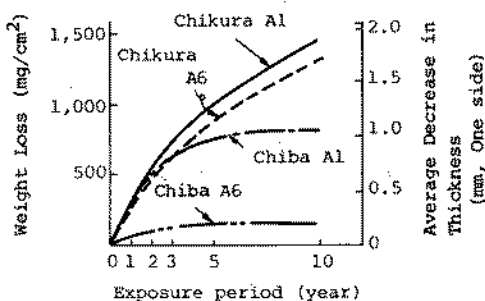


Fig. 4 Weight Loss of Mild Steel (A1) and Atmospheric Corrosion Resistant Steel (A6) in Atmospheric Zone at Chikura and Chiba

water corrosion resistant steel containing P, Cu and Ni (A8), in that order. Corrosion of these steels was always 1/5-1/6 that of mild steel.

Test results with coated specimens:

During exposure, film appearance was observed and photographed in the first, second, third, fourth, fifth, sixth, eighth and tenth years. After ten-year exposure tests were completed, appearance examination, measurement of defect area (degree of defect, in % of the entire surface area), surface hardness (pencil hardness), viscoelasticity and adhesive strength, observation by polarization microscope, infrared spectroscopic analysis, electron probe microanalysis (EPMA) and analysis of water in blister were conducted on specimens.

## (1) Results of appearance examination

Photo 1 shows coating deterioration after a ten-year exposure test of typical coating systems at Chikura.

Test result of Chiba is omitted because it is similar to that of Chikura. As shown in Photo 1, remarkable differences in corrosion protective performance were observed, depending on corrosive environment and coating system.

Photo 2 and 3 show age deterioration behaviour of coal-tar epoxy and epoxy films under each corrosive environment. In combination of epoxy zinc-rich primer and epoxy, there was only a little age deterioration, and all specimens were in good condition. In a combination of epoxy zinc-rich primer and coal-tar epoxy, however, a characteristic change in appearance was observed in each zone.

As film condition after ten years' exposure at Chikura (Photo 1) shows, the types of film deterioration differed with coating system, corrosive environment and test site.

## (2) Surface hardness

There was a certain difference among surface hardnesses after ten years exposure at Chikura, depending on corrosive environment and coating system. In the splash and atmospheric zones, surface hardness values were higher for all coating systems than those in the tidal and submerged zones. For coal-tar epoxy, the thicker the coating, the lower the surface hardness value; this corresponds to the results of viscoelasticity measurement mentioned below.

## (3) Results of viscoelasticity measurement

The viscoelasticity of coal-tar epoxy film from submerged and splash zones at Chikura was examined at temperatures from normal to 130°C. As shown in Table 5, the thicker the coated film, the lower the glass-transition temperature ( $T_g$ ), and all  $T_g$  were higher than the initial  $T_g$  (63°C). There was only a little difference in  $T_g$  between submerged and splash zones, the same as in the dynamic elastic modulus.

Table 5 Glass Transition Temperature ( $T_g$ )  
of Coal-tar Epoxy Film  
(after 10 years exposure, Chikura)  
(°C)

| Film Thickness<br>( $\mu\text{m}$ ) | Splash Zone | Submerged Zone |
|-------------------------------------|-------------|----------------|
| 200                                 | -           | 76             |
| 500                                 | 70          | 73             |
| 1,000                               | 67          | 65             |

(Note)  $T_g$  before exposure was 63°C at all film thickness

## (4) Adhesive strength

In submerged and tidal zones, adhesive strength of coal-tar epoxy coating on a shot-blasted surface was greatly influenced by film thickness. At thickness below 500 $\mu$ m, adhesive strength was approximately zero, while being 45 kg/cm<sup>2</sup> or more at 1,000 $\mu$ m. Epoxy on a shot-blasted surface displayed excellent adhesive strength in all corrosive environments.

## (5) Observation of cross section by polarization microscope

Photo 4 shows cross-sections of typical coating systems.

For coal-tar epoxy, the thicker the coating, the more rust was restricted (1 and 2 of Photo 4); Seawater corrosion resistant steel restricted rust more than did mild steel (2 and 3). With epoxy zinc-rich primer, no rust was observed (4). With epoxy and inorganic zinc-rich paint, no rust was observed (5, 6 and 8). With vinyl coating on shot-blasted surface, rust-blistering was observed (7).

## (6) Results of EPMA

Photo 5 shows the result of EPMA on cross section of typical coating systems. As shown in Photo 5, in coating system 1, in which coal-tar epoxy was coated on a shot-blasted surface, the rust layer contained a large amount of chlorine. In system 2 using epoxy zinc-rich primer and system 3 using epoxy, no rust layer was formed and chlorine accumulation was not observed.

## (7) Results of infrared spectroscopic analysis

Infrared spectroscopic analysis of typical coating systems showed that no remarkable change had occurred in chemical composition during the exposure test.

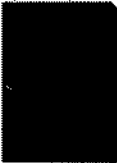
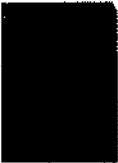

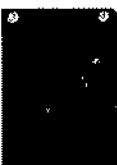

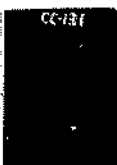

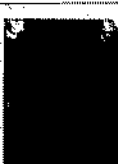

## (8) Analysis of water in blister

Table 6 Result of Atomic Absorption Spectro-photometer Analysis of Water in Blisters

|                                       | Fe     | Na     | Ca  | Mg    |
|---------------------------------------|--------|--------|-----|-------|
| Water in Blisters<br>(Coal-tar Epoxy) | 32,250 | 220    | 60  | 10    |
| Sea Water<br>(Chikura)                | 30     | 10,550 | 400 | 1,320 |

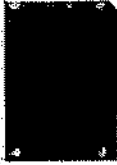

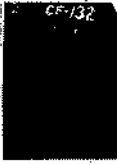

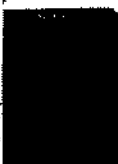
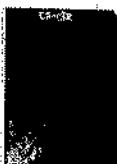
Table 6 shows the results of analysis of water extracted from blisters on coated film. Component ratio of water in blister differed from that of seawater.



| Zone             | Exposure Period (years)   |   |   |
|------------------|---|---|---|
|                  | 3   | 5   | 10  |
| Atmospheric Zone |  |  |  |
| Splash Zone      |  |  |  |
| Submerged Zone   |  |  |  |

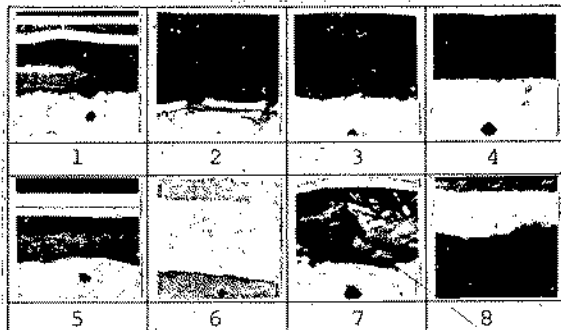
Mild Steel + Shot Blast + EBP (15  $\mu$ m) +  
TE (200  $\mu$ m)

Photo. 2 Appearance of Coal-tar  
Expoxy Film (Chikura)

| Zone           | Exposure Period (years)   |   |   |
|----------------|---|---|---|
|                | 3   | 5   | 10  |
| Splash Zone    |  |  |  |
| Submerged Zone |  |  |  |

Mild Steel + Shot Blast + EBP (15  $\mu$ m)  
+ EP (320  $\mu$ m)

Photo. 3 Appearance of Epoxy Film  
(Chikura)



1. Mild Steel + Shot Blast + TE (1200µm), Submerged Zone
2. Mild Steel + Shot Blast + TE (500µm), Submerged Zone
3. Sea Water Corr. Resist. Steel + Shot Blast + TE (500µm), Submerged Zone
4. Mild Steel + Shot Blast + IZP (15µm) + TE (1200µm), Submerged Zone
5. Mild Steel + Shot Blast + EP (180µm), Submerged Zone
6. Mild Steel + Shot Blast + EP (15µm) + EP (320µm), Submerged Zone
7. Mild Steel + Shot Blast + VX (150µm), Submerged Zone
8. Mild Steel + Sand Blast + IZP (7µm), Atmospheric Zone

Photo. 4 Cross Section of Typical Coating Systems  
(10 years, Chikura)

| Coating System  | Secondary Electron Image | Cl |
|---|--------------------------|----|
| 1<br>Coal-tar<br>Epoxy<br>(200 µm)  |                          |    |
| 2<br>Epoxy Zinc-<br>rich Primer<br>(15 µm) +<br>Coal-tar<br>Epoxy<br>(200 µm) |                          |    |
| 3<br>Epoxy<br>(180 µm)  |                          |    |

Mild Steel + Shot Blast

Photo 5 Result of EPMA of Typical Coating  
Systems (after 10 years exposure,  
submerged zone, Chikura)

## DISCUSSION

## Uncoated specimens:

It is well known that in a seashore area, a longer period is required for formation of stable rust layer on atmospheric corrosion resistant steel than in other areas 3). The influence of sea salt particles or seawater splashes on corrosion mechanism of steel has not been ascertained. However, it is supposed that corrosion acceleration and the delay in rust stabilization may be caused by destruction of the defected portion of rust layer by  $\text{Cl}^-$  ions 4, 5), water condensation by deliquescence of sea salt particles, and the promotion of rust reduction and reoxidation reaction by repeated dry and wet conditions caused by seawater splashes with high oxygen concentration. In these tests conducted in the atmospheric zones at Chikura and Chiba, rusting was accelerated by airborne sea salt particles and seawater splashes, and increased corrosion and delay in rust stabilization were observed. In particular, the atmospheric zone at Chikura, having so much seawater splash, was so severe an environment, more like a splash zone, that rust stabilization has not been observed for ten years even on atmospheric corrosion resistant steel, and there was only a slight difference in corrosion between steel grades.

At Chiba, stable rust layer was formed on atmospheric corrosion resistant steel and seawater corrosion resistant steel in two years, despite the considerable amount of airborne sea salt particles and seawater splashes. This may be because Chiba is located in a coastal industrial zone, and is therefore polluted with sulfur dioxide ( $\text{SO}_2$ ), which has more than sufficient effect upon rust stabilization to offset the bad influence of sea salt particles or seawater splashes 6).

## Coated specimens:

(1) Coating system and degree of defect

1) Influence of film thickness

In general, the rate of under-film corrosion depends on the transmission rate of water and oxygen 7). Therefore, it is believed that film thickness has a great influence on corrosion protective performance, so that effective thicknesses of specified coating systems and empirical equations of the relationship between durability and film thickness have been suggested 8, 9, 10). In this test, the influence of film thickness was researched with regard to coal-tar epoxy through various examinations; as a result, a notable influence was observed.

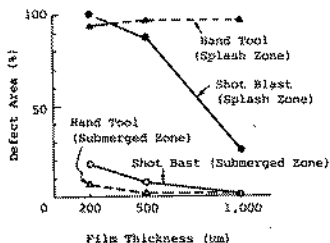


Fig. 5 Relation between Defect Area and Film Thickness of Coal-tar Epoxy (after 10 years' exposure, Chikura)

Fig. 5 shows the relation between film defect and thickness of coal-tar epoxy film after ten years' exposure at Chikura. In the submerged zone, increase in film thickness reduced the degree of film defect for both shot-blasted surfaces and hand-tool cleaned surfaces. In the splash zone, film thickness was observed to have a great influence on shot-blasted surfaces, while for hand-tool cleaned surfaces, the severity of film defect was very high, regardless of film thickness.

In such a severe environment as the splash zone, for example, film thickness had very little influence if surface preparation was insufficient. Film thickness also influenced surface hardness, viscoelasticity, adhesive strength and thickness of under-film corrosion. The result of infrared spectroscopic analysis did not show remarkable difference in chemical composition between before and after exposure. For coal-tar epoxy, however, surface hardness and  $T_g$  after ten-year exposure were reduced with increase in film thickness, so it is supposed that elusion of the plastic component in a coating differs according to film thickness.

## 2) Influence of coating system

Table 7 shows defect area of typical coating systems after ten years' exposure at Chikura. Epoxy (E1, E2, E3, E4 in Table 7) displayed excellent corrosion protective performance in both the tidal and submerged zones. Underwater hardening epoxy (E4) maintained good corrosion protective performance even in the splash zone, displaying the effect of super high build film (approx. 2,500 μm).

Coated films of inorganic zinc-rich paint (Z1 and Z2) were nearly exhausted by zinc elusion in such underwater environments as tidal and submerged zones, showing a high degree of film defect. In the atmospheric and splash zones, however, nearly perfect corrosion protective performance was maintained despite the large quantity of chlorine was recognized in the film by EPMA. For phenol MIO on a zinc-sprayed surface (M1), the degree of film defect after ten years' exposure in the atmospheric zone was zero, which proved the excellent corrosion protective performance of this system, as is evidenced in many huge bridges in Japan.



Table 7 Defect Area of Typical Coating Systems  
(after 10 years exposure, Chikura)

(4)

| System No. | Surface Preparation | Coating System                      | Atmospheric Zone | Splash Zone | Tidal Zone | Submerged Zone |
|------------|---------------------|-------------------------------------|------------------|-------------|------------|----------------|
| T1         | Shot Blast          | TE (200 $\mu$ m)                    | 98               | 100         | 9          | 30             |
| T1         | Hand Tool           | TE (200 $\mu$ m)                    | 93               | 95          | 4          | 8              |
| T4         | Shot Blast          | EZF (15 $\mu$ m) + TE (200 $\mu$ m) | 76               | 100         | 8          | 5              |
| T4         | Weld + Hand Tool    | EZF (15 $\mu$ m) + TE (200 $\mu$ m) | -                | 90          | 10         | 8              |
| E1         | Shot Blast          | EP (180 $\mu$ m)                    | -                | 83          | 1-2        | 1              |
| E2         | Shot Blast          | EZF (15 $\mu$ m) + EP (320 $\mu$ m) | -                | 0           | 1          | 3              |
| E3         | Shot Blast          | HEP (640 $\mu$ m)                   | -                | 33          | 2          | 1              |
| E4         | Shot Blast          | EP-Compound (2500 $\mu$ m)          | -                | 1           | 1          | 2              |
| V1         | Shot Blast          | VY (150 $\mu$ m)                    | -                | 92          | 9          | 20             |
| V2         | Shot Blast          | EZF (15 $\mu$ m) + VY (150 $\mu$ m) | 36               | 94          | 3          | 3              |
| C1         | Shot Blast          | CR (190 $\mu$ m)                    | -                | 100         | 88         | -              |
| C2         | Shot Blast          | EZF (15 $\mu$ m) + CR (190 $\mu$ m) | -                | -           | 44         | -              |
| T5         | Shot Blast          | TU (200 $\mu$ m)                    | 94               | 100         | 30         | 90             |
| M1         | Grit Blast          | Zinc Spray + PR-MIO (125 $\mu$ m)   | 0                | -           | -          | -              |
| Z1         | Sand Blast          | I2P (15 $\mu$ m) + I2P (75 $\mu$ m) | 1                | 1           | 38         | 99             |
| Z2         | Sand Blast          | I2P (75 $\mu$ m)                    | 1                | 1           | 100        | -              |
| -          | Grit Blast          | Zinc Spray (75 $\mu$ m)             | -                | 40          | 91         | 100            |

In coating systems combining epoxy zinc-rich primer with coal-tar epoxy, epoxy and vinyl corrosion protective performance was improved far more than in other systems using no epoxy zinc rich primer: in particular, combination with epoxy produced excellent results. This proves the superiority of coating systems combining epoxy with zinc-rich paint, which has been playing the main role in recent heavy duty coating. For example, a coating system in which 200  $\mu$ m or more of epoxy is applied over 75  $\mu$ m of zinc-rich paint may be expected to have a durability of ten years or more.

As shown in Table 7 and Fig. 5, the defect areas of coal-tar epoxy film on hand-tool cleaned surfaces were much smaller than those on shot-blasted surfaces, for film thickness of 500  $\mu$ m or less in the tidal and submerged zones. As mentioned above, however, sufficient surface preparation is basically preferable, considering that the efficacy of film thickness cannot be anticipated on hand-tool cleaned surfaces in the splash zone.

Examination of coal-tar epoxy showed that the welded seam had no effect on degree of film defect. However, pitting corrosion was locally observed on welded seam. Therefore, it is necessary to take tighten-up coating beforehand prior to all-over coating.

### 3) Defect area by year

Defect area by year differed according to various factors, including coating system and corrosive environment.

Fig. 6 shows defect areas by year of coal-tar epoxy on shot-blasted surface in splash and submerged zones. As shown in Fig. 6, film defect in the splash zone advanced at a faster rate than in the

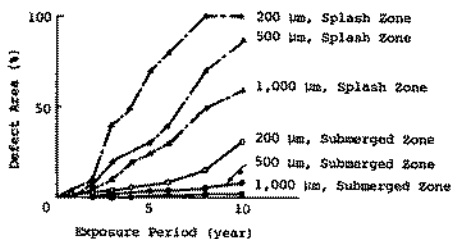


Fig. 6 Defect Area of Coal-tar Epoxy Applied on Shot Blasted Mild Steel (Chikura)

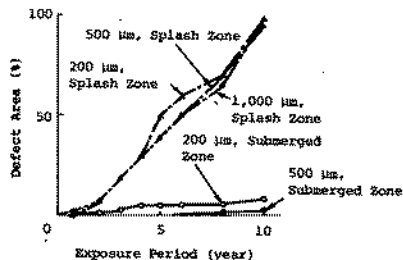


Fig. 7 Defect Area of Coal-tar Epoxy Applied on Hand Tool Cleaned Mild Steel (Chikura)

submerged zone, and film thickness was observed to have a strong influence in all environments. On the other hand, for hand-tool cleaned surfaces in the splash zone, film thickness had only slight influence on deterioration rate, as shown in Fig. 7.

Fig. 8 shows defect area by year for typical coating systems using coal-tar epoxy, epoxy and vinyl. The deterioration rate of coating system combining epoxy zinc-rich primer and epoxy was much lower than those of other coating systems. As shown in Fig. 6, 7 and 8, film defect advanced at a faster rate than ever when defect area reached 5 - 10% for any coat-

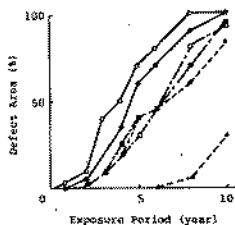


Fig. 8 Defect Area of Typical Coating Systems Applied on Shot Blasted Mild Steel (Splash Zone, Chikura)

ing system. Therefore, it is appropriate to do recoating at that point. In this report, it is assumed that the period before the defect area has reached 5% is the effective service life (durability), and the relation between the time at the first sign of film defect and the durability is shown in Table 8.

Considering the relation above in Table 8 will permit estimation of durability to fairly high accuracy, despite some deviation. However, values in Table 8 are for specimens whose coated films

Table 8 Relation between the Time at the First Sign on Film Defect and the Durability of Film

| Zone        | Time at the First Sign of Film Defect (year) | Durability   |                |
|-------------|--|--------------|----------------|
|             |  | Range (year) | Average (year) |
| Splash Zone | 0-1  | 1-2          | 1.1            |
|             | 1-2  | 2-3          | 2.4            |
|             | 2-3  | 4            | 4              |
|             | 3<   | 8            | 8              |
| Tidal Zone  | 0-1  | 3-6          | 4.7            |
|             | 1-2  | 2-8          | 5.4            |
|             | 2-3  | 4-10         | 8.3            |
|             | 3<   | 8-10         | 9.8            |

(Note) Durability shows the time when the defect area comes to 5% of the whole surface area

were scratched heavily, so it is necessary to note that effective service life values given in Table 8 are quite a bit shorter than would be the case with steel structures under actual use conditions.

## (2) Film defect and test environment

Film defect is greatly influenced by environment. Therefore in selecting a corrosion protective coating system, environmental intensity and expected durability of film should be considered for the most economical use of coating systems. Thus, it is important in terms of coating design to quantitatively understand the environmental intensity beforehand.

Table 9 Average Defect Area of Specimens (after 10 years exposure) (%)

| Zone             | Site    |       |
|------------------|---------|-------|
|                  | Chikura | Chiba |
| Atmospheric Zone | 51.5    | 25.8  |
| Splash Zone      | 86.4    | 86.2  |
| Tidal Zone       | 4.9     | 31.1  |
| Submerged Zone   | 4.6     | 9.0   |

Table 9 shows the average defect area of specimens at each zone in Chikura and Chiba. However, inorganic zinc-rich paint and zinc spray systems were excluded because they were entirely unlike other systems in deterioration behavior. As shown in this table, the splash zone has the largest defect area, followed by atmospheric, tidal and submerged zones in that order, at both Chikura and Chiba.

This result agrees with the measurement result of uncoated steel corrosion in Fig. 3, in tendency. Defect areas of the tidal and submerged zones at Chiba were larger than those at Chikura, presumably because the number of organisms adhering to the coated film was greater at Chiba. In the atmospheric zone, Chikura showed a larger defect area than Chiba, mainly because the splash volume of seawater and irradiation of ultra-violet ray were greater at Chikura.

## (3) Effect of steel grade on film defect

In tidal and submerged zones, steel grade had only a slight effect on film defect. Therefore, coating systems currently adopted for marine structures are readily applicable for atmospheric corrosion resistant steel and seawater corrosion resistant steel. As shown in Photo 4, seawater corrosion resistant steel restrained corrosion under its coating more than did mild steel. Thus, it may be neces-

sary to select the most suitable steel grade in taking corrosion protective measures in the marine environment.

In the splash zone, rust widely prevailed from scratches, and defect areas reached almost 100% after ten years exposure, presumably because scratches were too long; therefore it was impossible to recognize the actual effect of steel grade on film defect.

Table 10 Defect Area of Coal-tar Epoxy Film  
(after 10 years exposure, Atmospheric zone, Chiba) (%)

| Mild Steel | Sheet Pile | High Strength Steel |    | Atmospheric Corrosion Resistant Steel |    |    | Sea Water Corr. Resist. Steel |
|------------|------------|---------------------|----|---------------------------------------|----|----|-------------------------------|
| A1         | A2         | A3                  | A4 | A5                                    | A6 | A7 | A8                            |
| 98         | 97         | 100                 | 99 | 15                                    | 90 | 60 | 80                            |

Table 10 shows the relation between the defect area of coal-tar epoxy film and steel grade in the atmospheric zone at Chiba. In this environment, the effect of steel grade on film defect was clearly observed, and the results in Table 10 agreed well with the measurement of uncoated steel corrosion in Table 4.

#### (4) Film deterioration and steel corrosion

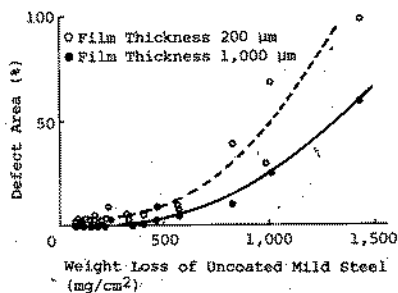


Fig. 9 Relation between Defect Area of Coal-tar Epoxy Applied on Shot Basted Mild Steel and Weight Loss of Uncoated Mild Steel

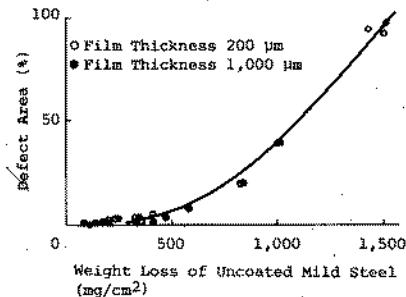


Fig. 10 Relation between Defect Area of Coal-tar Epoxy Applied on Hand-tool Cleaned Mild Steel and Weight Loss of Uncoated Mild Steel

Figs. 9 and 10 show the relation between defect area of coal-tar epoxy film and weight loss of uncoated mild steel. As shown in those two figures, the defect area of coated film is greatly dependent on steel corrosion. Thus corrosion, or weight loss, determined by a combination of two factors, environment and exposure period, can be taken as a parameter for the degree of film defect.

Film defect advanced rapidly when uncoated mild steel corrosion exceeded 500 mg/cm<sup>2</sup>. Therefore, the value 500 mg/cm<sup>2</sup> can be one of

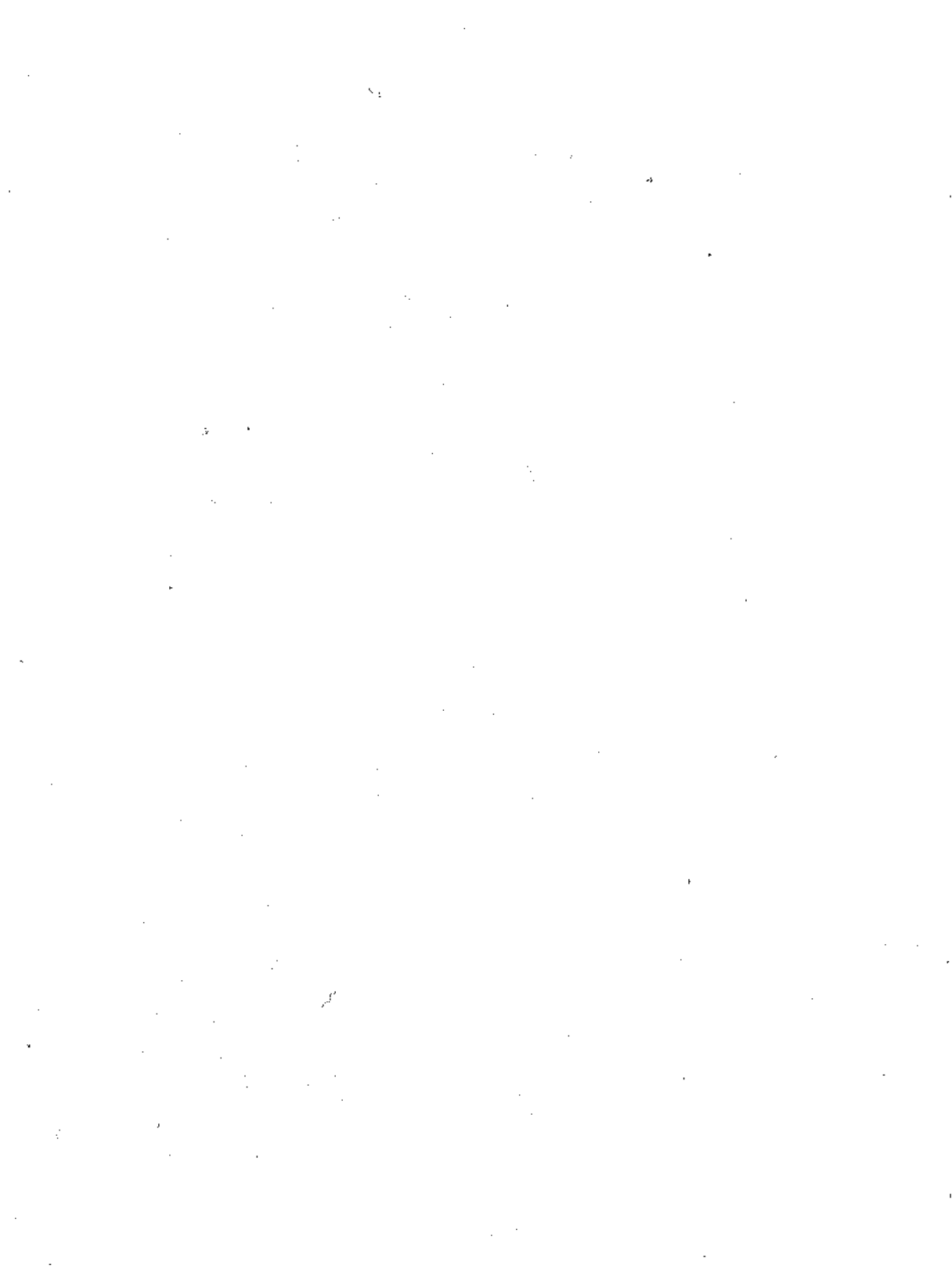
the main barometers for estimating the durability of coated film in each environment. On shot-blasted surfaces, it was observed that thicker film further restrained the advance of film defect accompanying increases in corrosion of uncoated steel. On hand-tool cleaned surfaces, however, no effect of film thickness was observed; thus, the effect of film thickness could not be fully displayed on an insufficiently prepared surface.

(5) Film defect and cathodic protection

It is generally admitted that the combination of coating and cathodic protection restrains the advance of corrosion at damage points such as scratches while get accelerating the occurrence of blistering or peeling around the damaged part, owing to cathodic disbonding. In this test of the effect of cathodic protection on coal-tar epoxy film, blistering due to cathodic disbonding was observed at the early stage. As a result of ten years exposure, there was only a slight difference in defect area between specimens with and without cathodic disbonding, partly because the zinc anodes had been exhausted during ten years exposure.

Literatures

- 1) J.E.O. Mayne, D.J. Mills: J. Oil Colour Chem. Assoc., 58 (1975) 5,155
- 2) S. Mizuki: Zairyo, 13 (1964) 7,490
- 3) C.P. Larrabee: Corrosion, 9 (1953) 8,259
- 4) J.F. Henriksen: Corros. Sci., 9 (1968) 8,573
- 5) T. Valad: Corros. Sci., 9 (1968) 8,577
- 6) T. Misawa, T. Kyuno, W. Suetaka, S. Shimodaira: Corros. Sci., 11 (1971) 1,35
- 7) K. Baumann: Plaste u. Kautschuk, 19 (1972), 694
- 8) T. Walter: Mater, Perform., 9 (1970) 9,37
- 9) Bosch: J.P.T., 41 (1969) 533,372
- 10) G. Menges: Kautschuk u. Gumi-Kunststoffe, 25 (1972) 5,213



A classification system for anti-fouling paints based on a dynamic  
flow test

Drs. F.H. de la Court

TNO PAINT RESEARCH INSTITUTE

P.O. Box 203, 2600 AE DELFT, HOLLAND

Abstract

In this paper a classification system for anti-fouling paints is presented. Paints are classified with regard to two criteria: anti-fouling performance after dynamic ageing on a rotor and toxicity to man and environment. To be classified paints must also meet some minimum paint technological requirements. The framework of the system has been tested with about 30 commercial paints. For most of these paints the anti-fouling performance has been investigated, their leaching rates have been determined, and their composition analysed.

It appeared that reliable classification by fouling tests is often difficult because of the variation of the anti-fouling performance of the paints. This problem has been overcome by determining the leaching curves of the paints, from which the leaching rate can be calculated. This shows whether the amount of toxins leaving the paint film at the time of testing was sufficient. Thus paints could be classified satisfactory, giving a clear indication of differences in quality.

With regard to toxicity paints were classified on the basis of the results of the analysis of the elements by röntgenmicro-analysis. This gives an indication of the kind of hazardous materials present and their concentrations. However, when all toxic materials present should be detected, a more detailed and complicated analysis procedure is necessary.

## Résumé:

Dans cet article un système de classification est donné des peintures antisalissures. Le système comporte une répartition des peintures selon 2 critères à savoir.

- a) l'effet antisalissure après vieillissement dynamique de la peinture applique sur un cylindre tournant (rotor) et
- b) la toxicité.

Pour classification une peinture doit répondre aux exigences techniques minimales par rapport à l'usage au pistolet, solidité de l'adhésion etc.

Le système est mis à l'épreuve de 31 peintures dite "de commerce". On a fait de toutes ces peintures des analyses: de la composition, de la capacité antisalissures et de la lixiviation des toxiques en fonction du temps.

Il appert, que la classification par essais salissures seule ne soit sûr, à cause de la non-stabilité du comportement anti-salissure au vieillissement de la peinture.

On a résolu ce problème à l'aide de la lixiviation en fonction du temps. Pour un effet efficace cette donnée la doit être maintenue d'une certaine valeur.

Avec ce système une classification est possible donnant une idée claire de la qualité des peintures diverses.

La classification selon la toxicité est faite par moyen des résultats d'une analyse élémentaire à rayons X.

Cette analyse indique sorte et quantité de toxiques.

Une analyse plus détaillée - plus complexe - peut révéler autres composants dangereux.

## 1. Introduction

For a shipowner it has always been a problem to decide what kind of anti-fouling paint to use on his ship in order to achieve optimal protection. When new paints are offered the normal procedure is to start ship trials. These trials appear many times difficult to keep under control and it takes a long time before the results are known. Furthermore the results are not always applicable to other ships in his company, with other sailing patterns. By the time the results are known paint-manufacturers may have developed better products, which suggest to him that former results are obsolete.

Of late years the problem became very pressing, due to the successful introduction of the so called "self polishing" anti-fouling. Therefore it has been decided to set up a "classification scheme" as a guide for the owner to make his choice.

In this paper a description of the scheme will be given. Furthermore the results of the investigation of some 30 paints are discussed. The investigation has been carried out to test the scheme and to improve it.



## 2. General considerations

Classification of an anti-fouling paint comprises in principle not only the duration of the anti-fouling activity of the dried paint film, but also a number of other properties e.g.:

- those of the wet paint, spraying characteristics, drying time, etc.
- the life time of the dried paint film in relation to adhesion, blister formation, wear, etc.
- the toxic properties in relation to occupational health and environmental problems.

Taking all these properties as criteria into account, would mean to design a very complicated classification system, which is badly manageable in practice and to our opinion not necessary. Apart from the life time with regard to anti-fouling activity, the toxic properties seem to be most important as a criterion for classification. The consequences of the toxic properties for labourers and environment are very well distinguished nowadays and legislation is increased accordingly. This legislation will make conditions as to the use of the paints and will forbid the use in a number of cases.

Though anti-fouling activity and toxic properties are the most important criteria for classification, it does not mean that the other properties mentioned are unimportant.

For instance a paint must have good application properties and must adhere well to the substrate. These are requirements to be met. In the other case classification is meaningless. A procedure for classification should therefore be started with an investigation into these properties. Detrimental phenomena such as lack of adhesion, blister formation etc. can be studied during the tests of the anti-fouling activity.

## 3. Framework of the classification system

### 3.1 Anti-fouling activity

As has been outlined already some time ago (1) there does not exist one uniform practice with regard to the life time of an anti-fouling paint.

The life time depends on:

- the time a ship is sailing relative to the time it lies stationary.
- the seawater composition.
- the sailing route, determining the kind and amount of fouling encountered.
- pollution of harbours etc.

Because these conditions vary for each ship, classification of anti-fouling paints by ship trials is very difficult, if not impossible. Therefore simulation of the ageing process on a ship's hull under controlled conditions is necessary.

For two reasons this should be done under dynamic flow conditions followed by a stationary test for fouling resistance (1, 2).

These are:

- a) leaching of toxins from anti-fouling paints is much higher when water flows along the surface (ship sailing) than under stationary conditions (2, 3, 4).
- b) fouling preferably takes place under stationary conditions (5, 6, 7).

For these reasons in our laboratory anti-fouling paints are aged in seawater on a rotor apparatus and subsequently tested on a raft against algal and barnacle fouling. Furthermore samples are taken and measurements performed to analyse the solution rate of the toxins in seawater, which occurs either by leaching or erosion.

The latter is done to support the fouling test results, considering that there is a direct relation between leaching rate and fouling prevention.

Rotor procedure including a picture of the rotor equipment, analysis of toxins and raft test have already been described earlier (1, 8, 9).

The above mentioned test procedure simulates a situation in which long periods of sailing are alternated with short stationary periods in which fouling can occur. Because these are the heaviest conditions as to ageing (solution of toxins in seawater) and fouling it must be expected that in practice otherwise the life time will be longer. "The procedure as described shows which paint gives the best relative anti-fouling activity under the same circumstances. It gives furthermore an indication for the real life time to be expected". Only when the circumstances in practice are quite different from the rotor test conditions, a prediction based on the latter may be erroneous. This may happen in a few cases, e.g., in the case of copper paints in the Baltic, with a lower salt concentration. The rotor test does not guarantee the life time in practice, because so many factors (pollution, bad application, etc.) are not considered.

### 3.2 Toxic properties

Classification according to toxic properties forms a special problem, because there are many toxic substances of which it is unknown how harmful they are and in which concentration. However, there are some guidelines which might be helpful:

- classify paints with toxins, of which the harmful character is well known, low or do not accept them for classification.

This applies for instance to paints containing mercury, lead, arsenic, antimony, PCB, PCT and DDT, which all are hazardous materials.

- classify paints with high toxic concentrations low and in reverse. In doing so a premium is put on the use of lesser amounts of toxins.

### 3.3 Description of the system

From the foregoing it seems that the most significant system would be the following:

- 1) Main classification on the basis of the results of the anti-fouling performance, as has been obtained after rotor ageing followed by a raft test. In case of doubt leaching and erosion curves can give additional evidence for the final decision.
- 2) Sub classification on toxic properties, determined by analysis of the toxic chemicals present.

With regard to main- and sub-classification, classes are distinguished as described in table 1 and 2. Paints will be tested for resistance against algae and barnacles because these organisms are most important. A classification for both species will be given. The number of classes can be extended if necessary. Before starting the experiments concerned it will be investigated whether the paints meet a number of minimum paint-technological requirements as sprayability, drying, thickness to be applied in one coat and recoatability. Furthermore the paints will be analysed for identification.

### 4. Testing of the system

To test the system described in the foregoing paragraphs, 31 anti-fouling paints have been selected from those offered for sale on the international market. For this purpose not only paints with a claimed long service time have been chosen, but also with a medium and short time of performance. Furthermore, apart from classical contact leaching types, also modern erodible paints have been investigated. From these 31 paints, 22 have been tested according to the system; 9 have been used to carry out more detailed investigations to answer questions especially with regard to the erosion aspect.

To test the anti-fouling activity the paints have been applied to the anti-corrosive substrate as recommended by the manufacturer. As far as could be observed all the paints did meet the minimum paint technological requirements, though no detailed tests were carried out. The paints have been rotated at a circumferential speed of 10 knots for times according to the class boundaries and tested then for their fouling resistance. The leaching has been determined by chemical and röntgenmicro-analysis, erosion by thickness decrease. To investigate the toxic properties the dry paint films have been analysed also by röntgenmicro-analysis.

#### 4.1 Anti-fouling results

In table 3 and 4 the results of the anti-fouling behaviour of 22 paints are reported.

Void places in the tables indicate that no tests were carried out. All tests were executed until a non-toxic panel was completely fouled.

Striking in both tables is in many cases the variation of the results with rotor time, especially for algae. Such a variation has been observed also on panels of the same paints which have been exposed continuously on the raft up to four years, without rotor ageing. The variation observed is well known (10) and takes place also on non-toxic substrates (11).

Analysis of all the information available has shown that the variability observed is neither increased nor induced by the rotor procedure (including application, drying, etc.). Anyhow the variation phenomenon makes unambiguous classification difficult.

#### 4.2 Leaching rate

An indication for the anti-fouling resistance of a paint film is the rate by which the toxins dissolve in seawater, from which algal zoospores, barnacle larvae etc take them up. Minimum rates are necessary to prevent settling. Because these are rather well known for the toxins normally used, a leaching curve can be of great help in classifying. Such a curve should include the toxins leaving the paint film by diffusion and/or erosion. Therefore the leaching of the paints from the 22 series has been determined for copper and tin, originating from the most important toxins present (cuprous-oxide, organotin derivatives). In table 5 the average leaching rate in a 200 days rotor period is reported. From this table it is clear that some paints can not have any resistance to fouling, because no leaching occurs at all. Most of the others have averages in the neighbourhood of the minimum rates and their resistance to fouling is doubtful, at least later then 200 days. A better insight into the life time to be expected is obtained from figures 1 (algae) and 2 (barnacles). In these figures the average amount of fouling observed in the 200 days period is plotted against the average leaching rate. If copper and tin were both present, the leaching rate of tin was always very low and has therefore been neglected. In the figures furthermore the minimum leaching rates are indicated, necessary for fouling protection. The minimum leaching rates for copper are slightly different from what normally is accepted in the literature ( $10 \mu\text{g Cu/cm}^2/\text{day}$ ). The values are based on our experience and reflect better the well known difference between algae and barnacles. For tin the values have been taken as found for tributyltinfluoride (8). For triphenyltinfluoride, another well-known tin toxin, the values are most probably much lower (12).

It appears that for algae most of the paints have average leaching rates below the minimum values. Most of them therefore foul. For barnacles the copper leaching is in most cases greater than the minimum rate and therefore no fouling occurs. The tin leaching is too low.

Apparently fouling occurs now and then, though the leaching rate is higher then needed.

This may be due to the fact that averages have been plotted. However, röntgenmicro-analysis has also shown that in these cases the leaching on one and the same paint film may be different on different places and therefore may be sometimes too low. In most of the cases (16) the leaching rate results confirm the fouling tests as discussed in 4.1. Deviations occur nearly always with regard to algae.

#### 4.3 Toxins

In order to determine the kind and amount of toxins, dried paint-films have been investigated by röntgenmicro-analysis. By this method in principle all the elements between nr. 5 and 92 can be detected. The amounts of copper, tin and zinc have been determined with the help of a standard paint. In table 6 the results for the most important elements in 25 paints are reported. Next to these silicium, aluminium, magnesium, calcium and titanium were found, in amounts of 0 - 10%.

Obviously no elements like mercury, arsenic, antimony or lead, pointing at hazardous toxins, are present. The method, however, is not suitable to detect organic compounds like PCB, PCT, etc. No other method has been applied at present to look for these materials. The most important toxic materials used seemed to be cuprous-oxide and organo tin derivatives. In some paints (10, 15, 17, 18, 23 through 25) the tin is, as tributyltinoxide, attached to an acrylic polymer. These have erodible properties. The presence of sulphur sometimes means (1, 2, 6, 10, 14, 23 through 25) that an organic algicide has been used. However, in other cases (15-1, 15-2 and 18-2) sulphur is, as copper, obvious present in copper thiocyanate. In this respect it is noteworthy that in two subsequent fouling seasons copper thiocyanate as such has shown no anti-fouling properties in a special test on our raft.

Further it has to be noted that nitrogen could not be detected. For this a slightly different method has to be used. Therefore algicides containing this element, remained unnoticed.

#### 4.4 Identification of paints

Basic for good functioning of the system is identification of the paints to be classified. This is necessary in order to determine whether the same paint as classified is offered after some time. Complete analysis for this purpose takes much time and is not necessary. Sufficient would be a "fingerprint-technique" by which the paint is unambiguously characterized.

For this purpose two such techniques are available.

In the first place röntgenmicro (REM-RMA) analysis, as mentioned in 4.3, which determines the pigmentcomposition. For identification it is sufficient to compare the X-ray spectrum of a new sample with that of a former one.

With the second technique, infrared spectroscopy, mixtures of polymers, plasticizers, etc., as used in paint media, are identified. In this method the pigments are separated from these materials, which remain in solution.

From the solution a film is cast on potassium bromide to make the infrared spectrum. As in the case of the pigments it is sufficient to compare the spectrum of a new sample with the one formerly taken.

## 5. Classification

On the basis of the results in the foregoing paragraphs, 21 paints have been classified. Because paint 22 showed loss of adhesion during the rotor tests this product was not considered. A number of paints were still foulfree after their test period. They have been placed in the corresponding class. However, on extending the rotor test, they could have scored higher.

### 5.1 Anti-fouling activity

Classification has been carried out on the basis of the results in table 3 and 4. In doing so one should remember that a qualification 1 with regard to fouling means that 0-10% of the surface is covered with algae or that 0-10 barnacles per  $\text{dm}^2$  occur. In both cases this will give a friction increase along the surface, which is not acceptable.

As can be observed from table 3 and 4 this guideline is often not easy to handle, because of the variation in the fouling results. To decide whether the fouling observed was just a coincidence or not, the leaching rate was used as a second guideline.

The following rules were adopted to classify the paints.

- a paint will be placed in the class, before the one in which for the first time fouling occurred.
- when fouling is qualified with a rating 1, this will be neglected when later on no fouling took place, on the condition that the leaching rate is not lower than the minimum rates discussed in 4.2.

Classification in relation to algal and barnacle fouling is reported in the following table.

| Class          | Algae             | Barnacles      |
|----------------|-------------------|----------------|
| not classified | 1, 2, 3, 4, 6, 14 | 2, 3, 6, 18    |
| 1              | 8, 9, 15, 18, 19  | 4, 14, 15      |
| 2              |                   | 10, 19         |
| 3              | 7, 10, 11, 16     |                |
| 4              | 5, 12, 13, 20, 21 | 11, 12, 13     |
| 5              | 17                | 1, 5, 7, 8, 9  |
| 6              |                   | 16, 17, 20, 21 |

As can be observed from this table the paints are reasonably well dispersed over the classes, which means that a difference in quality can thus be indicated. Classification in this way is only in a few cases somewhat doubtful.

## 5.2 Toxic properties

In this case classification has been done on the basis of the results reported in table 6.

Furthermore the following rules were adopted:

- copper has regarded to be present as cuprous oxide, unless it was clear that copper thiocyanate was used. In this case the amounts of copper and sulphur have been neglected, because CuCNS is not a toxin.
- tin has been calculated as tributyltin oxide.
- when sulphur is present as part of an algicide, the amount present has been multiplied with the average of 5 to find the percentage of that algicide
- the amounts of toxic materials have been taken together, without taking into account their specific toxicity.

(Sub)classification in relation to the amount of toxic material is reported in the following table.

| Sub class | division   |
|-----------|--|
| 1         | -  |
| 2         | 1, 2, 6, 7, 8, 11, 13, 14, 16-1, 16-2, 18-1, 19, 21  |
| 3         | 5, 9-2, 10-2, 12, 15-1, 15-2, 17-1, 17-2, 20-1, 20-2 |
| 4         | 3, 4, 9-1, 18-2                                      |

This table shows that many paints contain a high amount of toxin. Though a number of toxins can not be detected in the way the analysis was carried out so far (see 4.3), the system seems to give a rough but satisfactory impression of toxicity.

## 6. Influence of some test conditions

### 6.1 Circumferential speed of the rotor

Testing has been executed so far with a circumferential speed of the rotor of 10 knots. It has been shown earlier (3) that at higher speeds the leaching of conventional contact leaching paints is not increased. However, for modern erodible anti-foulings the erosion may be dependant on the water flow rate. In such a case a paint film would be eroded in an earlier stage and therefore give shorter fouling protection.

For this reason the erosion of 4 erodible anti-fouling paints was determined on a spinning disc (9). The results are shown in fig. 3. Instead of the varying speed the corresponding theoretically calculated friction has been plotted as independent variable. At the same time the erosion of the paints on the rotor has been determined at 17 knots. This has been plotted also in fig. 3.

As can be observed there is not a significant relation between erosion and friction. At least the effect of the friction will not be very high.

Nevertheless it seems sensible to increase the rotor speed to 17 knots, so that the friction in that case is at least within the range encountered on the disc. This range may also be expected on a ship's hull (9). To check this, the erosion of five erodible paints has been measured on the rotor at 17 knots as well as on a container ship. For the latter purpose the paints have been applied to panels which have been attached to the bilge keel. The paints have been exposed on the forward part of the bilge keel as well as on the rear end. Both places were about 60 m apart. The erosion on the rotor has been followed for a period of 3 months, on the ship for about 9 months. In the following table the results of the comparison of erosion on rotor and ship\* are presented.

| Paint | bilge Keel |      | Rotor |
|-------|------------|------|-------|
|       | front      | rear |       |
| 18    | 0.19       | 0.11 | 0.14  |
| 28    | 0.27       | 0.25 | 0.24  |
| 29    | 0.17       | 0.15 | 0.21  |
| 32    | 0.42       | 0.31 | 0.28  |
| 33    | 0.23       | 0.20 | 0.23  |

\*  $\mu\text{m/day}$ 

As can be seen they are very well in agreement. Only in one case, in front, the erosion rate was higher than on the rotor.

### 6.2 Rough surfaces

The question has been raised whether the roughness of a surface affects the erosion rate. For that purpose erosion measurements were done on the smooth part of the bilge keel panels (see 6.1) as well as on the artificial rough surface parts (peak to valley 500  $\mu\text{m}$ ).

The results\* have been summarized in the next table.

| Paint | Smooth | Rough |
|-------|--------|-------|
| 18    | 0.14   | 0.12  |
| 28    | 0.26   | 0.26  |
| 29    | 0.17   | 0.16  |
| 32    | 0.37   | 0.36  |
| 33    | 0.26   | 0.22  |

\*  $\mu\text{m/day}$ 

As is shown the differences between rough and smooth are only of minor importance.

### 6.3 Seawater condition during rotor tests

For the tests natural filtered seawater is used, with a pH of about 8 and a salinity of about 2,8‰; pH and salinity are continuously monitored. The temperature of the seawater is constant 20°C. The water is furthermore renewed continuously. The system may in some cases lead to erroneous results when the salinity is different from the figure quoted (see 3.1). The problem is restricted to cuprous-oxide containing paints. Lower salinities will occur in some seas and in estuaries.



Unless ships are always sailing in these areas, a constant deviation from the leaching rate found during the classification procedure will not occur. Thus the life time will not deviate considerably. At higher salinities the leaching is not so much affected (3) and therefore also in this case the life time will remain almost unchanged.

For contact leaching anti-foulings no influence of the temperature on leaching was found by the author (3), though this was not in agreement with other findings (13, 14).

In principle also the erosion rate may be influenced by the temperature. To the authors experience this is not the case, though no extensive experiments were carried out.

Continuous renewal of seawater is necessary to avoid accumulation of toxins in the rotor drum. Renewal takes place at a rate of 300 l/hour, which is 60% of the rotor's content. This rate keeps the concentration far below critical concentrations, which could affect the leaching rate.

### Conclusions

By the system as described in this paper, commercial anti-fouling paints can be classified in an adequate manner. Thus insight is obtained into anti-fouling life time differences and into the kinds and amounts of toxins.

The decision for anti-fouling classification in general is taken on the sole basis of the results of the fouling tests. However, a reliable classification can in many cases only be obtained when leaching curves are available.

For a more reliable classification as regards toxicity, it would be necessary to determine also nitrogen, so that algicides containing this element are detected. Furthermore hazardous materials like PCB, PCT etc. should be determined. No doubt this can be done. However, this asks for a more detailed and complicated analysis, of which the necessity at present is not clear. The same applies to the chemical structure of the algicides present.

### Acknowledgements

The research described in this paper was sponsored by the "National fundation for the coordination of maritime research in the Netherlands". Thanks are due to this organisation for their support.

Thanks are furthermore due to mr. A.C. Pycke, mr. A.A.A. ten Bruggencate, ir. H.C. Ekama, ir. J.N. Joustra, ir. E. Vossnack, and dipl. ing. H.F.M. Frohn for the stimulating discussions. The author is also greatly indebted to mr. J.J. Hink and mr. J.R. Roelofs for carrying out the experiments.

References:

1. F.H. de la Court. Fouling resistant coatings: mode of action and future development. Third International Conference in organic coatings science and technology, Athens 1977. Proceedings vol. 1- "Advances in Organic Coatings Science and Technol. Series". Technomic Publishing Co. Inc. Westport CT-USA, 170-188.
2. J.H. Bishop. Underwater Coatings under dynamic flow conditions. Australian OCCA Proceedings and News, December 1982, 8-12.
3. F.H. de la Court and H.J. de Vries. The leaching mechanism of cuprous oxide from anti-fouling paints. J. Oil Col. Chem. Assoc. 1973, 56, 388-395.
4. A.M. v. Londen. Testing and Investigation of ship bottom paints. J. Oil. Col. Chem. Assoc. 1969, 52, 141-157.
5. Woods Hole Oceanographic Institution. Marine Fouling and its prevention, United States Naval Institute Annapolis, Maryland, 1952.
6. A.O. Cristie and L.V. Evans. Shipping World and Shipbuilder, October 1975, 953.
7. D.R. Houghton. Third International Congress on Marine Corrosion and Fouling, Washington, October 1972, 682.
8. F.H. de la Court. The value of tributyltinfluoride as a toxicant in anti-fouling formulations. J. Oil. Col. Chem. Assoc. 1980, 63, 455-473.
9. F.H. de la Court. Measuring the erosion and friction of anti-fouling coatings in the laboratory and the significance of the results in practice. Proceedings of the Congress on Marine Corrosion and Fouling, Barcelone (Spain) 1980, 3-13.
10. P. de Wolf, A.M. van Londen, 1966. Anti-fouling compositions Nature. vol 209, no 5020, pp 272-274. January 15, 1966.
11. P. de Wolf, 1973. Ecological observations on the mechanisms of dispersal of barnacles larvae during planktonic life and settling. Netherlands Journal of Sea Research vol 6 (1-2), pp 1-129 (1973).
12. F.H. de la Court and H.J. de Vries. The leaching mechanism of some organotin-toxicants from anti-fouling paints. Proceedings of the Congress on Marine Corrosion and Fouling, Juan les Pins (France) 1976, 113-118.
13. A.M. van Londen. Report 54 C of the Netherlands Ship Research Centre TNO, Delft, 1963.
14. J.H. Bishop and F. Marson. Australian OCCA. Proc. and News 1971, 9.

Table 1.

Main classes  
Anti-fouling activity

| Class | Foulfree after:   |
|-------|---|
| 1     | One fouling season on a raft or <u>50</u> days on the rotor followed by a raft test |
| 2     | <u>100</u> days on the rotor followed by a raft test                                |
| 3     | <u>200</u> days on the rotor followed by a raft test                                |
| 4     | <u>300</u> days on the rotor followed by a raft test                                |
| 5     | <u>350</u> days on the rotor followed by a raft test                                |
| 6     | <u>400</u> days on the rotor followed by a raft test                                |

Table 2. Sub-classes  
Toxic material

| Class | Description  |
|-------|--|
| 1     | Paints containing Hg, As, Sb or chlorinated products like PCB, PCT or DDT  |
| 2     | Paints containing <u>more than 55 weight percent</u> toxic material calculated on the dry paint, not falling under heading 1 |
| 3     | As class 2, but containing <u>25-55 weight percent</u> toxic material.   |
| 4     | As class 2, but containing <u>less than 25 weight percent</u> toxic material.  |

Table 3. Algal resistance

| Paint nr. | after ageing on rotor (days) |      |      |      |      |      |
|-----------|------------------------------|------|------|------|------|------|
|           | 0/50                         | 100  | 200  | 300  | 350  | 400  |
| 1         | 1(B)                         | 1(G) | 4(G) | 1(G) | 0    | 2    |
| 2         | 1(G)                         | 0    | 4(G) | 4(G) |      |      |
| 3         | 3(G)                         |      | 4(G) |      |      |      |
| 4         | 1(B)                         |      | 4(G) | 2(G) | 4(G) |      |
| 5         | 0                            | 1(G) | 0    | 0    | 1(G) | 4(G) |
| 6         | 3(G)                         |      |      |      |      |      |
| 7         | 0                            | 1(G) | 0    | 1(G) | 4(G) |      |
| 8         | 1(G)                         | 0    | 4(G) | 4(G) | 2(G) |      |
| 9         | 0                            | 1(G) | 1(G) | 1(G) | 1(G) | 2(G) |
| 10        | 0                            | 0    | 0    | 1(G) | 0    | 4(B) |
| 11        | 0                            | 0    | 0    | 1(G) |      | 1(G) |
| 12        | 0                            | 0    | 0    | 0    |      | 1(G) |
| 13        | 0                            | 0    | 1(G) | 0    | 1(G) | 1(G) |
| 14        | 1(B)                         | 1(B) | 2(G) | 1(B) | 0    | 0    |
| 15        | 0                            | 1(B) | 1(G) | 4(B) | 1(G) | 1(G) |
| 16        | 0                            | 0    | 1(G) |      | 1(G) | 0    |
| 17        | 1(G)                         | 0    | 0    | 0    | 0    | 1(G) |
| 18        | 0                            | 1(B) | 1(G) | 1(G) | 1(G) | 2(G) |
| 19        | 0                            | 1(B) | 2(G) | 1(G) | 2(G) | 1(B) |
| 20        | 0                            |      | 1(G) | 0    | 3(G) | 0    |
| 21        | 0                            | 0    | 1(G) | 0    |      |      |
| 22        | 0                            | 0    | 0    | **   |      |      |

\* 0= 0% of surface covered (G) = green algae  
 1= 0-10% " " " (B) = brown algae  
 2= 10-20% " " "  
 3= 20-40% " " "  
 4= > 40% " " "

\*\* extensive detachment

Table 4. Barnacles resistance

| Paint nr. | After ageing on rotor (days) |     |     |     |     |     |
|-----------|------------------------------|-----|-----|-----|-----|-----|
|           | 0/50                         | 100 | 200 | 300 | 350 | 400 |
| 1         | 0                            | 0   | 0   | 0   | 0   | 3   |
| 2         | 2                            | 1   | 3   | 3   |     |     |
| 3         | 3                            | 1   | 2   |     |     |     |
| 4         | 0                            | 1   | 1   | 0   | 0   |     |
| 5         | 0                            | 0   | 1   | 0   | 0   | 1   |
| 6         | 1/4                          | 4   |     |     |     |     |
| 7         | 0                            | 0   | 0   | 0   | 0   |     |
| 8         | 0                            | 0   | 0   | 0   | 0   |     |
| 9         | 0                            | 0   | 0   | 0   | 0   | 2   |
| 10        | 0                            | 0   | 1   | 0   | 0   | 2   |
| 11        | 0                            |     | 0   | 0   |     | 1   |
| 12        | 0                            |     | 0   | 0   |     | 1   |
| 13        | 0                            | 1   | 0   | 0   | 3   | 3   |
| 14        | 0                            | 1   | 1   | 0   | 0   | 0   |
| 15        | 0                            | 1   | 1   | 0   | 1   | 1   |
| 16        | 0                            | 0   | 0   | 0   | 0   | 0   |
| 17        | 0                            | 0   | 0   | 0   | 0   | 0   |
| 18        | 1                            | 1   | 1   | 1   | 1   | 0   |
| 19        | 0                            | 0   | 1   | 1   | 1   | 0   |
| 20        | 0                            | 0   | 0   | 0   | 0   | 0   |
| 21        | 0                            | 0   | 0   | 0   |     | 0   |
| 22        | 0                            | 0   | 0   | **  |     |     |

\* code 0= no fouling observed  
 1= 0-10 barnacles per dm<sup>2</sup>  
 2= 11-25 " " "  
 3= 26-50 " " "  
 4= > 50 " " "

\*\* extensive detachment

Table 5. Average leaching rates over a 200 days rotor period

| Paint nr. | Toxicant | Average leaching rate* |            |              |
|-----------|----------|------------------------|------------|--------------|
|           |          | by diffusion           | by erosion | total amount |
| 2         | Cu       | 0                      | -          | 0            |
| 3         | Cu       | 8                      | -          | 8            |
| 6         | Cu       | 0                      | -          | 0            |
| 8         | Cu       | 12                     | -          | 12           |
| 4         | Cu       | 0                      | -          | 0            |
|           | Sn       | 5,5                    | -          | 5,5          |
| 5         | Cu       | 12                     | -          | 12           |
|           | Sn       | 1                      | -          | 1            |
| 7         | Cu       | 12                     | -          | 12           |
|           | Sn       | 2                      | -          | 2            |
| 9         | Cu       | 18                     | -          | 18           |
|           | Sn       | 2                      | -          | 2            |
| 11        | Cu       | 11                     | -          | 11           |
|           | Sn       | 1                      | -          | 1            |
| 12        | Cu       | 13                     | -          | 13           |
|           | Sn       | 2                      | -          | 2            |
| 13        | Cu       | 11                     | -          | 11           |
|           | Sn       | 0,2                    | -          | 0,2          |
| 16        | Cu       | 45                     | -          | 45           |
|           | Sn       | 0,3                    | -          | 0,3          |
| 19        | Cu       | 17                     | -          | 17           |
|           | Sn       | 0,2                    | -          | 0,2          |
| 20        | Cu       | 12                     | -          | 12           |
|           | Sn       | 0,3                    | -          | 0,3          |
| 21        | Cu       | 12                     | -          | 12           |
|           | Sn       | 0,7                    | -          | 0,7          |
| 22        | Cu       | 32                     | -          | 32           |
|           | Sn       | 0,1                    | -          | 0,1          |
| 4         | Sn       | 0,6                    | -          | 0,6          |
| 10        | Sn       | 1,2                    | 0,5        | 1,7          |
| 14        | Sn       | 3,3                    | -          | 3,3          |
| 17        | Sn       | 2,5                    | 2          | 4,5          |
| 15        | Sn       | 1,1                    | 3,2        | 4,3          |
| 18        | Sn       | 1,3                    | 1,1        | 2,4          |

\* in  $\mu\text{g./cm}^2$  day

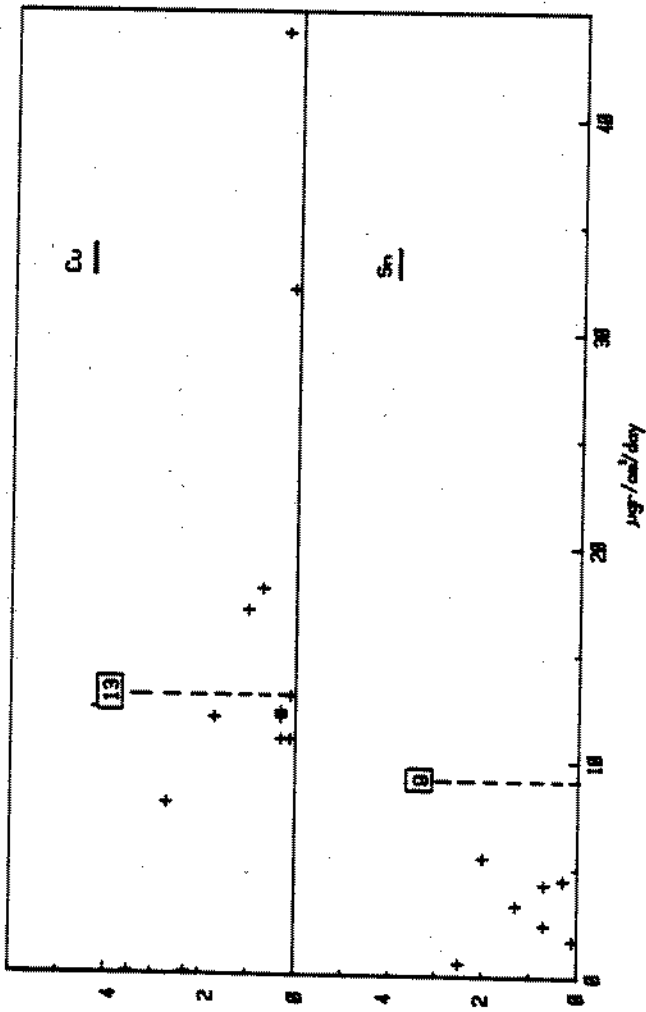
Table 6: Elements\* in the dried paint film

| Paint nr.** | Cu   | Sn   | S    | Zn   | Fe  |
|-------------|------|------|------|------|-----|
| 1           | 68,3 | 1,2  | 2,3  | 3,3  | -   |
| 2           | 53,0 | -    | 2,5  | 6,1  | 4,0 |
| 3           | 13,7 | -    | -    | 16,4 | 5,7 |
| 4           | -    | 1,7  | -    | 38,1 | 3,7 |
| 5           | 32,0 | 1,9  | -    | 24,6 | 5,0 |
| 6           | 64,1 | -    | 1,8  | -    | 4,4 |
| 7           | 48,8 | 2,4  | 0,7  | -    | 2,3 |
| 8           | 52,8 | -    | -    | 14,2 | -   |
| 9-1         | 1,1  | 5,6  | -    | 34,1 | -   |
| 9-2         | 34,6 | 1,6  | -    | 25,8 | 6,6 |
| 10-2        | 0,9  | 3,0  | 6,3  | 43,4 | 5,2 |
| 11          | 46,1 | 3,8  | -    | 6,0  | 3,6 |
| 12          | 36,1 | 3,4  | -    | 6,1  | 3,6 |
| 13          | 61,5 | 1,4  | 0,5  | -    | 2,6 |
| 14          | -    | 15,9 | 6,3  | -    | 9,5 |
| 15-1        | 17,4 | 11,8 | 11,0 | -    | -   |
| 15-2        | 19,3 | 11,3 | 12,0 | -    | -   |
| 16-1        | 60,7 | 1,1  | -    | 5,1  | -   |
| 16-2        | 57,3 | 1,3  | -    | 8,6  | -   |
| 17-1        | -    | 13,2 | -    | 42,0 | -   |
| 17-2        | -    | 12,6 | -    | 43,7 | -   |
| 18-1        | 69,1 | 6,0  | 1,3  | -    | 6,6 |
| 18-2        | 29,7 | 9,1  | 18,1 | -    | -   |
| 19          | 54,1 | 1,1  | 0,8  | 5,8  | 0,4 |
| 20-1        | 43,2 | 0,8  | -    | 16,0 | 5,9 |
| 20-2        | 43,8 | 1,2  | -    | 13,7 | 3,7 |
| 21          | 42,6 | 4,1  | -    | 2,8  | 4,5 |
| 22          | 50,2 | 1,6  | -    | -    | 4,3 |
| 23          | 5,7  | 3,4  | 7,0  | 41,1 | 4,1 |
| 24          | 5,6  | 3,1  | 9,6  | 41,4 | -   |
| 25          | 6,7  | 2,5  | 7,6  | 49,7 | -   |

\* % by weight

\*\* 9-1, 15-1 etc. means first coat of paint system.  
9-2, 15-2 etc. means top coat of paint system.

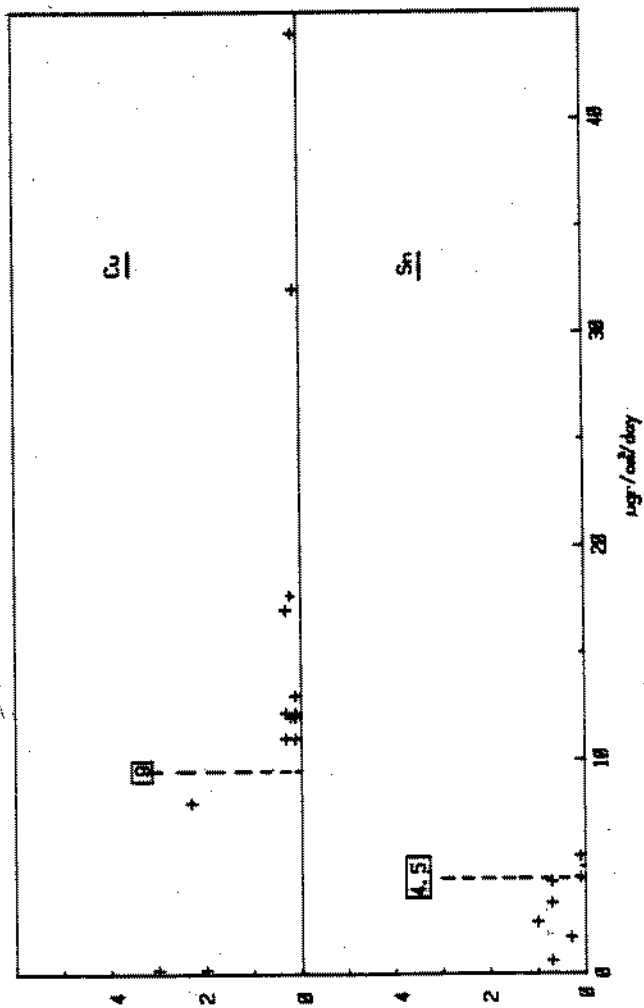
Fig. 1: Fouling (arbitrary scale)



Fouling with algae in relation to copper or tin leaching.  
average result in a 200 days rotorperiod



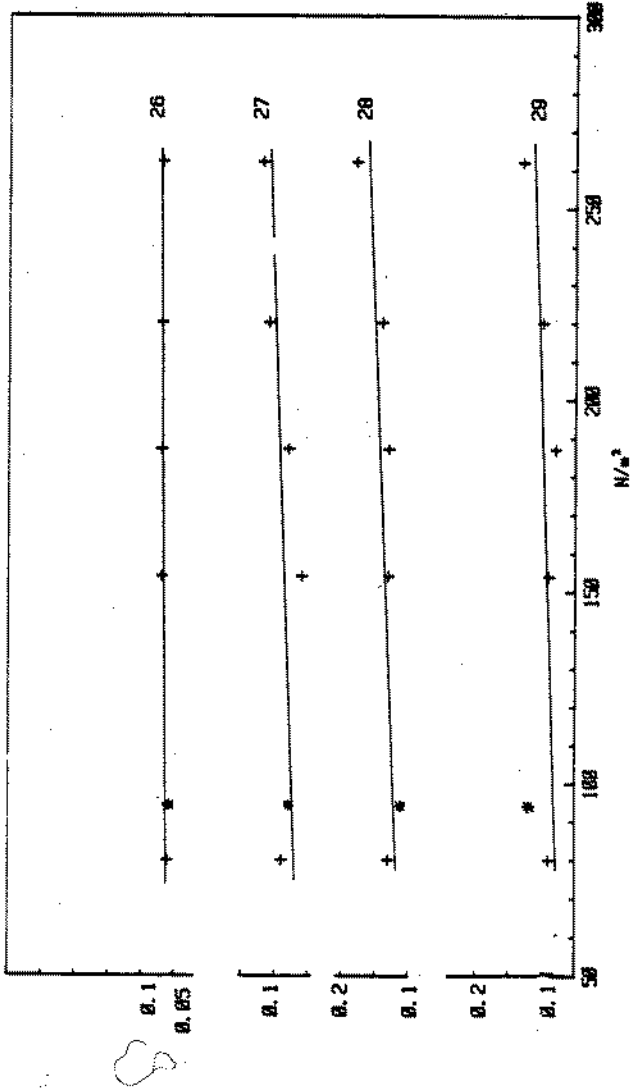
Fig. 2: Fouling (arbitrary scale)



Fouling with barnacles in relation to copper or tin leaching  
average result in a 200 days rotorperiode

PAINT

Fig. 3:  $\mu\text{m/day}$



Erosion on a smooth disc

circ. speed: 27 knots      Temp: 20° C  
+ disc      \* rotor (17 knots)

Application of the AC impedance measurements to predict paint systems performance in marine atmospheres

M. Morcillo, S. Feliu, J. Simancas and J.M. Bastidas

Centro Nacional de Investigaciones Metalúrgicas

Ciudad Universitaria, Madrid-3 Spain.

#### ABSTRACT

The performance of 8 typical paint systems is analyzed in the Spanish atmospheres of Vigo and El Pardo (Madrid), marine and rural respectively, after two years' exposure. Likewise, the effects of the degree of the surface preparation of steel (SIS 055900) and the presence of salt residues of sodium chloride in the metal/paint interface are studied with reference to the behaviour of chlorinated rubber system.

In the laboratory, possibilities offered by the electrochemical measurement technique of impedance vector for prediction of practical performances are also analysed.

#### RÉSUMÉ

Le comportement de 8 systèmes typiques de peinture est analysé dans les atmosphères espagnoles de Vigo et El Pardo (Madrid), atmosphères marine et rurale respectivement, après deux années d'exposition. Egalement, les effets du degré de préparation de la surface de l'acier (SIS 055900) et de la présence de résidus salins de chlorure de sodium dans la interface métal/peinture, sont étudiés dans le système de peinture de caoutchouc chloré pour la stabilité postérieure de revêtement organique.

## Introduction

Extensive research is being carried out in Spain (1) to ascertain: (a) protection requirements for paint systems (surface preparation grade; type and thickness of paint) according to the kind of predominant atmosphere, and (b) the effect of the contaminants  $\text{SO}_4^{2-}$  and  $\text{Cl}^-$  on the metal/coating interface in the performance of the paint. The results of this work pertain to the testing stations located in Vigo (marine atmosphere) and El Pardo, Madrid (rural atmosphere).

It is well known that outdoor exposure tests frequently need long periods of time, 10-20 years, in order to draw reliable conclusions. Nowadays the trend is towards the development of methods which enable early prediction of the future paint coating performance, even before the occurrence of any substantial changes in its appearance. In this paper the possibilities offered by electrochemical impedance measurement techniques are explored, which is lately having a great application in corrosion and protection studies.

## Experimental Procedure

Figure 1 shows a picture of Vigo's test station, located on the deck of a raft, built to conduct



Fig. 1.- View of Vigo's test station.

sea water immersion tests. The strong aggressiveness of this type of atmosphere as compared with El Pardo's rural atmosphere is shown in table I, where corrosion data of bare metal specimens obtained in both exposure sites are given.

Table I.- Corrosion data of bare metals in the atmospheres of Vigo and El Pardo

| Station                           | ANNUAL CORROSION RATE      |                           |                             |  |
|-----------------------------------|----------------------------|---------------------------|-----------------------------|--|
|                                   | Steel<br>( $\mu\text{m}$ ) | Zinc<br>( $\mu\text{m}$ ) | Copper<br>( $\mu\text{m}$ ) | Aluminium<br>( $\text{mg}/\text{dm}^2$ ) |
| Vigo<br>(marine<br>atmosphere)    | 58.2                       | 3.74                      | 2.92                        | 100.1                                    |
| El Pardo<br>(rural<br>atmosphere) | 15.1                       | 1.06                      | 1.11                        | 1.83                                     |

In Table II, the characteristics of the paints (applied by air spray) used in this study are shown.

Test samples have been prepared from a 3 mm hot-rolled steel sheet which showed an intact mill scale (degree A of Swedish Standards, SIS 055900). Thereafter, they were shot blasted with S-280 to reach the ASA 3 standard, previous to the application of the paint coating.

To study the effects of the steel surface preparation and the interface contamination by chlorides, two sets of panels were prepared to which only the chlorinated rubber system was applied. Surface preparation grades B Sa 3, B Sa 2 and B St 2 were obtained by shot blasting and wire brushing a steel sheet of grade B (SIS 055900), obtained in turn by oxidation of grade A sheet in El Pardo's contaminant free atmosphere. Contaminations with NaCl were prepared on A Sa 3 samples dosing amounts of 20, 100 and 500  $\text{mg}/\text{m}^2$  of NaCl, from solutions of NaCl

in distilled water and methanol (the last compound added to favour a quick evaporation of the solvent). Subsequently, the paint system was applied on these contaminated surfaces.

In laboratory studies, where the impedance technique was used, the panel testing consisted in two identical transparent plastic tubes (which permit a better visualization of coating evolution) stuck to the paint surface by means of a silicone sealer, leaving an interior surface area in contact with the electrolyte of 3.1 cm<sup>2</sup>. The tubes contained solutions of distilled water and NaCl (3%) in an attempt to simulate rural and marine atmospheric exposures, respectively.

Table II.- Characteristics of paint systems

| Paint System                  | SYSTEM DESIGNATION | Primer                 | Undercoat          | Topcoat         |
|-------------------------------|--------------------|------------------------|--------------------|-----------------|
| Oil/Alkyd                     | O /A               | INTA<br>164103         | ---                | INTA<br>164218  |
| Alkyd                         | A                  | INTA<br>164201         | ---                | INTA<br>164218  |
| Chlorinated Rubber            | CR                 | INTA<br>164705         | INTA<br>164701A    | INTA<br>164704A |
| Zinc Silicate/<br>Chl. Rubber | Zn/CR              | INTA<br>164408         | Tie Coat           | INTA<br>164704A |
| Vinyl                         | V                  | INTA<br>164604         | Tie Coat           | INTA<br>164603A |
| Zinc Silicate/<br>Vinyl       | Zn/V               | INTA<br>164408         | ---                | INTA<br>164603A |
| Polyurethane                  | P                  | R E N F E 03. 323. 125 |                    |                 |
| Epoxy/Polyurethane            | E/P                | MIL<br>C-82407         | RENFE 03. 323. 125 |                 |

A Hewlett-Packard Model 4800-A Vector Impedance Meter was used. The double electrode technique was applied. (2). As auxiliary electrode a 25 cm<sup>2</sup> platinized titanium sheet

was used, whose impedance can be considered negligible compared with the working electrode (painted sample).

The basis of this measurement technique has been analysed in numerous papers (3-5). The impedance measurements were carried out over a frequency range of 50 kHz to 5Hz. For each imposed frequency, the impedance modulus  $|Z|$  and the phase angle  $\varphi$  were measured. Periodic measurements of the impedance vector together with a visual evaluation of the coating appearance were made.

## EXPERIMENTAL RESULTS AND DISCUSSION

### Effect of the type of paint (on ASa 3)

Atmospheric exposure tests. After two years' exposure the different paint systems offer an excellent surface appearance.

Laboratory studies. Figure 2 shows the evolution of the impedance diagrams for the different paint systems concerning the various exposure times in a 3% NaCl solution. From the observation of these diagrams the following points can be drawn:

(i) Frequently, the diagram passes through three steps (Fig. 3). Initially (step I), when the paint film is in perfect condition, the diagram takes the shape of a straight line forming a certain angle with the imaginary axis. This response is similar to that of a capacitor, with phase angles near to  $90^\circ$  and very high values of the impedance modulus.

With time (step II), once the paths or channels of electrolyte penetration across the film are being established, the paint permeability decreases and the impedance diagram plots a semicircle arc. Finally (step III), when the paths in the film (which permits the movement of the chemical species to and from the metal substrate) have been completely established, other processes take place: corrosion, diffusion, etc.; the impedance plot in the complex plane shows a definite semicircle. Sometimes the semicircle does not intersect the real axis at low frequencies but draws a straight line of  $45^\circ$  slope.

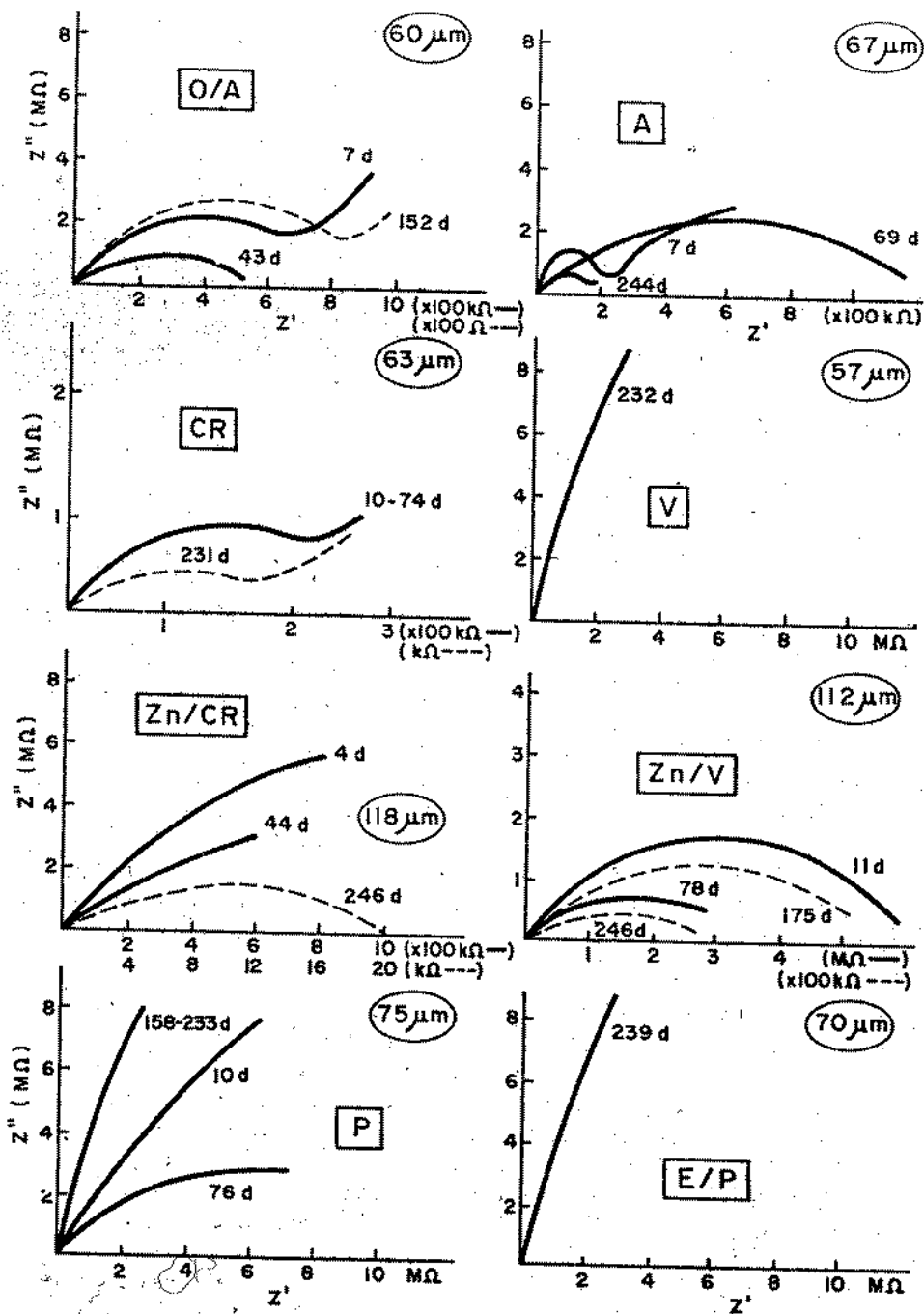


Fig. 2. - Time evolution of impedance diagram for the different paint systems. Electrolyte: 3% sodium chloride. Appearance after 250 days of testing: V, Zn/V and E/P (excellent), O/A and A (dense blistering and rusting), CR and P (medium dense blistering and rusting) and Zn/CR (medium dense blistering).



(ii) With this technique we can differentiate paint coating performances. Longer outdoor exposure times will tell if there exists or not a real correspondance between laboratory results and practical performances. A good correlation exists between the evolution of impedance plots and the deterioration visually observed on the coating in laboratory.

Observing Figure 2, it can be seen that only two systems - vinyl and epoxy/polyurethane- show, after 250 days of testing, an excellent performance, with an impedance diagram corresponding to a capacitor (Fig. 3, step I, with a very high resistance in parallel). In the remaining systems, the diagram reaches steps II or III (Fig. 3) and the damage of the coating starts to be important: blisters and rust (on perforated blisters) appear. So, the evolution of the diagram reflects, to some extent, the state (integrity) of the paint coating, anticipating in many cases, as commented before, visible deterioration.

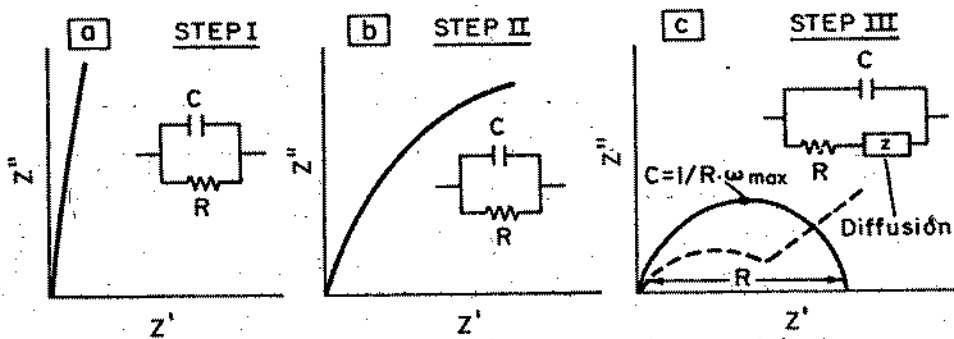


Fig. 3.- Schematic representative for the different steps of impedance diagrams evolution and associated equivalent electric circuits.

#### Quantitative information provided by the impedance measurements

The impedance diagram gives quantitative information of coating failure by means of the parameters  $R$ ,  $C$  and  $\tan \delta$ .  $R$  and  $C$  are obtained from analysis of diagram and  $\tan \delta$  ( $= \cotan \varphi$ ) at a frequency of 1 kHz.

R and C versus time. The equivalent electric circuit proposed by Randles (5), parallel R-C circuit (Fig. 3), explains quite well the frequency response of many electrochemical systems. Up to now, is not very well established the real meaning of C and R for the complex system metal/paint/electrolyte. In our opinion, at the beginning of the test, C could be related to the capacitance of the paint film (this working as a dielectric) and R to the ohmic electrical resistance of the film (which acts as a barrier to the permeation of substances across it). With time, new electrochemical processes would take place and the equivalent electric circuit would consequently change, involving now double layer capacitance and diffusion impedance, besides charge-transfer resistance. The time variation of parameters R and C is given in Tables III and IV.

Table III.- Variation of R versus time for the different paint systems.

| Time days | R, $\Omega \cdot \text{cm}^2 \times 10^5$ |      |      |     |       |      |     |     |
|-----------|---|------|------|-----|-------|------|-----|-----|
|           | O/A                                       | A    | CR   | V   | Zn/CR | Zn/V | P   | E/P |
| 10        | 27.9                                      | ---  | 49.6 | --- | 56    | 161  | --- | --- |
| 20        | 30.3                                      | 12.4 | 69.7 | --- | ---   | 87   | --- | --- |
| 40        | 14.8                                      | 6.2  | 22.6 | --- | ---   | 109  | --- | --- |
| 70        | 8.9                                       | 3.9  | 8.3  | --- | 0.22  | 99   | --- | --- |
| 100       | 1.2                                       | 3.4  | 3.0  | --- | 0.35  | 101  | --- | --- |
| 120       | 0.50                                      | 3.1  | ---  | --- | 0.40  | ---  | --- | --- |
| 150       | 0.025                                     | 1.0  | 15.7 | --- | 0.51  | 16   | --- | --- |
| 240       | ---                                       | 0.09 | 0.72 | --- | 0.41  | 9.4  | --- | --- |

Vinyl, polyurethane and epoxy/polyurethane systems perform like capacitors after 250 days of testing, not feasible to determine R. In the remaining systems a decreasing of R with time is observed (Table III), R being the controlling resistance of the process. At the

beginning, this resistance corresponds to the paint film resistance, but afterwards charge-transfer resistance can be the controlling factor.

The value of capacitance  $C$  has been calculated from the frequency corresponding to the top of the semicircle (Fig. 3c) or by extrapolation to high frequencies in the case the semicircle is not well defined (5). Generally, we can observe (Table IV) a continuous increase of capacitance with time. First of all, it shows an average value of  $200 \text{ pF} \cdot \text{cm}^{-2}$ , which is characteristic of a paint film in good condition. The capacitance tends to acquire higher values with time and simultaneously the coating loses its protection efficiency (6).

Table IV.- Variation of  $C$  versus time for the different paint systems.

| Time<br>days | $C$ , $\text{pF} \cdot \text{cm}^{-2}$ |      |      |     |       |      |     |     |
|--------------|--|------|------|-----|-------|------|-----|-----|
|              | O/A                                    | A    | CR   | V   | Zn/CR | Zn/V | P   | E/P |
| 10           | 129                                    | 198  | 110  | 100 | 189   | 391  | 144 | 136 |
| 20           | 143                                    | 181  | 120  | --- | ---   | 409  | --- | --- |
| 40           | 179                                    | 381  | 319  | 123 | ---   | 548  | 258 | 206 |
| 70           | 178                                    | 287  | 244  | 134 | 742   | 448  | 190 | 157 |
| 100          | 156                                    | 507  | 419  | 109 | 1050  | 515  | 208 | 148 |
| 120          | 152                                    | 397  | ---  | --- | 1013  | ---  | --- | --- |
| 150          | >12000                                 | 599  | 181  | 124 | ---   | ---  | 186 | 139 |
| 240          | ---                                    | 4762 | 1721 | 114 | 681   | 563  | 164 | 147 |

Dielectric loss factor ( $\tan \delta$ ) versus time. When a capacitor is in good condition, the phase angle ( $\gamma$ ) is close to  $90^\circ$ . On the contrary, as  $\gamma$  decreases, the dielectric losses of that capacitor will be higher.

Sato and other Japanese researchers ( 7-9 ) have conducted extensive studies in order to find correlations between  $\tan \delta$  (being  $\delta = 90 - \phi$ ) and current condition of the paint coating. According to them,  $\tan \delta$  acquires values less than 0.2 when paint film is in good protection condition. With time and simultaneously with film deterioration (loss of protection efficiency),  $\tan \delta$  acquires higher values.  $\tan \delta$  can also experiment changes because of water absorption, contraction and swelling of paint films and ionic interchange processes ( 7 ).

Figure 4 shows the time variation of  $\tan \delta$  for the different paint systems tested. Early,  $\tan \delta$  acquires values close to 0.1. Then,  $\tan \delta$  increases with time, depending on each paint system. The best performance corresponds to vinyl, polyurethane and epoxy/polyurethane systems, with values of  $\tan \delta$  after 250 days of testing of 0.07, 0.1 and 0.14 respectively, all of them below the critical value of 0.2. In the remaining systems  $\tan \delta$  increases with time, overpassing the threshold value of 0.2 and showing paint film damage (blisters, rust, etc.)

#### Effect of steel surface preparation

Figure 5 shows the evaluation of the impedance diagram for the chlorinated rubber system applied to steel surfaces with different degrees of cleaning (SIS 055900). In the same figure photographs of film appearance after 250 days (in the laboratory) and two years (in Vigo's atmosphere) are also shown. A clear correlation can be found between these different data. When the coating has been applied over grade A Sa3 (i.e. the cleanest tested surface), the appearance of the coating is excellent in both tests and impedance measurements indicate a capacitive behaviour (step I). However, when a paint film of similar thickness was applied on the BSt2 grade (i.e. the worst degree of cleanness) damage on the coating is important and the impedance diagram reaches step III. Intermediate degrees of cleaning show diagrams belonging to step II, but with the coating still being in excellent condition, probably indicating pending failures.

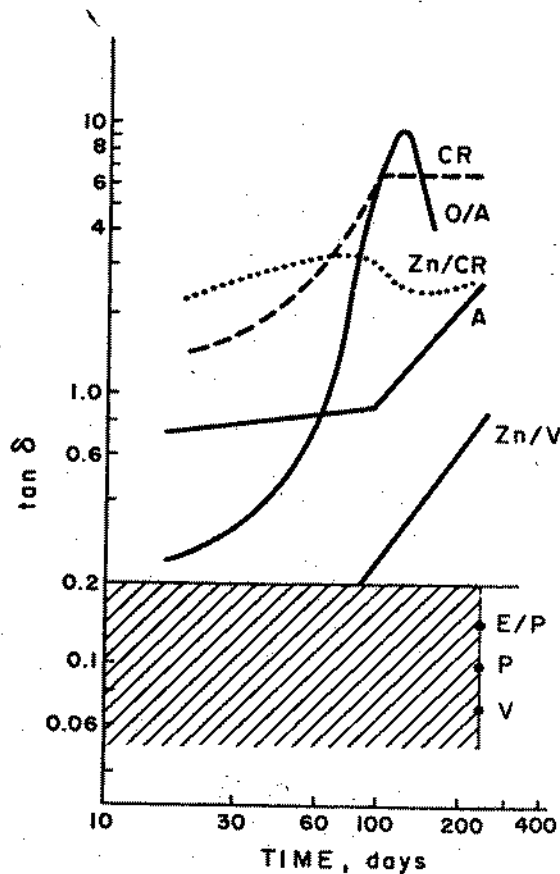


Fig. 4.- Time variation of  $\tan \delta$  (dielectric loss factor) for the different paint systems.

#### Effect of interface contamination by chlorides

Before the application of the chlorinated rubber paint system, different NaCl contamination levels were applied to a set of shot blasted (A Sa3) panels. These panels were exposed to the El Pardo's rural atmosphere, of

**EFFECT OF SURFACE PREPARATION**  
**PAINT SYSTEM: CHLORINATED RUBBER**

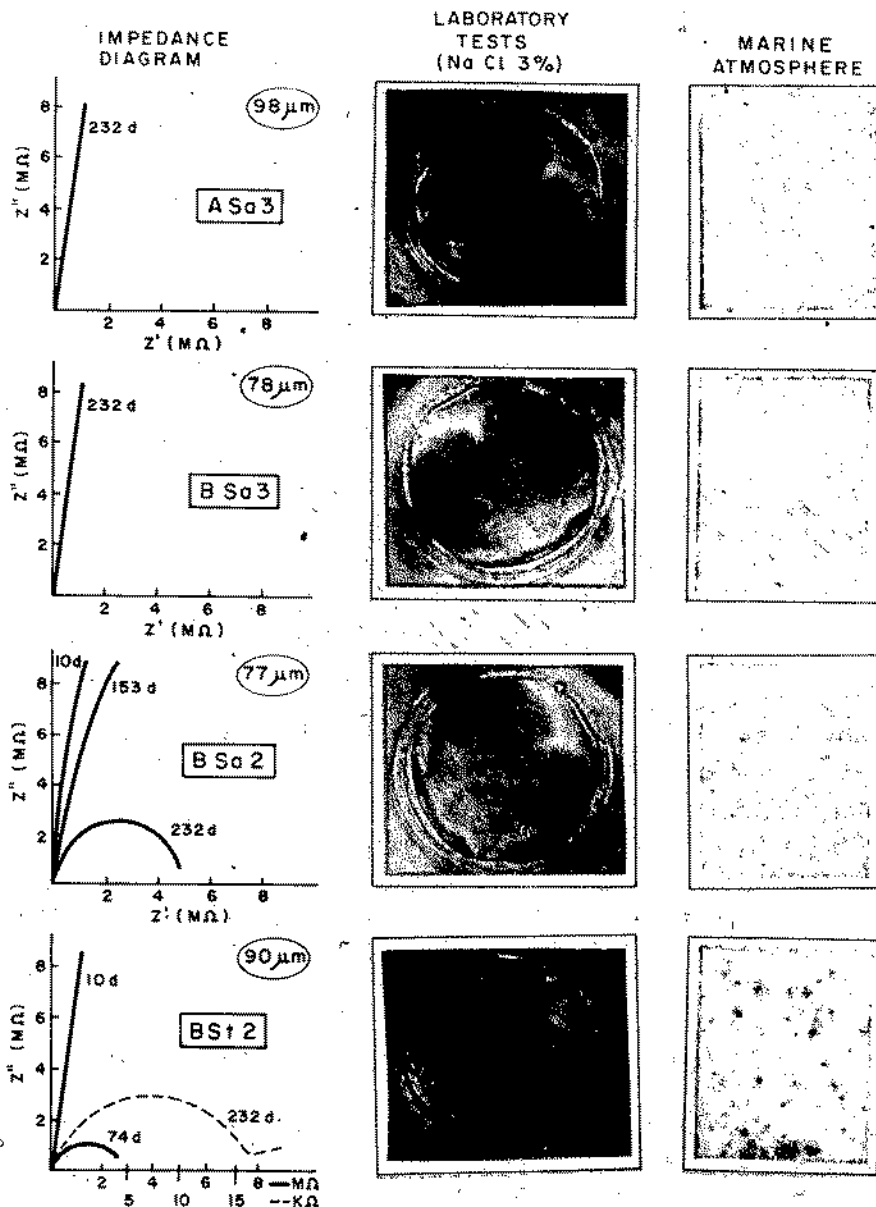


Fig. 5. - Effect of steel surface preparation. Field (marine atmosphere) and laboratory studies. System: Chlorinated Rubber.

very low aggressiveness, in order to evaluate the effect produced by this contaminant.

Figure 6 shows the close correlation between the evolution of impedance diagrams for the different contamination levels (0, 20, 100 y 500 mg/m<sup>2</sup> of NaCl) and visual deterioration of the sample's condition after laboratory and rural atmosphere tests.

From the results of the atmospheric exposure, the highest level (500 mg/m<sup>2</sup>) of chlorides causes an important blistering and rusting of the coating, similar to which was seen after one year of exposure. The corresponding impedance diagram shows the most advanced stage of evolution (smaller diameter of the semicircumference). For a 100 mg/m<sup>2</sup> contamination, blisters are seen in laboratory but not yet in the atmosphere. The diagrams for lower contaminations show the paint surface still intact in spite of belonging to step II. Once again, will these diagrams anticipate coming damages to the paint coating? Only a longer outdoor exposure time will be able to clarify this question.

### CONCLUSIONS

Considering the characteristics (type, thickness, etc.) of the tested paint systems, two years of exposure in a marine atmosphere is not enough time to notice major differences between paints. However, this exposure time was enough to show a pernicious effect when the chlorinated rubber system was applied on inadequately prepared rusty steel, or on contaminated steel with 500 mg/m<sup>2</sup> of NaCl.

The application (field or laboratory) of the electrochemical impedance technique seems to be a useful tool in order to follow and anticipate the real paint behaviours.

### ACKNOWLEDGEMENTS

The authors wish to express their acknowledgement to all the persons and organizations who collaborated in this project, particularly to the following firms: AESA, ANQUE,

**EFFECT OF INTERFACE CONTAMINATION BY CHLORIDES**  
**PAINT SYSTEM: CHLORINATED RUBBER.**

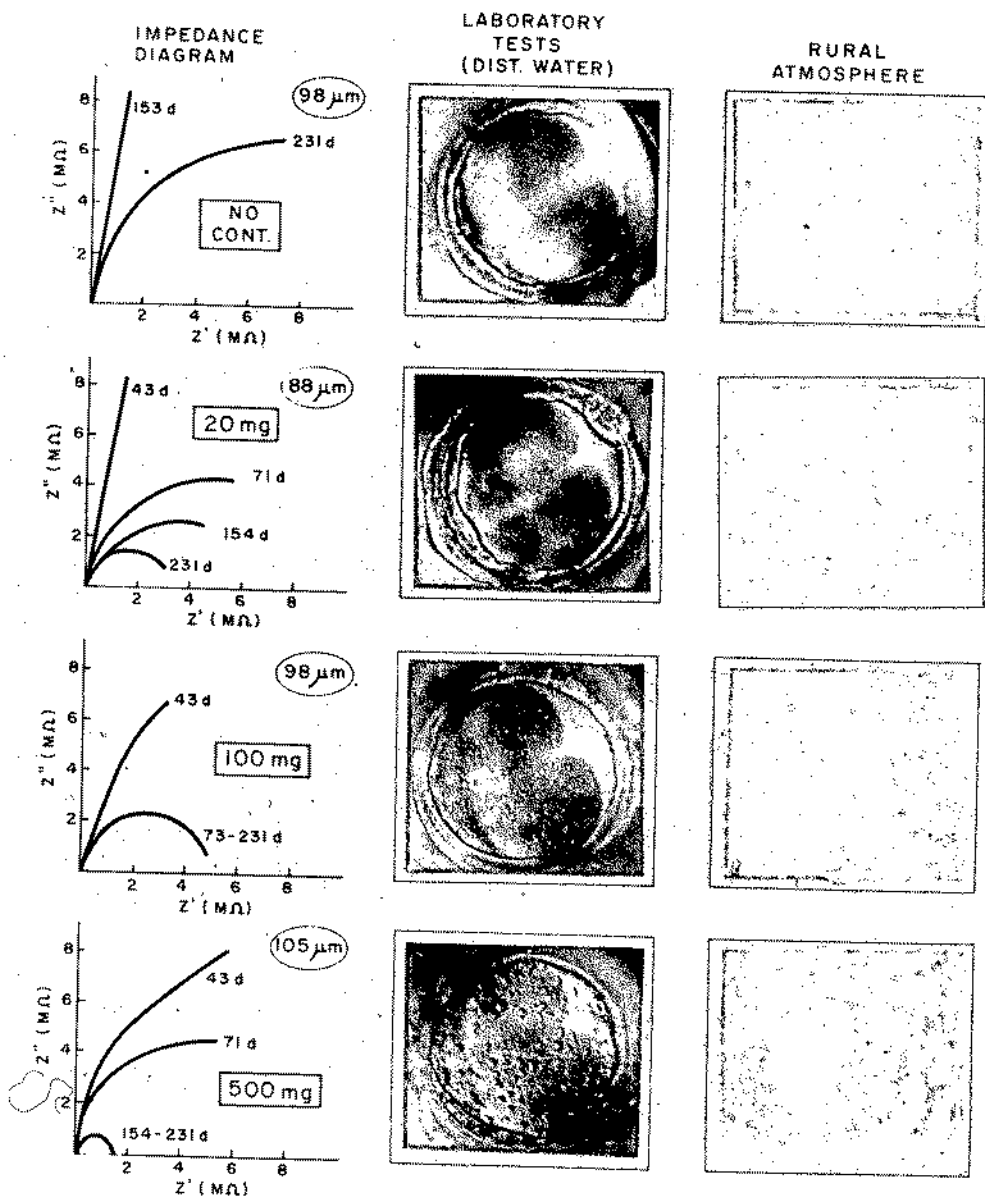


Fig. 6.- Effect of interface contamination by chlorides. Field (rural atmosphere) and laboratory studies. System: Chlorinated Rubber.



ASEFAPI, BECKER-PINER, BUFI Y PLANAS, CROS PINTURAS, EMP, ERT SA, FECSA, GLASURIT, HEMPEL, INTA, PROCOLOR, RESINOR D. VALENTINE.

#### REFERENCES

- (1).- M. Morcillo et al.: Rev. Iberoamericana de Corrosión y Protección. Special Issue (1983).
- (2).- J.D. Scantlebury and N. Ho: JOCCA, 62 (1979), 89-92.
- (3).- I. Epelboin et al.: Proced. 5th Int. Congress on Metal. Corrosion (1972), 90.
- (4).- S. Haruyama and T. Tsuru: "Electrochemical Corrosion Testing". ASTM STP 727 (1981), 167.
- (5).- S. Feliu, J.M. Bastidas and M. Morcillo: Rev. Química e Industria, 28, 9(1982), 635-639.
- (6).- F. Wormwell and D.M. Brasher: Journal of the Iron and Steel Institute, Feb. (1950), 141-148.
- (7).- Artículos cited by Y. Sato: Prog. Org. Coat, 9 (1981), 85.
- (8).- I. Sekine: "Corrosion Control by Organic Coatings", H. Leidheiser, Jr-Editor, NACE (1981), 130.
- (9).- S. Shimatani: "Standard for the preparation steel surface prior to painting" Report on the 4th International Congress on Marine Corrosion and Fouling. Antibes (Francia), 1976.



AN IMPEDANCE STUDY OF CATHODIC DELAMINATION IN MARINE  
PAINTS

S. Feliu, F. Utrilla and M. Morcillo

Centro Nacional de Investigaciones Metalúrgicas  
Ciudad Universitaria, Madrid-3, Spain

ABSTRACT

The performance of marine paint coatings on steel subjected to cathodic protection is studied with impedance techniques. The paper describes the experimental procedure adopted for carrying out the measurements on the rather large painted steel samples used in this laboratory research.

Evolution with time of the paint coating has been followed by the variation of: impedance modulus  $|Z|$  at 100 Hz, loss factor  $\tan \delta$  at 1000 Hz, and capacitance  $C$  of the parallel R-C circuit. It is found that each of these parameters offers a sensitive method for following the performance of the metal-paint system and, therefore, for a quantitative assessment of the deterioration of the painted metal when cathodic protection is applied.

Mention is made of the great effect of the cathodic potential level on the delamination phenomenon.

RÉSUMÉ

Il s'agit d'étudier le comportement des revêtements de peintures marines face à la protection cathodique

par l'entremise de l'utilisation de la technique d'impédance.

Ce présent travail expose la façon de résoudre le problème expérimental de la réalisation de mesures d'impédance avec des spécimens d'acier peint de dimensions non excessivement réduites.

Pour suivre la évolution du revêtement de la peinture avec le temps, furent pris en considération les trois paramètres suivants: le module d'impédance  $|Z|$  à 100 Hz, la tangente de perte  $\tan \delta$  à 1000 Hz et la capacité  $C$  du circuit R-C en parallèle. Une conclusion est que toutes se montrent sensibles au processus de détérioration du recouvrement de son exposition à la protection cathodique, et servent aussi à une suite quantitative.

Il est important de souligner la forte influence du très haut niveau de protection cathodique et de certaines peintures sur l'apparition du phénomène de délamination.

### Introduction

The susceptibility of paint coatings to delamination is an important matter, mainly because of its practical implications. For some time now studies are being carried out in order to determine this susceptibility (1-4). As a rule the behaviour of painted specimens is evaluated by visual inspection, a method which is generally subjective. Attempts have been made to use electrochemical measurements (5-9) to ascertain behaviour of painted surfaces.

The interest shown in electrochemical tests is related to the possibility of: (i) carrying out more objective evaluations than the visual ones, (ii) obtaining quantitative data on the corrosion rate of the metallic substrate and (iii) detecting variations in behaviour before failures in the coating are apparent. Both d.c. and a.c. techniques can be applied. The first comprises the determination of the polarization resistance  $R_p$ . A prominent place among the second techniques is held by the impedance measurements, i.e. determination of impedance diagrams, estimations of capacitance  $C$ , and of charge transfer resistance  $R_t$  in the assumption that the metal/paint

system can be represented by an equivalent circuit whose most simple expression is given in the upper part of Fig. 8. Resort can also be made to the determination of the value of loss factor,  $\tan \delta$ , and of the impedance modulus,  $|Z|$ , at certain frequencies. The a.c. techniques generally provide more information than the simple  $R_p$  measurement

Impedance measurements are performed by applying a sinusoidal signal of variable frequency to the specimens which had been subjected to the effect of the cathodic protection for given periods of time. The purpose is twofold: in the first place to get a better understanding of the possibilities of this technique for observing and predicting the behaviour of the metal/paint system with regard to the action of the cathodic protection and, in the second place, to establish the primary characteristics of the paint coating having greater influence on the behaviour of the metal/paint system.

### Experimental

Rectangular steel specimens of 15 by 10cm were subjected to shot blasting and painting under relatively similar conditions to those of the real practice.

Since the cathodic protection effects are intensified on the discontinuities of the coating, a circular holiday of 1.4 cm diameter was left on purpose on the centre of one of the two faces of each specimens. It should be pointed out that the introduction of this defect or other (for instance scratches) on the paint coatings to be exposed to the cathodic protection test constitutes a normal practice (10, 11).

Table 1 shows the various paint systems as applied to the steel specimens.

For carrying out the electrical measurements it is necessary to select a zone of the test specimens where there are no defective spots from the beginning. Otherwise the greater part of the alternating current applied would flow to them, principally at high frequencies. Therefore, impedance measurements were made in a zone of the coating far away from the edges but not far from the mentioned

holiday. The object of this was to detect the effects of the cathodic protection as soon as possible.

TABLE 1.- Type and thickness of coating

| PRIMER                                     | TOPCOAT                      | COATING DESIGNATION | TOTAL DRY FILM THICKNESS<br>$\mu\text{m}$ |                |               |
|--|------------------------------|---------------------|---|----------------|---------------|
|  |                              |                     | TESTS AT-1.20V                            | TESTS AT-0.85V | TESTS AT R.P. |
| WASH-PRIMER<br>Aprox. 15-20 $\mu\text{m}$  | COAL TAR EPOXY               | W.P./C.T.E.         | 120                                       | 135            | 140           |
|  | COAL TAR VINYL               | W.P./C.T.V.         | 135                                       | 190            | 190           |
|  | ALUMINIUM CHLORINATED RUBBER | W.P./A.C.R.         | 140                                       | 135            | 140           |
|  | CHLORINATED RUBBER           | W.P./C.R.           | 105                                       | 140            | 150           |
| Zinc Epoxy<br>Aprox. 20 $\mu\text{m}$      | COAL TAR EPOXY               | Z.E./C.T.E.         | 170                                       | 110            | 145           |
|  | COAL TAR VINYL               | Z.E./C.T.V.         | 130                                       | 190            | 205           |
|  | ALUMINIUM CHLORINATED RUBBER | Z.E./A.C.R.         | 150                                       | 150            | 140           |
|  | CHLORINATED RUBBER           | Z.E./C.R.           | 150                                       | 155            | 150           |
| Red Oxide Epoxy<br>Aprox. 20 $\mu\text{m}$ | COAL TAR EPOXY               | R.O.E./C.T.E.       | 140                                       | 115            | 155           |
|  | COAL TAR VINYL               | R.O.E./C.T.V.       | 170                                       | 150            | 205           |
|  | ALUMINIUM CHLORINATED RUBBER | R.O.E./A.C.R.       | 160                                       | 165            | 175           |
|  | CHLORINATED RUBBER           | R.O.E./C.R.         | 165                                       | 175            | 180           |

In order to limit the measurement surface area, it was decided to stick, by means of a silicone sealer, a small plastic cylinder (a section of a plastic tube) to the painted surface, on the same side as the holiday and at 0.2 cm from it.

This assembly, the small cylinder attached to the painted surface, see Fig. 1, is kept throughout the entire cathodic protection test. At the time of taking

the impedance measurements the painted steel specimen is temporarily removed from the cathodic protection cell (tank) and its surface is dried off. Then, the small cylinder on it is filled with synthetic sea water and a counter electrode is placed inside the cylinder. Once the measurements have been taken the painted specimen is again immersed in the tank in order to continue the application of the cathodic protection potential. It is recognized that the cylinder attached to the painted surface may introduce some distortion in the conditions prevailing in the specimen subjected to cathodic protection, mainly in the surface area within the cylinder, where the impedance measurements are made.

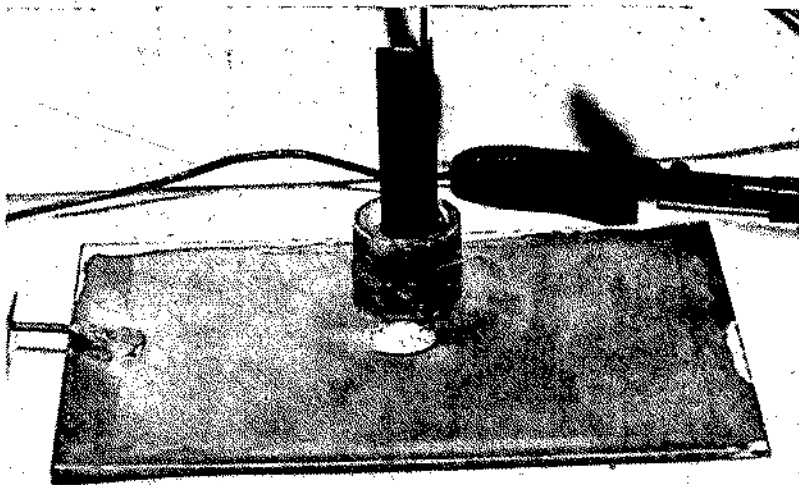


Fig. 1.

The determinations of impedance (modulus and phase angle) were performed with a H.P. (4800-A) Vector Impedance Meter. Frequency range was extended from 5 Hz to 55 kHz.

### Results

The graphs in Fig. 2-7 show the variation of parameters  $C$ ,  $\tan \delta$  and  $|Z|$  in terms of exposure time to cathodic protection. In the lower part of these figures

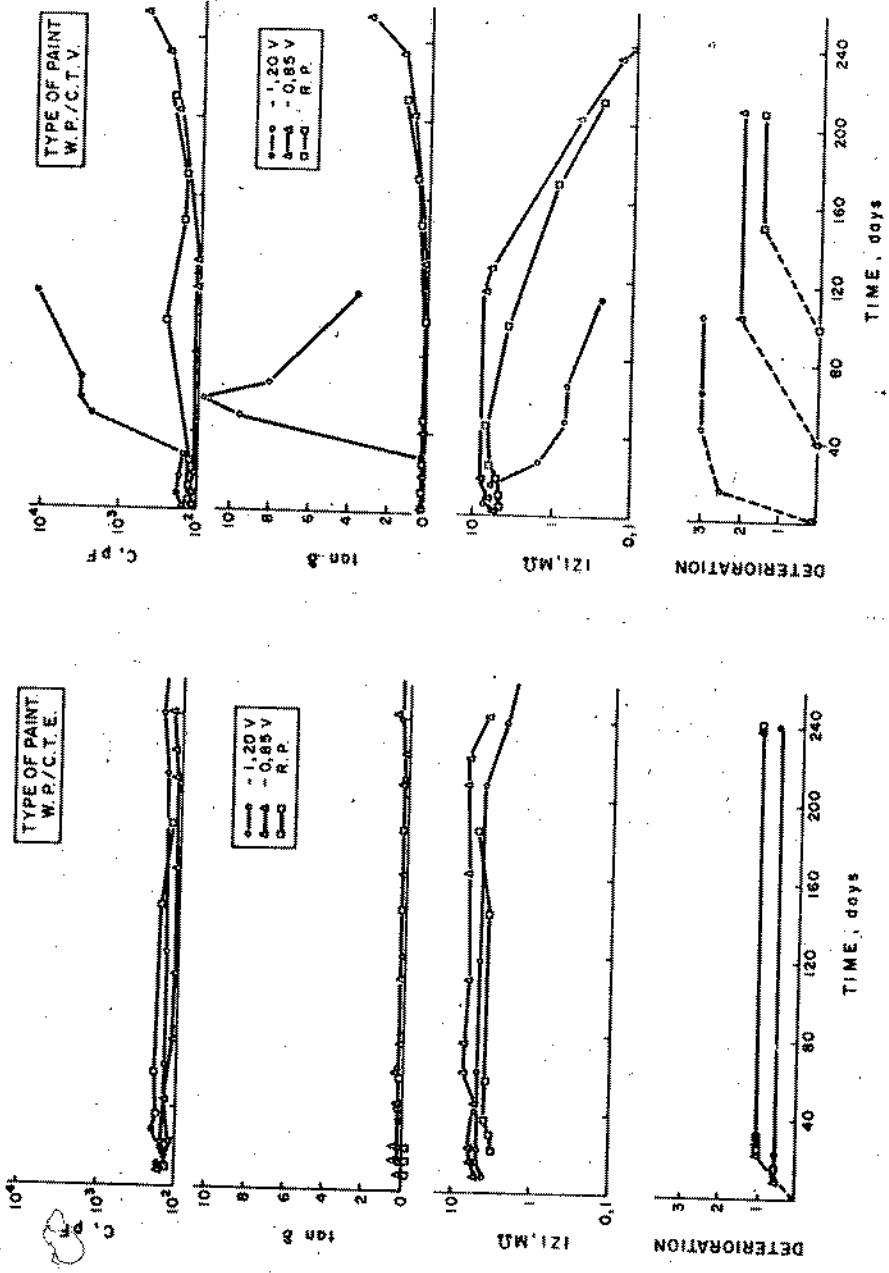


Fig. 2



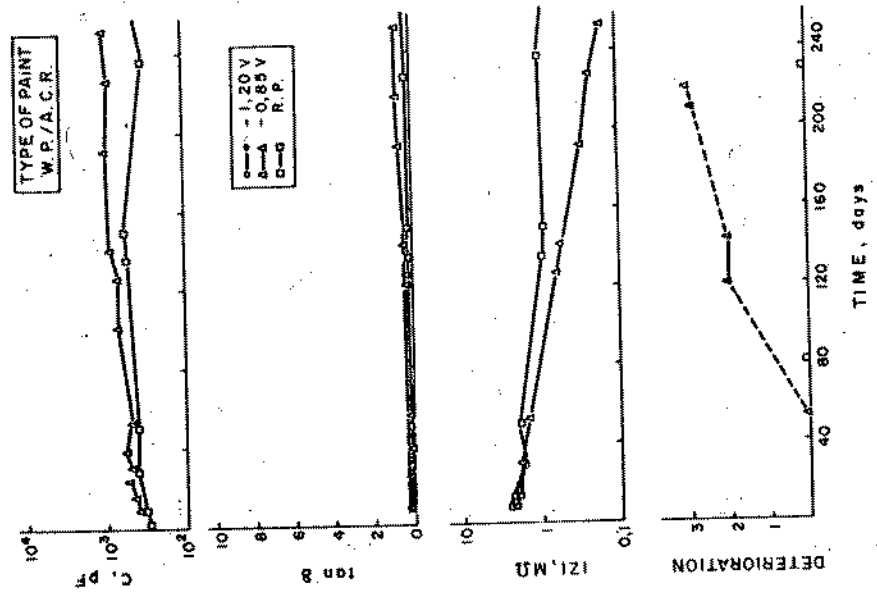
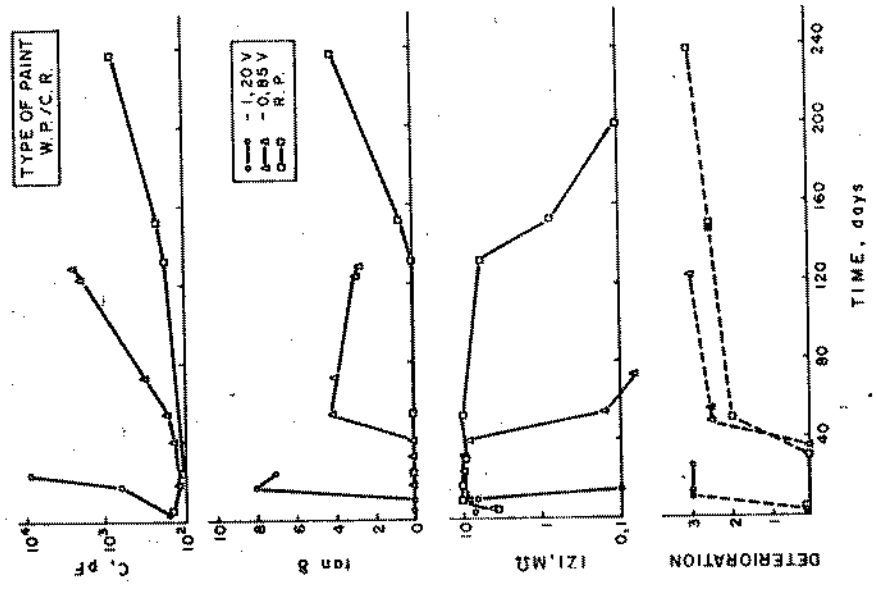


Fig. 3

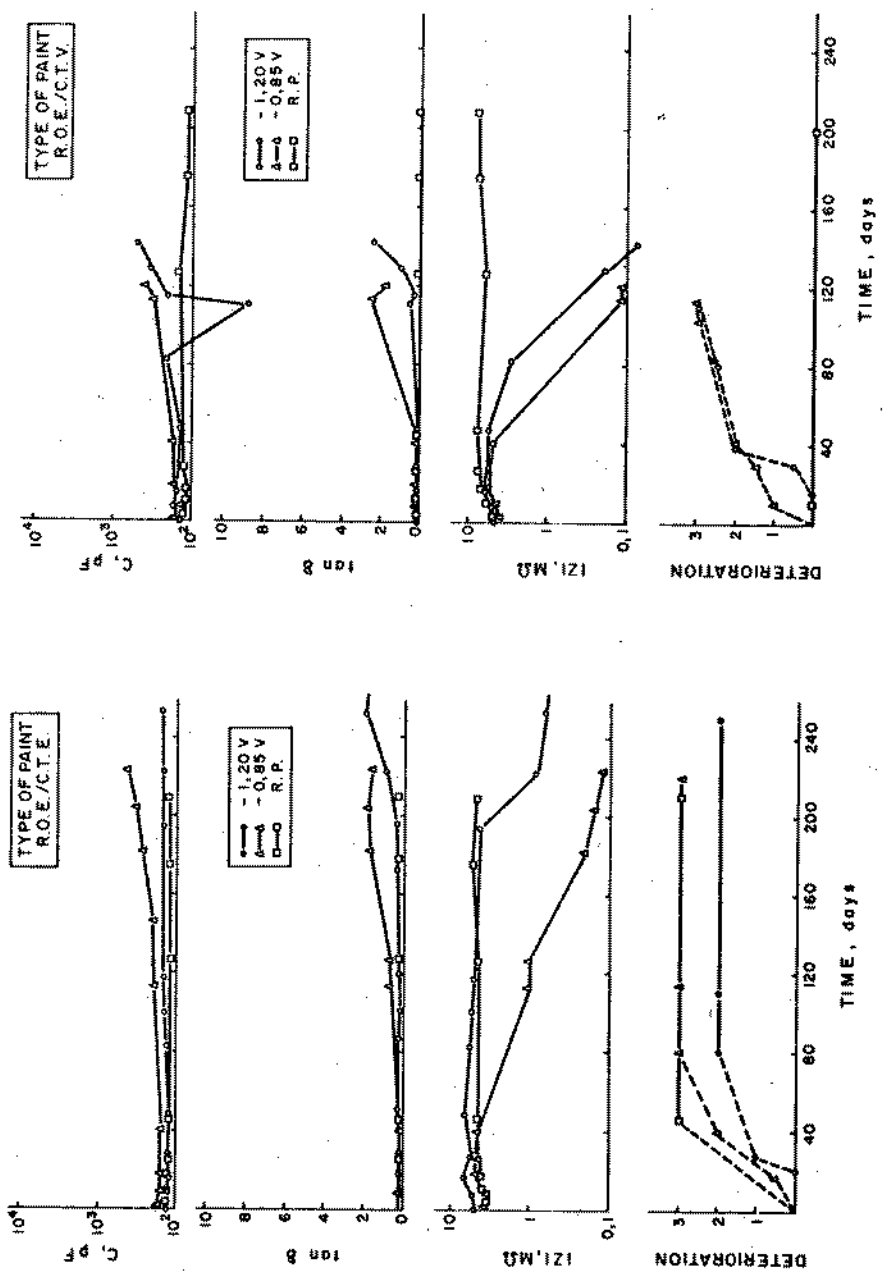


Fig. 4

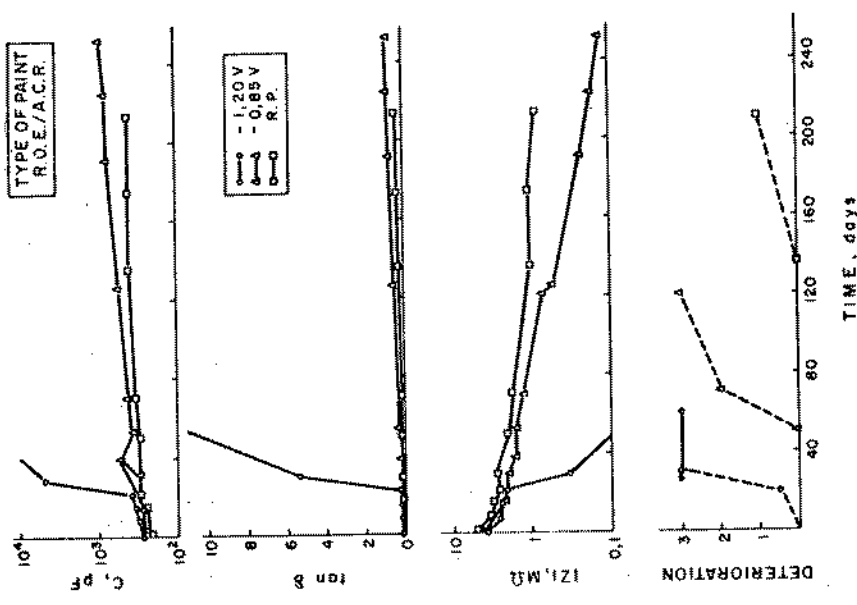
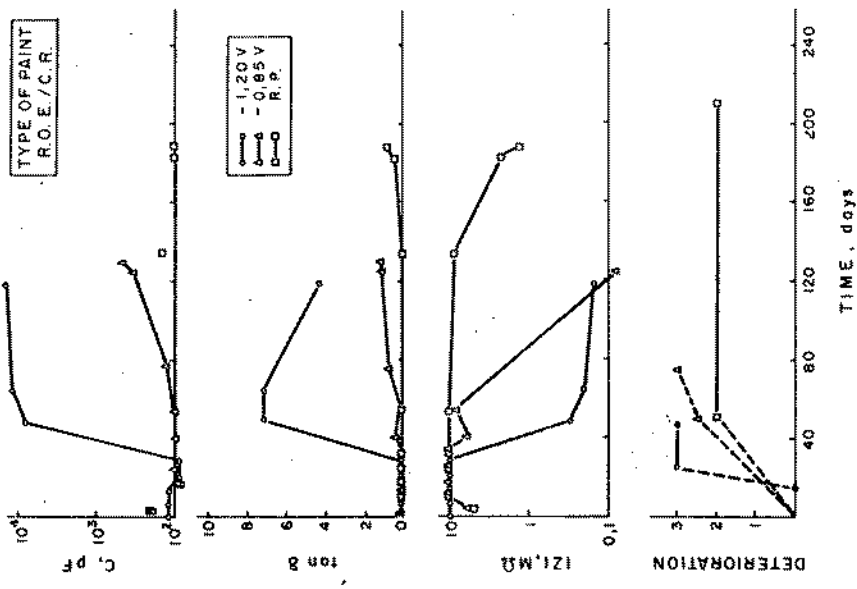


Fig. 5

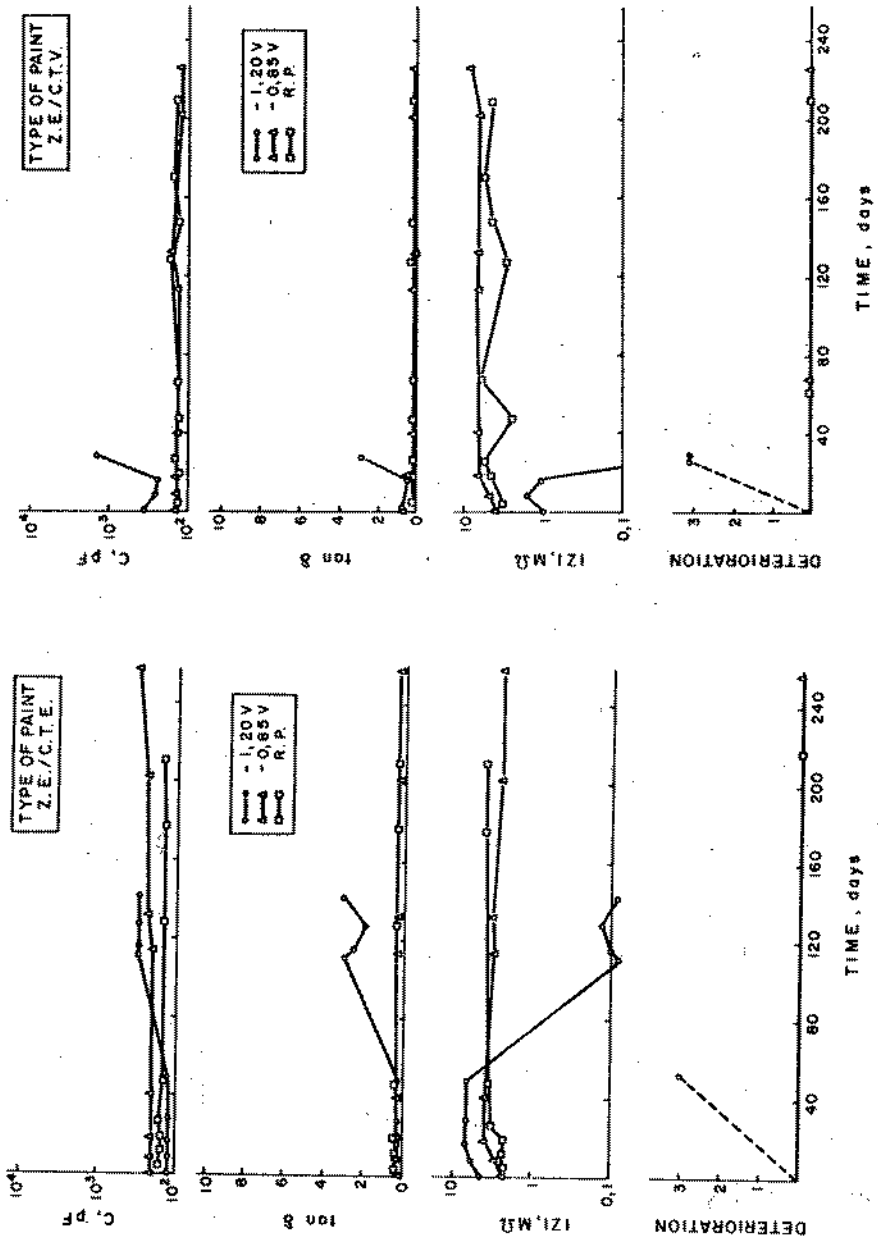


FIG. 6

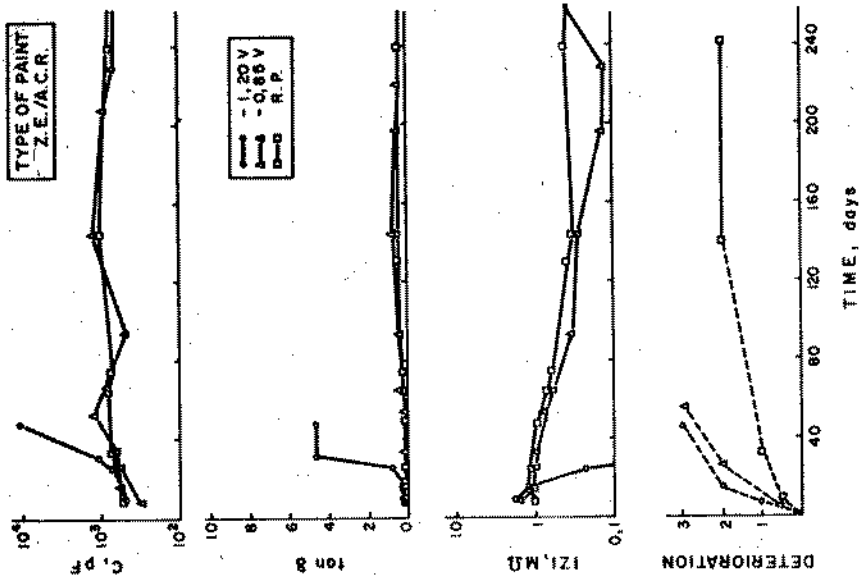
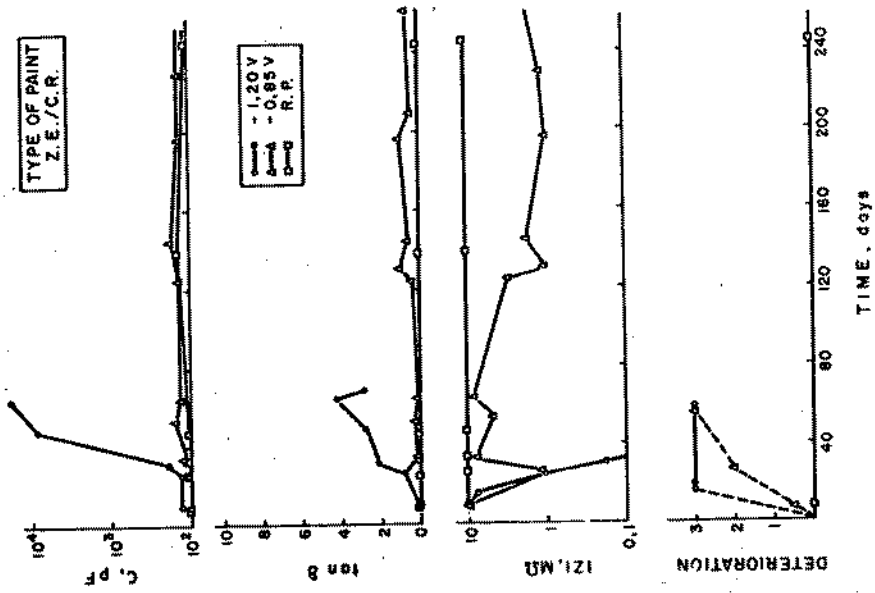


FIG. 7

an attempt has been made to show at the same time the degree of failure of the coating as evaluated visually.

The value of capacitance  $C$  was obtained from formula  $C = 1 / (2 \cdot \pi \cdot f \cdot Z'' )$  extrapolating to  $f \rightarrow \infty$ ,  $f$  being the frequency and  $Z''$  the value of the imaginary component of the impedance vector. In the event that Randles model is met, the value for  $C$  corresponds to that of the parallel capacitor in the R-C circuit (see Fig. 8). The value for  $\tan \delta$  is the loss factor of the impedance of painted specimens, which is equivalent to cotangent of the phase angle. In this report the values for  $\tan \delta$  refer to a frequency of 1000 Hz.

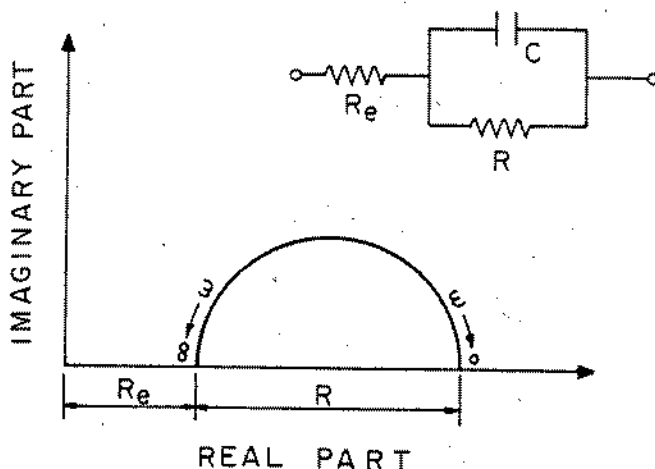


Fig. 8.

The value for  $|Z|$  in Figs. 2-7 corresponds to the impedance modulus at 100 Hz. With regard to the surface appearance of the coating, the deterioration was classified from 0 to 4 according to the following rating: 0 = no visible modification, 1 = slight deterioration, 2 = moderate deterioration and 3 = heavy deterioration. The deterioration may affect more rapidly the coating around the holiday than inside the perimeter limited by the plastic cylinder attached to the painted surface. To differentiate this case in the graphs relating to appearance of specimens, a black point has been used to

indicate the start of blistering inside the cylinder.

### Discussion

It was stated in the introduction that the main objective of this research was to verify the possibilities of the a.c. techniques for estimating the deterioration of the paint coating under cathodic protection. In Figs. 2-7 it is shown that, in effect, there is an evolution of the measured parameters as a function of exposure time to cathodic protection; to a certain extent, this variation is parallel to the degree of deterioration as verified by visual examination.

The three parameters determined, namely,  $C$ ,  $\tan\delta$  and  $|Z|$ , seem to be very sensitive to coating deterioration. Of these, the most sensitive perhaps is the modulus  $|Z|$  measured at comparatively low frequency (100 Hz). The practical interest of the measurements of  $\tan\delta$  and modulus  $|Z|$  at 1000 Hz and 100 Hz, respectively, is that they can be carried out with much less-sophisticated equipment than that required for determining the impedance diagrams or the value of  $C$ .

A question that is raised is whether such a.c. measurements permit obtaining information about the deterioration process earlier than by visual examination. According to the results of the present research the advantages of the a.c. tests are not very much in evidence in that sense, since the deterioration of the paint coating can be observed visually almost at the same time as it is detected by the analysis of the impedance data. In some cases these measurements have revealed a certain evolution in the characteristics of the coating before the visual defects appeared; doubts however exist as to the practical interest of these small differences in detecting time.

Another question is whether it would be possible to estimate the corrosion rate in the metal underneath the paint coating by means of the impedance measurements. This would be feasible if one could infer the charge transfer resistance ( $R_T$ ) from the impedance diagram. The curves in Fig. 9 provide some of these diagrams

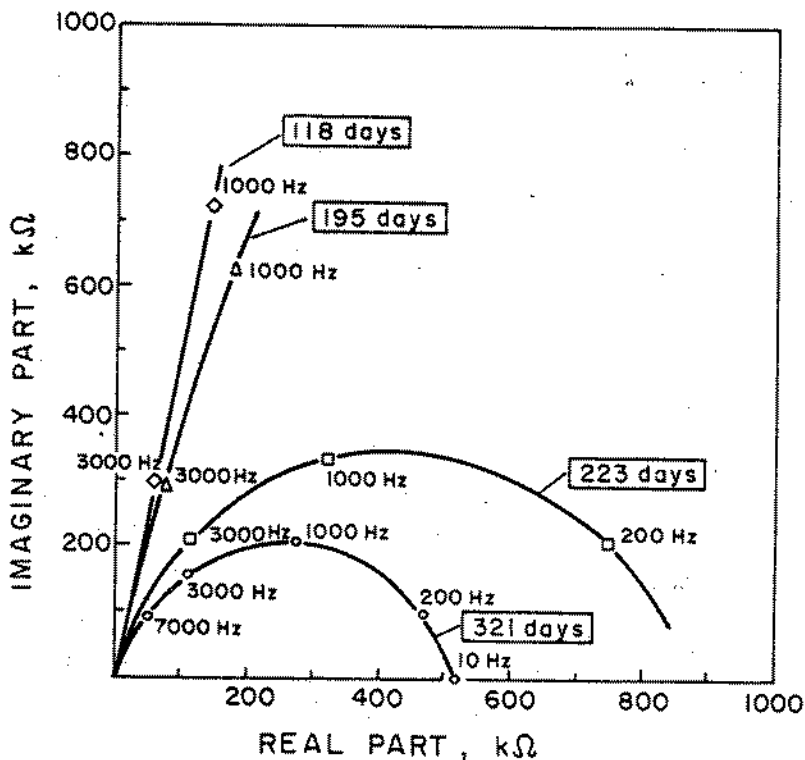


Fig. 9.

as an example. As is well known the frequency-dependence (complex impedance diagram) of the Randles model is shown by a semicircle (Fig. 8), and its diameter gives the value of the parallel resistance of the R-C circuit. However, it has not been verified whether this model fits, not even approximately, the metal/paint system, and whether the estimated resistance for this case corresponds entirely to the charge transfer resistance. It should be pointed out that the ohmic resistance of the paint coating is in series with the charge transfer resistance at the same branch of the parallel R-C circuit, the other branch being formed by the capacitor. Consequently, if the resistance thus inferred is substituted into the Stern-Geary equation, the true significance of the calculated "corrosion



current" value might be disputable. Logically, further research is required, such as the one performed with a specifically-designed test piece in order to separate in certain cases the contributions of the ohmic and charge transfer resistances (12).

In accordance with the results obtained, the behaviour of the painted steel panels when exposed to cathodic protection may depend substantially on coating composition, in particular when the highest level (-1.2V) of cathodic protection is applied. Of the 12 coatings tested the W.P./C.T.E. (Fig. 2) is the one which gives the more satisfactory results according to the evolution of curves in Fig. 2-7. The R.O.E./C.T.E. coating also shows quite good results. Stability of the other coatings appears to be markedly affected by the cathodic potential level; a given coating may show a remarkable behaviour at -0.85V and it may be quite unsatisfactory at -1.2 V. However, caution is necessary in drawing conclusions about the relative merits of the coatings listed in Table 1; it would be risky to extend these specific results to all coatings of similar generic composition since the factors that may modify paint behaviour without hardly changing their composition are numerous.

### References

1. Houston Society for Coatings Technology: J. Coating Technology, Vol. 47. No. 604, p. 57 (1975).
2. H. Leidheiser and W.J. Wang: J. Coating Technol., Vol. 53, No. 672, p. 77 (1981).
3. "Corrosion Control by Org. Coatings", Leidheiser Editor, NACE, Houston, Texas, 1981.
4. H. Leidheiser: Corrosion-Nace, Vol. 39, No. 5, p. 189 (1983).
5. A.R. Di Sarli, J.J. Podestá and A.J. Arvia: "5th International Congress on Marine Corrosion and Fouling", Barcelona, 1980, p. 484.
6. J.D. Scantlebury, K.N. Ho and D.A. Eden: "Electrochemical Corrosion Testing", Mansfeld/Bertocci Editors, ASTM-STP 727, 1981, p. 187.

7. J.C. Rowlands and D.J. Chuter: Corrosion Science, Vol. 23, No. 4, p. 331 (1983).
8. J.D. Kellner: Materials Performance, July, p. 25 (1983).
9. M. Kending, S. Tsai and F. Mansfeld: CORROSION '83, NACE Anaheim, California, 1983, Paper No. 31.
10. ASTM Standard 6-19-72, Annual Book of ASTM Standards, 27, 1979.
11. Travaux du Centre du Recherches et D'etudes Oceanographiques, Vol. 15, Fasc. 1, Nov. (1975).
12. S. Feliu, M. Morcillo and J.M. Bastidas ("The segmented test piece for studying the behaviour of the paint-metal system"): Meeting ETM-2, Genoa, April 1984.

## ABLATIVE ANTIFOULING COATING SYSTEMS

THEODORE DOWD

DEPARTMENT OF DEFENSE - U. S. NAVY

WASHINGTON, DC 20362

The widely used cuprous oxide antifouling paints are no longer able to meet the increasing demands of the Marine Industry. These paints were developed almost a century ago, and perform for about 18-24 months. In tropical waters we are lucky if we can get 12 months of service. When fuel and labor costs were cheap, this was an acceptable fact of life. Now that fuel and drydocking costs have soared, the marine industry is looking for antifouling paints that will permit extended drydocking intervals and perform foul-free between dockings to keep fuel costs to a minimum, and in addition, eliminate the costly underwater mechanical brushing. The new ablative antifouling coatings enable ship owners to achieve these results.

The marine industry, including the U.S. Navy and Coast Guard are beginning to obtain foul-free underwater hulls in excess of five years, and the clean hulls have produced a ten percent fuel saving per ship per year. In addition, the inherent, self-cleaning action will completely eliminate the expense of underwater brushing and the ensuing damage suffered by the antifouling coating by the mechanical process.

The U.S. Navy is service testing these ablative coatings on selected ships and comparing its findings with those obtained on ships in the commercial sector. The overall results show a very close correlation regarding fuel savings and foul-free performance over longer drydocking intervals.

## ABLATIVE ANTIFOULING COATING SYSTEMS

There are ever-increasing demands in the marine industry for antifouling paints that will extend drydocking intervals and improve resistance to marine fouling. The accumulation of fouling reduces a ship's speed and increases fuel consumption in order to overcome the resulting drag.

BACKGROUND:

The primary toxicants over the last 100 years have been copper salts added to vinyl and other paint resins. These paints have been marketed by every major paint company for the marine industry and sold in retail stores and marinas for pleasure boats. The U.S. Government's own version of cuprous oxide in vinyl has been designated as formula 121 and 129 under specification MIL-P-15931. This antifouling formulation has been used since 1952 on ships in the U.S. Navy and the Coast Guard.

Cuprous oxide salts perform through the gradual leaching of the toxicant through the paint film and prevent the attachment of marine fouling. However, at the very best, these materials perform anywhere from 18-24 months. In tropical waters, we're lucky if we get 12 months service.

The causes of this short service life are attributed to the following reasons:

1. Physical Properties - Since the toxicant is an additive, it is difficult to control the leaching process. At the outset, the leach rate is high due to the concentration of the toxicant in a fresh coat of paint. In the early stages after undocking, we have more toxicant exuding than is needed to control fouling. This fact also contributes to the rapid depletion of the toxicant and the early demise of the coating's effectiveness.
2. Chemical Properties - Cuprous oxide hydrolyzes in seawater and undergoes a chemical conversion to become a less

toxic copper complex salt consisting of hydroxide, carbonate, and oxychloride. This complex salt forms a hard crust which inhibits the further leaching of active cuprous oxide ions from the layer under the crust. As the concentration of copper salts diminishes, we begin to see the attachment of marine fouling in the following order:

- A. First we have the formation of slime. This begins to form in a few days after undocking.
- B. Second we note the seaweed, which starts to appear after 6 months to 1 year.
- C. Third is the attachment of tube worms, barnacles, and other crustacea.
- D. Fourth and last are the tunicates and sponges, the most sensitive of the fouling organisms, which in effect indicate the complete demise of the coating.

Once the hull fouls, the excess drag imposes a costly fuel penalty to maintain the ship's speed. When fuel was cheap, we accepted this as a way of life, and as the fouling accumulated, we turned up the fuel flow to overcome the drag. Now that fuel is costly, we cannot continue to overlook the problem.

In lieu of drydocking, we have an interim procedure of removing marine fouling with mechanical underwater brushes operated by divers.

This admittedly serves the immediate purpose to remove the fouling, restore ship's speed, and to reduce energy costs. But in so doing, there is a loss of film thickness and damage to the antifouling paint.

Once mechanical underwater cleaning is started, we're locked into it--it's like getting hooked on drugs--and the intervals between successive cleanings become progressively shorter due to the removal and damage of the antifouling coating.

Consequently, mechanical cleaning is only an interim method and a necessary evil until something

better comes along.

We are definitely in need of coating systems with a longer service life than a copper additive, and one which does not begin to accumulate fouling soon after the ship leaves the drydock.

Ideally too, is the need to supersede costly and damaging underwater brushing by having the inherent chemistry of the antifouling paint perform in an ablative fashion to continually provide a self-cleaning action to maintain a foul-free surface during the life-cycle of the antifouling coating.

#### IMPLEMENTATION OF ABLATIVE COATINGS

It appears that shipowners have finally found such a material in the commercially available ablative antifouling coatings, where the toxicant is chemically bonded to the resin. These coatings use either organotin, cuprous oxide, or a combination of organotin and copper salts. The self-cleaning action continually maintains a foul-free hull during the entire overhaul cycle of the ship.

We in the Navy certainly want to get the longest possible service life from our antifouling paints. This is emphasized in a non-classified directive issued in September 1981 by the Chief of Naval Operations who imposed drydocking intervals of up to 10 years for some classes of ships. Our plan of action is to evaluate ablative antifouling paints with extended life cycle properties.

The ablative paint system was introduced in Europe in 1974. I had an opportunity to assess its performance on commercial ships in 1978. I was convinced that the paint merited a service test and arranged for its application on the Coast Guard Cutter HAMMER in February 1979.

At the November 1980 drydocking the Coast Guard ship looked as good as the day it was painted. The companion barge with the control paint was heavily fouled.

The erosion rate is about 50 microns a year for this ship which operates at about 10 knots. Consequently, the projected service life for the 400 microns of antifouling paint is approximately 8 years. The ship's captain reports an annual average

of 10 percent fuel savings since 1980.

At the June 1983 drydocking, the antifouling coating was found to be in excellent condition after 4 years, 4 months in tropical waters off Florida. As in November 1980, the hull was washed and the ship was returned to the water without painting, except for touching up a few surfaces that had been mechanically damaged by grounding and rubbing against piers. The control coating on the barge was heavily encrusted with fouling, and was removed to base metal. This is the second time that the control coating had to be removed and replaced while the test coating continues to perform foul-free. This ship has now surpassed 5 1/2 years of foul-free service and is not scheduled for dry docking until February 1986.

At first ablative coating on a Navy ship was applied in November 1980 on USS SPRUANCE using the same material that was used on the Coast Guard Cutter. At the time, it was the first and only commercially available material and contained a combined organotin-copper salt toxicant.

At the October 1981 drydocking, the SPRUANCE antifouling coating was in excellent condition after 1 year. In October 1983, it was drydocked again and the ablative coating was still foul-free after 3 years service. It is now approaching 4 years and is still foul free.

In June 1981, another Navy ship, USS SAMPSON was coated with a similar ablative coating from a different vendor.

At the March 1982 drydocking, the ship was foul-free. It still remains that way after more than 3 years.

The two ships are operating respectively 46 and 40 months foul-free at a point in time when each of them would have required underwater brushing or drydocking to remove marine fouling if the standard cuprous oxide coatings were used. The performance of these coatings will be monitored, together with newer materials now available in the commercial sector, in order to determine which coatings satisfy our requirements.

The Navy estimates that if ablative organotin

paints are used fleet wide, they will reduce fuel costs by about 10 to 15 percent, or approximately \$300 million a year.

The earlier Navy ship, coated in November 1980 had reported that the \$100,000 extra cost of the materials and labor for the ablative coating was recouped from the fuel savings in 6 months of operation.

Continued fuel savings and elimination of underwater brushing will make this type of coating more cost effective for the Navy and other ship owners.

The overall performance of an ablative system depends on the erosion and leach rates which are affected by ship's speed, hull contour, temperature, and variations in ocean salinity.

As more new coatings become available, we are finding it expedient to apply a half dozen patches on one ship representing various manufacturers who passed preliminary screening tests in the laboratory. This was done on the destroyer USS BARNEY in June 1983.

Another method of multiple testing is to outfit the bilge keel of a ship with studs on which panels can be attached and tested under identical operational conditions. This type of testing was done on the aircraft carrier KITTY HAWK in August 1982 and repeated on BARNEY in June 1983. As a result of multiple testing, the Navy has also implemented 100 per cent ablative organotin for use on aluminum hulls, and 100 per cent ablative copper antifouling for use on steel. These paints are performing well for one to two years and will be closely monitored.

By using paints with the lowest leach rates of 0.2 to 0.4 micrograms per square centimeter per day, the Navy is minimizing any possible adverse impact on the environment. Low leach rates will keep the toxicant concentration levels in harbors to an absolute minimum.

In closing, I can safely say that ablative antifouling coating systems are accomplishing what conventional paints have failed to do, and we are hopeful that they can help us reduce our fuel costs



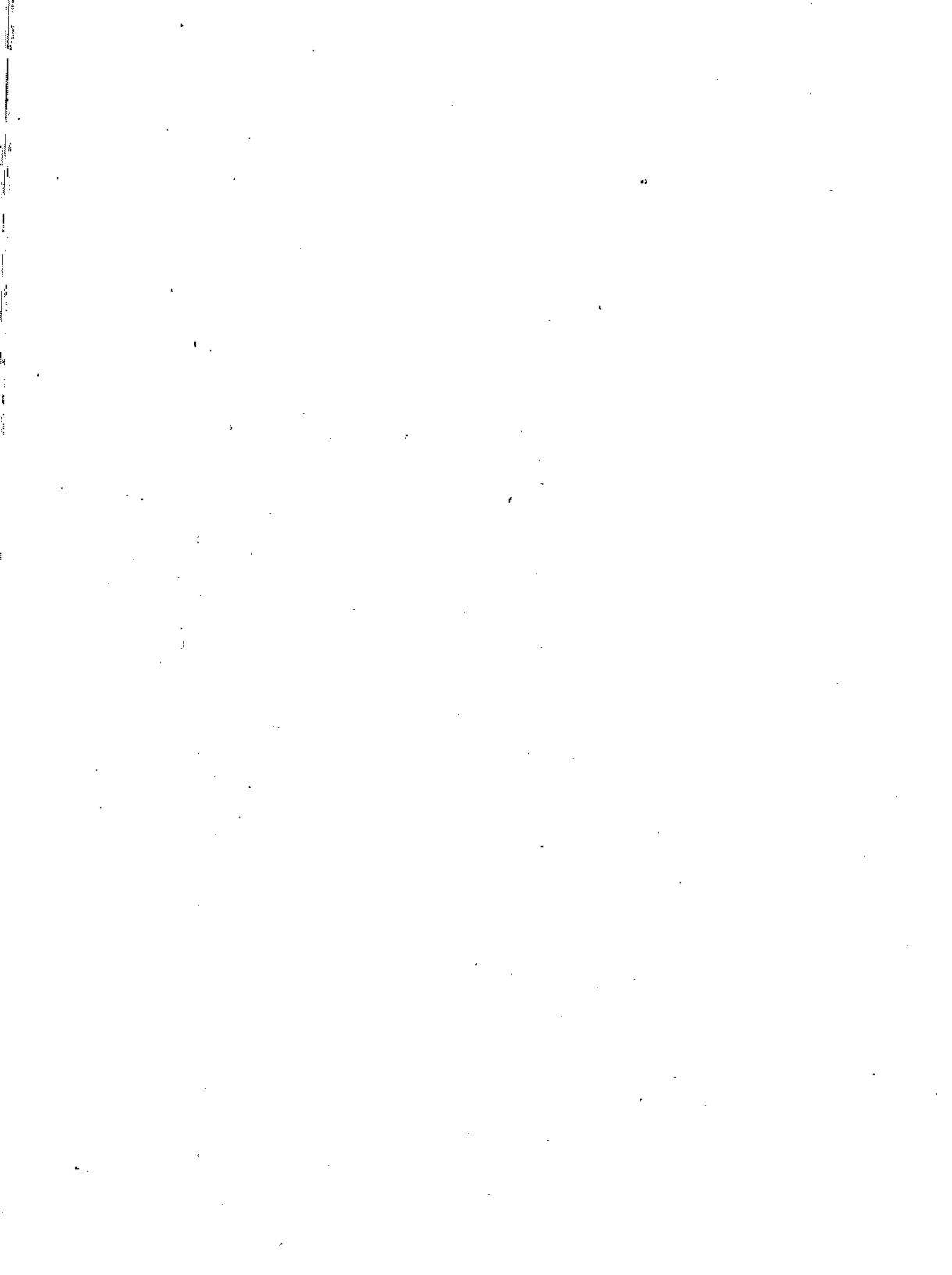
through foul-free operations, eliminate costly and damaging underwater cleaning, and increase the intervals between drydockings.

RESUME

Les peintures avec enduit préservatif à base d'oxide de cuivre d'usage généralisé ne sont plus à même de faire face aux exigences croissantes de l'industrie maritime. Ces peintures furent mises au point il y a environ un siècle et agissent au cours d'une durée de 18 à 24 mois. Il faut de la chance pour que dans les eaux tropicales elles puissent servir pendant 12 mois. Lorsque le combustible et la main d'oeuvre étaient bon marché ceci était une réalité acceptable. Maintenant que les coûts du combustible et de la cale sèche ont augmentés vertigineusement, l'industrie maritime a besoin de peintures à enduit préservatif qui permettront de longs intervalles entre séjours en cale sèche et empêcheront l'encrassement entre passages au radoub, ce qui maintient à un minimum les coûts de combustible. En outre, ceci permet d'éliminer les onéreux brossages mécaniques immergés. Les nouveaux enduits préservatifs décrassants permettent aux armateurs d'atteindre ces résultats.

L'industrie maritime, y compris la Marine des Etats-Unis et le Service de Garde-côte, commencent à obtenir des coques immergées sans encrassement pendant plus de cinq années, et les coques propres ont signifié une économie de dix pourcent en combustible par navire par an. En plus, l'effet inhérent d'auto-nettoyage éliminera totalement les frais de brossage immergé et les dommages qui s'ensuivent pour l'enduit préservatif à cause des procédés mécaniques.

La Marine des Etats-Unis procède actuellement à des essais en service de ces enduits décrassants sur des navires désignés, et compare les résultats à ceux des navires marchands. L'ensemble des résultats révèle un rapport très étroit entre les économies de combustible et l'effet anti-crasse des intervalles plus prolongés entre séjours en cale-sèche.



## BEHAVIOUR OF PIGMENTED FINISHES IN MARINE ENVIRONMENT

Š. SKLEDAR

Institute of Chemistry "Boris Kidrič"

Hajdrihova 19, YU-61115 Ljubljana, Yugoslavia

Finishes in four different media were pigmented with several organic and inorganic colour pigments at pastel tones and applied to the primed steel panels by spraying procedure. The panels were exposed in laboratory and out-of-doors. The laboratory exposures were performed in Marr accelerated weathering machine and in salt spray chamber, and the outdoor exposure in Adriatic marine climate. The tint resistance of finishes pigmented with Chrome Yellow, Disazo Yellow, and Phthalocyanine Green colour pigments was the best, and medium with Iron Blue, Indanthrone Scarlet, and a blend of Phthalocyanine Blue and Chrome Yellow colour pigments. The laboratory exposures gave useful first information in spite of more severe corrosion processes in salt spray chamber than in Adriatic environment.

### COMPORTEMENT DES FINITIONS PIGMENTÉES DANS L'ENVIRONNEMENT MARIN

Des finitions à quatre liants différents étaient pigmentées avec plusieurs pigments organiques et inorganiques colorés, en nuances dégradées dites pastel, et appliquées sur des tôles en acier, protégées par des peintures primaires, par projection au pistolet. Les tôles étaient soumises aux essais en laboratoire et dans la nature. Les essais en laboratoire étaient effectués dans la machine de Marr aux intempéries accélérées, et dans la chambre au brouillard salin, et les essais naturels dans le climat marin Adriatique. La résistance contre le blanchissement des finitions pigmentées avec des pigments colorants Jaune de Chrome, Jaune Disazoïque et Vert de Phthalocyanine était la meilleure, et médiocre avec des pigments colorants Bleu de Prusse, Ecarlate d'Indanthrone et un mélange au Bleu de Phthalocyanine et Jaune de Chrome. Les essais en laboratoire ont donné une information première utile, bien que les processus de corrosion dans la chambre au brouillard salin fussent plus sévères que dans l'environnement Adriatique.

## INTRODUCTION

Besides white finishes (1, 2), coloured finishing coats are also frequently used as a part of the protective coating systems in the marine climate (3, 4, 5). They impart a decorative effect to the surfaces on the ships' superstructures, coastal and offshore installations, appliances, and devices. However, they must be resistant to the climatic conditions in marine environment, especially to the solar radiation, where the ultraviolet part is the most active in the degradation processes of polymeric binder, and to the salt fog and wind. When finishes are tinted with colour pigments, fading can occur in various degrees, which depends on pigment and binder. In the present research work, a greater number of coated panels with coloured finishes were exposed to the Adriatic marine atmosphere for two years, and their durability investigated.

## EXPERIMENTAL

### MATERIALS AND SYSTEMS

Finishes in four different media were tinted with a gamut of nine organic and inorganic colour pigments: Chrome Yellow, Disazo Yellow, Indanthrone Scarlet, Permanent Red, Indanthrone Bordeaux, Quinacridone Violet, a non-bronze type Iron Blue, Phthalocyanine Green, and a mixed green pigment containing Chrome Yellow and Phthalocyanine Blue. All pigmentations were used at pastel tones. For comparison, white-pigmented finishes without colour pigments were also prepared. The binder employed in finish A consisted of a cellulose nitrate lacquer in combination with alkyd resin. The finish B represented an air-dried paint based on alkyd resins, the finishes C and D being stoving enamels with alkyd - melamine-formaldehyde resinous binders, stoved at temperatures of 343 K (2 hr.) and 403 K (0.5 hr.), respectively. The cleaned steel panels were primed with zinc chromate (systems B and C) and zinc chromate - red iron oxide (systems A and D) primers. Two different non-chalking grade rutiles were used as diluting white in all systems, so that two series were formed in each coating system. The characteristics of two rutile pigments are given in Table I. It can be seen that rutile I contains more titanium dioxide than rutile II whose whiteness is higher. Both of them are surface-treated with various amounts of aluminium and silicon compounds, and rutile II is additionally stabilized with zinc oxide. All finishes were applied to the primed surfaces by manual spraying procedure. The average thickness of dried coating systems was about 120  $\mu\text{m}$ . The hardness of coating films immediately before exposure in systems A and D was higher than in systems B and C, in latter being the lowest.

### EXPOSURES AND EXAMINATION METHODS

The coated panels were exposed in laboratory and out-of-doors. The laboratory exposures involved accelerated weathering in Marr weathering machine, and salt spray test at a temperature of 308 K. The out-door exposure was located on the shore of Adriatic near Crikvenica.

TABLE I  
CHARACTERISTICS OF RUTILE PIGMENTS USED

| Determination                      | Result   |           |
|------------------------------------|----------|-----------|
|                                    | Rutile I | Rutile II |
| TiO <sub>2</sub> (%)               | 94.9     | 93.7      |
| Al <sub>2</sub> O <sub>3</sub> (%) | 2.0      | 2.6       |
| SiO <sub>2</sub> (%)               | 1.9      | 1.2       |
| ZnO (%)                            | 0.0      | 0.8       |
| Whiteness (MgO = 100 %)            | 87.5     | 92.7      |
| Average particle size (μm)         | 0.25     | 0.25      |
| Density (g.cm <sup>-3</sup> )      | 4.2      | 4.2       |

The panels were placed on racks at an angle of 45° facing south. Since it was the combination of pigments and polymeric media under investigation, any change occurring on exposure was taken into account. The examinations included the measurements of gloss retention (system Lange), the ratings of the resistance to chalking (Kempf method), checking, cracking, erosion, flaking, blistering, rusting, and fading (ASTM Standard Methods D 610, D 660, D 661, D 662, D 714, and D 772). The measurements of tint resistance of finishes were performed using a reflectance filter colorimeter, which was calibrated using a set of porcelain enamel panels. The reproducibility of measurements was regarded as satisfactory, because only relative data were required to establish the colour changes. In order to better visualize the tint resistance of particular pigmentations in comparison to each other, the obtained data are represented in MacAdam's uniform chromaticity scale diagrams. The colour differences were computed according to Adams, Nickerson, and Stulz equation as combined with the Munsell value scale (6). In the computations, FORTRAN program was used in CDC 6600, CYBER 72 computer system (Control Data Corporation). The transformation of data into CIELAB colour differences is preparing (7).

#### RESULTS AND DISCUSSION

Figure 1 shows the results for finishes of system A, pigmented with rutile I and a gamut of colour pigments, from the exposure in Marr accelerated weathering machine. The results are presented in the form of uniform chromaticity scale diagram to better visualize the particular colour changes. The numbers of samples represent colour tones approximately according to DIN 6164 notation. Although there is no single accelerated weathering test which correlates absolutely with actual long-term performance in a marine environment, since there is no salt fog in the accelerated weathering machine used, still the first information can be got from this diagram. It can be seen that finishes tinted with Permanent Red and Quinacridone Violet colour pigments exhibit relatively low tint resistance, which is

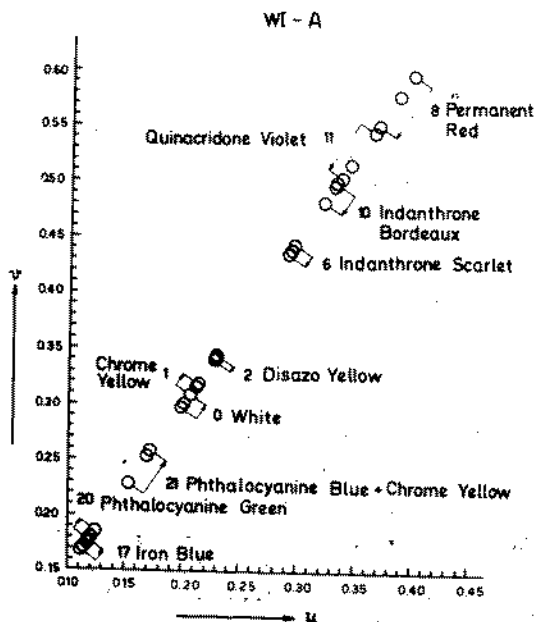


Fig. 1.—Colour changes of finishes in system A with rutile I during exposure in Marr accelerated weathering machine

better in the case of Indanthrone Scarlet than in pigmentation with Indanthrone Bordeaux. Furthermore, finishes pigmented with Disazo Yellow show the best tint resistance, which is better than that of Chrome Yellow pigment and even better of uncoloured white pigmentation. Moreover, it can be seen that pigmentation with Phthalocyanine Green resists to accelerated weathering better than pigmentation with a blend of Phthalocyanine Blue and Chrome Yellow. Finishes of system A, pigmented with rutile I and Iron Blue, show relatively good tint resistance. Generally, the colour changes are oriented towards white region in the diagram, with exception of two yellow coloured finishes, which become duller.

To evaluate the separate action of salt fog on the performance of pigmented finishes, an additional accelerated exposure was conducted in the salt spray chamber. Though there is no ultraviolet radiation, salt spray test is widely used to provide performance data for initial screening during formulation and development of coatings in spite of the fact that conditions in the salt spray chamber differ from those in a marine atmosphere due to the absence of ultraviolet radiation (8, 9). Thus other reactions take place in this accele-

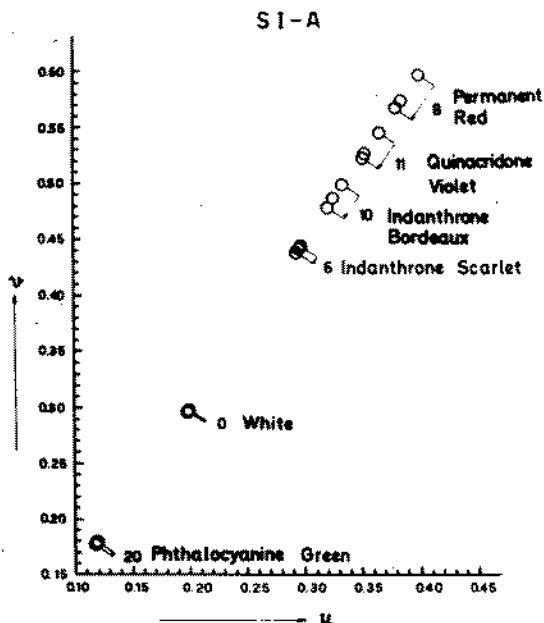


Fig. 2.—Colour changes of finishes in system A with rutile I during exposure in salt spray chamber

rated test than in outdoor exposure (10). Nevertheless, the results in Figure 2 from the salt spray chamber show a satisfactory correlation with the results from Marr accelerated weathering machine regarding tint resistance of finishes. Here too, though in smaller extent than in above mentioned machine, the tint resistance of finishes of system A containing rutile I as diluting white and pigmented with Permanent Red, Quinacridone Violet, and Indanthrone Bordeaux colour pigments is poorer than in the case of Indanthrone Scarlet and Phthalocyanine Green colour pigments. At the same time, the entire colour changes are directed to the white region. In the same system but with rutile II as diluting white, similar yet somewhat greater colour changes can be observed, which are also directed to the white region (Figure 3).

Figure 4 shows the colour changes of finishes in all four systems (A - D), containing rutile I, during outdoor exposure to Adriatic marine climate. Single points represent the computed results from the measurements after particular exposure time. Severe colour changes reveal in the case of Indanthrone Bordeaux being very small in finishes pigmented with Chrome Yellow and Disazo Yellow colour pigments. In all systems, the colour changes are oriented to the white region, except in the case of Chrome Yellow pigment. The greatest colour changes of finishes pigmented with a blend of Phthalocyanine Blue and Chrome Yellow are determined in system A, however, in case

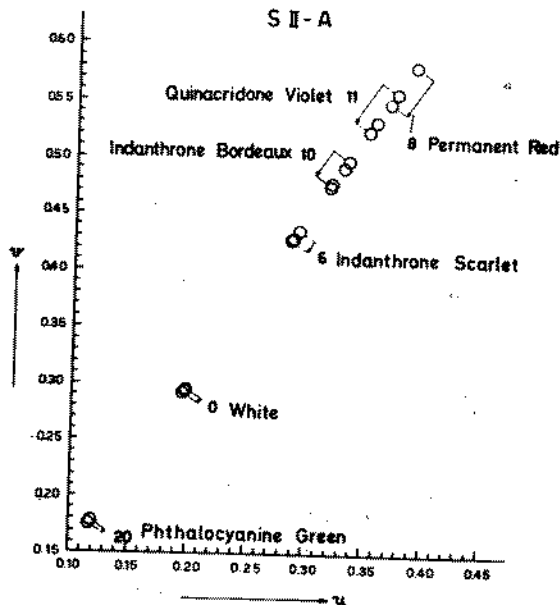


Fig. 3.—Colour changes of finishes in system A with rutile II during exposure in salt spray chamber

of Iron Blue pigment, these changes are the greatest in system B. The colour changes of finishes as pigmented with other four colour pigments and the same diluting white can be visualized from Figure 5. Finishes containing Indanthrone Scarlet exhibit much better tint resistance than those pigmented with Indanthrone Bordeaux, these changes being the smallest in system B. Similarly, the colour changes of finishes pigmented with Phthalocyanine Green are much smaller than those with a mixed green pigment containing Phthalocyanine Blue and Chrome Yellow, especially in system A. Considerable colour changes of finishes pigmented with Permanent Red can be observed, these being the greatest in system A, and the smallest in system C. The colour changes of finishes pigmented with Quinacridone Violet are smaller in all four systems as compared with Permanent Red pigmentation.

Comparable results are obtained using rutile II as diluting white in tinted finishes, as shown in Figure 6. The colour changes of finishes pigmented with Indanthrone Bordeaux are in systems A, C, and D even greater than using rutile I, but smaller in system B. Also here, the colour changes are much smaller in pigmentations with Iron Blue and a blend of Phthalocyanine Blue and Chrome Yellow, being the smallest in pigmentations with Disazo Yellow. The mixed



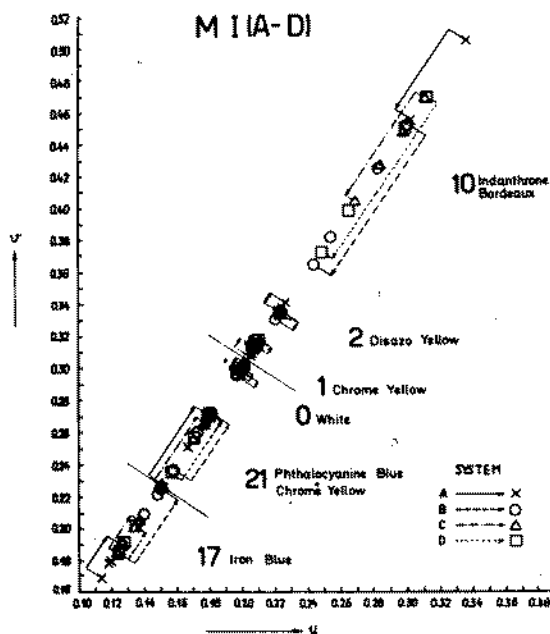


Fig. 4.—Tint resistance of finishes containing rutile I in Adriatic marine environment

green pigment shows here better tint resistance in systems A, B, and D, but somewhat smaller resistance in system C. The tint resistance of Iron Blue in finishes with rutile II is smaller than with rutile I in systems B, C, and D, remaining equal in system A. The entire colour changes are oriented to the white region, thus representing a constant-hue fading, i. e., at nearly constant dominant wavelength. The tint resistance of the next five colour pigments containing rutile II as diluting white pigment is demonstrated in Figure 7. Generally, similar impression can be got as in the case of finishes containing rutile I. Finishes pigmented with Indanthrone Scarlet show better tint resistance than those pigmented with Indanthrone Bordeaux, and Phthalocyanine Green behaves much better than mixed

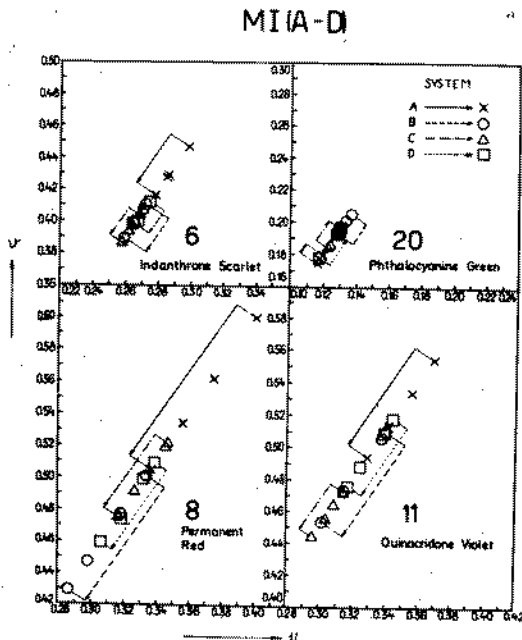


Fig. 5.-Tint resistance of finishes containing rutile I in Adriatic marine environment

green pigment containing Chrome Yellow and Phthalocyanine Blue. Chrome Yellow colour pigment exhibits superior stability against fading. On the other hand, finishes pigmented with Permanent Red show severe fading, especially in system A, where the colour changes are greater than in foregoing series containing rutile I, and smaller in systems B and C. Greater colour changes than in series with rutile I are also shown in finishes pigmented with Quinacridone Violet, with one exception in system D.

The effect of two diluting rutiles is better discernible in Figure 8 where the colour differences for two coloured pigmentations with Quinacridone Violet and Permanent Red in system A are plotted as a function of exposure time in Adriatic marine environment. Greater

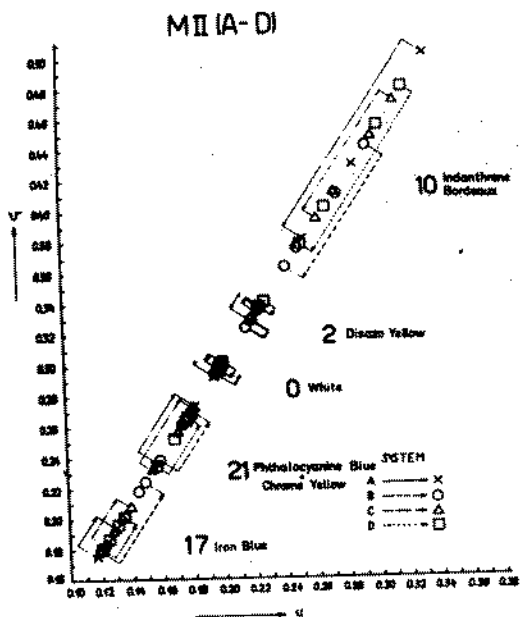


Fig. 6.—Tint resistance of finishes with rutile II in Adriatic marine environment

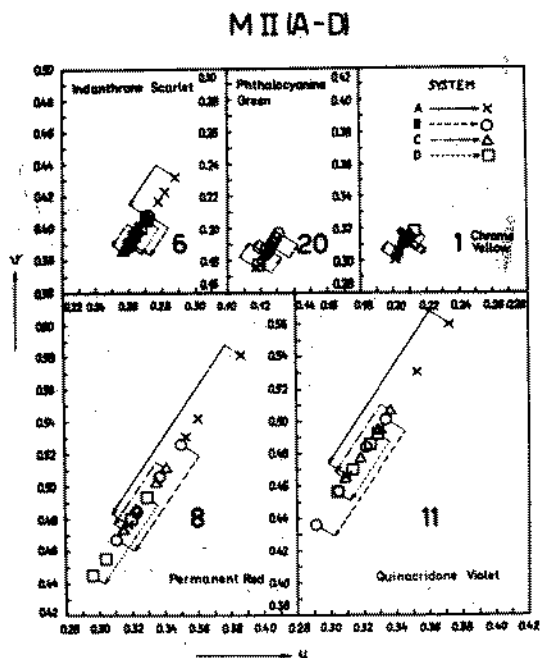


Fig. 7.—Tint resistance of finishes containing rutile II in Adriatic marine environment

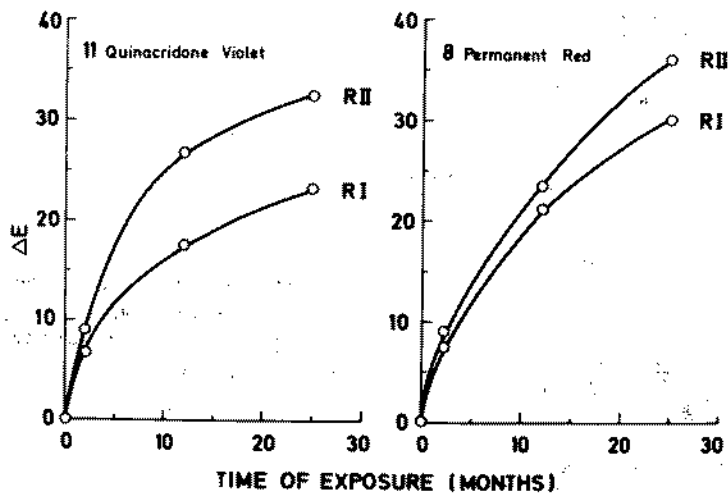


Fig. 8.—Colour differences of pigmented finishes in system A during two years' exposure to Adriatic marine atmosphere (R I - rutile I, R II - rutile II)

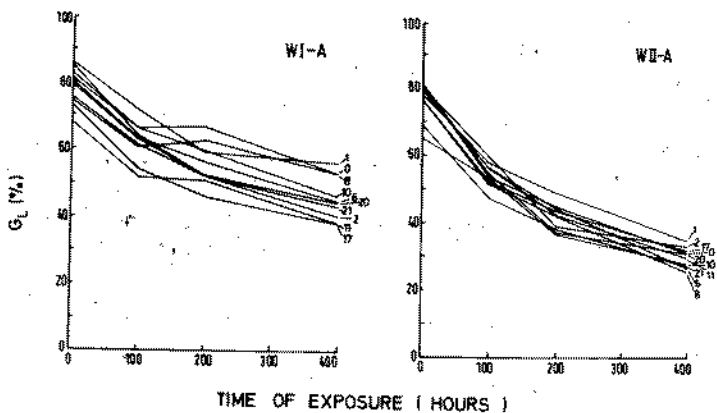


Fig. 9.—Gloss retention of pigmented finishes in system A during exposure to accelerated weathering (I - rutile I, II - rutile II, numbers of curves represent various colour pigments)

TABLE II  
AVERAGE GLOSS RETENTION OF FINISHES IN VARIOUS EXPOSURES

| System | Rutile | Percentage surface gloss retention in exposures |                          |                      |                     |
|--------|--------|---|--------------------------|----------------------|---------------------|
|        |        | Marr<br>(400 hr.)                               | Salt spray<br>(3000 hr.) | Marine<br>(2 months) | Marine<br>(2 years) |
| A      | I      | 58.0  | 77.4                     | 58.9                 | 3.9                 |
| B      | I      | 80.8  | 84.7                     | 92.8                 | 3.5                 |
| C      | I      | 75.0  | 75.5                     | 94.1                 | 8.5                 |
| D      | I      | 78.4  | 86.9                     | 88.2                 | 5.6                 |
| A      | II     | 35.0  | 77.3                     | 40.4                 | 3.9                 |
| B      | II     | 63.3  | 74.0                     | 93.2                 | 3.5                 |
| C      | II     | 69.4  | 81.8                     | 89.5                 | 13.4                |
| D      | II     | 79.7  | 86.0                     | 89.5                 | 15.2                |

effect is shown with Quinacridone Violet than with Permanent Red, however, in both coloured pigmentations, better tint resistance results with rutile I than with rutile II. But this is not a general rule, because the behaviour of investigated finishes varies depending on particular pigmentation and system.

Figure 9 shows the gloss retention of pigmented finishes in system A separately for rutile I and rutile II when exposed in Marr accelerated weathering machine. In spite of more pronounced divergence of curves for particular colour pigment in case of rutile I as diluting white pigment (left diagram), the gloss retention is better in former one. In this exposure, the gloss retention of finishes containing rutile I is also better in systems B and C, as shown in Table II representing average gloss retention of finishes in various exposures. In salt spray chamber, the gloss retention is much better than in accelerated weathering machine for lack of ultraviolet radiation, thus the absence of photochemical degradation of the polymeric binder. In Adriatic marine atmosphere, the average gloss retention of finishes in system A after two months' exposure is also better when using rutile I, however, after two years' exposure, the results are quite the same for both rutilies not only in system A, but also in system B. Moreover, after two years' outdoor exposure to Adriatic marine atmosphere, the gloss retention is generally better in systems C and D than in systems A and B, these results being much better when using surface-treated and stabilized rutile II. These results correlate well with rating of chalking shown in Table III, where higher level of chalking can be observed in systems A and B than in systems C and D.

TABLE III

## CHALKING OF WHITE PIGMENTED FINISHES IN ADRIATIC ENVIRONMENT

| System | Rutile | Percentage chalking* during exposure (yr.) |    |    |
|--------|--------|--|----|----|
|        |        | 3/4  | 1  | 2  |
| A      | I      | 14   | 22 | 30 |
| B      | I      | 9  | 19 | 25 |
| C      | I      | 0  | 1  | 14 |
| D      | I      | 0  | 6  | 23 |
| A      | II     | 12   | 19 | 25 |
| B      | II     | 0  | 9  | 23 |
| C      | II     | 0  | 1  | 17 |
| D      | II     | 0  | 1  | 14 |

\* Erichsen Chalking Scale

The protective efficiency of steel surfaces by the investigated coating systems in the course of two years' exposure to Adriatic marine atmosphere was satisfactory. No corrosion of steel surfaces appeared except on the edges of steel panels. Slight checking was observed in system A. With respect to the general appearance of coatings, their quality increased in the direction from system A to system D. On the other hand, coatings exposed to salt spray fog showed more visible corrosion processes on the edges of steel panels, which were accompanied by blistering, especially in the system A. In spite of the fact that this short-term testing procedure cannot simulate completely the Adriatic marine climate, it can give a useful information on the durability of coating systems, particularly when combined with the exposure to ultraviolet radiation in an accelerated weathering machine.

## CONCLUSION

The tint resistance of finishes in Adriatic marine environment is the best when pigmented with Chrome Yellow, Disazo Yellow, and Phthalocyanine Green, and medium with Iron Blue, Indanthrone Scarlet, and a mixed green pigment comprising Phthalocyanine Blue and Chrome Yellow, being much lower with Indanthrone Bordeaux, Permanent Red, and Quinacridone Violet colour pigments. The influence of different vehicle systems and diluting rutiles on this behaviour is not always uniform. Nevertheless, it is found that the average gloss retention of finishes upon two years' exposure to the Adriatic marine climate is better in melamine-formaldehyde vehicles combined with alkyd resin (systems C and D) than in cellulose nitrate

lacquer combined with alkyd resin (system A) and an alkyd vehicle (system B). The data from the chalking measurements correlate well with the above results. The laboratory short-term exposures in Marr accelerated weathering machine and in salt spray chamber give an initial useful information regarding the behaviour of pigmented coatings.

#### REFERENCES

1. SKLEDAR, Š.: J. Polym. Sci., Part C, No. 16: 3309, 1968.
2. SKLEDAR, Š.: Proc. 4th Intern. Congr. on Marine Corr. Fouling, Antibes, Juan-Les-Pins, 499, 1976.
3. SKLEDAR, Š.: XXXIV<sup>e</sup> Congr. Intern. Chimie Industrielle, Belgrade, 1963 (conf.).
4. SKLEDAR, Š.: Chim. Ind., 90, No. 3 bis: 181, 1963.
5. SKLEDAR, Š.: Peint. Pigm. Vern., 45: 783, 1969.
6. JUDD, B. and WYSZECKI, G., Color in Business, Science, and Ind., John Wiley & Sons, Inc., New York, 1963.
7. BILLMEYER, F. W., Jr.: J. Coatings Technol., 54, No. 694: 65, 1982.
8. KEANE, J. D., BRUNO, J. A., and WEAVER, R. E.: PACE, Phase I Report, Steel Structures Painting Council, Mellon Institute, Pittsburgh, 1979.
9. SKLEDAR, Š.: Proc. XVith FATIPEC Congr., Liège, 335, 1982.
10. APPLEMAN, B. R. and CAMPBELL, P. G.: J. Coatings Technol., 54, No. 686: 17, 1982.





CATHODIC PROTECTION  
PROTECTION CATHODIQUE



ANALYSIS OF THE TIME-DEPENDENT DEVELOPMENT OF CATHODIC  
PROTECTION WITHIN PIPES

D.J. TIGHE-FORD and J.N. McGRATH

Royal Naval Engineering College

Manadon, PLYMOUTH, UK

It is shown that cathodic protection can be impressed down pipe interiors and that development is time-dependent. The behaviour may be quantitatively described by a two stage mechanism approximated by a step function and linear transport. The rate of the second stage is determined by a coefficient of potential development which is approximately  $5 \times 10^{-5} \text{ m}^2 \text{ s}^{-1}$  for copper pipes. Possible mechanisms for a transport-dependent phenomenon are discussed and a preliminary theoretical expression for the proposed coefficient is presented.

Cet article montre que la protection cathodique peut être imprimée à l'intérieur de tuyaux et que son développement varie en fonction du temps. Son fonctionnement peut être décrit quantitativement par un mécanisme à deux phases qui ressemble approximativement à une fonction à paliers et un transport linéaire. La vitesse de la deuxième phase est déterminée par un coefficient des variations du potentiel d'un peu près  $5 \times 10^{-5} \text{ m}^2 \text{ s}^{-1}$  pour des tuyaux en cuivre. On cherche enfin quels pourraient être les mécanismes qui opéraient ce phénomène de transport et on avance une expression préalable du dit coefficient.

INTRODUCTION

Although impressed current cathodic protection systems are widely used for the protection of structures immersed in or carrying electrolytes it has been maintained until recently that it is impossible to protect a pipe for more than a few diameters from its mouth. Experimental trials in Langstone Harbour<sup>1</sup> showed that after approximately six weeks cathodic protection had

## CATHODIC PROTECTION WITHIN PIPES

developed along the length of a one metre long annulus formed between a copper pipe and an inner core.

LaQue<sup>2</sup> attributed the spread of protection over an 18in. radius circular steel plate, with a central sacrificial magnesium anode, to the deposition of an insulating, calcareous film. The development of potential was a slow process with protection not being attained right across the plate until approximately five weeks. Recent studies of galvanic and impressed current cathodic protection of pipes (Astley<sup>3</sup> and Schwenk<sup>4</sup>) and plane surfaces (Munn<sup>5</sup>) have resulted in mathematical models. These models, however, provide a quantitative description of the distribution of potential (or current) either at particular times or after "equilibrium conditions" have been obtained. The present authors have approached this field of research ab initio as a time-dependent phenomenon. The aim is to investigate and quantify the nature of the time-dependency, to determine the mechanisms involved and to produce a model to predict the behaviour of systems in a way useful to an engineer.

## EXPERIMENTAL

Fig. 1 shows the experimental system. A one metre long pipe was immersed in a tank of electrolyte and subjected to impressed current cathodic protection. The outside of the pipe was painted to reduce current demand and one end was sealed as preliminary studies shows that this effectively doubled the length. The pipe was made the cathode in the system, with a carbon rod as the inert anode; impressed potential was controlled by a precision potentiostat with reference to a silver/silver chloride (SSC) reference electrode. The potentials at different points within the length of the pipe were measured by miniature versions of the reference electrode connected via a multi-position switch to a high-impedance digital voltmeter. Throughout, the following terminology has been used:

- $E_{INIT}$  - the initial potential (SSC) of the pipe
- $E_{IMP}$  - the potential (SSC) imposed upon the pipe
- $E_{MEAS}$  - the potential (SSC) measured at any one of the mini-electrodes.

## RESULTS

Typical results for a copper pipe in sea water are shown in

## CATHODIC PROTECTION WITHIN PIPES

Fig. 2. The curves show the distribution of potential at different distances from the open end of a pipe at different times after the system was switched on. In this case the initial potential of the pipe was  $-210$  mV and the imposed potential was  $-850$  mV.

The curves show how potential varied down the inside of the pipe and at any one point became more negative, ie cathodic, with time. If the potential required to protect copper from corrosion is ca  $-350$  mV, then it can be seen that the pipe was protected along its entire length, ie 26 diameters, at some time between 900 seconds (15 minutes) and 3600 seconds (one hour). The potential attained along the pipe after one day is shown in the bottom curve. Closely similar results were obtained using 3% NaCl solution as the electrolyte (Fig. 3).

Fig. 4 shows typical results for a mild steel pipe in sea water with an initial potential of  $-700$  mV and the same imposed potential of  $-850$  mV. In this case protection may be assumed at a potential of ca  $-775$  mV; it took approximately 25 hours to achieve this value along the entire length of the pipe interior. The more negative initial potential of the steel pipe, compared with copper, limits the available driving potential and it is not possible to increase this significantly, as imposed potentials more negative than approximately  $-900$  mV are likely to result in electrolysis of the sea water. Again, however, it is clearly possible to establish a protective cathodic potential down the interior of a pipe, in this case for some 37 diameters.

In addition to studies of the distribution of potential under a variety of conditions total current demands in the impressed system have been measured. Fig. 5 shows results for two diameters of copper pipe in sea water and 3% sodium chloride solution. Current demand decreased with time, approaching a limiting value and results were closely similar in both electrolytes. Although absolute current demands differed for the two pipe diameters the current densities were virtually identical.

Events following the removal of the protective potential were also monitored. From Fig. 6a it can be seen that there is a steady decay of potential within the pipe after the current is switched off. If this decay is examined at a specific electrode (Fig. 6b), it will be seen that the potential decays exponentially with a time constant of 1500s to a condition some 100 mV more negative than the initial potential.

## THEORETICAL ANALYSIS

The shape of the potential/distance/time curves suggested similarities to those from studies of solid state diffusion or heat transfer. As transport phenomena are certainly involved

## CATHODIC PROTECTION WITHIN PIPES

in the development of cathodic potential an empirical approach has been developed employing a potential analogue of Fick's Second Law, in which concentration (C) is replaced by potential (E) and the diffusion coefficient (D) by a parameter the present authors have named the Coefficient of Potential Development ( $\mathcal{D}$ ).

Diffusion

$$\frac{\partial C}{\partial t} = D \frac{\partial^2 C}{\partial x^2}$$

Potential Development

$$\frac{\partial E}{\partial t} = \mathcal{D} \frac{\partial^2 E}{\partial x^2}$$

(x = distance, t = time)

To use this model it is necessary to convert the raw potential data to fractional change in potential, which has been

termed  $\epsilon$ , where  $\epsilon = \frac{E_{MEAS} - E_{INIT}}{E_{IMP} - E_{INIT}}$ .

As a first attempt at quantitative analysis the semi-infinite medium was chosen as an approximate model of the physical system. Analysis suggested that  $\mathcal{D}$  values of approximately  $10^{-4} \text{ m}^2 \text{ s}^{-1}$  and  $5 \times 10^{-6} \text{ m}^2 \text{ s}^{-1}$  described the changes of potential within copper and steel pipes, respectively. There was an apparent variation of  $\mathcal{D}$  in that experimental development of potential although initially faster than predicted, later became slower<sup>6</sup>. These results encouraged an investigation of the solution for a plane sheet which is believed to be a closer approximation to the experimental geometry. Using three non-dimensional groups;

$\epsilon$  = fractional change in potential

$x/l$  = fractional change in distance where  $l$  = tube length

$\eta = \mathcal{D} t/l^2$  (for constant  $\mathcal{D}$  and  $l$ , this is equivalent to time),

a solution of the following form is obtained:

## CATHODIC PROTECTION WITHIN PIPES

$$\epsilon = 1 - \frac{4}{\pi} \sum_{n=0}^{\infty} \frac{(-1)^n}{(2n+1)} e^{-(2n+1)^2 \pi^2 l^2 / 4} \cos \frac{(2n+1)\pi (x/l)}{2}$$

As with the semi-infinite medium solution<sup>6</sup> the phenomenon was originally treated as a single stage mechanism based upon linear transport; a comparison of theoretical curves from the plane sheet solution and typical results (Fig. 2) is shown in Fig. 7. Up to one hour the fit is not very close but thereafter there is a marked improvement. There was an apparent variation in  $\epsilon$  similar to that observed with the semi-infinite medium model<sup>6</sup>.

Results from Figs. 2 and 6b indicated that a condition some 100 mV more negative than  $E_{INIT}$  is rapidly attained, which apparently has a considerable degree of stability. Accordingly, a two stage mechanism has been postulated involving an initial rapid change to around -310 mV, a value termed E background, taking place after the application of an impressed current, followed by linear transport. In this case  $\epsilon = \frac{E_{MEAS} - E_{BKGD}}{E_{IMP} - E_{BKGD}}$  and the rapid potential change is approximated by a step function. Using a two stage mechanism there is close agreement between practical results and theoretical predictions (Fig. 7). Analysis of these curves shows that much of the apparent variation of the coefficient of potential development has been removed - values  $\epsilon$  or  $\epsilon$  are presented in Table 1.

TABLE 1. VALUES FOR THE COEFFICIENT OF POTENTIAL DEVELOPMENT - COPPER PIPE, TWO STAGE MECHANISM

|                  |                      |                      |                      |                      |                      |                      |                      |
|------------------|----------------------|----------------------|----------------------|----------------------|----------------------|----------------------|----------------------|
| time (s)         | 360                  | 900                  | 1800                 | 3600                 | 10800                | 14400                | 28800                |
| ( $m^2/B^{-1}$ ) | $1.1 \times 10^{-4}$ | $6.7 \times 10^{-5}$ | $5.6 \times 10^{-5}$ | $3.3 \times 10^{-5}$ | $3.7 \times 10^{-5}$ | $4.2 \times 10^{-5}$ | $2.8 \times 10^{-5}$ |

Mean:  $5.3 \times 10^{-5} m^2 s^{-1}$

## DISCUSSION

From such results and analysis it is possible to examine

## CATHODIC PROTECTION WITHIN PIPES

mechanisms which may contribute to the development of potential within a pipe by a transport-dependent phenomenon; the following four are considered to be the strongest contenders:

- |                     |  |
|---------------------|--|
|                     | Calcareous deposits, as suggested by LaQue <sup>2</sup> and others       |
| IONIC TRANSPORT     | Protective films, other than calcareous deposits                         |
|                     | Double layers, formed at the metal/electrolyte interface                 |
| MOLECULAR TRANSPORT | Oxygen, as the major cathodic reactant under the experimental conditions |

Of these it is possible to eliminate chalking - at least, as a short-term mechanism. Results from studies carried out using 3% sodium chloride solution as the electrolyte (Fig. 3) show that the time-dependent development of potential is closely similar to that in sea water (Fig. 2). Obviously, NaCl solution contains none of the elements, such as calcium and magnesium, which have been described by LaQue<sup>2</sup> as the major components of an insulating layer of "cathodic chalk". It is, of course, possible that other kinds of films on the surface of the pipe could contribute to the development of cathodic protection.

An investigation of the nature of other possible films was carried out by X-ray crystallography of deposits formed on copper discs immersed in sea water and solutions of NaCl, MgCl<sub>2</sub> and CaCl<sub>2</sub> for 6 hours at an impressed potential of -450 mV. The only constituent identified in the deposits was cuprous oxide, with the exception of CaCl<sub>2</sub> solution where Ca(OH)<sub>2</sub> was also present. It would seem likely that such surface deposits form as a result of the increased alkalinity at the cathode and it is suggested that they are an effect of the development of cathodic protection, rather than a cause. It must, however, be emphasised that the composition and density of surface films can be dependent upon potential and current density. That these films



## CATHODIC PROTECTION WITHIN PIPES

are not by themselves protective, at least under the experimental conditions, is shown by the exponential decay of cathodic potential when the impressed current is switched off (Figs. 6a & b). Such behaviour lends support not only to the belief that discharge and build-up of electrochemical double layers at the cathode surface may be involved in the development and decay of cathodic protection but also to the idea of a metastable interface state some 100 mV more negative than the free corrosion potential. The time constant of decay to this state is 1500s.

As far as molecular transport as a mechanism is concerned oxygen, which is the major cathodic reactant ( $O_2 + 2H_2O + 4e \rightarrow 4OH^-$ ) in alkaline or near neutral electrolytes is the most likely contender. This factor has been examined in pipes and in a parallel series of studies on plane surfaces. These latter studies<sup>7</sup> have been illuminating, showing that development of impressed potential (Fig. 8) is much faster in situations where the supply of dissolved oxygen to the cathode surface is reduced either by increasing electrolyte depth, providing a physical barrier or deaerating with an inert gas. Clearly oxygen is one factor which must be allowed for in any expression for  $\mathcal{D}$ .

Typical experimental values for  $\mathcal{D}$  for copper pipes, of about  $5 \times 10^{-5} \text{ m}^2 \text{ s}^{-1}$  need to be accounted for in a theoretical expression. As the most mobile ionic species,  $H^+$  and  $OH^-$ , have diffusivities of approximately  $10^{-8}$  and  $5 \times 10^{-9} \text{ m}^2 \text{ s}^{-1}$ , respectively, the problem has been approached by considering  $\mathcal{D}$  to be the product of the diffusivity of a key ion and a non-dimensional group composed of those factors known or suspected to influence the spread of potential. The expression at present being examined is:

$$\mathcal{D} = (\text{diffusivity of key ion}) \times \{ (\text{electrical conductivity of electrolyte}) \times (\text{potential gradient}) \times (\text{current density})^{-1} \times (1 - \text{function of oxygen concentration}) \}$$

Values are available for all these quantities with the exception of potential gradient and the function of oxygen concentration. Present work is directed to evaluating these two parameters.

## CONCLUSIONS

1. It has been established that there is a time-dependent development of cathodic protection within pipes.

## CATHODIC PROTECTION WITHIN PIPES

2. The phenomenon has been quantitatively described by a two stage mechanism involving an initial step change of potential followed by a transport phenomenon.
3. The transport phenomenon has been described using a potential analogue of Fick's Second Law. The coefficient of potential development has been shown to be approximately  $5 \times 10^{-5} \text{ m}^2 \text{ s}^{-1}$  for copper.
4. The oxygen content of the electrolyte is a major factor in the rate at which potential develops.
5. The coefficient of potential development is suspected to be the product of the diffusivity of a key ion and a non-dimensional group composed of factors affecting the spread of potential.
6. The formation of calcareous deposits is not a major mechanism for the spread of cathodic protection - at least in the short term. Such other films which may form appear to be the result of the increased alkalinity in the vicinity of the cathode rather than a cause of protection.

## REFERENCES

1. SAWYER, L.J.E, Private communication.
2. LAQUE, F.L., "Marine corrosion, causes and prevention", New York, John Wiley & Sons, 1975, pp. 104-109.
3. ASTLEY, D.J., "A Method for calculating the extent of galvanic corrosion and cathodic protection in metal tubes assuming unidirectional current flow", Corrosion Science, Volume 23(8), 1983, pp. 801-832.
4. SCHWENK, W., "Current distribution during the electrochemical corrosion protection of pipes", Corrosion Science, Volume 23(8), 1983, pp. 871-886.
5. MUNN, R.S., "A Mathematical model for a galvanic anode cathodic protection system", Materials Performance, August, 1982, pp. 28-36.
6. McGRATH, J.N., and TIGHE-FORD, D.J., "Corrosion", in press.
7. TIGHE-FORD, D.J. and McGRATH, J.N., in preparation.

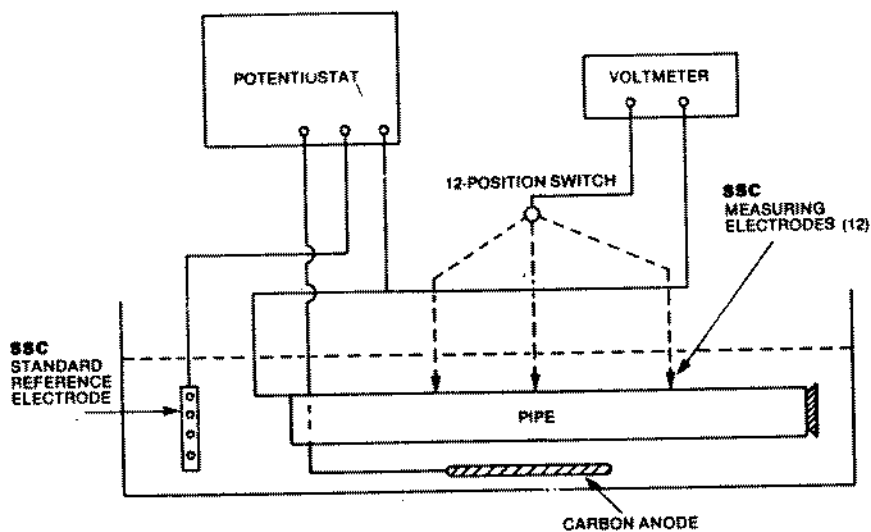


Fig. 1. Experimental system.

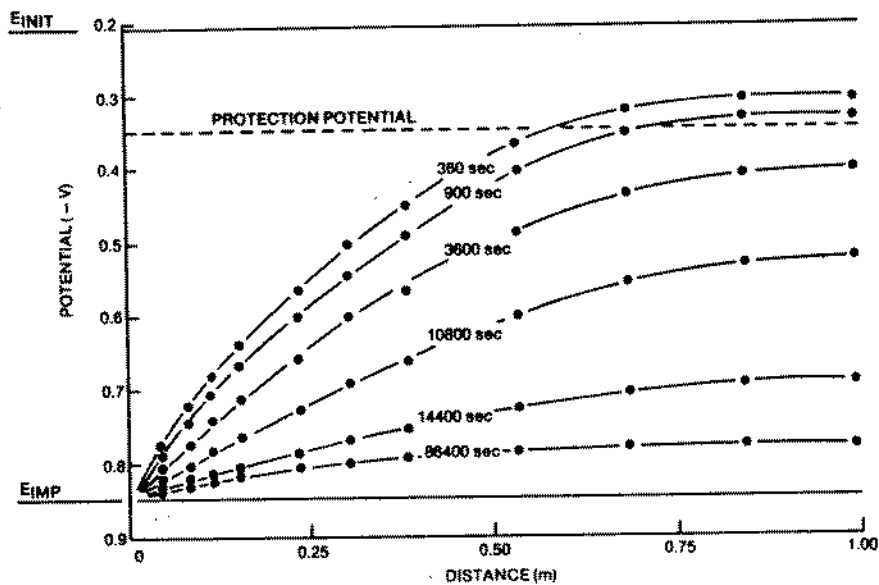


Fig. 2. Development of potential within a 38 mm diameter copper pipe in sea water.

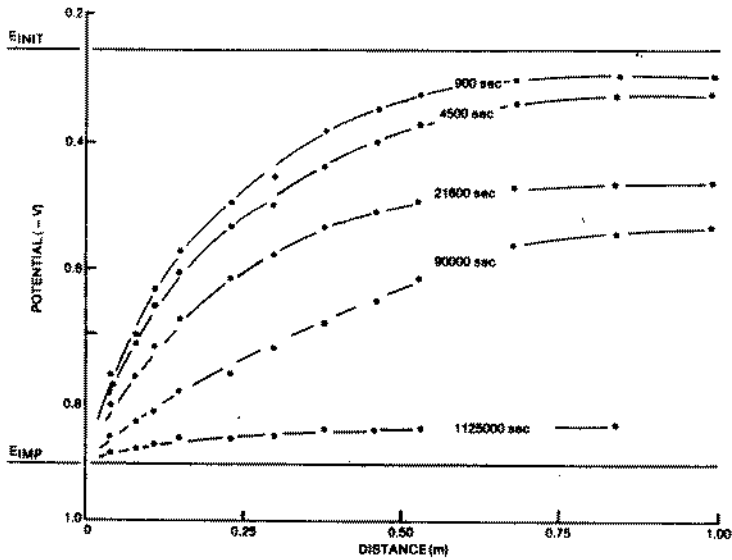


Fig. 3. Development of potential within a copper pipe in 3% NaCl solution.

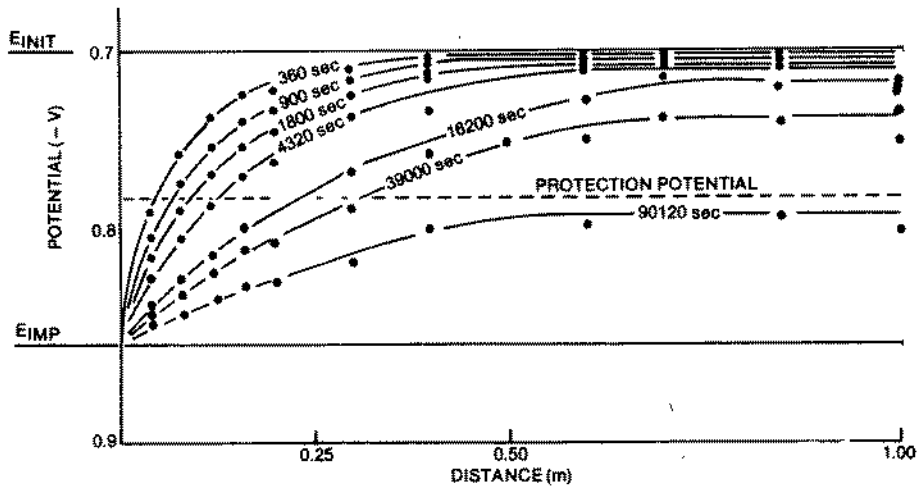


Fig. 4. Development of potential within a 27 mm diameter mild steel pipe in sea water.

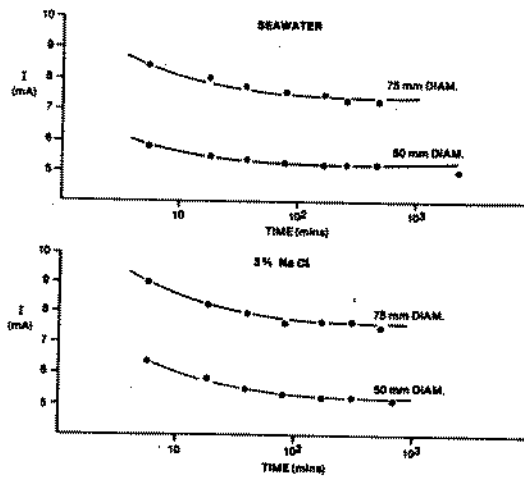


Fig. 5. Current demand for copper pipes in different electrolytes.

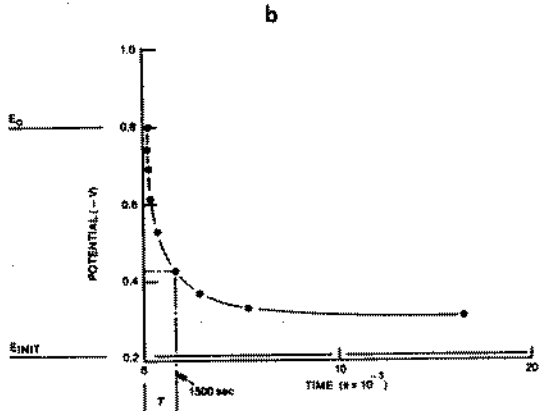
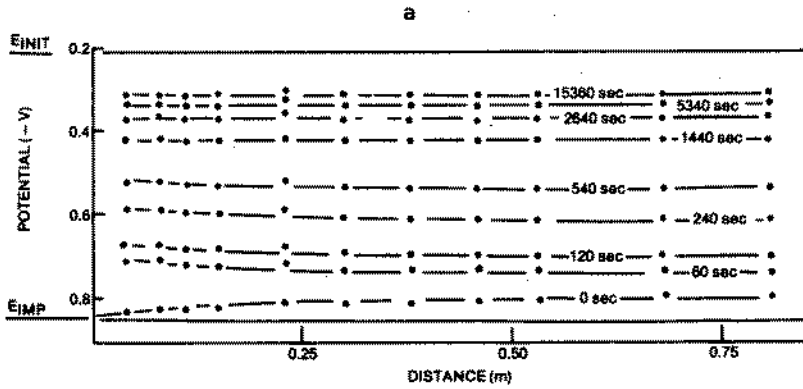


Fig. 6. Decay of impressed potential after impressed system has been switched off; a, full pipe; b, at electrode 0.53 m from mouth.

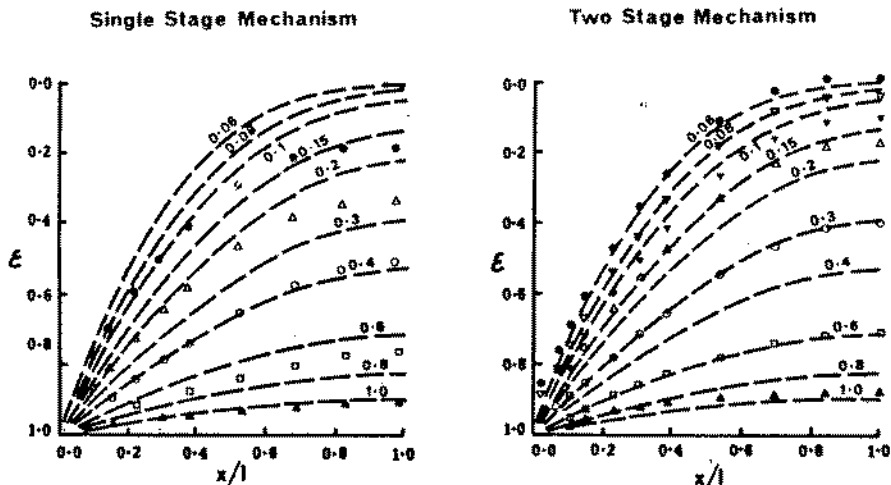


Fig. 7. Theoretical predictions (dotted) and experimental results (symbols) for a 38 mm diameter copper pipe; plane sheet solution.  $\varepsilon$  = fractional potential,  $x/l$  = fractional distance,  $\eta$  (no. on theoretical curves) =  $D t/l^2$ . ● 360s, ▽ 900s, ▼ 1800s, △ 3600s, ○ 10800s, □ 14400s, ▲ 28800s.

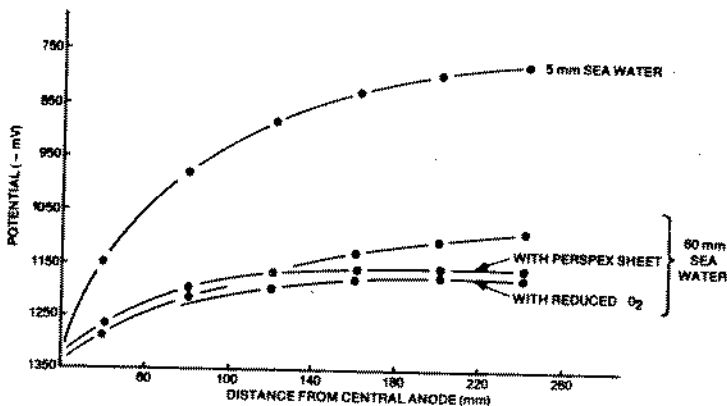


Fig. 8. Effect of oxygen upon development of impressed potential over a circular copper plate in sea water.

AN INITIAL INVESTIGATION OF pH CHANGES CLOSE TO THE SURFACE OF  
ALUMINIUM WITH PROLONGED CATHODIC POLARISATION IN SEA WATER

D. EUROF DAVIES and K.G. WATKINS

DEPARTMENT OF METALLURGY AND MATERIALS TECHNOLOGY

UNIVERSITY COLLEGE OF SWANSEA, SWANSEA, SA2 8PP, U.K.

ABSTRACT

The change in the pH of sea water with distance from the surface of cathodically polarised HS30 aluminium alloy and the effect on the deposition of calcareous deposits has been investigated. It was found that both calcium and magnesium compounds were deposited only after prolonged polarisation and at values of pH in excess of the theoretical values for the deposition of these compounds from sea water. Once formed magnesium compounds were more effective than calcium compounds in buffering the electrolyte near the surface against increase in pH under the conditions of the test.

RÉSUMÉ

La variation de pH de l'eau de mer en fonction de la distance à la surface d'un alliage d'aluminium HS30 cathodiquement polarisé, et son effet sur le dépôt de calcaire à la surface de l'alliage ont fait l'objet de la présente étude.

Il a été mis en évidence que les composés calciques et magnésiques ne se déposent qu'après une polarisation prolongée, à des valeurs de pH supérieures aux valeurs théoriques calculées.

Les composés magnésiques une fois formés se sont révélés avoir, dans les conditions expérimentales, un effet tampon sur l'électrolyte, à proximité de la surface, plus marqué que les composés calciques.

## INTRODUCTION

Changes in the pH of the electrolyte close to the surface of aluminium with prolonged cathodic polarisation are of fundamental importance in the cathodic protection of the metal in marine environments.

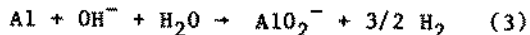
The cathodic protection of aluminium is achieved by cathodically polarising the metal to such a potential that passivity results, a condition also achieved when the aluminium is coupled with zinc.

The predominant form of attack on aluminium in aqueous chloride solutions is that of pitting corrosion. This may be inhibited, however, when the metal is cathodically polarised, but the application of a cathodic current results in the production of  $\text{OH}^-$  ions by the oxygen reduction and/or hydrogen evolution reaction. (1)



At potentials slightly more negative than the free corrosion potential the predominant cathodic reaction is diffusion controlled oxygen reduction, but as the potential becomes more negative the predominant cathodic reaction is the activation controlled hydrogen evolution.

The accumulation of hydroxyl ions in the electrolyte close to the metal surface may lead to a localised increase in pH. This is unfavourable in the case of aluminium which, because of its amphoteric nature, may suffer cathodic corrosion - a specialised form of attack resulting in the formation of aluminate ions.

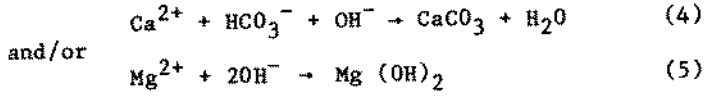


Depending upon environmental conditions, some cathodic corrosion will generally take place and thus the effectiveness of cathodic protection on aluminium depends upon the application of cathodic polarisation sufficient to inhibit pitting while minimising cathodic corrosion. (2)

The magnitude of the pH close to the surface of aluminium during cathodic protection is important since the corrosion rate of the metal in alkaline environments increases sharply with increasing pH. Factors which mitigate against a localised increase in pH will similarly be important. In sea water such localised increase in pH may result in the solubility product of sparingly



soluble alkaline earth compounds such as CaCO<sub>3</sub> and Mg(OH)<sub>2</sub> being exceeded:



Theoretical estimates of the pH at which CaCO<sub>3</sub> and Mg(OH)<sub>2</sub> are deposited from sea water are 8.7 and 9.7 respectively.

The formation of such compounds may be beneficial, in buffering the electrolyte against further rise in pH (3) and, upon deposition on the aluminium surface, in reducing the current required for polarisation and thus limiting the rate of production of OH<sup>-</sup> ions (in (1) and/or (2)) (1,4,5,6). Calcareous film formation has also been found to be of importance in the cathodic protection of steel in marine environments, an area which has been recently reviewed. (7)

The purpose of this investigation is the preliminary study of the pH changes close to the surface of an aluminium alloy in sea water during prolonged cathodic polarisation, and the macroscopic observation of the effect of such changes on the deposition of calcium and magnesium compounds.

EXPERIMENTAL

Specimens of size 4.5 x 2.2 x 0.20 cm were prepared from HS30 aluminium alloy strip. The composition of the alloy was as follows:

|    |      |    |         |
|----|------|----|---------|
| Si | 0.86 | Ti | 0.018   |
| Mg | 0.65 | Zn | 0.015   |
| Mn | 0.42 | B  | 0.003 % |
| Fe | 0.39 | Al | balance |
| Cu | 0.03 |    |         |

Sea water was collected from deep water off Swansea Bay and filtered through a 0.2µm micropore filter.

The apparatus shown schematically in Figure 1 was developed to enable the pH of the sea water close to the cathodically polarised aluminium alloy specimen to be determined. The specimen was mounted horizontally and secured between the perspex frame, (A) and the base-plate, (B) by means of six stainless steel screws. Water-tightness was ensured by the incorporation of grease-coated rubber gaskets between the specimen, the frame and the base-plate. Electrical connection was made to the specimen by means of a sprung copper strip (C) secured to the base-plate to which was soldered an insulated wire.(D)

The pH of the sea water was determined by the use of an antimony micro electrode, (E) in conjunction with a saturated calomel probe\*, (F). Calibration was carried out in buffer solutions of pH 8.0, 9.2 and 10.0 and, in this range, a straight-line relationship between pH and the potential difference of the electrodes was obtained.

The apparatus which was employed to hold the pH electrode system and move it accurately with respect to the surface of the aluminium specimen is also shown schematically in Figure 1. This arrangement has been adapted from an experimental apparatus used by Kobayashi (8) to determine the pH close to the surface of cathodically polarised steel in NaCl solution.

The electrodes were secured in the plate G which could move freely on the stainless steel rods, H against the springs I. Plate G, and hence the electrode assembly, could be moved accurately in the vertical direction by means of the micrometer barrel, J, rigidly mounted in the fixed plate K. The aluminium specimen was cathodically polarised by means of the current supplied by the Marston MA 84 platinised titanium rod, L. The potential of the aluminium was monitored by the saturated calomel reference electrode, M and was regulated by means of a Chemical Electronic TR-70-2A potentiostat. The cell was filled with 200cm<sup>3</sup> of sea water of initial pH 8.2. Cathodic polarisation was carried out under quiescent conditions at room temperature (20°C) at potentials of -1.0, -1.1, -1.2, -1.3, -1.4 and -1.5V for periods up to 5 days. The detection of the formation of calcium or magnesium compounds on the aluminium surface was limited to the macroscopic appearance of these compounds and where these were observed they were investigated by means of S.E.M. and X-ray microprobe analyses.

---

\* both manufactured to specification by Probion Ltd., Glenrothes, Fife, Scotland.

## RESULTS AND DISCUSSION

The pH of the sea water as a function of distance from the surface of the aluminium alloy during cathodic polarisation at potentials of -1.0, -1.1, -1.2, -1.3, -1.4 and -1.5V is shown in Figures 2-7.

At potentials of -1.0 and -1.1V the pH close to the surface (0.05mm) has risen to 9.6 after 20 hrs. This is in excess of the theoretical estimate of the pH for calcium carbonate deposition from sea water (8.7) yet there was no evidence of deposit formation on the aluminium alloy surface, suggesting that the process might also depend on factors such as nucleation and growth. (7)

Calcareous deposit formation at a potential of -1.2V was slight and was only apparent towards the end of the 5 day polarisation period. The deposit took the form of small spheroids (Figure 8) which had incompletely covered the aluminium surface. X-ray microprobe analysis determined the deposit as  $\text{Ca}^{++}$  with  $\text{Mg}^{++}$  absent. Despite the formation of a calcium compound the pH of the sea water close to the surface remained high after 5 days at 10.3 (Figure 4).

At potentials of -1.3, -1.4 and -1.5V (Figures 5, 6 and 7, respectively), deposit formation was more pronounced and resulted in a film which completely covered the surface of the specimens for testing times up to 5 days. But after 20 hours, before the deposits had formed, the pH close to the surface was not prevented from rising to values as high as 10.8. After 5 days (4 days in the case of the specimen polarised at -1.4V) when the deposits had formed, the pH near the surface had decreased to 10 or below and was close to the theoretical value for the deposition of magnesium compounds (9.7) (i.e. 9.7 at -1.3V; 10.0 at -1.4V (after 4 days), 9.8 at -1.5V). S.E.M. observations (Figures 9, 10, 11) revealed the presence of small spheroids embedded in a more uniform matrix. X-ray microprobe analysis determined the spheroids as  $\text{Ca}^{++}$  with  $\text{Mg}^{++}$  absent (as at -1.2V) and the more uniform matrix as  $\text{Mg}^{++}$  with  $\text{Ca}^{++}$  absent, suggesting  $\text{CaCO}_3$  spheroids in a matrix of  $\text{Mg}(\text{OH})_2$ .

These results suggest that under these conditions, while calcium compounds are deposited from the sea water at a lower pH than magnesium compounds, they are less effective in buffering the sea water close to the aluminium surface against rise in pH. One explanation is that the magnesium compounds, once a suitable pH for their deposition has been established, nucleate and grow more effectively than calcium compounds.

## CONCLUSIONS

The following conclusions are reached concerning the cathodic polarisation of HS30 aluminium alloy in sea water under the given conditions:

1. The deposition of calcium and magnesium compounds limit the rise in pH close to the surface only after prolonged polarisation (up to 5 days) and at potentials more negative than  $-1.2V$ .
2. Calcium and magnesium compounds are deposited at pH values greater than the theoretical estimate of the limiting pH for their deposition from sea water, possibly because of factors connected with nucleation and growth.
3. Once formed, magnesium compounds are more effective in limiting the rise in pH close to the surface although a higher pH is initially required for their formation.

The effect of calcium compound formation alone (i.e. at  $-1.2V$ ) over longer periods of testing merits investigation.

## REFERENCES

1. H J Engell and P Forchhammer, "Variation of the pH value at metal surfaces during cathodic protection in sea water" (in German), Corrosion Science, 1965, 5, 479-488.
2. M Cerny, "Present State of Knowledge about Cathodic Protection of Aluminium", Protection of Metals, 1975, 11, 645-654.
3. I B Ulanovskii, "Cathodic Protection of Aluminium in Sea Water", Protection of Metals, 1970, 6, 550-552.
4. J T Crennell, "Cathodic Protection - its Application to Ships and Establishments of the Royal Navy", Chemistry and Industry, February 1954, 204-209.
5. J H Morgan, "Cathodic Protection", (Leonard Hill, London, 1959), p 28 ff; p 170 ff.
6. G Butler and H C K Ison, "Corrosion and its Prevention in Waters", (Leonard Hill, London, 1966), pp 21, 227.
7. S Pathmanaban and B J Phull, "Calcareous Deposits on Cathodically Protected Structures in Sea Water", paper presented at UK National Corrosion Conference 1982, London.
8. T Kobayashi, "Effect of Environmental Factors on the Protective Potential of Steel", Proceedings of N.A.C.E. Fifth International Congress on Metallic Corrosion, Tokyo, Japan, 1972, 627-630.

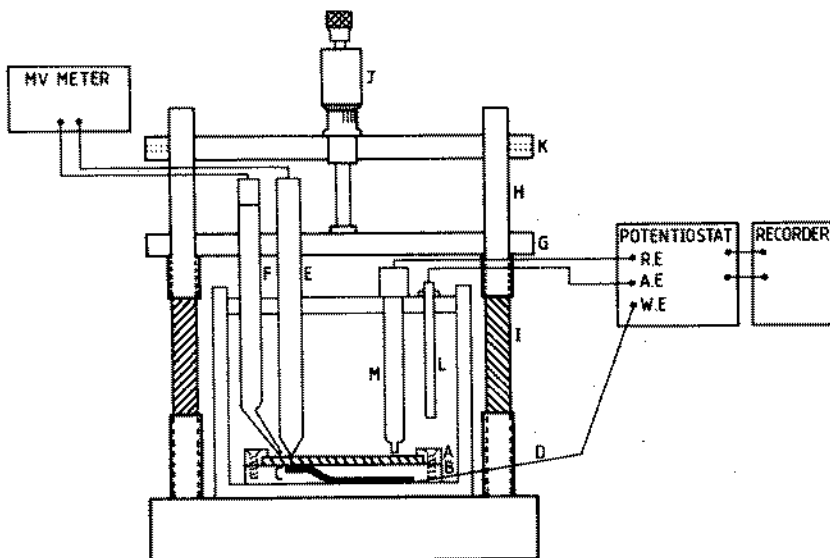


FIGURE 1. Schematic diagram of apparatus for the determination of the pH of the sea water close to the surface of a metal during cathodic polarisation.

[Key: A - perspex frame; B - base plate; C - sprung copper contact strip; D - insulated wire; E - antimony electrode; F - saturated calomel probe; G - movable plate; H - stainless steel rods; I - springs; J - micrometer barrel; K - fixed plate; L - platinised titanium counter electrode; M - saturated calomel reference electrode].

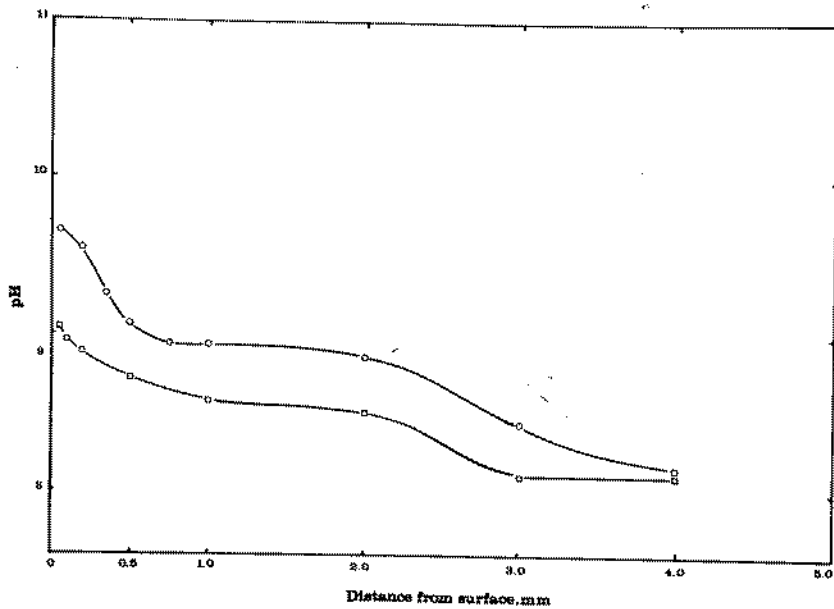


FIGURE 2. The variation of the pH of the sea water with distance from the surface of HS30 aluminium alloy cathodically polarised at  $-1.0V$ .

[KEY:  $\square$  after 1 hour;  $\circ$  after 20 hours]

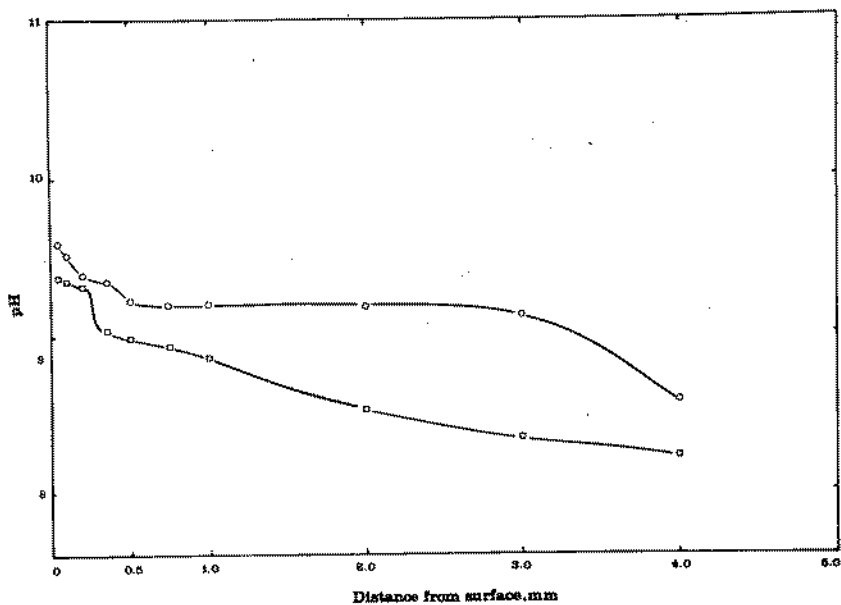


FIGURE 3. The variation of the pH of the sea water with distance from the surface of HS30 aluminium alloy cathodically polarised at  $-1.1V$ .  
[KEY □ after 1 hour; ○ after 20 hours]

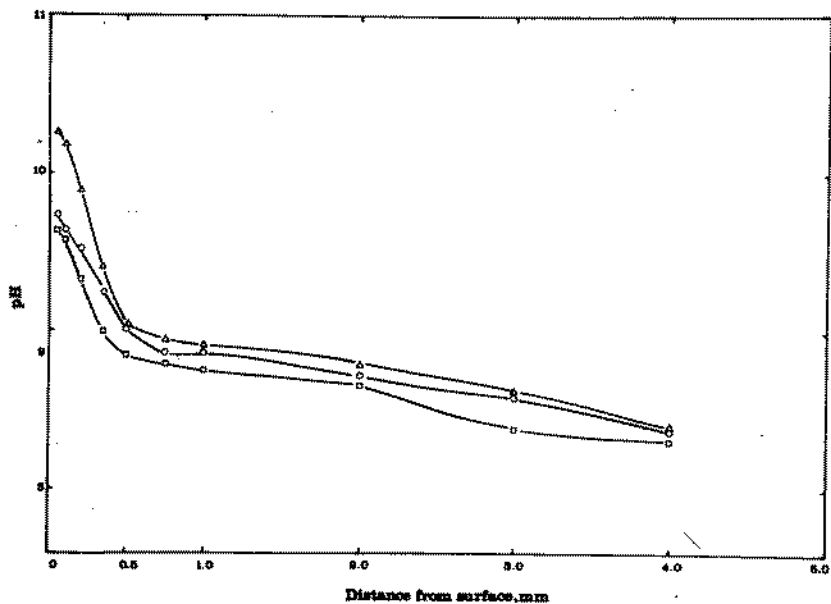


FIGURE 4. The variation of the pH of the sea water with distance from the surface of HS30 aluminium alloy cathodically polarised at  $-1.2V$ .

[KEY:  $\square$  after 1 hour;  $\circ$  after 20 hours;  
 $\triangle$  after 5 days]



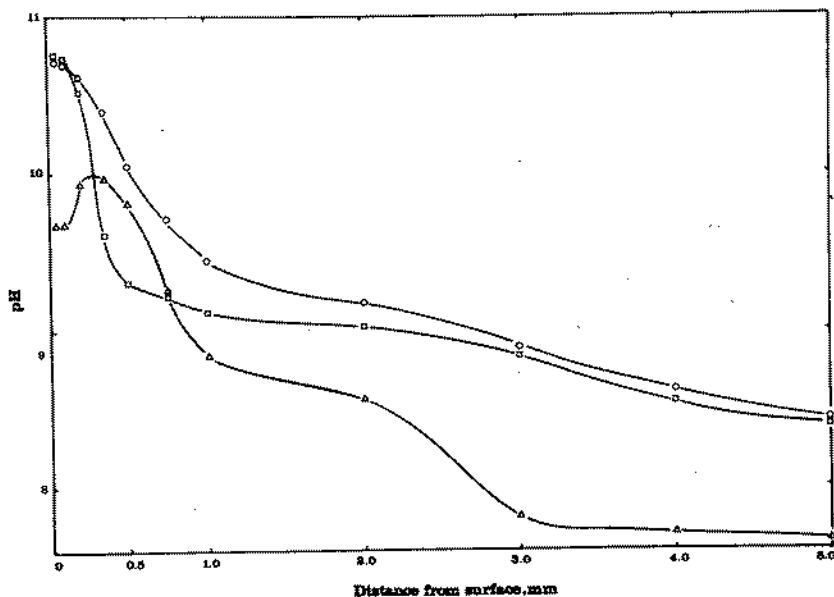


FIGURE 5. The variation of the pH of the sea water with distance from the surface of uncoated HS30 aluminium alloy cathodically polarised at  $-1.3V$ .

[KEY:  $\square$  after 1 hour;  $\circ$  after 20 hours;  
 $\triangle$  after 5 days]

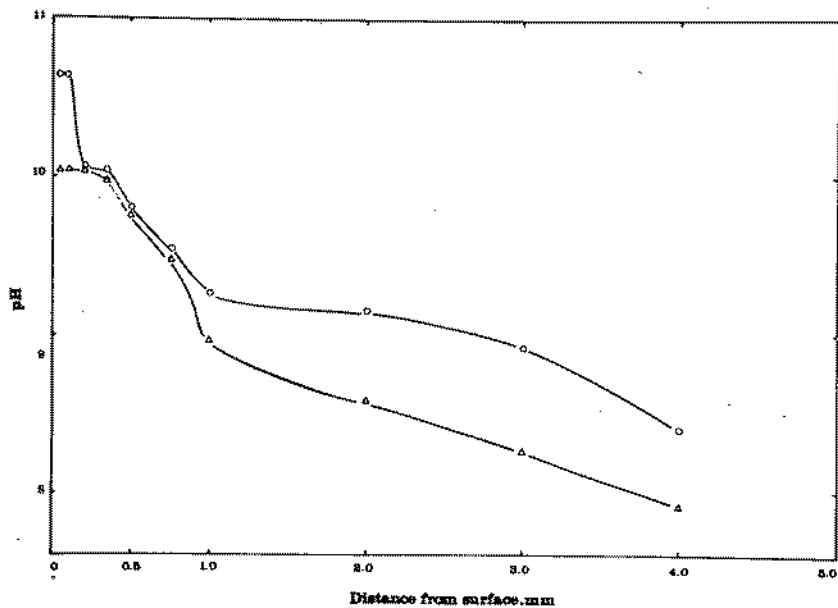


FIGURE 6. The variation of the pH of the sea water with distance from the surface of HS30 aluminium alloy cathodically polarised at  $-1.4V$ .

[KEY: ○ after 20 hours; △ after 4 days]

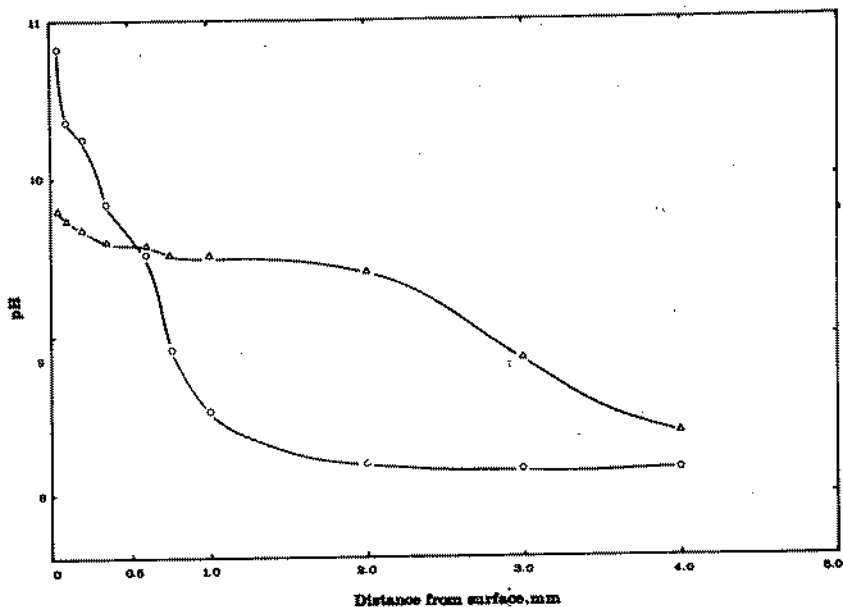


FIGURE 7. The variation of the pH of the sea water with distance from the surface of HS30 aluminium alloy cathodically polarised at  $-1.5V$ .  
[KEY: O after 20 hours; Δ after 5 days]

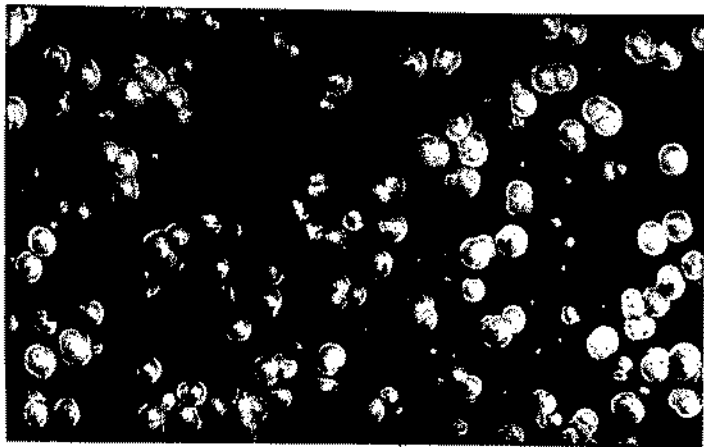


FIGURE 8. Scanning electron micrograph of the surface of HS30 aluminium alloy after cathodic polarisation at  $-1.2V$  in sea water for 5 days

(x 50)

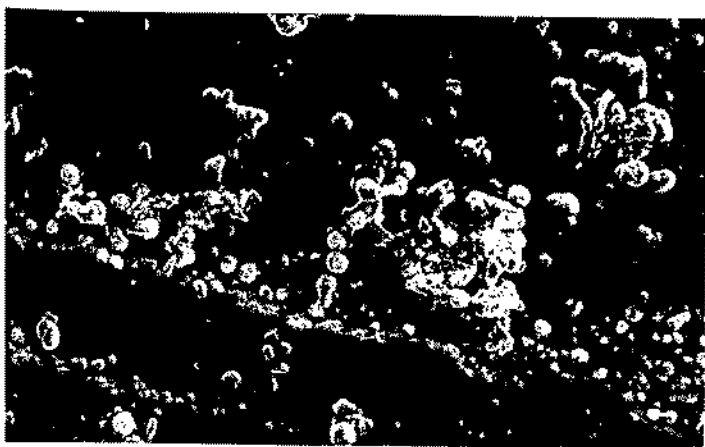


FIGURE 9. Scanning electron micrograph of the surface of HS30 aluminium alloy after cathodic polarisation at  $-1.3V$  in sea water for 5 days

(x 50)

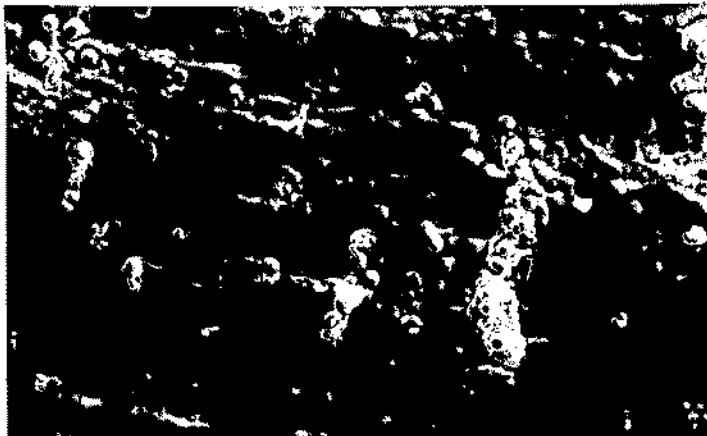


FIGURE 10. Scanning electron micrograph of the surface of HS30 aluminium alloy after cathodic polarisation at  $-1.4V$  in sea water for 4 days

(x 50)

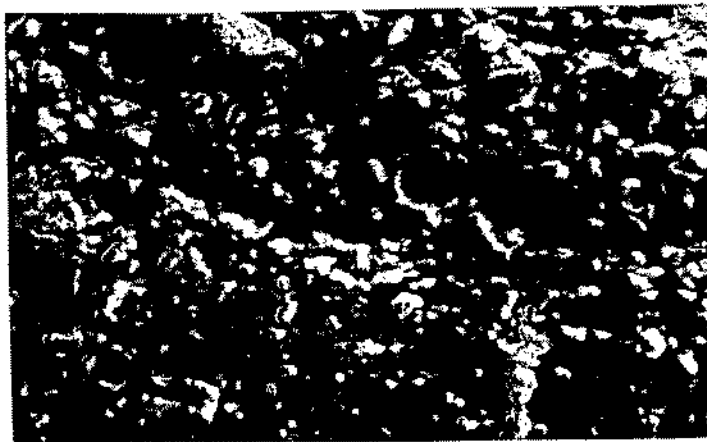


FIGURE 11. Scanning electron micrograph of the surface of HS30 aluminium alloy after cathodic polarisation at  $-1.5V$  in sea water for 5 days

(x 50)



ROLE DE L'INDIUM DANS LA DEPASSIVATION DES  
ANODES Al-Zn-In UTILISEES EN PROTECTION CATHODIQUE

J.J. RAMEAU<sup>\*</sup>, Ph. GIMENEZ<sup>\*\*</sup> et M. C. REBOUL<sup>\*\*</sup>

<sup>\*</sup>Laboratoire d'Energétique Electrochimique LA CNRS 265  
ENS Electrochimie Electrometallurgie de Grenoble INPG  
Domaine Universitaire, BP 75 -38402 SAINT-MARTIN D'HERES-

<sup>\*\*</sup>Aluminium Pêchiney, Centre de Recherches et de Développement,  
B.P. 24 -38340 VOREPPE-

RESUME

L'alliage Al-Zn 5% - In 0,02% est utilisé sous forme mou-  
lée comme anode sacrificielle pour la protection cathodique  
de structures en acier immergées dans l'eau de mer(1). En  
effet, le potentiel imposé par l'alliage mis en court-cir-  
cuit avec l'acier est - 1,1V/ECS, inférieur de 0,3V environ  
au potentiel de l'acier dans l'eau de mer. A ce potentiel,  
l'alliage ne se passive pas mais se dissout de façon régu-  
lière. L'indium joue donc un rôle sur la dépassivation de l'  
alliage, comme le font le mercure(2), l'étain(3) ou le gal-  
lium(4). Pour expliquer ce rôle, nous avons étudié l'influ-  
ence de l'addition d'indium à l'aluminium pur et aux allia-  
ges aluminium-zinc sur la structure métallique, sur les pro-  
priétés électrochimiques et la morphologie de la dissolu-  
tion, et sur les caractéristiques de la couche d'oxyde.

ABSTRACT

The Al-Zn 5%-In 0.02% alloy is employed formed as a mold  
as a sacrificial anode for the cathodic protection of steel  
structures in the sea water(1). Thus the imposed potential  
on the structure is - 1.1V/ECS between the alloy short-cir-  
cued with the steel, less than 0.3V than steel in the  
sea water. In this potential, the alloy does not passivate  
but it dissolves in a regular way. Indium plays a role in  
the dépassivation of the alloy, as the Hg, Sn or Ga. In or-  
der to explain this role we have studied the influence with  
the indium addition in the pure aluminium and Al-Zn alloy  
in the metallic structure, the electrochemical properties  
in the morphology of the dissolution, and in the characte-  
ristics of the oxygen layer.

## I. STRUCTURE METALLIQUE DE L'ALLIAGE Al-Zn 5 % - In 0,02 %

L'indium est très peu soluble dans l'aluminium pur (5) ; il n'existe pas de composés définis Al-In (fig. 1).

L'étude de l'alliage Al-Zn 5 % - In 0,02 % au microscope électronique en transmission (M.E.T.) révèle la présence de précipités de la phase  $Al_3Fe$  et de nodules renfermant des éléments lourds (fig. 2). Au microscope électronique à balayage (M.E.B.), les nodules apparaissent également ; ils ont un diamètre d'environ 1  $\mu m$  et sont localisés dans la zone interdendritique (fig. 3). L'analyse X dispersive en énergie (E.D.A.X.) indique que ces nodules renferment principalement de l'indium (fig. 4) qui existe également en solution solide dans la matrice.

## II. PROPRIETES ELECTROCHIMIQUES DE L'ALLIAGE Al-Zn 5 % - In 0,02 %

La courbe de polarisation anodique de l'alliage dans une solution désaérée contenant 30  $g.l^{-1}$  de chlorure de sodium a été tracée par la méthode galvanocinétique quasistationnaire. On observe que le potentiel d'abandon  $E_a$  de l'alliage  $E_a = -1,34$  V/ECS (fig. 5a) est inférieur à celui de l'aluminium A85  $E_a = -1,02$  V/ECS (fig. 5b) et à celui d'un alliage Al-Zn 5 %  $E_a = -1,1$  V/ECS (fig. 5c). Le potentiel critique de piqure  $E_c$  de l'alliage  $E_c = -1,015$  V/ECS est également plus faible que celui de l'A85 ( $E_c = -0,72$  V/ECS) et que celui de l'alliage Al-Zn 5 % ( $E_c = -0,94$  V/ECS).

Lorsqu'on impose une densité de courant anodique égale à 6,2  $A.dm^{-2}$  (norme ASTM), le potentiel en débit  $E_d$  de l'alliage Al-Zn 5 % - In 0,02 % est égal à  $E_d = -1,1$  V/ECS, très voisin du potentiel critique de piqure  $E_c$ . Ce potentiel est très affecté par la teneur en indium dans les alliages Al-Zn 5 % - In : pour des teneurs inférieures à 80 ppm, il est de 0,955 V/ECS, alors que pour des teneurs supérieures à 80 ppm, il est égal à -1,1 V/ECS (fig. 6).



Le rendement de dissolution des alliages Al-Zn 5 % - In dépend également de la teneur en indium : pour des teneurs inférieures à 80 ppm, ce rendement est inférieur à 60 % par suite d'une importante autocorrosion de l'alliage ; pour des teneurs In > 80 ppm le rendement atteint 92 % (fig. 7). Après dissolution pendant 10 jours sous  $6,2 \text{ A.dm}^{-2}$ , il existe à la surface de l'alliage Al-Zn 5 % - In 0,02 % de larges cavités circulaires à fond plat, peu nombreuses, qui coalescent rapidement par propagation latérale, engendrant une corrosion uniforme avec attaque plus prononcée des joints de grains (fig. 8). La différence de morphologie est importante par rapport à l'aluminium A85 qui présente une attaque sous forme de piqûres profondes à aspect cristallographique (fig. 9) et par rapport à l'alliage AZ5 qui présente une corrosion par piqûres qui se développent préférentiellement dans la zone interdendritique (fig. 10).

Le diagramme d'impédance électrochimique relatif à l'alliage Al-Zn 5 % - In 0,02 % en solution aérée NaCl  $30 \text{ g.l}^{-1}$  est, à la tension d'abandon  $E_a$ , de même forme (fig. 11a) que celui relatif à l'aluminium A85 (fig. 11b). Toutefois les valeurs de la résistance, caractéristique du circuit électrique équivalent R-C parallèle correspondant aux hautes fréquences, sont très différentes : environ  $60.000 \text{ } \Omega \cdot \text{cm}^2$  pour l'aluminium A 85 et seulement  $7000 \text{ } \Omega \cdot \text{cm}^2$  pour l'alliage Al-Zn 5 % - In 0,02 %. Ces résistances sont caractéristiques des réactions qui se produisent à l'électrode car elles évoluent avec la tension anodique ou cathodique imposée à l'électrode. Le rapport des 2 résistances est sensiblement le même que le rapport des résistances de polarisation déterminées à partir des courbes de polarisation (fig. 5a et 5b) et indique donc le rôle de l'indium dans la diminution de cette résistance. La partie basses fréquences des diagrammes d'impédance (fig. 11a et 11b), qui se situe dans le

demi-plan inductif, est significatif de l'adsorption qui se produit à la surface des échantillons, probablement adsorption des ions  $\text{Cl}^-$ .

Nous avons précisé les propriétés électrochimiques de l'indium métallique en solution  $\text{NaCl}$   $30 \text{ g.l}^{-1}$  désaérée, par le tracé de la courbe de polarisation (fig. 12). A  $-1,1 \text{ V/ECS}$ , tension critique de piqûre de l'alliage  $\text{Al-Zn}$   $5\%$  -  $\text{In}$   $0,02\%$ , l'indium ne peut que se trouver à l'état métallique et on à l'état d'ions  $\text{In}^{3+}$ . Lorsqu'on ajoute des ions  $\text{In}^{3+}$  à la solution  $\text{NaCl}$   $30 \text{ g.l}^{-1}$ , on constate que le potentiel de l'aluminium A85 est déplacé vers une valeur plus négative, quelle que soit la quantité de chlorure d'indium ajoutée (fig.13). L'aluminium se recouvre d'indium métallique. C'est donc la présence de  $\text{In}^{3+}$  en solution qui est responsable de la dépassivation de l'alliage  $\text{Al-Zn}$   $5\%$  -  $\text{In}$   $0,02\%$ .

### III. PROPRIETES DE LA COUCHE PASSIVE DE L'ALLIAGE $\text{Al-Zn}$ $5\%$ - $\text{In}$ $0,02\%$

Les épaisseurs, déterminées par ellipsométrie, de la couche naturelle d'oxyde sur l'alliage  $\text{Al-Zn}$   $5\%$  -  $\text{In}$   $0,02\%$  et sur l'aluminium A85 sont très voisines et augmentent avec le temps (respectivement  $45 \text{ \AA}$  et  $38 \text{ \AA}$  après 5 jours,  $87 \text{ \AA}$  et  $80 \text{ \AA}$  après 4 mois).

En présence d'ions  $\text{In}^{3+}$  dans la solution  $\text{NaCl}$   $30 \text{ g.l}^{-1}$ , la couche d'oxyde adhère mal au substrat et s'en détache facilement.

L'analyse E.D.A.X. d'une couche d'oxyde, d'épaisseur  $0,2 \mu\text{m}$  obtenue par anodisation, montre un enrichissement en indium d'un facteur 20 environ par rapport à la teneur de l'alliage. Ces résultats sont confirmés par spectrométrie de masse d'ions secondaires (S.I.M.S): les profils de l'élément indium (fig. 14a) et de l'élément zinc (fig. 14b) dans la couche d'oxyde de l'alliage montrent un enrichissement en ces deux éléments.

Des essais de traction d'alliages  $\text{Al-Zn}$   $5\%$  -  $\text{In}$   $0,02\%$  anodisés, montrent que l'allongement  $A$  à la rupture du film d'oxyde est plus faible ( $A = 1,88\%$ ) que dans le cas de l'aluminium A85

(A = 3,08 %). La couche est donc fragilisée par la présence d'indium.

La mesure des caractéristiques électriques (résistivité  $\rho$ , permittivité  $\epsilon$  et fréquence de relaxation  $f_r$ ) de ces couches d'oxydes par la méthode d'impédance (fig. 15a et 15b) montre que la résistivité de l'alliage de la couche sur l'alliage Al-Zn 5 % - In 0,02 % est environ 1000 fois plus faible que celle relative à la couche sur l'aluminium A85.

#### IV. MECANISMES DE LA DEPASSIVATION DE L'ALLIAGE Al-Zn 5 % - In 0,02 %

---

D'après AKIMOV (6), lorsqu'on oxyde une solution solide métallique, l'alliage se dissout de façon homogène et tous les éléments passent en solution. Ainsi lors de la polarisation anodique de l'alliage Al-Zn 5 % - In 0,02 %, le zinc et l'indium en solution solide dans l'aluminium sont oxydés en  $Zn^{2+}$  et  $In^{3+}$ . Les nodules d'indium ne sont pas oxydés. L'attaque s'initie aux défauts de la couche d'oxyde.

En présence d'aluminium, les ions  $In^{3+}$  sont réduits selon la réaction  $Al + In^{3+} \rightarrow Al^{3+} + In$  ; au cours de cette réaction la couche d'oxyde devient moins adhérente au substrat et elle peut s'en séparer pour laisser l'alliage à nu, qui continue alors à se dissoudre. L'enrichissement en indium de la couche d'oxyde diminue sa résistance mécanique et sa résistivité électrique.

Le mécanisme de dépassivation est autocatalytique puisque la dissolution est activée par les ions  $In^{3+}$  qui sont produits dans les zones actives de dissolution. Le zinc, qui augmente la solubilité de l'indium dans l'aluminium facilite ce mécanisme ; il augmente également la fragilité des couches d'oxyde.

## R E F E R E N C E S

- =====
- (1) W.B. MACKAY  
Sacrificial anodes in "Corrosion" edited by L.L. SHREIR,  
Newnes - - Butterworths, London, 1979.
  - (2) M. REBOUL , M.C. DELATTE  
Materials Performance, 19(5), (1980), 35.
  - (3) D.S. KEIR , M.J. PRAYOR , P.R. SPERRY  
J. Electrochem. Soc., 114(8), (1967), 777.
  - (4) W. BOHNSTED  
J. of Power Source, 5 (1980), 245.
  - (5) L.M. MONDOLFO  
Aluminium alloys structure and properties, Butterworths-London  
(1976).
  - (6) G.W. AKIMOV  
Corrosion Nace, 11 (1955), 474.

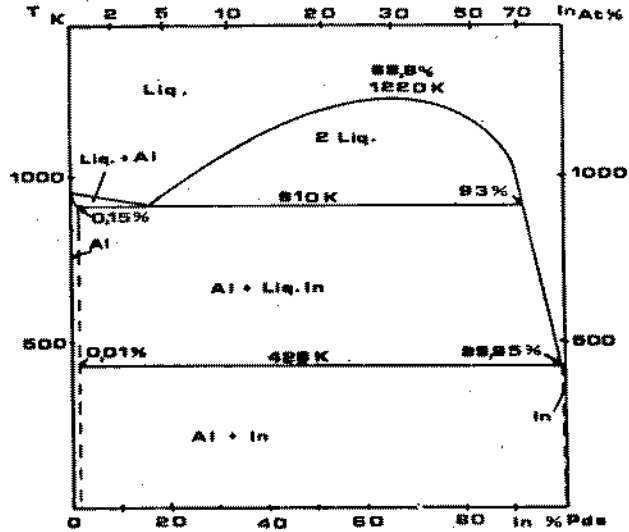


Fig. 1 : Diagramme de phases Al-In (6)

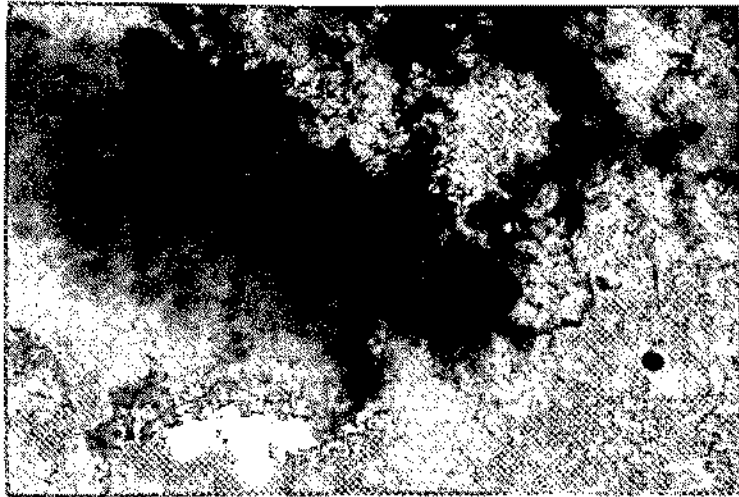


Fig. 2 : Image électronique des nodules d'indium de l'alliage Al-Zn 5 % - In 0,02 %. M.E.T. (X 17800)



Fig. 3 : Image électronique des précipités d'indium dans l'alliage Al-Zn 5 % - In 0,02 %. M.E.B. (X 550)

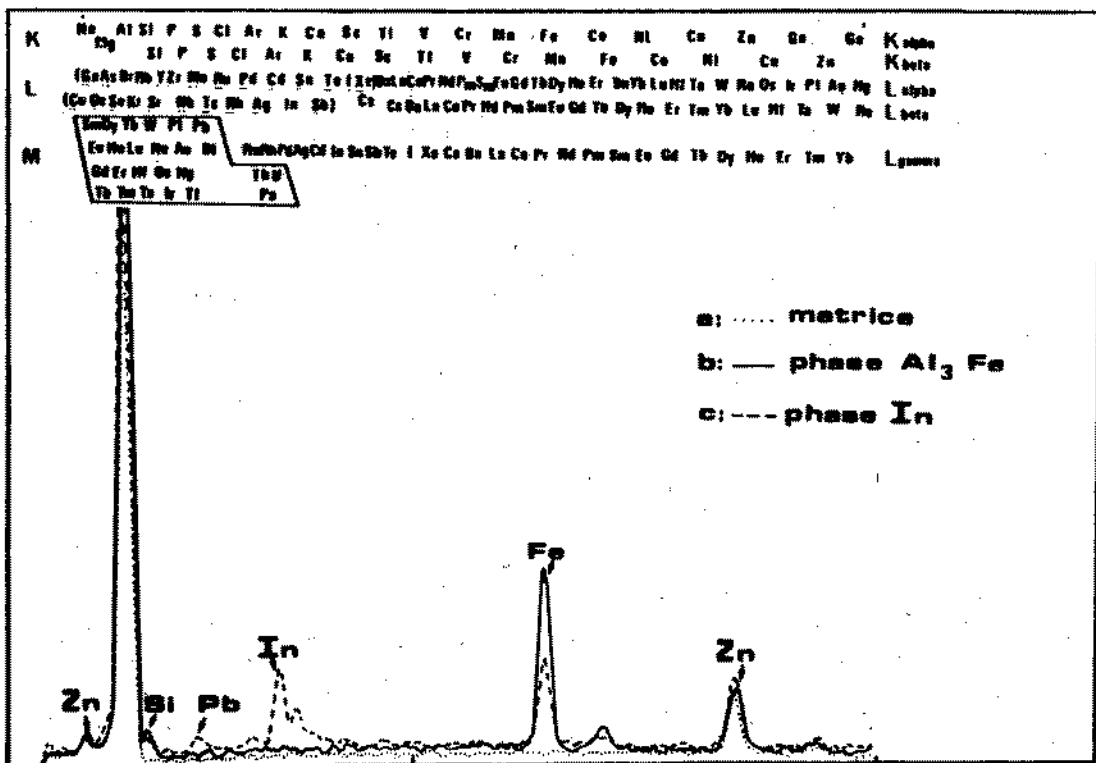


Fig. 4 : Spectres E.D.A.X. de l'alliage Al-Zn 5 % - In 0,02 %  
 a : matrice    b : phase  $Al_3Fe$     c : phase In

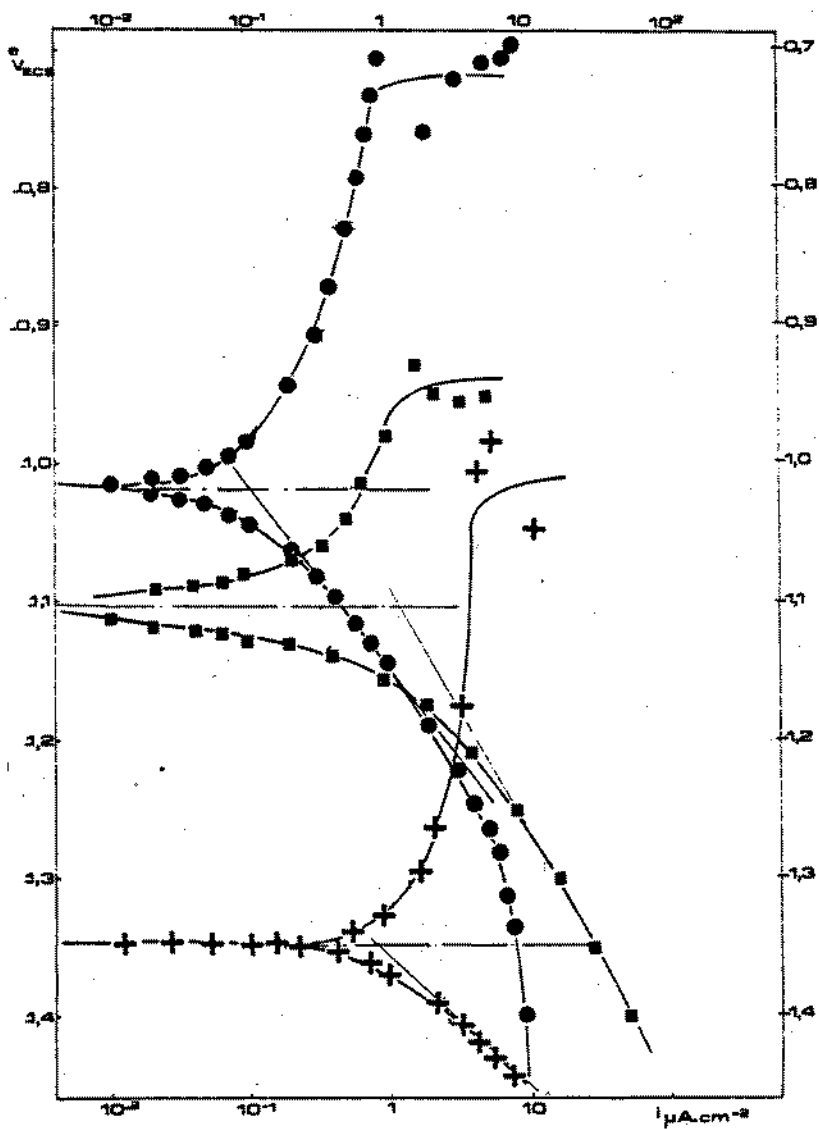


Fig. 5 : Courbe de polarisation des alliages Al-Zn 5 % - In 0,02 % (a) A85 (b) , AZ5 (c)

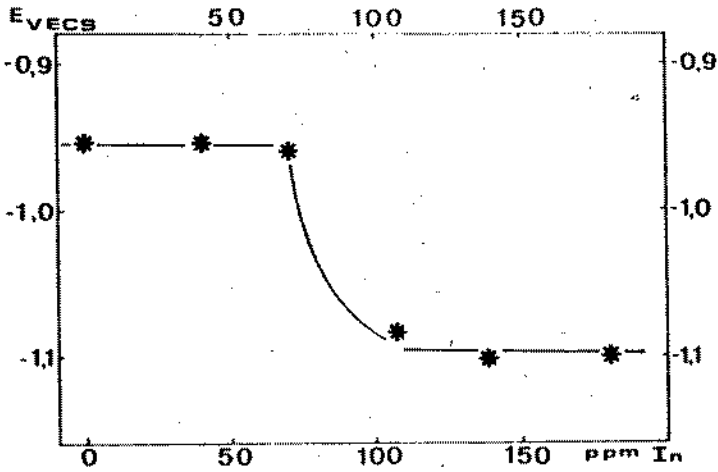


Fig. 6 : Influence de l'addition d'indium sur le potentiel en débit de l'alliage AZ5.

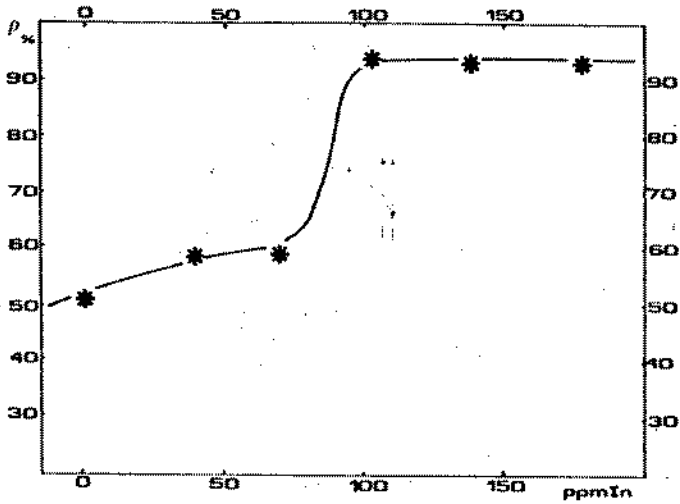


Fig. 7 : Influence de l'addition d'indium sur le rendement de dissolution de l'alliage AZ5





Fig. 8 : Morphologie de la dissolution de l'alliage Al-Zn 5 % - In 0,02 %. Coupe micrographique, attaque Keller (x 200)



Fig. 9 : Morphologie de la dissolution de l'alliage A85. Coupe micrographique, attaque Keller (x 50)

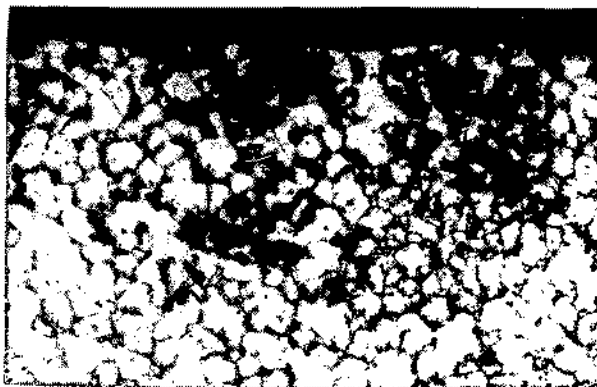


Fig. 10 : Morphologie de la dissolution de l'alliage AZ5. Coupe micrographique, attaque Keller (x 50)

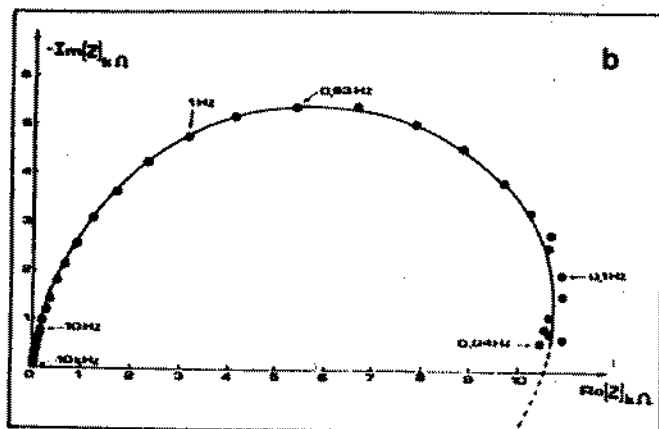
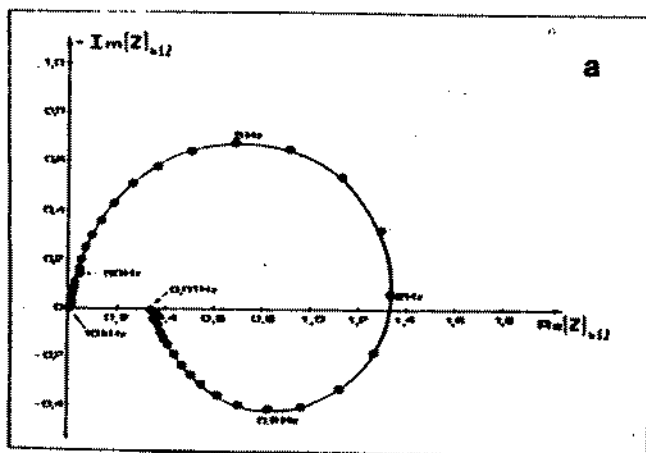


Fig. 11 : Diagramme d'impédances au potentiel de corrosion  
 (a) alliage Al-Zn 5 % - In 0,02 %  
 (b) alliage A85

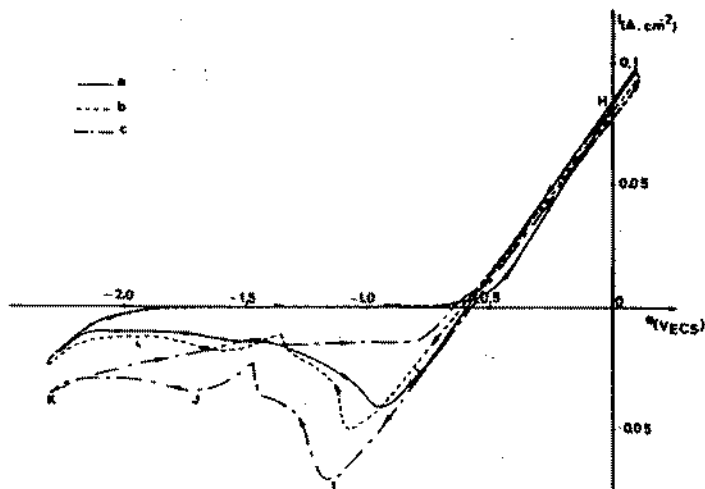


Fig. 12 : Comportement électrochimique de l'indium pur dans la solution  $\text{NaCl } 30 \text{ g.l}^{-1}$ . Electrode de travail indium.  
Balayage  $-0,59 \text{ V/ECS} \rightarrow +0,1 \text{ V/ECS} \rightarrow -2,4 \text{ V/ECS} \rightarrow -0,59 \text{ V/ECS}$   
Vitesse de balayage (a)  $0,01 \text{ V.s}^{-1}$  ; (b)  $0,05 \text{ V.s}^{-1}$  ;  
(c)  $0,1 \text{ V.s}^{-1}$

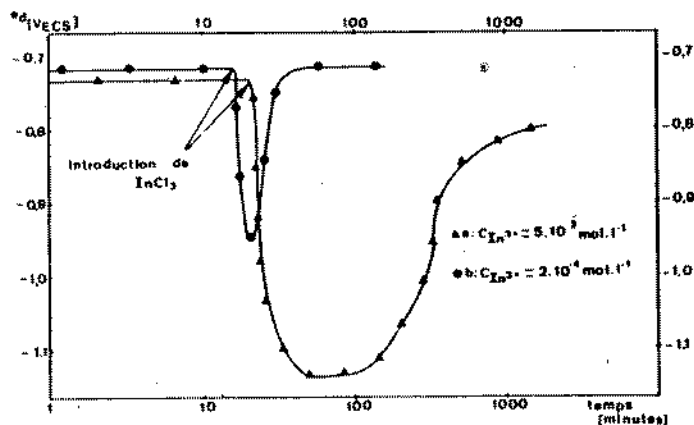


Fig. 13 : Evolution de  $E_0$  de l'alliage A85 après introduction de chlorure d'indium dans la solution  $\text{NaCl } 30 \text{ g.l}^{-1}$   
(a)  $C_{\text{In}^{3+}} = 5.10^{-2} \text{ mol.l}^{-1}$  (b)  $C_{\text{In}^{3+}} = 2.10^{-4} \text{ mol.l}^{-1}$

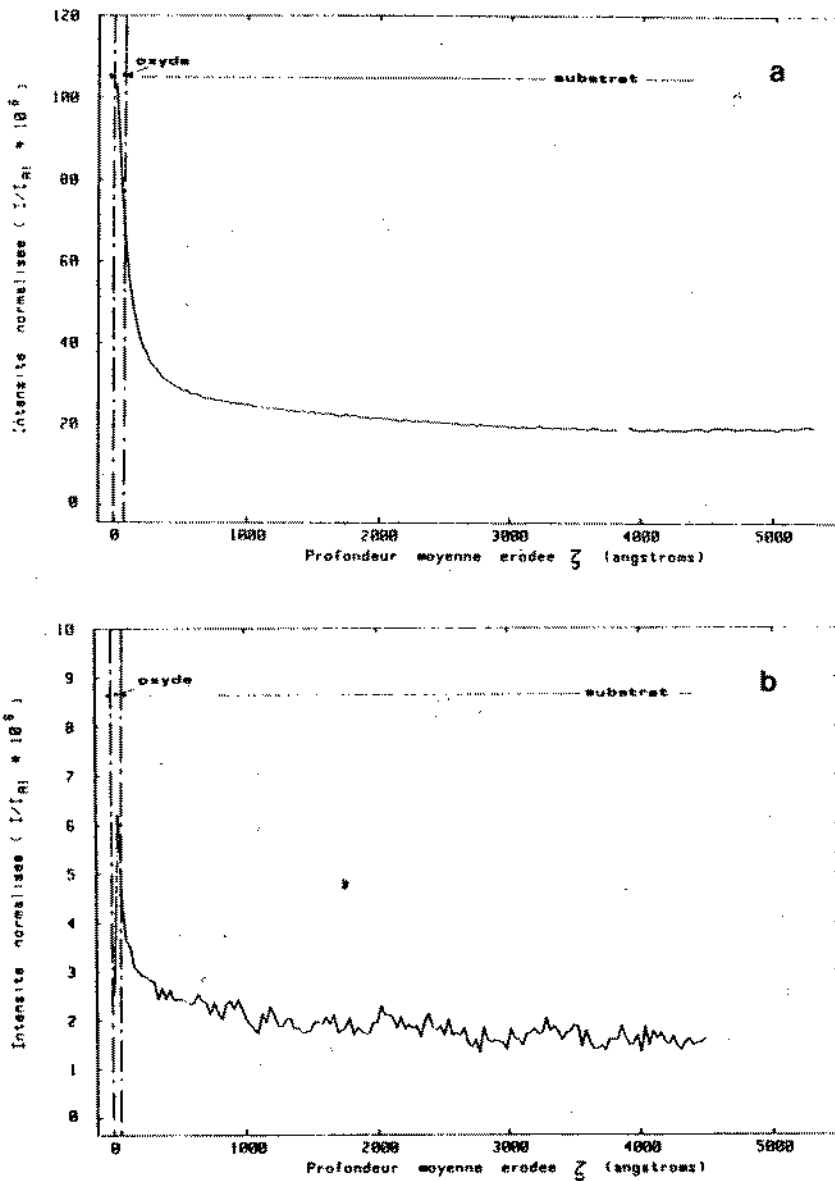


Fig. 14 : Profils de concentration dans l'alliage Al-Zn 5 % - In 0,02 % (S.I.M.S.) (a) indium, (b) zinc

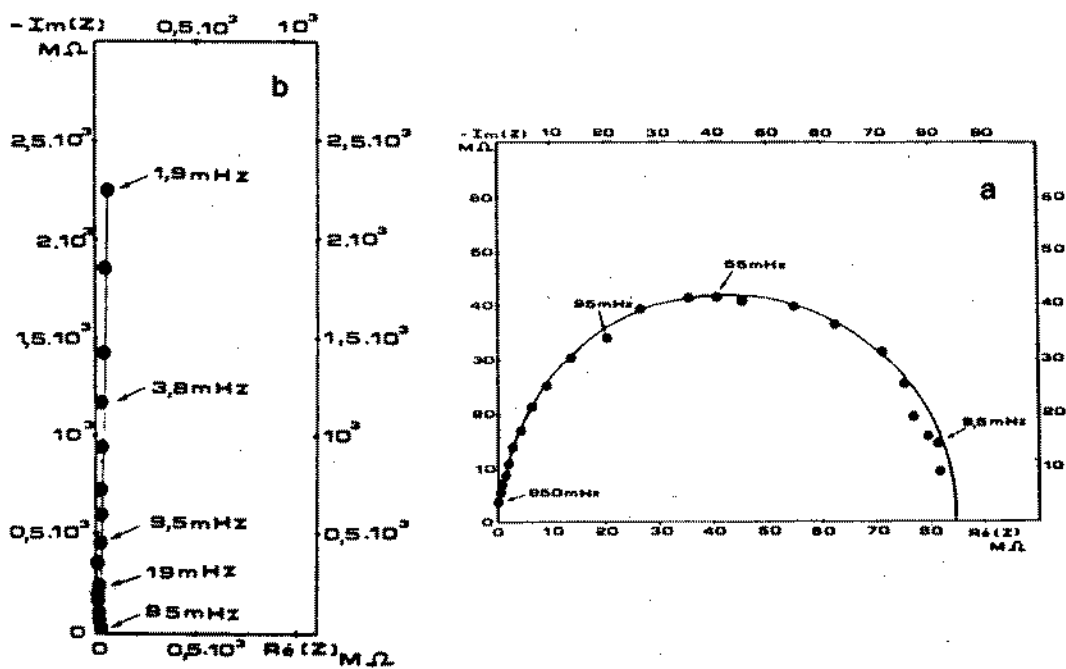


Fig. 15 : Diagrammes d'impédance de la couche d'oxyde  
 (a) alliage Al-Zn 5 % - In 0,02 % ; (b) alliage A85



CALCULATION OF CURRENT DENSITY DISTRIBUTION FOR A CORRECT APPLICATION  
OF CATHODIC PROTECTION

A. Colombo - G. Rocchini

ENEL (Italian Electricity Board)

Via Rubattino, 54 - 20134 MILANO ITALY

ABSTRACT

With reference to an electrochemical system where only two processes under activation energy control are present, some criteria are developed which can be used as a guide-line when designing the cathodic protection of a structure. These criteria are based on the use of corrosion current density and polarization resistance. Very useful is the concept of the protection effectiveness attained after polarization of the structure under investigation, which is founded on common practice in the field of inhibition.

Some classical electrodynamic concepts leading to the Laplace equation for the determination of the potential in a region subject to current flow are also examined.

Ritz's version of the method of finite elements is introduced and the PEVACO three-dimensional code is briefly described through three different applications. The first refers to a classical electromagnetic problem, the second to an electrolytic cell and the third to an experimental structure installed by ENEL at one of its thermal power stations for the purpose of setting up a computerized cathodic protection system.

1. INTRODUCTION

The importance and interest of the methods used for calculating potential and current density distribution in electrochemical systems in relation to corrosion processes and metal electrodeposition have

been particularly emphasized in the review /1/ giving an exhaustive bibliography that includes as many as two hundred references.

As explained in that paper, the problem can be tackled from two different standpoints using either mathematical-physical techniques or empirical relationships directly derived from experimental observations.

It is well known that to calculate the electric field in an electrochemical system with accuracy it is necessary to solve the Laplace equation /2/ with boundary conditions that should take into account the true nature of all interactions occurring between the metal and the solution. The physical model of the metal/solution interface gives a non-linear current-voltage characteristic whose form may be further complicated by the presence of kinetic controls other than activation energy. Hence, an analytical solution is impossible for most of these problems, except for very simple geometries, as illustrated by Wagner /4/.

Therefore, for problems of industrial interest, like the cathodic protection of condenser water box and tube sheet in a thermal power station, recourse must be had to numerical methods, especially if the subject is to be dealt with in three-dimensional space.

In view of these considerations and in order to optimize anode positioning in the case of cathodic protection by impressed currents, ENEL-CRTN has developed PEVACO, a three-dimensional code based on the finite elements method which will be described further on.

At present the code is being used for mapping the current density on an experimental structure installed in one of our thermal power stations with the aim of setting up a computerized cathodic protection system.

The positioning of anodes is a crucial problem, if the current density value is to be practically the same in all the zones of the structure to be protected.

## 2. GENERAL

The possibility of preserving the integrity of a metal material dipped in an aggressive medium by cathodic protection depends on the electrochemical nature of the corrosion process which allows separation of the two partial anodic and cathodic reactions through external intervention. A very interesting qualitative description of the phenomenon can be found in Akimov's book /5/ where the kinetics of a global reaction are discussed. In that case the reaction included several processes which were activated in different intervals of the electrode overvoltage. In this paper, however, reference will be made to a current-voltage characteristic of the following type:



$$i = I_c [\exp(\alpha \Delta E) - \exp(-\beta \Delta E)] = i_a - i_c \quad (1)$$

which describes a global process under activation energy control and contains, as a limiting case, diffusive control with constant current corresponding to  $\beta=0$ . Of course,  $\Delta E$  is the potential difference referred to the mixed potential of the system under investigation, while  $I_c$  is its corrosion current density.

Eqn (1) can be rewritten as:

$$i = -I_c \exp(-\beta \Delta E) \cdot [1 - \exp(\alpha + \beta) \Delta E] \quad (2)$$

which will prove much more useful for our discussion.

From eqn(2) it follows that if the metal/solution interface is to be chiefly subject to the cathodic process alone, the inequality:

$$|(\alpha + \beta) \Delta E| \gg 1 \quad (3)$$

must be satisfied.

If the polarization resistance,  $R_p$  /6/ is introduced, the relationship will become:

$$\frac{1}{R_p} \cdot \left| \frac{\Delta E}{I_c} \right| \gg 1 \quad (4)$$

which shows that the criterion of the sole presence of the cathodic reaction can be expressed using more intuitive physical quantities, like  $R_p$  and  $I_c$ .

It should be noted that condition (4) is exclusively related to the method used for neglecting the anodic process in respect of the cathodic process. The inequality (3) is a step forward as compared with the common tendency towards neglecting the first term of the second member of eqn (1).

The advance of (4) is that it helps determine the protection potential, if the polarization resistance and the corrosion current density values are known. Of these, the polarization resistance can be determined very easily, while for the corrosion current density a direct method can be used.

A very useful concept is that of the protection effectiveness,  $P$ , which, by analogy with the inhibiting efficiency, can be defined by:

$$P = \left( 1 - \frac{i_a}{I_c} \right) \cdot 100 \quad (5)$$

By eqn (1) and using the  $R_p$  and  $I_c$  quantities eqn (5) becomes:

$$P = \left[ 1 - \exp \left[ \left( \frac{1}{R_p I_c} - \beta \right) \Delta E \right] \right] \cdot 100 \quad (6)$$

For a corrosion process controlled by the limiting diffusion current ( $\beta=0$ ), the preceding relationship will become:

$$P = \left[ 1 - \exp \left( \frac{\Delta E}{R_p I_c} \right) \right] \cdot 100 \quad (6')$$

From eqn (6') one may infer that cathodic protection is complete when the whole amount of the oxidated species diffusing towards the surface is reduced by the external current. The same conclusion was reached by Engell and Forchhammer in /7/.

Yet, although the definition of the protection effectiveness, (6) is physically satisfactory in that it is related to  $I_c$ , the presence of the parameter  $\beta$  limits its practical application to approximate calculations. An alternative definition in line with (4) is given by:

$$P = \left( 1 - \frac{i_a}{i_c} \right) \cdot 100 \quad (7)$$

From this definition and the current-voltage characteristic (1) it is evident that the overvoltage  $\Delta E$  of the electrode, in order to obtain the protection effectiveness  $P$ , is given in any case by:

$$\Delta E = R_p \cdot I_c \cdot \ln (1 - P \cdot 10^{-2}) \quad (8)$$

Moreover, by definition (7), between the external current density,  $i$ , and the cathodic current density,  $i_c$ , there exists the relationship:

$$i = -P \cdot 10^{-2} \cdot i_c \quad (9)$$

from which follows the well-known result that complete cathodic protection cannot be achieved by simply applying an external current whose density equals  $I_c$  in absolute value.

In one of his works /8/ Schwerdtfeger proved experimentally that for the protection of sample buried in a medium of very high electric resistivity a current density corresponding to about  $3 \cdot I_c$  is required.

Of course, the foregoing applies only to an ideal electrochemical system. In a real case, the reference electrode is positioned at a certain distance from the working electrode and the current-voltage characteristic takes a more complicated form /6/ :

$$i = I_c [\exp [\alpha (\Delta E - RiS)] - \exp [-\beta (\Delta E - RiS)]] \quad (10)$$

In eqn(10) R is the electric resistance of the solution between the reference electrode and the working electrode and S is the surface area of the latter. Thus, in place of (3) we have:

$$|(\alpha + \beta) (\Delta E - RiS)| \gg 1 \quad (11)$$

which shows that the effect of the ohmic drop must not be neglected if an optimal cathodic protection is desired.

### 3. POSITION OF THE PROBLEM

#### 3.1 Mathematical developments

The previous section has stressed the importance of knowing the current density distribution in an electrochemical system in that it controls the kinetics of the corrosion process and determines its subdivision into the anodic and the cathodic zone.

The starting point for the determination of the current density vector,  $\vec{J} = \vec{J}(x, y, z)$ , is the continuity equation /9/ :

$$\operatorname{div} \vec{J} + \frac{\partial \rho}{\partial t} = 0 \quad (12)$$

which, under stationary conditions, becomes:

$$\operatorname{div} \vec{J} = 0 \quad (13)$$

In this paper reference will be made only to eqn(13) which can be applied to an electrolytic solution solely if the concentration of the electrolyte is independent of time or its variation is so slow that it can be practically neglected.

Significant variations requiring the application of eqn(12) may well occur in the double layer /10/ where all electrochemical processes develop.

Yet, to avoid unnecessary complications, the physical structure of the metal/solution interface will not be considered. It will only be depicted from the mathematical point of view by use of convenient non-linear boundary conditions. In this depiction the extension of the interface is assumed to be equal to zero. According to Ohm's law /9/,  $\vec{J} = \sigma \vec{E}$ , where  $\sigma$  is the conductivity of the electrolytic solution and is considered an isotropic quantity, eqn(13) can be transformed into:

$$\operatorname{div} \sigma \vec{E} = \operatorname{div} \vec{E} + \operatorname{grad} \sigma \vec{E} = 0 \quad (14)$$

If the conductivity,  $\sigma$ , is not a point function, by introducing the potential,  $\Phi$ , eqn(14) turns into the Laplace equation /9/ :

$$\frac{\partial^2 \Phi}{\partial x^2} + \frac{\partial^2 \Phi}{\partial y^2} + \frac{\partial^2 \Phi}{\partial z^2} = 0 \quad (15)$$

By the variational methods /11/, the solution of this equation is amenable to the determination of the stationary value of the functional:

$$F = \frac{1}{2} \iiint_V \left[ \left( \frac{\partial \Phi}{\partial x} \right)^2 + \left( \frac{\partial \Phi}{\partial y} \right)^2 + \left( \frac{\partial \Phi}{\partial z} \right)^2 \right] dV \quad (16)$$

where  $V$  is the volume of domain  $D$  to which (15) refers. The advantage of this formulation is that the function  $\Phi$  can be approximated by polynomial forms of the following type:

$$\Phi = a + bx + cy + dz + exy + \dots \quad (17)$$

and the solution can be replaced by the determination of the values of the coefficients of polynomial (17) which render the functional,  $F$ , stationary.

Ritz's version of the method of finite elements /12/, which has already been applied to analogous problems /13/, consists in subdividing domain  $D$  into a finite number of subdomains, where polynomial (17) provides a more adequate approximation of the unknown function, and in expressing the coefficients as a function of the values of  $\Phi$  for a given number of points, called nodes, taken on the surface delimiting an elementary volume element. The number of nodes should be equal to the number of terms of the polynomial. The advantage of this procedure is that it imposes the continuity of the function automatically, as the nodes are common to more than one volume element.

Substantially, by the method of finite elements the partial differential equation (15) is equivalent to a linear system of equations. It should be remembered that an approximate solution of eqn (15) can be achieved also by the method of finite differences /14/ and the method of finite boundary elements /15/.

### 3.2 Boundary conditions

For the boundary conditions to be added to eqn(15) in order to

attain to a physically satisfactory solution of the problem under consideration, reference should be made to Fig. 1 where domains D1, D2 and D3 respectively refer to the cathode, the anode and the other surfaces which delimit the electrolytic cell and are not subject to current flow.

Thus, the condition to impose on these surfaces is given by:

$$\frac{d}{dn} \varphi = 0, \quad (x, y, z) \in D_3 \quad (18)$$

where  $\vec{n}$  denotes the unit vector normal to them. The derivative being equal to zero indicates that the surfaces are not crossed by a current flow.

As to the boundary conditions to be imposed on the surfaces of the electrodes, they depend on the nature of the electrochemical processes that take place on them. If they can be considered unpolarizable [16], the case becomes very simple. The current density distribution is known as primary distribution. It should be noted, however, that this model cannot be applied in practice because the current passage induces polarization on the electrodes. In this work only the electrochemical reactions that are governed by activation energy will be considered, diffusive control requiring the introduction of the time variable, at least as a parameter.

Another approximation, which does not prejudice the final result and helps save calculating time, consists in considering the anode unpolarizable. This depiction is based on the fact that overvoltage on the anode may be regarded as negligible in respect of the voltage applied from the outside, which sometimes amounts to several volts.

On the basis of the previous choice, the condition to be applied on the anodic surface is given by:

$$\varphi(x, y, z) = \text{const}, \quad (x, y, z) \in D_2 \quad (19)$$

For the description of the electrochemical process taking place on the cathode the current-voltage characteristic (1) will be adopted. Thus, if  $\varphi_c$  denotes the cathode potential, the boundary condition to be applied on it will be :

$$\varphi_c = \varphi(x, y, z) + |\Delta E|, \quad (x, y, z) \in D_1 \quad (20)$$

where the value of  $\Delta E$  is determined either by solving eqn(1) or by resorting to a polynomial representation of the relationship  $\Delta E = \Delta E(i)$ .

Eqn(20) shows how the double layer is treated mathematically.

The depiction practically consists in introducing a potential discontinuity on the cathodic surface, the values of  $\Phi_c$  and  $\Phi$  referring to the same points.

If a non-linear condition is to be imposed also on the anode, eqn(20) will become:

$$\Phi_a = \Phi(x, y, z) - |\Delta E_a| \quad (21)$$

### 3.3 Description of the PEVACO program

For the numerical solution of eqn(15) with boundary conditions (18), (19) and (20) use was made of the method of finite element in Galerkin's formulation /17/ which, as everybody knows, is a particular form of the weighted residual methods /17/ where weight functions are equal to shape functions. It may be useful to remember that in this case Galerkin's formulation coincides with the variational method developed by Ritz and briefly illustrated in a previous section, while shape functions are discussed in detail in /12/.

The PEVACO code can make use of the 8-, 20- and 32-node isoparametric elements shown in Fig. 2. They are taken from /18/ where the analytical expressions of the shape functions for the individual cells are given in detail. An element is termed "isoparametric" when form functions coincide with the functions that define its geometry /19/. Lattices are generated automatically by a procedure based on the Bergen code /20/ which generates lattices for three-dimensional structures and was developed in connection with the calculation programs of the Bersafe family /21/.

The use of the Bergen code has been considerably simplified because the application of the PEVACO program is foreseen for structures of well-defined geometry. In investigations of this kind, whose main purpose is to determine an anode space distribution that will ensure uniform protection of the structure, lattice generation is of great importance in that it facilitates the examination of different configurations and helps choose the one that best suits the circumstances. Therefore, particular attention was given to this aspect of the problem whose developments are described in /22/ which illustrates also the procedure set up for this particular case and all the operations.

In its present configuration, the PEVACO code can be readily applied to a structure containing up to ten anodes distributed at random but subject to the condition of having all the same form and dimensions. A detailed description of the code, which would go beyond the scope of the present paper, can be found in the user's

handbook /23/ where the algorithms employed and the architecture of the code are examined in detail. It will suffice here to remember that the code is written in FORTRAN IV, it consists of 26 subprograms mutually connected and the algebraic system of equations for the determination of the potential nodal values is solved by the frontal method /24/. It can be added that for the use of this code six data-sets are envisaged to be located either on a disc or on a tape.

The output foreseen in the code is of three different types which could be summed up as follows: 1) printing of potential at nodes, cathodic overvoltage and current density values; 2) a graph of equipotential curves on the printer; 3) same information on a plotter /22/.

#### 4. APPLICATIONS

##### 4.1 Analytical case

To check the validity of the PEVACO code we considered a problem for the determination of the potential,  $\Phi(x,y,z)$ , whose analytical solution was known. As a test case we chose the classical problem of the determination of the potential in a rectangular box discussed in /25,26/. For the sake of simplicity, the box was assumed to be cubic. With reference to Fig. 1, the boundary conditions were:  $\Phi=C_1$ ,  $\Phi=C_2$ , on faces ABCD and EFGH respectively, while for the remaining faces  $\Phi$  was assumed to be equal to zero.

The results obtained for the line segment perpendicular to plane  $z = 0$  and passing through point (0.1; 0.1; 0) are given in Fig. 3 together with the analytical trend of the solution. The edge of the cube was 0.3 cm long and the whole volume was divided into 27 elements. Considering the discontinuity of the potential on some cube edges, the potential values for their respective nodes were assumed to be equal to zero. Examination of this figure shows that the accuracy of the numerical solution increased with the number of nodes, which was to be expected owing to the fixed volume of the elements, and that, except for the two nodes in the vicinity of planes  $z = 0$  and  $z = 0.3$ , the 32-node lattice is a faithful reproduction of the analytical behaviour. In this case, the results obtained for the 8-node lattice were unsatisfactory.

It should be added that when the function was given values other than zero at discontinuous points, the results were less satisfactory, especially for the 20-node lattice.

##### 4.2 Electrolytic cell

A very important problem in the corrosion field is the knowledge of the distribution of current density on the working electrode. If

the distribution is not reasonably uniform all over the surface, the information about electrochemical parameters, which concerns the global trend of the process, may be incorrect unless special devices are used to obtain local data.

On the basis of this observation, we thought of applying the PEVACO code to an electrolytic cell we often use in our laboratory. For the occasion the cell was considered to be of cylindrical symmetry and the reference electrode was neglected. As can be seen in Fig. 4, which shows also the trend of current density, the cell has a height of 10 cm and a 7.5 cm radius just like the anode.

The ARMCO iron working electrode was 3 cm high and had a radius of 0.7 cm. The solution was  $\text{H}_2\text{SO}_4$  1N at 25°C. The values of the electrochemical parameters were:  $I_c=0.666 \mu\text{A}/\text{cm}^2$ ,  $b_a=86.79 \text{ mV}$ ,  $b_c=102.67 \text{ mV}$ . They were derived from a polarization curve of the galvanostatic pulse type. The electric conductivity of the solution was assumed to be equal to  $3.52 \cdot 10^{-3} \Omega^{-1}\text{cm}^{-1}$ . The bases of the working electrode were considered as being electrically insulated from the solution, as is the rule in experimental procedures. For reasons of symmetry, the calculation was limited to one fourth of the cylinder and a 20-node lattice was employed. Complete convergence was achieved after 10 iterations. Fig. 4 shows that the values of the primary current density are higher than those of the true current density corresponding to the polarized electrode. This confirms the well-known concept that polarization of a metal is a form of self-protection. However, the most interesting feature is the fact that the distribution of current density along the z axis is not uniform and tends to assume higher values at the two bases of the working electrode. This situation can be mended by choosing such dimensions for the counter electrode that the length of the central zone, which presents a constant current density value and is therefore best suited for a study of the corrosion process mechanisms, will be extended.

#### 4.3 Experimental structure

A cathodic protection experiment was undertaken in the past by ENEL's Construction Management and Società DE NORA on a condenser of Monfalcone thermal power station. The results of this application based on a industrial system can be found in a paper /26/. Although some experience had already been gained in the operation of a cathodic protection with impressed current by an industrial system, it was decided to start a specific research program in order to improve the technology and investigate the physical phenomenon more closely.

Thus, with the cooperation of the Production and Transmission Management, a research programme was embarked on, which brought to



the realization of a computerized cathodic protection system and an experimental structure installed at Piombino thermal power station. In this field ENEL is moving in the same direction as other electric utilities, like the British Electricity Board which we understand has already implemented analogous systems.

A schematic representation of the experimental structure can be seen in Fig. 5 which shows also the positioning of the platinum-plated titanium anodes. The structure consists essentially of a rectangular steel-plate box, 3 mm thick, a dipped pump sucking sea water from the same cooling system as the condenser and a set of tubes. The dimensions of the water box are: 1.5 m high x 3 m long x 2 m wide. With a delivery of about 5 m<sup>3</sup>/h the pump ensures a continuous change of water inside the box. This is of great importance for the study of calcareous deposits resulting from local alcalinization near the cathodic zone in consequence of current flow. The design of the water box provides for occasional modifications to solve specific problems associated with the operation of steam condensers.

The first part of the experimental work will be a study of the behaviour of the condenser tube sheet under cathodic protection. To this purpose, all the walls of the water box, except BFGC to be replaced by a copper alloy, will be covered with a protective coating. For the numerical application, that refers to this case, one copper wall has been considered.

For the sake of simplicity, the rectangle AEHD has been assumed to belong to plane  $y = 0$ . In the case on hand both anodes are perpendicular to this plane and the points at which their axes intersect the plane are  $P = (75, 0, 75)$  and  $P_1 = (225, 0, 75)$ , the distances being expressed in centimetres.

The total length of each anode is 30 cm, while the useful length is 16 cm only, the remaining part being electrically insulated. The external diameter is 1.9 cm. The anodes are hollow cylinders and the maximum current they can withstand is 5A. For the calculations, however, they were considered solid cylinders and the possible current contribution due to their inner surface was neglected. A more realistic depiction would have been more onerous and probably not worth the effort. The whole volume was divided into 294 20-node elements.

As to the boundary conditions for the cathodic surface, reference was made to the paper of TrabANELLI, ZUCCHI and GARASSITI /28/ concerning the behaviour of some materials in sea water. The polarization curve, quoted in Fig. 6 of their paper, was discretized and the numerical values thus obtained were processed by the NOLI method /29/, which gave the following electrochemical parameters:

$$I_c = 104 \mu\text{A}/\text{cm}^2, \quad b_a = 69 \text{ mV}, \quad b_c = 575 \text{ mV}.$$

It should be remembered that according to the above authors the behaviour of the copper/sea water system does not appear to be of the Tafel type and that the NOLI method was applied by us as an example of best-fitting of an experimental polarization curve. A 5V voltage was applied to the anodes while the sea water conductivity was assumed to be equal to  $5 \cdot 10^{-2} \Omega^{-1} \text{cm}^{-1}$ . As in the previous case, convergence was achieved after 10 iterations. The total calculation time was 27 minutes; of these, 2 minutes were for lattice generation.

From Fig. 6, which shows some isopotential curves for the cathodic zone, it is evident that in the case considered protection was fairly uniform, the minimum and the maximum overvoltage values,  $E$ , being  $-444 \text{ mV}$  and  $-429 \text{ mV}$ , respectively. The corresponding current density values,  $615 \mu\text{A}/\text{cm}^2$  and  $579 \mu\text{A}/\text{cm}^2$ , confirm this observation. The protection effectivenesses derived from formulae (5) and (7) are equal to 100% for the whole cathodic surface. This result is understandable, considering the value of the anodic Tafel slope.

The fact that the total current value exceeds 10A should not surprise, for the example was studied only for illustrative purposes. In practice, the protection effectiveness we aim at is not so high. At present, the real case, for which 4 anodes are foreseen, is being examined in detail.

The example we have illustrated clearly shows how useful a three-dimensional calculation code can be for the design of a power system to be used for the cathodic protection of industrial structures. By means of preliminary calculations it is possible to define the total current required for a certain protection effectiveness, which is generally based either on direct investigation into the behaviour of a given metal in its working environment or on data from literature. The use of non-linear boundary conditions is justified in that the indications given by the primary distribution of current density are by far superior to actual needs.

Another consideration concerning the space distribution of anodes and deriving from the calculation performed is that to ascertain if current density distribution over the cathodic zone is uniform one need not use a very complex structure. A simpler case, which among other things allows a considerable saving of calculation time, often serves the purpose just as well.

#### REFERENCES

- 1 YU.YA. IOSSEL', G.E. KLENOV, Prot. of Metals 9, p.565, 1973.
- 2 J.D. JACKSON, Classical Electrodynamics, John Wiley and Sons, Inc., New York-London, 1962.
- 3 T.N. ANDERSEN, H. EYRING, The electrical double layer in physical chemistry, an advanced treatise, Vol. IX A, Academic Press, New

- York-London, 1970.
- 4 G. WAGNER, J. Electr. Soc., 99, p.1, 1952.
  - 5 G.V. AKIMOV, Théorie et méthodes d'essai de la corrosion des métaux, Dymod, Paris, 1957.
  - 6 G. ROCCHINI, ENEL-DSR/CRTN, Report n. G6/83/06.
  - 7 H.J.ENGELL, P. FORSCHHAMMER, Curr. Sci.,5,p.479, 1965.
  - 8 W.J. SCHWERDTFEGER, Corrosion, 16, p.2095, 1960.
  - 9 L. LANDAU, E. LIFCHITZ, Electrodynamique des milieux continus, Editions de Moscou, 1969.
  - 10 L. ANTROPOV, Theoretical Electrochemistry, MIR Publishers, Moscow 1977.
  - 11 P.M. MORSE, H. FESHBACH, Methods of theoretical physics, McGraw-Hill, New York, Vol. I, 1953.
  - 12 D.H. NORRIE, G. DE VRIES, The finite element method, Academic Press, New York-London, 1973.
  - 13 H.P.E. HELLE, G.H.M. BEEK, J.TH. LIGTELIJN, Corrosion, 37, p. 522, 1981.
  - 14 K.J.BINKS, P.J. LAWRENSON, Analysis and computation of electric and magnetic field problems, Pergamon Press, New York, 1963.
  - 15 C.A. BREBBIA, The boundary element method for engineers, John Wiley And Sons, Inc., New York-London, 1978.
  - 16 K. O'M. BOCKRIS, A.K.N. REDDY, Modern electrochemistry, Vol. 2, Plenum Press, New York, 1970.
  - 17 R.H. GALLAGHER, Finite element analysis, Prentice-Hall, Inc., Englewood Cliffs, New Jersey, 1975.
  - 18 T.K. HELLEN, CEGB, Research Department, Report n° RD/B/N.1975, June 1971.
  - 19 D.C. ZIENKIEWICZ, The finite element method in engineering science, McGraw-Hill, London, 1971.
  - 20 B.K. NEALE, CEGB, Research Department, Report n° RD/B/N.2432, October 1972.
  - 21 T.K. HELLEN, CEGB, Research Department, Report n° RD/B/N.1761, Ottobre 1970.
  - 22 ENEL Contract N. 74779/12930. Final Report MTC/FL37/83, November 1983.
  - 23 ENEL Contract N. 82481/8580. Final Report MTC/FL30/83, February 1983.
  - 24 B. IRONS, S. AHMAD, Techniques of finite elements, John Wiley and Sons, New York, 1980.
  - 25 H.S. CARSLAW, J.C. JAEGER, Conduction of heat in solids, Clarendon Press, Oxford, 1959.
  - 26 E. WEBER, Electromagnetic theory, Dover Publications, Inc., New York, 1965.
  - 27 G.L. MUSSINELLI, Giornata di studio sulla protezione catodica,

- organizzata dal Centro Corrosione dell'AIM, Milano, February 1984.
- 28 G.A. NICHOLS, A cathodic protection system for C.E.G.B. Cooling water systems. C.E.G.B. Scientific Services Department. Report N°SSD/SW/78/N.151, December 1978.
- 29 G. TRABANELLI, F. ZUCCHI, V. CARASSITI, 2ème Congrès International de la corrosion marine, et des salissures, Athènes, Septembre 1968.
- 30 G. ROCCHINI, ENEL-DSR/CRTN, Report n°G6-1, 1979.

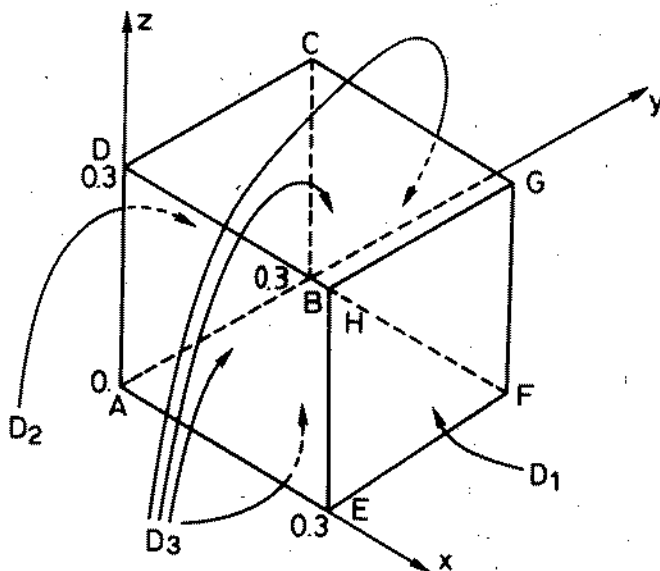


Fig. 1: Reference sketch for boundary conditions.

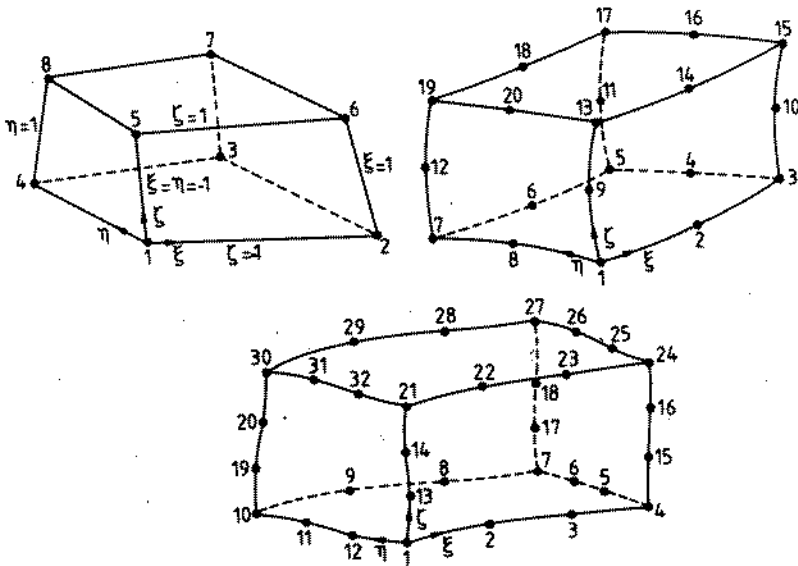


Fig. 2: 8-, 20-, 32-node elements.

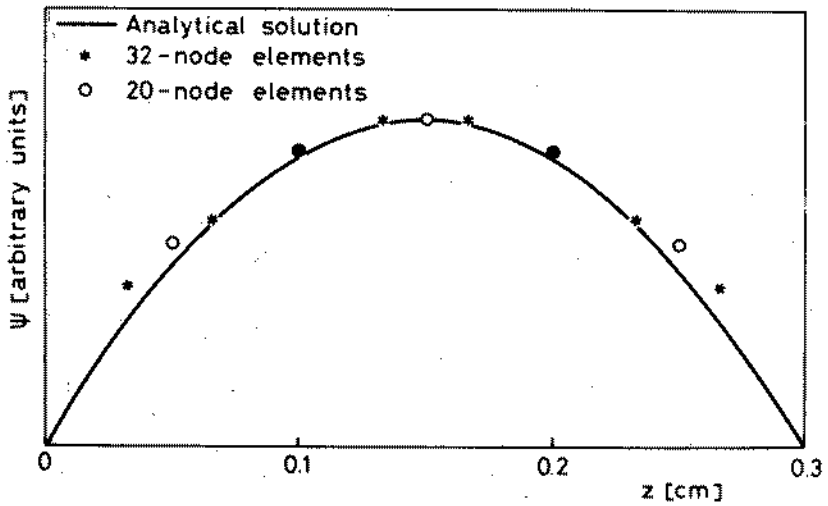


Fig.3 : Potential distribution along the straight line  $x=y=0.1$

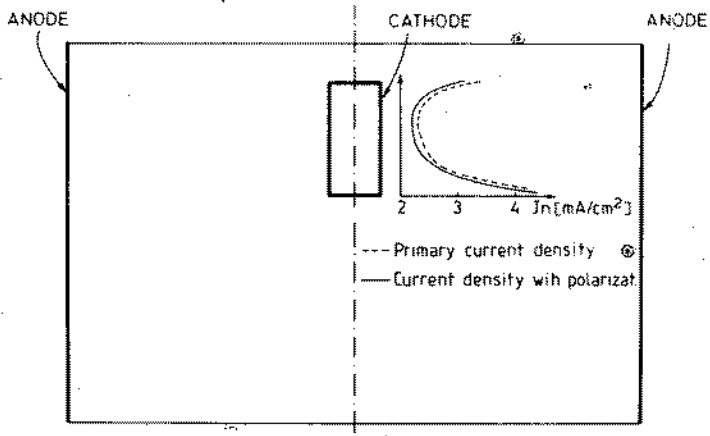


Fig. 4 : Electrolytic cell and current density distribution along the cathode.

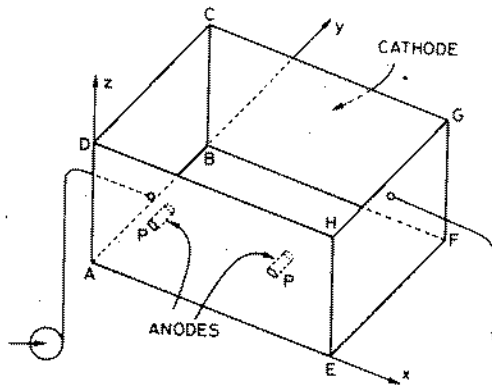


Fig. 5 : Experimental structure.

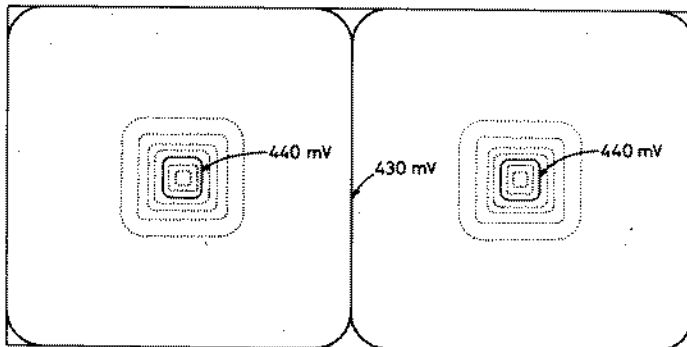


Fig. 6 : Isopotential curves for the cathodic zone.

## CATHODIC PROTECTION WITH DEEP ANODE GROUND BEDS

Joe F. Tatum, P.E. and Joseph F. Tatum, Jr., P.E.

Cathodic Engineering Equipment

P.O. Box 1089 Hattiesburg, MS 39401

This paper describes the use of deep anode impressed current groundbeds, their development, use, and reliability. A replaceable deep anode system is described as a method to reduce anode ground bed loss and as a research tool for material evaluation. The paper describes anode "end effect" with a developed method of center tapping as a means to minimize anode loss. A method of segmenting the anode surface to obtain more uniform current distribution, as a means to control the "end effect" phenomena, is described.

Ce document décrit l'utilisation de bases terrestres à anode profonde dans le cas de courant imprimé ainsi que leur développement, leur utilisation, et leur sécurité de fonctionnement. Un système remplaçable d'anode profonde est décrite comme étant une méthode de réduction des pertes de connection à l'anode ainsi qu'un outil de recherche pour l'évaluation des matériaux. Le dossier donne une description de "l'effet d'extrémité" à l'anode et développe une méthode de pris centrale de courant comme étant un moyen de minimiser les pertes à l'anode. Une méthode de segmentation de la surface de l'anode afin d'obtenir une distribution de courant plus uniforme est développée comme étant un moyen de contrôle du phénomène "d'effet d'extrémité."

The first recorded installation of a deep anode system was in 1949. Since that time there had been thousands of deep anode installations made around the world. The design for deep anode systems by corrosion engineers has been far from consistent. The different types of deep anode systems are almost as numerous as the number of installations, with some exception. This paper will describe deep anode systems, development work thereon and anode systems of a replaceable design utilizing carbonaceous backfill as a conductive medium between the anode surface and the earth. The anode systems described herein are for land based installations.

In August, 1971, an installation was developed which enabled deep groundbeds to be replaced without the necessity of drilling a new bore hole. A schematic of the design utilized from which the data in this paper was gathered is shown as Figure I (Replaceable Deep Anode System)\*.

When the first replaceable deep anode systems were installed, they were designed to give adequate, dependable service for a period of ten to fifteen years. Most of the systems installed are still giving excellent service. However, as might be expected, some systems failed early and this inspired the development work reported in this paper. The replacement deep anode design enabled the components of the deep anode system to be retrieved, the cause of failure determined, and with indicated design changes to improve service life and make the systems more dependable.

It was not anticipated that the anodes or wire would have early failure, but failures did occur and rejuvenation was made possible by the fluidization of the carbonaceous backfill within the plastic casing enabling the removal of the anodes wire and backfill, once the components were removed, they were observed and analyzed, corrections were made and new components reinstalled incorporating the new designs.

One of the main disadvantages to deep anode systems has been the fact that they were not easily replaced. Once the replaceable system was developed utilizing carbonaceous backfill which could be fluidized so that the components there could be easily removed, we created an enormous research tool to study the failure of the various components.

Figure II (Round Low Resistivity Carbonaceous Backfill Magnified 15 Times)\* Figure III (Cutaway of Backfill Magnified 100 Times Showing Small Interval Voids) The type of backfill used is the low resistivity calcined round carbon type with additives. This backfill contains few internal voids enabling it to sink readily in water. The round shape facilitates pumping and causes the coke to be fluidized readily. Additives of different types give the coke to develop properties depending on

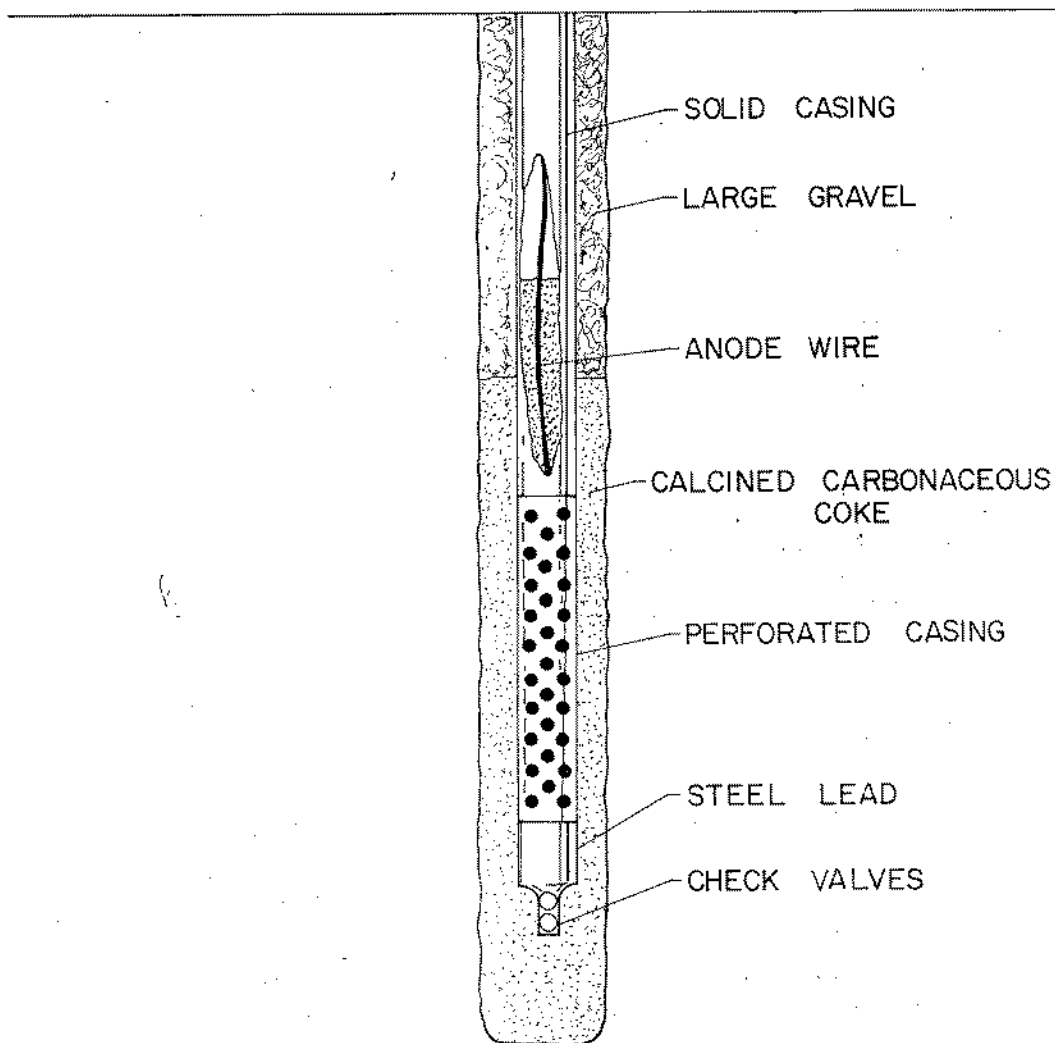
---

\* U.S. Patent No. 3,725,669

\* U.S. Patent No. 4,018,715



FIGURE I  
REPLACEABLE DEEP ANODE SYSTEM



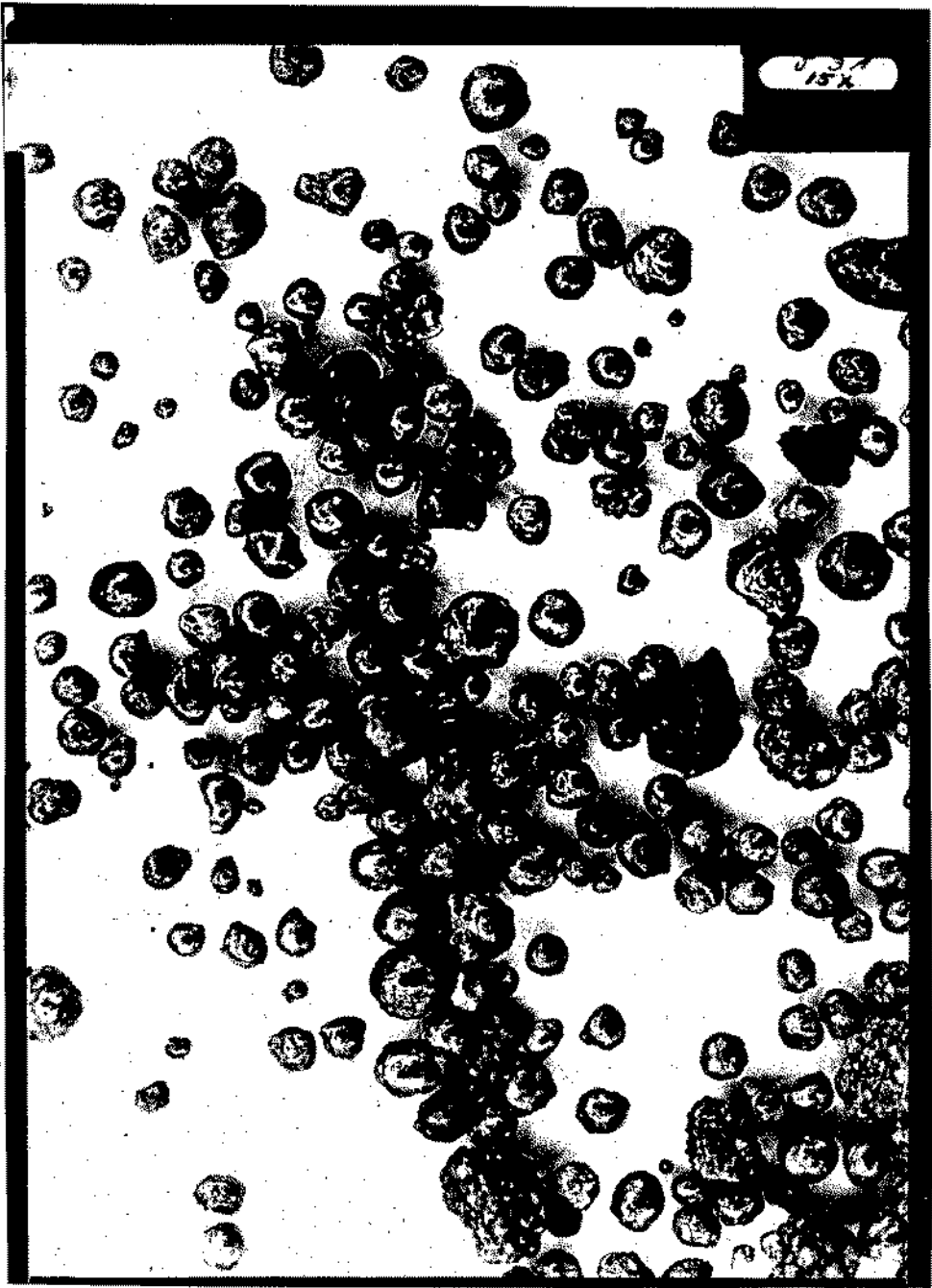


Figure II  
Round Low Resistivity  
Carbonaceous Backfill  
Magnified 15 Times

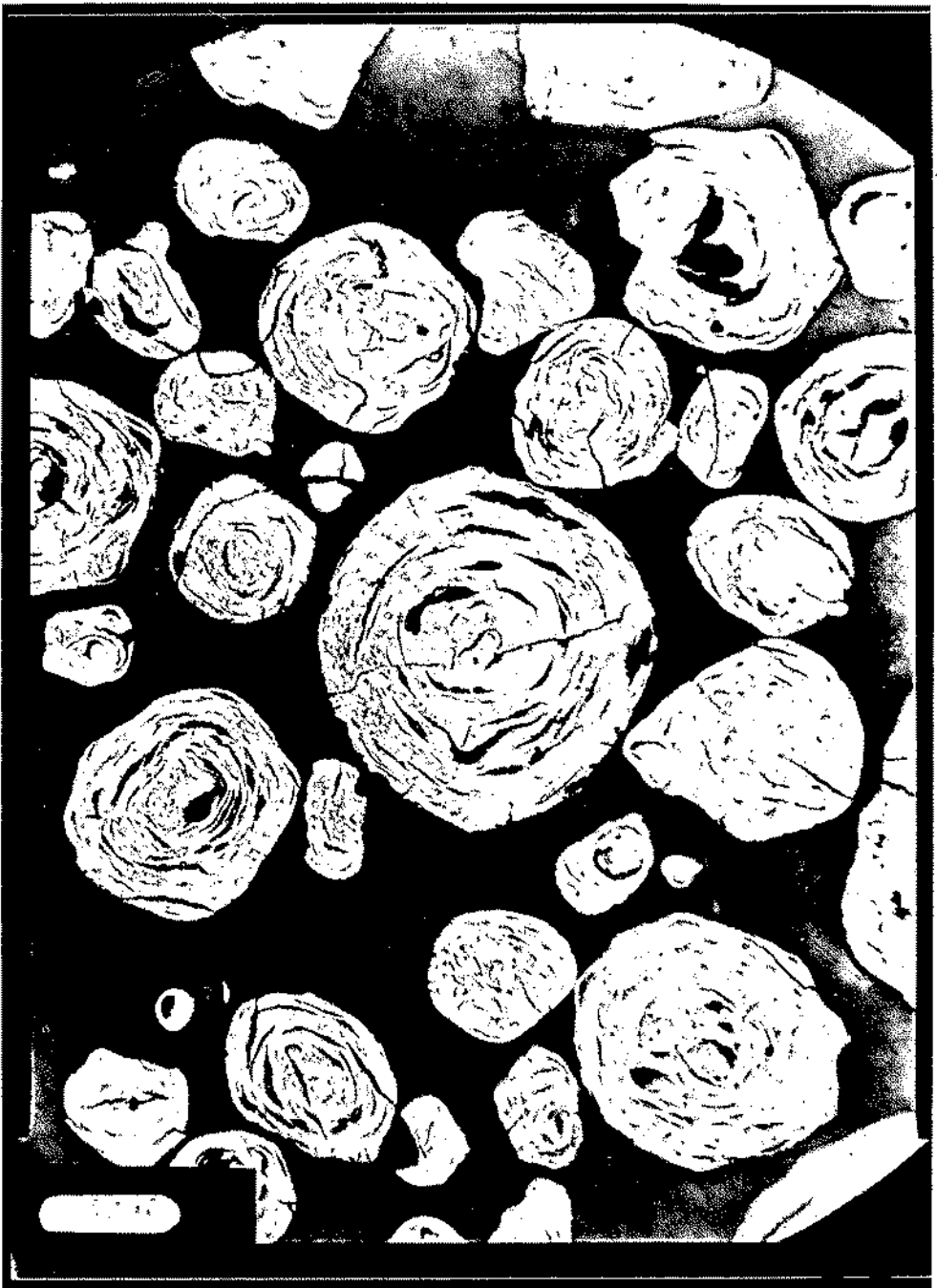


Figure III  
Cutaway of Backfill  
Magnified 100 Times Showing  
Small Internal Voids

the end use requirement. The Chemical Analysis is as follows:

|        |           |
|--------|-----------|
| 92.47% | Carbon    |
| 5.39%  | Sulfur    |
| 2.06%  | Ash       |
| 0.06%  | Silicon   |
| 0.02%  | Iron      |
| 0.00%  | Volatiles |
| 0.00%  | Moisture  |

The weight is 74 pounds per cubic foot. The Particle Analysis is as follows:

|                  |       |
|------------------|-------|
| 16 mesh          | 0%    |
| 28 mesh          | 2.1%  |
| 48 mesh          | 21.1% |
| 100 mesh         | 60.3% |
| 200 mesh         | 15.0% |
| 200 plus<br>mesh | 1.5%  |

The coke has a resistivity of 0.1 ohms per cubic centimeter under a pressure of 150 pounds per square inch. Additives enable the coke to pump readily and develop lower resistivity.

In the earlier replaceable deep anode systems, there was approximately a 25 percent failure rate. One of the principal causes was the loss of anode material, anode passivity or loss of anode contact to the conductive backfill. There are several types of anode materials utilized in replaceable designs. These are High Silicon cast iron, platinum clad, or platinum plated anodes with a passive substrate, steel and graphite. This paper will cover the development work on only one type of anode material, graphite. In graphite systems, the reason for failure is not a long list. Failures were caused by anode surface properties, connection failures, sealant failures and "end effect". In the majority of the systems studied, the wire insulation was high molecular weight polyethylene. The failure because of wire insulation was not a factor in any of the deep anode systems reviewed for this paper.

Graphite anodes were utilized in some of the first replaceable deep anode systems. The initial systems had wire top connections and lined oil treated anodes. The current densities of the installations varied between 800 to 1000 milliamperes per square foot. Failure on some systems occurred after two or three years of operation. Of the systems removed, normally only the epoxy cap, the lead wires and some anode material could be retrieved from the deep anode system. Large pieces of the graphite anode would sometimes break off and drop to the bottom of the casing to be ground and flushed out of the hole.

An installation was made in 1971 in Mississippi. The installation was of the replaceable deep anode type and employed three 2 x 2 x 72 linseed oil treated, top end connected graphite anodes. The wire insulation was of the high molecular polyethylene type. In 1974, two of the three anodes in this installation showed zero current output. A decision was made to remove the components of the groundbed and replace. Upon removing the anodes it was observed that all of the anodes were experiencing a penciling type failure on the bottom end and some were experiencing a penciling on the top end. One of the anodes was completely lost in the hole because of this penciling effect. This phenomena is called "end effect". The reason for the failure of the anodes was because the current density at the ends of the anode exceeds the current density in the center by a ratio of 7:1. Although the anodes are computed by their surface to carry a current designs limitation such as 1000 milliamps per square foot. The "end effect" caused the current density to far exceed the design.

Research was conducted to determine actually how much current was being discharged from the end and how much was being discharged from the center. These tests were conducted in a tank of uniform resistivity water. It was readily observed by taking potential measurements that the current on the ends was approximately seven times the current from the center. Figure IV (Anode Current Discharge "End Effect") This has a two-fold effect. By the current density being at such a high level, hydrogen or oxygen gas was evolved from the anode's surface and this gas evolution caused the backfill to become separated from the anode and therefore the anode material would be consumed as though the anodes were in an aqueous environment. Studies were being conducted at the time for providing a more even current distribution in the anodes but these studies were not available at this particular time. Therefore, the best way to extend the anode life would be to connect the anode at the center and this was done by gun drilling the anode from one end and installing a brass stud connected to the wire in the center of the anode. Thus the anode could be consumed on both ends without losing contact to the wire connection. Figure V (Graphite Anode Center Connection)\* One other solution would be to install more anodes and therefore have them closer together causing a mutual interference between the anodes on the ends and thereby reducing the end effect, but this method requires the expanded use of anode materials and therefore increased the cost of the anode bed considerably. The anodes for this bed were center connected and reinstalled with carbonaceous backfill. Additional life of the deep anode life system was experienced, but another problem developed.

---

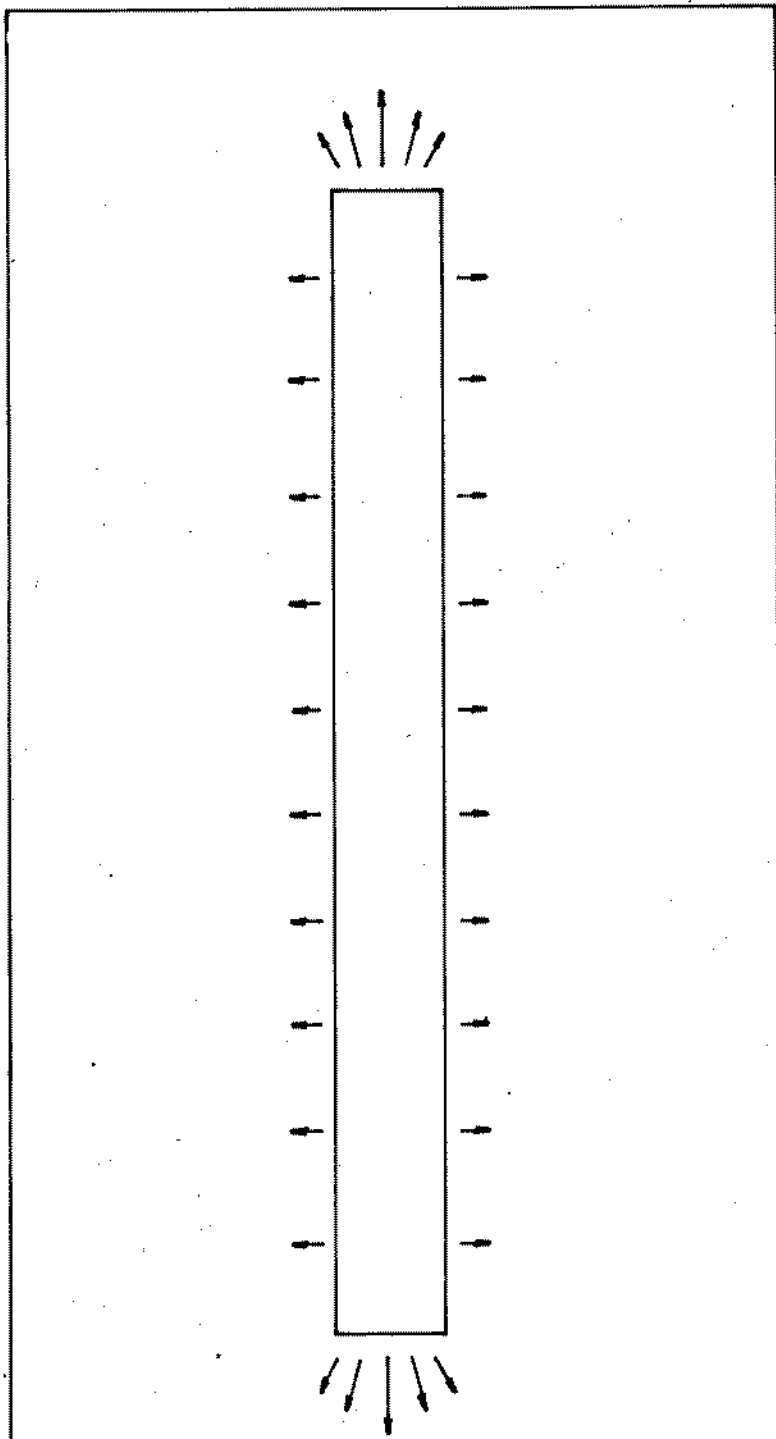
\*U.S. Patent No. 4,265,725

FIGURE V  
GRAPHITE ANODE CENTER CONNECTION



FIGURE IV

ANODE CURRENT DISCHARGE "END EFFECT"



This major development occurred because of two replaceable deep anode installation failures which occurred in Louisiana. These systems were installed in 1975. The two systems contained five 3 x 3 x 72 center tap linseed oil treated graphite anodes and were designed to discharge approximately 25 amps. The systems were in operation until early 1982 when it became obvious that there were large fluctuations in the current discharge and a decision was made to replace the two systems. The systems were removed and they were typical of deep anode systems observed elsewhere which contained linseed oil treated graphite. Typically when a system containing oil treated anodes is retrieved, oil is observed in the fluidization when the anode column vicinity is reached by the fluidization. The fluidization is conducted by pumping water down a hole into the casing and into discharge area of the anodes and will cause the coke to be fluidized, the anodes will become loose and may be removed for replacement. When the water goes into the fluidization tanks with oil impregnated anodes, oil is observed on the top of the water. Tests revealed that the carbonaceous backfill which is retrieved from the vicinity of the anodes has a substantially higher resistivity (15 times greater) because of the contamination by the oil. This contaminated high resistivity coke decreased the electronic conductivity and resulted in the anodes behaving in a manner similar to anodes having no backfill. The anodes removed from the Louisiana wells had a 50 percent higher material consumption rate.

Examination of the anodes removed from the Louisiana deep anode systems revealed two important points. First was that the practice of center tapping the anodes would greatly extend the life. Second, the problem of the insulating effect caused by the linseed oil migration into the backfill was apparent. This caused the anodes to become separated electronically from the conductive carbonaceous backfill and caused the anodes to behave as though suspended in fresh water with resulting premature failure. Research indicated that to solve the problem of surface insulation and high carbon consumption because of impregnation could best be done by using an untreated graphite. The reason for impregnating graphite anodes with an oil such as linseed or other oxidizable oil was because of the pores developed within the graphite particles. The pores developed in the graphite caused gases to be accumulated within the anode and the expansion of these gases caused the graphite to spall off in large chunks rather than be consumed in a uniform manner. In experimentation, it was demonstrated that an untreated graphite surface exposed to lubricated calcined fluid petroleum coke would greatly decrease the anode consumption rate. The theory is that electronic conduction between coke particles results in the gas being generated at the coke periphery instead of at the anode and this conduction results in lower anode material consumption. After the research studies were completed, installations containing untreated graphite anodes were center



tapped and placed in deep anode systems. The anodes were constructed from high density graphite which contained fewer pores than lower density graphite, therefore, treating was not as critical. Installations with the untreated high density graphite were observed after two or three years of operation and showed an improved consumption rate. There remained the problem of "end effect".

Research was begun in 1978 on a method to improve current distribution over the anode surface. This was done by installing insulating segment bands on the anode resulting in multiple ends and thereby gave a more uniform current density. Figure VI (Anode with Insulating Segmented Strips)\* Laboratory tests to determine current density by the use of the segmented anode concept showed the current density could be maintained at a fairly uniform rate over the anode surface, this resulted in longer anode life.

In 1978, a replaceable deep anode system was installed in Mississippi. The ground bed site was chosen because of its uniform underground strata resistance from the surface to below the 222 foot depth. The deep anode system was to consist of two segmented and two conventional graphite anodes. The anodes were identical except for the segmentation to decrease end effects. They were constructed of high density graphite and contained no oil or pore impregnation. The system was operated for five years and the anodes removed each year for observation and weight. Testing of anodes was terminated on June, 1983, and new anodes of the same configuration and type were reinstalled in the test groundbed. Initially, the deep anode system was energized for a total current output of ten amperes and each anode was monitored so as to carry one-fourth of the current output. The anode currents were observed once each month and kept within a tolerance of 10 percent. The anodes were removed for inspection and observation for the first time on August, 1979. Additional inspections and observations were made in October, 1980, January, 1982, July, 1982, and June of 1983. The observation at each point indicated that there was very minor consumption on the segmented anodes. The two unsegmented graphite anodes showed very noticeable consumption on their ends with some pits being developed in the body section.

The total consumption of the unsegmented anodes showed a 20 percent loss of material by weight whereby the segmented anodes had only a 2.6 percent loss in weight during the same operational period. This resulted in a 90 percent reduction in anode consumption by using the segmented design.

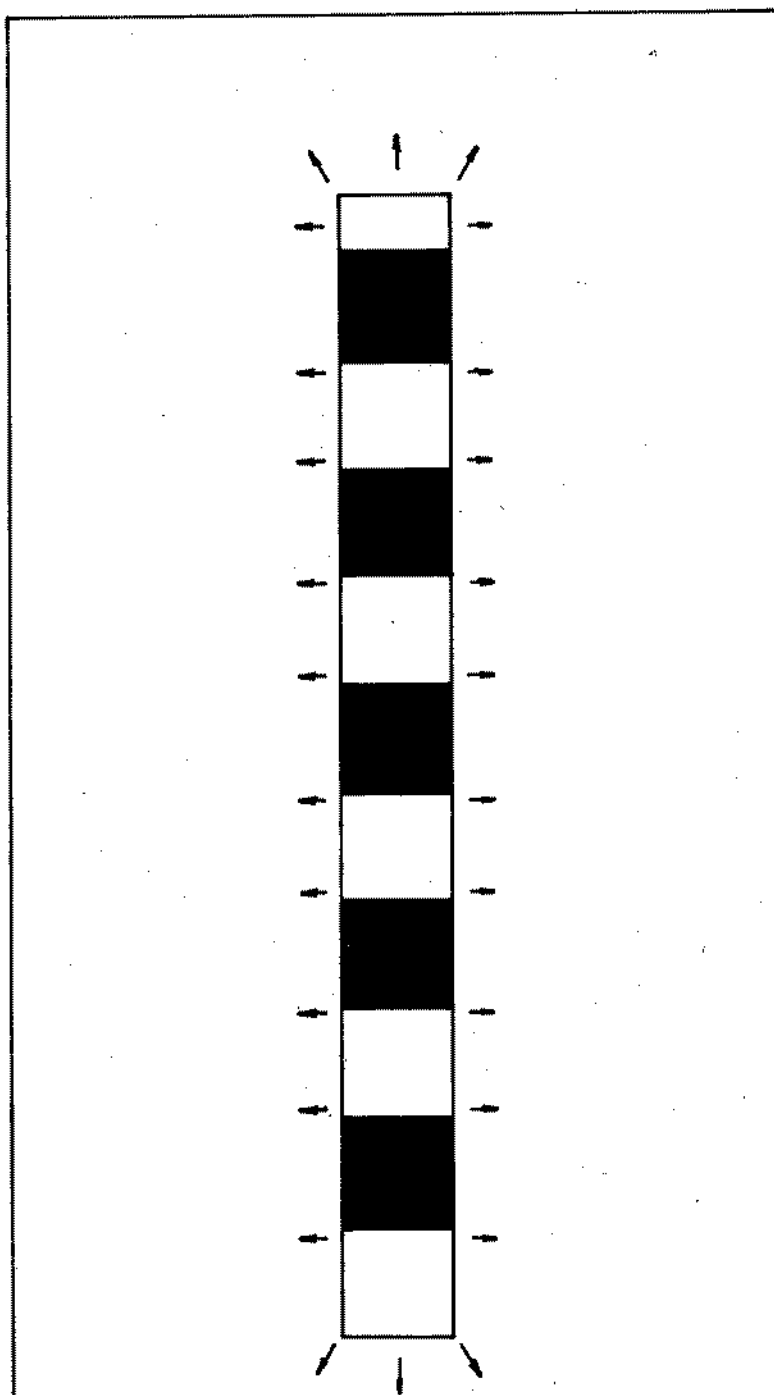
At the present time, the deep anode systems being installed by our company are the center tapped high density

---

\*U.S. Patent No. 4,175,021

FIGURE VI

ANODE WITH INSULATING SEGMENTED STRIPS



\*U.S. PATENT NO. 4,175,021

graphite segmented type. The failure rate has shown a very noticeable decrease and the reliability of deep anode systems have been greatly improved.

The development of the replaceable deep anode system has resulted in a tool giving the corrosion engineer an opportunity to observe causes of failure in deep anode systems. The observation and testing resulted in a greatly improved anode performance. A side benefit has been observation of the loss of anodes because of wire insulation failure and this has resulted in an improved anode insulation and a decrease in failures because of this factor. Deep anode systems may now be installed by using graphite anodes with a high reliability factor capable of giving dependable service over their design life.

## BIBLIOGRAPHY

1. Lewis II. West, "Cathodic Protection of Buried Pipelines in Congested Areas," MATERIALS PROTECTION, February, 1963, p. 11.
2. J.R. Gates, "Deep Well Ground Beds for Cathodic Protection of Multiple Lines in Highly Congested Industrial Areas." CORROSION, July, 1961, p. 75.
3. Joe F. Tatum, "Theory and Application of Deep Ground Anode Beds," CORROSION, August, 1961, p. 27.
4. Robert Pope, "Interference from Forced Drainage," CORROSION, January, 1950.
5. Francis W. Binger, "Solution of Cathodic Protection Interference Problems," CORROSION, March 5, 1955.
6. Irving A. Denison, "Geometric Factors in Electrical Measurements Relating to Corrosion and Its Prevention," CORROSION, October, 1955.
7. Joe F. Tatum, "Impressed Current Anodes Installed and Backfilled at Depth of 350 Feet," CORROSION, April, 1958.
8. F.E. Costanzo, "Use of Graphite Anodes in Deep Groundbeds," NACE 26th Annual Conference, March 2-6, 1970.
9. Don Boles, "Evaluation of Heavy Duty Deep Well Groundbeds," presented at the 1962 NACE Southern Region Symposium, San Antonio, Texas, October 18, 1962.
10. Richard L. Seifert, "Cathodic Protection Interference Mitigation Currents Exposed," published in two parts in PIPELINE ENGINEER, June and August, 1968.
11. A.W. Peabody, "Use of Steel Anodes in Deep Ground Beds," presented at the NACE 26th Annual Conference, March 2-6, 1970, Philadelphia, Pennsylvania.
12. NACE Standard RP-05-83, "Recommended Practice--Design, Installation, Operation, and Maintenance of Impressed Current Deep Groundbeds".
13. Joe F. Tatum, "Replaceable Deep Groundbed Evaluation," MATERIALS PERFORMANCE, Volume 14, Number 12, pp. 12-16, December, 1975.

"SUSCEPTIBILITY TO MARINE CORROSION OF AN INDUSTRIAL STEEL SUBJECTED  
TO ANODIC PULSES, DURING CATHODIC PROTECTION"

"ETUDE DE LA SUSCEPTIBILITE A LA CORROSION MARINE D'UN ACIER INDUSTRIEL  
SOU MIS A DES IMPULSIONS ANODIQUES, SOUS PROTECTION CATHODIQUE"

S. GRENET, J. GALLAND, M. GROOS

Laboratoire de Corrosion et Fragilisation par l'Hydrogène

Ecole Centrale des Arts et Manufactures

CHATENAY-MALABRY - FRANCE -

ABSTRACT

The behaviour of an industrial mild steel used for construction of off shore platforms, relatively to marine corrosion was studied. We have observed the influence of anodic pulses, with different conditions of polarisation, during the cathodic protection, in presence of calco-magnesium deposits. So we achieved always an acceleration of the corrosion process. No acceptable corrosion rate could be found in these conditions.

RESUME

Le comportement d'un acier doux industriel, utilisé dans la construction des plate-formes off shore a été étudié vis-à-vis de son comportement à la corrosion en milieu de type marin. Nous avons observé l'influence de pulses anodiques, pour différentes conditions de polarisation, au cours de la protection cathodique, en présence de dépôts calcomagnésiens. Nous avons ainsi toujours obtenu une accélération plus ou moins notable du processus de corrosion. Aucune vitesse acceptable de corrosion n'a pu être trouvée, dans ces conditions.

"ETUDE DE LA SUSCEPTIBILITE A LA CORROSION MARINE D'UN ACIER INDUSTRIEL  
SOU MIS A DES IMPULSIONS ANODIQUES, SOUS PROTECTION CATHODIQUE"

S. GRENET, J. GALLAND, M. GROOS

Laboratoire "Corrosion et Fragilisation par l'Hydrogène"  
Ecole Centrale des Arts et Manufactures 92290 CHATENAY-MALABRY

Nous avons étudié le comportement à la corrosion d'un acier industriel pour construction "off shore" placé sous protection cathodique, avec pour conséquence création d'un dépôt calco-magnésien (1) (2), et soumis périodiquement à des impulsions anodiques en potentiel. Ce traitement devant ainsi entraîner un processus forcé de corrosion, nous avons observé dans quelle mesure cette corrosion pouvait être d'un niveau acceptable et si le dépôt formé pouvait jouer un rôle inhibiteur vis-à-vis de la corrosion.

Le matériau.

L'acier utilisé est un acier de construction faiblement allié de type "E 355", et a la composition chimique suivante :

|       |       |       |       |       |       |       |
|-------|-------|-------|-------|-------|-------|-------|
| C     | Si    | Mn    | P     | S     | Al    | N     |
| 0,16  | 0,3   | 1,36  | 0,019 | 0,023 | 0,047 | 0,007 |
| Ni    | Cr    | Mo    | Cu    | Sn    | V     | Fe    |
| 0,048 | 0,029 | 0,009 | 0,445 | 0,01  | 0,011 | Reste |

(Composition en poids %)

Ses caractéristiques mécaniques, à l'état normalisé, déterminées pour une vitesse de déformation  $\dot{\epsilon} = 10^{-4} s^{-1}$  sont :

|                    |          |        |               |                             |
|--------------------|----------|--------|---------------|-----------------------------|
| Re<br>à 0,2% (MPa) | R<br>MPa | A<br>% | $\Sigma$<br>% | H <sub>v</sub><br>(Vickers) |
| 445                | 707      | 33,7   | 70,6          | 170                         |

Un examen métallographique révèle une structure ferrito-perlitique. Les grains de perlite se répartissent en couches parallèles à la direction de laminage. Vis-à-vis de la corrosion en milieu de type marin, le métal réagit de manière uniforme et homogène.

#### Comportement en milieu marin (en l'absence de polarisation).

Le matériau, après polissage, est placé dans une solution de NaCl 0,6 M (35 g/l) ou une solution d'eau de mer artificielle (norme ASTM D1141) pendant 160 heures sans agitation. La perte de poids enregistrée est alors de 3 mg, pour une surface immergée de 1 cm<sup>2</sup>. On calcule ainsi le taux de corrosion généralisée qui est de 0,25 mm/an.

#### Comportement en milieu marin (sous polarisation).

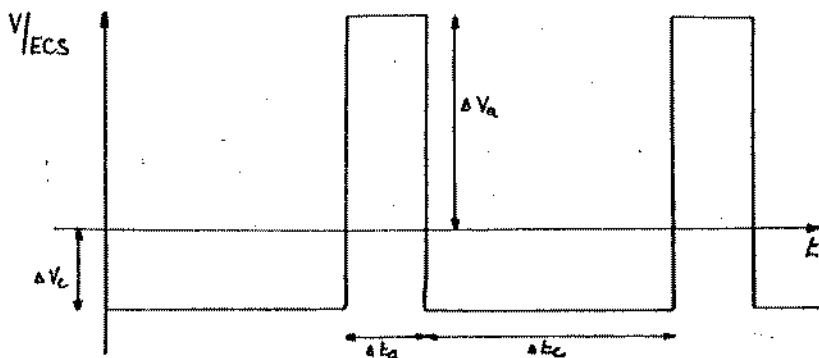
L'étude électrochimique a été faite à partir de la détermination de la courbe intensité-potentiel représentée figure 1.

On remarque, au retour, un épaulement caractérisant une redéposition du fer qui avait été dissous dans le domaine anodique, par suite de l'enrichissement localisé au voisinage de l'électrode en ions Fe<sup>++</sup> puisque le milieu n'est pas agité. On retrouverait un comportement similaire dans le cas où un dépôt calco-magnésien existerait, puisque dans les pores de ce dépôt on peut également considérer que l'électrolyte est stagnant.

#### Etude de la corrosion forcée.

##### Essais préliminaires

Le signal électrique obtenu sur l'échantillon répond schématiquement au profil ci-dessous :



Avec  $\Delta V_c$  : potentiel de protection cathodique choisi entre -1100 mV et -1250 mV

$\Delta V_a$  : hauteur de l'impulsion anodique qui doit être suffisamment grande pour être significative. Elle est au moins égale à +1200 mV.

$\Delta t_a$  : est la durée de l'impulsion anodique comprise entre 5 et 10 secondes.

$\Delta t_c$  : temps de maintien sous polarisation cathodique. Il doit être assez important pour que l'action bénéfique du dépôt calco-magnésien se fasse sentir. Nous avons choisi  $\Delta t_c = 2$  heures.

La durée totale d'un essai est de l'ordre de une à deux semaines, pour qu'un état moyen stationnaire puisse être observé et que la dispersion des résultats ne soit pas trop importante. Les essais ont été réalisés en utilisant un générateur de signaux arbitraires pilotant un potentiostat à réponse rapide de façon à éviter une déformation du signal de pilotage. La cellule d'électrolyse contient une électrode au calomel saturée (ECS) une contre-électrode de platine et l'échantillon d'acier de surface  $1 \text{ cm}^2$ .

Les chutes ohmiques dues à la résistance de l'électrolyte et à la géométrie de la cellule sont négligeables.

Un test d'immunité, au potentiel cathodique choisi, a été effectué dans les conditions suivantes :

- après polissage, une impulsion anodique à +1200 mV/ECS pendant dix secondes est appliquée au métal soumis ensuite à une polarisation cathodique de -1100 mV/ECS pendant quatre jours.

Aucune perte de poids n'est enregistrée, après que le dépôt formé en surface ait été éliminé.

#### Expériences avec polarisation anodique temporaire.

De nombreuses valeurs de  $\Delta V_c$ ,  $\Delta V_a$ ,  $\Delta t_c$ ,  $\Delta t_a$ , ont été envisagées. Nous ne décrivons ici qu'un petit groupe d'expériences significatives, mettant plus particulièrement en évidence le rôle du dépôt calco-magnésien et son adhérence en fonction de l'orientation de la surface (verticale ou horizontale).



a) L'échantillon est en position verticale et subit une prépolarisation cathodique de 16 heures à  $-1100$  mV/ECS.

Les impulsions anodiques de 8 secondes à  $1375$  mV/ECS sont espacées de deux heures pendant lesquelles on maintient une polarisation cathodique de  $-1150$  mV/ECS. Les résultats des essais d'une durée de plusieurs jours sont résumés dans le tableau ci-dessous.

| Durée de l'essai | Vitesse de corrosion |
|------------------|----------------------|
| 144 heures       | 0,83 mm/an           |
| 176 heures       | 0,93 mm/an           |
| 192 heures       | 1,25 mm/an           |

On voit sur les enregistrements correspondants  $V(t)$  et  $I(t)$  que le retour à l'état stable dans le domaine cathodique s'effectue en deux minutes environ (Figures 2 et 3). On observe un épaulement sur la courbe cathodique pouvant être dû à une redéposition du fer (non adhérent) à l'intérieur du dépôt calco-magnésien poreux.

Il faut remarquer au cours de l'essai un certain nombre de décollements du dépôt calco-magnésien, en relation avec la présence des pulses anodiques. Cela accentue donc l'importance de la corrosion.

Des essais complémentaires de trois heures entre impulsions anodiques ne nous ont pas permis d'abaisser de façon appréciable la vitesse de corrosion qui reste élevée, en comparaison avec les valeurs observées en corrosion libre.

b) La surface utile de l'échantillon est horizontale.

On a alors utilisé les conditions suivantes :

- polarisation cathodique de 16 heures à  $-1100$  mV/ECS ;
- impulsions anodiques de 10 secondes à  $+1400$  mV/ECS ;
- intervalle de temps de deux heures à  $-1250$  mV/ECS ;
- durée totale de l'expérience : 178 heures.

Dans ces conditions le dépôt ne peut plus tomber en se détachant de la surface du métal et son importance vis-à-vis de l'inhibition de la corrosion est plus grande.

On obtient alors une vitesse de corrosion plus faible de 0,49 mm/an seulement, qui a diminué de 50% environ, mais qui reste encore assez élevée en valeur absolue.

Ces résultats sont confirmés à l'aide de la comparaison des enregistrements  $I(t)$  mettant en évidence une diminution de l'intensité du courant dans les domaines anodique et cathodique lorsque la surface est recouverte d'un dépôt épais.

Une étude de celui-ci au microscope électronique à balayage n'a pas permis d'observer de différence sensible sur la morphologie du dépôt calco-magnésien obtenu en présence ou non d'impulsions anodiques.

#### DISCUSSION DES RESULTATS

Cette étude montre le danger qu'il y a à envisager la possibilité de polarisation anodique temporaire d'une structure en acier destinée à la construction off-shore. La quantité d'électricité mise en oeuvre au cours de la perturbation de potentiel donne un bilan global, dans le sens anodique, de 0,2 à 0,4 coulomb par pulse suivant l'importance du dépôt calco-magnésien présent au moment du pulse (voir figure). Il en résulte un bilan anodique moyen de 3 à 6 coulombs par jour, qui est à comparer à la valeur de 1 coulomb par jour, correspondant à la dissolution naturelle d'un acier ordinaire dans l'eau de mer. On retrouve bien ainsi l'accentuation de la vitesse de corrosion observée après mesure de la perte de poids de l'échantillon.

#### CONCLUSION

Les polarisations anodiques effectuées sur un acier de construction en milieu marin ont provoqué une accentuation importante de la corrosion du matériau. Cependant les conditions de polarisation anodique étaient sévères.

Elles avaient pour but d'envisager la production au cours du pulse anodique d'espèces chimiques biocides, telles que chlore ou ions hypochlorites, qui peuvent permettre le nettoyage des salissures marines déposées sur les structures off shore (3) (4). Nous n'avons pas conduit cette étude jusqu'à ce niveau, par suite du risque encore trop élevé de corrosion.

Les modifications apportées au cours de notre étude aux conditions de polarisation, ont fait diminuer la vitesse de corrosion d'un facteur supérieur à 5. Il est certainement possible d'aller encore plus loin dans ce domaine et de trouver des conditions d'emploi où ce procédé de nettoyage chimioélectrique des structures off shore en acier pourrait être mis en oeuvre.

Nous remercions la Société ORCAL de l'aide financière qu'elle nous a apportée au cours de cette étude.

#### BIBLIOGRAPHIE

- (1) "Formation de dépôts calcomagnésiens sur un acier protégé cathodiquement". G. PHILIPPONNEAU, C. DAGBERT, J. GALLAND, L. LEMOINE  
5<sup>ème</sup> Congrès International de Corrosion Marine et des Salissures.  
Barcelone, mai 80, p. 596-602.
- (2) "Cathodic polarisation effects on magnesium calcium deposits formation at fatigue crack root of mild steel in sea water".  
G. PHILIPPONNEAU, S. WIDANSKY, M. HABASHI, J. GALLAND,  
Int. Congr. "Fracture Prevention in Energy Systems" Rio de Janeiro,  
(novembre 83).
- (3) "A technique for prevention or removal of biofouling, from surfaces exposed to the marine environment".  
T.R. KRETSCHMER, A.P. SMITH and B.C. STREETS. Proceedings of "off-shore. Technology Conference 1980.
- (4) "Nettoyage par action d'un produit toxique dégagé au contact du métal d'une structure "off-shore" par un procédé d'électrolyse". M. GROOS, J. GALLAND, L. PICARD. Rapport ORCAL, Ecole Centrale des Arts et Manufactures, 1983.

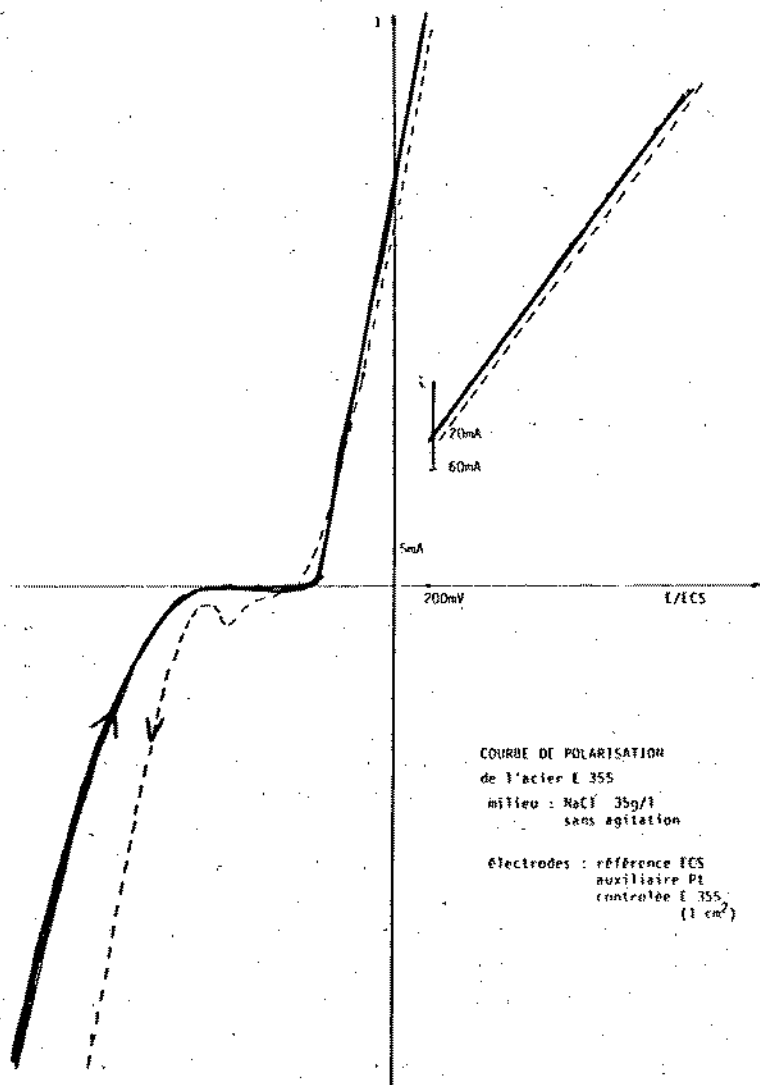


Figure 1

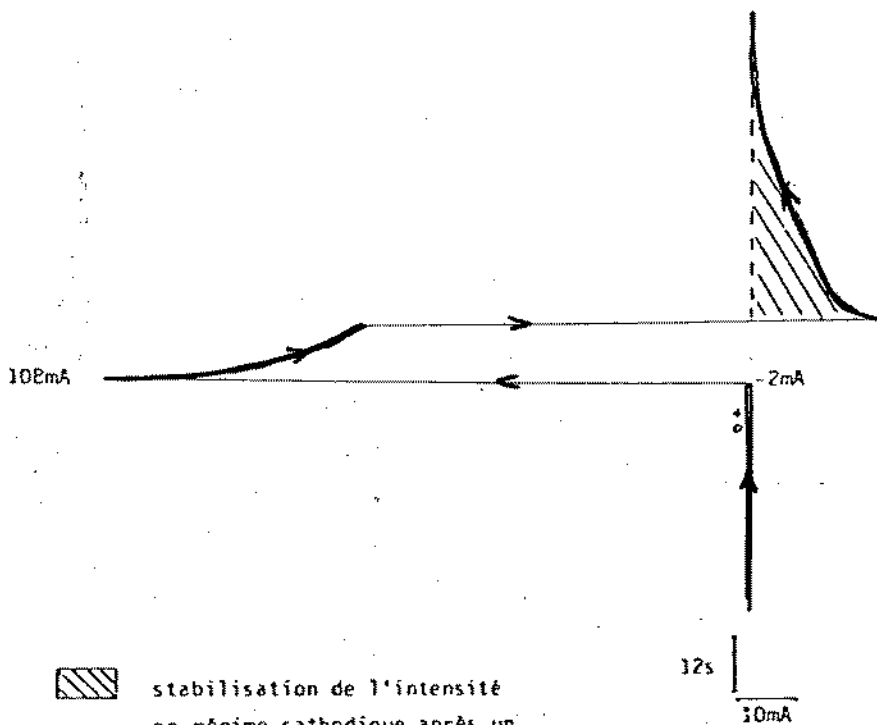


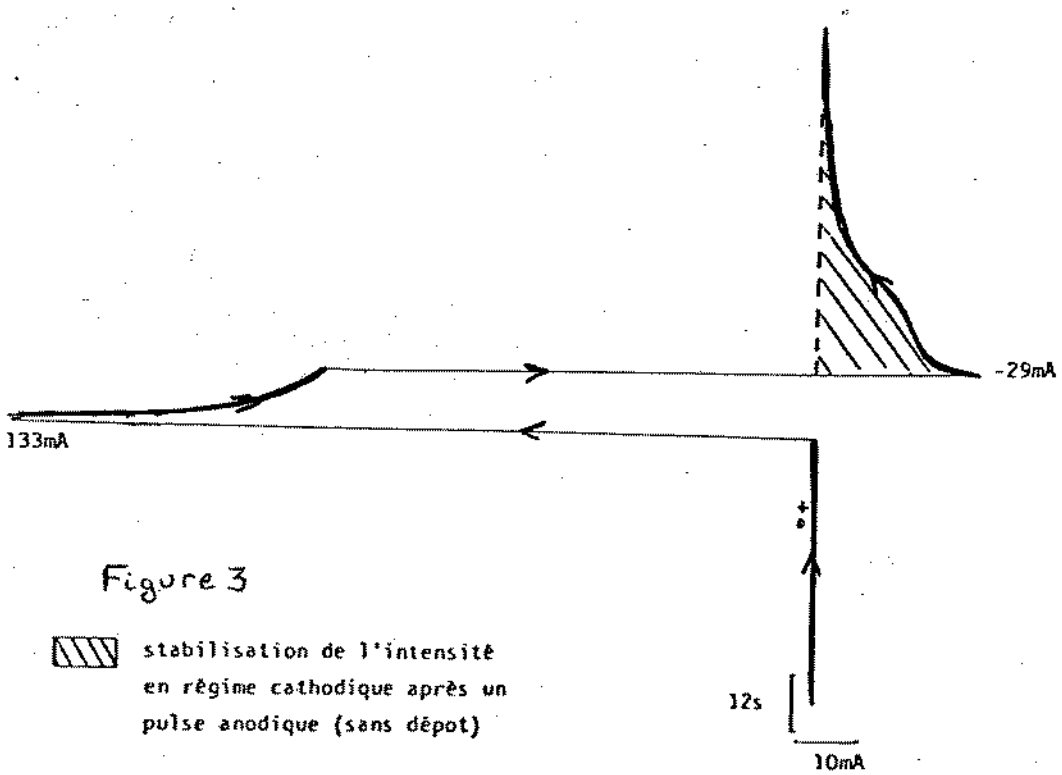
Figure 2



stabilisation de l'intensité  
en régime cathodique après un  
pulse anodique (dépôt épais)

12s

10mA



19924

